Magnetism in Metals

A symposium in Memory of Allan Mackintosh

Copenhagen, 26–29 August 1996

Invited Review Papers

Edited by D. F. McMorrow, J. Jensen *and* H. M. Rønnow

Preface

The Symposium on Magnetism in Metals took place at The Royal Danish Academy of Sciences and Letters in Copenhagen on 26-29 August 1996. The Symposium was conceived by Allan Mackintosh with the aim of bringing together a wide group of international experts in the field to discuss and review recent developments and new perspectives in magnetism research. The Programme Committee comprised Allan, Leo Falicov, Jens Als-Nielsen, Ole Krogh Andersen and myself, but Allan steered us skillfully in the choice of invited speakers. 1996 was to be the year of his sixtieth birthday and he was proud that Copenhagen had been chosen as that year's European Capital City of Culture. He had planned the programme, and had secured generous financial support for the meeting.

Alas, it was not to be. We were greatly saddened by the death of Leo Falicov in January 1995. The news of Allan's sudden death in December 1995 was a further dreadful shock for us all. We believed that Allan would have wanted us to go ahead with the Symposium, and Jette Mackintosh encouraged us to do so. I was asked to take over as Chairman of the Organising Committee: the programme was modified to include a memorial session on the first day, but otherwise was largely as Allan had planned.

The splendid conference room of the Royal Danish Academy was filled with more than 80 participants: the memorial session was a deeply moving occasion with reminiscences and tributes to Allan from his brother Ian and son Poul, and from some of his closest collaborators and friends, Hans Bjerrum Møller, Ole Krogh Andersen, Jens Jensen, Kurt Clausen and myself. The Symposium continued with the review talks, which are published in this volume. There were also a number of contributions presented as posters, which are not included here. These Proceedings begin with an obituary of Allan together with a list of his impressive range of scientific achievements and his publications.

Allan had also arranged a comprehensive social programme for the participants. The highlight of this was the magnificent Conference Banquet in Tivoli's Nimb Restaurant. We also toured the historic cathedral of Roskilde and the Viking Ship Museum before visiting Risø National Laboratory, our hosts for an excellent dinner.

The success of the Conference resulted from the collective efforts of many people. I would like to take this opportunity to thank Kurt Clausen and Ca Thi Studinski, who looked after all the financial affairs and the organisation of the participants, and Jens Als-Nielsen for the local arrangements at the Academy. Thanks go also to Des McMorrow, Jens Jensen and Henrik Rønnow for transforming the authors' manuscripts into this volume as a permanent record of the Symposium dedicated to Allan's memory.

Keith McEwen

Contents

General:

Allan Roy Mackintosh, 1936–1995

Allan Roy Mackintosh, who died on 20 December 1995 as a result of a car accident in Denmark, devoted much of his life to the study of the behaviour of electrons in solids. He made major contributions to our understanding of the fundamental electrical and magnetic properties of the rare earth metals. In Denmark, where splendid traditions had been established in astronomy, atomic, nuclear and particle physics half a century earlier, Allan Mackintosh will be remembered for his successful efforts in developing modern solid state physics. Through the European Physical Society and, more recently, within the context of the European Union, he strove to improve the quality and efficiency of physics research through international collaboration.

Born in Nottingham on 22 January 1936, he was educated at Nottingham High School and Peterhouse, Cambridge. His doctoral research was carried out in the Cavendish Laboratory, under the supervision of Sir Brian Pippard, where he investigated the Fermi surface of metals, using ultrasonic attenuation methods. It was also in Cambridge that he met Jette, his Danish wife.

On leaving Cambridge in 1960, he became Associate Professor of Physics at Iowa State University. This move was to shape the direction of his future scientific career. The University's Ames Laboratory had begun to make single crystals of the rare earth metals. The chemical properties of these elements are very similar, and consequently they had only recently been separated into pure form. However, their physical properties, particularly their magnetic behaviour, are very diverse and were, at that time, unexplored territory for the inquisitive physicist. Allan Mackintosh took up this challenge and soon established himself as a leading expert in this new field. His major contributions included the discovery (together with his student Dan Gustafson), by an elegant positron annihilation experiment, that the number of $4f$ electrons in cerium does not change significantly at the α–γ transition. Showing that Ce is a $4f$ band metal disproved the then widely accepted promotional model, and was an early contribution to heavy-fermion physics.

In 1963, he spent a sabbatical at the Risø National Laboratory, in Denmark,

where a new research reactor had just become operational. Danish physicists led by Hans Bjerrum Møller were constructing a triple-axis neutron spectrometer to measure phonons in solids. Allan Mackintosh quickly realised the scientific potential of applying this technique to measure spin waves in the rare earth metals. This was the beginning of a most fruitful collaboration that was to contribute substantially to our understanding of rare earth magnetism, and which lasted until the last hours of Allan's life.

In 1966, Allan Mackintosh moved permanently to Denmark and became Research Professor at the Technical University, Lyngby, where he remained until 1970. He brought with him from Ames not only precious rare earth crystals but also T. L. Loucks' relativistic APW programs for performing electronic structure calculations. Allan used them to demonstrate the relevance of computing Fermi surfaces to describe magnetic ordering. He soon taught Danish students how to perform such calculations and asked them to compute the Fermi surfaces of the transition metals, whose complicated d-band sheets were currently being mapped out by the de Haas–van Alphen technique. It had been known only since 1964 that, unlike the localized $4f$-electrons in the rare earth metals, the magnetic electrons in the $3d$-transition metals contribute to the Fermi surface; the role of the Coulomb correlation between them was a much discussed topic. Allan had a deep understanding of the behaviour of electrons in metals, and a profound scepticism towards oversimplified theories. Leo Falicov was his life-long discussion partner and close friend. Allan's work not only helped to establish the boundaries of the usefulness of density-functional calculations for d- and f-bands systems, but also inspired his students to develop new computational methods.

In 1970 Allan became Professor of Experimental Solid State Physics at the University of Copenhagen. Soon afterwards, at the age of 35, he was appointed Director of the Risø National Laboratory. Prompted by the oil crisis, Denmark had embarked on a national debate about the development of nuclear power for electricity generation. In this frequently heated debate, Allan Mackintosh needed all his diplomatic skills to steer the discussion with factual rather than emotional persuasion.

After 1976, he returned to his Chair in Copenhagen, where he remained until his death. He made many more important contributions to the understanding of the magnetism of the rare earths, which led to him being awarded (jointly with Hans Bjerrum Møller) the prestigious Spedding Prize in 1986. He inspired and motivated all his collaborators and students, and his scientific papers, with their carefully constructed prose, are a pleasure to read. The culmination of his research was the publication (with Jens Jensen) of Rare Earth Magnetism, a superbly written exposition of the subject that has already become a classic text. His achievements were further recognised by his election in 1991 to Fellowship of the Royal Society

of London. In Denmark, he was made a Knight of the Dannebrog Order. He was also a Fellow of the Royal Danish Academy of Sciences and Letters, the Danish Academy of Technical Sciences, the Royal Norwegian Scientific Academy and the American Physical Society. Upsalla University awarded him an honorary doctorate of philosophy in 1980.

Although research was always Allan Mackintosh's main priority, his leadership skills were much in demand. His period as director of the Risø Laboratory has already been mentioned, and from 1986 to 1989 he directed NORDITA, with its close connections to the renowned Niels Bohr Institute. He also played an increasingly important role on the European physics scene. A strong believer in the need for international collaboration, he was President of the European Physical Society from 1980 to 1982. Later, he played an important role within the EU Large Scale Facilities programme: he emphasised scientific excellence as the principal criterion for funding.

Allan Mackintosh took great pleasure in music, travelling and his comprehensive collection of malt whiskies. He disguised his enjoyment of sport and physical activity behind a facade of feigned mediocrity. On hill-walking holidays, he divided his energies between humorous discourses as to the pointlessness of climbing the next hill, and making certain that he was the first to the top. Numerous friends will also remember the warmth of the welcome extended to them by Allan and Jette at their home in Denmark.

In later years, his keen interest in the history of physics led him to investigate the mutual influence of Ernest Rutherford and Niels Bohr. He revealed important, but often overlooked, achievements of less well-known scientists, such as John Vincent Atanasoff's key role in the invention of the computer. In one of his last papers, he showed the contribution of Charles Ellis to the discovery of the neutrino. It is symbolic of his interest in the past as well as the future of physics, that he spent the last day of his life selecting experiments to be carried out in 1996 at Risø under an EU - financed programme, and then gave an eloquent seminar on the discovery of the neutrino some 60 years ago.

We have lost one of the finest physicists in magnetism and neutron scattering: the tragic nature of Allan Mackintosh's sudden death makes this loss all the more acute amongst his world-wide circle of friends and colleagues.

Allan Mackintosh's scientific achievements

Allan worked at Iowa State University between 1960 and 1966, and became interested in the rare earths and electronic structure calculations. During this period, he and his students made the following main contributions:

(a) The discovery of magnetic superzones [4].

(b) The first systematic studies of conduction-electron scattering by localized moments [5].

(c) The demonstration by positron annihilation that the number of $4f$ electrons in Ce does not change significantly at the α–γ transition [15]. This disproved the validity of the then generally accepted "promotional" model. Since the $4f$ electrons are itinerant at low temperatures, and have very large masses, this was one of the first contributions to heavy-electron physics. Throughout his life, Allan returned to the problem of understanding the transition between and the duality of the itinerant and localized character of the $4f$ electrons in Ce and Pr. He motivated his former students in the field of electronic structure calculations to push the border of validity of the itinerant picture [64,80] and, shortly before his death, he and his experimental colleagues succeeded in observing in Pr a new magnetic excitation of itinerant character [79–81].

(d) The observation of the positive or negative magnetoresistance associated with changes of the magnetic structures in Ho and Dy [16], which allowed a systematic study of the effect of magnetic superzones and spin-wave scattering, and revealed intermediate phases, later identified as helifans [73].

(e) The determination of the spin-wave energy gap in Tb from resistivity measurements [12]. The deduced value was close to that later measured by neutron scattering [39,42].

(f) The first direct observation, by positron annihilation, and interpretation, by electronic structure calculation, of the highly distorted Fermi surfaces in the heavy rare earths [23].

In 1963, Allan Mackintosh spent a sabbatical year at Risø and initiated the study of rare earth magnetism in Denmark. On returning permanently to Europe in 1966, he began a long-lasting study, with Hans Bjerrum Møller and their colleagues, of the spin waves in Tb. These experiments resulted in the following advances:

(a) The first complete study of the spin-wave spectrum for any magnetic system [35,42], allowing the deduction of the magnon density of states, the ther-

modynamic properties, and the detailed form of the exchange interaction in reciprocal and real space, in the ferromagnetic phase.

(b) Measurements of the magnons in the helical phase, the first detailed studies of the excitations of an incommensurate system [25]. Such phasons, or Goldstone modes, have since proved to be of interest in a number of incommensurate systems. From the dispersion relations, the exchange and its temperature dependence were deduced, clarifying the driving mechanism for the helical-ferromagnetic transition.

(c) Measurement of the single-ion anisotropy parameters, distinguishing between the crystal-field and magnetoelastic contributions [39].

(d) Experimental demonstration of the "frozen-lattice" effect, that the energy gap does not vanish when the hexagonal anisotropy is cancelled by a magnetic field [39].

(e) The observation of anisotropic two-ion coupling [43].

(f) Detailed studies of the interactions of magnons with phonons [25], with magnetic impurities [28], with each other [42], and with conduction electrons [50].

In recent years, Allan Mackintosh turned his attention to holmium. Together with Jens Jensen, he explained old observations and predicted new effects. The major results are:

(a) The discovery of the helifan structures [73]. These structures, which are stable in a range of intermediate fields, have many interesting features. This work has solved mysteries in the magnetization, neutron diffraction and transport properties of Ho which have been unexplained for decades, and has excited wide interest.

(b) The investigation of the effects of commensurability on magnetic excitations [69]. They established that commensurability causes an energy gap in the spin-wave spectrum of Ho at $\mathbf{q} = \mathbf{0}$, and that the dipole interaction produces a discontinuity in the dispersion relation, and thereby stabilizes the cone structure at low temperatures. The long-standing mystery of the stability of the cone structure was thereby solved.

The culmination of Allan's research in the rare earths was the book, co-authored with Jens Jensen [75], which contains many predictions of new effects and suggestions for experimental studies. These have given a considerable stimulus to rare earth research, and a number of such studies have already been initiated.

His most recent research was in examining a possible breakdown of the *standard model* of rare earth magnetism in praseodymium, where a new magnetic excitation was observed [79,81]. This new form of magnetic excitation is interpreted as arising from the dynamical response of the conduction electrons, and is thus the first observed example of a propagating paramagnon.

In 1966 at the Technical University in Lyngby, Allan Mackintosh initiated what later became a school of electronic structure calculation. He and his students were among the first to calculate the electronic structures of transition and rare earth metals, and to demonstrate that the Fermi surfaces obtained with what he called the standard single-particle potential, agree in detail with experimental results [26,27,29,37,41]. For the fcc transition metals Rh, Pd, Ir, and Pt, the excellent agreement with the extremal areas of orbits on the Fermi surface measured via the de Haas–van Alphen effect, allowed him to deduce for each orbit, the mass enhancement due to electron–phonon and electron–electron interactions, and thus to provide the first reliable estimate of the spin-fluctuation enhancement in Pd [26].

The nearly perfect agreement of the complicated Fermi surfaces obtained with this Slater-exchange potential was a strong hint that the local approximation (LDA) to density-functional formalism proposed three years earlier by Kohn and Sham for ab initio computation of ground-state properties might work. This motivated Allan's former students to develop methods for charge- and spin-selfconsistent LDA calculations. In 1975, as a first application, Allan Mackintosh et al. applied the LMTO method with the standard potential to the heavy hcp transition metals [47]. Apart from demonstrating again excellent agreement with de Haas–van Alphen measurements, they proved the efficiency of the new method and showed how it made the complicated relativistic hcp band structures intelligible in terms of "canonical" *s*-, *p*-, and *d*-bands.

During the second half of the seventies, LDA-LMTO calculations were performed for all elemental 3*d*, 4*d*, and 5*d* metals and the cohesive and magnetic ground-state properties obtained ab initio were surprisingly accurate. In a review of the electronic structure of transition metals, Mackintosh and Andersen [53] explained the LDA bands and their relation to the pressure-volume curves, the crystal structures, and the occurrence of itinerant magnetism. Furthermore, they reviewed the experimental and computed Fermi-surface and optical properties. For the much studied noble metals, Mackintosh et al. [55] investigated whether a local potential exists, which will reproduce not only the experimental ground-state properties, but also the band structures. The answer was: No, but almost.

The influence of Allan Mackintosh on the field of electronic structure calculations went far beyond the research papers he authored. He continued to provoke and motivate his large, international electronic-structure family, but usually refused to put his name on the publications. He preferred writing reviews in which

he also pointed out what to do next [58,64,70,80].

Allan Mackintosh also made important contributions to the history of both physics [82] and computing [67,72].

Publications by Allan Mackintosh

[1] *Magnetoacoustic Effects in Lead and Tin*, A.R. Mackintosh, in The Fermi Surface, eds. W.A. Harrison and M.B. Webb (John Wiley and Sons, New York, 1960), 233.

[2] *Shear Wave Attenuation in Normal and Superconducting Tin*, A.R. Mackintosh, in Proceedings of the Seventh International Conference on Low Temperature Physics (University of Toronto Press, 1960), 12.

[3] *The Electronic Structure of the Rare Earth Metals*, A.R. Mackintosh, in Rare Earth Research, eds. J.F. Nachman and C.E. Lundin (Gordon and Breach, New York, 1962), 272.

[4] *Magnetic Ordering and the Electronic Structure of Rare Earth Metals*, A.R. Mackintosh, Phys. Rev. Lett. **9**, 90 (1962).

[5] *Scattering of Conduction Electrons by Localized Moments in Metals*, A.R. Mackintosh and F.A. Smidt, Phys. Lett. **2**, 107 (1962).

[6] *Ultrasonic Attenuation in Lead*, A.R. Mackintosh, Proc. Roy. Soc. A **271**, 88 (1963).

[7] *Magnetoacoustic Effects in Longitudinal Fields*, A.R. Mackintosh, Phys. Rev. **131**, 2420 (1963).

[8] *Model for the Electronic Structure of Metal Tungsten Bronzes*, A.R. Mackintosh, J. Chem. Phys. **38**, 1991 (1963).

[9] *Magnetoresistance and Fermi Surface Topology of Thallium*, A.R. Mackintosh, L.E. Spanel and R.C. Young, Phys. Rev. Lett. **10**, 434 (1963).

[10] *Positron Annihilation in Liquid and Solid Mercury*, D.R. Gustafson, A.R. Mackintosh and D.J. Zaffarano, Phys. Rev. **130**, 1455 (1963).

[11] *Electronic Structure of Liquid Gallium by Positron Annihilation*, D.R. Gustafson and A.R. Mackintosh, Phys. Lett. **5**, 234 (1963).

[12] *Energy Gaps in Spin Wave Spectra*, A.R. Mackintosh, Phys. Lett. **4**, 140 (1963).

[13] *The Thermoelectric Power in Chromium and Vanadium*, A.R. Mackintosh and L. Sill, J. Phys. Chem. Solids 24, 501 (1963).

[14] *The Fermi Surface of Metals*, A.R. Mackintosh, Scientific American **209**, 110 (1963).

[15] *Positron Annihilation in Rare Earth Metals*, D.R. Gustafson and A.R. Mackintosh, J. Phys. Chem. Solids **25**, 389 (1964).

[16] *Magnetoresistance in Rare Earth Single Crystals*, A.R. Mackintosh and L.E. Spanel, Solid State Commun. **2**, 383 (1964).

[17] *Magnetic Scattering of Neutrons in Chromium*, H. Bjerrum Møller, K. Blinowski, A.R. Mackintosh and T. Brun, Solid State Commun. **2**, 109 (1964).

[18] *Interaction of Long Wavelength Phonons with Electrons*, A.R. Mackintosh, in Phonons and Phonon Interactions, ed. T.A. Bak (W.A. Benjamin, New Work, 1964), 181.

[19] *Open-Orbit Resonances in Tin*, R.J. Kearney, A.R. Mackintosh and R.C. Young, Phys. Rev. **140**, 1671 (1965).

[20] *Inelastic Scattering of Neutrons in Chromium*, H. Bjerrum Møller and A.R. Mackintosh, in Inelastic Scattering of Neutrons (IAEA, Vienna, 1965), Vol.I, 95.

[21] *Antiferromagnetism in Chromium Alloy Single Crystals*, H. Bjerrum Møller, A.L. Trego and A.R. Mackintosh, Solid State Commun. **3**, 137 (1965).

[22] *Observation of Resonant Lattice Modes by Inelastic Neutron Scattering*, H. Bjerrum Møller and A.R. Mackintosh, Phys. Rev. Lett. **15**, 623 (1965).

[23] *Positron Annihilation and the Electronic Structure of Rare Earth Metals*, R.W. Williams, T.L. Loucks and A.R. Mackintosh, Phys. Rev. Lett. **16**, 168 (1966).

[24] *Antiferromagnetism in Chromium Alloys. I. Neutron Diffraction*, W.C. Koehler, R.M. Moon, A.L. Trego and A.R. Mackintosh, Phys. Rev. **151**, 405 (1966).

[25] *Magnetic Interactions in Rare Earth Metals from Inelastic Neutron Scattering*, H. Bjerrum Møller, J.C. Houmann and A.R. Mackintosh, Phys. Rev. Lett. **19**, 312 (1967).

[26] *Fermi Surfaces and Effective Masses in FCC Transition Metals*, O. Krogh Andersen and A.R. Mackintosh, Solid State Commun. **6**, 285 (1968).

[27] *Electronic Structure of Rare Earth Metals II. Positron Annihilation*, R.W. Williams and A.R. Mackintosh, Phys. Rev. **168**, 679 (1968).

[28] *Magnetic Interactions in Tb and Tb-10% Ho from Inelastic Neutron Scattering*, H. Bjerrum Møller, J.G. Houmann and A.R. Mackintosh, J. Appl. Phys. **39**, 807 (1968).

[29] *Energy Bands and Magnetic Ordering in Terbium.* A.R. Mackintosh, Phys. Lett. **28A**, 217 (1968).

[30] *Antiferromagnetism in Chromium Alloys. II. Transport Properties*, A.L. Trego and A.R. Mackintosh, Phys. Rev. **166**, 495 (1968).

[31] *Investigation of Localized Excitations by Inelastic Neutron Scattering*, A.R. Mackintosh and H. Bjerrum Møller, in Localized Excitations in Solids, ed. R.F. Wallis (Plenum Press, New York, 1968), 721.

[32] *The Fermi Surface*, A.R. Mackintosh, in Theory of Condensed Matter (IAEA, Vienna, 1968), 783.

[33] *Neutron Scattering Conference Summary*, A.R. Mackintosh, In Neutron Inelastic Scattering (IAEA, Vienna, 1968), Vol.II, 243.

[34] *Electronic Structure and Magnetic Excitations in Rare Earth Metals*, A.R. Mackintosh, in Magnetism in Metals and Alloys, Kjeller Report KR-132 (1969).

[35] *Exchange Interactions in Rare Earth Metals*, H. Bjerrum Møller, M. Nielsen and A.R. Mackintosh, in Les Eléments des Terres Rares (CNRS, Paris, 1970) Vol.II, 277.

[36] *Magnon Interactions in Terbium*, M. Nielsen, H. Bjerrum Møller, and A.R. Mackintosh, J. Appl. Phys. **41**, 1174 (1970).

[37] *Electronic Structure and Phase Transitions in Yb*, G. Johansen and A.R. Mackintosh, Solid State Commun. **8**, 121 (1970).

[38] *Crystal Fields and the Magnetic Properties of Pr and Nd*, T. Johansson, B. Lebech, M. Nielsen, H. Bjerrum Møller, and A.R. Mackintosh. Phys. Rev. Lett. **25**, 524 (1970).

[39] *Magnetic Anisotropy in Rare Earth Metals*, M. Nielsen, H. Bjerrum Møller, P.A. Lindgård and A.R. Mackintosh, Phys. Rev. Lett. **25**, 1451 (1970).

[40] *Magnetism in the Light Rare Earth Metals*, A.R. Mackintosh, J. Phys. (Paris) **32**, C1-482 (1971).

[41] *Electrons and Spin Waves in Heavy Rare Earth Metals*, A.R. Mackintosh, Critical Reviews in Solid State Sciences **3**, 165 (1972).

[42] *Spin Waves*, A.R. Mackintosh and H. Bjerrum Møller, in Magnetic Properties of Rare Earth Metals, ed. R.J. Elliott (Plenum Press, London, 1972), 187.

[43] *Anisotropic Coupling between Magnetic Ions in Terbium*, H. Bjerrum Møller, J.G. Houmann, J. Jensen, and A.R. Mackintosh, in Neutron Inelastic Scattering (IAEA, Vienna, 1972), 603.

[44] *High Field Magnetization of Light Rare Earth Metals*, K.A. McEwen, G.J. Cock, L.W. Roeland and A.R. Mackintosh, Phys. Rev. Lett. **30**, 287 (1973).

[45] *Mechanisms of Magnetic Anisotropy in Rare Earth Metals*, A.R. Mackintosh, in Magnetism and Magnetic Materials - 1972 (AIP, New York, 1973).

[46] *Magnetic Excitations and Magnetic Ordering in Praseodymium*, J.G. Houmann, M. Chapellier, A.R. Mackintosh, P. Bak, O.D. McMasters and K.A. Gschneidner, Phys. Rev. Lett. **34**, 587 (1975).

[47] *Electronic Structure of hcp Transition Metals*, O. Jepsen, O. Krogh Andersen and A.R. Mackintosh, Phys. Rev. B **12**, 3084 (1975).

[48] *The Magnetism of Rare Earth Metals*, A.R. Mackintosh, Physics Today **30**, 23 (1977).

[49] *Central Peaks and Soft Modes in Praseodymium*, J.G. Houmann, B. Lebech, A.R. Mackintosh, W.J.L. Buyers, O.D. McMasters and K.A. Gschneidner, Physica **86-88B**, 1156 (1977).

[50] *Magnon Lifetimes in Terbium at Low Temperatures*, H. Bjerrum Møller and A.R. Mackintosh, J. Phys. (Paris) **40**, C5-28 (1979).

[51] *Magnetic Excitations in Praseodymium*, J.G. Houmann, B.D. Rainford, J. Jensen, and A.R. Mackintosh, Phys. Rev. B **20**, 1105 (1979).

2

[52] *Magnetic Excitations in Rare Earth Systems*, A.R. Mackintosh, J. Magn. Magn. Mater. **15-18**, 326 (1980).

[53] *The Electronic Structure of Transition Metals*, A.R. Mackintosh and O. Krogh Andersen, in Electrons at the Fermi Surface, ed. M. Springford (Cambridge University Press, 1980), 149.

[54] *From Chaos to Order - Solid State Physics in the Twentieth Century* (in Danish), A.R. Mackintosh, Royal Danish Academy of Sciences and Letters (1980), **24**.

[55] *Potentials, Band Structures and Fermi Surfaces in the Noble Metals*, O. Jepsen, D. Glötzel and A.R. Mackintosh, Phys. Rev. B **23**, 2684 (1981).

[56] *Energy Bands and Mass Enhancement in Yttrium*, H.L. Skriver and A.R. Mackintosh, Inst. Phys. Conf. Ser. **55**, 29 (1981).

[57] *Atomic Structure with a Programmable Calculator*, A.R. Mackintosh and P.E. Mackintosh, Eur. J. Phys. **2**, 3 (1981).

[58] *Conference Summary: Perspective on Nordic Solid State Physics*, A.R. Mackintosh, Physica Scripta **25**, 901 (1982).

[59] *Hyperfine Interactions, Magnetic Impurities and Ordering in Praseodymium*, H. Bjerrum Møller, J.Z. Jensen, M. Wulff, A.R. Mackintosh, O.D. McMasters and K.A. Gschneidner, Phys. Rev. Lett. **49**, 482 (1982).

[60] *Neutron Scattering and Magnetism*, A.R. Mackintosh, Inst. Phys. Conf. Ser. **64**, 199 (1983).

[61] *Excitations of Neodymium Ions in Praseodymium*, M. Wulff, J. Jensen, A.R. Mackintosh, H. Bjerrum Møller, O.D. McMasters and K.A. Gschneidner, J. Magn. Magn. Mater. **31-34**, 601 (1983).

[62] *The Stern-Gerlach Experiment, Electron Spin and Intermediate Quantum Mechanics*, A.R. Mackintosh, Eur. J. Phys. **4**, 97 (1983).

[63] *Quantum Correlations and Measurements*, A.R. Mackintosh and J. Jensen, Eur. J. Phys. **4**, 235 (1983).

[64] *Cerium and Cerium Intermetallics: 4f-Band Metals?*, A.R. Mackintosh, Physica **130B**, 112 (1985).

[65] *Rare Earth Solutes and the Magnetic Properties of Terbium*, C.C. Larsen, A.R. Mackintosh, H. Bjerrum Møller, Sam Legvold and B.J. Beaudry, J. Magn. Magn. Mater. **54-57**, 1165 (1986).

[66] *Foundations of Rare Earth Magnetism*, A.R. Mackintosh and H. Bjerrum Møller, J. Less Common Metals **126**, 1 (1986).

[67] *The First Electronic Computer*, A.R. Mackintosh, Physics Today **40**, (3), 25 (1987).

[68] *Electronic Structure of Cubic Sodium Tungsten Bronze*, N.E. Christensen and A.R. Mackintosh, Phys. Rev. B **35**, 8246 (1987).

[69] *Magnetic Excitations in Commensurable Periodic Structures*, C.C. Larsen, J. Jensen and A.R. Mackintosh, Phys. Rev. Lett. **59**, 712 (1987).

[70] *Magnetic Metals*, A.R. Mackintosh, Europhysics News **19**, 41 (1988).

[71] *Spin Dynamics of Thulium Ions in Terbium*, C.C. Larsen, J. Jensen, A.R.Mackintosh and B.J. Beaudry, J. Phys. (Paris) **49**, C8-331 (1988).

[72] *Dr. Atanasoff's Computer*, A.R. Mackintosh, Scientific American **256**, 90 (1988).

[73] *Helifan: A New Type of Magnetic Structure*, J.Jensen and A.R. Mackintosh, Phys. Rev. Lett. **64**, 2699 (1990).

[74] *Commensurable Spin Structures and their Excitations*, A.R. Mackintosh and J. Jensen, in Disorder in Condensed Matter Physics, eds. J.A. Blackman and J. Taguena (Clarendon Press, Oxford, 1991), 213.

[75] *Rare Earth Magnetism: Structures and Excitations*, J. Jensen and A.R. Mackintosh (Clarendon Press, Oxford, 1991), pp 403.

[76] *Novel Magnetic Phases in Holmium*, J. Jensen and A.R. Mackintosh, J. Magn. Magn. Mater. **104-107**, 1481 (1992).

[77] *Magnetic Structures and Excitations in Rare Earth Metals: Old Problems and New Solutions*, A.R. Mackintosh and J. Jensen, Physica B **180-181**, 1 (1992).

[78] *Neutrons and X-Rays in Magnetism*, A.R. Mackintosh, Physica B **192**, 200 (1993).

[79] *New Mode of Magnetic Excitation in Praseodymium*, K.N. Clausen, K.A. McEwen, J. Jensen and A.R. Mackintosh, Phys. Rev. Lett. **72**, 3104 (1994).

[80] *Localized and Itinerant f-Electrons*, A.R. Mackintosh, in New Trends in Magnetism, Magnetic Materials, and their Applications, eds. J.L. Morán-López and J.M. Sanches (Plenum Press, London, 1994).

[81] *Crystal Fields and Conduction Electrons in Praseodymium*, K.N. Clausen, S. Aagaard Sørensen, K.A. McEwen, J. Jensen and A.R. Mackintosh, J. Magn. Magn. Mater. **140-144**, 735 (1995).

[82] *The Third Man: Charles Drummond Ellis, 1895-1980*, A.R. Mackintosh, Notes Rec. R. Soc. Lond. **49**, 277 (1995).

[83] *Neutrons and Rare Earth Magnetism*, A.R. Mackintosh, Neutron News **6**, (4), 22 (1995).

Hans Bjerrum Møller
Kurt N. Clausen
Jens Jensen
Ole Krogh Andersen
Keith A. McEwen

Developments in Magnetism
Since the Second World War

R. J. Elliott

Department of Physics, Theoretical Physics,

1 Keble Road, Oxford, England.

1   Introduction

I was given this task by Allan Mackintosh. Against his unique combination of charm, wit, and determination it was impossible to refuse. Only later when I realised the size of the task did I begin to wonder why his choice had fallen on me. In looking back I found that Casimir had expressed my sentiments precisely at the beginning of a talk he had given 20 years ago. He said "as a young physicist I regarded an interest in the history of physics as an unmistakable sign of either incompetence or beginning senility. Today I am inclined to regard a lack of interest in the history of our science as a mark of deplorable immaturity". But, perhaps unfairly, I began to suspect that Allan had some deeper motive. As we all know his tremendous curiosity and energy had recently led him to take an interest in, and write articles about, some aspects of the history of science. I believe that Allan had something special he wanted to tell us about the development of magnetism, and I was the straw man who was introduced to set the scene.

Alas, we shall never know what Allan had in mind. You are left with only my dry bread for the sandwich and the spicy filling that he would have provided is missing. Such feelings of loss spread far beyond the subject of this talk. For 30 years I have talked physics with him, and together we have watched and contributed to the development of our understanding of the rare earths. In recent years, because of other distractions, these meetings have been less frequent but he remained a good friend – one of the few people of whom one could honestly say that you were really pleased to see him whatever the circumstances. All our lives, and our subject, have been made irretrievably the poorer by his death.

2   Background

Turning to the subject it was necessary to find some definition which would restrict the topic to manageable proportions. I decided to define "Magnetism" as the material covered in the regular International Conferences on Magnetism which have been held every 3 years since Grenoble in 1958 to the 13th of the series in Warsaw in 1994. The proceedings of these meetings are listed in the References (Proc. I.C.M., 1959, 1962, 1964, 1968, 1971, 1974, 1977, 1980, 1983, 1986, 1988, 1992, 1995). Although not technically part of the sequence there were two earlier meetings with a similar format in 1950 also in Grenoble (Colloque Int. de Ferro et Antiferromagnetisme, 1951) and in 1952 in Maryland (Magnetism Conference, 1953). These were landmarks in the development of the subject because the changes brought by the war, both in new techniques like magnetic resonance and neutron diffraction, and also in the greatly increased support for research in this area, were already being felt. These changes can be thrown into sharp relief by comparison with the only other major international conference of this type ever held, that in Strasbourg in May 1939 (Le Magnetisme, 1940).

To be complete there had been one other major international conference devoted to Magnetism at an earlier date, the Solvay Meeting of 1930 (Le Magnetisme, 1932), but I do not think we ordinary mortals would have recognised it as such, although I believe we would have been at home in all the later meetings. Only about a dozen papers were presented to the Solvay Conference but the roll-call of participants sounds more like that for a scientists Valhalla. It included Bohr and Einstein, Heisenberg and Dirac, Sommerfeld and Pauli, Fermi and Kapitza as well as Langevin, Weiss, Zeeman and van Vleck. The actual papers seem much more prosaic. It is hard for us to understand the enormous leaps of comprehension which were necessary to apply the new quantum mechanics. But after its dramatic success in atomic physics, magnetism proved one of the most fruitful areas of applicability. van Vleck's book "The Theory of Electric and Magnetic Susceptibilities" (van Vleck, 1932) and Stoner's "Magnetism and Matter" (Stoner, 1934) remain classics to this day.

In 1939 the fundamental ideas which underpin our understanding of magnetic phenomena today were largely in place. The Strasbourg conference of that year was able to look back also to the triumphs of the classical era. Weiss was its Chairman and although Langevin was too ill to attend his comments on the development of magnetism during the preceding 50 years were included in the paper by his colleague Bauer. Langevin's work at the turn of the century (Langevin, 1905) on diamagnetism and paramagnetism, and his derivation of the famous formula of the magnetisation of an assembly of classical magnetic dipoles had, together with Curie's empirical law (Curie, 1895) for the susceptibility, proved a significant

milestone in our understanding of magnetic materials. Weiss' brilliant concept of the molecular field not only provided a basic understanding of ferromagnetism but gave us a prototype theory for all phase transitions. In spite of red herrings like the existence of a fundamental (Weiss) magneton, quantum mechanics now provided a sound basis for the explanation of these phenomena while at the same time removing many of the difficulties which had become apparent in the detailed application of classical theory, particularly to magneto-optic effects.

One of the most bizarre of these was Miss van Leeuwen's theorem (van Leeuwen, 1921) which demonstrated that in classical statistical mechanics the magnetic susceptibility must be zero. (Bohr in his 1911 dissertation had already gone some way towards a similar result). The reason why Langevin's formula violated this theorem, while giving the physically correct result, lay in his assumptions about fixed magnetic dipole moments which were at variance with the strictly classical conditions.

In 1939 several papers were presented giving detailed properties of paramagnetic salts using both static and optical measurements while Simon and Casimir discussed their use in adiabatic demagnetisation. Néel gave a paper on antiferromagnetism and there were references to other types of magnetic order. Kramers discussed both crystal fields and exchange for magnetic ions in insulators. The difficulty in understanding the most important of all magnetic materials, ferromagnetic iron remained much to the fore and Mott's paper on "Recent Progress and Difficulties in the Electron Theory of Metals" was a prototype of many more to come.

Two articles discussing the history of the development of magnetism have appeared in recent years as part of the International Project on the History of Solid State Physics (Keith and Quédec, 1992) and in the Institute of Physics comprehensive history of 20th Century Physics (Stevens, 1996).

3   Post-war growth

At the first post-war conference in Grenoble in 1950 there were 49 contributed papers and by the first ICM in that City in 1958 the number had grown to 78. The next time ICM met in Grenoble in 1970 the number was approaching 500; it passed a thousand in Paris in 1988 and was almost 2000 in Warsaw in 1994. The growth shown in Fig. 1 is not quite exponential but is highly non-linear. At various times there have been attempts to analyse the growth of different aspects of the subject. Figs. 2 and 3 show the distribution between nine rather arbitrary groups of topics made in 1979 and 1985. It is in practice rather difficult to define meaningful categories and to allocate all papers between them.

The rise and fall of some topics is clearly shown, but others are hidden within
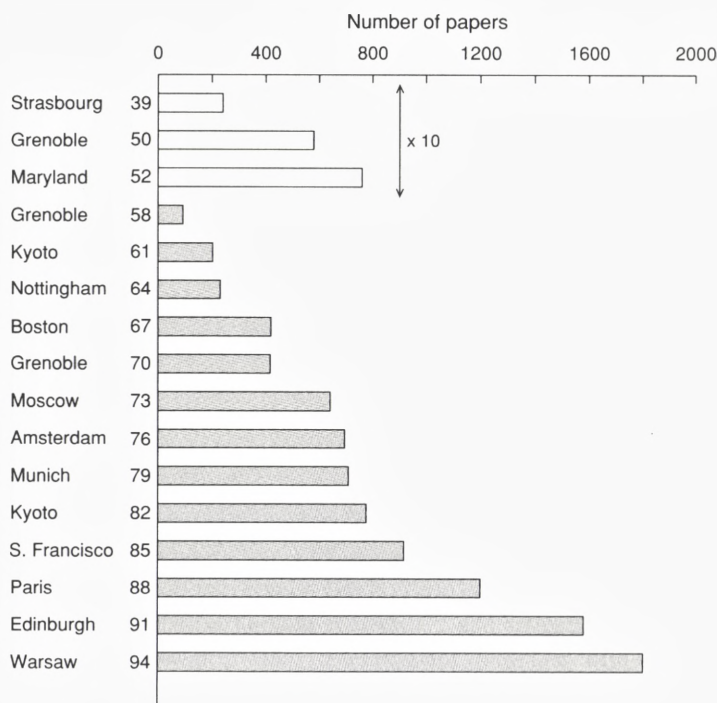
Figure 1. Numbers of published papers at the International Conferences on Magnetism – together with three earlier meetings. The latter are on an enhanced (×10) scale.

their broader allocation. Perhaps the most dramatic is the rise in interest in disordered spin systems in the 1970's. Until that time, apart from metallic alloying, efforts had concentrated on studying systems which were as pure and regular as possible. This new upsurge of research was partly driven by widespread interest in the newly defined concept of a spin glass. A similar rise in research into phase transitions and in particular into critical phenomena also occurred across this period as improved theories using the renormalisation group, and much more accurate experiments became possible. On the other hand the upsurge of interest in mixed valent and heavy fermion systems, or the impact of new techniques like the Mössbauer effect are less obvious in the numbers.

Throughout the period practical uses of magnetic materials have, of course, attracted the attention of the research community. The improved understanding of magnetic domains extensively described by Bozorth (Bozorth, 1951, see also Colloque Int. de Ferro et Antiferromagnetisme, 1951) has allowed great improve-

ment in the performance of permanent magnets for electric motors, generators, loudspeakers, etc., and of soft magnetic materials for transformers and inductors. In addition the technology of tape recording has been dramatically improved although the basic principles remain unchanged. Attempts to use magnetic materials for data storage has, however, largely lost out to semiconductor materials so that the study of ferrites and garnets which was such an important feature in the 50's and 60's has been attenuated after that period. As a result of these fluctuating fortunes for industrial application the proportion of papers submitted to ICM from industrial laboratories has reduced over the years.

It is almost impossible to know where to start to summarise all this effort. Since this is a conference about Magnetism in Metals I should certainly give that area attention, although it was not in my brief to confine myself to that field. I therefore propose to discuss first the development of our understanding of magnetic insulators, in order to highlight the differences between them and the metals. After that I shall pass to metallic systems with particular reference to the transition metals and finally to the rare earths. I make no apology for emphasising the latter since their properties reflect both those of insulators and metals, of localised and itinerant electrons. They also provide a thread of my own Odyssey through these years – I attended many of the ICM Meetings starting with Maryland in 1952 where I went as a newly graduated D.Phil on my way to a post-doc in Berkeley with Kittel, but they also provide a thread for my longstanding contacts with Allan Mackintosh who was also to be found at these meetings from 1964 onwards. I met him in Warsaw in 1994 and know he was planning to attend the meeting in 1997. His book with Jens Jensen "Rare Earth Magnetism: Structures and Excitations" (Jensen and Mackintosh, 1991) summarises much of our knowledge of the Rare Earths which has been accumulated since the war.

4   Insulators

As has been said the basic properties of the insulating salts of the $3d$ transition metals and the rare earths were broadly understood by the beginning of the period under review, and similar compounds from the $4d$ and $5d$ series, together with the actinides, could also be accounted for by extensions of the basic model. In its simplest form this regarded the transition metal ion as an isolated entity interacting with its surroundings only by a crystalline electric field derived from the Coulomb forces of the charges on the surrounding ions. In the case of the rare earths the $4f$ electrons lay inside the outer shells and hence experienced only a weak field. As a result their magnetic properties closely resembled those of the free ions, although significant changes were observed at low temperatures due to the splitting of the
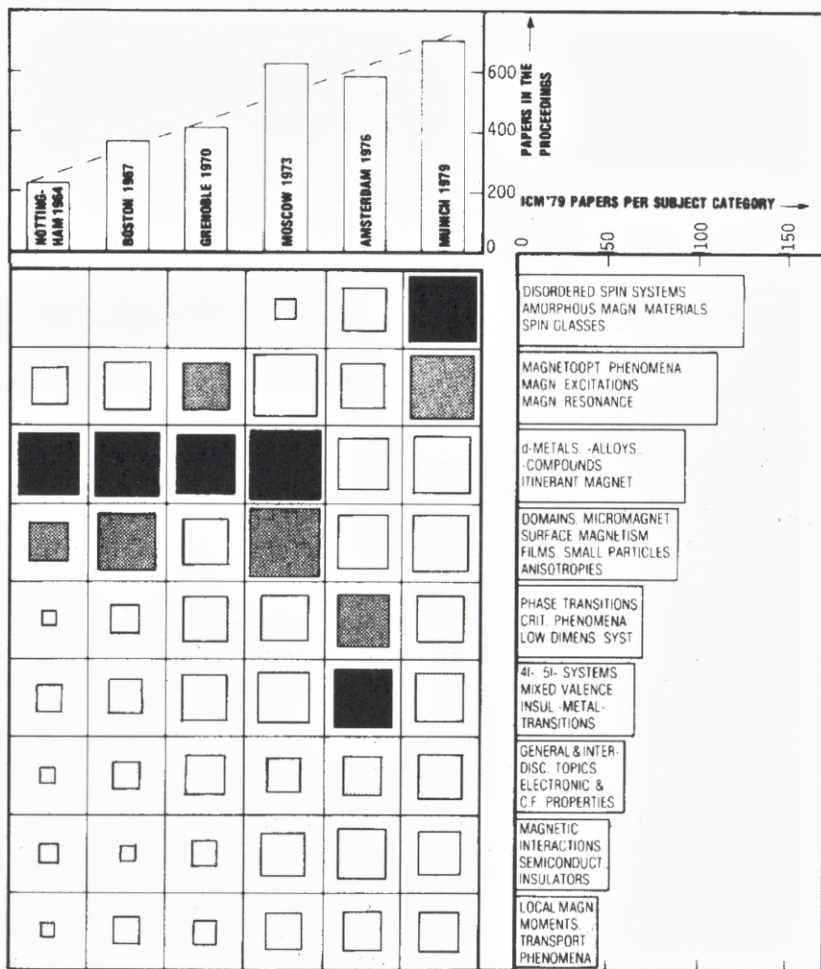
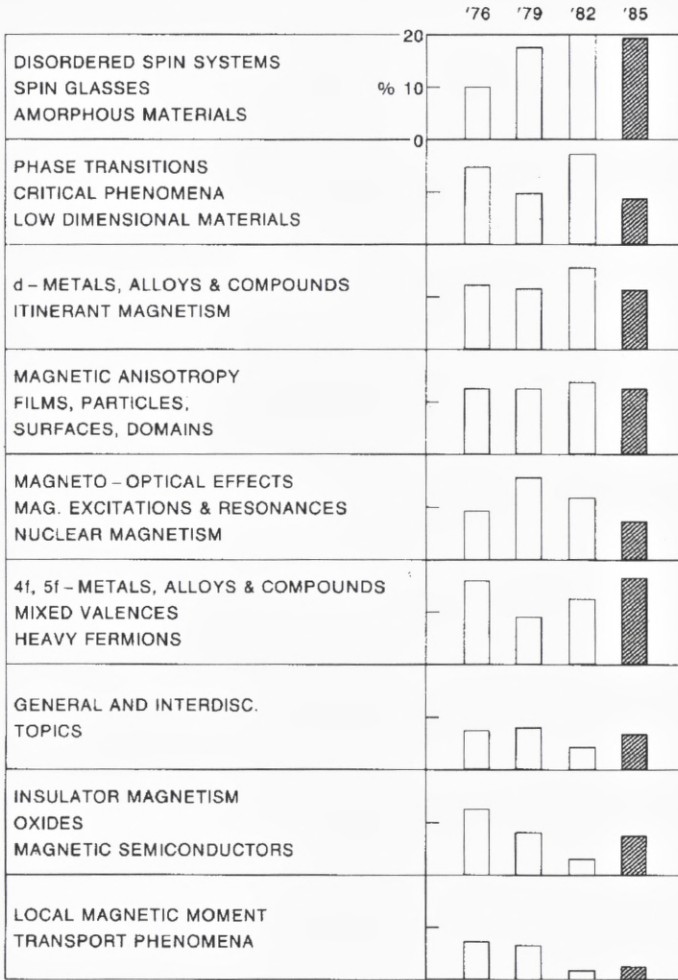Figure 2. Distribution of papers at various ICMs in various categories (after Proc. I.C.M., 1980).

Figure 3. Distribution of papers at various ICMs in various categories (after Proc. I.C.M., 1986).

spin–orbit multiplets with total angular momentum J by the field. However, the salts of the transition metals usually exhibited a spin–only magnetic moment. Here, the larger crystalline field was believed to split the energy levels of the lowest Russell–Saunders multiplet so that the degeneracy arising from the total angular momentum L was removed while the degeneracy from the total spin S remained. The actual splitting depended on the nature of the field but the lowest level was normally a singlet since any symmetry induced degeneracy was expected to be split by the spontaneous distortion of the Jahn–Teller effect (Jahn and Teller, 1937; van Vleck, 1939; Ham, 1968).

This picture was confirmed by detailed experimentation in the 1950's when, in particular, paramagnetic resonance allowed detailed investigation of the lowest lying states. Originally pioneered by Zavoisky it was brought to maturity by Bleaney and his group in Oxford (Abragam and Bleaney, 1970) using higher frequency microwave sources derived from the wartime radar programme. This work was assisted by parallel theoretical developments. It was Bloch (1946) who had first written down the equations governing the motion of spins driven by an oscillating field which gave the underlying description not only of this phenomenon but that of nuclear magnetic resonance which was to become even more ubiquitous. While its impact in chemistry and beyond has been far greater than that of paramagnetic resonance, it has been more peripheral to the development of magnetism as defined in this talk. It is therefore one of the many topics which must be excluded.

The Bloch equations emphasised the importance of relaxation times in determining the conditions under which resonance could be observed and identified two times, spin–spin relaxation giving the time for the magnetic systems to reach equilibrium, and spin–lattice relaxation giving the time for the magnetic system to come into equilibrium with the heat bath. Gorter and others had also emphasised this problem in connection with adiabatic demagnetisation and van Vleck gave detailed treatments of both phenomenon (see Abragam and Bleaney, 1970).

One of the new features of paramagnetic resonance, first observed by Penrose in 1949 before his untimely death, showed that in dilute crystals hyperfine structure due to the interaction between the magnetic electrons and the nuclear spin could be observed. Observations of these fields at the nucleus were later to be extended using the Mössbauer effect to materials like ferromagnetic metals (Frauenfelder, 1962).

These detailed experiments rapidly demonstrated the shortcomings of the simple crystal field model. It was obvious from a chemical point of view that the d-electrons were involved in covalent bonding with the surrounding ions. It was therefore preferable to regard the transition metal ion and its surrounding ligands which were usually arranged in an octahedral form, as a single complex molecule. The unpaired magnetic electrons occupy antibonding states of the complex with

wave functions concentrated on the magnetic ion but with significant overlap on to the neighbouring ligands (see Fig. 4). This model was essential for the $4d$ and $5d$ systems in order to predict the correct ground state. The spatial extent of the magnetic electrons was further confirmed by the clever experiments of Feher and others (Feher, 1956; see also Abragam and Bleaney, 1970) who showed by ENDOR that they could measure the hyperfine field at the nuclei beyond the initial shell.
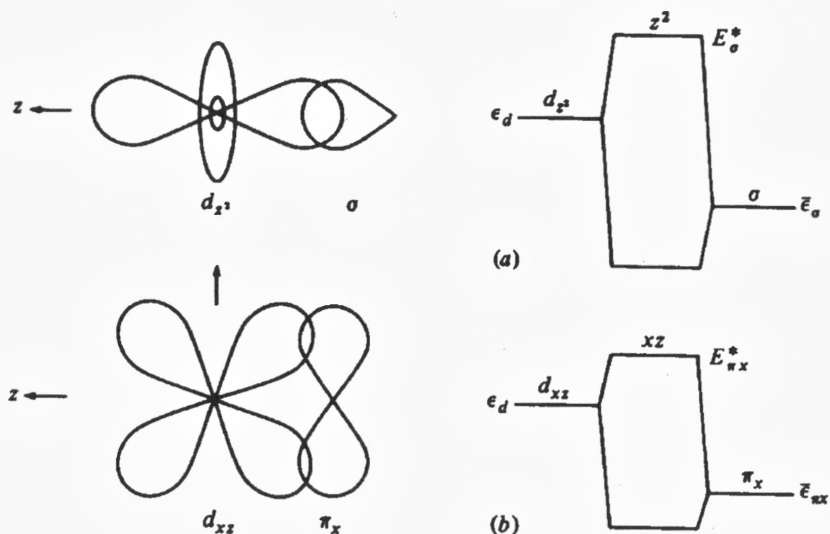

Figure 4. Schematic representation of bonding between d orbitals of two different symmetry types and $s - p$ orbitals on a single ligand. A symmetric combination of these orbitals on the six octahedral neighbours gives bonding and antibonding states with relative energy E^*.

Further complications were revealed by a detailed study of the hyperfine interaction on the magnetic ion. The most striking effect occurred in Mn^{++} ions where the $3d^5$ configuration has an $^6S_{\frac{5}{2}}$ ground state which should give zero magnetic field at the nucleus. The large observed result was interpreted by Abragam and Pryce (see Abragam and Bleaney, 1970) as due to admixture of s wave functions which had a density at the nucleus and hence a hyperfine interaction through the contact term.

Thus, although the general behaviour of the energy levels of the paramagnetic ion could be interpreted on the crystal field model, in particular using the symmetry

reflected there, the actual situation was much more complicated and the values of the parameters such as the crystal field splitting itself and the g-factors which gave the Zeeman splitting, together with the hyperfine coupling terms could not easily be calculated from simple models. These parameters were often summarised by a spin Hamiltonian. For example the lowest energy levels of a divalent manganese ion in many salts can be described as follows ($S = 5/2$)

$$\mathcal{H} = \mu \boldsymbol{H} \cdot \bar{\bar{g}} \cdot \boldsymbol{S} + D[3S_z^2 - S(S+1)] + F[S_x^4 + S_y^4 + S_z^4 - (1/5)S(S+1)(3S(S+1)-1)]$$

$$+ \boldsymbol{S} \cdot \bar{\bar{A}} \cdot \boldsymbol{I},$$

where $\bar{\bar{g}}$ and $\bar{\bar{A}}$ are tensors with axial symmetry while the D and F terms reflect the residual results of the crystalline field.

This phenomenological model of the low lying energy states of an isolated paramagnetic ion was further extended by consideration of the exchange interaction between pairs of such ions. Exchange interactions between electrons within an atom were already well understood and detailed calculations were well known in diatomic molecules such as H_2. In an attempt to find a better analogy for the magnetic systems Slater had made an exhaustive investigation of O_2 which has a $S = 1$ ground state (Magnetism Conference, 1953). But detailed calculations for the magnetic systems were more difficult to make for detailed comparisons with the experimental results which became available from a variety of sources. Heisenberg and Dirac had pointed out that the effect of exchange between two atoms with spin S but no orbital degeneracy could also be written as a spin Hamiltonian

$$\mathcal{H} = -2J(1,2)\boldsymbol{S}(1) \cdot \boldsymbol{S}(2),$$

where the sign is conventional so that positive J leads to a preferred parallel alignment. In most cases J turns out to be negative. Also residual orbital effects lead to anisotropy so that J becomes a tensor and $\mathcal{H} = -2\boldsymbol{S}(1) \cdot \bar{\bar{J}}(1,2) \cdot \boldsymbol{S}(2)$. An extreme model which is simpler for theoretical investigation is the Ising model

$$\mathcal{H} = -2I(1,2)S_z(1)S_z(2).$$

Sometimes direct information on J can be obtained from isolated pairs such as occur naturally in copper acetate (Abragam and Bleaney, 1970). In a more normal crystal with a periodic array of magnetic ions the sum of the pairwise interactions leads to a well defined magnetic order.

The magnetic neutron diffraction experiments of Shull and colleagues (1951) showed for the first time the details of the antiferromagnetic order predicted by Néel, from which values of the exchange interactions could be derived. It was clear that the largest interaction came not necessarily between those ions which were

closest as a direct overlap of d wave functions would suggest, but between those ions which had a bridging ligand (see Fig. 5). Thus the overlap of the magnetic electrons onto the neighbouring anions was crucial in explaining the origin of the exchange interaction as discussed originally by Kramers and subsequently developed by Anderson (1950, 1963) and others. It was given the name of superexchange and again it was possible to explain the results phenomenologically by assuming an exchange interaction which was largely isotropic of the Heisenberg type though it also contained some elements of anisotropy. However, fundamental first principle calculations of the value of these exchange parameters proved extremely difficult.
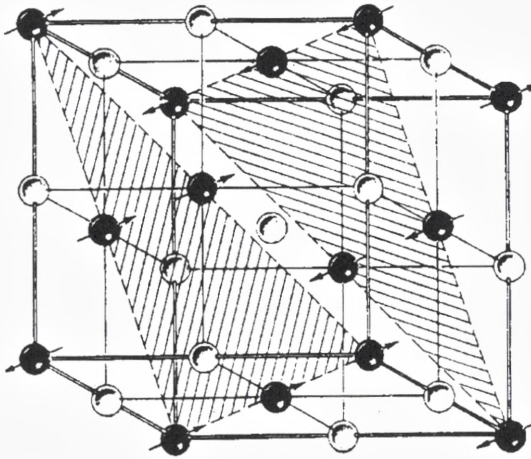

Figure 5. Antiferromagnetic order in MnO. The most strongly coupled spins are antiparallel and have an intervening oxygen ion.

Further information about the detailed value of the exchange parameters became available with experiments which measured the low energy excitations of the ordered magnetic systems. These spin waves which were originally postulated for ferromagnets by Bloch (1930), had been discussed in the antiferromagnetic structures by Kittel and others (Keffer, 1966). Those excitations with wave vector $k = 0$ could be observed by resonance techniques but gave limited information. With the use of the triple axis neutron spectrometer developed by Brockhouse it became possible to observe the spectrum of spin waves across the Brillouin zone and derive the values of the exchange parameters directly from them (see Fig. 6).

One of the other areas which was developed extensively in the 1960's was the
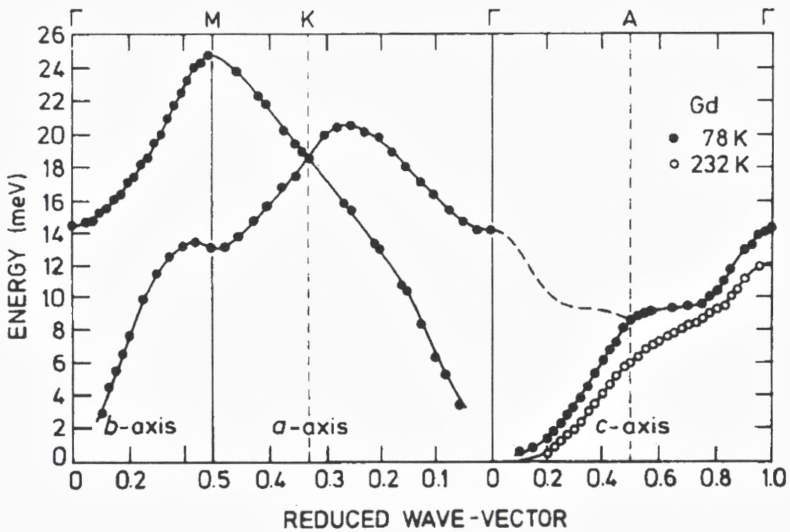
Figure 6. A remarkable example of the complete spin wave spectrum of Gd. (after Koehler et al., 1970).

theoretical and experimental study of the thermodynamic properties of these co-operatively coupled spin systems. The Weiss molecular field theory gave an overall description containing a high temperature paramagnetic phase where the susceptibility was given by the Curie–Weiss law, a transition temperature below which the magnetic order appeared and grew continuously to saturate at $T = 0$. Expansion of the thermodynamic functions in power series of $(1/T)$ gave a more detailed treatment of the high temperature phase (Domb and Green, 1974), while study of the excitations such as spin waves gave a description at low T. In the case of the Ising model, where the low temperature parameter is $\exp(-J/T)$ it was possible to obtain many terms in both expansions, but for the Heisenberg model even the first few terms required a remarkable tour de force (Dyson, 1956). Much effort was expended on extrapolating these expansions towards the singularity which occurred at the transition temperature where fluctuations are important (Fig. 7). The introduction of renormalisation group methods (see Fisher, 1974) allowed a detailed treatment of this singular critical region and magnetic systems proved to be the most appropriate experimental testing ground for these theories. The non-classical behaviour in the region of the critical temperature is more pronounced in low dimensional arrays and so two-dimensional magnetic systems have been extensively studied. In one dimension the fluctuations dominate and no transition
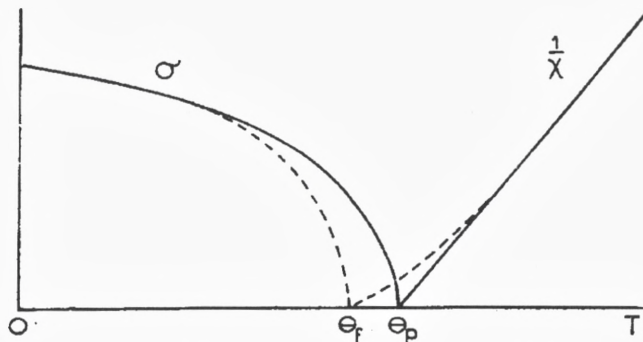
Figure 7. An early representation after Néel in Le Magnetisme (1940) of "effect des fluctuations du champ moleculaire..." At $T \to T_c (= \Theta_f)$ the critical effects give $\chi^{-1} \sim (T - T_c)^\gamma$ with $\gamma > \gamma_o = 1$ and $\sigma \sim (T_c - T)^\beta$ with $\beta < \beta_o = 1/2$ where β_o, γ_o are the mean field values.

occurs although interesting effects occur as $T \to 0$.

Thus the standard model of individual magnetic ions described basically in terms of their atomic d and f electrons but having some overlap into orbitals on neighbouring ions, and interacting with neighbours through an exchange interaction mediated via that overlap, was developed to give a full and sophisticated description of the magnetic properties of insulators. Its spectacular success tended to divert attention away from the fundamental assumptions which went into the model, which some workers found difficult to accept. This was particularly true for those who came from groups which focussed their attention on understanding the magnetism of the transition metals. Here it was clear, looking no further than the saturation moment of Ni at 0.6 μ_B, that an assembly of paramagnetic ions could not provide a satisfactory description. Such work started naturally from band theory where the conduction electrons occupied, to a first approximation, independent states which covered the whole crystal. The answer, of course, lay in the correlation energy brought about by the interaction between the electrons. At the 1952 conference there was an extended and heated discussion summarised by Smoluchowski (Magnetism Conference, 1953). [Although not recorded there it included, if my memory serves me correctly, an extensive discussion of the rhetorical question – why is NiO an insulator? It has an odd number of electrons per unit cell and hence cannot have an integral number of filled bands. The doubling of the size of unit itself from antiferromagnetic order is not relevant since the conductivity does not change at the transition temperature. The answer lies in the energy penalty which is required to change a pair of Ni^{2+} ions into Ni^+ and Ni^{3+}.] In the standard model of insulator magnetism it is assumed that this correlation energy is so great that all

such states can be ignored, while at the other end of the scale simple band theory of non interacting electrons assumes that there is no energy penalty at all. Clearly the true situation lies between but because it is so difficult to deal with much of the early period involved discussion between workers who began from one extreme or the other and were unable to meet in the middle.

5   Transition metals

As early as 1934 Stoner (1934) had shown that a plausible model of ferromagnetism in Ni and Fe could be made by introducing the Weiss molecular field into a simple band theory and, moreover, by appropriate choice of parameters it could account non integral saturation moments. This idea was made more realistic by Mott and others by the introduction of both s and d bands which were hybridised, while the relevant exchange interaction was assumed to act on the d components. These ideas could account to a large extent for the properties of alloys as systematised in the Slater–Pauling curves (see Fig. 8). Attempts to calculate the exchange energy were confined to the Hartree–Fock method using simplified concepts introduced by Wigner and others to allow for the fact that the exclusion principle kept electrons of like spin at a greater distance than those of opposite spin. This helped increase the ferromagnetic component of exchange. After the war calculations of band structure gradually improved with the increase in computer power, but even then calculations of the exchange energy were difficult and unreliable even in respect of the sign. The situation was further complicated by the discovery that Cr had a small antiferromagnetic moment while Mn also showed unusual magnetic order patterns (Wilkinson et al., 1962).

Furthermore, the new experimental techniques were providing information which it was easier to interpret in terms of localised moments, similar to those in insulators, than from the simple band theory. Neutron diffraction revealed moment distributions in both elements and alloys which were similar to those observed in salts while spin waves observed initially by ferromagnetic resonance in films and then by inelastic neutron scattering were also found to have properties similar to those in insulators (Lowde, 1956; Seavey and Tannenwald, 1958). Moreover, the behaviour characteristic of localised moments persisted in the fluctuations which were observed around the transition temperature and above. This lead to some further controversy between those theoreticians who approached the problem from opposite ends. It was clear that a better treatment of the correlation energy was needed and various models were put forward to try to bridge the gap. van Vleck suggested that this could be achieved by restricting the configurations of the d-electrons allowed on each atom but a specific formulation of the problem which
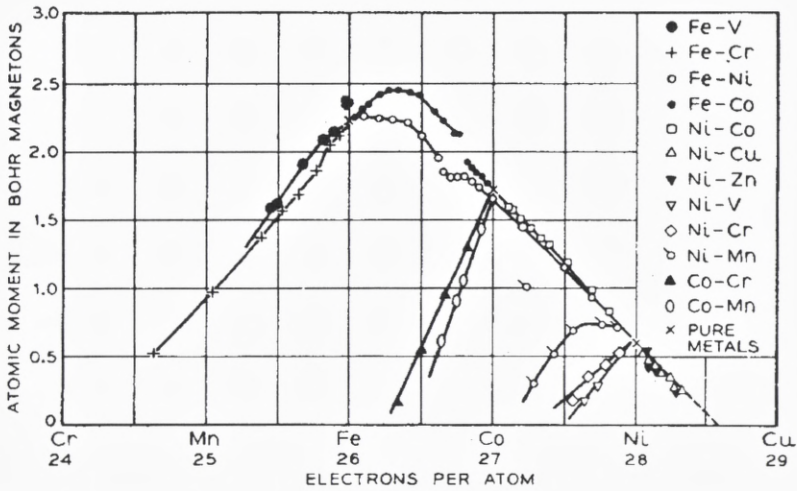
Figure 8. The Slater–Pauling curve of the saturation magnetisation in transition metal alloys plotted as a function of electron concentration which can be broadly interpreted in terms of band filling (after Bozorth, 1951).

allowed detailed evaluation was lacking. Zener (1951) proposed that it was the interaction between the conduction electrons and the *d*-shells which was mainly responsible for ferromagnetism.

The first major step in resolving this dilemma came from the study of the free electron gas without specific reference to magnetism. The use of diagrammatic techniques in many particle physics began in the early 1950's soon after their introduction into field theory. Using Feynmann diagrams and the Greens function methods of Schwinger the theory of the homogeneous electron gas was worked out by many contributors during the period 1957–8 (Mahan, 1981). Very crudely, the main understanding derived from this was that the long range Coulomb interaction gave rise to collective excitations, the plasmons, at high frequency leaving a gas of effectively free particles with a Fermi distribution and a residual short range screened interaction which resulted in both a further direct and an exchange energy. The low frequency excitations of this system could be regarded as the promotion of quasi particles across the Fermi surface giving rise to what has been described as a Fermi liquid.

The second important step was to concentrate on electrons in bands, as opposed to free electrons, interacting via the short range screened interaction. A great deal was clarified by the Hubbard model (Hubbard, 1963, 1966) which used a single band with electrons in orbitals which were localised around each site (Wannier

3*

functions). If the residual interaction was of sufficiently short range that it was confined to a single atomic site its only component coupled electrons of opposite spin since electrons of the same spin were forbidden by the exclusion principle. The simple Hubbard Hamiltonian takes the form

$$\mathcal{H} = \sum_{\ell} \left[\sum_{\delta} t(\delta) a_{\sigma}^{+}(\ell) a_{\sigma}(\ell + \delta) + U n_{\sigma}(\ell) n_{-\sigma}(\ell) \right],$$

where $a_{\sigma}^{+}(\ell)$ creates an electron on site ℓ with spin σ and $n_{\sigma}(\ell) = a_{\sigma}^{+}(\ell) a_{\sigma}(\ell)$ is the number of such electrons. This has two essential parameters, the band width determined by t and the interaction energy U. A somewhat more realistic model was proposed by Anderson (1961), included both s and d electrons which were hybridised while the interaction energy was assumed to act only between the d-electrons. Here

$$\mathcal{H} = \sum_{\ell\sigma} \epsilon_{d\sigma} n_{d\sigma}(\ell) + U_{\sigma\sigma'} n_{d\sigma}(\ell) n_{d\sigma'}(\ell) + \sum_{k} \epsilon_s(k) a_s^{+}(k) a_s(k)$$

$$+ \sum_{k\ell\sigma} A_{sd\sigma}(k) e^{ik.R(\ell)} [a_s^{+}(k) a_{d\sigma}(\ell) + a_{d\sigma}^{+}(\ell) a_s(k)],$$

where $\epsilon_s(k)$ are the band energies of the s electrons and $A(k)$ gives the hybridisation. By a number of innovative techniques Hubbard obtained approximate solutions to this problem which showed that if t/U was small, i.e. U was large, an insulator was obtained with an effective exchange interaction in the form t^2/U When U was small the system was effectively still a Fermi gas.

Further evaluation of this model showed that it predicted both individual particle excitations across the Fermi surface and between the Fermi surfaces of different spin, as well as collective excitations in the form of spin waves. It therefore produced, from a single model, properties which were thought to be typical of both the extreme localised and band models. This was important because it was shown (Gold et al., 1971) by de Haas–van Alphen measurements that the ferromagnetic metals did indeed show Fermi surfaces and that these were different for the two spin types. These detailed measurements required further refinement of the band structure calculations but with the rapid evolution of improved numerical techniques reasonable agreement between theory and experiment has been obtained.

A thorough discussion of all aspects of this problem was given by Herring (1966) in his book entitled "Exchange Interactions Among Itinerant Electrons". In particular he reviews the controversy of the itinerant versus localised spin models of ferromagnetic metals and the experimental properties which require explanation.

6   Rare earth metals

The study of the magnetism of the rare earth metals has proved one of the most interesting and satisfying topics of the post-war years. In the 1930's it had been established that these materials showed, at room temperature, a paramagnetism similar to their salts but that things were much more complicated at low temperatures. In particular gadolinium had been found to be ferromagnetic below room temperature. After the war the topic was boosted by the availability of relatively pure elements obtained by improved separation techniques by Spedding and his colleagues at Ames. But the real breakthrough came in 1960 when Koehler and Wollan showed by neutron diffraction (Koehler et al., 1961) that these materials displayed a wealth of interesting types of magnetic order which had hitherto been unexpected. The heavy metals Gd–Tm showed various magnetic phases where components of the magnetisation varied sinusoidally as one moved from layer to layer along the c axis to give simple helices in Tb, Dy, a cone in Er, and longitudinal wave in Tm (Fig. 9). Moreover, these phases changed as the temperature was lowered in a way which appeared to be controlled by magnetic anisotropy. At high temperatures the wave vector q of the wave varied continuously and was incommensurate with the lattice dimension, at lower temperatures the system locked in to commensurate structures. There was also a distortion reflecting the crystallographic symmetry and a tendency towards ferromagnetic order at the lowest temperature. The magnetic moments were, by and large, those expected for the free ions.

Later experiments elucidated the more complex orderings found in Pr, Nd, and to some extent in Sm. Here the q of the modulation was parallel to the basal plane and had three equivalent axis arising from the hexagonal symmetry. Further complications were induced by the double hexagonal close packed crystal structure which gives two types of ionic site. The elements at the ends and in the middle of the series were anomalous because it was energetically preferred to change the f configuration to a full shell in Lu and a half filled shell in Eu. Ce proved even more interesting since it exists in two phases which broadly correspond to the configuration for f^0 and for f^1.

The essential outlines of this remarkable behaviour could be broadly understood on the basis of a "standard model" (Jensen and Mackintosh, 1991) in which the magnetism was carried by the f electrons which were strongly correlated so that the configuration was fixed. As in the salts these were subjected to a crystal field reflecting the symmetry of the surroundings. In the heavy rare earths this was predominantly axial with a smaller hexagonal component. The many electron nature of the atomic f^n wave functions meant that for a charge distribution which energetically favoured a quadrupole moment for the electron cloud which lay in the
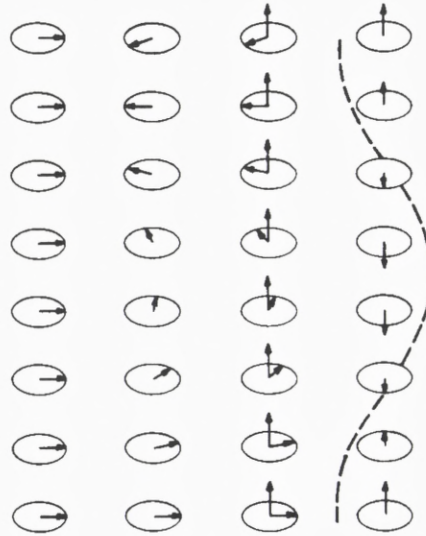
Figure 9. Simple magnetic structures found in the heavy rare earth metals. The moments within each hexagonal layer are parallel and these may be arranged to give a ferromagnet, helix, cone and longitudinal wave respectively. In real systems these are distorted at lower temperature by anisotropy and phase pinning effects.

equatorial plane, the preferred direction of the moments would change from planar to axial between Ho and Er as observed in the magnetic structures. The hexagonal component was responsible for the distortion of the simple helical patterns as the temperature was lowered.

The results suggested that hybridisation between the f electrons and the s-d conduction bands must be small and the main candidate for the origin of the exchange interaction was the polarisation of this conduction electron cloud. Rudermann and Kittel (1954) had shown earlier that the most important coupling between nuclear spins in a metal was of this form and the idea had been extended by Kasuya (1956) and Yosida (1957) to magnetic d and f electrons. In order to favour the observed magnetic ordering it was necessary that the spin susceptibility of the electron gas should peak not at $q = 0$ which would favour ferromagnetism or at the q for a zone boundary which would favour antiferromagnetism but at some intermediate point. This would be facilitated if there was nesting of the Fermi surface where two or more areas were parallel. Over the years calculations of the band structure of these materials have improved to a point where such properties are plausibly predicted Freeman (1972).

Further details of the relevant parameters were evaluated by other methods,

notably the observation of spin waves and the effects of strong applied magnetic fields. These required a number of refinements including anisotropic exchange and magnetostrictive effects but the basic model remained intact as a broad picture. In some ways it is simpler than the transition metals since the f electrons remain strongly correlated and have properties very similar to those in salts while the conduction electrons have well defined Fermi surfaces as has been shown from de Haas–van Alphen measurements (Mattocks and Young, 1977; Wulff et al., 1988) on Gd and Pr.

In all this Allan Mackintosh played a central role. His interest derived from his period in Ames and he made significant contributions to the theory of resistivity and to improved band structure calculations. Later, at Risø, he and his colleagues pushed forward a number of neutron diffraction studies including the observation of magnetic order in Pr which only exists because of the coupling of the nuclear spins to the singlet electronic ground states. All of this is splendidly summarised through his long standing collaboration with Jens Jensen in their book (Jensen and Mackintosh, 1991).

Hybridisation of the f electrons with the conduction electrons is observed in compounds of those elements where the valence is known to vary; notably Ce, Tm, and particularly in uranium in the actinides which exists in compounds with valence varying between three and six. The narrow f bands so generated give rise to a number of interesting effects, the most striking of which is the huge electronic heat capacity associated with large effective masses and hence to the title of heavy fermion compounds, as an alternative to mixed valence compounds. As will be seen from the analysis in Sect. 2 these have enjoyed a significant vogue during the period under review.

Another important phenomena for isolated local moments which have strong interactions with the conduction electrons is the effect named after Kondo (1969) which we can only mention here.

7   Conclusion

The period since the war has seen an enormous growth in the study of magnetism. Ever more sophisticated experiments on a wider and wider group of materials has shown the remarkable richness of the phenomena. The number of people working in the field and the extent of the results available continues to grow. Naturally occurring materials are being overtaken by artificially constructed systems with enhanced desired properties, for example the compounds which give improved hard and soft ferromagnets, the spin glasses, and most recently the multilayers of different magnetic species which show among other effects giant magneto-resistance

(Proc. I.C.M., 1995). But underlying all this are relatively simple concepts which are underpinned by quantum mechanics. For magnetic salts these derive from the unfilled shell configurations d^n, f^n and their interactions with the crystalline electric field of their surroundings and bonding to nearby ligands. The molecular field of Weiss derives from exchange interaction between pairs of such ions. In metallic systems the essential ingredient is the band structure but it must include a treatment of correlation effects in order to give the interesting magnetic properties. The initial success of the theory of insulators based on a phenomenological spin Hamiltonian tended to obscure this point, but more recent work has shown its essential validity. For both models, actual numerical calculations from first principles of the parameters which can be derived from experiment is difficult and has only been achieved in a relatively few cases.

In giving this talk I am conscious of its superficiality and of the large number of areas which it has not been able to address. An obvious one is the magnetism of conduction electrons in semiconductors and metals outside the transition groups. Here much work has been done to elucidate the Fermi surface in metals and to study the Landau ladder of levels expected in semiconductors. The most dramatic consequence of the latter has been the quantum Hall effect but somehow this has not been considered to be "magnetism". One area which does have a magnetic component is the study of high T_c superconductors and these have been extensively reported at Magnetism Conferences. The key element has proved to be CuO planes where the d bands are narrow and the system is almost "mixed valent". At perfect stoichiometry the d holes on the Cu display antiferromagnetism, and only with doping does the superconductivity become apparent.

This paper represents a necessarily personal and idiosyncratic view of the development of magnetism over the last 50 years, coloured as it is by my own perspective and experience. I hope, nevertheless that I have discharged the last request that Allan Mackintosh made to me in a manner which he would have approved – and that it provides an appropriate background for this conference.

References

Abragam A and Bleaney B, 1970: *Electronic Paramagnetic Resonance of Transition Metals* (Oxford University Press, Oxford)

Anderson P, 1950: Phys. Rev. **79**, 950

Anderson P, 1961: Phys. Rev. **124**, 41

Anderson P, 1963: *Magnetism* (Academic Press, New York) Vol. 1

Bloch F, 1930: Z. Phys. **61**, 206

Bloch F, 1946: Phys. Rev. **70**, 460

Bozorth R, 1951: *Ferromagnetism* (Van Nostrand)

Colloque Int. de Ferro et Antiferromagnetisme, 1951: J. Phys. Rad. **12**, 149

Curie P, 1895: Ann. Chim. Phys. (7 series) **5**, 289

Domb C and Green M, 1974: *Phase Transitions and Critical Phenomena*, (Academic Press, London) Vol. 3

Dyson F, 1956: Phys. Rev. **102**, 1717

Feher G, 1956: Phys. Rev. **103**, 824

Fisher M, 1974: Rev. Mod. Phys. **46**, 597

Frauenfelder EH, 1962: *The Mössbauer Effect* (Benjamin, New York)

Freeman A, 1972: in *Magnetic Properties of Rare Earth Metals* (Plenum, New York) p. 245

Gold A et al., 1971: Int. J. Magn. **2**, 357

Ham F, 1968: Phys. Rev. **166**, 307

Herring C, 1966: *Exchange Interactions among Conduction Electrons* (Academic Press, New York) *Magnetism*, Vol. IV

Hubbard J, 1963: Proc. Roy. Soc. **276**, 238

Hubbard J, 1966: Proc. Roy. Soc. **296**, 82; *ibid.*, 100

Jahn H and Teller E, 1937: Proc. Roy. Soc. **A161**, 220

Kasuya T, 1956: Prog. Theor. Phys. **16**, 45

Keffer F, 1966: *Handbuch der Physik* (Springer Verlag, New York) Vol. 18

Keith S and Quédec P, 1992: *Out of the Crystal Maze* (Oxford University Press, Oxford) Chap. 6

Koehler W, Wollan EO, Wilkinson MK and Cable JW, 1961: *Rare Earth Research* (Macmillan, New York) p. 149

Koehler W, Child HR, Nicklow RM, Smith HG, Moon RM and Cable JW, 1970: Phys. Rev. Lett. **24**, 16

Kondo K, 1969: *Solid State Physics* (Academic Press, New York) Vol. 23

Langevin P, 1905: Ann. Chim. Phys. (8 series) **5**, 70

Le Magnetisme, 1932: 6th Cons. de Solvay, (Gauthier-Villars, Paris)

Le Magnetisme, 1940: 3rd Coll. Sci. de C.N.R.S. (Paris)

Lowde R, 1956: Proc. Roy. Soc. **235**, 305

Jensen J and Mackintosh AR, 1991: *Rare Earth Magnetism: Structures and Excitations* (Oxford University Press, Oxford)

Magnetism Conference, 1953: Rev. Mod. Phys. **25**, 1

Mahan G, 1981: *Many Particle Physics* (Plenum, New York)

Mattocks P and Young R, 1977: J. Phys. F **7**, 1219

Proc. I.C.M., 1959: J. Phys. Rad. **20**

Proc. I.C.M., 1962: J. Phys. Soc. Japan **17** (Suppl. B1)

Proc. I.C.M., 1964: (Institute of Physics, Bristol)

Proc. I.C.M., 1968: J. App. Phys. **39**, 363

Proc. I.C.M., 1971: J. Phys. (Paris) **32** (Suppl. C1)

Proc. I.C.M., 1974: (Nauka, Moscow) 5 Vols.

Proc. I.C.M., 1977: Physica **86–88**

Proc. I.C.M., 1980: J. Magn. Magn. Mater. **15–18**

Proc. I.C.M., 1983: J. Magn. Magn. Mater. **31–34**

Proc. I.C.M., 1986: J. Magn. Magn. Mater. **54–57**

Proc. I.C.M., 1988: J. Phys. (Paris) **49–51**(C8)

Proc. I.C.M., 1992: J. Magn. Magn. Mater. **104–107**

Proc. I.C.M., 1995: J. Magn. Magn. Mater. **140–144**

Rudermann M and Kittel C, 1954: Phys. Rev. **96**, 99

Seavey M and Tannenwald P, 1958: Phys. Rev. Lett. **1**, 168

Shull C, Wollan E and Strausen W, 1951: Phys. Rev. **83**, 333

Stevens K, 1996: *Twentieth Century Physics* (Institute of Physics, Bristol) Chap. 14

Stoner E, 1934: *Magnetism and Matter*, (Methuen, New York)

van Leeuwen J, 1921: J. Phys. (Paris) (6 series) **2**, 361

van Vleck JH, 1932: *The Theory of Electric and Magnetic Susceptibilities* (Oxford University Press, Oxford)

van Vleck JH, 1939: J. Chem. Phys. **7**, 72

Wilkinson M et al., 1962: Phys. Rev. **127**, 2080

Wulff M, Lonzarich GG, Fort D and Skriver H, 1988: Europhys. Lett. **7**, 629

Yosida K, 1957: Phys. Rev. **106**, 893

Zener C, 1951: Phys. Rev. **81**, 440

Magnetic Structures of Rare Earth Metals

Roger A. Cowley

Oxford Physics, Clarendon Laboratory,

Parks Rd, Oxford OX1 3PU, UK

and

Jens Jensen

Ørsted Laboratory, Niels Bohr Institute,

Universitetsparken 5, 2100 Copenhagen, Denmark

Abstract

The recent development in the understanding of the magnetic structures of two rare earth elements are described. These include the observation of distortions in the structures which can only be explained by interactions which break the symmetry between the two superlattices and which have a trigonal form. The observation of a connection between the commensurate modulation, the ordered basal-plane moment and the c/a ratio, and the difference in the magnetic structures of epitaxial grown materials compared with the bulk. The structures of alloys of Ho with non-magnetic Y and Lu and for the alloys of Ho and Er are also reviewed.

1 Introduction

The study of the magnetic structures and interactions in the rare earth metals was one of the topics to which Allan Mackintosh made a major contribution and in which he was most interested. This interest culminated in his book with one of us (Jensen and Mackintosh, 1991) which described in detail both the experimental results and theories of the magnetism of rare earths. In this article our intention is to discuss some of the developments which have taken place since 1991. These developments have arisen even though the basic principles of rare earth magnetism were well established, partly because of the development of new experimental techniques but also because the book provided a stimulus to new work on the rare earth metals. In a short article we cannot discuss the progress made in the whole of rare earth magnetism. We have therefore chosen to concentrate on the magnetic structures of two of the heavy rare earth metals, Ho and Er, of alloys of Ho with the

non-magnetic elements Y and Lu and of alloys of Ho with Er. In the book it was proposed that trigonal interactions may have significant effects on the magnetic structures in these systems. Since then the studies of the long-periodic complex structures in the Ho and Er based materials have confirmed that this is the case.

Nevertheless, there are still some topics which we shall not discuss in detail. One of these is the extensive set of experiments performed particularly with x-ray and neutron scattering techniques to study the properties of the paramagnetic to incommensurately modulated structure by Wang et al. (1991), Gaulin et al. (1988), Thurston et al. (1993, 1994), Lin et al. (1992), Hagen et al. (1992) and Helgesen et al. (1995). Briefly the exponents measured in these experiments are not in agreement with the predictions of any of the theories. Furthermore, the observation of two length scales (Thurston et al., 1993, 1994) in Ho were the first to show that this behaviour occurred in magnetic systems and, although it is now established that the long length scale is associated with the surface, there is still no detailed understanding of the results (Cowley, 1997).

In this paper we shall describe in detail the new results for the low-temperature structures and their implications for the nature of the magnetic interactions. In the next section we describe results and theory for the magnetic structure of holmium and in Sect. 3 similar results for Er. Both of these sets of results demonstrate that the properties of the rare earths cannot be understood solely in terms of single-ion anisotropy and exchange interactions between pairs of spins which depend only quadratically on the spin components. In Sect. 4 we summarise the results obtained on the properties of Ho/Y and Ho/Lu alloys and the information they provide about the magnetic interactions. In Sect. 5 we describe the magnetic structures of Ho/Er alloys and then in a final section summarise the results and outstanding problems.

2   Magnetic structures of holmium

The magnetic structure of Ho was determined initially by Koehler et al. (1966). They showed that between the Néel temperature of 132 K and about 19 K, the magnetic structure consisted of ferromagnetically coupled moments within each basal plane and that the orientation of the moments rotated in successive basal planes giving a helical structure. The average angle of rotation is described by a wavevector $\mathbf{q}$, which has the value of 0.275 $\mathbf{c}^*$ at T_N and reduces on cooling. Below about 19 K the wavevector $\mathbf{q}$ locks in to 1/6 $\mathbf{c}^*$ and the structure develops a ferromagnetic moment along the c axis giving a cone structure. Koehler et al. (1966) and Felcher et al. (1976) showed that the structure was not a homogeneous helix but distorted so as to produce a bunching of the magnetic moments around the easy b axes. The 12-layered commensurable structure in the $1/6\,\mathbf{c}^*$ phase consists of

pairs of layers with the moments nearly along the same b axis, while the moments rotate 60° from one pair to the next. The bunching angle between the moments in the pairs and the nearest b axis was found to approach 5.8° in the zero temperature limit.

Gibbs et al. (1985) used x-ray resonant scattering techniques to study Ho and showed that the wavevector did not change smoothly with temperature but that below 30 K there were a series of lock-ins to commensurable structures. They proposed the long-period commensurable structures to be the 12-layered structure modified by regularly spaced spin slips at which only one plane was associated with an easy axis instead of two planes. These spin-slip structures give rise to a characteristic pattern of the neutron scattering which was measured (Cowley and Bates, 1988) and then used to produce detailed models of these structures. These
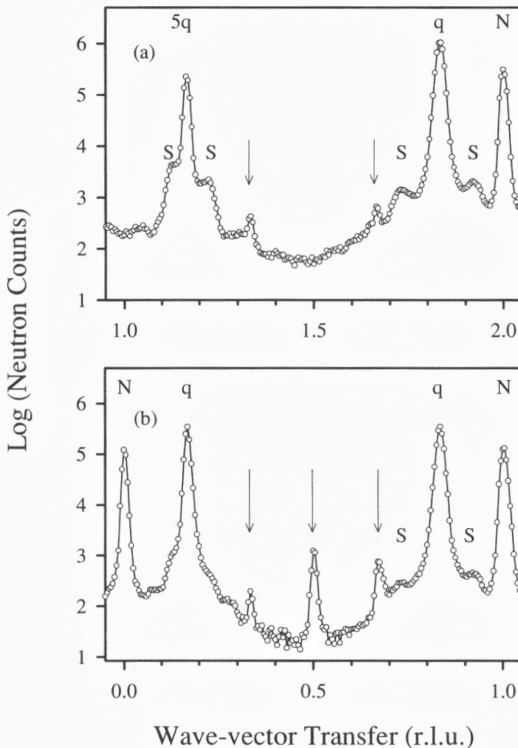

Figure 1. The neutron scattering from Ho at 10 K when the wavevector transfer is varied along (a) [00ℓ] and (b) [10ℓ]. The peaks marked with arrows cannot be accounted for by an undistorted cone structure while the peaks marked S are spurious (Simpson et al., 1995).
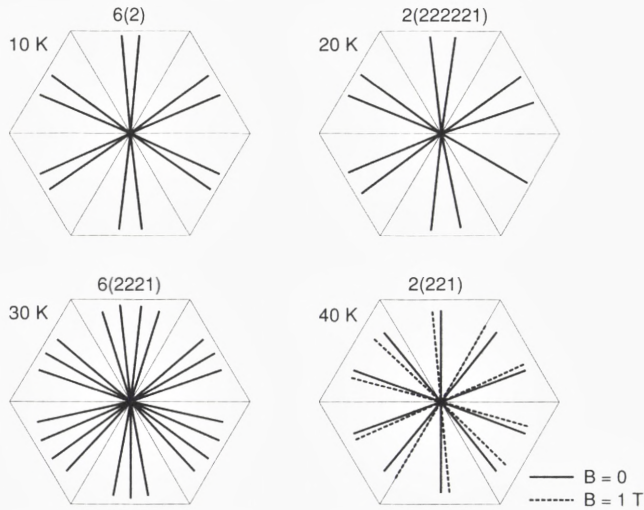
Figure 2. Spin-slip structures in Ho with $\mathbf{q} = 1/6$, $2/11$, $4/21$, and $1/5$ $\mathbf{c}^*$ calculated at 10, 20, 30, and 40 K respectively. The 10-layered structure at 40 K is both calculated at zero field and at a field of 1 T along the c axis.

models compared well with the results obtained later from mean-field calculations (Mackintosh and Jensen, 1991).

Recently Simpson et al. (1995) have performed further neutron scattering studies on Ho to study in particular the structure of the low-temperature cone phase and the transition from it to the basal-plane helix. The results for the scattering observed when the wavevector transfer is varied along $[00\ell]$ and $[10\ell]$ are shown in Fig. 1 at 10 K in the cone phase. The peaks marked N arise from the nuclear setting, the ones marked q from the $q = 1/6 \, c^*$ helical structure, the one marked $5q$ from the bunching of the moments around the easy axes, and the weaker ones with arrows are previously unreported peaks with $\mathbf{Q} = (001\frac{1}{3})$, $(001\frac{2}{3})$, $(10\frac{1}{3})$, $(10\frac{1}{2})$ and $(10\frac{2}{3})$. The usually assumed structure of the cone phase cannot account for these peaks as they can only arise if the conventionally assumed symmetry of the cone phase is broken. Figure 2 shows a possible structure which can account for the observations. In the structure shown at 10 K the bunching angle differs for successive easy axes by about $1.3°$ giving rise to the scattering with $\mathbf{q} = (00\frac{1}{3})$ and the cone tilt angle varies for successive easy axes by about $2.3°$ giving rise to the $(10\frac{1}{2})$ scattering.

The symmetry breaking arises because the environment of a rare earth atom differs for each of the two sublattices in the hcp structure. Both sublattices have

trigonal, not hexagonal, symmetry, and the trigonal axes are rotated by 60° for one sublattice compared with the other. As pointed out by Jensen and Mackintosh (1991), the lowest order pair-interactions which have this reduced symmetry are of the fourth rank, and one example is:

$$\mathcal{H}_3 = \sum_{ij} \mathcal{K}_{31}^{21}(ij) \left[O_3^2(i) J_y(j) + O_3^{-2}(i) J_x(j) \right], \tag{1}$$

where the Stevens operators are $O_3^{\pm 2} = \frac{1}{2}(J_z O_2^{\pm 2} + O_2^{\pm 2} J_z)$ with $O_2^2 = J_x^2 - J_y^2$ and $O_2^{-2} = J_x J_y + J_y J_x$. The x-, y-, and z-axes are assumed to be along the a-, b-, and c-axes of the hcp lattice, respectively. All of the three fourth-rank terms are similar in that they couple the spin components $J_x^2 J_y J_z$ and $J_y^3 J_z$ but with different components associated with the two sites i and j.

Calculations by Simpson et al. (1995) and by Jensen (1996) using the mean-field model (Larsen et al., 1987) and the data shown in Fig. 1 and other similar results at higher temperatures and in applied magnetic fields, suggests that the largest contribution arises from the $\mathcal{K}_{31}^{21}$ term given by Eq. (1) and that this interaction is about 2% of that of the two-spin exchange interaction.

The effect of the trigonal interaction on the $2/11\,c^*$ commensurate phase was also studied and scattering was observed for $\mathbf{Q} = (0, 0, m/11)$ with m an odd integer. This scattering would be absent if both sublattices had the same symmetry. The contribution of the trigonal coupling to the free energy is of second order in the helical case. The effect is larger for the cone structure, as observed for the $2/11\,c^*$ phase when a c-axis magnetic field of 2 T is applied (Cowley et al., 1991). In the cone phase all three components of the moments have non-zero expectation values leading to a first-order contribution to the free energy which is

$$\Delta F \propto \sum_p (-1)^p J_{\parallel} J_{\perp}^3 \cos(3\phi_p). \tag{2}$$

$J_{\parallel}$ and $J_{\perp}$ are the components of the magnetic moments parallel and perpendicular to the c axis, respectively, and ϕ_p is the angle the perpendicular component of the moments in the pth layer makes with the x- or a-axis. Thus if only the trigonal anisotropy is important for the cone structure, then every second a axis is an easy axis in one of the sublattices and the other three a axes are the easy axes in the other sublattice.

The experiment of Simpson et al. (1995) also clarified the nature of the lock-in to the cone phase at 19 K. As first noted by Sherrington (1971) there is no reason that the lock-in to $\mathbf{q} = 1/6\,\mathbf{c}^*$ should occur at the same temperature as the c-axis moment develops in the cone phase. Furthermore, specific-heat measurements by Stewart and Collocott (1989) and ultrasonic measurements by Bates et al. (1988) suggested that there might be two transitions. Unfortunately, the measurements

are difficult because of hysteresis, but a study of the temperature dependence of the $(10\frac{1}{3})$ reflections which effectively measure the average cone angle and the $(10\frac{1}{2})$ reflections which measure the existence of the $1/6\,c^*$ phase, showed quite different behaviour and that between 18 K and 19 K the crystal was in a $\mathbf{q} = 1/6\,\mathbf{c}^*$ basal-plane helix with no net ferromagnetic moment, and that below 18 K the crystal underwent a second transition to the cone phase.
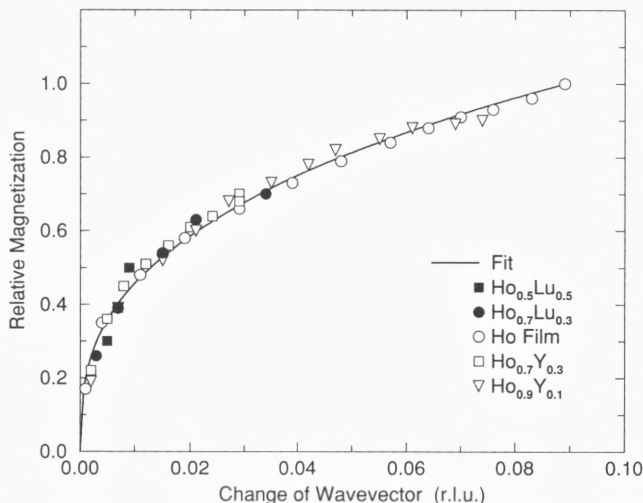

Figure 3. The change in the ordering wavevector of a holmium film, of Ho/Y alloys (Cowley et al., 1994) and of Ho/Lu alloys (Swaddling et al., 1996) as a function of the basal-plane ordered moment.

The variation of the ordering wavevector with temperature has been re-examined by Helgesen et al. (1994) and their results are shown in Fig. 3. Close to T_N the change in the wavevector is proportional to the square of the ordered moment M, as might be expected from the theory of Elliott and Wedgwood (1963), where the change in wavevector results from a change in the position of the superzone gaps at the nesting Fermi-surface. Over much of the temperature range the change in the ordering wavevector is proportional to M^3, but this behaviour is as yet not understood. A further correlation is with the c/a ratio for which Andrianov (1992) discovered that the ordering wavevector was given by

$$q = q_0 \left[(c/a)_0 - c/a \right]^{\frac{1}{2}}, \tag{3}$$

where $(c/a)_0$ is 1.582. This result shows that the Fermi-surface properties are strongly correlated with the c/a ratio. Because of these effects any modeling of

the structures by using exchange constants between neighbouring planes must inevitably require temperature-dependent exchange constants.

The mean-field model developed for Ho utilizes the spin-wave measurements at different temperatures to obtain a phenomenological account of the temperature dependence of the exchange coupling. The model has been used for analysing the commensurable effects displayed by the helical ordered basal-plane moments in Ho (Jensen, 1996). At low temperatures the hexagonal anisotropy energy is large and the model predicts strong commensurable effects of the spin-slip structures in consistency with the experiments. Figure 4 shows a comparison between the calculated results and the field experiment of Cowley et al. (1991). The model accounts well for the overall shift of the ordering wavevector with the c-axis field at a constant temperature, and there seems to be no need for invoking a field dependence of the exchange coupling. As shown in Fig. 4 the experiments of Cowley et al. indicated that metastable states appear frequently at low temperatures. They found by measuring the position of the higher harmonics rather than the first harmonic, that the diffraction pattern was determined in many cases by a superposition of neutrons scattered from domains with different commensurable periods.

The hexagonal anisotropy energy decreases very quickly with the magnetisation M, approximately like M^{21}, whereas the change of the trigonal anisotropy energy $\sim M^7$ is more moderate. This means that around 40 K ($M \simeq 0.925 M_0$) the hexagonal anisotropy energy has decreased by a factor of 5 whereas the trigonal anisotropy is only reduced by a factor of 1.7, compared with the zero-temperature values. The trigonal contribution is strongly enhanced by a c-axis field, Eq. (2). In combination the two effects imply that although the trigonal distortions of the helix at 40 K are small at zero field, they dominate in a c-axis field of 1 T. At this field the 10-layered structure is predicted to be the one shown in Fig. 2, where the moments in the two spin-slip layers are oriented along an a axis instead of a b axis as at zero field. This modification leads to a strong increase of the commensurability of the 10-layered structure. At zero field the model indicates that this structure is stable within a temperature interval around 42 K of about 2.2 K, which increases to about 10 K at a c-axis field of 1 T, whereupon the lock-in interval stays more or less constant between 1 and 5 T. The hysteresis effects detected by Cowley et al. (1991) below 35 K may possibly explain why the lock-in intervals determined by Tindall et al. (1993) are somewhat smaller than predicted by the theory. They only studied the behaviour of the first harmonic which did not indicate any lock-in at zero field, and at 3 T the lock-in interval was found to be 2–3 K.

Around 100 K the spin-slip model no longer applies. The hexagonal anisotropy only manages to rotate the moments by about one tenth of a degree. At this temperature the ordering wavevector is close to $1/4 c^*$, but the model indicates only a marginal lock-in to the 8-layered structure. In the presence of a c-axis field of 3 T,
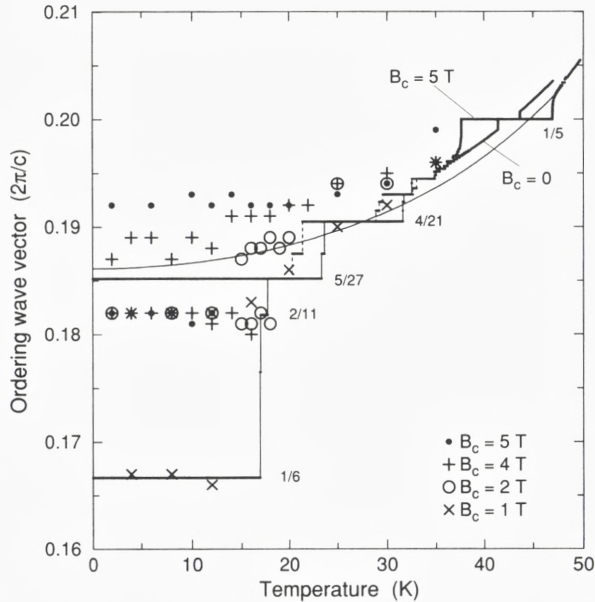
Figure 4. The ordering wavevector in Ho. The calculated results are shown by the horizontal solid lines connected with vertical thin solid or thin dashed lines corresponding respectively to the results obtained at zero or at a field of 5 T applied along the c axis. The symbols show the experimental results of Cowley et al. (1991) obtained at the various values of the c-axis field defined in the figure. The smooth curve shown by the thin solid line is the temperature dependent position of the maximum in the exchange coupling assumed in the model.

the trigonal coupling increases the bunching effect by a factor of 4, but the lock-in interval is still estimated to be very small, about 0.1 K. In analogy with the fifth and seventh harmonics induced by the hexagonal anisotropy, the first-order term in the free energy due to the trigonal coupling induces a second and a fourth harmonic. Because of the factor $(-1)^p$ in Eq. (2) these harmonics are translated a reciprocal lattice vector along the c axis (half of a reciprocal lattice vector in the double-zone scheme), which means that the fourth harmonic appears at zero wavevector when $\mathbf{q} = 1/4\ \mathbf{c}^*$. In other words, in the case of a cone structure with a period of 8 layers the trigonal coupling leads to a ferromagnetic component perpendicular to the c axis. Although it is small, this component has a determining effect in forming the commensurable structure. The lock-in interval increases proportionally to $\sqrt{\theta}$, where θ is the angle the field makes with the c axis, and even the slightest deviation

of the field from perfect alignment along the c axis will produce a sizable lock-in effect. The lock-in interval is calculated to be 2.7 K at $\theta = 1°$ at the field of 3 T. Both this value and the very weak lock-in effect at zero field are consistent with the observations (Noakes et al., 1990; Tindall et al., 1991). In the experiments the field was applied nominally along the c axis but with an uncertainty of about $2°$ corresponding to an effective $\theta \simeq 1°$. At a larger tilt angle of the field the lock-in interval is estimated to increase up to a value of 8–12 K.

The increased stability of the 10-layered periodic structure around 42 K and of the 8-layered one around 96 K, observed when applying a field along the c axis can not be explained without the trigonal anisotropy term. If this term is neglected the anisotropy effects and therefore also the commensurable effects on the helical structures, decrease rapidly with a field applied in the c-direction (misalignment effects are estimated to be unimportant in this situation). The model including the trigonal interactions explains most of the commensurable effects observed in Ho except for the lock-in of the $5/18\,c^*$-structure observed in an interval of 5 K just below T_N in a b-axis field of 3 T (Tindall et al., 1994). The model only predicts a marginal lock-in in this case, which discrepancy is most likely a consequence of the limited validity of the mean-field approximation in this close neighbourhood of the phase transition.

One further set of measurements on the magnetic properties of holmium has been the result of the growth of Ho films grown by molecular beam epitaxy. Usually the films have been grown by the techniques developed by Kwo et al. (1985) in which a Nb film is deposited on a sapphire substrate, to provide a chemical buffer and then a seed layer of a non-magnetic material such as Y or Lu is deposited. The holmium is then grown to the appropriate thickness with the c axis as the growth direction and the samples are capped with Y or Lu to prevent oxidation of the holmium layer. This procedure typically leads to samples with a mosaic spread of about $0.15°$. The films are single crystals and the basal-plane lattice constants are different from those of the seed layer or capping layer and very similar to those of the lattice constant of bulk holmium above T_N.

The magnetic structures have been determined for Ho films grown on Y (Jehan et al., 1993; Swaddling, 1995), Lu (Swaddling, 1995) and Sc (Bryn-Jacobsen et al., 1997). In the case of Y films of thickness 1500 Å, 5000 Å, and 15000 Å have been studied, while for a Lu seed the thickness was 5000 Å and for the Sc seed, 2500 Å. The wavevector for the onset of ordering was the same as for bulk holmium but, the wavevector at low temperature was in some cases larger than that of the bulk: $1/5\,c^*$ and $5/27\,c^*$ for the 15000 Å film on Y, $1/5\,c^*$ and $4/21\,c^*$ for the 5000 Å film on Y, $1/6\,c^*$ and $7/39\,c^*$ for the 5000 Å film on Lu and $7/39\,c^*$ for the 2500 Å film on Sc. The results for the films on Y show that there is little change in wavevector with film thickness for these thick films. There is a change in the

behaviour with substrate and hence strain but that all the films have on average larger wavevectors than the bulk even though for the Y seeds, the basal planes of the Ho are expanded while for the Sc and Lu seed layers, they are compressed. In all the films the ferromagnetic cone phase is suppressed except for the 15000 Å film for which the c-axis moment is much less than for the bulk. These results and the differences from the bulk behaviour are not understood in detail but presumably arise from the clamping of the basal-plane lattice parameter of the films.

3   Magnetic structures of erbium

The crystal-field interactions in erbium are of opposite sign to those of holmium so that the structures have a c axis or longitudinal component to the magnetic ordering. The magnetic structures were determined by Cable et al. (1965) as

(i) between $T_N = 84$ K and $T'_N = 52$ K, a roughly sinusoidal variation of the longitudinal component of the magnetisation with a wavevector of about $\mathbf{q} = 0.277$ $\mathbf{c}^*$.

(ii) between T'_N and $T_C = 18$ K the wavevector decreases to $\mathbf{q} = 0.25$ $\mathbf{c}^*$ and transverse basal-plane components of the moments are ordered with the same wavevector as the longitudinal ones.

(iii) below T_C the magnetic structure is a cone with a basal-plane modulation of $\mathbf{q} = 5/21$ $\mathbf{c}^*$ and a ferromagnetic c-axis component.

Subsequent measurements by Habenschuss et al. (1974) showed that the structures were distorted from the simple ones. High-resolution x-ray scattering measurements by Gibbs et al. (1986) showed that in phase (ii) the wavevector locked into a series of commensurate wavevectors with $\mathbf{q} = 1/4, 6/23, 5/19$ and $4/15$ $\mathbf{c}^*$ and proposed that these structures resulted from there being either 4 or 3 successive basal-planes having their moments along the positive or negative c axis.

More recently high-resolution neutron scattering measurements have been performed to study these phases in more detail (Cowley and Jensen, 1992). Measurements were made of the higher harmonics and the results interpreted to deduce the structures. The results shown in Fig. 5 were obtained for the $\mathbf{q} = 4/15$ $\mathbf{c}^*$ phase at 35 K and show a large number of higher harmonics. Initially the data showed that phase (ii) could be described approximately as a cycloidal structure in which the moments rotate in an a–c plane. Nevertheless this structure cannot describe the data shown in Fig. 5 because, if both sublattices are identical, the peaks with $\mathbf{Q} = (0, 0, n/15)$ with n odd should be absent and although they are weak, their intensity is clearly non-zero. The origin of these peaks is distortions of the structure arising from the trigonal terms already discussed in Sect. 2. The structure is not a planar cycloid in the a–c plane but a wobbling cycloid in which the
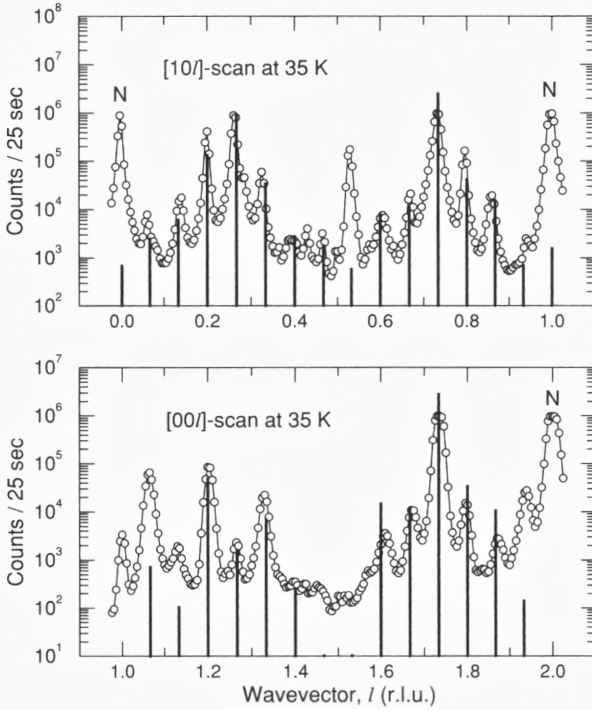
Figure 5. Neutron scattering from Er at 35 K. The upper part shows the results obtained when the wavevector transfer was scanned along $[10\ell]$ and along $[00\ell]$ in the lower figure. The peaks marked N are from nuclear scattering and the others are magnetic scattering. The wavevector of the cycloidal phase is $\mathbf{q} = 4/15\ \mathbf{c}^*$. The thick vertical lines are the intensities predicted by the mean-field calculations including the trigonal interactions. The experimental data have not been corrected for extinction or spurious scattering effects (Cowley and Jensen, 1992).

structure has deviations away from the plane (Cowley and Jensen, 1992; Jensen and Cowley, 1993). A mean-field calculation and a careful comparison with the experimental results suggested that the dominant trigonal term was $\mathcal{K}_{31}^{21}$ as also found for holmium, Sect. 2, and that the interaction is about 15% of the two-spin exchange interaction. The agreement for the $4/15\,c^*$ phase between the observed scattering and that calculated by the model is illustrated schematically in Fig. 5. Similar results were obtained for five other commensurable structures in the intermediate phase and for the cone structure below T_C (Cowley and Jensen, 1992). The trigonal interactions are also possibly responsible for the lock-in of the cone phase to $\mathbf{q} = 5/21\ \mathbf{c}^*$. In erbium the cone angle is small so that the basal-plane anisotropy makes only a small contribution to the energy and it is more likely that the lock-in energy arises from the trigonal interactions.

There is also still some uncertainty about the behaviour of Er between T_N and T'_N. In principle, there is the possibility of the longitudinal and transverse moments ordering at different temperatures and, if the exchange is anisotropic, at different wavevectors. Since the single-ion anisotropy favours the longitudinal ordering this ordering occurs at the higher temperature T_N, and the basal-plane components might then order at a lower temperature. As the moments increase entropy effects would then cause a lock-in between the longitudinal and transverse components into a cycloidal phase. Experimentally there is some suggestion that above T'_N but below T_N the basal-plane components show short-range order into a helical structure with a slightly different wavevector from the longitudinal components. This indicates that the transverse moments may be close to order at the different wavevector just above the transition to the cycloidal phase, and thus that the exchange coupling is anisotropic. The intensities are, however, very small and further work is needed to confirm these results.
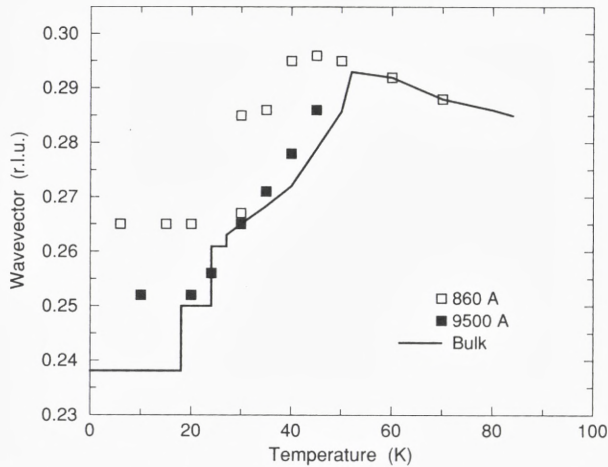

Figure 6. The temperature dependence of the ordering wavevector for bulk Er and for 860 and 9500 Å thick Er films (Borchers et al., 1994).

The ordering wavevector for bulk Er is shown as a function of temperature in Fig. 6 (Gibbs et al., 1986). It differs from that of bulk Ho in that in the longitudinal phase, the wavevector increases with decreasing temperature. This increase is characteristic also of Tm which has a longitudinally modulated phase. Once the basal-plane components order below T'_N, the wavevector decreases with

decreasing temperature as found for Ho. This shows that the decrease is most strongly correlated with the basal-plane component of the magnetic ordering. The same is valid though to a lesser extent also for the changing of the c/a ratio.

Er thin films grown on a Y seed have been studied by Borchers et al. (1991a, 1991b). They studied films with thicknesses between 375 Å and 14000 Å and found that T_N only slightly decreased as the film thickness decreased. In all the films the structure was a longitudinally modulated structure below T_N and there was an ordering of the basal-plane components below about 45 K. In Fig. 6 we show the measured wavevectors for the moments in a 9500 Å thick film, and the results are very similar to those of bulk Er except for the suppression of the cone phase. The results for the thinner films are similar except that the wavevectors tend to lie above those of bulk Er and that the low-temperature structures are commensurate phases with $\mathbf{q} = 5/19$ or $4/15$ $\mathbf{c}^*$. The suppression of the cone phase is presumably, as for Ho films, due to the clamping of the basal planes by the substrate and seed layers.

4 The magnetic properties of Ho-Y and Ho-Lu alloys

One of the advantages of the development of artificial growth facilities like molecular beam epitaxy, is that it enables the growth of high quality uniform alloy samples. The samples are grown in the same manner as described for the Ho films in Sect. 2 but with the sample being produced by using the fluxes from two sources controlled so as to produce a constant composition alloy. Using these techniques, measurements have now been made of Ho/Y alloys (Cowley et al., 1994), Ho/Lu alloys (Swaddling et al., 1996) and Ho/Sc alloys (Bryn-Jacobsen et al., 1997). Earlier experiments on bulk powdered alloy samples were performed by Child et al. (1965). The results of measurements on single-crystal films and on powdered bulk samples are in general agreement with one another but the accuracy obtainable with powdered samples is not sufficient to test this in detail. In all the cases the thin-film samples have mosaic spreads of about 0.15°.

For all of the samples, the magnetic structures are found to be basal-plane helices with a wavevector dependence as illustrated in Fig. 7 for Ho/Y alloys. The wavevector for the onset of magnetic ordering is independent of concentration and decreases with decreasing temperature but by amounts which decrease with increasing Y concentration. The results for the Ho/Lu alloys are also shown in Fig. 7, and the behaviour is qualitatively similar but differs in that the wavevector for the onset of magnetic order decreases as the Lu concentration increases. Figure 8 shows the behaviour of T_N as a function of Ho concentration. These results can be compared
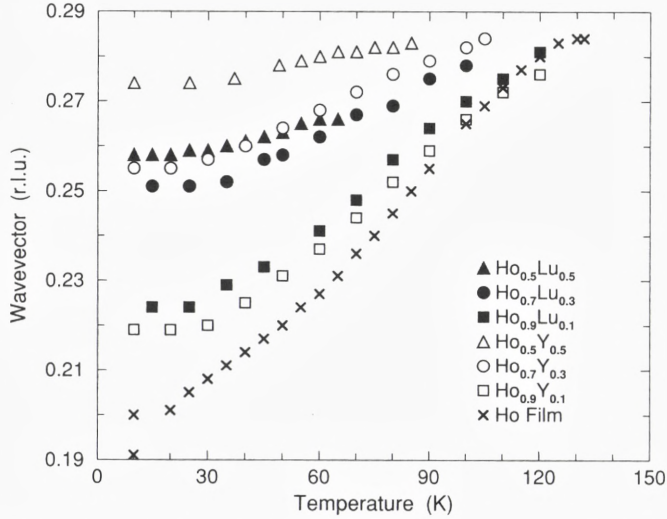
Figure 7. The wavevector for the basal-plane ordering of Ho/Y and of Ho/Lu alloys as a function of temperature and compared with a similar Ho film (Swaddling et al., 1996; Cowley et al., 1994).

with those of Child et al. (1965) for a range of bulk alloy systems which suggested that T_N was a universal function of the de Gennes factor $x = c(g-1)^2 J(J+1)$ and that T_N was proportional to $x^{2/3}$. This empirical result has little theoretical basis because mean-field theory suggests that T_N is proportional to x and even then the theory would only be valid if the conduction-electron susceptibility of all rare earth metals was the same. Although this result is successful at describing the overall trends, it cannot be expected to describe the detailed behaviour of particular systems and indeed, as shown in Fig. 8, fails for Ho/Lu alloys and to a lesser extent for Ho/Y alloys.

A more reasonable description of the alloys is to assume an average or virtual crystal model of the conduction-electron susceptibility when

$$T_N(c) = c\big[cT_{\mathrm{Ho}} + (1-c)T_\gamma\big], \tag{4}$$

where T_γ is T_N for bulk Ho if it had the conduction-electron susceptibility of the alloying element γ. As shown in Fig. 8, Eq. (4) provides a good description of the results with $T_{\mathrm{Ho}} = 132 \pm 2$ K, $T_Y = 207 \pm 3$ K and $T_{\mathrm{Lu}} = 144 \pm 2$ K. This then suggests that the peak in the conduction-electron susceptibility for Y is 1.64 times larger than for Ho while that for Lu is 1.09 times larger. It is similarly possible to
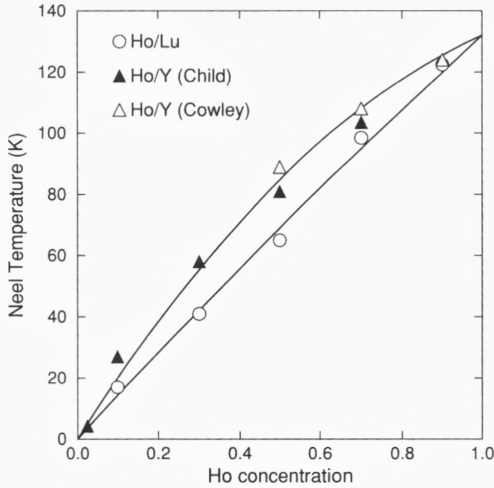
Figure 8. The dependence of T_N on concentration for Ho/Y and Ho/Lu alloys (Swaddling et al., 1996).

extrapolate the wavevector for the onset of magnetic order to give the wavevector for the peak of the susceptibility for Ho as $0.282 \pm 0.004 \; \mathbf{c}^*$, Y as 0.282 ± 0.004 $\mathbf{c}^*$ and Lu as $0.235 \pm 0.015 \; \mathbf{c}^*$. This analysis assumes an average crystal model and neglects critical fluctuations, but its success suggests that there is considerable validity in the approach.

Figure 3 of Sect. 2 shows that the change in wavevector with temperature is correlated with the ordered moment in Ho. The figure also shows a similar relationship for Ho/Lu and Ho/Lu alloys, and that $\Delta q \sim M^\alpha$ with $\alpha = 2.8 \pm 0.3$ from a combined fit to all of the results.

At low temperatures all of the alloy samples lock-in to commensurate structures: $\mathbf{q} = 2/9 \; \mathbf{c}^*$ for $c = 0.9$, $\mathbf{q} = 1/4 \; \mathbf{c}^*$ for $c = 0.7$, $\mathbf{q} = 8/31 \; \mathbf{c}^*$ for $c = 0.5$ in Ho/Lu alloys and $\mathbf{q} = 3/11 \; \mathbf{c}^*$ for Ho/Y alloys. Clearly, therefore, the concepts developed for the bulk rare earth materials can be taken over to the alloy systems. Of particular interest is the phase diagram of the Ho/Y alloy with $c = 0.7$ in an applied basal-plane field which shows not only the low-field helical phase and a high field fan phase but between these phases at low temperatures an exceptional clear example of a helifan phase (Jensen and Mackintosh, 1990; Mackintosh and Jensen, 1991, 1992) which is stable over a considerable range of parameters.

5   The magnetic structure of Ho/Er alloys

Ho/Er alloys are of interest because of the competing anisotropy of the Ho and Er atoms. The first experiments on this system were by Pengra et al. (1994) who studied a bulk crystal with $c = 0.5$. The experiments reported below (Simpson et al., 1997) were obtained by studying thin-film alloy samples grown as described in Sect. 2 and the results obtained are different from those obtained on bulk samples. Further work is needed to find out the reasons for these differences.

Three alloy systems have been studied as thin films of $Ho_c Er_{1-c}$ with $c = 0.8$, 0.5 and 0.3. In all cases the neutron scattering intensity was measured along $[00\ell]$ to determine the basal-plane ordering, and along $[10\ell]$ to determine the longitudinal ordering. No evidence was found of scattering from higher harmonics suggesting that the moments are ordered in a largely sinusoidal pattern.

For $c = 0.8$, the ordering wavevector decreases with decreasing temperature until it locks in to $\mathbf{q} = 1/5\ \mathbf{c^*}$ below 20 K. The magnetic structure is a basal-plane spiral until surprisingly below 20 K the moment tilts out of the plane to form a cone phase with a cone angle of $75° \pm 2°$. This is unexpected because films of Ho, Ho/Y and Ho/Lu alloys have not shown cone phases. Preliminary measurements on bulk crystals of $Ho_c Er_{1-c}$ with $c = 0.9$ and 0.5 indicates that T_C is higher in the alloy systems than in either Ho or Er, and this is found to be in accord with mean-field predictions (Rønnow, 1996). The opposite signs of the single-ion axial anisotropy in Ho and in Er imply that the average or effective axial anisotropy changes its sign at a higher temperature in the alloy systems than in pure Ho.

The behaviour of the sample with $c = 0.5$ is more complex. The basal-plane moments order below 110 ± 2 K with a wavevector $\mathbf{q} = 0.282\ \mathbf{c^*}$. The wavevector then reduces steadily with decreasing temperature with the possibility of lock-ins to structures with $\mathbf{q} = 8/31\ \mathbf{c^*}$, $1/4\ \mathbf{c^*}$, $8/33\ \mathbf{c^*}$, and $3/13\ \mathbf{c^*}$. The structure is a basal-plane spiral above 50 K and then becomes at least partially a cycloid until 30 K when the structure becomes a cone phase with a cone angle of $67°$ at 20 K.

The third sample with $c = 0.3$ developed magnetic order as a basal-plane helix with $\mathbf{q} = 0.288\ \mathbf{c^*}$ at $T_N = 94 \pm 2$ K. The structure remained a basal-plane helix down to 80 K while the wavevector reduced. On further cooling there was ordering in the longitudinal moments and the structure developed a cycloidal phase below 60 K. Between 35 K and 22 K the magnetic structure was a $\mathbf{q} = 1/4\ \mathbf{c^*}$ cycloidal phase, and below 22 K the wavevector became $\mathbf{q} = 5/21\ \mathbf{c^*}$ and the structure became a cone with a cone angle of $44° \pm 5°$.

These results are summarised in the schematic phase diagram in Fig. 9. The unexpected feature is that in all the systems the low-temperature phase is a cone phase unlike thin films of Er or Ho, Sects. 2 and 3. The basal-plane helical ordering presumably of the Ho moments dominates at temperatures above T_N of bulk
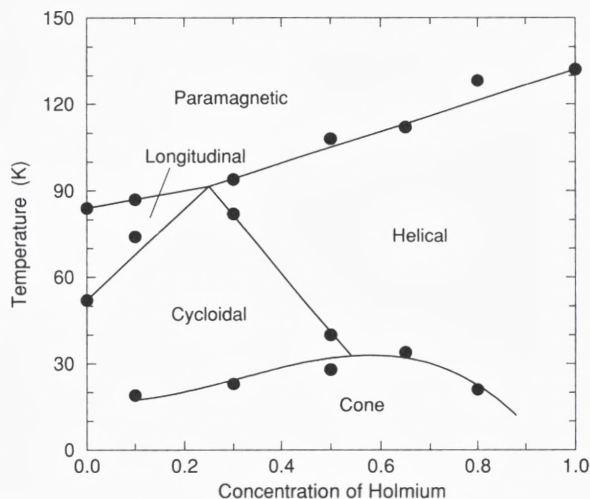
Figure 9. A schematic phase diagram for thin films of Ho/Er alloys deduced from the measurements of Simpson et al. (1997).

erbium. On cooling for larger concentrations of Er the structure becomes a cycloid with the possibility of commensurate phases similar to those of Er before forming a cone phase at low temperature. This behaviour is at least qualitatively consistent with the approximate cancellation of the axial and basal-plane crystal-field anisotropy in Ho/Er alloys with $c = 0.5$.

6 Summary and Conclusions

The results described in the previous sections show that there have been considerable developments in our understanding of the rare earth metals particularly on the experimental side. The strongest magnetic interactions are the well known single-ion crystal fields and the exchange interactions conveyed through the conduction electrons. Nevertheless, there are now many experiments (Sects. 2 and 3) which show that some important aspects also require there to be trigonal interactions between sites. These terms must arise from the effect of the spin-orbit interactions on the conduction electrons, but there is as yet no quantitative understanding.

The ferromagnetic structures (Gd and the low-temperature phases in Tb and Dy) or the longitudinally polarized c-axis modulated structures (Tm and Er between T_N and T_N') are not affected by the trigonal coupling. Therefore the only remaining candidates among the elemental heavy rare earths to be investigated for

the possible structural effects of the trigonal coupling, are Tb and Dy in their high-temperature helical phases. Of these two only Dy may be a realistic possibility, because the helical phase in Tb only occurs in a narrow temperature range.

Ho and Er and their alloys are found to have commensurate locked-in structures not only at low temperatures, but, in Ho, even very close to T_N. Except for the lock-in of Ho close to T_N at $\mathbf{q} = 5/18\,\mathbf{c}^*$ in a b-axis field, the mechanisms behind the commensurable effects are now well understood. The lock-in temperature interval of the $1/5\,c^*$ phase in Ho is predicted to be larger than indicated by the variation in the position of the first harmonic, and a study of the behaviour of the fifth or seventh harmonics will be useful for a clarification of the experimental situation. The strong lock-in of the 8-layered structure in Ho around 96 K indicated by the mean-field model, deserves further studies in which the field is applied by purpose in a direction making a non-zero angle with the c axis or with the basal plane.

The neutron diffraction experiments show that Ho may contain several domains with different commensurable structures below 40 K. In this spin-slip regime there is also the possibility that the positions of the spin-slip layers in the different domains are disordered to some extent. The x-ray experiments (Helgesen at al., 1990, 1992) indicate that this is the case by showing a reduction of the longitudinal correlation length between 40 and 20 K by a factor of 3, a reduction which is partly removed when the spin-slip layers disappear at the lock-in to the 12-layered structure at about 20 K. In the alloy $Ho_{0.9}Er_{0.1}$ the $7/36\,c^*$ structure is stable at the lowest temperatures, and Rønnow (1996) has observed that the widths of the neutron diffraction peaks in this phase are much larger for the higher harmonics than for the first one. The $7/36\,c^*$ spin-slip structure consists of alternating two and three pairs of layers between the spin-slip planes, (2212221), and Rønnow has found that a structure in which the succession of the two sequences is completely random, predicts a diffraction spectrum close to the observed one. Hence the large hexagonal anisotropy in Ho at low temperatures strongly resists a rotation of the moments from one easy direction to the next and may cause a spin-glass like situation.

It is now also empirically known that there is a strong correlation between the ordering wavevector, the c/a ratio and the ordered moment but as yet there is no theory of this connection. Maybe now, with the increasing computer power, is the time for a more realistic calculation of $\mathcal{J}(\mathbf{q})$ mediated by the conduction electrons in the rare earths and for the changes in $\mathcal{J}(\mathbf{q})$ on ordering, using realistic wavefunctions rather than the free electron model of Elliott and Wedgwood (1963). There is a steadily increasing amount of experimental information which could be compared with such calculations.

Finally, there has been much recent interest in artificially grown thin films, alloys and superlattices. The experiments on the alloys have led to a better knowledge of the conduction-electron susceptibilities in Y and Lu, and to a better knowledge of

the phase diagrams and the effects of competing interactions. As yet there has not been much theoretical work performed with which these results can be compared.

Acknowledgements

References

Andrianov AV, 1992: JETP Lett. **55**, 666

Bates S, Patterson C, McIntyre GJ, Palmer SB, Mayer A, Cowley RA and Melville R, 1988: J. Phys. C **21**, 4125

Borchers JA, Salamon MB, Erwin RW, Rhyne JJ, Du RR, and Flynn CP, 1991a: Phys. Rev. B **43**, 3123

Borchers JA, Salamon MB, Erwin RW, Rhyne JJ, Nieuwenhuys GJ, Du RR, Flynn CP and Beach RS, 1991b: Phys. Rev. B **44**, 11814

Bryn-Jacobsen C, Goff J, Cowley RA, McMorrow DF, Wells MR and Ward RCC, 1997: (to be published)

Cable JW, Wollan EO, Koehler WC and Wilkinson MK: 1965, Phys. Rev. **140**, A 1896

Child HR, Koehler WC, Wollan EO and Cable JW, 1965: Phys. Rev. **138**, A 1655

Cowley RA, 1997: Proc. of 15th Conference on Condensed Matter of the European Physical Society, Physica Scripta, (to be published)

Cowley RA and Bates S, 1988: J. Phys. C **21**, 4113

Cowley RA and Jensen J, 1992: J. Phys. Condens. Matter **4**, 9673

Cowley RA, Jehan DA, McMorrow DF and McIntyre GJ, 1991: Phys. Rev. Lett. **66**, 1521

Cowley RA, Ward RCC, Wells MR, Matsuda M and Sternlieb B, 1994: J. Phys. Condens. Matter **6**, 2985

Elliott RJ and Wedgwood FA, 1963: Proc. Phys. Soc. **81**, 846

Felcher GP, Lander GH, Ari T, Sinha SK and Spedding FH, 1976: Phys. Rev. B **13**, 3034

Gaulin BD, Hagen M and Child HR, 1988: J. Phys. (Paris) Coll. **49**, C8-327

Gibbs D, Moncton DE, D'Amico KL, Bohr J and Grier BH, 1985: Phys. Rev. Lett. **55**, 234

Gibbs D, Bohr J, Axe JD, Moncton CE and D'Amico KL, 1986: Phys. Rev. B **34**, 8182

Habenschuss M, Stassis C, Sinha SK, Deckman HW and Spedding FH, 1974: Phys. Rev. B **10**, 1020

Hagen M, Child HR, Fernandez-Baca JA and Zaretsky JL, 1992: J. Phys. Condens. Matter **4**, 8879

Helgesen G, Hill JP, Thurston TR, Gibbs D, Kwo J and Hong M, 1994: Phys. Rev. B **50**, 2990

Helgesen G, Hill JP, Thurston TR and Gibbs D, 1995: Phys. Rev. B **52**, 9446

Jehan DA, McMorrow DF, Cowley RA, Ward RCC, Wells MR, Hagmann N and Clausen KN, 1993: Phys. Rev. B **48**, 5594

Jensen J, 1996: Phys. Rev. B **54**, 4021

Jensen J and Cowley RA, 1993: Europhys. Lett. **21**, 705

Jensen J and Mackintosh AR, 1990: Phys. Rev. Lett. **64**, 2699

Jensen J and Mackintosh AR, 1991: *Rare Earth Magnetism: Structures and Excitations* (Oxford University Press, Oxford)

Koehler WC, Cable JW, Wilkinson MK and Wollan EO, 1966, Phys. Rev. **151**, 414

Kwo J, Gyorgy EM, McWhan DB, DiSalvo FJ, Vettier C and Bower JE, 1985: Phys. Rev. Lett. **55**, 1402

Larsen CC, Jensen J and Mackintosh AR, 1987: Phys. Rev. Lett. **59**, 712

Lin H, Collins MF, Holden TM and Wei W, 1992: Phys. Rev. B **45**, 12873

Mackintosh AR and Jensen J, 1991: in *Disorder in Condensed Matter Physics*, eds. J.A. Blackman and J. Taguena (Clarendon Press, Oxford) p. 213

Mackintosh AR and Jensen J, 1992: Physica B **180&181**, 1

Noakes DR, Tindall DA, Steinitz MO and Ali J, 1990: J. Appl. Phys. **67**, 5274

Pengra DB, Thoft NB, Wulff M, Feidenhansl R and Bohr J, 1994: J. Phys. Condens. Matter **6**, 2489

Rønnow HM, 1996: *Magnetic Properties of Holmium–Erbium Alloys*, Thesis (University of Copenhagen)

Sherrington D, 1971: Phys. Rev. Lett. **28**, 364

Simpson JA, McMorrow DF, Cowley RA and Jehan DA, 1995: Phys. Rev. B **51**, 16073

Simpson JA, McMorrow DF, Cowley RA, Ward RCC and Wells MR, 1997: (to be published)

Stewart AM and Collocott SJ, 1989: J. Phys. Condens. Matter **1**, 677

Swaddling PP, 1995: *The Chemical and Magnetic Structure of Rare Earth Superlattices and Thin Films*, Ph.D. thesis (University of Oxford)

Swaddling PP, Cowley RA, Ward RCC, Wells MR and McMorrow DF, 1996: Phys. Rev. B **53**, 6488

Thurston TR, Helegesen G, Gibbs D, Hill JP, Gaulin BD and Shirane G, 1993: Phys. Rev. Lett. **70**, 3151

Thurston TR, Helegesen G, Hill JP, Gaulin BD and Simpson PJ, 1994: Phys. Rev. B **49**, 15730

Tindall DA, Adams CP, Steinitz MO and Holden TM, 1994: J. Appl. Phys. **75**, 6318

Tindall DA, Stenitz MO and Holden TM, 1993: Phys. Rev. B **47**, 5463

Tindall DA, Stenitz MO, Kahrizi M, Noakes DR and Ali N, 1991: J. Appl. Phys. **69**, 5691

Wang J, Belanger DP and Gaulin BD, 1991: Phys. Rev. Lett. **66**, 3195

Magnetism in the Actinides

G. H. Lander

European Commission, Joint Research Center, Institute for Transuranium Elements,

Postfach 2340, D-76125 Karlsruhe, Germany

Abstract

Magnetism involving $5f$ electrons in the actinides exhibits a bewildering diversity that is difficult to fit within any conventional framework. In this article I review briefly some of the significant work that has been performed during the last 5 years. From itinerant $5f$ systems such as UFe_2, to heavy-fermions exhibiting non-Fermi-liquid behaviour such as $(U,Y)Pd_3$, to quasi-localized materials such as $NpBi$, to fully localized compounds such as UPd_3, the magnetism continues to provide both richness and surprises. Neutron scattering, especially inelastic scattering, provides the surest method to help define the "state of hybridization" in these compounds. Heavy-fermion superconductivity remains the most difficult aspect to understand. I argue that the communities working on both "conventional" actinides and heavy-fermion compounds would benefit from greater contact with each other.

1 Introduction

Characteristically, the title for my talk was chosen by Allan Mackintosh without consulting me. I say characteristically because every time we talked about $5f$ magnetism he was searching for a framework into which he could put my remarks. Being one of the pioneers in establishing a framework, and a highly successful one as the elegant book by Jens Jensen and him (Jensen and Mackintosh, 1991) shows, for $4f$ magnetism, he felt (even insisted) that we must find the framework for $5f$ magnetism. He recognized many years ago, of course, that it was not the same as that for the lanthanides, but his orderly mind refused to accept what appears to be a great heap of unconnected facts in $5f$ magnetism. Thus, I shall accept that challenge, difficult though it is.

One of the principal techniques for elucidating the magnetic properties of compounds in both the $4f$ and $5f$ series is neutron scattering. The results for $4f$ systems, with the exception of Ce and some other materials that exhibit intermediate valent behaviour, are for the main part understood (Jensen and Mackintosh, 1991). The framework of localized moments interacting with each other through the conduction electrons and subject to the crystal-electric fields (CEF) from the

surrounding ions, explains not only the neutron results, but also almost all the bulk property measurements. Of course, neutrons are never the first technique to be applied to a system, especially the actinides, and they have never, and will never, discover new heavy-fermion compounds, for example. In the end, however, until the neutron scattering results can be placed in a framework, the materials are not understood. The reason for this in magnetism is simple. The neutrons couple to magnetic moments so they can give us the magnetic structures, which is an important manifestation of the ground state, and the energy scale of neutron spectroscopy is from 1 to 100 meV, thus allowing information about the excited states to be extracted. Given the narrow bandwidths (as opposed to the many eV of the transition-metal compounds) of f electrons, whether they be $4f$ or $5f$, this is exactly the energy range of importance to learn about the ground and first excited states.

Some start has been made in establishing such a framework in the recent reviews in the Rare Earth Handbook series (Lander, 1993; Holland-Moritz and Lander, 1994; Aeppli and Broholm, 1994). I shall not repeat information already discussed, which represent the situation in ~ 1992, and refer to these chapters rather than the original references to save space, but without any intention to slight the original authors!

Before starting with the neutron experiments, it is worth mentioning the "arrival" of x-ray resonant scattering into the study of the magnetism of the actinides (Isaacs et al., 1989, 1990). This technique is a very exciting one, and one with great promise for the future, both from the scattering and the dichroism aspects (Lander, 1996). So far, the scattering technique has added to our knowledge about the coherent lengths in magnetically ordered compounds (Isaacs et al., 1990), about the nature of phase transitions (for example, the presence (Langridge et al., 1994a,b; Watson et al., 1996a), or absence (Nuttall et al., 1995), of "two length scales" in the development of the critical correlations just above the ordering temperature), and on the details of the magnetic ordering processes (Langridge et al., 1994c; Perry et al., 1996). Most of these discoveries are a consequence of the better (than neutrons) q-space resolution of the x-ray technique. No new structures have yet been discovered by x-rays, but the small samples that can be used in x-ray experiments should allow diffraction studies of the heavier ($> Am$) actinides, and also the examination of thin films and multilayers. In dichroism, the first experiments have been reported (Collins et al., 1995), but, again, the element specificity and the information on the electron states (Tang et al., 1992) have not been exploited yet to any appreciable extent. Recently, the first measurement of surface antiferromagnetism has been reported (Watson et al., 1996b,c) with grazing-incidence x-rays on a polished sample of UO_2. This is an important new frontier, but it addresses questions of surface rather than of actinide physics. Inelastic magnetic scattering using the
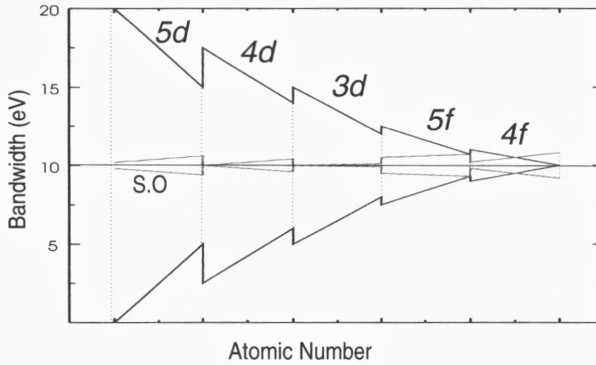
Figure 1. A schematic of the bandwidth, W, and spin–orbit splitting, Δ_{so}, for the d and f series elements. (Taken from Lander, 1993)

strong resonances is another subject that has not been explored very much (Ice et al., 1993).

We shall, no doubt, hear more from this competitive (or complementary would probably be a better word) microscopic technique in actinide research, but at the moment the surest information on the physics of actinides is still coming from neutron scattering experiments.

2   Band $5f$ electrons

Figure 1 shows the energy scale of two of the most important interactions in the magnetism of the various electron series (Lander et al., 1991). In the actinides it may be seen that the spin–orbit and bandwidths are of comparable magnitude. This is one of the fundamental reasons that the model I discussed earlier is so difficult to characterize. The $5f$ electrons fit neither into the schemes devised for the d-transition metals, where the spin–orbit interaction is a small perturbation on the bandwidth parameter, nor into those applicable to the rare earths, where the reverse is true. We find that actinides have characteristics of both series.

To illustrate this point I start with a compound that can surely be best described by the band approach, UFe_2. This compound has the cubic fcc Laves phase structure, and some years ago extensive calculations of the properties by the single-electron band-structure approach, including spin–orbit coupling and orbital polarization, showed that the main properties could be understood if the $5f$ electrons were treated as band electrons (Brooks et al., 1988). This paper even went so far as to predict an unusual form factor for the U $5f$-electrons in this material

associated with the cancellation of the orbital and spin contributions to the U magnetic moment. This was experimentally verified (Wulff et al., 1989; Lebech et al., 1989), although the magnitudes of the individual contributions to the moment at the uranium site were smaller than the calculations suggested.

Recently, we studied the dynamics of UFe_2 with a large single crystal and neutron inelastic scattering (Paolasini et al., 1996a,b). Following the extensive work on the isostructural Laves phases of the rare earths, we would expect three modes at low energy. However, only one mode, involving the Fe spins only was found. Some data from an experiment with full polarization analysis at the Institut Laue Langevin (ILL) are shown in Fig. 2. Exhaustive searches were made for the two other modes, but without success. That the "crystal-field like" mode of the U moment in the molecular field of the Fe moments was not observed is not a surprise – this is an itinerant system. More of a surprise was our inability to find the low-energy acoustic mode involving both the U and Fe spins. Elementary spin-wave theory tells us that this mode must be present, but it is probably strongly damped, perhaps by the strong coupling to the single-particle (Stoner) modes, or because of the unusual coupling of the spin and orbital moments on the uranium site.

The dispersion of the Fe only mode in UFe_2 was found to very steep. Figure 3 shows a plot of the energy of the excitation as a function of q^2. In a ferromagnetic the spin wave energies (E) for small q may be written as $E = E_0 + Dq^2$, where E_0 is the spin-wave gap, and the slope of the line gives the value of D, the spin-wave stiffness. The gap in UFe_2 is small, consistent with the small overall anisotropy of this material, but the D values are even bigger than found in pure Fe. In linear spin-wave theory D can be taken to be a measure of the direct exchange and does not have a strong T dependence, so by this analogy we would expect UFe_2 to have an ordering temperature even greater (or at least similar to) that found in pure Fe. That is not the case, T_C of UFe_2 is a low value of 165 K. Diluting Fe with U (if that is a justifiable way to consider the Laves phase compound UFe_2) has then had two important effects:

1. To increase the direct exchange interactions between the Fe spins, thus suggesting that high Curie temperature materials with uranium can be made.

2. To increase the temperature dependence of D (see the values in the figure caption), which, put another way, indicates that linear spin-wave theory is no longer applicable because of the strength of the higher-order interactions.

More studies are planned on UFe_2. At the moment the spin-wave energies of the Fe mode have not been observed much above ~ 7 meV, and certainly extending this in energy may give more information on whether the single-particle modes play an important role in this itinerant system.
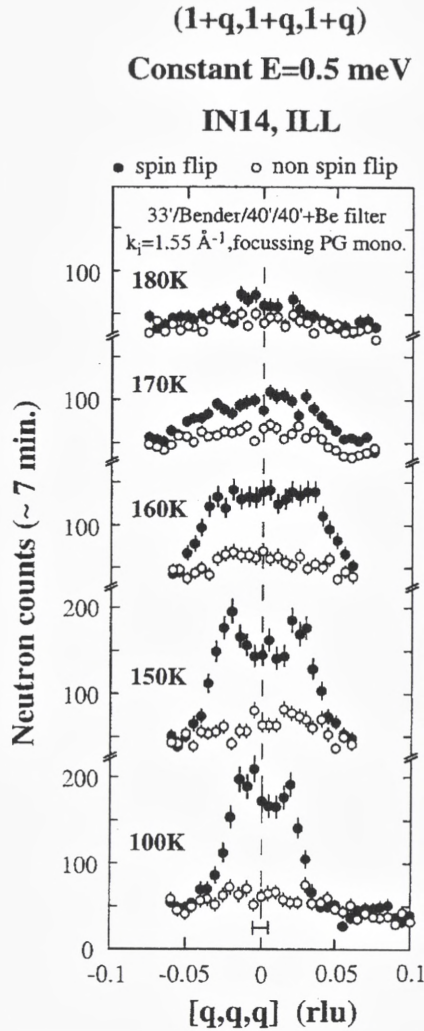
Figure 2. Data taken on UFe₂ single crystal near the (111) zone center and with full polarization analysis using the IN14 triple-axis spectrometer at the Institut Laue Langevin, Grenoble. The incident neutron wavevector is 1.55 Å^{-1}. A horizontal field of 1 T was used to saturate the sample along a ⟨111⟩ direction. The energy transfer is 0.5 meV in neutron energy loss. The instrumental resolution in q-space is shown as a horizontal bar in the lower panel. Solid points are spin flip (magnetic) and open points are non-spin-flip (non magnetic). (Taken from Paolasini et al., 1996a,b)
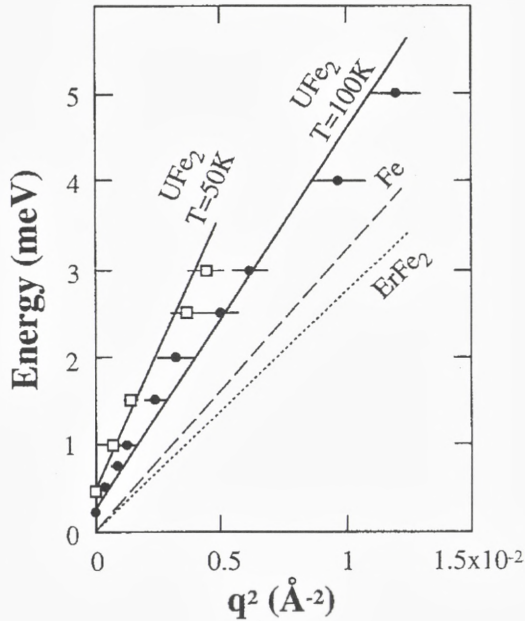
5*

Figure 3. Analysis of the low-q region for various materials. Dashed line is best fit for pure Fe giving $D = 325(10)$ meV^{-2}. The dotted curve represent $D = 280$ meV^{-2} as found for ErFe$_2$ at 295 K; note that a large gap E_0 has been suppressed in this plot. The two solid lines are fits to UFe$_2$ at 100 and 50 K giving values of $D = 440(30)$ and $630(50)$ meV^{-2}, respectively. (Taken from Paolasini et al., 1996a,b)

Of course, many of the actinide compounds that can be described as band systems (including the light actinide elements) do not order magnetically because the Stoner criterion is not fulfilled. Compounds with Fe, Co, and Ni are an exception because there is strong exchange involving the d electrons that drives the magnetic ordering. Other examples of band systems include the 1:1:1 compounds, such as URhAl and URuAl. In these compounds polarized neutrons (Lander, 1993) have shown that an important characteristic is that the d electrons on one of the Rh (or Ru) atoms are strongly polarized, and give $\sim 30\%$ of the total moment (Paixão et al., 1993). This means that the hybridization involves a planar interaction (this plane being perpendicular to the easy direction of magnetization) and gives a possible explanation of the large bulk anisotropy found in these materials. Unlike the itinerant system UFe$_2$, these 1:1:1 itinerant systems exhibit a large anisotropy that must originate from the large orbital moment of the $5f$ electrons. Understanding

the dynamics of such systems is clearly the next step after the experiments on UFe_2 (at least as far as band-like systems are concerned) and we have attempted such experiments on URhAl. No low-energy spin waves were found. Experiments at the ISIS spallation source (Hiess et al., 1996b) show a wide magnetic contribution centered around ~ 90 meV, see Fig. 4. There is little theoretical framework within which to interpret spectra of this sort; we can speculate that the magnetic contribution arises from the mixed $5f$–$4d$ band from the hybridization of the U and Rh electrons. If this can be considered as the spin-wave gap, see above, then it corresponds to an anisotropy field of ~ 700 T, which is clearly beyond the reach of laboratory magnetic fields, and represents a quite new mechanism of anisotropy.
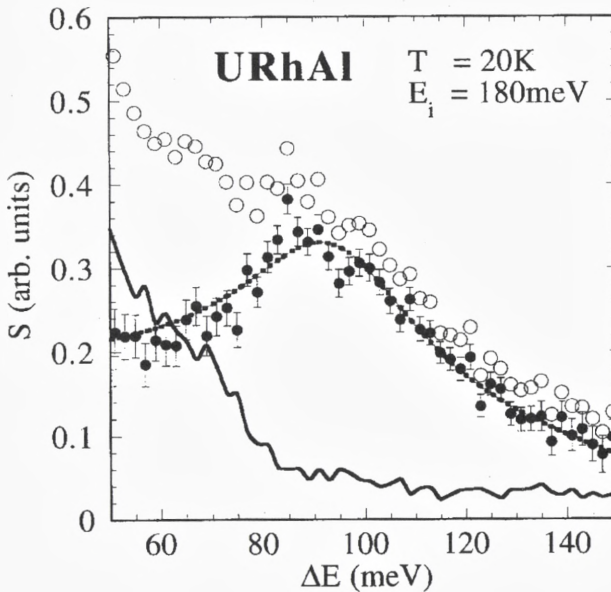

Figure 4. Results of experiments with $E_i = 180$ meV and $T = 20$ K on URhAl. Open circles are data from the low-angle detectors, the solid line the data from the high-angle detectors. The closed circles are the difference. The broken line gives a fit to a Lorentzian centered at 94(5) meV and with a $\Gamma/2 = 22(3)$ meV. The broken line is asymmetric because the uranium form factor changes appreciably over this range of energy transfer because of the variation in Q. A sloping background is also required to give a good fit. This could either be magnetic or from multiphonon contributions. (Taken from Hiess et al., 1996b)

3 Heavy-fermion compounds and the non-Fermi-liquid state

The correlations that develop, particularly at low temperature, in heavy-Fermion (HF) compounds continue to be at the center of much research in condensed-matter science. The understanding of such compounds falls outside the scope of the conventional band-structure approach as their most important feature are the correlation effects, which are neglected in single-electron theory. A more complete discussion of all the neutron experiments performed on single crystals of HF compounds up to ~ 1992 can be found in Aeppli and Broholm (1994).

3.1 Two new HF superconductors

Two new superconducting HF compounds have been found recently, UP_2Al_3 and UNi_2Al_3 (Geibel et al., 1991; Krimmel et al., 1992), both which exhibit magnetic order and then become superconducting at a lower temperature. UPd_2Al_3 is the most studied, and has a surprisingly large moment of $0.85\ \mu_B$. The magnetic structure consists of a simple arrangement of alternating $+--+-$ sheets of ferromagnetic planes stacked along the hexagonal c-axis. The wavevector is $q = (0, 0, 1/2)$, and the magnetic moments lie in the basal plane. Experiments on single crystals have shown that the moments probably lie along the a-axis (Kita et al., 1994; Paolasini et al., 1994). No sign of any incommensurate component has been found, unlike the case of UNi_2Al_3, in which the magnetic ordering is more complicated and the ordered moment is smaller (Schröder et al., 1994). UPd_2Al_3 becomes superconducting at ~ 2 K. Although the ordered magnetic structure seems well established of the UPd_2Al_3, the presence (if any) of an interaction between the magnetism and superconductivity has been more difficult to find (Petersen et al., 1994; Sato et al., 1996), and this is an area of considerable current activity. Clearly on the scale of the superconducting temperature $T_C \sim 2$ K, one might expect effects at the energy scale of less than 1 meV.

On a different energy scale is the question of whether UPd_2Al_3 might exhibit crystal-field (CF) levels, which have been deduced from bulk-property measurements (Böhm et al., 1993; Grauel et al., 1992). Recently, Krimmel et al. (1996) have reported on a series of experiments at the HET spectrometer at the ISIS spallation source. We reproduce a key figure from their paper in Fig. 5. It is important to realize that these data have been corrected for the phonon contribution, which have definite peaks in them, so that given these uncertainties it seems safe to make the statement that there is really no hard evidence for CF levels in this material. Of course, there are CF interactions in all these uranium materials. However, the crucial point about the neutron spectroscopy is that it shows that the CF levels
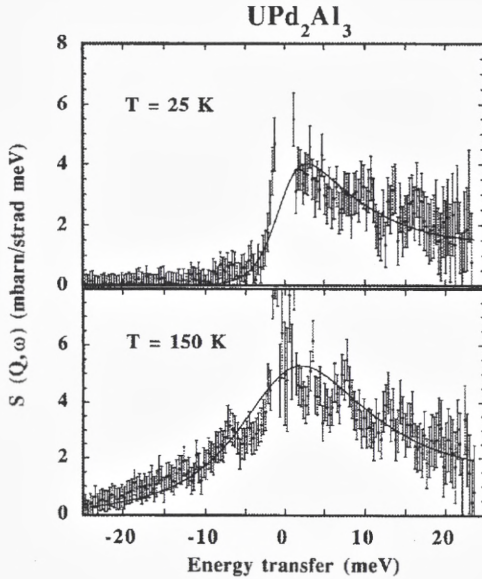
Figure 5. Corrected spectra of UPd_2Al_3 with an incident neutron energy of $E_i = 25$ meV showing the magnetic intensity at $T = 25$ K and $T = 150$ K. The data are fitted (solid lines) by two Lorentzians, one centered at $E = 0$ (quasielastic scattering) and $\Gamma/2 = 2.5$ meV at 25 K, and 5.7 meV at 150 K, and the other Lorentzian centered at 23.4 meV with $\Gamma/2 \sim 5$ meV, and thus being inelastic in origin. The detailed balance factor is included in the fit. (The FWHM of the Lorentzians is Γ, consistent with the nomenclature in Holland-Moritz and Lander (1994); figure taken from Krimmel et al., 1996)

are broadened, perhaps changed substantially, and the rare-earth model does not work. The values of $\Gamma/2$ (~ 3 meV at 25 K and ~ 6 meV at 150 K) in UPd_2Al_3 are rather small for uranium compounds, see Table 5 of Holland-Moritz and Lander (1994) where one can see that the values of $\Gamma/2$ for uranium compounds range between 5 and 15 meV. Indeed one is tempted by the data of Fig. 5 to try just one Lorentzian of a larger width ($\Gamma/2$ at least 8 meV at 25 K) and it is unfortunate that the authors do not show how such a fit looks.

One of the more intriguing theories about UPd_2Al_3 and its superconductivity is that there are two electron systems that are relevant, both involving $5f$ electrons. The first gives the ordered moment, the normal behaviour for the susceptibility, the CF level structure, and the second $5f$ electron system is relevant for the superconductivity at ~ 2 K (Caspary et al., 1993; Feyerherm et al., 1994). Corroborating

evidence for this idea comes from the polarized-neutron study (Paolasini et al., 1993) of single crystals. In this work the most interesting results were that the ratio of the orbital to spin orbital moments (μ_L/μ_S) was somewhat below the free-ion value, and that there is an appreciable positive conduction-electron polarization. Normally in U compounds (and in all compounds with the lighter actinides) there is a negative conduction-electron polarization (Lander, 1993), so that the situation in UPd_2Al_3 is unusual. In contrast to the studies cited earlier on URhAl and URuAl, no induced moment is found on the Pd site in UPd_2Al_3. Certainly, this material is a long way from the band $5f$ electrons discussed in the Introduction above.

3.2   New experiments on HF systems

3.2.1   UPt$_3$

A key question in the superconductivity of the HF compounds is whether it is of the s- or d-wave form. UPt$_3$ is perhaps the most-studied compound, and increasing evidence suggests that the superconductivity is unconventional (i.e. not of the s-wave form) (Fisk and Aeppli, 1993). Related to this question is how the magnetic ordering found in UPt$_3$ (Aeppli et al., 1988) interacts with the superconductivity. The earlier experiments (Aeppli and Broholm, 1994) had shown that the amplitude of the magnetic moment appeared to be reduced when UPt$_3$ becomes superconducting, however, it was also possible that there was a change in the magnetic structure that went unobserved in the early work. The AF state of UPt$_3$ has therefore been re-examined (Isaacs et al., 1995) with both neutron and resonant x-ray techniques. This study finds that the correlations in the AF state of UPt$_3$ are definitely smaller than in a classic long-range ordered materials and range from ~ 300 to ~ 500 Å, as was found also for URu$_2$Si$_2$. Furthermore, there is definitely a slight reduction in the ordered moment when the material becomes superconducting, but neither a change in the direction of the moment nor a different magnetic structure. The intensities reduce by about 10% when $T < T_C$. This is important as it shows a coupling between magnetism and superconductivity. Further than that takes us into the realm of the newest theories for d-wave superconductivity.

The inelastic response for UPt$_3$ has been measured and consists of at least two energy scales. At the highest energy, corresponding to a $\Gamma/2 \sim 9$ meV, each U moment is correlated antiferromagnetically with its six nearest neighbours (Aeppli and Broholm, 1994). On a smaller energy scale (longer time scale) of $\Gamma/2 \sim 0.2$ meV another characteristic response has been found (Aeppli and Broholm, 1994), and this has been examined in some detail recently by Bernhoeft and Lonzarich (1995) especially as a function of q at low q. The main result is that in this region of q-space the form of the function $\chi''(q,\omega)$ cannot be understood in terms of a single-

pole model with a wavevector-independent relaxation spectrum. The response at very low energies, which is associated with the quasiparticles that establish the HF state, accounts for about 20% of χ'', with the remainder coming in the higher-energy region. Unfortunately, there is no theory yet that attempts to account for the two energy scales observed in UPt_3, UBe_{13}, and USn_3 (Holland-Moritz and Lander, 1994) so it is not easy to make further remarks.

3.2.2 URu_2Si_2

In this material the major question is also related to the co-existence of super-conductivity and magnetism. There are two major problems to reconcile in URu_2Si_2 and they derive from the fact that in the ordered state an interpretation of the in-tensity of the magnetic Bragg peaks indicates that the ordered magnetic moment is only 0.04 μ_B. However, there is a large jump in the specific heat at T_N and this is an order of magnitude greater than can be accounted for by the mean-field ordering of such a weak magnetic moment. The second problem is that in the neutron inelastic spectrum there is a gap in the energy spectrum, and the lon-gitudinal fluctuations across this gap have matrix elements that correspond to a moment of $\sim 1.2\ \mu_B$, and yet the final ordered moment, as we have seen, is much smaller. These difficulties have led to suggestions that the real order parameter may be much more complex, and has not yet been found. In the last 3 years a number of theoretical papers have been published following this idea, and at least 2 experimental papers published (Walker et al., 1993; Mason et al., 1995) trying to establish whether any of these theories can be verified. Unfortunately, the exper-iments have failed to find any indication that the ordering is anything other than simple dipole. The mystery remains.

3.2.3 UBe_{13} and $NpBe_{13}$

UBe_{13} is a superconductor at about 0.9 K and, so far, is the only HF superconductor in which no magnetic ordering or magnetic correlations have been found. That in itself is odd, and weakens attempts to build consistent theories for these materials. Hiess and collaborators (Hiess et al., 1996a,b) have recently performed experiments on $NpBe_{13}$ that sheds some light on the problem of the magnetic response function in metal–Be_{13} compounds. Some of the data from this study, performed on both a polycrystalline sample and a small (~ 1 mg) single crystal, are shown in Fig. 6. By using the Mössbauer (on ^{237}Np) and neutron techniques they were able to establish the interesting magnetic structure for the Np atoms shown in Fig. 7. The data clearly show that the ordering wavevector is $q = \langle \frac{1}{3}, 0, 0 \rangle$ in this cubic system, and this is the same wavevector that is found for the lanthanide–Be_{13} compounds. It is unusual to find any similarity between magnetic structures of
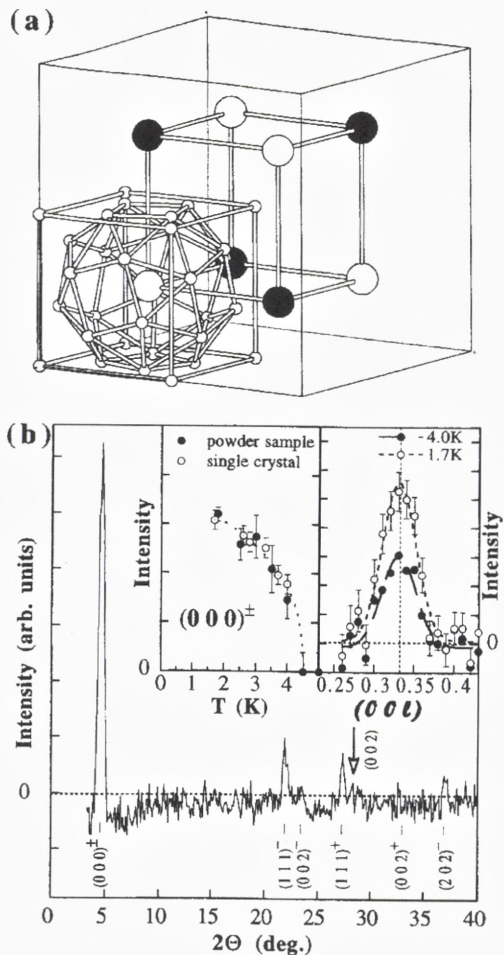
Figure 6. (a) Chemical structure of the MBe_{13} compounds. The two different Bravais lattices of the M atoms are shown as black and open spheres. Each M atom is surrounded by a polyhedron of 24 Be atoms (smaller gray spheres) at a distance of 3.0 Å. The nearest M–M distance is $a_0/2 = 5.12$ Å. (b) The main figure shows the low-angle part of the difference pattern $I(T = 1.5$ K$) - I(T = 10$ K$)$ obtained from the polycrystalline sample. The magnetic reflections are indexed and the position of the nuclear (002) peak marked. The insets show (left) the intensity of the $(000)^\pm$ satellite as a function of temperature, and (right) the intensities from the single crystal as a function of wavevector at two different temperatures. (Taken from Hiess et al., 1996a)
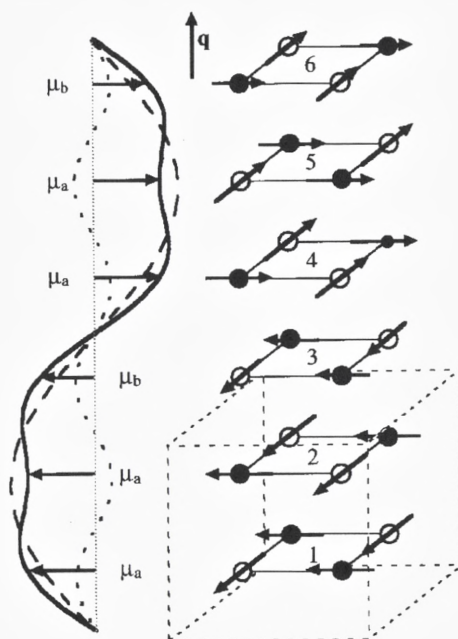
Figure 7. The magnetic structure of NpBe$_{13}$. On the left hand-side are shown the wave forms of the modulations for one Bravais lattice. The long-dashed line is the $(p = 1)$ first and the short-dashed the $(p = 3)$ third harmonic. They combine together to give the modulation shown by the solid line, which is the envelope describing the magnitudes of the magnetic moments. On the right-hand side are shown three chemical unit cells (the first outlined). The moments are perpendicular to the propagation direction, and the two sublattices (see Fig. 6a) have their moments perpendicular to each other. (Taken from Hiess et al., 1996a)

chemically isostructural lanthanide and actinide compounds because the magnitude of the interactions are normally quite different in the two series. However, the conduction-electron response, which is an important parameter in defining the ordering wavevector, comes in these compounds primarily from the Be electrons so that it is not too surprising that the ordering wavevector is a general property of MBe$_{13}$ systems, provided that the metal ions have a valence of three. So this suggests where to begin the search for such correlations in UBe$_{13}$. The magnetic structures of the lanthanide–Be$_{13}$ are, however, quite different from that found in NpBe$_{13}$. The lanthanide–Be$_{13}$ follow a helical arrangement (Becker et al., 1985), with all the moments in a plane perpendicular to the propagation direction (see Fig.

7) ferromagnetically aligned and simply turning from plane to plane. In $NpBe_{13}$ the arrangement is such that both a ferro and an antiferro component exist. The most likely structure is shown in Fig. 7. An interesting aspect of this structure is that each Np moment is surrounded by 6 moments that are perpendicular to the initial one. Thus, the direct exchange term $\mathbf{J} \cdot \mathbf{J}$ is actually zero. The $NpBe_{13}$ structure does not appear to "square" down to 1.5 K. This probably indicates the importance of the Kondo effect in stabilizing an oscillatory component of the moment – a similar situation has been found in $NpRu_2Si_2$ (Bonnisseau et al., 1988). Both of these compounds have large terms in the specific heat and are thus heavy fermions, although there is no indication (yet) that they are superconductors. It would be interesting to extend the diffraction study of this compound down to lower temperatures.

3.3   The non-Fermi liquid state

Over the last several years increasing evidence has pointed to the fact that in many electronic systems the thermodynamic, magnetic, and transport properties are not adequately described by conventional Fermi-liquid (FL) theory. One of the most important predictions of the latter theory, is that at low temperature the specific heat can be written $C = \gamma T + AT^3 + \cdots$, so that as $T \to 0$ the quantity C/T should tend to a constant, the so-called Sommerfeld coefficient, that gives the electronic contribution to the specific heat. This theory is based on the assumption that the quasiparticles, which in the HF compounds consist of states involving both the f and conduction electrons, are only weakly interacting. In many respects the FL theory is found to work for the heavy-fermions, although when the measurements are extended to very low temperatures, important deviations are found from FL theory. A similar situation is found in the layered superconductors, and this has given rise to many experiments trying to shed further light on this intriguing problem. UBe_{13} is one of the systems that do not obey FL theory (Ramirez et al., 1994), as are compounds based on the solid solutions $U_xY_{1-x}Pd_3$ and $UCu_{5-x}Pd_x$.

Neutrons give important information on the development of the non-FL ground state and some rather interesting experiments have been done on the compound UCu_4Pd (Aronson et al., 1995). Some of the data is shown in Fig. 8. The most striking property of Fig. 8(a) is the temperature independence of the data. Because of detailed balance considerations, this constant signal means that the imaginary part of the dynamic susceptibility, $\chi''(\omega, T)$, must have a special form. $S(\omega)$ and $\chi''(\omega, T)$ are related by $S(\omega) = [n(\omega) + 1]\chi''(\omega, T)$, where $n(\omega) + 1$ is the thermal occupation factor (Holland-Moritz and Lander, 1994). Since for $T \gg \omega$, $[n(\omega)+1] \sim T/\omega$, then $\chi''(\omega, T) \sim (\omega/T)G(\omega)$ and for $T \ll \omega$, $[n(\omega)+1] \sim 1$, $\chi''(\omega, T) \sim G(\omega)$.
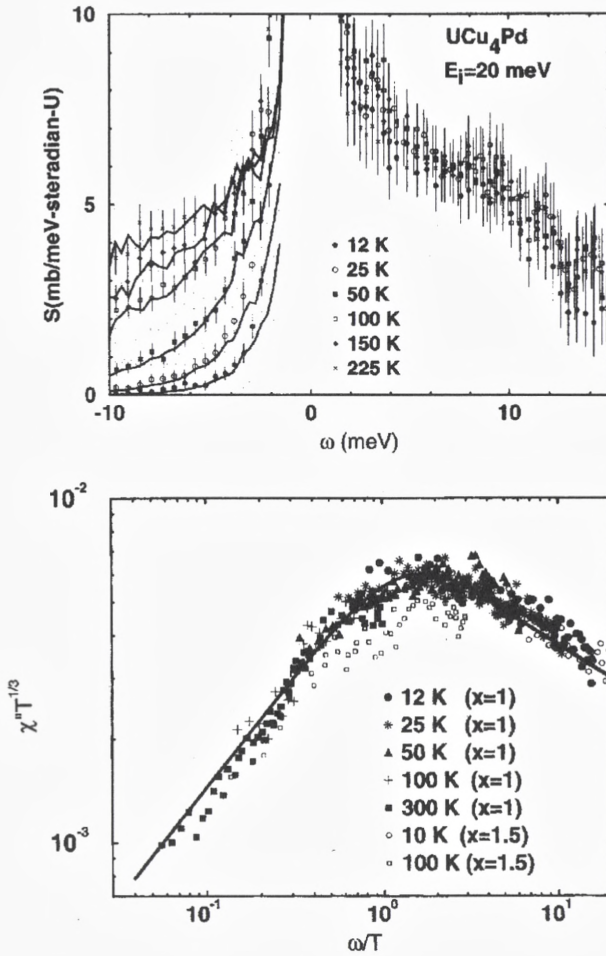
Figure 8. (a) $S(\omega)$ of UCu$_4$Pd at fixed temperatures ranging from 12 to 225 K. The incident energy is 20 meV. Solid lines for energy gain (left-hand side) are calculated from the energy loss part of the neutron spectrum by the detailed balance factor. (b) A plot of $\chi''T^{1/3}$ against ω/T showing almost universal scaling properties for compounds UCu$_{5-x}$Pd$_x$ ($x = 1$ and 1.5). Data with $\omega > 25$ meV are not included. Solid line: $\chi''(\omega, T)T^{1/3} \sim (T/\omega)^{1/3}\tanh(\omega/1.2T)$. (Taken from Aronson et al., 1995)

For energies below a characteristic energy ω^* it is found that $G(\omega) \sim \omega^{-1/3}$, and this idea is at the basis for the representation of the data in Fig. 8(b). The major result of this study is that the magnetic response depends only on temperature, rather than depending on some characteristic energy – usually associated with the Kondo temperature. The inference from these results is that there is a divergence at $T = 0$, a so-called quantum phase transition.

A rather similar situation of a non-FL ground state has been found in the solid solution $U_x Y_{1-x} Pd_3$ (Seaman et al., 1991, 1992; Andraka and Tsvelik, 1991). At low uranium concentration ($x < 0.2$) these compounds were thought to be spin glasses. Since these materials are related to UPd_3, which I shall discuss later, there has been an expectation that they exhibit sharp crystal-field transitions between different states. In fact, as shown by McEwen et al. (1995a), the picture is more complex. Whereas for $x = 0.45$, crystal-fields can be readily seen, they get much more difficult to observe when the uranium concentration is reduced (and this is not simply a dilution effect) as they become much broader in energy space. Initially, the bulk property measurements were interpreted in terms of the quadrupolar Kondo effect (Cox, 1987, 1988a,b). This theory, which has also been applied to UBe_{13} (see Ramirez et al., 1994), requires that the ground state be non-magnetic. In particular, for a non-Kramers ion such as U^{4+} there exists the crystal-field state Γ_3 that meets these requirements. Although the work of McEwen et al. (1995a) firmly established CF transitions at ~ 5 and ~ 36 meV in both the $x = 0.2$ and 0.45 samples, these measurements were not able to determine the ground state. More recently, experiments by Dai et al. (1995) have shown that there is a substantial amount of quasielastic scattering in both the $x = 0.45$ and 0.2 samples and this is inconsistent with the non-magnetic doublet Γ_3 as the ground state, but rather point to the triplet Γ_5 being the ground state. They did not consider any possible $5f^3$ CF configurations. In addition, and perhaps quite surprising considering the number of people who have studied these samples, they found that the $x = 0.45$ sample orders magnetically with a simple doubling of the unit cell. The magnetic structure is identical to that found in UPd_4, which also has the same $AuCu_3$ structure, and the ordered moments of both compounds are ~ 0.7 μ_B. Interestingly, the muon experiments (Wu et al., 1994) had already indicated that the $x = 0.4$ system contained a magnetic moment, but in the absence of direct diffraction evidence for its long-range order, there was a belief that the compound was a spin glass. This study by Dai et al. (1995) went on to observe elastic magnetic correlations in the $x = 0.2$ sample at the same reciprocal-lattice vector as the ordering was found in the $x = 0.45$ sample, so that the $x = 0.2$ material is certainly close to a magnetic instability. Furthermore, fluctuations were still seen at $E = 0$ meV in the $x = 0.2$ sample, so that the CF scheme is probably the same for both values of x, although the scattering is much reduced in the $x = 0.2$ sample, in agreement with the finding

of McEwen et al. (1995a). This study by Dai et al. (1995) is a good example of how a careful neutron study can change completely the ideas about the physics of a certain material.

4 The progression towards localized $5f$ electrons

The discussion about how to define localized $5f$ electrons has been one that has been at the center of actinide research for many years. In many respects the answer depends on the measuring technique. As far as neutron scattering is concerned the answer is relatively simple: the $5f$ electrons can be described as localized when sharp and clear CF excitations can be seen with neutron spectroscopy. This is a definition that follows the framework of defining compounds containing the lanthanide elements, and has the advantage of simplicity. Most compounds containing lanthanides exhibit sharp, or relatively sharp, CF transitions; compounds containing cerium being the one notable exception (Holland-Moritz and Lander, 1994). Unfortunately, the only metallic actinide compound (so far) that has been found to fit readily into this classification is UPd_3. We do not include here a discussion of the oxides, which are without doubt localized, even though they exhibit many unusual properties (Holland-Moritz and Lander, 1994).

4.1 Compounds with the NaCl crystal structure

Certainly the most studied examples of compounds in this class are those with the NaCl crystal structure and comprising the monopnictides and monochalcogenides. However, there a number of exceptions. The most notable are the first member of this series, UN, which is itinerant (Holland-Moritz and Lander, 1994), and the Pu–chalcogenides, which are still the subject of much debate, and have been proposed as showing intermediate-valent behaviour (Wachter et al., 1991). However, with these caveats, the remainder of the compounds, e.g. USb, UTe, NpAs, NpBi, NpTe, PuSb, may be regarded as quasi-localized. Although they do not, for the most part, exhibit CF excitations, relatively sharp excitations involving the uranium moments have been found in most of them. A recent review (Lander et al., 1995) has focused on these compounds so that I will not repeat what is written there. Experiment and theory are in modest agreement; the latter having to include a considerable amount of hybridization between the $5f$ and conduction-electron states. Recently, Bourdarot and colleagues (Bourdarot et al., 1995) have succeeded in seeing sharply defined spin-wave modes in NpBi, but an experiment on an equally good single crystal of NpTe failed to find any excitation. The localization is certainly more important for the pnictides (N, P, As, Sb, and Bi) than for the chalcogenides (S, Se, and Te), and there is always a trend for more localization as one proceeds to

heavier actinides or anions. The failure, so far, to find excitations in a material like NpTe would seem to be contrary to the above rules since excitations have been measured in UTe (Lander et al., 1995). However, if we are approaching an intermediate valent behaviour in the Pu-chalcogenides, then the Np-chalcogenides may exhibit precursor effects.

The last few years have seen a number of new studies of the phase diagrams of the AnX compounds, both with neutrons and with resonant x-rays (Lander, 1996). With neutrons two different types of investigations merit discussion. A significant study of the NpX compounds with elastic neutron scattering has been performed by Bourdarot (1994) as part of his thesis work at the Centre d'Etudes Nuclaires, Grenoble; unfortunately, most of this remains unpublished. A new capability has been developed at the Laboratoire Leon Brillouin, Saclay, to look at single crystals at low temperature and high pressures up to 8 GPa. Initial studies have performed on UAs and USb (Goncharenko et al., 1994; Braithwaite et al., 1996), and are very promising in trying to understand the development of the complex magnetic structures (Lander and Burlet, 1995) as a function of pressure, and thus give information on changes in hybridization as a function of volume.

4.2   Compounds with the $AuCu_3$ structure

The UX_3 compounds have been of interest for many years and a full discussion of their properties, as known so far, may be found in the chapters of the Vol. 17 and 19 of the Rare Earth Handbook (Lander, 1993; Holland-Moritz and Lander, 1994; Aeppli and Broholm, 1994). In these compounds, as in the NaCl series, the $5f$ hybridization with the conduction electrons and the anion p states is critical in determining the magnetic properties. Like the NaCl compounds they exhibit increased hybridization for the lighter anions. UGa_3 is classified as a band antiferromagnet, UGe_3 as a band paramagnet, USn_3 as a spin-fluctuation system, and UPb_3 close to a localized antiferromagnet. Recently, an effort in the Cadarache Laboratories of the CEA has led to the production of a number of single crystals of the NpX_3 compounds, and provided the opportunity for neutron experiments to extend our knowledge of the systematics into the Np series. This work is not yet complete, but initial reports are summarized by Sanchez et al. (1993), with brief details on $NpAl_3$ (Oddou et al., 1994), $NpGa_3$ (Bouillet et al., 1993), $NpIn_3$ (Colineau et al., 1995), and $NpSn_3$ (Charvolin et al., 1994). Large enough single crystals of $NpSn_3$ are now available for inelastic neutron experiments, and these will be performed at the ILL shortly. At the moment it is clear that the Np samples are more "magnetic" than their uranium analogues, which is consistent with our general picture that, for an isostructural series, the hybridization reduces as one substitutes a heavier actinide.
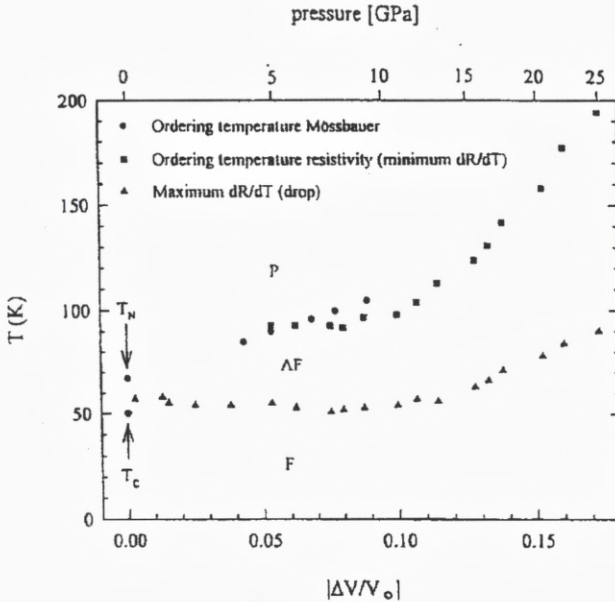
Figure 9. The ordering temperature deduced from Mössbauer spectroscopy (circles) and from resistance measurements (squares) versus volume reduction (pressure on the top scale) for NpGa$_3$. The maximum of the derivative dR/dT of the low-temperature drop in resistance is also plotted (triangles). The phase diagram, P = paramagnetic, AF = antiferromagnetic, and F = ferromagnetic is proposed. (Taken from Zwirner et al., 1996)

Within the AnX$_3$ compounds a rather complete experiment (except for the use of neutrons) has been performed on NpGa$_3$ under pressure (Zwirner et al., 1996). We reproduce from this study the tentative phase diagram under pressure in Fig. 9. Perhaps the most startling aspect of this phase diagram is the dramatic increase in the ordering temperature T_N as a function of pressure above 10 GPa. The increase has been confirmed directly by Mössbauer spectroscopy up to this pressure, but the technique is not easily applicable above 10 GPa, and T_N is taken from a change of slope seen in the resistivity. The authors explain their many measurements by assuming that the Np $5f$-electrons are initially only weakly hybridized at ambient pressure, and the increase in T_N may be ascribed to the increase of exchange as the atoms are pushed closer together. This is consistent with a decrease in both the iso-mer shift and the quadrupole interaction as measured by the Mössbauer technique with applied pressure. Of course, at higher pressures the hybridization should start

to increase, and this must eventually lead to a $5f$ band that is too wide to fulfill the Stoner criterion, and thus a reduction of the ordering temperature. Such an effect of observing first a dramatic increasing in T_C and then, with further pressure, a reduction, occurs in UTe (Link et al., 1992). Theory (Cooper et al., 1994) and experiment are in reasonable accord for UTe, and the extent of hybridization required is consistent also with the neutron inelastic measurements and the observation of broadened spin waves (Holland-Moritz and Lander, 1994). Other pressure studies have been reported on NpSb (Amanowicz et al., 1994), and are in preparation for NpAs (Ichas et al., 1996). As the studies of UTe and NpGa$_3$ illustrate, the use of pressure gives a considerable amount of new information. These are hard experiments with neutrons. The higher pressures can only be obtained with samples almost too small to be useful for neutron scattering. It is an area that in future may be exploited by using the resonant x-ray technique, except that this too has its disadvantages. At the resonant energy of ~ 4 keV photons are strongly absorbed, and it will require great ingenuity to make a pressure cell inside a cryostat and still allow such photons to enter and diffract from the single crystals. However, the advantage is that the x-ray intensity from modern synchrotron sources is much greater than can ever be conceived with neutrons.

4.3 Localized $5f$ electrons in UPd$_3$

UPd$_3$ stands out as an extraordinary exception in the actinides (Holland-Moritz and Lander, 1994) as it clearly can be described starting from a localized $5f^2$ configuration. Crystal fields were first observed many years ago and much of the work at Chalk River National Laboratories is published in Buyers and Holden (1985). The structure of this material is not cubic AuCu$_3$ as discussed in the last section, but rather has the double hexagonal close-packed structure in which there are two different sites for the uranium ions.

In the last few years the transitions at low temperature have been examined in more detail by McEwen and his colleagues and the theory has been worked out by Walker and colleagues. Steigenberger et al. (1992)and McEwen et al. (1993, 1995b) have reported both inelastic and elastic neutron scattering. Two transitions take place at low temperature; the first at $T_1 \sim 6.7$ K involves the ordering of the quadrupoles of the uranium ions; the second at $T_2 \sim 4.5$ K involves magnetic ordering with a very small magnetic moment. The superlattice reflections that appear on cooling at T_1 arise from the modulated ionic displacements which accompany the quadrupolar modes: neutrons do not couple directly to the quadrupolar moments. This phase transition has been examined from a group theoretical point of view in a series of papers (Walker et al., 1994; Kappler et al., 1995; Luettmer-Strathman et al., 1995), and special attention has been given to the results of

experiments when a symmetry breaking field (either magnetic or uniaxial stress, for example) is applied. The combination of theory and experiment have now led to the triple-k quadrupole ordering given by Fig. 10. Quadrupolar ordering has also been observed in UO_2 (Lander, 1993), but occurs at the same temperature as the magnetic ordering. However, such orderings at higher temperatures than the magnetism are not confined to the actinides; they may be found for a number of lanthanide compounds (Morin and Schmitt, 1990). This work on UPd_3 illustrates the extreme complexity when the quadrupolar moments are the driving force for the phase transitions. Such quadrupole moments are large in f systems (Morin and Schmitt, 1990), and may significantly affect both the final magnetic structure as well as the nature of the transitions. That these quadrupolar effects have not (yet) been observed in systems such as UBe_{13} is only because there are other, more important, interactions involving the hybridized f-conduction-electron states in that material.
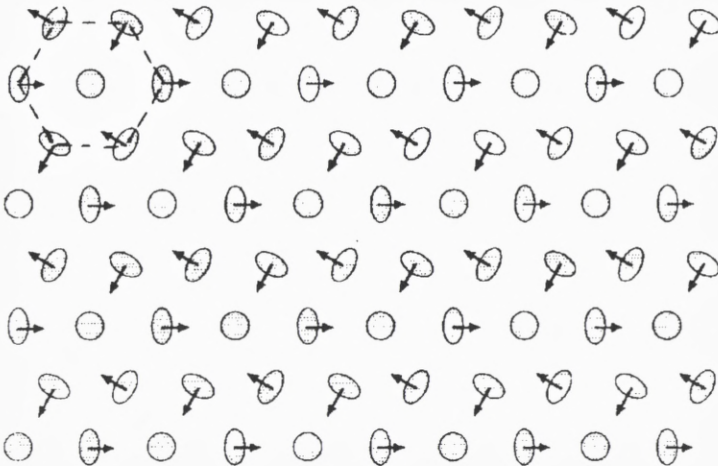
Figure 10. Basal plane projection of the antiferroquadrupolar structure on the cubic sites of UPd_3 below T_1 as described in the text. The unit cell of the structure is indicated. The ordering has the $3k$ symmetry. (Taken from McEwen et al., 1993, 1995b)

5   Discussion

A framework for the magnetism of the $5f$ electrons in the actinides still eludes us. A key parameter is the extent of hybridization, $\mathfrak{F}$. Unfortunately, this may take place either with the conduction-electron states (as, for example, dominates in most of the heavy fermions) or with the p- or d-states of neighbouring anions (as, for example, is believed to be the basic mechanism in the AnX_3 compounds), and it is difficult to distinguish which is the most important for any particular property that is being measured. Certainly introducing a single parameter $\mathfrak{F}$ is too naive. However, what I have tried to show in this article is that if we start from the Jensen-Mackintosh (1991) picture of localized f electron behaviour, then the hybridization is zero (or very small) and this explains the magnetism of UPd_3. With increasing $\mathfrak{F}$ we come to the compounds of the form AnX and AnX_3. A still further increase of $\mathfrak{F}$, especially with respect to the conduction-electron states, takes us to a magnetic instability and the possibility of the heavy-fermion state. Why some of these materials should be superconducting remains a mystery, but is believed to be due to the quasi-particles (involving hybridized $5f$ and conduction states) forming unconventional (i.e. non s-state) pairs at the lowest temperature (Aeppli and Broholm, 1994; Aeppli et al., 1988; Cox and Maple, 1995; Lonzarich, 1996). A further increase in $\mathfrak{F}$ takes us to the truly itinerant $5f$ electron states, such as UN, UFe_2, possibly UGa_3, and allows the reduction of the orbital moment (Lander et al., 1991), and the understanding of the magnetism in terms of the local-density approximation (Johansson and Skriver, 1996; Brooks, 1996).

Many different factors determine where a particular actinide may fit into this loose framework. More work, both experiment and theory, lies ahead to attempt to make such a framework quantitative.

Acknowledgements

References

Aeppli G et al., 1988: Phys. Rev. Lett. **60**, 615

Aeppli G and Broholm C, 1994: in *Handbook on the Physics and Chemistry of Rare Earths*, eds. K.A. Gschneider, L. Eyring, G.H. Lander and G.R. Choppin (Elsevier Science, Amsterdam) Vol. 19, Chap. 131, p. 122

Amanowicz M et al., 1994: Phys. Rev. B **50**, 6577

Andraka B and Tsvelik AM, 1991: Phys. Rev. Lett. **67**, 2886

Aronson MC et al., 1995: Phys. Rev. Lett. **75**, 725

Becker PJ et al., 1985: Mol. Cryst. Liq. Cryst. **125**, 405

Bernhoeft NR and Lonzarich GG, 1995: J. Phys. Condens. Matter **7**, 7325

Böhm A et al., 1993: Int. J. Mod. Phys. B **7**, 34

Bonnisseau D et al., 1988: J. Phys. (Paris) **49**, C8–491

Bouillet MN et al., 1993: J. Magn. Magn. Mater. **125**, 113

Bourdarot F, 1994: Thesis (University of Grenoble, France)

Bourdarot F et al., 1995: (unpublished experiments at the ILL)

Braithwaite D et al., 1996: Europhys. Lett. **35**, 121

Brooks MSS, 1996: (see paper at this conference)

Brooks MSS et al., 1988: J. Phys. F **18**, L33

Buyers WJL and Holden TM, 1985: in *Handbook on the Physics and Chemistry of the Actinides*, eds. A.J. Freeman and G.H. Lander (North Holland, Amsterdam) Vol. 2, p. 239

Caspary R et al., 1993: Phys. Rev. Lett. **71**, 2146

Charvolin T et al., 1994: J. Magn. Magn. Mater. **132**, 46

Colineau E et al., 1995: Physica B **206-208**, 528

Collins SP et al., 1995: J. Phys. Condens. Matter **7**, 9325

Cooper BR et al., 1994: J. Alloys and Compounds **213-214**, 120

Cox DL, 1987: Phys. Rev. Lett. **59**, 1240

Cox DL, 1988a: Physica C **153**, 1642

Cox DL, 1988b: J. Magn. Magn. Mater. **76**, 56

Cox DL and Maple MB, 1995: Physics Today, 32

Dai P et al., 1995: Phys. Rev. Lett. **75**, 1202

Feyerherm R et al., 1994: Phys. Rev. Lett. **73**, 1849

Fisk Z and Aeppli G, 1993: Science **260**, 38

Geibel C et al., 1991: Z. Phys. B **81**, 1

Goncharenko IN et al., 1994: Physica B **199-200**, 625

Grauel A et al., 1992: Phys. Rev. B **46**, 5818

Hiess A et al., 1996a: Phys. Rev. Lett. **77**, 3917

Hiess A et al., 1996b: SCES Conference (Zürich), Physica B (in press)

Holland-Moritz E and Lander GH, 1994: in *Handbook on the Physics and Chemistry of Rare Earths*, eds. K.A. Gschneider, L. Eyring, G.H. Lander and G.R. Choppin (Elsevier Science, Amsterdam) Vol. 19, Chap. 130, p. 1

Ice GE et al., 1993: Phys. Rev. B **47**, 6241

Ichas V et al., 1996: (to be published)

Isaacs ED et al., 1989: Phys. Rev. Lett. **62**, 1671

Isaacs ED et al., 1990: Phys. Rev. Lett. **65**, 3185

Isaacs ED et al., 1995: Phys. Rev. Lett. **75**, 1178

Jensen J and Mackintosh AR, 1991: *Rare Earth Magnetism: Structures and Excitations* (Clarendon Press, Oxford)

Johansson B and Skriver H, 1996: (see paper at this conference)

Kappler C et al., 1995: Phys. Rev. B **51**, 11319

Kita H et al., 1994: J. Phys. Soc. Jpn. **63**, 726

Krimmel A et al., 1992: Z. Phys. B **86**, 161

Krimmel A et al., 1996: J. Phys. Condens. Matter **8**, 1677

Lander GH, 1993: in *Handbook on the Physics and Chemistry of Rare Earths*, eds. K.A. Gschnei-
    der, L. Eyring, G.H. Lander and G.R. Choppin, (Elsevier Science, Amsterdam) Vol. 17, Chap.
    117, p. 635
Lander GH, 1996: Invited talk at Rare-Earth Research Conference, Duluth, Minesota, J. Alloys
    and Compounds (in press)
Lander GH et al., 1991: Phys. Rev. B **43**, 13672
Lander GH et al., 1995: Can. J. Phys. **73**, 718
Lander GH and Burlet P, 1995: Physica B **215**, 7
Langridge S et al., 1994a: Europhys. Lett. **25**, 137
Langridge S et al., 1994b: Phys. Rev. B **49**, 12022
Langridge S et al., 1994c: Phys. Rev. B **49**, 12010
Lebech B et al., 1989: J. Phys. Condens. Matter **1**, 10229
Link P et al., 1992: J. Phys. Condens. Matter **4**, 5585
Lonzarich G, 1996: (see paper at this conference)
Luettmer-Strathman J et al., 1995: Phys. Rev. B **52**, 6285
Mason TE et al., 1995: J. Phys. Condens. Matter **7**, 5089
McEwen KA et al., 1993: Physica B **186-188**, 670
McEwen KA et al., 1995a: Physica B **206-207**, 112
McEwen KA et al., 1995b: Physica B **213-214**, 128
Morin P and Schmitt D, 1990: in *Ferromagnetic Materials*, ed. K.H.J. Buschow (Elsevier Science,
    Amsterdam) Vol. 5, p. 1
Nuttall WJ, 1995: Phys. Rev. B **52**, 4409
Oddou JL et al., 1994: J. Magn. Magn. Mater. **135**, 183
Paixão JA et al., 1993: Europhys. Lett. **24**, 607
Paolasini L et al., 1993: J. Phys. Condens. Matter **8**, 8905
Paolasini L et al., 1994: Phys. Rev. B **48**, 7072
Paolasini L et al., 1996a: Europhys. Lett. **34**, 459
Paolasini L et al., 1996b: Phys. Rev. B **54**, 7222
Perry S et al., 1996: Phys. Rev. B (in press)
Petersen T et al., 1994: Physica B **199-200**, 151
Ramirez AP et al., 1994: Phys. Rev. Lett. **73**, 3018
Sanchez JP et al., 1993: Physica B **186-188**, 675
Sato N et al., 1996: (preprint)
Schröder A et al., 1994: Phys. Rev. Lett. **72**, 136
Seaman CL et al., 1991: Phys. Rev. Lett. **67**, 2882
Seaman CL et al., 1992: J. Alloys and Compounds **181**, 327
Steigenberger U et al., 1992: J. Magn. Magn. Mater. **108**, 163
Tang CC et al., 1992: Phys. Rev. B **46**, 5287
Wachter P et al., 1991: Phys. Rev. B **43**, 11136
Walker MB et al., 1993: Phys. Rev. Lett. **71**, 2630
Walker MB et al., 1994: J. Phys. Condens. Matter **6**, 7365
Watson GM et al., 1996a: Phys. Rev. B **53**, 686
Watson GM et al., 1996b: Physica B **221**, 405
Watson GM et al., 1996c: Phys. Rev. Lett. **77**, 751
Wu WD et al., 1994: Phys. Rev. Lett. **72**, 3722
Wulff M et al., 1989: Phys. Rev. B **39**, 4719
Zwirner S et al., 1996: Phys. Rev. B **54**, 12283

Crystal Fields in Metallic Magnetism

K. A. McEwen

Department of Physics, Birkbeck College, University of London,

Malet Street, London WC1E 7HX, UK

Abstract

The magnetic structure and excitations of praseodymium are reviewed. Two phenomena which cannot be understood within the standard model of rare earth magnetism are discussed. These are the quasielastic peak which is present in both the paramagnetic and antiferromagnetic phases, and the excitations which accompany the crystal field excitations near the Brillouin zone centre. We also review the properties of the localised moment compound UPd₃, and discuss the nature of the quadrupolar phases observed in this system.

1   Introduction

The crystal field interaction is an essential component of the standard model of rare earth magnetism, which Allan Mackintosh put forward. In this model, the $4f$ electrons are localised, with ground state multiplets determined by Hund's rules. Their magnetic moments interact with their surroundings through the single-ion crystalline electric field (CEF) interaction, which removes the degeneracy of the $|J, J_z\rangle$ ground multiplet. The f-electrons and the conduction electrons are weakly coupled, leading to the two-ion indirect RKKY exchange. Other interactions, such as the magnetoelastic and hyperfine interactions, and the classical dipolar couplings, are assumed to be relatively weak. A full account of the standard model and its application to the structures and excitations of the rare earths was given by Jens Jensen and Allan Mackintosh in their book (Jensen and Mackintosh, 1991), which reviews the field up to 1991.

CEF effects play a profound role in the magnetism of the light rare-earth metals, and in this paper I will examine new results which have been discovered since 1991. Some of these results provide a stringent test for the standard model, and suggest that the model breaks down when the coupling with the conduction electrons becomes sufficiently strong that the $4f$ states develop a significant band-like component. Indeed Allan Mackintosh recognised this effect was central to an understanding of cerium, which he called a $4f$ band metal (Mackintosh, 1985). I shall

also discuss some actinide compounds in which clear evidence for localised moment magnetism and CEF effects have been observed.

2   Praseodymium

Pr is in many respects the apotheosis of the standard model of rare earth magnetism: although it has been extensively studied for many years, new aspects of its magnetic behaviour have been discovered in the past five years. In particular, there are now two well-established phenomena which cannot be understood within the standard model, and we shall discuss them in some detail, after a brief outline of the essential properties of this element.

The crystal structure of Pr is double-hexagonal close-packed, with locally hexagonal and cubic sites. The first model for the CEF splitting of the $4f^2$, $J = 4$ ground multiplet, was put forward by Bleaney (1963), based on heat capacity and susceptibility data from polycrystalline samples. Singlet ground states at both sites were proposed. With the advent of single crystals in the 1970s, the magnetic excitations and bulk properties (magnetisation, susceptibility) were studied. The level scheme of Rainford and Houmann (1971), subsequently refined by Jensen (1979), accounts well for the observed properties. On the hexagonal sites, the ground state is $|J_z = 0\rangle$ with the first excited (doublet) states of $|J_z = \pm 1\rangle$ at 3.5 meV. On the cubic sites the ground state is also a singlet separated by 7.5 meV from the excited Γ_4 triplet. The overall splitting of the $J = 4$ multiplet is about 15 meV. This level scheme accounts for a large anisotropy of the moments on the hexagonal sites in a magnetic field. At low temperatures, there is thus no moment induced on the hexagonal sites by a field along the c-axis until the Zeeman splitting brings about a level crossing of one of the excited states with the singlet state. Such a metamagnetic transition, resulting in a large increase in the magnetisation, was found by McEwen et al. (1973) to take place at 32 tesla.

The criterion for magnetic ordering in a singlet ground state system may be easily seen from the inverse magnetic susceptibility in a mean field approximation:

$$\chi^{-1}(\boldsymbol{q}) = \left[\frac{2g^2\mu_B^2\alpha^2}{\Delta}\right]^{-1} - \mathcal{J}(\boldsymbol{q})$$

where Δ is the energy gap between the ground and first excited CEF state, and α is the matrix element $\langle e|J_\xi|g\rangle$ connecting them. The criterion for the divergence of χ^{-1} and hence magnetic ordering is

$$\frac{2\mathcal{J}(\boldsymbol{q})g^2\mu_B^2\alpha^2}{\Delta} \geq 1$$

i.e. the exchange energy divided by the crystal field splitting must exceed a critical ratio. A comprehensive study of the magnetic excitations in Pr at 6 K was carried out at Risø by Houmann, Rainford, Jensen and Mackintosh in the 1970s. Their measurements (Houmann et al., 1979) revealed a strong dispersion of the crystal field excitations (called magnetic excitons) with a well defined minimum along the ΓM direction. From the energy of this incipient soft mode, it was deduced that the exchange is some 92% of the critical value for ordering.

Magnetic ordering in Pr thus requires either a reduction in the CF splitting (Δ) or an increase in the exchange $J(\boldsymbol{Q})$. Jensen's suggestion that a suitably applied uniaxial stress might induce ordering in Pr was exhaustively investigated by McEwen, Stirling and Vettier in experiments (McEwen et al., 1978, 1983a, 1983b) at the ILL. These demonstrated that only a very modest uniaxial pressure, e.g. 1 kbar (100 MPa), along the a-axis is required to split the excited doublet and produce a large ordered moment ($\approx 1\ \mu_B$). In the pressure-induced magnetic structure the moments are longitudinally polarised along the real-space b direction in an incommensurable structure whose wave vector is $\boldsymbol{q} = 0.13\boldsymbol{\tau}_{100}$, and are also coupled antiferromagnetically along the c-axis. Under pressure, the excitations showed a pronounced softening, and became overdamped around the critical wave vector (Jensen et al., 1987).

Magnetic ordering in Pr may also be produced by another mechanism, via the hyperfine coupling. Since the nuclear spin of Pr (which exists naturally only as the single isotope ^{141}Pr) is $I = \frac{5}{2}$, the Curie susceptibility of the nuclear spins will diverge at sufficiently low temperatures and the coupling $A\boldsymbol{I} \cdot \boldsymbol{S}$ to the electronic moments will eventually lead to their order, as predicted by Murao (1971, 1975, 1979). Experiments at ILL (McEwen and Stirling, 1981) and Risø (Bjerrum Møller et al., 1982) in the 1980s demonstrated this effect in principle, but cryogenic difficulties restricted the range of the measurements to just below the Néel temperature of $T_N \approx 50$ mK.

The onset of magnetic ordering in Pr is, however, most unusual. Already at temperatures far above T_N, fluctuations appear at a wave vector of $\boldsymbol{q}_1 = 0.105\boldsymbol{\tau}_{100}$, as seen in the neutron scattering data shown in Fig. 1. These fluctuations grow as the temperature is reduced, and then a second peak appears at $\boldsymbol{q}_2 = 0.13\boldsymbol{\tau}_{100}$. It is this latter peak which is eventually the signature of the long-range order, but the first peak continues to grow, albeit at a slower rate, and coexists in the ordered phase. Its q-width is greater than the experimental resolution so it is not truly long range: it is known as the broad, central or quasielastic peak, and it cannot easily be understood within the standard model. The coexistence in the ordered phase of a resolution limited magnetic satellite peak at one wave vector, and a broader peak at a different wave vector is a phenomenon unique to Pr.

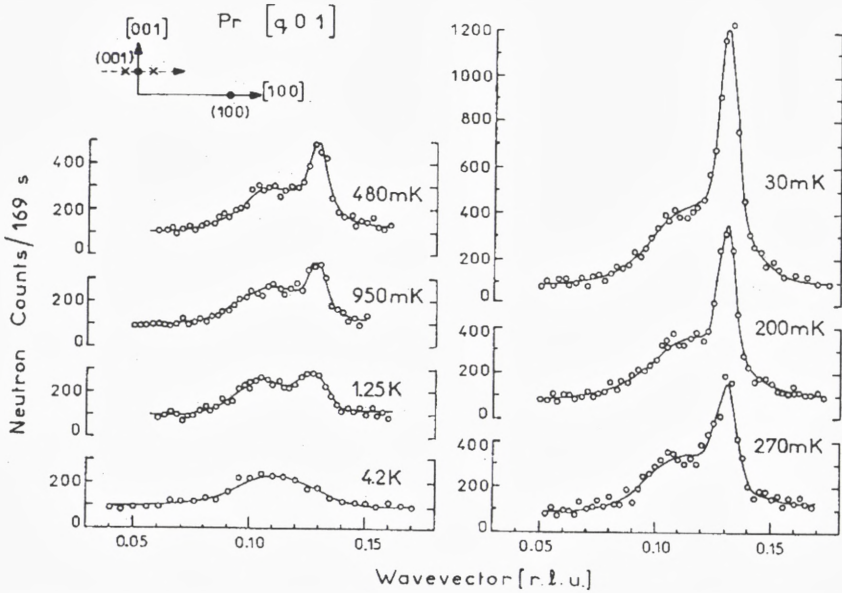More recently, we have extended these studies to temperatures well below T_N

Figure 1. Elastic neutron scattering scans through $(q, 0, 1)$ in Pr as a function of temperature, measured on the IN2 spectrometer at the ILL, Grenoble, from McEwen and Stirling (1981). The data have been fitted to two gaussians. It is now clear that the lowest sample temperature was significantly above 30 mK.

in a collaboration with the group at HMI Berlin, and have succeeded in carrying out both elastic and inelastic neutron scattering measurements on Pr at temperatures down to 9 mK (Moolenaar et al., 1997). We have confirmed that the central peak coexists with the satellite peak in the truly long-range ordered phase, and were at last able to measure the saturation intensities of the magnetic satellite and central peaks. Figure 2 shows elastic scattering scans through the $(q, 0, 3)$ position, which may be directly compared with the earlier ILL data. We see that at 175 mK, the broad peak is centred around $q_1 = 0.105\tau_{100}$, as in Fig. 1, although it is clear that this part of the scattering function is not particularly well modelled by a single Gaussian, and the satellite peak is centred at $q_2 = 0.13\tau_{100}$. However, at lower temperatures, the broad peak component is best fitted by a Gaussian function whose centre moves steadily towards the satellite wave vector, which remains essentially fixed at $0.13\tau_{100}$.

Figure 3 presents the temperature dependence of the ratio of the integrated intensity of the $(q_2, 0, 1)$ and $(q_2, 0, 3)$ magnetic satellite peaks, normalised to the intensity of the $(1, 0, 0)$ nuclear Bragg reflection. There is good agreement between
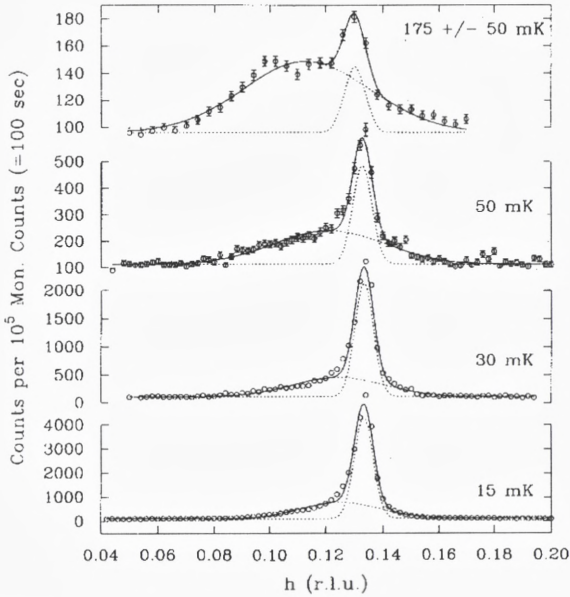
Figure 2. Elastic neutron scattering scans through $(q, 0, 3)$ in Pr as a function of temperature, measured on the V2 spectrometer at the HMI, Berlin, from Moolenaar et al. (1997). The data have been fitted to two gaussians.
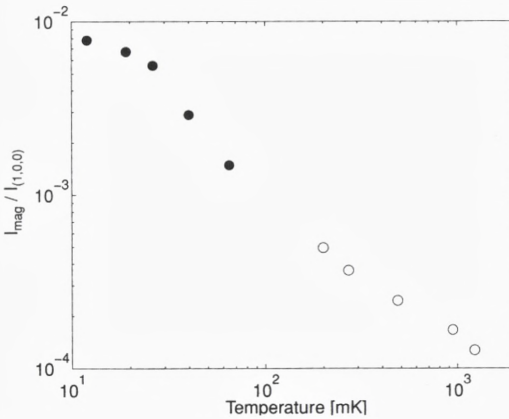

Figure 3. Temperature dependence of the integrated intensity of the satellite peaks at $(q_2, 0, 1)$ and $(q_2, 0, 3)$, normalised to the intensity of the $(1, 0, 0)$ Bragg peak, from the data of (o) McEwen and Stirling (1981) and (•) Moolenaar et al. (1997).
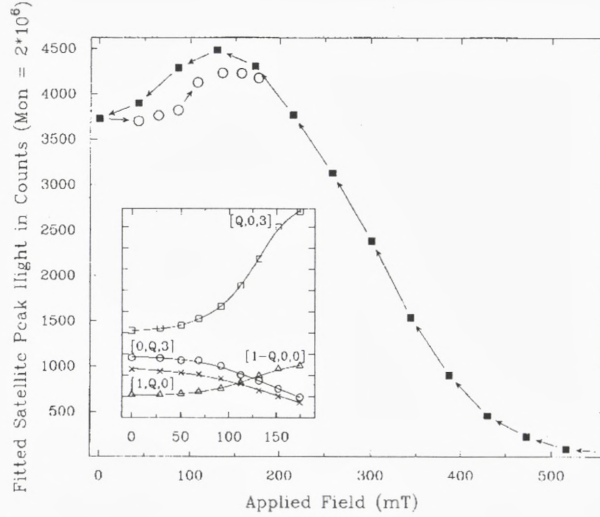
Figure 4. The magnetic field dependence of the in-plane and out-of-plane satellites in Pr, measured at $T = 10$ mK, on the V1 diffractometer at the HMI, Berlin, from Moolenaar et al. (1997).

the measurements at HMI and at ILL, which were made 15 years apart. We deduce the saturation moment to be 0.54 ± 0.1 μ_B, assuming that the magnetic structure comprises three equally populated domains. This is in reasonably good agreement with the $T = 0$ moment of 0.6 μ_B, calculated by Jensen (Jensen and Mackintosh, 1991).

The magnetic structure may be described by

$$\boldsymbol{m}\left(\boldsymbol{r}_i\right) = m_{\parallel}\hat{\boldsymbol{b}}\sin\left(\boldsymbol{Q}\cdot\boldsymbol{r}_i + \phi_b\right) + m_{\perp}\hat{\boldsymbol{a}}\sin\left(\boldsymbol{Q}\cdot\boldsymbol{r}_i + \phi_a\right)$$

where $m_{\parallel}$ denotes a moment parallel to one of the three real-space b directions ([100] in reciprocal space), and $m_{\perp}$ is a moment along the perpendicular a direction. The ordering wave vector $\boldsymbol{Q}$ is that of the magnetic satellites, i.e. $\boldsymbol{q}_2 = 0.13\boldsymbol{\tau}_{100}$.

The results discussed above have shown that the intensity of the broad peak follows that of the satellite peak, as a function of temperature. A particularly interesting new result was the discovery that the magnetic field dependence of the two peaks differs. In the experimental configuration used for these studies, the Pr single crystal was mounted with (real-space) b and c directions in the horizontal scattering plane of the neutron spectrometer. In this way, diffraction peaks from one domain of the magnetic structure lie in the scattering plane (the *in-plane satellites*). The magnetic moments of the other two domains lie at $\pm 60°$ out of the horizontal plane, but some of their diffraction peaks (the *out-of-plane satellites*)
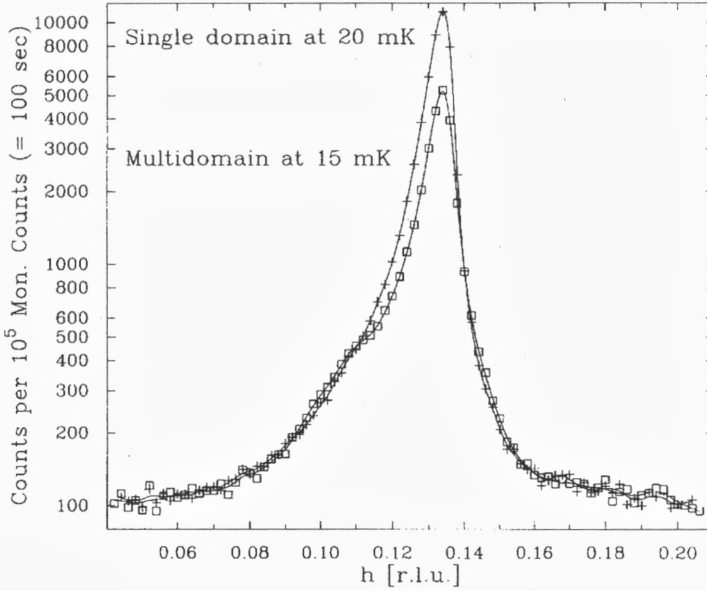
Figure 5. Comparison of $(q, 0, 3)$ scans for Pr at $T = 15$ mK, prepared in the multi-domain (zero-field cooled) and single-domain (field cooled) states, from Moolenaar et al. (1997).

may nevertheless be accessed by an appropriate tilt of the cryostat or the detector. With the sample at a temperature well below T_N, a magnetic field was applied in the vertical direction selecting, as expected for an antiferromagnet (see, for example, McEwen and Walker, 1986), the domain for which the magnetic moments were perpendicular to the field. Figure 4 shows the consequent increase in intensity of the in-plane satellite reflection, and the concomitant decrease of the out-of-plane reflections. At 10 mK, a field of 0.2 tesla suffices to produce a single domain structure. A single domain phase can also be prepared by cooling the sample through T_N in a magnetic field and then reducing the field to zero. Figure 5 illustrates the results of a $(q, 0, 3)$ scan for the single domain sample of Pr at 15 mK, prepared by field cooling, together with a similar scan for the multi-domain state, measured after the sample had been cooled in zero field. Whilst the satellite component has an intensity in the single domain state close to three times that of the multi-domain sample, as expected, the intensity of the broad peak component is clearly the same in both the single domain and multi-domain cases. This result is undoubtedly significant, and requires further theoretical understanding.

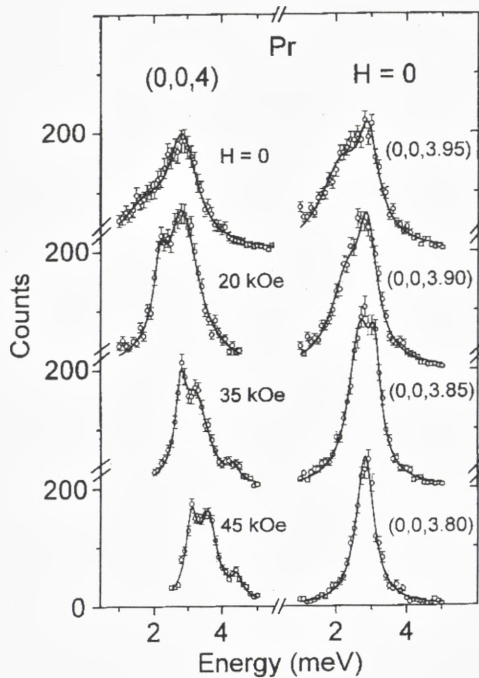The field dependence shows that a field in the basal plane leads to a rapid

Figure 6. Inelastic neutron scattering spectra for Pr at $T = 4.2$ K, for wavevectors from $(0, 0, 4)$ to $(0, 0, 3.80)$, measured on the TAS7 spectrometer at Risø, from (Clausen et al., 1994a, 1994bb). The data have been fitted to Lorentzian functions convoluted with the experimental resolution.

reduction in satellite intensity. At 10 mK the magnetic moment is quenched in a applied field of 0.5 T. The effect of the magnetic field is twofold. Firstly the energy of the crystal field excitations is increased slightly, leading to a reduction in the ratio of exchange to crystal field splitting. The second effect is more significant: the nuclear moments are strongly polarised by the applied field since the effective field seen by the nuclei is enhanced by a factor of about 40 (see p. 351 of Jensen and Mackintosh, 1991). Due to this strong polarisation the susceptibility of the nuclear moments is substantially reduced. The combined effect of these factors is to reduce T_N to below 10 mK and hence the satellite intensity due to long range order disappears.

Another feature of Pr which cannot be understood within the standard model was discovered in a series of experiments at Risø which were carried out shortly after the redevelopment of the cold neutron guide produced a major increase in the neutron flux at the triple-axis spectrometer TAS7. In the paramagnetic phase, the
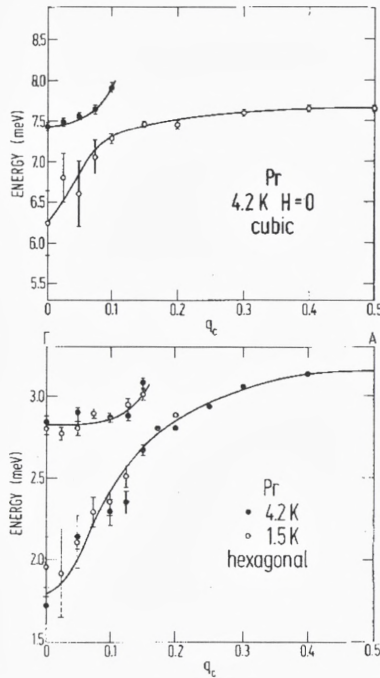
Figure 7. Dispersion relations for the magnetic excitations in Pr in the c-direction, as a function of q in units of τ_{001}, from (Clausen et al., 1994a, 1994b). For both the cubic and hexagonal sites, a lower energy *satellite excitation* hybridizes with the single branch of crystal field excitations predicted by the standard model.

crystal field excitations (magnetic excitons) broaden at wave vectors q approaching the zone centre, as was first reported by Houmann et al. (1979), and discussed in Jensen and Mackintosh (1991). This broadening is most easily observed along the c-direction, where the standard model predicts only one mode on each of the hexagonal and cubic sites. However, a careful study of the linewidths of these excitations at 4.2 K, made after the flux increase, revealed evidence of a second mode, as shown in Fig. 6, for wave vectors from $q = 0$ to $q = 0.15$ (Clausen et al., 1994a, 1994b). This second mode (the mode has been named a "satellite excitation", but this name is a source of potential confusion, since the mode is not directly linked to the elastic satellite peaks) appears to have an energy of 1.0 meV less than the $4f$ mode at the zone centre, but rises rapidly to hybridise with it. Similar behaviour was found around $q = 0$ for the cubic site excitations. The relevant dispersion relations are illustrated in Fig. 7.

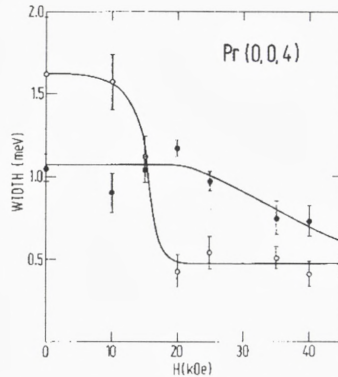Measurements of these excitations in a field along the a-axis showed that their

Figure 8. Magnetic field dependence of the width of the hexagonal site excitations in Pr at $(0, 0, 4)$, from (Clausen et al., 1994a, 1994b). The open circles correspond to the lower branch (satellite excitation) in Fig. 7, and the closed circles to the upper branch (standard model crystal field excitation).

width is rapidly reduced in an applied magnetic field (Clausen et al., 1994a, 1994b). In particular the width of the lower energy excitation shows a sharp drop between 1 and 2 tesla (see Fig. 8). It is interesting to note that this corresponds to the magnetic field at which the central peak is quenched (see Fig. 9).

Neither the broad peak observed close to the magnetic satellite wave vector, nor the extra excitations found in the paramagnetic phase of Pr can be explained within the standard model of rare-earth magnetism. The most plausible explanation for these phenomena is that they have their origin in a hybridization of the $4f$ electrons and the conduction electron states: a calculation of $\chi(\boldsymbol{q}, \omega)$ with this hybridization is therefore required, and we hope that our experiments will stimulate further progress in this direction.

3   Crystal fields in the actinides

The standard model developed for the rare-earth metals cannot be generally applied to the interpretation of the magnetism of the actinides. The strong spd–f hybridization present in these materials means that the basic assumption of the standard model, of localised moments and conduction electrons relatively weakly coupled to them, is not normally valid. However, there are a small number of actinide compounds which do exhibit a good approximation to localised moment magnetism and it is interesting to examine how far the standard model can be applied in these cases. One particularly important example of such a system is the uranium intermetallic compound UPd_3.
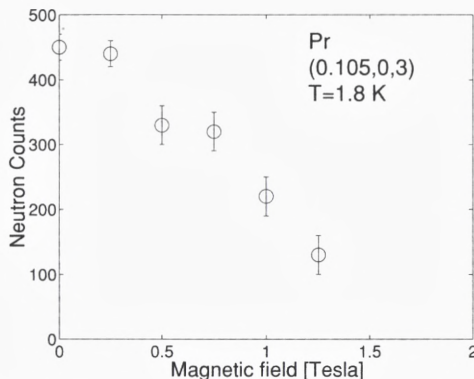
Figure 9. Magnetic field dependence of the intensity of the broad peak in Pr at $q_1 = 0.105\tau_{100}$, measured in the paramagnetic phase at 1.8 K.

3.1   UPd$_3$

Like Pr, the crystal structure of UPd$_3$ is double-hexagonal close-packed. The electronic configuration is $5f^2$, as confirmed by the intermultiplet transitions observed in high energy neutron spectroscopy (Bull et al., 1996). The peak at 380 meV is attributed to transitions from the $^3H_4$ ground multiplet to the excited $^3F_2$ multiplet. This result may be compared with the heavy-fermion compound UPt$_3$, where inelastic neutron spectroscopy showed the equivalent transition to be very much weaker, as expected due to the band-like character of its $5f$ electrons. Magnetic excitations at lower energies (1–20 meV) were first observed in UPd$_3$ by Buyers and Holden (1985) who interpreted them as crystal field excitations. As in the case of Pr, there appear to be singlet ground states on both the hexagonal and cubic site ions, but in contrast to Pr, the higher lying modes (at 15–20 meV) arise from transitions on the hexagonal sites, whilst the modes at 1–3 meV originate on the cubic sites. The overall splitting of the ground multiplet is some 40 meV, considerably greater than found in Pr or other rare-earths.

The presence of at least two phase transitions in UPd$_3$ has been known for some time: heat capacity (Andres et al., 1978) and thermal expansion measurements (Ott et al., 1980) indicated transitions around 7K and 5K. More recent thermal expansion (Zochowski and McEwen, 1994) and magnetization (McEwen et al., 1994; Park and McEwen, 1997) measurements on single crystals have confirmed these transitions and revealed the existence of a third transition near 8 K.

The magnetic susceptibility of the hexagonal and cubic site ions may be determined separately, by polarised neutron diffraction measurements in a magnetic field. Figure 10 shows the magnetic moment on the two uranium sites of UPd$_3$, in
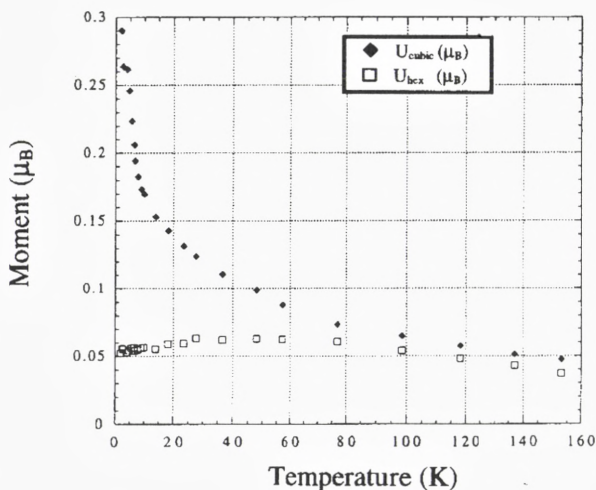
Figure 10. Magnetic moment on the hexagonal and cubic sites in UPd$_3$ in a field of 4.6 T along the a-axis, as a function of temperature, measured on the D3 diffractometer at the ILL, from Park et al. (1997).

a field of 4.6 tesla along the a-axis, measured with the D3 diffractometer at the ILL (Park et al., 1997). The anisotropy between the two sites is striking: whilst the moment on the hexagonal sites varies little below 100 K, the cubic site moment increases steadily as the temperature is reduced. This behaviour of the moments can be understood within the crystal field scheme described above. The relatively small values of the magnetic moments (particularly on the hexagonal sites) means that it is not practical to determine accurately the details of the moment variations on the two sites near phase transitions. However, the bulk magnetization measurements on UPd$_3$ single crystals, shown in Fig. 11 (McEwen et al., 1994) clearly reveal the phase transitions at $T_1 = 7$ K and $T_2 = 4.5$ K in the measurements for fields along the a-, b- and c- axes.

In their early neutron diffraction experiments at Chalk River, Buyers and Holden (1985) discovered new reflections below T_1 at positions $\left(h + \frac{1}{2}, 0, \ell\right)$ in reciprocal space. Subsequently, Steigenberger et al. (1992) carried out a more detailed investigation, using polarised neutron diffraction techniques. They found that the temperature dependence of reflections such as $\left(\frac{1}{2}, 0, 3\right)$ and $\left(\frac{1}{2}, 0, 4\right)$ also showed anomalies at the transition at T_2. Most significant was the finding that the scattering cross-section for these superlattice reflections was *non-spin-flip*, demonstrating that their origin was structural, rather than magnetic.

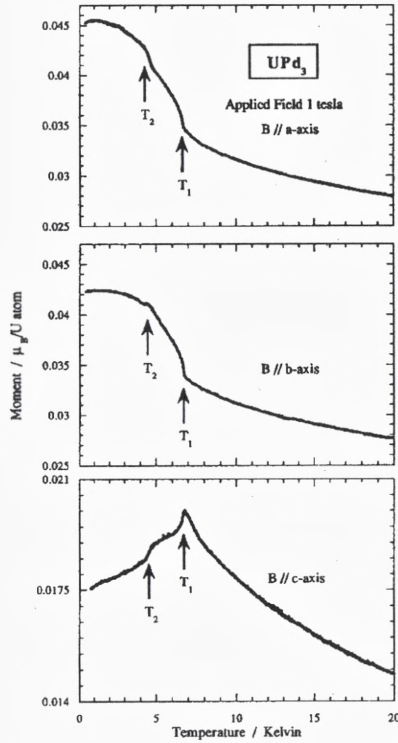This result indicates that the primary order parameter is quadrupolar. It is the

Figure 11. Magnetization of UPd$_3$ in a field of 1 T applied along the a-, b- and c-axes, from McEwen et al. (1994).

periodic lattice distortions produced by the ordering of the quadrupolar moments which couple to neutrons and give rise to the superlattice reflections. The development of quadrupolar ordering is consistent with a crystal field model for UPd$_3$ in which the ground states at both the hexagonal and cubic sites are singlets. Each uranium ion may have, in general, five independent quadrupole moments which we denote by Q_{zz}, $Q_{x^2-y^2}$, Q_{xy}, Q_{yz} and Q_{zx}. Above the ordering temperature, the only quadrupole moment which has a non-zero expectation value is Q_{zz}. With four uranium ions per unit cell in the dhcp crystal structure, there are 20 linearly independent quadrupolar symmetry modes. The group theory analysis of Walker et al. (1994) showed that this permits 8 possible order parameters. By comparing the observed intensities of the $\left(h + \frac{1}{2}, 0, \ell\right)$ superlattice reflections with those expected for the possible order parameters, it was deduced that the order parameter has B$_{2g}$ symmetry. The doubling of the unit cell means that the structure is, of course, antiferroquadrupolar (AFQ), and B$_{2g}$ symmetry implies that the possible
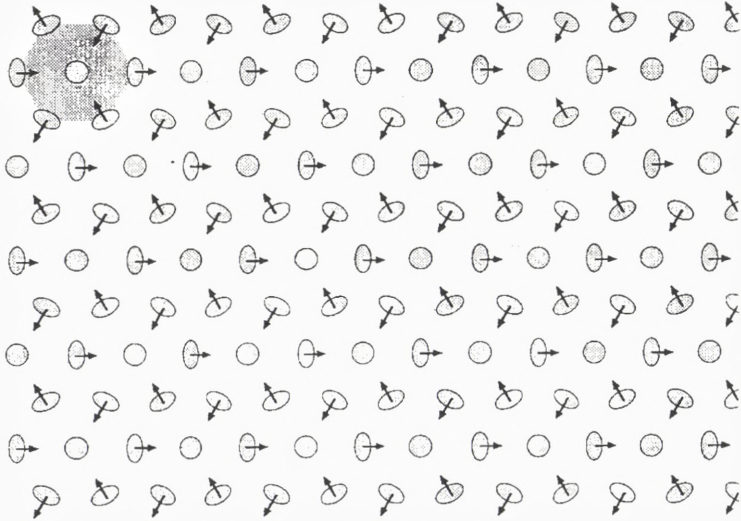
7*

Figure 12. The antiferroquadrupolar structure of UPd$_3$, as described in the text.

components of the structure are a combination of $Q_{x^2-y^2}$, Q_{zx} and Q_{zz} quadrupolar moments on the cubic sites and Q_{zz} quadrupolar moments on the hexagonal sites. The presence of weak reflections at $\left(\frac{1}{2}, 0, 0\right)$ was attributed to the structure being triple-q, and the AFQ structure is illustrated in Fig. 12. In this figure, the shaded ellipsoids represent the charge densities of the $5f^2$ electrons at the uranium sites, for a section of the basal plane. The doubling of the chemical unit cell and the triple-q nature of the structure are obvious. The arrows do not denote dipolar moments, which are of course absent in this phase, but indicate the direction about which the charge densities are tilted out of the basal plane to produce Q_{zx} components. The charge densities without arrows are not spherical, but rather are spheroidal due to the Q_{zz} component.

The magnetic phase diagrams for UPd$_3$ have been deduced from thermal expansion measurements made in constant magnetic fields (Zochowski and McEwen, 1994) and magnetization studies (McEwen et al., 1994; Park et al., 1997). It is now clear that there exist three transitions, at temperatures (in zero magnetic field) of 7.8 ± 0.2 K, 6.8 ± 0.1 K and 4.4 ± 0.1 K. We shall denote these temperatures by T_0, T_1 and T_2, respectively. The transition at T_0 is most apparent in the thermal expansion (Zochowski and McEwen, 1994) but careful examination shows it is present also in the susceptibility data (Park and McEwen, 1997). A re-examination of the neutron scattering data published in Steigenberger et al. (1992), confirmed in more recent measurements, reveals that the $\left(\frac{1}{2}, 0, 3\right)$ peak appears at a higher

temperature than the $\left(\frac{1}{2}, 0, 4\right)$ peak. The magnetic field dependence of the three
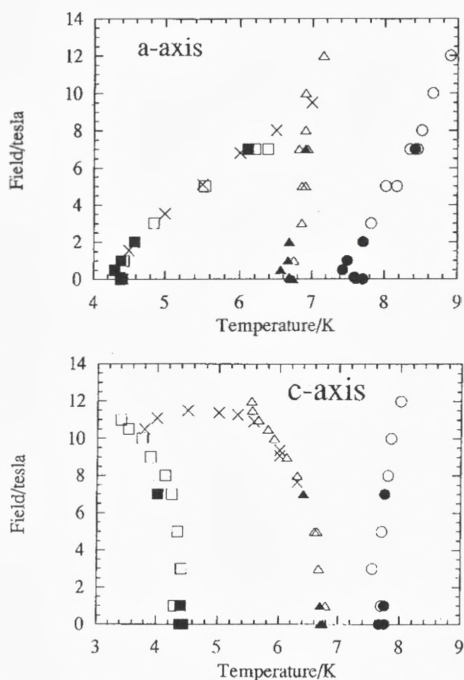

Figure 13. Magnetic phase diagrams of UPd$_3$ for fields along the a-axis and c-axis, from (Park and McEwen, 1997).

transition temperatures has been mapped out by following the anomalies associated with each of them. Figure 13 shows the phase diagrams for fields along the a-axis and c-axis (Park and McEwen, 1997).

Having mapped out the phase diagrams by macroscopic measurement techniques, we have begun to investigate them by neutron diffraction studies in a magnetic field. Figure 14 shows measurements made at Risø of the temperature dependence of the $\left(\frac{1}{2}, 0, 1\right)$ and $\left(\frac{1}{2}, 0, 2\right)$ peaks for UPd$_3$ in a field of 4 tesla applied along the vertical a-axis perpendicular to the horizontal scattering plane McEwen et al. (1997). It is clear that the scattering at $\left(\frac{1}{2}, 0, 1\right)$ develops below T_0, with a small but distinct anomaly at T_1, whereas the much less intense $\left(\frac{1}{2}, 0, 2\right)$ peak develops only below T_1. The intensity of this latter peak drops precipitously at T_2, as shown in the figure.
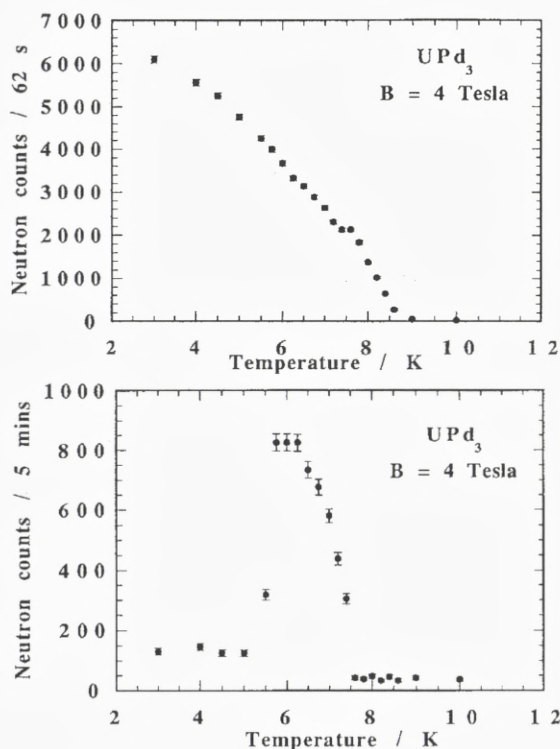
Figure 14. Temperature dependence of the $\left(\frac{1}{2}, 0, 1\right)$ and $\left(\frac{1}{2}, 0, 2\right)$ reflections in UPd₃ in a field of 4 T applied along the a-axis perpendicular to the scattering plane, measured on the TAS7 spectrometer at Risø, from McEwen et al. (1997).

The intensities of these reflections in a magnetic field are greatly enhanced over their zero field values, indicating the presence of magnetic scattering in this case. Again we have employed polarised neutrons to determine the origin of the superlattice reflections. Experiments at ILL have demonstrated that the $\left(\frac{1}{2}, 0, 1\right)$ scattering between T_0 and T_1 is entirely *non-spin-flip* (Steigenberger et al., 1997). In the experimental configuration used (which was as for the measurements shown in Fig. 14), this result implies that the neutron scattering for $T_0 > T > T_1$ may arise both from structural components and from magnetic moments parallel to the direction of the neutron polarisation (i.e. the a-axis direction of the magnetic field). Since the intensity of the $\left(\frac{1}{2}, 0, 1\right)$ reflection is so much greater than in zero field, where it is due to the structural distortion only, we may deduce that the magnetic field has induced a *ferrimagnetic* structure with the moments parallel to the field direction. When an a-axis magnetic field is applied to a quadrupolar structure of

symmetry B_{2g}, the induced magnetic structure is expected to have A_g symmetry (Walker, private communication), and a detailed analysis of the diffraction data confirms that this is indeed the case.

As mentioned earlier, UPd_3 is a rare example of a metallic actinide system for which well-defined magnetic excitations have been observed, and this evidence provides important justification for using a crystal field model to interpret its magnetic properties. The excitations with energies in the 1–3 meV range arise from crystal field transitions propagating on the cubic sites. Their dispersion and temperature dependence through the phase transitions has been studied (McEwen et al., 1993).

In our consideration of uranium compounds, we have concentrated on UPd_3. However, it should be noted that crystal field effects have been considered in a few other uranium intermetallic compounds. The system $U_x Y_{1-x} Pd_3$ has attracted much attention because of its non-Fermi liquid behaviour for compositions near $x = 0.2$. However, clear evidence for crystal field like excitations at energies of 2–5 meV and 36–40 meV has been found in $U_{0.45} Y_{0.55} Pd_3$, and the evolution of these with uranium composition has been studied (McEwen et al., 1995). Another system in which crystal field excitations have been observed is the heavy fermion compound URu_2Si_2 (Broholm et al., 1987, 1991). The nature of the order parameter at the 17.5 K phase transition in URu_2Si_2 is the subject of current investigation by several groups. A crystal field model has been employed (Santini and Amoretti, 1994) to understand the transition but this explanation remains controversial.

4   Acknowledgements

References

Andres K, Davidov D, Dernier P, Hsu F, Reed WA and Nieuwenhuys GJ, 1978: Solid State Commun. **28**, 405

Bjerrum Møller H, Jensen JZ, Wulff M, Mackintosh AR, McMasters OD and Gschneidner Jnr KA, 1982: Phys. Rev. Lett. **49**, 482

Bleaney B, 1963: Proc. Roy. Soc. A **276** 39

Broholm C, Kjems JK, Buyers WJL, Matthews PT, Palstra TTM, Menovsky AA and Mydosh
    JA, 1987:   Phys. Rev. Lett. **58**, 1467
Broholm C, Kjems JK, Buyers WJL, Matthews PT, Palstra TTM, Menovsky AA and Mydosh
    JA, 1991:   Phys. Rev. B **43**, 12809
Bull MJ, McEwen KA, Osborn R and Eccleston RS, 1996:   Physica B **223&224**, 175
Buyers WJL and Holden TM, 1985: *Handbook on the Physics and Chemistry of the Actinides*,
    eds. G.H. Lander and A.J. Freeman, (North Holland, Amsterdam) Vol. 2, p. 239
Clausen KN, McEwen KA, Jensen J and Mackintosh AR, 1994a: Phys. Rev. Lett. **72**, 3104
Clausen KN, Sørensen SAa, McEwen KA, Jensen J and Mackintosh AR, 1994b: J. Magn. Magn.
    Mater. **140–144**, 735
Houmann JG, Rainford BD, Jensen J and Mackintosh AR, 1979:   Phys. Rev. B **20**, 1105
Jensen J and Mackintosh AR, 1991: *Rare Earth Magnetism: Structures and Excitations* (Claren-
    don Press, Oxford)
Jensen J, McEwen KA and Stirling WG, 1987:   Phys. Rev. B **35**, 3327
Jensen J, 1979: J. Phys. (Paris) **40**, C5-1
Mackintosh AR, 1985:   Physica B **130**, 112
McEwen KA, Steigenberger U and Clausen KN, 1997: (to be published)
McEwen KA, Bull MJ, Eccleston RS, Hinks D and Bradshaw AR, 1995:   Physica B **206&207**,
    112
McEwen KA, Ellerby M and de Podesta M, 1994:   J. Magn. Magn. Mater. **140–144**, 1411
McEwen KA, Steigenberger U and Martinez JL, 1993:   Physica B **186–188**, 670
McEwen KA and Walker MB, 1986:   Phys. Rev. B **34** 1781
McEwen KA and Stirling WG: 1981: J. Phys. C **14**, 157
McEwen KA, Stirling WG and Vettier C, 1978:   Phys. Rev. Lett. **41**, 343
McEwen KA, Stirling WG and Vettier C, 1983a: Physica B **120**, 152
McEwen KA, Stirling WG and Vettier C, 1983b: J. Magn. Magn. Mater. **31–34**, 599
McEwen KA, Cock GJ, Roeland LW and Mackintosh AR, 1973:   Phys. Rev. Lett. **30**, 287
Moolenaar AA, Metz A, McEwen KA, Ellerby M, Schröder-Smeibidl B and Steiner M, 1997: (to
    be published)
Murao T, 1971: J. Phys. Soc. Japan **31**, 683; *ibid* 1975: **39**, 50; *ibid* 1979: **46**, 40
Ott HR, Andres K and Schmidt PH, 1980:   Physica B **102**, 148
Park JG and McEwen KA, 1997: (to be published)
Park JG, McEwen KA and Tasset F, 1997: (to be published)
Rainford BD and Houmann JG, 1971:   Phys. Rev. Lett. **26**, 1254
Santini P and Amoretti G, 1994:   Phys. Rev. Lett. **73**, 1027
Steigenberger U, McEwen KA, Martinez JL and Fort D, 1992:   J. Magn. Magn. Mater. **108**, 163
Steigenberger U, McEwen KA and Kulda J, 1997: (to be published)
Walker MB, Kappler C, McEwen KA, Steigenberger U and Clausen KN, 1994:   J. Phys. Condens.
    Matter **6**, 7365
Zochowski SW and McEwen KA, 1994:   J. Magn. Magn. Mater. **140–144**, 416

Rare Earth Superlattices

D. F. McMorrow

Department of Solid State Physics, Risø National Laboratory,

DK-4000 Roskilde, Denmark

Abstract

A review is given of recent experiments on the magnetism of rare earth superlattices. Early experiments in this field were concerned mainly with systems formed by combining a magnetic and a non-magnetic element in a superlattice structure. From results gathered on a variety of systems it has been established that the propagation of magnetic order through the non-magnetic spacer can be understood mostly on the basis of an RKKY-like model, where the strength and range of the coupling depends on the details of the conduction electron susceptibility of the spacer. Recent experiments on more complex systems indicate that this model does not provide a complete description. Examples include superlattices where the constituents can either be both magnetic, adopt different crystal structures (Fermi surfaces), or where one of the constituents has a non-magnetic singlet ground state. The results from such systems are presented and discussed in the context of the currently accepted model.

1 Introduction

The first rare earth superlattices were produced by molecular beam epitaxy (MBE) a little over a decade ago. The initial results from these systems had an immediate impact on the field of magnetism in metals, in that they provided a new window on the nature of the magnetic coupling in the metallic state. This early work also helped to stimulate studies of transition metal superlattices, which eventually resulted in the discovery of the giant magneto-resistance effect (Baibich et al., 1988).

Two of the key early papers in the field of rare earth superlattices were both concerned with the magnetism of a system formed from a magnetic element interleaved with a Y spacer block. (Y is an almost ideal element for these studies as it has the hcp structure and is well latticed matched ($\approx$ 2%) with the heavy rare earths.) The idea behind these experiments was to investigate how the magnetic order is transmitted through the spacer block. In the case of Dy/Y it was discovered by Salamon et al. (1986) that the helical order adopted by the Dy $4f$ moments propagates coherently through the Y block. A natural explanation for

this observation was an RKKY-like coupling between the Dy blocks through the Y (see, for example, Yafet et al., 1988). Although Y is itself non-magnetic it does have a large peak in its conduction susceptibility, $\chi(\mathbf{q})$, at about the same position as the ordering wave vector in Dy (Liu et al., 1971). Thus, when the $4f$ moments in the Dy block order, they spin polarize the conduction band of the Y to form a spin-density wave, and it is this spin-density wave that carries information on the order from one magnetic block to the next. In this view, the range over which the order can be propagated coherently (the magnetic coherence length) is determined by the width and height of the peak in the conduction susceptibility of the spacer layer. A second important result of this work was that the helical-to-ferromagnetic transition of bulk Dy is suppressed in the superlattice. This was shown to be a consequence of the clamping of the Dy blocks by the Y. At about the same time as the work on Dy/Y was published, Majkrzak et al. (1986) reported the results of an investigation of Gd/Y. For this system it was found that the Gd within an individual block ordered ferromagnetically (as in the bulk), and that the coupling between successive blocks of Gd oscillated between being ferro- or antiferromagnetic depending on the thickness of the Y spacer. The period of the oscillation was also found to be consistent with that expected on the basis of an RKKY-like coupling.

The study of rare earth superlattices has continued to develop, with several dedicated MBE plants around the world now producing samples, but with a change of emphasis to investigate more complex systems, such as fabricating superlattices from two magnetic elements. All of the examples presented here result from a collaboration between the Clarendon Laboratory and Risø National Laboratory. For more comprehensive accounts of the work on rare earth superlattices the reader is referred to the reviews by Majkrzak et al. (1991), and Rhyne et al. (1993). The development of this subject has relied extensively on neutron scattering results, and this is reflected in this review, where all of the examples given have used this technique.

2   Sample growth

The samples of interest here are all produced using MBE techniques, and a schematic of a superlattice is shown in Fig. 1. In MBE the material to be grown is evaporated from a source (usually a crucible that is heated in some way) so that it is deposited on a substrate, with an evaporation rate that allows for the control of the growth down to the sub-monolayer level. The main requirements for the production of good quality superlattices, with flat interfaces between the constituents, are that the substrate must be atomically flat, there must be as close a match as possible
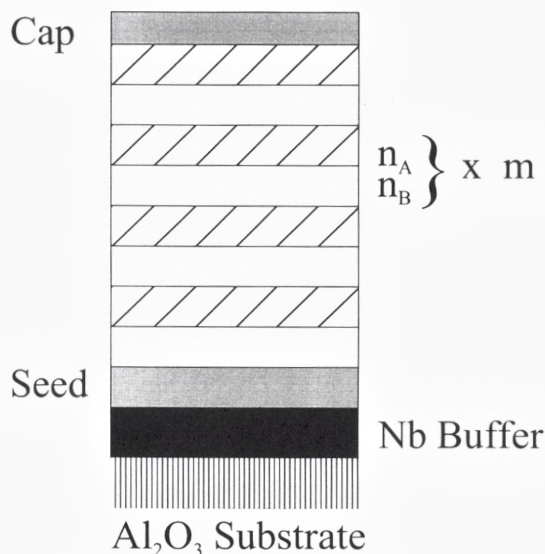
Figure 1. A schematic of the structure of a rare earth superlattice. For all of the superlattices of interest here the growth direction is parallel to the c axis of the rare earth metal. Each superlattice unit cell is made up from n_A atomic planes of element A and n_B planes of element B, with the unit cell repeated m times, so that the complete superlattice can be designated as $(A_{n_A}/B_{n_B})_m$. The seed layer is normally one of the non-magnetic elements Y, Lu or Sc.

between the lattice parameters of the substrate and the deposited material, and they should not react chemically. These requirements are often difficult to realize in practice, and the rather elaborate foundation of the superlattice shown in Fig. 1 is the best solution that has been found to date for the rare earths (Kwo et al., 1985, 1987). In fact the mosaic spread of the completed superlattice can be as little as $\approx 0.15°$, which is low compared to typical values for bulk crystals of the rare earths, and from this point of view the superlattices may be regarded as good single crystals. X-ray diffraction experiments also show that the interfaces are well defined, with interdiffusion limited to approximately four atomic planes (McMorrow et al., 1996, and references therein).

In what follows we shall refer to the superlattice unit cell as a bilayer, which is composed of n_A atomic planes of element A and n_B atomic planes of element B. This bilayer unit is then repeated m times, so that the superlattice may be written as $(A_{n_A}/B_{n_B})_m$. Values for n are chosen to lie in the range of 5 to 50, while m is usually around 100 or fewer. This means that the superlattice is at best 1 μm thick, and for a 1 cm^2 substrate there is less than one 1 milligram of sample.

3   Magnetism in a system with a large lattice mis-match: Ho/Sc superlattices

In addition to using either Y there is also the possibility of exploring what happens when other non-magnetic elements are used to form the spacer layer. Several systems have been grown with Lu as the spacer, and these include Dy/Lu (Beach et al., 1992), Ho/Lu (Swaddling et al., 1993, 1996). Sc is another obvious choice as it also adopts the hcp structure, while band structure calculations (Lui et al., 1971) suggest that it has a peak in its conduction electron susceptibility qualitatively similar to that in Y, albeit weaker and broader. The main problem in using Sc, however, is that it has lattice parameters that are approximately 7% smaller than those of the heavy rare earths such as Ho. In spite of this it proved possible to produce superlattices of Dy/Sc (Tsui et al., 1993), which did not display any long-range magnetic order, but had instead short-range ferromagnetic correlations at temperatures well above T_C of bulk Dy. More recently Bryn-Jacobsen et al. (1997) have studied a series of Ho/Sc superlattices, which display a number of interesting structural and magnetic properties.

We shall first consider their structural properties. When attempting to produce a superlattice from two constituents that have a lattice mis-match, it may occur that the mis-match is so large that the lattice parameters of the individual blocks within the superlattice relax back to their bulk values. This occurs if the critical thickness for the formation of misfit dislocations is comparable to or smaller than the desired thickness of the block. Its signature is the appearance of two distinct peaks in a scan of the wave vector in the plane of the film, one for each of the constituents. Using a combination of x-ray and neutron scattering techniques, Bryn-Jacobsen et al. (1997) established that this was indeed the situation for Ho/Sc, as shown schematically in Fig. 2. (For other systems studied, where the lattice mismatch is smaller, only a single peak representative of the average lattice parameter has been found.) Thus, Ho/Sc superlattices are essentially composed of blocks of Ho and Sc with almost their respective bulk lattice parameters. While there is a strong correlation in the the position of the close packed planes from block to block, the hcp stacking sequence (ABAB···) is not maintained from one block to the next.

These unusual structural features also express themselves when we come to consider the magnetic structure. In Fig. 3 two scans are shown with the wave vector transfer **Q** scanned parallel to the c^* direction for a Ho_{30}/Sc_{10} superlattice. In the top panel the scan direction is [00ℓ]. Around the position of the (002) Bragg peak (in the range 2.2 to 2.35 Å^{-1}) sharp satellite peaks are evident. These arise from the contrast in the nuclear scattering lengths of Ho and Sc. Symmetrically

X

(002) ●

X

          X   ● $^{●}$ (101)
                  ●

[001]   X

     ↑
     │
     └──→   ●   ●   ● (100)
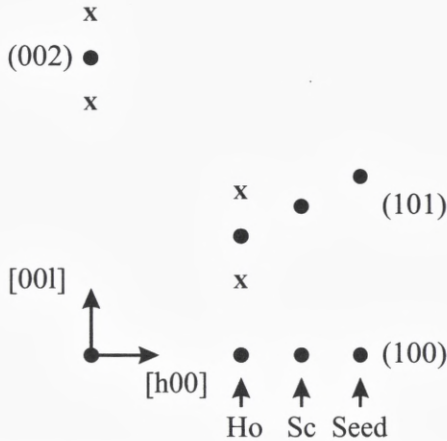   [h00]   ↑   ↑   ↑
                 Ho Sc Seed

Figure 2. A schematic (not to scale) of the reciprocal space in the ($h0\ell$) plane of Ho/Sc superlattices. Filled circles represent nuclear Bragg peaks from the hcp lattice, while crosses indicate regions where magnetic scattering would be detected for a helical arrangement of the moments. (For clarity the positions of the magnetic satellites around the origin are not shown.) The width of the scans for **Q** along [00ℓ] is a measure of the coherence in the stacking of the close-packed planes. Scans of **Q** along [$h00$] reveal the existence of more than one a lattice parameter (Bryn-Jacobsen et al., 1997).

displaced either side of the (002) peak is the magnetic scattering, which is only seen when the sample is cooled below $\approx$ 132 K, the bulk ordering temperature of Ho (Koehler et al., 1966), and which indicates that the Ho moments within an individual Ho block form a helix. In contrast to the nuclear scattering, the magnetic scattering is extremely broad, showing that the magnetic correlations are short-ranged. In fact the magnetic correlations just extend between nearest-neighbour blocks of Ho ($\approx$ 150 Å for this sample). One of the unusual aspects of the magnetic structure, deduced from fits to the scattering data by Bryn-Jacobsen et al. (1997), is that while individual Ho blocks are helically ordered, the coupling between blocks is antiferromagnetic. Whether this results from the effect of a dipolar coupling, or from some other type of coupling has yet to be established.

In the bottom panel of Fig. 3 the scan direction is [10ℓ] (see Fig. 2) through the position of the $(101)_{Ho}$ peak. (The Ho subscript refers to the fact that the value of h was set for the position of the (100) for the Ho blocks.) As this scan direction has a component **Q** in the basal plane, it is sensitive to the stacking sequence of the hcp planes. As the scattering at the position of $(101)_{Ho}$ is broad, it is clear that this stacking sequence is disordered. This is also reflected in the magnetic scattering at $(1\,0\,1-q)_{Ho}$ and $(1\,0\,1+q)_{Ho}$, which is well described by a broad Gaussian line
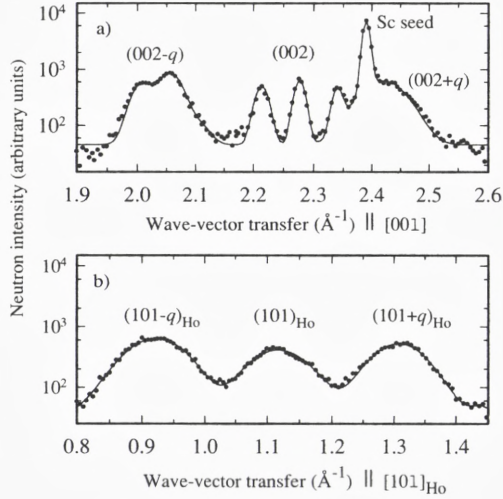
Figure 3. The neutron scattering observed at 4 K from Ho_{30}/Sc_{10}. (a) A scan of **Q** along $[00\ell]$ showing nuclear superlattice peaks around (002). The peaks at positions $(002\pm q)$ are magnetic in origin, and can be identified with helical ordering of the Ho moments. (b) A scan along $[10\ell]_{Ho}$ with an absence of any nuclear superlattice peaks around $(101)_{Ho}$. The peaks at positions $(101\pm q)_{Ho}$ arise from a helical configuration of the moments (Bryn-Jacobsen et al., 1997).

shape.

It is also instructive to compare the systematic dependence of the magnetism as the spacer material is varied. Perhaps the parameter that is most readily obtained from a scattering experiment, and one that does not depend on any modelling of the structure, is the magnetic coherence length, ζ. Here ζ is defined by $\zeta = 2\pi/\Delta Q$, where ΔQ is the width (FWHM) of the magnetic peak. The results for the Ho/X series, with X = Y, Lu or Sc are collected in Fig. 4. For the cases of Y and Lu it can be seen that the coherence length is as large as 1000 Å for spacer layers below about 10 atomic planes, and that it decreases rapidly (roughly as $1/r$) as the spacer thickness is increased. There is a marked tendency for the magnetic coherence to persist to greater distances in Y-based systems than those with Lu. In contrast, the Sc-based systems exhibit short-range order for all thicknesses of Sc investigated. These results may be considered to be in qualitative agreement with what is expected on the basis of an RKKY model of the coupling, and the known properties of the conduction electron susceptibilities $\chi(\mathbf{q})$ of the spacer layer, either derived from calculations or experiments. The calculations of Liu et al. (1971) show that the for the three spacer elements considered here, the peak in $\chi(\mathbf{q})$ is strongest
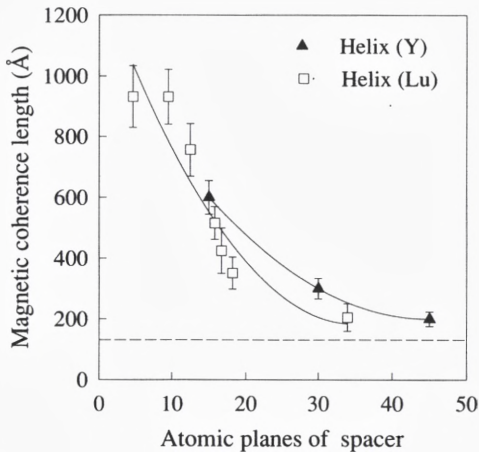
Figure 4. A comparison of the dependence of the magnetic correlation length as a function of the spacer layer thickness for Ho/X superlattices, where X = Y (Jehan et al., 1993), Lu (Swaddling et al., 1996) or Sc (Bryn-Jacobsen et al., 1997). The solid lines are guides for the eye, whereas the dotted line represents an average of the results for Sc.

and sharpest for Y, and is weaker, and possibly broader, for Sc and Lu. The peak in $\chi(\mathbf{q})$ for Sc is, however, predicted to be similar to that of Lu, and so it is not immediately clear why the coherence length in the former is so small. It could well be that another factor, such as an enhanced scattering of the conduction electrons from the greater concentration of defects in the Sc based systems plays a part in limiting the development of long-range order. More accurate calculations of $\chi(\mathbf{q})$ for these elements would be of obvious use in trying to resolve this question.

4   Persistence of helical order in Dy/Ho superlattices

As a first example of a system fabricated from two magnetic rare earths, we will consider the Dy/Ho system studied by Simpson et al. (1996) using time-of-flight neutron diffraction. This work is of interest as it illustrates how simple ideas based on modifications of the magnetic structure through strain can be misleading.

Previous studies of Dy-based superlattices include Dy/Y (Salamon et al., 1987; Erwin et al., 1987) and Dy/Lu (Beach et al., 1992), where very different behaviour was found for the temperature dependence of the turn angle ψ_{Dy} in the Dy blocks. Due to the lattice mis-match between the Dy and spacer blocks, in the former there

is an expansive basal-plane strain of the Dy, which results in the ferromagnetic phase found below $T_C = 78$ K in bulk Dy being suppressed at all temperatures. In contrast, there is a compressive strain for the Dy blocks in Dy/Lu, and T_C is slightly enhanced. The strain for the Dy layers in Dy/Ho is the same sign as that for Dy/Lu, although the lattice mis-match is much smaller: 0.4% compared to 2.5%. If strain alone was the sole factor in determining the modification of the magnetic structure of Dy in a superlattice, then it would be expected that the Dy in Dy/Ho would have a slightly higher T_C than the bulk.

Two superlattices of Dy/Ho were studied of composition Dy_{32}/Ho_{11} and Dy_{16}/Ho_{22}. Both samples studied were found to order magnetically at a temperature consistent with that of bulk Dy (179 K) (Wilkinson et al., 1961). From this temperature down to approximately the bulk ordering temperature of Ho, a good description of the scattering was obtained by assuming that the $4f$ moments in the Dy blocks formed a helix, while those in the Ho blocks remained paramagnetic. Moreover, the coupling of the Dy through the disordered Ho was long range, with an effective turn angle per layer through the Ho that was essentially the same as that found in bulk Ho at its ordering temperature. As the temperature was lowered below T_C of Dy no dramatic change in the scattering was noted. In particular the intensity of the (002) peak did not increase on cooling through T_C, as would be expected if the Dy moments collapsed into a basal-plane ferromagnet. A representative scan below T_C is shown in Fig. 5. Here it is evident that the scattering is qualitatively consistent with that expected from a system in which there is helical order in both components of the superlattice; the superlattice sub-structure in the magnetic (M) peaks results from the fact that the magnitude of the ordered moment in the Dy and Ho blocks is not identical.

The results of fitting the data to extract the individual turn angles (or equivalent wave vectors) are summarised in Fig. 6, where they are compared to the behaviour of the bulk. For the case of Dy, it can be seen that above T_C, the wave vector of the Dy blocks in the superlattice is slightly higher than that in the bulk, and that below T_C it appears to lock in to a value of $(1/6)c^*$. The wave vector in Ho is essentially independent of temperature above $T_N(\text{Ho})$, and then decreases below this temperature.

The fact that the Dy remains in a helical phase at all temperatures below $T_N(\text{Dy})$ in Dy/Ho superlattices is clearly at variance with what would have been predicted if the system was considered to be isolated, but strained, blocks of Dy and Ho. This indicates that the magnetic structure assumed by the Dy must depend on the magnetic structure of the superlattice taken as a whole. The reduction in energy from the formation of a coherent helical structure in both materials, without the disruption that would occur at the interface if the Dy were ferromagnetic, must then more than offset the energy cost of Dy remaining helical.
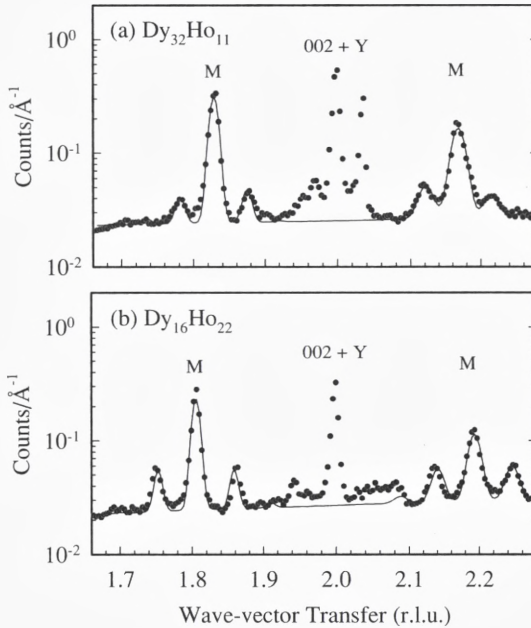
Figure 5. The neutron scattering with the wave-vector transfer along $[00\ell]$ observed at $T = 40$ K from (a) Dy_{32}/Ho_{11} and (b) Dy_{16}/Ho_{22}. The solid line is a fit to the data of a model with basal-plane helical ordering of both the Dy and Ho moments. The peaks near $Q = 2c^*$ are the (002) nuclear Bragg peaks and are not included in the model of the magnetic structure. M indicates the position of the main magnetic satellites, each of which is seen to have its own superlattice side peaks. (Simpson et al., 1996).

We also not that interesting results have also been reported recently for other superlattices containing two magnetic elements, including Ho/Er (Simpson et al., 1994) and Dy/Er (Dumensil et al., 1994).

5   Magnetism in a mixed hcp/dhcp superlattice

So far we have restricted ourselves to a consideration of the heavy rare earths only. For the present considerations, there are two salient features of the light rare earths compared to the heavies: they have more complex crystal structures, and the nesting features of the Fermi surface may be such that $\chi(\mathbf{q})$ is peaked at
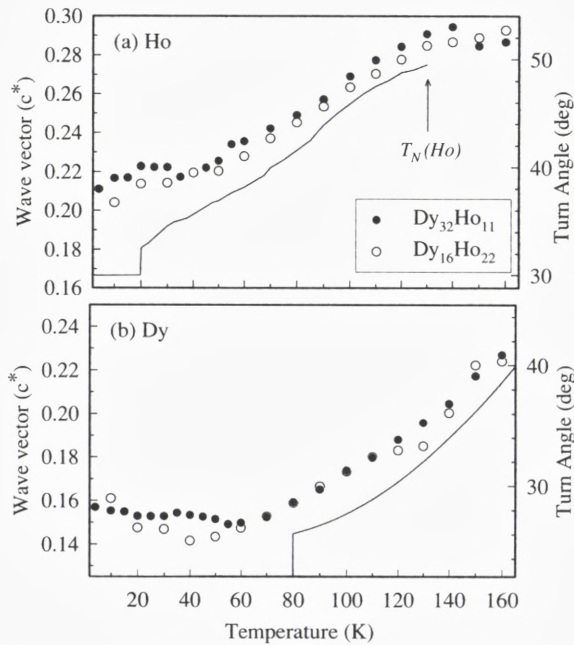
Figure 6. The wave vector (and equivalent turn angle) for (a) Ho and (b) Dy moments deduced from the model described in the text (o Dy_{16}/Ho_{22}; • Dy_{32}/Ho_{11}). The variation of the bulk value for each element is shown by the solid lines. (Simpson et al., 1996).

finite $\mathbf{q}$ along a^*, instead of along c^* as found in the heavy rare earths. By way of example, Nd and Pr both adopt the dhcp structure, and order magnetically with a propagation wave vector within the hexagonal basal planes (Jensen and Mackintosh, 1991). The motivation in producing a mixed hcp/dhcp superlattice is then to determine its structural and magnetic properties. In particular, it is interest to study the consequences of the mis-match in the Fermi surfaces [or equivalently the mis-match in $\chi(\mathbf{q})$] on the propagation of magnetic order.

As far as we are aware, there have been only two reports of work on mixed hcp/dhcp superlattices: Nd/Y by Everitt et al. (1995), and Ho/Pr by Simpson et al. (1995). In total three different superlattices were investigated by Simpson et al. (1995), with nominal compositions of Ho_{20}/Pr_{20}, Ho_{30}/Pr_{10}, and Ho_{24}/Pr_6. From scans of $\mathbf{Q}$ performed along the $[10\ell]$ direction at room temperature it was deduced that the Pr blocks in the superlattice retain their dhcp stacking (ABAC···), but as might be expected, the dhcp stacking was not coherent from one Pr block to the next.
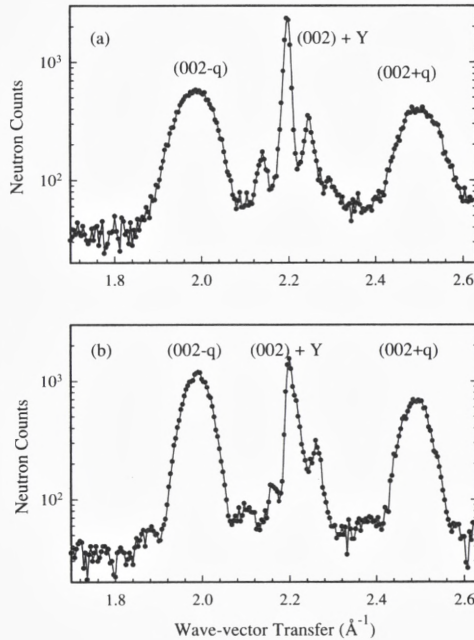
Figure 7. The neutron scattering observed at 10 K with the wave-vector transfer along $[00\ell]$ for (a) the Ho_{20}/Pr_{20} and (b) Ho_{30}/Pr_{10}. The broad magnetic peaks occur at q from the nuclear peaks and indicate short-range helical magnetic order in the Ho blocks (Simpson et al., 1995).

The key results relating to the magnetic structure of the Ho/Pr superlattices are summarised in Fig. 7. This shows the scattering at 10 K from the Ho_{20}/Pr_{20} (top panel) and Ho_{30}/Pr_{10} (bottom panel) superlattices when **Q** was scanned along the $[00\ell]$ direction through the (002). As with the previous examples of Ho-based superlattices in Sect. 3 and Sect. 4, the gross features of the magnetic scattering is consistent with those expected from a basal-plane helix: there are magnetic peaks displaced $\pm q$ from the (002) nuclear peak. The (002) has sharp superlattice peaks, reflecting the good coherence in the stacking of the close-packed planes. The broad magnetic scattering, however, is well described by a single Gaussian line shape, and the coherence length extracted from its width indicates that the magnetic correlations are completely confined to lie within the individual Ho blocks. In some ways this is reminiscent of the scattering from the Ho/Sc superlattices shown in Fig. 3. The difference, however, is that in that particular case there was a short-range antiferromagnetic coupling between the Ho blocks. For Ho/Pr there

is no coupling between adjacent Ho whatsoever. (We note that the strain in the Ho/Pr system is considerably smaller than in Ho/Sc.) From the neutron scattering it has not proved possible to determine whether or not the Pr ions retain the non-magnetic ground state of the bulk (McEwen and Stirling, 1981; Bjerrum Møller et al., 1982).

Thus, it appears that the effect of the Pr blocks is to completely decouple the magnetic correlations between blocks of Ho. The most plausible explanation for this effect is the differences in the nesting features of the Fermi surfaces of the two constituents, which in Ho produce a peak in $\chi(\mathbf{q})$ along the c^* axis, whereas in Pr it is peaked in the a^* direction. Any conduction-electron-mediated coupling of the Ho blocks along c would then depend on the details of the Pr conduction electron susceptibility along that direction. The calculations by Liu et al. (1971) suggest a ferromagnetic coupling should be favoured in Pr, whereas in fact an antiferromagnetic structure occurs. It seems clear, therefore, that without a better description of $\chi(\mathbf{q})$ for Pr it is difficult to draw any further conclusions.

6   Induced magnetic order in Nd/Pr superlattices

The final example is taken from some very recent work on superlattices formed from the two light rare-earths Nd and Pr (Goff et al., 1996). In their bulk form both Pr and Nd adopt the dhcp structure, which has two inequivalent sites in the chemical unit cell of approximately cubic and hexagonal symmetry.

Although Nd and Pr sit next to each other in the periodic table their magnetic properties are very different. The $4f$ moments on the hexagonal sites in bulk Nd order below about 20 K to form an incommensurable structure (Moon et al., 1964). Both the wave vector describing the order and the moments themselves are confined to the basal plane, and hence are perpendicular to c, the superlattice modulation direction. Below about 8 K in Nd the cubic sites also order. Pr on the other hand has a non-magnetic singlet groundstate and only orders spontaneously below 0.05 K (McEwen and Stirling, 1981; Bjerrum Møller et al., 1982).

In Fig. 8 results of the scattering from the hexagonal sites of two superlattices of Nd/Pr are compared. The top panel shows the magnetic scattering from Nd_{33}/Pr_{33}, where well defined superlattice peaks are evident either side of the main magnetic peak. The width of the individual peaks is a direct measure of the magnetic coherence length and it can be immediately deduced that the magnetic order in the Nd blocks propagates coherently through the Pr to form a long-range structure. The fact that the superlattice peaks are readily observed also shows that there is a large contrast between the size of the magnetic moments in the Nd and Pr blocks. The solid line through the data is the result of a calculation where it
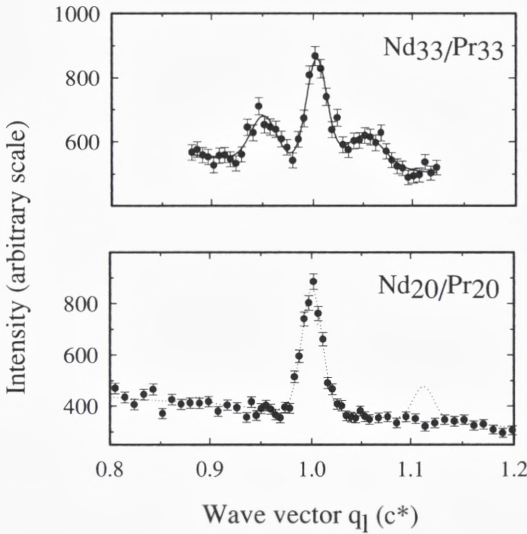
Figure 8. Scans along the c^* direction through the magnetic reflections in Nd/Pr from the hexagonal sites at 10 K from (a) Nd_{33}/Pr_{33} and (b) Nd_{20}/Pr_{20}. The solid line in (a) is the result of a calculation assuming that there is no ordering of the $4f$ moments in the Pr, while in (b) a similar calculation is given by the dotted line which does not go through the experimental points. For (a) and (b) the scan direction was along q_l through $(q_h^{hex} \, 0 \, q_l)$ with $q_h^{hex} \approx 0.14$ r.l.u. (Goff et al., 1996).

has been assumed that there is a negligible moment in the Pr blocks, as would be expected if the Pr ions retained the non-magnetic singlet groundstate of the bulk. When the thickness of the Pr spacer is reduced a quite different result is obtained, as shown in Fig. 8(b) for Nd_{20}/Pr_{20}. Here just a single magnetic peak is observed, even though calculations of the magnetic scattering, performed assuming no ordering of the local moments in the Pr, predict that superlattice substructure should be visible. What in fact is happening in this sample is that the Nd moments have induced the local Pr moments to order so that a uniform magnetic structure is established throughout the superlattice. This is shown more clearly in the top panel of Fig. 9, where the temperature dependence of μ_{Pr}/μ_{Nd}, the ratio of the Pr to Nd moments, is plotted for Nd_{20}/Pr_{20} and Nd_{33}/Pr_{33}. For the former sample with the thinner layers the Pr and Nd moments have, within error, the same magnitude at all temperatures below T_N, whereas for the latter the Pr moment is small until the sample is cooled below 6 K. It is worth noting that for the Nd_{33}/Pr_{33} sample this temperature coincides with a marked decrease in the coherence length of the
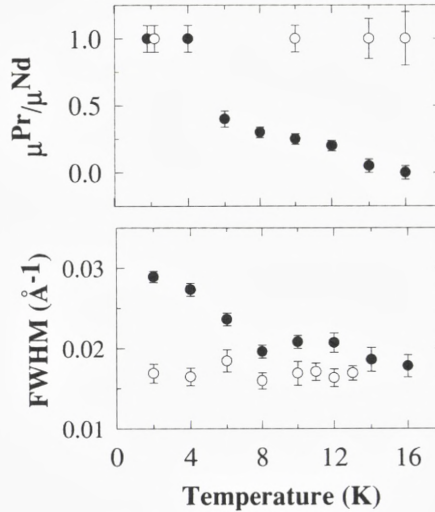
Figure 9. Temperature dependence of (a) the ratio of the Pr to Nd moment and (b) the width of the magnetic reflection along c^* for two Nd/Pr superlattices. Key: o Nd_{20}/Pr_{20}, ● Nd_{33}/Pr_{33} (Goff et al., 1996).

hexagonal site order (as shown in the lower panel of Fig. 10), and the onset of order on the cubic sites. The cubic sites in Nd_{20}/Pr_{20} were not observed to order for temperatures down to 2 K.

One further interesting feature of the Nd/Pr system is shown in Fig. 10. For the same Nd_{33}/Pr_{33} superlattice that displayed coherent magnetic order on the hexagonal sites, the order on the cubic sites is short range (as attested to by the very broad peak) and restricted to a single block of Nd.

7   Summary

The examples in this review have been chosen to illustrate current trends in the study of rare earth superlattices. It is has been emphasised that while the coupling mechanism that determines the magnetic structures undoubtedly has many of the features associated with an RKKY-like interaction, there are difficulties in using such an approach to explain all of the experimental results. This is in part due to the fact that more accurate calculations of the conduction electron susceptibilities of the rare earths are needed before it can be judged finally whether or not this type of approach provides an adequate description. A more profound difficulty is that a
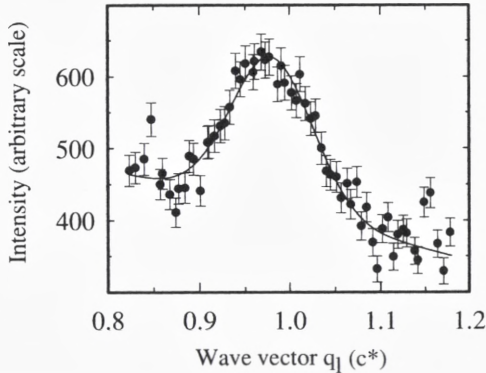
Figure 10. Representative scan along the c^* direction through the magnetic reflections in Nd/Pr from the cubic sites. The scan direction was along q_l through $(q_h^{cubic}\, 0\, q_l)$ with $q_h^{cubic} \approx 0.19$ r.l.u. (Goff et al., 1996).

full description of the magnetic interactions in the rare earth superlattices requires due consideration of the localised $4f$ electrons (single-ion anisotropy, etc) as well as the nature of the conduction electron states in a superlattice. This remains a formidable challenge.

Acknowledgements

References

Baibich MN, Broto JM, Fert A, Nguyen Van Dau F and Petroff F, 1988: Phys. Rev. Lett. **61**, 2472

Bryn-Jacobsen C, Cowley RA, McMorrow DF, Goff JP, Ward RCC and Wells MR, 1997: Phys. Rev. B (In press)

Beach RS, Borchers JA, Erwin RW, Flynn CP, Mathney A, Rhyne JJ and Salamon MB, 1992: J. Magn. Magn. Mater. **104-107**, 1915

Bjerrum Møller H, Jensen JZ, Wulff M, Mackintosh AR, McMasters OD and Geschneider Jr. KA, 1982: Phys. Rev. Lett. **49**, 482

Dumesnil K, Dufour C, Vergnat M, Marchal G, Mangin P, Hennion M, Lee WT, Kaiser H and Rhyne JJ, 1994: Phys. Rev. B **49**, 12274

Erwin RW, Rhyne JJ, Salamon MB, Borchers JA, Sinha S, Du R, Cunningham JE and Flynn CP, 1987: Phys. Rev. B **35**, 6808

Everitt BA, Borchers JA, Salamon MB, Rhyne JJ, Erwin RW, Park BJ and Flynn CP, 1995: J. Magn. Magn. Mater. **144**, 769

Goff JP, Bryn-Jacobsen C, McMorrow DF, Ward RCC and Wells MR, 1996: J. Magn. Magn. Mater. **156**, 263

Jehan DA, McMorrow DF, Cowley RA, Wells MR, Ward RCC, Hagman N and Clausen KN, 1993: Phys. Rev. B **48**, 5594

Jensen J and Mackintosh AR, 1991: *Rare Earth Magnetism: Structures and Excitations* (Clarendon Press, Oxford)

Koehler WC, Cable JW, Wilkinson MK and Wollan FO, 1966: Phys. Rev. **151**, 414

Kwo J, Gyorgy EM, McWhan DB, Disalvo FJ, Vettier C, and Bower JE, 1985: Phys. Rev. Lett. **55**, 1402

Kwo J, 1987: *Thin Film Growth Techniques For Low Dimensional Structures*, eds. R.F.C. Farrow, S.P. Parkin, P.J. Dobson, J.H. Neave and A. Arrott (Plenum, London)

Liu SH, Gupta RP and Sinha SK, 1971: Phys. Rev. B **4**, 1100

Majkrzak CF, Cable JW, Kwo J, Hong M, McWhan DB, Yafet Y, Waszczak JV, Grimm H and Vettier C, 1986: Phys. Rev. Lett. **56**, 2700

Majkrzak CF, Kwo J, Hong M, Yafet Y, Gibbs D, Chien CL and Bohr J, 1991: Adv. Phys. **40**, 99

McEwen KA and Stirling WG, 1981: J. Phys. C **14**, 157

McMorrow DF, Swaddling PP, Cowley RA, Ward RCC and Wells MR, 1996: J. Phys. Condens. Matter **8**, 6553

Moon RM, Cable JW and Koehler WC, 1964: J. Appl. Phys. **35**, 1041

Rhyne JJ and Erwin RW, 1993: *Magnetism in Aritificial Metallic Superlattices of Rare Earth Metals*, in Magnetic Materials **8**, ed. K.H.J. Buschow

Salamon MB, Sinha S, Rhyne JJ, Cunningham JE, Erwin RW, Borchers J and Flynn CP, 1986: Phys. Rev. Lett. **56**, 259

Simpson JA, McMorrow DF, Cowley RA, Jehan DA, Wells MR, Ward RCC and Clausen KN, 1994: Phys. Rev. Lett. **73** 1162

Simpson JA, McMorrow DF, Cowley RA, Wells MR and Ward RCC, 1995: J. Phys. Condens. Matter **7**, L417

Simpson JA, Cowley RA, McMorrow DF, Ward RCC and Wells MR, 1996: J. Phys. Condens. Matter **8**, L187

Swaddling PP, McMorrow DF, Simpson JA, Wells MR, Ward RCC and Clausen KN, 1993: J. Phys. Condens. Matter **5**, L481

Swaddling PP, Cowley RA, Wells MR, Ward RCC and McMorrow DF, 1996: Phys. Rev. B **53**, 6488

Tsui F, Flynn CP, Beach RS, Borchers JA, Erwin RW and Rhyne JJ, 1993: J. Appl. Phys. **73**, 6904

Yafet Y, Kwo J, Hong M, Majkrzak CF and O'Brien T, 1988: J. Appl. Phys. **63**, 3453

Wilkinson MK, Koehler WC, Wollan EO and Cable JW, 1961: J. Appl. Phys. **32**, 48S

Magnetotransport in Transition Metal Multilayered Structures

S. S. P. Parkin

IBM Research Division, Almaden Research Center,

650 Harry Road, K11/D2, San Jose, CA 95120-6099, USA

Abstract

Metallic multilayered structures comprising alternating ferromagnetic and non-ferromagnetic layers exhibit enhanced magnetoresistance values compared with the magnetoresistance of the individual magnetic layers. The largest changes in resistance are found in sputter-deposited 110 oriented crystalline Co/Cu multilayers in which the Co layers are doped with small amounts of Fe. Values of *giant magnetoresistance* (GMR) of ∼110% at room temperature and ∼220% at 4.2 K are found. The origin of the magnetoresistance relates to spin-dependent scattering at the interfaces between the Co and Cu layers. These very large MR values make GMR materials attractive for a variety of applications for which magnetic field sensors are required. Simple exchange-biased sandwich structures (*spin-valve* sandwiches) are described which exhibit large changes in resistance in very small fields.

1 Introduction

In recent years there has been a great deal of interest in the magnetic and transport properties of metallic multilayered thin film structures composed of thin $3d$ transition metal ferromagnetic layers separated by thin non-ferromagnetic spacer layers. These systems display unique properties, notably an oscillatory indirect exchange coupling of the ferromagnetic (FM) layers via the non-ferromagnetic spacer layers, and enhanced magnetoresistance. The latter has come to be called *giant magnetoresistance* (GMR). In this brief report the properties of these systems are reviewed with an emphasis on recent results in sputtered crystalline multilayers containing copper spacer layers.

2   Giant magnetoresistance in polycrystalline Co/Cu multilayers

Typical $3d$ ferromagnetic metals or alloys display only small changes in their resistance when subjected to magnetic fields at room temperature (McGuire and Potter, 1975). Maximum magnetoresistance values of about 5–6% are found in Ni–Co and Ni–Fe alloys. In magnetic fields large enough to saturate the magnetic moment of such metals their resistance primarily depends on the orientation of their magnetic moment with regard to the direction of the sense current passing through the sample. Thus they display an *anisotropic* magnetoresistance (AMR) such that their resistance can be written as $\rho = \rho_0 + \Delta\rho\cos^2\theta$, where θ is the angle between the magnetic moment of the sample and the direction of the current (McGuire and Potter, 1975; Rossiter, 1987). The resistance is typically higher when the magnetic moment of the sample is aligned orthogonal to the sense current. In magnetic fields not large enough to saturate the magnetization of the metal the resistance depends on the detailed magnetic domain structure. In thin ferromagnetic films the magnitude of the AMR effect becomes even smaller as the thickness of the FM layer is decreased because scattering of the conduction electrons from the outer boundaries of the film increases the resistance of the film. These scattering processes do not give rise to AMR.

The same AMR phenomenon is displayed by thin ferromagnetic layers in metallic multilayers but the magnitude of the effect is further reduced. By contrast certain magnetic multilayers, containing very thin ferromagnetic layers can display very large or *giant* changes in resistance with magnetic field of a different origin (Parkin, 1994; Fert and Bruno, 1994; Parkin, 1995; Levy, 1994). The largest GMR effects have been found in multilayers, prepared by sputter deposition, composed of alternating thin Co and thin Cu layers. In such polycrystalline Co/Cu multilayers GMR effects as large as 70–80% at room temperature have been reported (Parkin et al., 1991b). An example is shown in Fig. 1.

The origin of the giant magnetoresistive effect is quite different from that of AMR. GMR is found in multilayered and other inhomogeneous magnetic structures in which the magnetic layers [or other entities such as magnetic granules in magnetic granular metals (Chien, 1995)] are oriented non-parallel to one another for some range of magnetic field, and, such that, with application of a sufficiently large magnetic field, the magnetic moments of the layers (or entities) become oriented parallel to one another. It is the change in the magnetic configuration which affects the scattering of the conduction electrons propagating between the magnetic layers or entities and which thereby gives rise to GMR. In Co/Cu multilayers, for certain thicknesses of Cu, the moments of the Co layers are arranged antiparallel to one
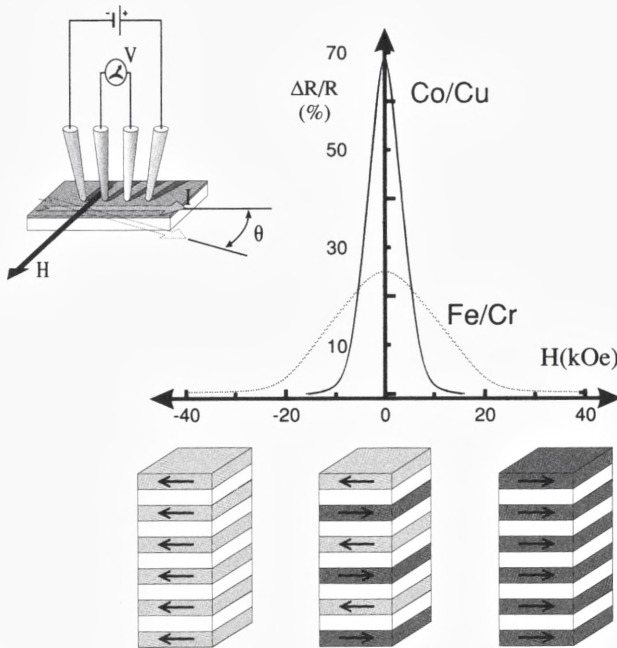
Figure 1. Resistance versus in-plane magnetic field curve for a polycrystalline Co/Cu multilayer exhibiting nearly 70% change in resistance at room temperature (Parkin et al, 1991b). The measurement geometry is shown in the top left corner. A schematic diagram of the Co/Cu layer is shown for large negative, zero and large positive fields.

another in small fields because of an antiferromagnetic (AF) coupling of the Co layers mediated via the Cu spacer layers. When a magnetic field is applied, large enough to overcome the AF interlayer coupling, the Co moments become aligned parallel to each other and to the applied field. This is shown schematically in Fig. 1.

Polycrystalline Co/Cu multilayers are usually (111) textured for thin Co and Cu layers, although the texture changes to (100) for thick Cu layers (Parkin et al., 1993), or when the multilayer is grown on thick Cu buffer layers (Lenczowski et al., 1994). Polycrystalline multilayers usually display little in-plane magnetic anisotropy. Consequently the resistance of such multilayers typically varies continuously with magnetic field independent of the orientation of the magnetic field in the plane of the sample (Parkin et al., 1990, 1991b,c). For strongly antiferromagnetically coupled multilayers, as the magnetic field is increased, the angle between neighbouring magnetic layers, ~180° in small fields, smoothly decreases

until at magnetic fields large enough to overcome the antiferromagnetic interlayer exchange coupling the magnetic moments become aligned parallel to the magnetic field and to each other. When multilayers are crystalline and have significant magnetic anisotropy the dependence of resistance on magnetic field is more interesting and can display quite unusual behaviour as discussed in Sect. 3.

As shown in Fig. 2 the magnitude of the giant magnetoresistance effect oscillates as a function of copper thickness. The oscillation in saturation magnetoresistance
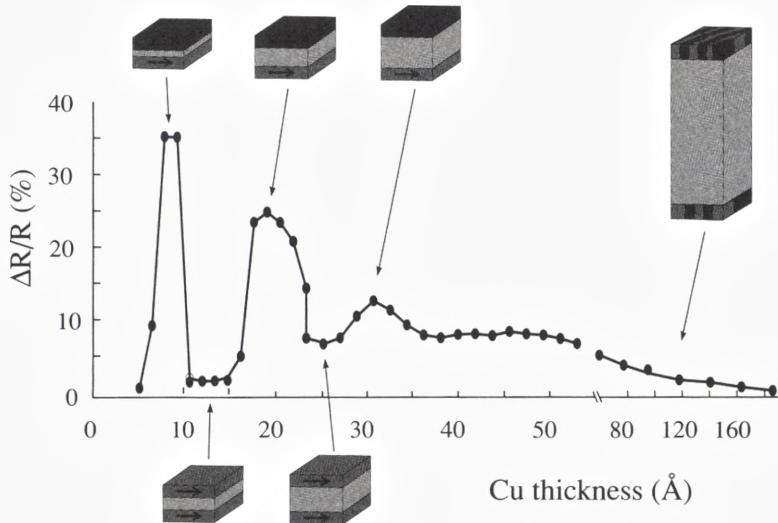

Figure 2. Room temperature saturation magnetoresistance versus Cu spacer layer thickness for a series of Co/Cu multilayers (Parkin et al, 1991a). The magnetic state of the multilayers are shown schematically for various Cu spacer layer thicknesses (only two Co layers are shown).

is related to an oscillation in the interlayer coupling between antiferromagnetic (AF) coupling and ferromagnetic (F) coupling as the Cu spacer thickness is varied. This is shown schematically in Fig. 2. Similar oscillations in magnetoresistance and interlayer coupling were first observed in Fe/Cr and Co/Ru multilayers (Parkin et al., 1990).

The coupling via Cu, Cr, Ru and other transition and noble metals is long-range and of the RKKY type. In polycrystalline Co/Cu multilayers the oscillation period is ~10 Å. The first observation of oscillatory interlayer coupling in transition

metal multilayers was in Fe/Cr and Co/Ru sputtered polycrystalline multilayers (Parkin, 1994). Subsequently it was shown that oscillatory interlayer coupling is exhibited by nearly all of the 3d, 4d, and 5d non-ferromagnetic transition and noble metals (Parkin, 1991). Later oscillatory coupling was observed in single-crystalline Fe/Cr and Co/Cu films grown by evaporation techniques in ultra-high vacuum chambers (Pierce et al., 1994; Johnson et al., 1992). For (100) Fe/Cr and (100) Co/Cu the interlayer exchange coupling oscillates with Cr and Cu spacer layers with two superposed oscillation periods, one long and one short (Unguris et al., 1991; Weber et al., 1995). For Fe/Cr the short period corresponds remarkably to just 2 monolayers of Cr (Unguris et al., 1991; Rührig et al., 1991). The magnitude of the oscillation periods for noble metal spacer layers can be well accounted for by examination of the Fermi surfaces of the noble metals. The oscillation periods are related to wave-vectors which span or nest the Fermi surface (Bruno and Chappert, 1992; Mathon et al., 1995).

3   Giant magnetoresistance in [110] crystalline Co/Cu and Co-Fe/Cu multilayers

3.1   Structure

There has been a great deal of work in the past few years to optimize the magnitude of the magnetoresistance in magnetic multilayers but especially Co/Cu and related systems because Co/Cu exhibits the largest GMR effects at room temperature. The magnitude of the GMR is increased with increasing number of Co/Cu bilayers and for very thin Co and Cu layers (the Cu thickness has to be one which gives rise to well defined anti-parallel orientation of the Co layers). Figure 3 shows a plot of resistance versus magnetic field for a Co-Fe/Cu multilayer displaying by far the highest GMR yet found. The film displays a value of room temperature magnetoresistance (MR) of $\Delta R/R_s \sim 110\%$, where R_s is the saturation resistance in large fields. At 4.2K the MR is even higher $\Delta R/R_s \sim 220\%$. The Co-Fe/Cu sample in Fig. 3 is composed of 120 bilayers of [9.5Å Co$_{95}$Fe$_5$/ 8.5Å Cu] grown by seeded epitaxy (Farrow et al., 1993; Harp and Parkin, 1994, 1996) on a MgO(110) single crystal substrate. Seed layers of 6Å Fe/ 45Å Pt are first deposited at $\sim$450 °C. The Co$_{95}$Fe$_5$/Cu multilayer is grown after cooling the substrate to $\sim$40 °C to reduce interdiffusion of the metal layers. Specular x-ray diffraction and cross-section transmission electron microscopy (XTEM) characterization of the structure of the multilayer show that the Fe/Pt seed layers and the multilayer grow highly oriented with respect to the substrate crystallographic axes. By using (100) oriented MgO and (0001) Al$_2$O$_3$ substrates, (100) and (111) oriented fcc Co/Cu and Co-Fe/Cu
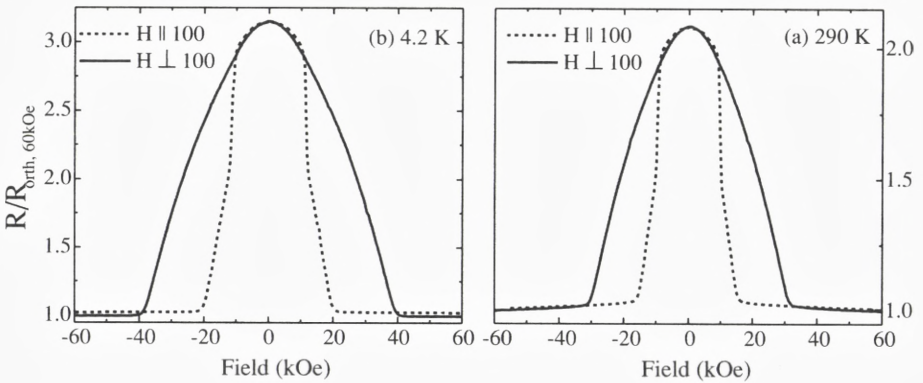
Figure 3. Resistance versus field curves at (b) 4.2 K and (a) 290 K of a magnetic multilayer of the form MgO(110)/ 6Å Fe/ 45Å Pt/ 9.5Å Cu/ [9.5Å $Co_{95}Fe_5$/ 8.5Å Cu]$_{120}$/ 12Å Pt. Curves are shown for the magnetic field applied in the plane of the film parallel and perpendicular to [100]. The current is applied along the [100] direction.

multilayers can be grown. Identical (100), (110) and (111) Co(Fe)/Cu multilayered structures can be prepared by simultaneous deposition onto these various MgO and sapphire substrates (Smith et al., 1997).

The structure of representative Co/Cu multilayers (grown without Fe seed layers) was characterized in detail with specular and off-specular x-ray scattering measurements using wiggler beam line VII-2 at the Stanford Synchrotron Radiation Laboratory (Smith et al., 1997). The weak scattering contrast between Co and Cu was enhanced by utilizing the Co scattering factor resonant modification obtained for 7692 eV photons close to the 7709 eV Co K absorption edge. Modeling of low angle specular scattering data, using an optical recursion formulation of the reflectivity (Parratt, 1954; Toney and Thompson, 1990), revealed that the Co/Cu interfaces had a typical root mean square width of ~4.5 Å where the averaging is over the spectrometer in-plane coherence length (~5000 Å). Peaks in the slightly off-specular diffuse scattering at the multilayer periodicity demonstrate that significant long wavelength interfacial roughness is conformally replicated throughout the multilayer (Sinha et al., 1991; Lurio et al., 1992).

The epitaxy, mosaicity and structural coherence of various Co/Cu films was explored by large-angle Bragg scattering. Figure 4 shows azimuthal x-ray scans (rotation about the multilayer normal) through off-specular Bragg peaks for three Co/Cu multilayers, which demonstrate both the symmetry of the films and the excellent in-plane orientational order with respect to the substrate crystallographic axes. Whilst orientationally ordered, the films are not strictly epitaxial as the
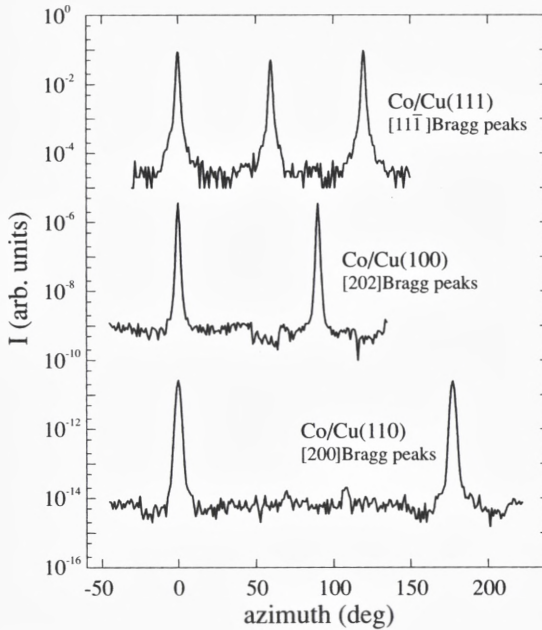
Figure 4. Azimuthal scans through off-specular Bragg peaks: six-fold symmetric (twinned three-fold) [11$\bar{1}$] peaks from a Co[10Å]/Cu[9Å] (111) oriented film, four-fold symmetric [202] peaks from a Co[20Å]/Cu[20Å] (100) oriented film, and two-fold symmetric [200] peaks from a Co[10Å]/Cu[9Å] (110) oriented film. Successive scans are scaled by 10^{-5}.

Co/Cu lattices are relaxed relative to that of the underlying seed film, although the largest observed Co/Cu in-plane strain relative to the bulk metals is $< 0.2\%$. Note that when the very thin Fe seed layer is omitted, for growth on (100) and (110) MgO, the Pt seed layer, and consequently the multilayer, may grow with mixed orientations, and typically some (111) orientation is then obtained. Interestingly, the (111) phase grows oriented with respect to the substrate crystal axes. The Co/Cu films exhibit modest structural coherence lengths as summarized in Table I for four representative films. Although the data in Table I correspond to Co/Cu multilayers grown without Fe seed layers, of the films examined, only one grew with mixed orientation.

Figure 5(a) shows a high resolution XTEM image of a (100) Co/Cu multilayer grown on MgO(100) with an Fe/Pt seed layer. The sample was prepared for electron microscopy using standard procedures of mechanical polishing and dimpling, followed by Ar$^+$ ion milling at 77 K. The microscopy was carried out using a JEM-
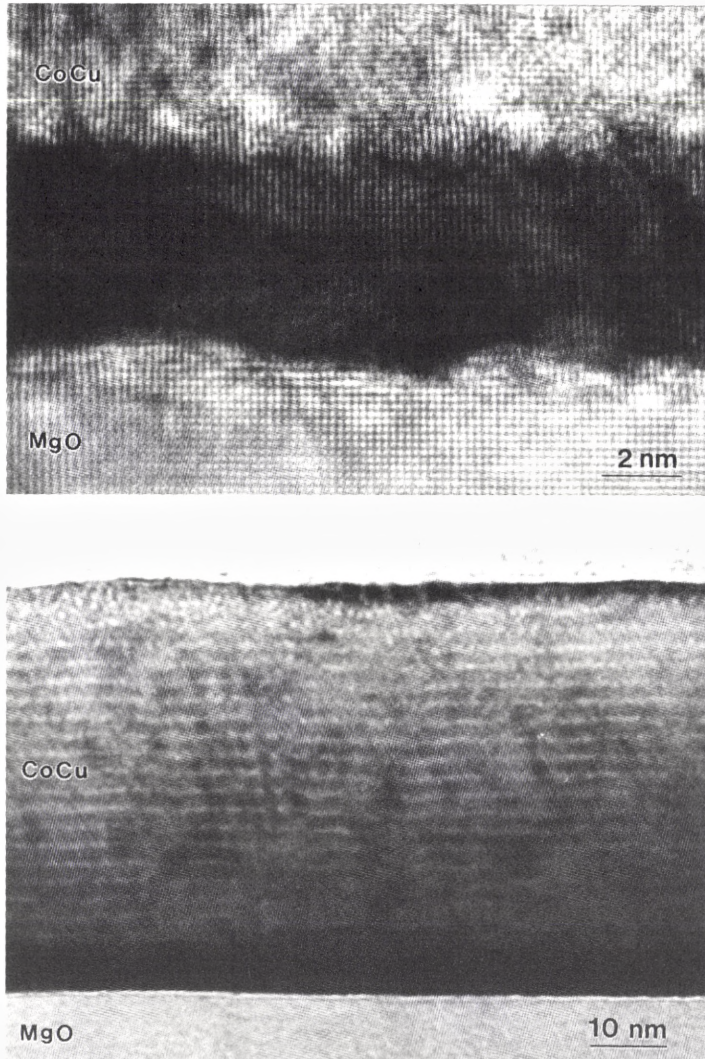
Figure 5. (a) High-resolution cross-section transmission electron micrograph of a MgO(100)/ 5Å Fe/ 50Å Pt/[11Å Co/ 13Å Cu] 19/ 11Å Co/ 15Å Pt multilayer. (b) Low magnification electron micrograph showing cross-section of the same multilayered structure as in Fig. 3(a) but deposited on a MgO(100) substrate. The image is deliberately defocussed to enhanced layer contrast. A section of the structure including, MgO substrate, Fe/Pt seed layer and a lower portion of the multilayer is shown.

Table I. Structural characteristics of four representative multilayers. Only one sample displayed mixed orientation. Tabulated mosaics are multilayer normal ($\perp$) or in-plane ($\parallel$) Bragg peak rocking full widths at half maximum. Coherence lengths ($\xi_\perp$, $\xi_\parallel$) are resolution corrected Bragg peak inverse half widths at half maximum.

Substrate	Orientation	Mosaic$_\perp$ (Deg.)	$\xi_\perp$ (Å)	Mosaic$_\parallel$ (Deg.)	$\xi_\parallel$ (Å)
Al_2O_3 (0001)	111	1.1	227	1.5	37
MgO (110)	110	1.4	61	1.2	47
MgO (100)	100	1.0	96	0.8	89
MgO (110)	100	2.2	41	1.6	42
MgO (110)	111	0.7	184	2.0	44

4000EX high-resolution electron microscope operated at 400 keV. The micrograph shows that the Pt seed layer and Co/Cu are epitaxially oriented with the MgO(100) substrate, and that the multilayer is of high crystalline quality with few defects. Under optimum imaging conditions the Co and Cu layers cannot be distinguished. However by deliberately defocussing the image the contrast between the Co and Cu layers is enhanced (Smith et al., 1994). Fig. 5(b) shows an XTEM of exactly the same multilayered structure as in Fig. 5(a) but grown, at the same time, on a MgO(110) substrate. The low resolution image shows that the Co and Cu layers are well defined and essentially flat. High resolution microscopy of the same sample shows that the crystal perfection is not as great as for the (100) oriented multilayer but that there are a substantial number of stacking faults along the $\langle 111 \rangle$ planes.

3.2 Magnetic properties: bilinear and biquadratic interlayer coupling

For crystalline multilayers with significant in-plane magnetic anisotropy the resistance varies in a complicated manner with magnetic field as first observed in (100) Fe/Cr/Fe sandwiches (Binasch et al., 1989). The magnetic properties of (100) and (211) Fe/Cr multilayers, which exhibit a two-fold (uniaxial) and a four-fold magnetic anisotropy respectively, have been examined in great detail (Fullerton et al., 1993, 1995; Azevedo et al., 1996). The magnetic moment versus field hysteresis loops of multilayers with different crystalline symmetries (and thus possessing two-fold, four-fold or higher-order magnetic anisotropies) and both bilinear and biquadratic interlayer coupling of adjacent magnetic layers has been extensively modeled (Folkerts, 1991; Dieny et al., 1990; Fujiwara, 1995; Almeida and Mills, 1995). The bilinear interlayer coupling varies as $\cos\theta$ where θ is the angle between the magnetic moments of adjacent magnetic layers, and favours parallel or antipar-

allel alignment of the magnetic moments. By contrast, the biquadratic interlayer coupling varies as $\cos^2 \theta$, thereby favouring perpendicular orientation of neighbouring magnetic moments. The bilinear coupling can be understood in terms of RKKY models but the biquadratic coupling strength (which similarly oscillates with spacer layer thickness) is too large to be accounted for within conventional models. A variety of models have been proposed to account for biquadratic coupling (Slonczewski, 1995). These are generally based on competition between competing ferromagnetic and antiferromagnetic interlayer interactions resulting, for example, from variations in individual layer thicknesses on the atomic length scale. For Fe/Cr, as mentioned above, the interlayer coupling oscillates with a period of just 2 monolayers of Cr which means the sign of the coupling can change from F to AF when the thickness of Cr is increased or decreased by just one atomic monolayer. Other models propose a competing interaction between an RKKY AF coupling and a F coupling derived from pinholes or perhaps significant local thickness variations in the spacer layer which lead to F coupling (Fulghum and Camley, 1995). For Fe/Cr the spin density wave in the Cr layers themselves has been invoked in yet another model (Slonczewski, 1995).

The dependence of the magnetic moment with magnetic field of the (110) Co/Fe/Cu sample shown in Fig. 3 is exhibited in Fig. 6 for a field oriented in-plane along (100). This sample exhibits a significant two-fold in-plane magnetic anisotropy as shown by the strong orientation dependence of the resistance versus in-plane magnetic field curves shown in Fig. 3. The field required to saturate the resistance is smallest when the field is applied parallel to $\langle 100 \rangle$ and largest when applied perpendicular to $\langle 100 \rangle$ along $\langle 011 \rangle$. The energy, E_i, of the ith magnetic layer in the multilayer per unit area can be written as

$$E = -\frac{1}{2} \left[J_1^{i,i+1} \cos \theta^{i,i+1} + J_1^{i,i-1} \cos \theta^{i,i-1} \right] + K_u \sin^2 \theta \qquad (1)$$

where $\theta^{i,i\pm1}$ is the angle between the ith magnetic moment and the two neighbouring magnetic moments, and θ is the angle between the applied magnetic field and the easy magnetic anisotropy axis. J_1 and K_u are the bilinear interlayer exchange coupling, and the uniaxial magnetic anisotropy energies respectively. The relative strengths of these energies can be determined from the magnetic fields required to saturate the magnetization of the multilayer along the magnetic easy and hard axes. From Fig. 3 it is readily deduced that K_u is large and is about 1/3 the size of J_1.

The data in Fig. 6 show that there are two distinct field regions of magnetization for the (110) CoFe/Cu multilayer. At low fields the moment of the multilayer is close to zero consistent with the magnetic moments of adjacent layers being coupled antiferromagnetically (Cebollada et al., 1989; Parkin et al., 1991a). The
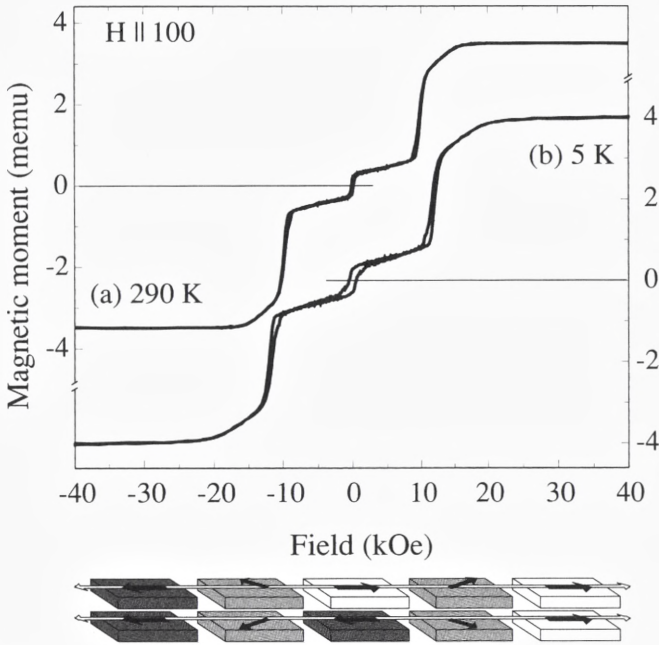
Figure 6. Magnetic moment versus field curves at (a) 300 K and (b) 5 K of a magnetic multilayer of the form MgO(110)/ 6Å Fe/ 45Å Pt/ 9.5Å Cu/[9.5Å Co$_{95}$Fe$_5$/ 8.5Å Cu]$_{120}$/ 12Å Pt for magnetic field applied in the plane of the film parallel to [100].

small residual moment may indicate that some small portion of the Co layers are coupled ferromagnetically, perhaps because of defects in the multilayer, or because of a small biquadratic interlayer coupling contribution. As the field is increased the moment of the multilayer increases slowly until at about 10 kOe the moment increases abruptly. The system undergoes a spin-flop transition at this field in which the moments reorient themselves from being aligned largely along ⟨100⟩ and antiparallel to one another to being aligned largely parallel to the applied field and each other (see sketch of magnetic configurations in Fig. 6). The sudden decrease in the angle between neighbouring moments results in a significant decrease in the resistance of the multilayer (see Fig. 3). For field oriented along the ⟨110⟩ in-plane axis, the magnetic hard axis, both the magnetization (not shown) and resistance (Fig. 3) vary monotonically with magnetic field. Similar results have been obtained for (211) Fe/Cr multilayers (Fullerton et al., 1993).

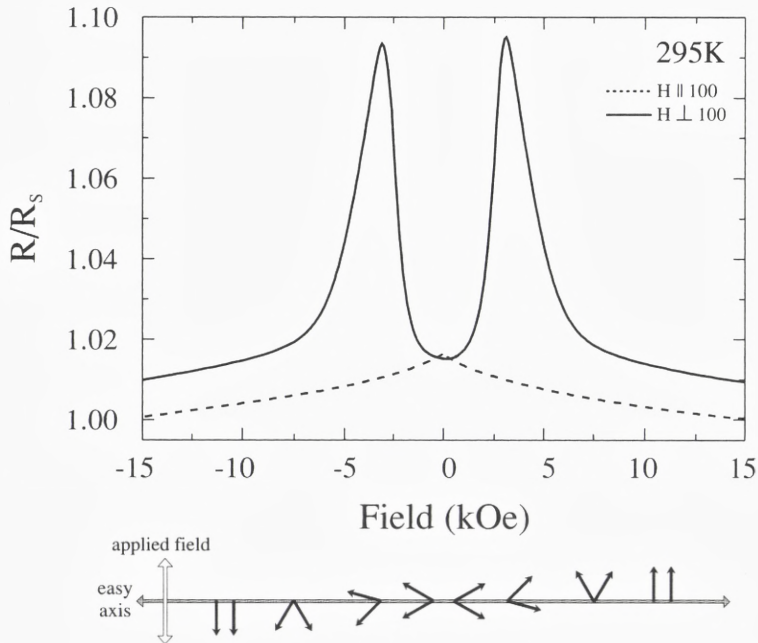Figure 7 shows an unusual example of the magnetoresistance curve of a (110) MgO/ 9Å Fe/ 50Å Pt/ 10Å Cu/[8.5Å Co$_{85}$Fe$_{15}$/ 12Å Cu]$_{40}$ multilayer. In this

Figure 7.   Resistance curve of a (110) MgO/ 9Å Fe/ 50Å Pt/ 10Å Cu/[8.5Å Co$_{85}$Fe$_{15}$/ 12Å Cu]$_{40}$ multilayer for field applied along the easy and hard in-plane axes.

case the resistance varies little when the magnetic field is applied along the easy axis (100) but when the field is applied along the hard axis the resistance, which is low in small fields, exhibits two peaks at fields of $\sim \pm 4$ kOe. This behaviour can only be accounted for by including a biquadratic interlayer exchange coupling contribution in addition to a ferromagnetic bilinear term and a uniaxial magnetic anisotropy (Pettit et al., 1997).

4   Giant magnetoresistance in sandwiches

The phenomena of giant magnetoresistance and oscillatory interlayer coupling have captured much attention, not only because they allow the basic transport and electronic properties of transition metals to be probed in a novel manner, but because it was immediately recognized that they may have useful properties for certain applications. In particular magnetoresistive materials can be used to measure magnetic fields. An important application is in magnetic recording disk drives in which in-

formation is stored in the form of magnetic bits written in thin magnetic films deposited on circular platters or discs. Bits correspond to small longitudinally magnetized regions or, rather, transitions between regions magnetized in opposite directions. An important parameter describing the performance of a disk drive is the number of magnetic bits which can be stored in a given area. In modern disk drives areal densities are in excess of 1 Gbit/in^2. In recent years the areal density has been increasing at a compound growth rate of approximately 60%/year (Grochowski and Thompson, 1994). This is reflected in decreased magnetic bit sizes which makes them increasingly difficult to read (as well as write). The most advanced magnetic recording read heads today use magnetoresistive technology based on the AMR effect in thin permalloy (Ni$_{81}$Fe$_{19}$) films (Ciureanu, 1992; Tsang et al., 1990). In order to achieve higher areal densities the thickness of the AMR sense film has to be decreased from approximately 150 Å at 1 Gbit/in^2 to well below ~100 Å at densities of > 5 Gbit/in^2. As mentioned previously the AMR effect is decreased in thin ferromagnetic films such that it is predicted that within the near future AMR metals will no longer provide sufficient signal for MR read head devices. Thus new materials are needed to allow ever greater areal densities in magnetic recording disk drives. Novel spin-valve sensors based on the GMR in magnetic sandwiches have been proposed (Dieny et al., 1991).

The spin-valve device is composed of two thin ferromagnetic layers separated by a thin Cu layer. The device relies on the exchange-biasing of one of the ferromagnetic layers to magnetically pin this layer. This effect, of ancient origin, is described schematically in Fig. 8. The magnetic hysteresis loop of a ferromagnetic layer is centered symmetrically about zero field. However certain combinations of thin ferromagnetic and antiferromagnetic layers display hysteresis loops which are displaced from zero field by an *exchange bias field* (Yelon, 1971). The origin of the effect is related to an interfacial exchange interaction between the AF and F layers and the fact that the magnetic lattice of the AF layer is essentially rigid, and little perturbed by even large external magnetic fields. Assuming the simplest possible AF structure of successive ferromagnetically ordered atomic layers whose moments alternate in direction from one layer to the next, one can readily appreciate that the uncompensated magnetic moment in the outermost AF layer at the AF/F interface will give rise to a exchange field which the F layer is subjected to. A long standing puzzle is why any exchange bias field is observed at all since one supposes that the interface between the F and AF layers is rough on an atomic scale (Malozemoff, 1988). As shown in Fig. 8, if the interface consists of atomic terraces whose length is less than the exchange length in the F metal there will be no net exchange anisotropy field. Note that similarly, if the AF layer is composed of randomly oriented magnetic domains, then this alone would quench the exchange bias field. In order to establish an exchange bias field the AF layer is usually de-

Ferromagnet

H=0

Exchange biased Ferromagnet

Interface terrace length >> exchange length   Terrace length < exchange length ⇒ No net exchange

F

AF

H≠0   H=0
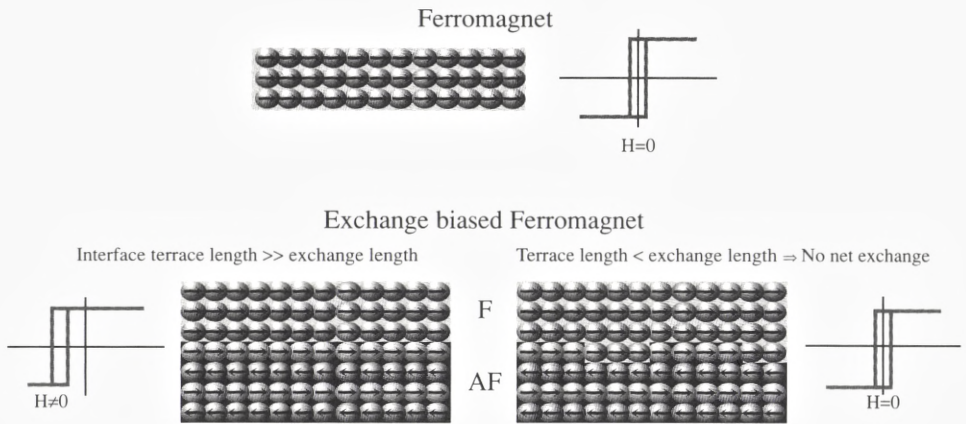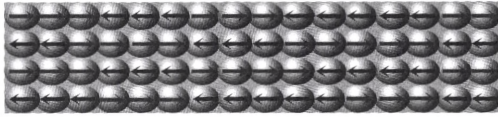
Figure 8. Schematic depiction of exchange biasing of a ferromagnetic layer by an antiferromagnetic layer on cooling through the blocking temperature of the AF layer.

posited on a magnetized F layer such that the interfacial exchange anisotropy leads to a preponderance of domains in the AF layer contributing to a net exchange bias field. Alternatively by heating the F/AF combination above the so-called blocking temperature of the AF layer where the AF spin system is no longer rigid, and subsequently cooling the bilayer couple in a magnetic field, an exchange bias field can be established in the direction of the applied field (see Fig. 9). This is a useful method to orient the exchange bias field in different directions in different magnetic layers in more complicated magnetic structures. By using AF layers with different blocking temperatures different, F layers can thereby be exchange biased in different directions. This is useful for engineering magnetic structures for various applications. A variety of models have been proposed to account for an exchange bias field even in the presence of rough interfaces (Malozemoff, 1988; Koon, 1997).

By combining an exchange biased ferromagnetic layer with a simple ferromagnetic layer it is thereby possible to engineer the magnetic moments of the two layers to be either parallel or antiparallel to one another as a function of magnetic field without relying on interlayer exchange coupling. Examples of such spin-valve GMR sandwiches are shown in Fig. 10 (Parkin, 1993). In each case a thin Co or permalloy layer, *pinned* by exchange biasing to a thin MnFe antiferromagnetic layer, is separated from an unpinned or *free* thin Co or permalloy layer by Cu layers ∼20 Å thick. The interlayer coupling via the Cu layer is weak. As shown in Fig. 10, well defined magnetic states of the sandwich are obtained in small positive and negative fields with the magnetic moments of the pinned and free layers parallel or anti-parallel to one another. This leads, via the GMR effect, to a step-wise change

An antiferromagnet grown in the absense of
a magnetic field has no long-range magnetic order

A disordered antiferromagnet layer adjacent to a hard ferromagnetic layer
may be magnetically ordered by heating above its blocking temperature
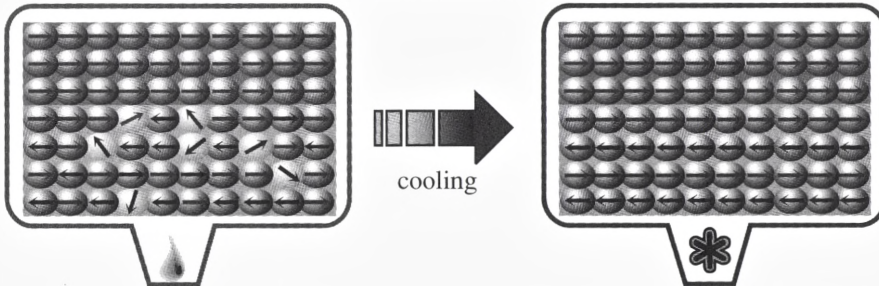and subsequently cooling

cooling

Figure 9. Schematic depiction of exchange biasing of a ferromagnetic layer by an antiferromagnetic layer.

in the resistance of the sandwich in small magnetic fields. The magnitude of the GMR effect in such sandwiches is very small, 3–7%, as compared with more than 100% in the Co–Fe/Cu multilayer shown in Fig. 3. A great deal of the GMR effect has been sacrificed to engineer a structure useful for MR head applications. The magnitude of the GMR in the sandwich is reduced for various reasons, including that there are only two magnetic layers (Parkin, 1995), and that the Cu spacer layer and the magnetic layers themselves are relatively thick leading to increased dilution of the GMR effect (Parkin et al., 1993). By using additional magnetic layers such that the free FM layer has two pinned magnetic layers on either side of it, GMR values of more than 20% have been obtained at room temperature (Egelhoff et al., 1995).

The origin of the GMR effect has been much debated since its discovery a few years ago (Binasch et al., 1989; Baibich et al., 1988). Much discussion has related to the role of spin-dependent scattering of the conduction electrons at the interfaces between the F and spacer layers. Early models emphasized the role of spin-dependent scattering within the interior of the F layers (Camley and Barnas, 1989; Levy, 1994) but subsequent work has revealed that the interfacial scattering
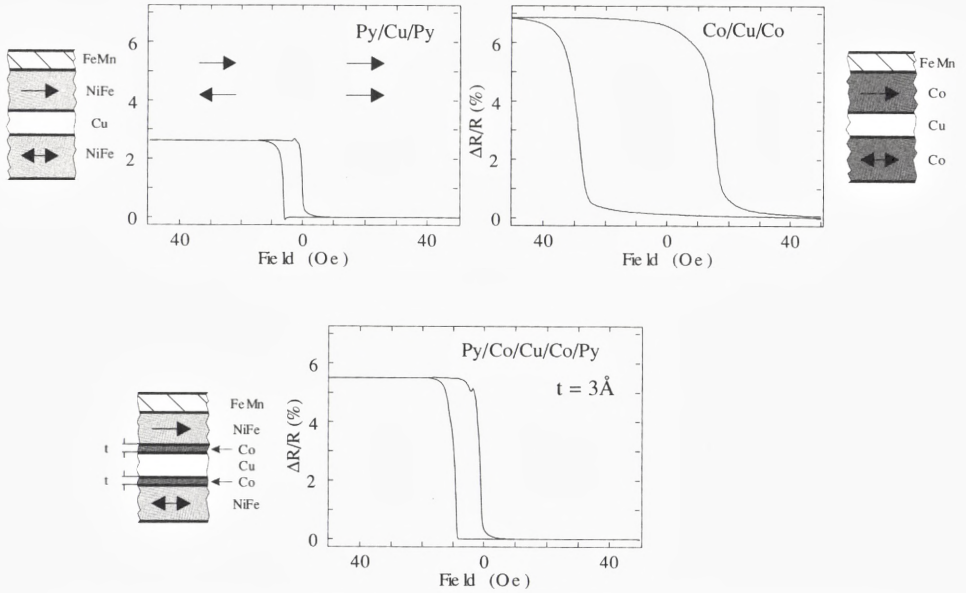
Figure 10. Resistance versus field curves for three spin-valve GMR exchange-biased structures: Py/Cu/Py, Co/Cu/Co and a Py/Cu/Py sandwich with 3 Å Co interface layers. (Py=permalloy).

is the dominant contribution (Parkin, 1992, Parkin, 1993). This is clearly demonstrated in Fig. 10 in which room temperature resistance versus field curves are shown for three spin-valve sandwiches. Fig. 10(a) shows data for Si/ 53Å Py/ 32Å Cu/ 22Å Py / 90Å FeMn/ 10Å Cu, where Py is permalloy ($Ni_{81}Fe_{19}$). The Py free layer in the Py/Cu/Py sandwich exhibits a very small switching field so that the structure is very sensitive to small fields. Data for a similar structure with the Py layers replaced by Co is shown in Fig. 10(b). The MR of the sandwich with Co layers is about twice as large as that of the Py/Cu/Py structure. However the Co free layer displays a significantly higher switching field than Py since Co has a much higher anisotropy. By simply dusting each of the Py/Cu interfaces in structure (a) with very thin layers of Co a structure with MR comparable to that of the Co/Cu structure but with low switching fields corresponding to the Py/Cu structure is obtained. Data for a sandwich with the same structure as in (a) but with 3 Å thick Co layers added at each Py /Cu interface is shown in Fig. 10 (c). Only 1–2 atomic layers of Co, just sufficient to completely cover the Py/Cu interface is required to obtain the enhanced GMR of the Co/Cu structure (see Fig. 11) (Parkin, 1993).

Finally another example of the dominant role of interface scattering in magnetic
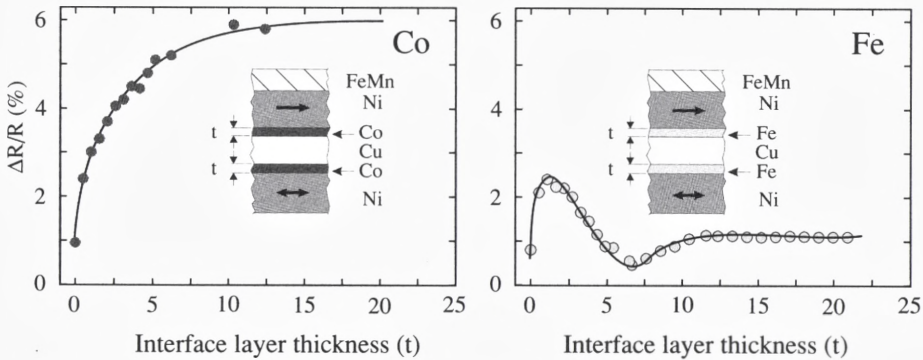
Figure 11. Saturation magnetoresistance versus thickness of Co and Fe layers inserted at the Ni/Cu interfaces in an exchange biased Ni/Cu/Ni spin valve GMR structure.

multilayers is shown in Fig. 11. The figure shows the results of dusting the Ni/Cu interfaces in Ni/Cu/Ni exchange biased sandwiches with Co and Fe. For Co interface layers the MR systematically increases as the Co interface layer is thickened, increasing by about a factor of six for Co layers about 10 Å thick. By contrast the MR of Ni/Cu/Ni structures has a complicated dependence on the thickness of Fe interface layers. The MR initially increases with the insertion of 1–2 Å Fe, then decreases and finally increases with thicker Fe layers. The dependence of the MR on Fe thickness can be accounted for by changes in the crystal structure, and consequently the magnetic moment of the Fe layer. For very thin Fe layers the Fe takes up a tetragonally distorted fcc phase which is ferromagnetic. For intermediate Fe thicknesses the Fe takes up an undistorted fcc phase which has no net magnetic moment and, finally, for thicker Fe layers, the Fe structure changes to a bcc phase which again is ferromagnetic. Details of the structure and magnetism of the Fe layers has been explored in related sputter-deposited crystalline (100) Ni/Fe superlattices (Kuch and Parkin, 1997).

5 Summary

Transition metal magnetic multilayers display fascinating properties. These include the indirect magnetic exchange coupling of thin $3d$ ferromagnetic layers of Co, Fe, Ni and their various alloys via intervening spacer layers of almost any of the non-ferromagnetic transition or noble metals. The indirect coupling is long-range and oscillates between ferro- and antiferromagnetic coupling as the spacer layer thickness is varied. Antiferromagnetically coupled multilayers display enhanced

magnetoresistance values. These giant magnetoresistance values have magnitudes of as much as $\sim 110\%$ and $\sim 220\%$ at room temperature and helium temperatures, respectively. The oscillatory interlayer coupling makes possible the *spin* engineering of magnetic multilayers with all sorts of possible magnetic structures (Parkin and Mauri, 1991). Simple sandwich structures composed of two ferromagnetic layers separated by thin Cu layers can be optimized, using interfacial dusting, to give large changes in resistance in very small magnetic fields. Such structures show great potential for magnetic recording read head sensors.

Acknowledgements

References

Almeida NS and Mills DL, 1995: Phys. Rev. B **52**, 13504
Azevedo A, Chesman C, Rezende SM, Aguiar FMD, Bian X and Parkin SSP, 1996: Phys. Rev. Lett. **76**, 4837
Baibich MN, Broto JM, Fert A, Dau FNV, Petroff F, Etienne P, Creuzet G, Friederich A and Chazelas J, 1988: Phys. Rev. Lett. **61**, 2472
Binasch G, Grünberg P, Saurenbach F and Zinn W, 1989: Phys. Rev. B **39**, 4828
Bruno P and Chappert C, 1992: Phys. Rev. B, **46**, 261
Camley RE and Barnas J, 1989: Phys. Rev. Lett. **63**, 664
Cebollada A, Martinez JL, Gallego JM, Miguel JJD, Miranda R, Ferrer S, Batallan F, Fillion G and Rebouillat JP, 1989: Phys. Rev. B **39**, 9726
Chien CL, 1995: in Annu. Rev. Mater. Sci., ed. B.W. Wessels (Annual Reviews Inc., Palo Alto) Vol. 25, p. 129–160
Ciureanu P, 1992: in *Thin Film Resistive Sensors*, eds. P. Ciureanu and S. Middelhoek (Institute of Physics Publishing, Bristol)
Dieny B, Gavigan JP and Rebouillat JP, 1990: J. Phys. Condens. Matter **2**, 159
Dieny B, Speriosu VS, Parkin SSP, Gurney BA, Wilhoit DR and Mauri D, 1991: Phys. Rev. B **43**, 1297
Egelhoff WF, Ha T, Misra RDK, Kadmon Y, Nir J, Powell CJ, Stiles MD, Michael RD, Lin CL, Silvertsen JM, Judy JH, Takano K, Berkowitz AE, Anthony TC and Brug JA, 1995: J. Appl. Phys. **78**, 273
Farrow RFC, Harp GR, Marks RF, Rabedeau TA, Toney MF, Weller D and Parkin SSP, 1993: J. Cryst. Growth **133**, 47
Fert A and Bruno P, 1994: in *Ultrathin Magnetic Structures*, eds. B. Heinrich and J.A.C. Bland (Springer-Verlag, Berlin) Vol. II, p. 82
Folkerts W, 1991: J. Magn. Magn. Mater. **94**, 302
Fujiwara H, 1995: IEEE Trans. Magn. **31**, 4112

Fulghum DB and Camley RE, 1995: Phys. Rev. B **52**, 13436

Fullerton EE, Conover MJ, Mattson JE, Sowers CH and Bader SD, 1993: Phys. Rev. B **48** 15755

Fullerton EE, Riggs KT, Sowers CH, Berger SD and Berger A, 1995: Phys. Rev. Lett. **75**, 330

Grochowski E and Thompson DA, 1994: IEEE Trans. Magn. **30**, 3797

Harp GR and Parkin SSP, 1994: Appl. Phys. Lett. **65**, 3063

Harp GR and Parkin SSP, 1996: Thin Solid Films **288**, 315

Johnson MT, Coehoorn R, Vries JJD, McGee NWE, Stegge JAD and Bloemen PJH, 1992: Phys. Rev. Lett. **69**, 969

Koon NC, 1997: (preprint)

Kuch W and Parkin SSP, 1997: Europhys. Lett. **37**, 465

Lenczowski SKJ, Gijs MAM, Giesbers JB, van de Veerdonk RJM and Jonge WJM, 1994: Phys. Rev. B **50**, 9982

Levy PM, 1994: in *Solid State Physics*, eds. H. Ehrenreich and D. Turnbull (Academic Press, New York) Vol. 47, p. 367

Lurio LB, Rabedeau TA, Pershan PS, Silvera IF, Deutsch M, Kosowsky SD and Ocko BM, 1992: Phys. Rev. Lett. **68**, 2628

Malozemoff AP, 1988: J. Appl. Phys. **63** 3874

Mathon J, Villeret M, Muniz RB, Castro JDAE and Edwards DM, 1995: Phys. Rev. Lett. **74**, 3696

McGuire TR and Potter RI, 1975: IEEE Trans. Magn. **MAG-11**, 1018

Parkin SSP, 1991: Phys. Rev. Lett. **67**, 3598

Parkin SSP, 1992: Appl. Phys. Lett. **61**, 1358

Parkin SSP, 1993: Phys. Rev. Lett. **71**, 1641

Parkin SSP, 1994: in *Ultrathin Magnetic Structures*, eds. B. Heinrich and J.A.C. Bland (Spinger-Verlag, Berlin) Vol. II, p. 148

Parkin SSP, 1995: in *Annual Review of Materials Science*, ed. B.W. Wessels (Annual Reviews Inc., Palo Alto) Vol. 25, p. 357–388

Parkin SSP, Bhadra R and Roche KP, 1991a: Phys. Rev. Lett. **66**, 2152

Parkin SSP, Li ZG and Smith DJ, 1991b: Appl. Phys. Lett. **58**, 2710

Parkin SSP, Mansour A and Felcher GP, 1991c: Appl. Phys. Lett. **58**, 1473

Parkin SSP and Mauri D, 1991: Phys. Rev. B **44**, 7131

Parkin SSP, Modak A and Smith DJ, 1993: Phys. Rev. B **47**, 9136

Parkin SSP, More N and Roche KP, 1990: Phys. Rev. Lett. **64**, 2304

Parratt LG, 1954: Phys. Rev. B **95**, 359

Pettit K, Gider S, Salamon MB and Parkin SSP 1997: (preprint)

Pierce DT, Unguris J and Celotta RJ, 1994: in *Ultrathin Magnetic Structures*, eds. B. Heinrich and J.A.C. Bland (Spinger-Verlag, Berlin) Vol. II

Rossiter PL, 1987: *The electrical resistivity of metals and alloys* (CUP, Campridge)

Rührig M, Schäfer R, Hubert A, Mosler R, Wolf JA, Demokritov S and Grünberg P, 1991: Phys. Status Solidi A **125**, 635

Sinha SK, Sanyal MK, Gibaud A, Satija SK, Majkrzak CF and Homma H, 1991: in *Science and Technology of Nanostructured Magnetic Materials*, eds. G.C. Hadjipanayis G.A. and Prinz (Plenum Press, New York) Vol. B259, p. 145

Slonczewski JC, 1995: J. Magn. Magn. Mater. **150**, 13

Smith DJ, Li ZG, Modak AR, Parkin SSP, Farrow RFC and Marks RF, 1994: Scr. Metall. Mater. **30**, 689

Smith DJ, Modak AR, Rabedeau TA and Parkin SSP, 1997: (submitted)

Toney MF and Thompson C, 1990: J. Chem. Phys. **92**, 3781

Tsang C, Chin MM, Togi T and Ju K, 1990: IEEE Trans. Magn. **26**, 1689

Unguris J, Celotta RJ and Pierce DT, 1991: Phys. Rev. Lett. **67** 140

Weber W, 1995: Europhys. Lett. **31** 491

Yelon A, 1971: in *Physics of Thin Films: Advances in Research and Development*, eds. M. Francombe and R. Hoffman (Academic Press, New York) Vol. 6, p. 205

Recent Progress in First Principles Investigations of Magnetism of Surfaces and Thin Films

Ruqian Wu

Department of Physics & Astronomy, California State University,

Northridge, CA 91330-8268, USA

and

A. J. Freeman

Department of Physics & Astronomy, Northwestern University,

Evanston, IL 60208-3112, USA

Abstract

The present state of the art of theoretical studies of magnetism in artificial low dimensional transition metal materials, e.g., surfaces, overlayers and multilayers, is reviewed here by means of some illustrative examples. Strong magnetic moment enhancements are found for Fe, Co and Ni atoms at surfaces or interfaces contacting with inert substrates. By contrast, the spin polarization is strongly frustrated in systems with strong hybridization, which usually leads to more complex antiferromagnetic ground states. As a major progress for first principles determination of the magneto-crystalline anisotropy, the state tracking and the torque approaches enable us to obtain very stable and reliable results of the MCA energy and other subsequent effects such as magnetostriction. The x-ray magnetic circular dichroism and its application for determination of spin, orbital and dipole moments at surfaces and interfaces are also discussed.

1 Introduction

As Allan Mackintosh understood and applauded, magnetism research has been undergoing a renaissance over the last decade following the discovery of a variety of new scientific phenomena associated with man-made transition metal thin films. Among them are the theoretical prediction of enhanced magnetic moments in ultrathin films and at surfaces (Freeman et al., 1991), the discovery of perpendicular magnetic anisotropy (Garcia et al., 1985) in layered structures, and the discovery of giant magnetoresistance (GMR, Baibich et al., 1988 and Binasch et al., 1989) and accompanying oscillatory exchange coupling in multilayers made by alternating magnetic and "nonmagnetic" metals (Parkin et al., 1990). Some of these discoveries

are expected to have a major impact on the magnetic recording industry. An example is the so-called spin-valve sensor (Dieny et al., 1991), which is about to be used as a magnetic recording head. Other applications are multilayers with out-of-plane anisotropy which show promise as "blue" magneto-optical media (Hurst et al., 1993), or GMR based structures which offer non-volatile alternatives to semiconductor based DRAM (Daughton et al., 1992).

As was also known to him, the great success of first principles electronic structure studies based on local spin density functional theory, which performs extremely complex simulations of ever increasingly realistic systems, plays a very important role in explaining magnetism in thin films and has led to the facing of even more challenging problems (Freeman et al., 1991). Theoretical calculations predicted the large enhancement of the magnetic moment for $3d$ transition metal (TM) surfaces or overlayers deposited on inert substrates, and the possible magnetization in some normally non-magnetic materials – for which some results have already been verified experimentally. Complex magnetic structures, especially some anti-ferromagnetic (AFM) configurations, can now be predicted by comparing total energies with their equilibrium atomic geometries (including multilayer relaxations and reconstructions at surfaces and interfaces) optimized very efficiently using the atomic force approach. Significant progress has been made very recently for the treatment of the weak spin-orbit coupling (SOC) and now we are able to obtain (i) very reliable results for the magneto-crystalline anisotropy (MCA) energies and magnetostrictive coefficients for transition metal thin films using the state tracking (Wang et al, 1993) and the torque (Wang et al., 1996) approaches; (ii) magneto-optical Kerr effect (MOKE) and soft x-ray magnetic circular dichroism (MCD). Using a linear response theory, magnetic transport properties, such as GMR, can also be determined from the ground state band structures.

The aim of the present review, dedicated to Allan Mackintosh, is to present the main lines of important theoretical developments in this exciting area in recent years with an emphasis on our own full potential linearized augmented plane wave (FLAPW) (Wimmer et al., 1981) calculations. Examples presented here indicate that high quality *ab initio* calculations of magnetic systems can achieve high accuracy/precision for a wide range of magnetic properties of transition metal and rare-earth metal systems. The new level of performance and the capability of modern computational simulations can help to alleviate many expensive experimental procedures, and can gradually build up effective tools to search for new magnetic materials.

2 $3d$ Overlayers

As determined by Hund's rules, most of the free transition metal atoms possess
a net spin moment. In the solid state, their magnetic moments decrease because
the interatomic Coulomb repulsion diminishes the parallel spin alignment in the
region between the atoms. Naturally, a reduced dimensionality, e.g., in 2D (i.e.,
monolayer) or 1D (i.e., linear chain) systems, is expected to restore the free atom
nature of the atom in question and thus to enhance the local magnetic moment.
Indeed, the calculated magnetic moments of $3d$ transition metals increase with
the decreasing dimensionality of system in going from bulk, surface and to a free
monolayer (Freeman et al., 1991).

To realize the predicted strong magnetic moment in monolayers, supporting
substrates should be lacking electronic states at the Fermi energy so as to minimize
the overlayer-substrate hybridization. As listed in Table I, the magnetic moments
of Fe and Co atoms are reduced by only about 0.1–0.2 μ_B on Ag(001) or Au(001)
compared to those in their free-standing monolayers. Surprisingly, Cu(001) exhibits
very strong proximity effects; the overlayer magnetic moments are reduced by 0.5
μ_B from those in the free standing case. A benign substrate, namely MgO(001),
was found on which the spin moment of an Fe monolayer is as large as 3.07 μ_B –
almost unchanged from the value for the free standing Fe monolayer, 3.10 μ_B. Since
MgO(001) has no states in the gap at E_F even for the surface layer, Fe/MgO(001)
is almost free of chemical interactions.

With strong interfacial interactions, e.g., in Fe/W(001) and Fe/Ru(0001), we
found that AFM ordering prevails since the FM state is frustrated by the d-band
hybridization. For example, Fe/W(001) has no stable, or even metastable, FM
states. By contrast, the AFM state ($M = 0.7$ μ_B) is about 0.01 eV/cell lower
than the PM state. Very interestingly, the FM ordering of the "dead" Fe layer
can be activated by an additional Fe overlayer and the magnetic moments in the
interface and surface layers jump to 1.68 μ_B and 2.43 μ_B, respectively. Therefore,
the observations of magnetism in Fe/W(001) should vary dramatically between one
and two layers.

On the diamond (001) surface, we found that a large Fe and Co magnetic
moment can be sustained (1.93 μ_B and 1.56 μ_B, respectively), whereas the magnetic
moment of a Ni monolayer is reduced to zero. It was found that the magnetic
moments strongly depend on the interlayer distance due to the interaction with
the dangling bond surface states on C(001). Interestingly, Fe and Co magnetic
layers induce almost zero magnetic moments at the interfacial C sites and a sizable
magnetic moment at the subinterfacial C sites (0.04 μ_B).

A strong interplay between magnetism and atomic structure was found for
Mn/Fe(001). The antiparallel alignment in the Mn plane with a large (3.1 μ_B)

Table I. Magnetic moment (μ_B) and magnetic ground state of magnetic monolayer and overlayer systems.

System	Monolayer		Overlayer	
	state	moment	state	moment
Fe/Ag(001)	FM	3.20-3.4	FM	2.96-3.01
Fe/Au(001)	FM	–	FM	2.97
Co/Ag(001)	FM	2.20	FM	2.03
Ni/Ag(001)	FM	1.02	FM	0.57-0.65
Fe/MgO(001)	FM	3.10	FM	3.07
Fe/Cu(001)	FM	3.20	FM	2.69-2.85
Co/Cu(001)	FM	2.05	FM	1.79
Ni/Cu(001)	FM	1.01	FM	0.39
Ni/Cu(111)	FM	1.01	FM	0.34
Fe/C(001)	FM	2.96	FM	1.93
Co/C(001)	FM	2.06	FM	1.56
Ni/C(001)	FM	1.03	PM	0.00
Pd/Ag(001)	FM	0.40	PM	0.00
Pd/MgO(001)	FM	0.34	PM	0.00
Pd/C(0001)	FM	0.14	PM	0.00
Rh/Au(001)	FM	1.56	FM	1.09
Rh/Ag(001)	FM	1.45	FM	0.95
Rh/MgO(001)	FM	1.45	FM	1.21
Rh/C(0001)	FM	1.35	FM	0.24
Ru/Ag(001)	FM	2.12	FM	1.57
Ru/MgO(001)	FM	2.14	FM	1.95
Ru/C(0001)	FM	2.48	FM	0.28
Fe/W(110)	FM	2.98	FM	2.18
Fe/W(001)	FM	3.10	AFM	0.93
Fe/Ru(0001)	FM	2.90	AFM	2.23
Mn/Fe(001)	AFM	4.32	AFM	3.15

magnetic moment is found to drive a $c(2 \times 2)$ buckling reconstruction in the Mn overlayer. Due to hybridization with the magnetic Fe(001) substrate, the valence bands of the two different Mn atoms differ substantially and thus FM signals can be detected from the AFM Mn monolayer using techniques such as spin-polarized photoemission. For the bilayer Mn/Fe(001) (i.e., 2Mn/Fe(001)), we found that the surface Mn layer (instead of the interfacial Mn layer) appears to couple antiferromagnetically with the underlying Fe substrate. This unusual behaviour was also found in experiments for Cr/Fe(001) and Mn/Fe(001) (Roth et al., 1995). Again, we found that the magnetic ordering in 2Mn/Fe(001) is very sensitive to the atomic structure and thus the positions of all the atoms need to be well optimized for such

a system.

3   Possible 4d magnetism

It was found that some 4d elements, namely Pd, Rh and Ru, can possess magnetic moments in certain circumstances. In an isolated monolayer geometry, the calculated magnetic moments for Pd, Rh and Ru are 0.35 μ_B, 1.45 μ_B and 2.12 μ_B, respectively (Zhu et al., 1990; Wu et al., 1992). Physically, the density of states at E_F of paramagnetic Ru and Rh monolayers is found to increase by 450% over their corresponding bulk values, which results in a large Stoner factor (1.45 and 1.89 for Ru and Rh monolayers, respectively) and thus a Stoner instability.

Strikingly, the magnetism of the free Rh monolayer is found to remain when placed on Ag(001) and Au(001) substrates. However, verification experiments using the surface magneto-optic Kerr effect (SMOKE) failed to find any evidence of ferromagnetism in Rh/Ag(001) at temperatures down to 40 K. (Mulhollan et al., 1991; Liu et al., 1992). To understand this discrepancy, FLAPW calculations were carried out for the Rh/Ag(001), Ru/Ag(001), Ag/Rh/Ag(001) and Ag/Ru/Ag(001) systems. The overlayer relaxation is found to be very small and to have no significant effect on the electronic and magnetic properties. Further, we found that the ferromagnetism of Rh/Ag(001) can be destroyed by an additional Ag layer – which attributes the lack of ferromagnetism in recent SMOKE experiments to the surface segregation between Rh and Ag atoms. By contrast, Ru/Ag(001) is predicted to be ferromagnetic with both a larger magnetic moment and larger magnetic energy even after being covered by a Ag layer, and thus is more suitable for experimental verification. In addition, the considerably stronger overlayer-substrate Coulomb repulsion indicates that Ag is no longer the "benign" substrate for 4d overlayer magnetism that it is for the 3d metals.

As expected, large magnetic moments are predicted for Ru and Rh monolayers on MgO(001) (1.95 μ_B and 1.21 μ_B for Ru and Rh, respectively) – indicating, in principle, the potential application of MgO(001) as a benign substrate for 4d monolayer magnetism. Significantly, according to our atomic force determinations, the metal overlayers induce a sizable *buckling* reconstruction in the interfacial MgO layer, which enhances the M–MgO binding energy by 0.1 eV. The weak M–O interaction is mainly via tail effects; however, it affects the density of states at the Fermi level for Pd/MgO(001) significantly and completely eliminates the small magnetic moment of the free Pd monolayer (0.34 μ_B).

A nonzero in-plane spin polarization was observed for Ru/C(0001) below 250 K, using spin-polarized secondary electron emission (SPSEE) techniques (Pfandzelter et al., 1995). This first evidence of 4d monolayer magnetism is very encouraging and

deserves theoretical verification. Surprisingly, the calculated magnetic moments of Rh/C(0001) and Ru/C(0001) are only 0.24 μ_B/adatom and 0.28 μ_B/adatom even in a very sparse structure. Furthermore, the magnetic moments are found to depend strongly on the overlayer/substrate interlayer distance. The calculated magnetic moment of Ru jumps discontinuously to a value as large as 1.1 μ_B just slightly away from the equilibrium position. It can even reach a value of 1.5 μ_B if the interlayer distance is 10% larger than the equilibrium one. Such a discontinuous behaviour suggests the co-existence of several high- and low-spin moment states.

4   Magneto-crystalline anisotropy

As is known, the strength of spin-orbit coupling (SOC) in $3d$ transition metal systems is very weak (30–50 meV, or 100 times smaller than that of the crystalline field) and thus can be well treated using a perturbative framework. As stated in the often-used MCA force theorem, the MCA energy can be approximately taken as the *band* energy

$$E_{\mathrm{MCA}} = E(\rightarrow) - E(\uparrow) = \sum_{\mathrm{occ}'} \varepsilon_i(\rightarrow) - \sum_{\mathrm{occ}''} \varepsilon_i(\uparrow) + O(\delta\rho^n). \tag{1}$$

Very recently, we proved that the order of n goes up to 4 for thin film systems, and thus the force theorem should be able to provide sufficient accuracy for MCA energy determinations. However, several numerical uncertainties have been inherent in most previous *ab initio* MCA calculations because the sets of occupied states, i.e., $\{\mathrm{occ}'\}$ and $\{\mathrm{occ}''\}$, were determined through the Fermi filling scheme which relies on the very limited information from the eigenvalues, ε_i.

Recently, we proposed the state tracking approach in which the $\{\mathrm{occ}'\}$ and $\{\mathrm{occ}''\}$ states are determined according to their projections back to the occupied set of the unperturbed states. Since this procedure ensures minimum change in the charge and spin densities as required by the force theorem and excludes the possible randomness in the Brillouin zone (tracking at a given k-point) (Wang et al., 1993), very stable MCA results have been obtained for magnetic thin films such as Fe, Co and Ni monolayers in the free standing case as well as on various substrates (Cu and Pd, etc) with relatively small number of k-points. Perhaps more importantly, the behaviour of MCA for transition metal thin films can now be related to more fundamental properties, such as band structures and wave functions. This enables us to explore the underlying physics and, furthermore, to figure out a way to tune the MCA for transition metal systems: For example, the strong in-plane MCA of a free standing Co monolayer is found to originate from the coupling between the occupied $d_{xz,yz}$ and unoccupied d_{z^2} and $d_{x^2-y^2}$ states at the $\bar{M}$ point. When adsorbed onto the Cu substrate, for example, the $d_{xz,yz}$ state is lowered in energy

due to the interfacial hybridization and thus the MCA energy becomes less negative in the Co/Cu overlayer systems and even positive in Co/Cu sandwiches.

More recently, we proposed a torque (Wang et al., 1996) method which can further depress the remaining uncertainties resulting from the SOC interaction between near-degenerate states around the Fermi level (so called surface pair coupling). To demonstrate the idea of the torque method, recall that the total energy of an uniaxial system can be well approximated in the form

$$E = E_0 + K_2 \sin^2\theta + K_4 \sin^4\theta \,, \tag{2}$$

where θ is the angle between the normal axis and the direction of magnetization. It is easy to find that the MCA energy is equal to the angular derivative of the total energy (torque) at a "magic angle" of $\theta = 45°$ as

$$E_{\mathrm{MCA}} \equiv E(\theta = 90°) - E(\theta = 0°) = K_2 + K_4 = dE/d\theta\big|_{\theta=45°} \,. \tag{3}$$

If we apply the Feynman-Hellman theorem, E_{MCA} can be evaluated finally as (note only $H^{\mathrm{soc}} = \xi\, \mathbf{s} \cdot \mathbf{L}$ depends on θ in the Hamiltonian)

$$E_{\mathrm{MCA}} = \sum_{\mathrm{occ}} \langle \Psi_i' | dH/d\theta | \Psi_i' \rangle \big|_{\theta=45°} = \sum_{\mathrm{occ}} \langle \Psi_i' | \partial H^{\mathrm{soc}}/\partial\theta | \Psi_i' \rangle \big|_{\theta=45°} \tag{4}$$

where Ψ_i' is the ith perturbed wave function.

The advantage of the torque method is obvious since in this approach we only have to deal with one particular magnetic orientation and thus only one Fermi surface is required for the k-integration. In addition, the MCA energy is expressed as the expectation value of the angular derivative of H^{soc} and therefore it is much more insensitive to the surface pair coupling. With the aid of the state tracking and torque methods, very stable results have been obtained for various transition metal systems and so we are able to attack the long standing problem of magnetostriction in transition metals.

As a first illustration, consider isolated monoatomic iron and cobalt layers with the same square lattice so that their electronic bands are very similar. Despite these similarities, in-plane and perpendicular surface MCA are expected for Co and Fe, respectively, from both experiment and theoretical calculations. According to our calculation and analysis, this is caused by the different occupation of the spin-down d bands due to the difference in the valence electron number. For example, for the Co monolayer, two bands consisting of xz and yz states are all occupied in a large region near $\bar{M}$. They are coupled through either l_y or l_x angular momentum components to the empty z^2 states, and this contributes to the in-plane MCA. The variation of the surface MCA for different atomic (Co vs Fe) layers amounts to about 3 meV, depending on the lattice strain.

In an overlayer system, the MCA energy depends mainly on the hybridization between its out-of-plane states, namely the xz and yz states, and the orbitals of the substrates. At the Co–Pd interface of a Pd/Co/Pd sandwich, for example, the Co xz and yz states have been appreciably pushed up to higher energy which results in perpendicular interface MCA. We found that the effects of different substrates can affect the MCA energy by 2 to 3 meV. These interfacial effects are well described using an effective ligand interaction model.

5 Magnetostriction

In general, the size of the (magnetostrictive) strain induced by rotation of the magnetization of a magnetic material depends on the direction of the measured strain and magnetization with respect to the crystalline axes of the material. For a cubic material, the directional dependence of the fractional change in length can be expressed in terms of the direction cosines of the magnetizations (α_i) and those of the measurement direction (β_i) with respect to the crystalline axes

$$\frac{\Delta l}{l} = \frac{3}{2}\lambda_{100}\left[\sum_{i=1}^{3}\alpha_i^2\beta_i^2 - \frac{1}{3}\right] + 3\lambda_{111}\sum_{i\neq j}\alpha_i\alpha_j\beta_i\beta_j\,. \tag{5}$$

If the measurement is carried out along the (001) direction for example, $\beta_x = \beta_y = 0$ and $\beta_z = 1$, Eq. (5) can be simplified as

$$\frac{\Delta l}{l} = \frac{3}{2}\lambda_{100}\left[\alpha_z^2 - \frac{1}{3}\right] \tag{6}$$

and

$$\lambda_{100} = \frac{2}{3}\frac{\Delta l_z - \Delta l_{x,y}}{l}\,. \tag{7}$$

Clearly, λ_{100} represents the change in length along (001) when the magnetization turns from the the x–y plane to the z direction.

The equilibrium length l can be obtained by fitting the calculated total energy as a quadratic function of l ($l_0 = -b/2a$) as

$$E = al^2 + bl + c\,. \tag{8}$$

If the MCA energy is a linear function of l (as will be demonstrated)

$$E_{\mathrm{MCA}} = E(x,y) - E(z) = k_1 l + k_2 \tag{9}$$

then we finally have

$$\lambda_{001} = -2k_1/3b\,. \tag{10}$$

Obviously, while the value of b can be easily calculated with high precision, the bottleneck for the determination of λ is the value of k_1, i.e., the strain dependence of the MCA energy.

For cubic bulk magnetic transition metals, the in-plane lattice constants are expected to change when the strains are applied along the vertical direction. Here, we consider two modes of distortion, namely (i) constant volume (i.e., γ_1 mode) and (ii) constant area in the lateral plane, when we change l to determine the magnetostrictive coefficients. For the γ_1 mode, the calculated total energies and MCA energies are plotted in Fig. 1. For bulk bcc Fe and fcc Co and Ni, the total energy can be well-fitted by a parabola and the MCA energy exhibits a good linearity with respect to the change of l – indicating the high precision of the present calculations and also justifying the huge range of strain ($\Delta l/l \sim 5\text{--}20\%$) used in the calculations relative to saturation magnetostrictive strains ($\Delta l/l \sim 10^{-5}$).

For both the constant volume and constant area modes, the calculated λ_{001} is *positive* for bcc Fe and fcc Co – meaning that the dimension expands along the direction of magnetization; by contrast, the calculated λ_{001} for bulk fcc Ni is opposite in sign. For the constant area mode, the values of λ_{001} decrease substantially from the results obtained for the constant volume mode. These zero temperature results are of the correct sign and set a satisfactory range for the measured values of λ_{001}. They thus serve to validate this new approach for determining the tiny magnetostriction in transition metal systems.

To extend this approach to thin films consisting of a magnetic monolayer and a thick non-magnetic substrate, one should bear in mind that the lattice constant in the lateral plane is fixed by the substrate and so only strains along the vertical direction can be observed. The l in Eqs. (8) and (9) should therefore be considered as the interlayer distance between the magnetic overlayer and the non-magnetic substrate. The orientation of the substrate is used as a subscript for λ, e.g., λ_{100} stands for systems with (100) substrates. To simulate Co/Cu(001) and Co/Pd(001), a slab consisting of seven ideally constructed fcc Cu or Pd layers ($a_{Cu} = 6.83$ a.u. and $a_{Pd} = 7.35$ a.u.) with a pseudomorphic Co overlayer on each side is used.

For each system, the total energy curve can be well fitted by a parabola and the MCA energy exhibits a fairly good linearity as functions of the overlayer/substrate distance. We found for Co/Cu(001) that b and k_1 are equal to -4390 meV/a.u. and -0.376 meV/a.u., respectively; thus, the calculated λ_{100} at the Co/Cu(001) interface is -5.7×10^{-5}. The negative sign means that the Co–Cu interlayer distance contracts when the direction of magnetization changes from in-plane to normal to the surface. Dramatically, we found that the MCA energy for Co/Pd(001) becomes more *negative* when the Co–Pd distance shrinks and thus λ_{001} becomes *positive*, $+2.3 \times 10^{-4}$, just opposite to that for Co/Cu(001).
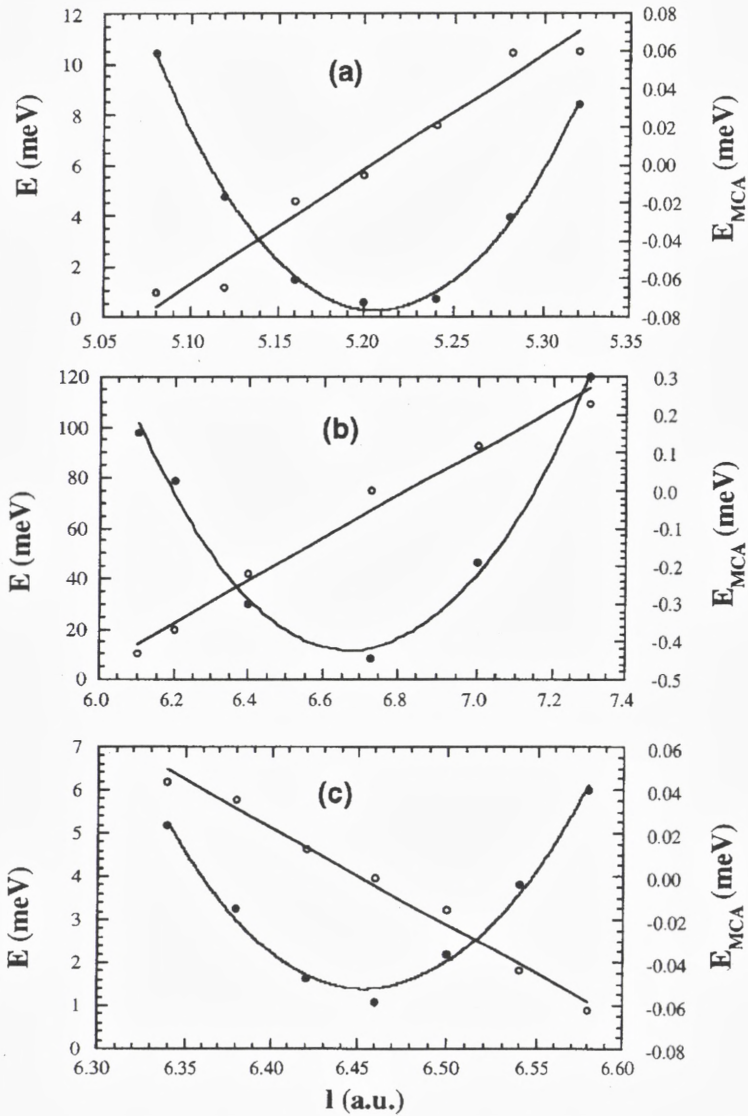
Figure. 1. The calculated total energy (left scale) and MCA energy (right scale) as a function of the length of the c-axis for (a) bcc Fe, (b) fcc Co and (c) fcc Ni.

6   Strain-induced MCA in Ni/Cu(001)

In many cases, the origin of perpendicular magnetic anisotropy (PMA) in ultra thin films is still not very clear today. It is believed that PMA originates from the altered hybridization, reduced symmetry or the stronger spin-orbit coupling (SOC) interaction at the interfacial region when heavier substrate atoms (Pd or Pt) are involved. It is hard, however, to explain the observation for Ni/Cu(001) in which the PMA occurs only when the Ni film becomes thicker than seven atomic layers (Baberschke, 1996). To understand this unusual result, we calculated the MCA energies of bulk fct Ni (lattice matched with Cu(001)) and of the mono- and bi-layer Ni/Cu(001) overlayer systems. We find that the lattice strain in bulk fct Ni leads to a large positive MCA energy (an inverse effect of magnetostriction), whereas the interfacial contribution to the MCA energy is negative (-1.1 meV per Ni atom). Thus, the PMA in Ni/Cu(001) is clearly due to strain-induced effects in the bulk, rather than interfacial effects, as was believed in the literature.

Similar to that in Fig. 1, the calculated MCA energies for bulk fct Ni can be well fitted by a linear function of the length of the c-axis. When c is equal to 6.83 a.u. (ideal fcc Cu lattice), the MCA energy is smaller than 1 μeV/atom – a result which indicates the precision of the present approach for the determination of the MCA energy for bulk magnetic transition metals. At the position corresponding to the measured structure ($c = 6.44$ a.u.), the MCA energy reaches 65 μeV/atom. This result agrees well with recent experimental data extrapolated to zero temperature, i.e., 70 μeV/atom (Baberschke, 1996). In bulk fct Ni, with a magnetic moment of 0.65 μ_B, the calculated shape (so-called volume) anisotropy energy due to the magnetostatic dipole interactions is less than 0.6 μeV/atom for a wide range of lattice distortion (10%). Thus, the MCA contribution is the dominant part of the PMA.

The strain-induced MCA energy is found to originate from the shift of the unoccupied $d_{xz,yz}$ states ($m = 1$) into a higher energy region when the lattice is compressed along the vertical direction. This weakens the spin-orbit interactions between the $d_{xz,yz}$ and the occupied non-bonding $d_{x^2-y^2}$ and d_{z^2} states (which yield a negative MCA energy). Meanwhile, almost no change is found for the unoccupied states with $m = 2$ and $m = 0$. The SOC interactions between the $d_{x^2-y^2}$ and d_{xy} states (which give a positive MCA energy) are therefore almost unaffected. This results in a positive MCA energy since the SOC interactions with the same m prevail over that with different m.

We have also determined the MCA energies of mono- and bi-layer Ni/Cu(001) thin films; they are -0.69 meV/atom and -0.30 meV/atom, respectively. Again, the shape anisotropy is negligible even for these overlayer systems (e.g., it is 0.023 meV/atom for the monolayer Ni/Cu(001)). The net MCA energy is strongly nega-

tive so that in-plane magnetization is preferred for the ultra-thin overlayer system. Thus, at least for Ni/Cu(001), the observed PMA for thick overlayers does not come from surface/interface effects as was believed before, but appears to be due to the strain-induced bulk contribution.

7   MCD at surfaces and interfaces

The possibility to determine both the spin and orbital moments (denoted as $\langle S_z \rangle$ and $\langle L_z \rangle$, respectively) directly from x-ray magnetic circular dichroism (MCD, Schütz et al., 1987; Stöhr, 1993, 1995) spectra by applying recently proposed simple but powerful MCD sum rules has attracted considerable excitement and attention (Thole et al., 1992; Carra et al., 1993). Since these sum rules have been derived from a single ion model, their validity for complex materials (e.g., transition metals) with strong multi-shell hybridization (excluded in the original derivation) needs to be verified. As is well known, MCD measures the difference in absorption between right- and left-circularly polarized incident light during the process of electric transitions from core states to unoccupied valence states. Due to the spin-orbit coupling between valence states, the MCD signals of σ_m ($= \sigma_+ - \sigma_-$) for the L_2 and L_3 absorption edge for $3d$ transition metals no longer cancel each other as they do in the absence of SOC where the integrated L_2 and L_3 signals are equal and opposite. Here, σ_+ and σ_- represent the absorption cross sections for left- and right-circularly polarized light, respectively.

As stated in the MCD sum rules, integrations of the MCD and total absorption spectra relate directly to $\langle L_z \rangle$, $\langle S_z \rangle$ and $\langle T_z \rangle$ for the unoccupied states

$$\frac{I_m}{I_t} = \frac{\int_{L_3+L_2} \sigma_m dE}{\int_{L_3+L_2} \sigma_t dE} = \frac{\langle L_z \rangle}{2N_h} \; ; \quad N_h = \int \rho(E) dE \tag{11}$$

and

$$\frac{I_s}{I_t} = \frac{\int \sigma_s dE}{I_t} = \frac{\int (\sigma_{m,L_3} - 2\sigma_{m,L_2}) dE}{\int_{L_3+L_2} \sigma_t dE} = \frac{\langle S_e \rangle}{N_h} = \frac{\langle S_z \rangle + 7\langle T_z \rangle}{3N_h}, \tag{12}$$

where $\sigma_m = \sigma_+ - \sigma_-$ and $\sigma_t = \sigma_+ + \sigma_- + \sigma_z$. **T** is the spin magnetic dipole operator, i.e., $\mathbf{T} = \frac{1}{2}[\mathbf{S} - 3\hat{r}(\hat{r} \cdot \mathbf{S})]$, ($T_z = S_z(1 - 3\cos^2\theta)/2$ for **S** aligned along the z direction). The number of valence holes, N_h, can be obtained from an integration over the unoccupied density of states ($\rho(E)$).

There are two assumptions in the derivation of the sum rules: (i) the radial matrix elements are constant for all transitions, and (ii) no hybridization exists between different l shells (i.e., l is a good quantum number). As is well-known, both assumptions fail in real materials and thus weak $s, p-d$ hybridization (which

Table II. Calculated values of $\langle L_z \rangle$, $\langle S_z \rangle$, $\langle T_z \rangle$, $\langle S_e \rangle$ and N_h and sum rule errors $R_1 = \frac{I_m}{I_t} / \frac{\langle L_z \rangle}{2N_h} - 1$, $R_2 = \frac{I_s}{I_t} / \frac{\langle S_e \rangle}{N_h} - 1$ and $R_3 = \frac{I_m}{I_s} / \frac{\langle L_z \rangle}{2S_e} - 1$ for Ni(001), Co(0001) and Fe(001) surface (S) and bulk-like centre (C) layers.

Atom	$\langle L_z \rangle$	$\langle S_z \rangle$	$7\langle T_z \rangle$	$\langle S_e \rangle$	N_h	R_1	R_2	R_3
Ni(S)	−0.069	−0.67	−0.082	−0.250	1.81	0.27	0.52	−0.10
Ni(C)	−0.051	−0.62	−0.027	−0.215	1.66	0.20	0.36	−0.11
Co(S)	−0.090	−1.61	0.240	−0.457	2.60	0.11	0.24	−0.09
Co(C)	−0.078	−1.52	0.014	−0.502	2.55	0.09	0.22	−0.10
Fe(S)	−0.111	−2.71	0.230	−0.828	3.70	0.10	0.16	−0.04
Fe(C)	−0.063	−2.10	0.028	−0.691	3.34	0.04	0.15	−0.09

affects both assumptions) is important for the validity of the sum rule. Since the effects of s, p states are inherent in real materials and thus in the experimental spectra, the validity of these sum rules needs to be checked. To this end, FLAPW calculations were carried out to obtain both the MCD spectra (I_m, I_s and I_t) and ground state properties ($\langle S_z \rangle$, $\langle L_z \rangle$, $\langle T_z \rangle$ and N_h).

In a series of investigations (Wu et al., 1993; 1994), we found that the main mechanism affecting the validity of the sum rules is the hybridization between the d states and the high-lying s, p states. Significantly, the I_t and N_h are not well defined quantities since they do not converge with respect to the upper-limit of the energy integration, and thus an arbitrary energy cut-off has to be applied in order to stay within the d band region. Thus, we proposed a criterion for the choice of the energy cut-off, i.e., cut the integrations for I_t and N_h at the energy where the MCD counterpart becomes acceptably close to zero. Based on this criterion, we adopted an energy cut-off of 6 eV above E_F for the calculated results for Fe, Co and Ni (bulk and surfaces).

As listed in Table II, the validity of the spin and orbital sum rules is denoted by $R_1 = \frac{I_m}{I_t} / \frac{\langle L_z \rangle}{N_h} - 1$, and $R_2 = \frac{I_s}{I_t} / \frac{\langle S_e \rangle}{N_h} - 1$. Obviously, the orbital sum rule is seen to work very well (within 10%) for Fe and Co systems, and the error becomes larger for Ni since the number of s, p holes is almost equal to that of d holes (we used an energy cutoff of 6 eV above E_F). By contrast, the errors of the spin sum rule are much larger; it actually fails severely for the Ni surface since R_2 is as large as 52%.

In addition, the $\langle T_z \rangle$ term in the spin sum rule is negligible only for atoms with cubic symmetry. For atoms in non-cubic environments such as surfaces and interfaces, as seen from Table II, its importance is obvious, since its magnitude becomes 8.5%, 12% and 15% of $\langle S_z \rangle$ at E_F for Fe(001), Ni(001) and Co(0001),

respectively. The hybridization between different l shells is the main mechanism causing the failure of the MCD spin sum rule for transition metals. Without s, p states, the error of the MCD spin sum rule can be reduced to within 10% even for the Ni surface.

We have emphasized the need for a proper energy cut-off for the integrations in order to eliminate the error introduced by the high lying s, p states through the normalizing denominators. A better way is to combine the $\langle L_z \rangle$ and $\langle S_z \rangle$ sum rules, as was done recently in some experiments on bulk transition metals. From our first principles calculations, we found that the error in the ratio $R_3 = \frac{I_m}{I_s} / \frac{\langle L_z \rangle}{\langle S_e \rangle} - 1$, is 10% or so for all systems studied.

8   Conclusions

In summary, state-of-the-art *ab initio* LSD electronic structure calculations have achieved great success in the exciting field of thin film magnetism, in both explaining existing phenomena and, more importantly, in predicting the properties of new systems. Illustrative results demonstrate that: (1) the lowered coordination number at clean metal surfaces leads to enhanced magnetic moments; (2) noble metal and MgO substrates do not affect the magnetism in most cases, but show significant effects on $4d$ overlayers; (3) the strong interaction (hybridization) with nonmagnetic transition metals diminishes (entirely in some cases) the ferromagnetism and usually leads to AFM ordering; (4) the magnetic anisotropy and magnetostriction can be predicted correctly using the state-tracking and torque procedures; and (5) x-ray magnetic circular dichroism can be explained in the framework of interband transitions. In the future, electronic structure theory is expected to continue to play a predictive role by considering more practical systems, by eliminating the limitation of the local spin density approximation and developing more efficient and precise methods.

9   Acknowledgement

References

Baberschke K, 1996: Appl. Phys. A **62**, 417

Baibich MN, Broto JM, Fert A, Dau A, Petroff F, Eitenne P, Creuzet G, Friederich A, and
  Chazelas J, 1988: Phys. Rev. Lett. **61**, 2472

Binasch G, Grunberg P, Saurenbach F and Zinn W, 1989: Phys. Rev. B **39**, 4828

Carra P, Thole BT, Altarelli M and Wang XD, 1993: Phys. Rev. Lett. **70** 694

Carcia PA, Meinholdt AD and Suna A, 1985: Appl. Phys. Lett. **47**, 178

Daughton JM, 1992: Thin Solid Films, **216**, 162

Dieny B, Speriosu VS, Parkin SSP, Gurney AB, Wilhoit DR and Mauri D, 1991: Phys. Rev. B
  43, 1279

Freeman AJ and Wu RQ, 1991: J. Magn. Magn. Mater. **100**, 497

Hurst JE Jr. and Kozlovsky WJ, 1993: Jpn. J. Appl. Phys. **32**, 5301

Liu C and Bader SD, 1992: Phys. Rev. B **44**, 12056

Mulhollan GA, Fink RL and Erskine JL, 1991: Phys. Rev. B **44**, 2393

Parkin SSP, More N and Roche KP, 1990: Phys. Rev. Lett. **64**, 2304

Pfandzelter R, Steierl G and Rau C, 1995: Phys. Rev. Lett. **74**, 3467

Roth C, Kleeman Th, Hillebrecht FU and Kisker E, 1995: Phys. Rev. B **52**, 15691

Schütz G, Wagner W, Wilhelm W, Kienle P, Zeller R and Materlik G, 1987: Phys. Rev. Lett. **58**,
  737

Stöhr J, 1993: Science **259**, 658

Stöhr J, 1995: J. Electron Spectroscopy and Rel. Phenom. **75**, 253

Thole BT, Carra P, Sette F and Van der Laan G, 1992: Phys. Rev. Lett. **68** 1943

Wang DS, Wu RQ and Freeman AJ, 1993: Phys. Rev. Lett. **70**, 869

Wang XD, Wu RQ, Wang DS and Freeman AJ, 1996: Phys. Rev. B **54**, 61

Wimmer E, Krakauer H, Weinert M and Freeman AJ, 1981: Phys. Rev. B **24**, 864

Wu RQ and Freeman AJ 1992, Phys. Rev. B. **45**, 7222

Wu RQ, Wang DS and Freeman AJ, 1993: Phys. Rev. Lett. **71** 3581

Wu RQ and Freeman AJ, 1994: Phys. Rev. Lett. **73** 1994

Zhu MJ, Bylander DM and Kleinman L, 1990: Phys. Rev. B **42**, 2874

Spin Dynamics in Strongly Correlated Electron Compounds

Yasuo Endoh

Department of Physics, Graduate School of Science, Tohoku University,

Aramaki Aza Aoba, Aoba-ku, Sendai, 980-77, Japan

Abstract

The recent neutron magnetic scattering results from strongly correlated electron compounds are reviewed. We have elucidated the spin fluctuations in the $3d$ transition metal oxides including the high temperature superconductors, the colossal magneto-resistance materials and related compounds. One important conclusion obtained from our studies is that spin dynamics or thermal spin fluctuations in these correlated electron systems are quite similar to those characterising itinerant electron magnetism.

1 Introduction

In the past decade, we have been interested in the physics of strongly correlated electron systems as the most fascinating subject in modern condensed matter physics. Materials of the strongly correlated electron systems commonly show unconventional properties as the result of nonlinear many-body electron forces plus various competing interactions acting on not only electrons and spins but also phonons. Among these we focus on transition metal oxides presented in this paper, which belong to the family of either a cubic perovskite of ABO_3, with A = Alkaline (-earth) metal cation, B = transition metal cation or their modified lattices.

The cubic perovskite of high symmetry is well known for its structural instabilities and it exhibits the distorted lower symmetry structure coupled with other freedoms such as electrons, (pseudo-)spins etc. (Samuelsen et al., 1972). Eventually it has become the important class of the 'strongly correlated materials' for not only the research of solid state physics but industrial application. The colossal magneto-resistance system of $La_{1-x}Sr_xMnO_3$ can be included in this category. On the other hand, the high T_c superconductors of the single layered copper oxide, $La_{2-x}Sr_xCuO_4$, have an A_2BO_4 unit lattice, where units of A_2O_2 plus BO_2 layers stack alternately. Therefore the lattice structure is quasi two dimensional (2D),

and in fact the physical properties are of mostly 2D character.

Another important aspect of these transition metal oxides presented here is the 'Mott transition' upon doping charges (holes) into the parent material. The insulating state is realized by the effect of the strong electron correlation. In other words, the half-filled band is split by the electron correlations and then the lower split band becomes fully occupied, hence an insulator. The insulating state of this category exhibits the antiferromagnetic long-range order due to the strong electron correlation. La_2CuO_4 and $LaMnO_3$ are both considered to be realizations of the Mott insulator or Mott–Hubbard insulator (Hubbard, 1963; Kanamori, 1963; Gutzwiller, 1963).

Spin fluctuations in the strongly correlated electron systems have become a central issue for the mechanism of the high T_c superconductivity: how strong the 2D antiferromagnetic interaction governs the metallic state of these high T_c superconducting copper oxides, which might be extended from the 2D quantum antiferromagnetism in the insulating state of La_2CuO_4. Furthermore it must be clarified experimentally how the unique spin fluctuations play a key role in the mechanism of the unconventional superconductivity.

Among many recently discovered high T_c superconductors of the copper oxides, the single layered copper oxide materials of $La_{2-x}Sr_xCuO_4$ have been focussed on in our group mainly due to the fact that this system is the simplest material among the high T_c superconductors and also the fact that undoped La_2CuO_4 ($x = 0$) is the most ideal 2D quantum ($S = 1/2$) Heisenberg antiferromagnet in our long standing interest. The main stream of our research activities for a decade have been summarized in several review papers (Birgeneau and Shirane, 1989; Endoh, 1990; Shirane et al., 1994). Therefore the first half of this paper deals with the most recent progress in our investigation of spin fluctuations in the superconducting phase of $La_{2-x}Sr_xCuO_4$ with $x = 0.15$, which gives the highest transition temperature ($T_c = 37.3$ K) in this particular system of the single layered superconductors. We also present the doping (x) dependence of the wave vector (δ) of the incommensurate spin fluctuations in the following section.

In the latter half, we discuss spin dynamics in the colossal magneto-resistance materials of $La_{1-x}Sr_xMnO_3$, with $x < 0.3$ (Martin et al., 1996). Spin correlations were predicted to be unusual reflecting the colossal magneto-resistance effect, which is the gigantic jump in resistivity associated with the long range magnetic order. The transition from the antiferromagnetic insulator to ferromagnetic metal at around $x \approx 0.15$ is induced by the double exchange interaction due to the spin canting (de Gennes, 1960). A dimensional crossover behaviour in $La_{1-x}Sr_xMnO_3$ at around $x \approx 0.1$ (Hirota et al., 1996) will also be interpreted by the double exchange interaction. Finally we will show that the characteristics of spin dynamics in the metallic phase of $La_{1-x}Sr_xMnO_3$ can be mapped onto the ferromagnetic

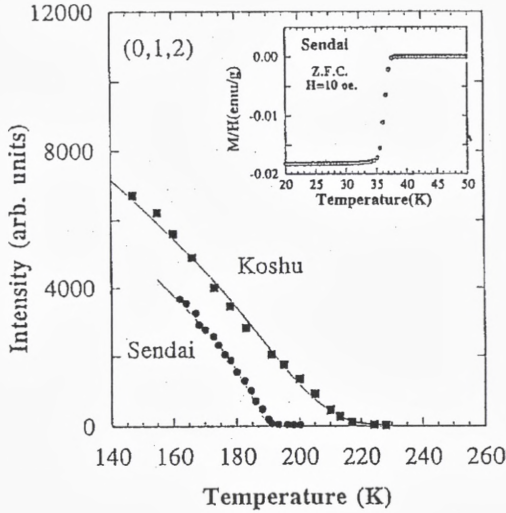Figure 1. Temperature dependence of peak intensities of (0,1,2) superlattice reflection near and below the structural phase transition of $La_{1.85}Sr_{0.15}CuO_4$ single crystals of 'Sendai' ($T_c = 37.3$ K) and 'Koshu' ($T_c = 33$ K). Insert is given the superconducting transition of Sendai crystal (Yamada et al., 1995).

transition metals, such as MnSi (Ishikawa et al., 1985), Ni (Steinvoll et al., 1984), Fe (Wicksted et al., 1984), Pd_2MnSn (Shirane et al., 1985), EuO (Boni and Shirane, 1986) or recently studied CoS_2 (Hiraka, 1996).

Note that the neutron scattering results very much depend on the quality as well as the size of the single crystals, and naturally the single crystal growth is one of the most important research activities in our group. Most of the oxide crystals used for our neutron scattering experiments were grown by the Traveling Solvent Floating Zone (TSFZ) method using the lump-image focusing furnace (Hosoya et al., 1994). This method is very useful for the production of pure and large samples because any impurity can be excluded during the melting and the oxygen atmosphere can be readily controlled as desired. A typical size of the single crystal is 7 mm in diameter and 3–4 cm in length of each rod.

The homogeneity of the grown single crystal of $La_{2-x}Sr_xCuO_4$ was characterized by the sharpness of the tetragonal-orthorhombic structural phase transition as shown in Fig. 1 (Yamada et al., 1995). The temperature dependence of the peak intensities at $(0, 1, 2)$ (Bamb notation) superlattice is shown in our studies, which is proportional to the square of the orthorhombic order parameter. It is well known that the data are described by the rounded power laws of $(T'_t - T)^{2\beta}$,

where the structural phase transition temperature T'_t has a Gaussian distribution with the mean value T_t and a half width $\sigma_{1/2}$; β was held fixed at the 3D XY value of 0.35. $\sigma_{1/2}$ was determined to be 1.4 K and $dT_t/dx = -2600$ K. Thus the experimental result corresponding to an inhomogeneity was determined to be 6×10^{-4} in x. $T_c = 37.3$ K as well as the sharpness in ΔT_c prove the highest quality among existing single crystals used at least for neutron scattering studies. For instance, the other crystals used in the previous experiments show $T_c \approx 33$ K and the inhomogeneity of 4×10^{-3} in x (Matsuda et al., 1994).

The lower energy neutron scattering experiments have been carried out on the triple axis spectrometers of both TOPAN installed at the JRR3 in JAERI and H7 installed at the HFBR in BNL. The high energy time of flight (TOF) neutron scattering experiments have been also made on the chopper spectrometer installed at the pulsed spallation neutron source of ISIS in DRAL.

2 Dynamical susceptibility in superconducting $La_{2-x}Sr_xCuO_4$

2.1 Incommensurate spin fluctuations

Dynamical magnetic susceptibility in low energies, typically less than 20 meV in the superconducting $La_{2-x}Sr_xCuO_4$ is well characterized by the incommensurate spin fluctuations: sharp peaks appear at $Q_\delta = (\pi(1 \pm \delta), \pi)$ and $(\pi, \pi(1 \pm \delta))$ in the 2D reciprocal space of the square lattice representation (Matsuda et al., 1994; Mason et al., 1992). As shown in Fig. 2, the magnetic peaks which correspond to four rods extending along $[0, 0, L]$ intersect the $(H, K, 0)$ plane at Q_δ. First, we present the doping effect of the wave vector of the incommensurate spin fluctuations, i.e. x–δ relationship.

As mentioned earlier, the experimental data specifying a relation between spin correlations and/or fluctuations and electronic properties, such as the carrier densities of the doping holes, should be very sensitive to the crystal quality. Systematic experiments combining careful neutron scattering measurements with precise bulk measurements can only provide the reliable determination of the wave vector (δ) of the incommensurate spin fluctuations, the development of the spin correlations, chemical composition, the super-conducting temperature (T_c), and consequently x–δ. Since we must determine these values for the crystals of different x, we tried to keep the identical single-crystal growth condition of the TSFZ method and post-growth heat treatment, as well. We have also minimized possible errors in various stages of the experimental process. The experimental error was determined to be no more than 0.008 in nominal x, which is accurate enough for the present purpose.
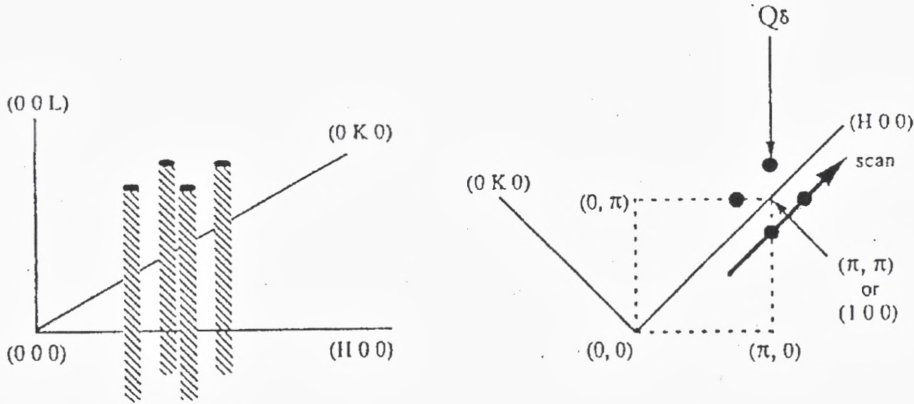
Figure 2. The schematic drawing of the 2D incommensurate spin fluctuations. 4 rods are located at $Q_\delta = (\pi, \pi(1 \pm \delta))$ and $(\pi(1 \pm \delta), \pi)$ in the c plane. δ is 0.24 rlu for $x = 0.15$.

The accuracy of δ is seen in the following figures (Yamada et al., 1996).

We have already presented a nonlinear x–δ relation (Endoh et al., 1992). We can now show unambiguously the nonlinearity, which is shown in Fig. 3. It must be emphasized here that the double peaked spectra become noticeable above $x = 0.05$, approximately corresponding to the superconducting phase boundary. Precisely speaking, x–δ is approximately linear in $x > 0.05$ with slight deviation downwards occurring beyond $x \approx 0.12$. Note that previous neutron scattering studies with the most recent result show the single peaked spectra centered at (π, π) at $x < 0.04$. We have also obtained a surprising result that δ is proportional to T_c in the latest investigation, which is presented in the same figure. We argue that this result should be a direct evidence of a causal relation of the superconductivity and incommensurate spin fluctuations in the single layered superconductors of the $La_{2-x}Sr_xCuO_4$ crystals.

As for the result of the incommensurate spin correlations in the superconducting state of the $La_{2-x}Sr_xCuO_4$ crystals, several models are proposed. The first model is the nesting of the large hole band at the Fermi energy (Si et al., 1993). The second is the possible existence of a stripe phase of doped holes with the periodic antiferromagnetic regions in between (Kievelson and Emery, 1996) and finally the third is the frustration of the Cu^{2+} spins caused by doped holes (Aharony et al., 1989), which eventually induces the periodic modulated spin structure. Related to the first model of the d–p band picture, the incommensurate spin fluctuations was
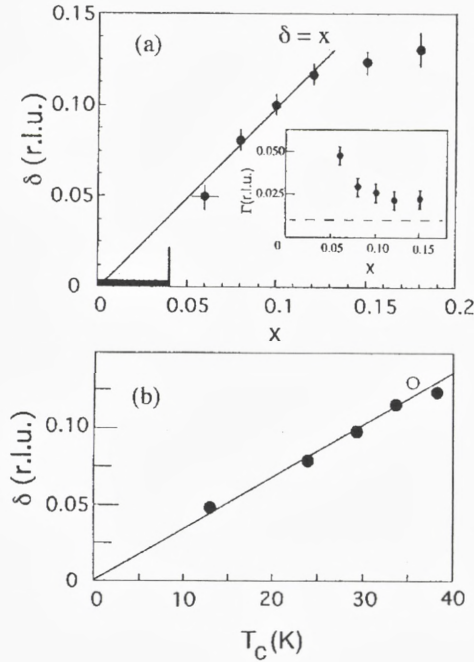
Figure 3. Incommensurability, δ plotted with respect to x in top. $\delta = 0$ for $x < 0.04$ is represented by thick line in the figure. The insert is the line width in q for $\omega = 2$ meV scan. The bottom panel shows the relationship between δ and the superconducting transition temperature, T_c (Yamada et al., 1996).

also predicted by the model started from the t-J model (Zhang and Rice, 1988). The d-band nature of $La_{2-x}Sr_xCuO_4$ is introduced and therefore it is defined as an extended t-J model (Fukuyama et al., 1994). Then an enhanced peak appears at the wave vectors, $Q_\delta = (\pi(1 \pm \delta), \pi)$ and $(\pi, \pi(1 \pm \delta))$, instead of (π, π) for the t-J model only. The relation of x–δ calculated by the extended t-J model quite resembles the experimental observation, except the δ which starts finite from $x = 0.1$ in calculation (Tanamoto, 1995). In the second model, the phase separation ascribes the competition between the long range Coulomb interaction and the broken exchange bond energy. This model became lively because of its successful interpretation of the charge ordering and modulated antiferromagnetic structure in the insulating phase of $(La_{0.6}Nd_{0.4})_{0.88}Sr_{0.12}CuO_4$ and La_2NiO_{4+y} (Tranquada et al., 1995). As far as we understand, δ in this model is mainly controlled by the concentration of the doped charge. In this respect, we observed that δ in the insulating La_2NiO_{4+y} or $La_{2-x}Sr_xNiO_4$ (Nakajima et al., 1996) is proportional to the doping

concentration of either y or x. Note that in these nickelate oxides, the charge ordering was confirmed experimentally together with the oxygen staging of the regular stacking along the crystalline c axis. On the other hand, there has been no detection of the moving domain walls in superconducting $La_{2-x}Sr_xCuO_4$. Therefore it seems to us very difficult to extend this phase separation model straightforwardly to the superconducting phase.

2.2   Hierarchical structure in spin dynamics in superconducting phase

The magnetic scattering at 4 K is buried in the experimental background, though the sharp peaks appear at Q_δ in the normal state above T_c as mentioned above (Yamada et al., 1995). We searched the careful temperature dependence of the scattering showing the exponential decay of the scattering intensity towards $\omega = 0$, and $T = 0$, and then we evaluated the energy gap, ω_c, in spin excitations to be 3.5 meV at $\delta = 0.24$ in the superconducting state, shown in Fig. 4. The superconducting gap energy, Δ_0 is estimated at 11 meV by the following equation proposed by the t-J model (Tanamoto et al., 1994)

$$\omega_c = \Delta_0 \sin(\pi\delta/2)\,.$$

This evaluation also directly brings a conclusion for the long time issue concerning the symmetry of the superconducting wave function in a high T_c superconductors. The t-J model predicted that the unconventional superconductivity gives rise to the $d_{x^2-y^2}$ wave symmetry and the ratio of $2\Delta_0/T_c$ is about seven, which is consistent with the experimental results as well.

Let us proceed to another aspect of higher energy excitations which have been studied to comprehend the overall feature of the unique spin fluctuations in the superconducting state (Yamada et al., 1994). Our experimental data are essentially the same as are shown in the recent publication (Hayden et al., 1996), but the most recent data are much improved with a good signal to noise ratio. Magnetic excitations in the superconducting state well below T_c show that the strong 2D antiferromagnetic spin correlations in the undoped La_2CuO_4 (Hayden et al., 1992; Itoh et al., 1993) is not drastically renormalized by doping of holes even in the superconducting state. This phenomenon is expressed from a different point of view such that the low energy spin dynamics influenced by the conduction electrons of doped holes change to the dynamics of localized spins at Cu^{2+} sites in a higher energy range.

Unlike the magnetic excitation or $S(q,\omega)$ in $YBi_2Cu_3O_7$ (Fong et al., 1995), $La_{1.85}Sr_{0.15}CuO_4$ has a featureless spectra in which the broad peak centered at (π,π) extends to the cut-off energy of 280 meV. It must be noted that we can hardly
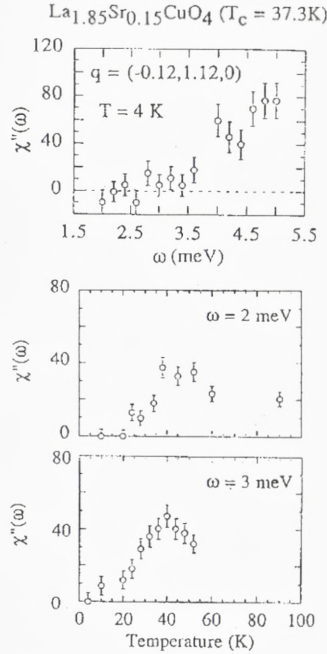
La$_{1.85}$Sr$_{0.15}$CuO$_4$ (T$_c$ = 37.3K)

Figure 4. $\chi''(q = Q_\delta, \omega)$ is plotted as the function of transfer energy, ω at $T = 4$ K (top). Temperature dependence for $\omega = 2$ meV (middle), and 3 meV (bottom) are also shown (Yamada et al., 1995).

determine any specific structure in energy, though Hayden et al. (1996) claimed a shallow peak at around 20 meV in $\chi''(\omega)$. The cut off energy determined to be as high as 280 meV is essentially the same as the zone boundary energy of spin-wave excitation, just above 300 meV in La$_2$CuO$_4$ taking account of the considerable energy broadening in the doped crystal. We argue that we could define another type of crossover or a hierarchical structure in spin dynamics clarifying from the metallic character in the low energy to the localized one in high energy.

Related to this particular point, the qualitatively resembled magnetic excitation spectra have been observed in the Spin Density Wave (SDW) state of Cr at low temperatures well below the ordering temperature (T_N) (Endoh et al., 1994; Fukuda et al., 1996). In energies lower than about 15 meV, the sharp peaks appear at $Q = (\pi/a)(1 \pm q_{\text{SDW}}, 0, 0)$ where q_{SDW} is the SDW wave vector. In this case of the SDW, another peak centered at $Q = (1, 0, 0)$ of the antiferromagnetic reciprocal reflection takes over the incommensurate peaks at higher energies. (Fig. 5) The
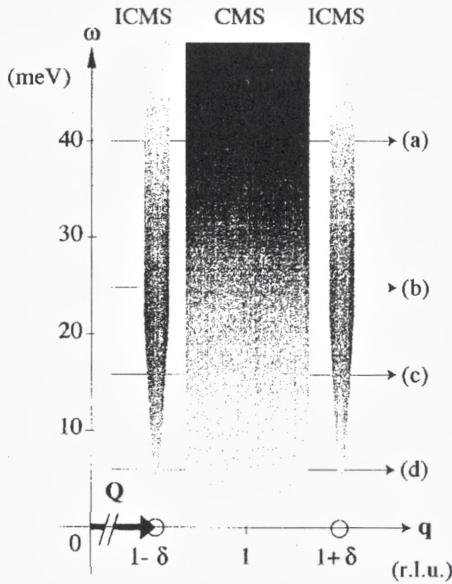
Figure 5. Schematic drawing of magnetic excitations from the SDW state in Cr. ICMS and CMS, respectively represent incommensurate and commensurate magnetic scattering. δ is the SDW wave vector in rlu unit.

magnetic excitations are still distinguishable from the background in very higher energies above 500 meV. Since the excitation energy goes up to eV regions, the cut off energy of the excitation could hardly be determined in the current experimental conditions. Although the phenomena are very much similar in two cases, the physics does not seem to be quite identical. In the present case of the high T_c superconductor, we look at the excitations from the magnetically disordered state. On the other hand, the magnetic excitation in Cr are from the ordered SDW. Usually any RPA calculation based on the two band model could predict spin wave mode which is presented by the linear dispersion relation of $w^\pm = A(q_{\text{SDW}} \pm q)$ from the SDW ordered state. In fact, the observed magnetic excitations are not so simple. As just mentioned above, the excitations have a triple peak structure. The energy spectra or $\chi''(\omega)$ of the SDW state in Cr gives a broad peak around 20 – 50 meV. Although we cannot find a reasonable interpretation, we can point out a remarkable similarity that both materials exhibit the sharp excitation peaks centered at the incommensurate wave vector dominates in lower energy and the single broad peak centered at the commensurate wave vector takes over as the excitation energy increases. The cut off energy is very large of the order of 1000 K or above

in both cases.

3 Spin dynamics in colossal magnetoresistance oxides

Tokura et al. (1995) first claimed that the colossal magnetoresistance phenomena in the metallic $La_{1-x}Sr_xMnO_3$ ($x < 0.3$) near below T_c should inherit the concept that the $LaMnO_3$ is the Mott–Hubbard insulator. Since then, this system became the important class of materials in the 'strongly correlated electron systems'. We have started neutron scattering experiments in order to elucidate the physical origin of the strange properties of the colossal magnetoresistance (CMR) from a view point of the strongly electron correlation effect, which should be active in the dynamical spin structure. It must be emphasized here that in a narrow range of x for $A_{1-x}M_xMnO_3$, where A = divalent alkaline metal cations, M = trivalent alkaline earth cations, there appear many complicated phase transitions. It should also be noted here that the classical neutron diffraction experiments studied by Wollan and Koehler (1955) from powdered samples of $La_{1-x}Sr_xMnO_3$ are still valuable, since all the complicated magnetic structures and lattice symmetries for the whole x range were determined. Nevertheless, mutual competing interactions among spins, charge and lattice as well as the change of the electron correlations upon doping of holes are naturally expected.

We understand well that the double exchange interaction leads to the transition from antiferromagnetic insulator to ferromagnetic metal upon doping of Sr (de Gennes, 1960), associated with increase of the spin canting. Furthermore the lattice structure at $x \approx 0.175$ shows a successive structural phase transition in thermal evolution, where the largest CMR effect is observed (Urushibara et al., 1995).

We first present here well defined spin-wave scattering in the ordered state of all the crystals of $La_{1-x}Sr_xMnO_3$ with $x = 0$, 0.05, 0.12, 0.2 and 0.3. The spin-wave dispersion in the antiferromagnetic phase of $LaMnO_3$ ($x = 0$) is very anisotropic as shown in Fig. 6 (Hirota et al., 1996). It is like a 2D dispersion relation; a typical ferromagnetic curve in the $(H\,K\,0)$ plane in the orthorhombic notation. The zone boundary energy is larger than the energy corresponding to $T_N = 140$ K. On the other hand, the observed dispersion curve along $[0\,0\,L]$ is a typical antiferromagnetic spin-wave dispersion relation with a remarkably lower zone boundary energy than the other. This anisotropic spin-wave dispersion reflects the order parameter of the staggered magnetization near below T_N. The critical index of the order parameter, β is about 0.2, which is far smaller than any of those of 3D antiferromagnets. Therefore $LaMnO_3$ is considered to be a quasi 2D antiferromagnet; the 2D ferromagnetic lattices stacking along the c axis antiferromagnetically. Note that
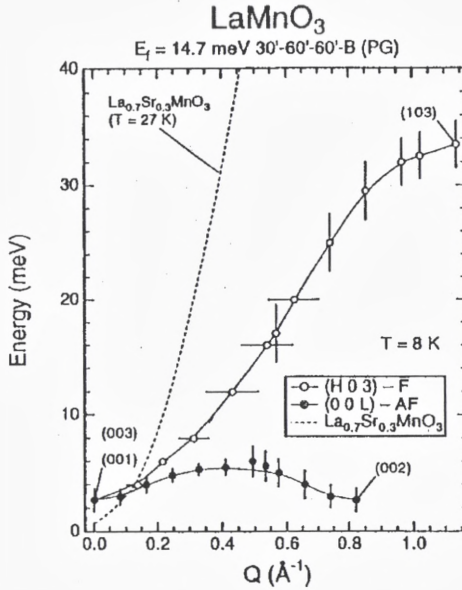
Figure 6. Spin-wave dispersion curves of LaMnO$_3$ along (100) and (001) directions (orthorhombic notation). The isotropic ferromagnetic spin-wave dispersion of La$_{0.7}$Sr$_{0.3}$MnO$_3$ is shown as the reference (Hirota et al., 1996).

the crystal structure is nearly isotropic with orthorhombic distortions as mentioned below. The 2D magnetic character should reflect the orbital order of $(3x^2 - r^2)$ and $(3y^2 - r^2)$ in the e_g band (Goodenough, 1955). Although the real lattice structure of LaMnO$_3$ is distorted to orthorhombic, Pbnm as the result of the Jahn-Teller effect, the orbital order itself as well as the 2D ferromagnetic character was predicted by Kanamori who considered extensively the superexchange mechanism in various $3d$ orbitals in the cubic crystalline field (Kanamori, 1959). It should be remarked that there is a considerable energy gap in the spin wave, about 2.5 meV at $q = 0$.

At elevated temperatures, only low energy spin excitations in small q are renormalized, as expected, leaving the higher energy part a little changed. This means that the antiferromagnetic order is controlled by $\sqrt{J'J}$, where J', interlayer exchange and J, intralayer exchange interaction. The strong intralayer magnetic interaction is the consequence of the squared ferromagnetic lattice with the 180° superexchange interaction. The magnetic excitations in $x = 0.05$ crystal are essentially similar to those of the undoped crystal, but the energy dispersion along the c axis is nearly constant; more complete 2D character.

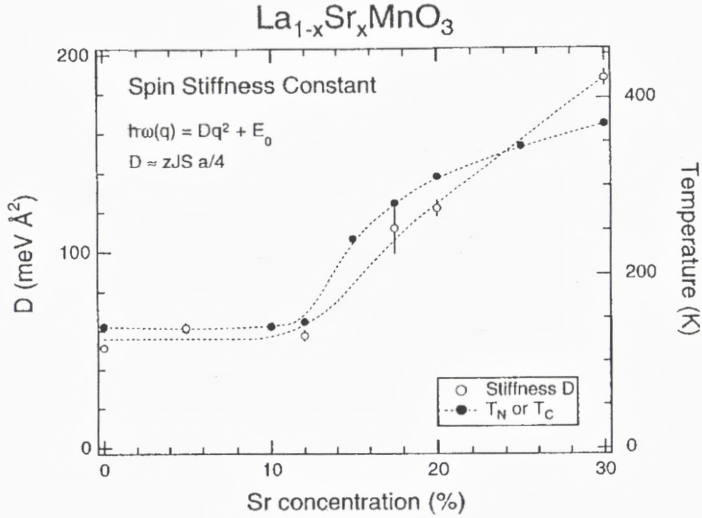On the contrary, we found the very isotropic 3D ferromagnetic spin-wave dis-

$$La_{1-x}Sr_xMnO_3$$

Figure 7. Spin-wave stiffness constant, D and the magnetic transition temperature $(T_N$ or $T_c)$ are plotted with respect to doping concentration of Sr.

persion curve when x reaches approximately 0.1. The zone boundary energies are beyond the experimental condition of the triple axis spectroscopy with thermal neutrons, but the exchange integral could be well estimated from the lower part of spin-wave dispersion or spin-wave stiffness constant D, which was reproduced by the motion of equation in terms of the model Heisenberg Hamiltonian with nearest neighbour exchange only. An important finding here is the fact that the exchange integral or the nearest neighbour interaction increases steadily with x, which almost coincides with the change in T_c as the function of x (Fig. 7).

The 2D ferromagnetic feature characterized the magnetism of the insulating $LaMnO_3$ reflects the orbital order of $3x^2 - r^2$ and $3y^2 - r^2$ in e_g band. Therefore this gives rise to the evidence of the orbital order and furthermore that the crossover effect becomes evident from the 2D ferromagnetic feature to 3D ferromagnetic character of metallic phase, besides the antiferro- to ferromagnetic transition. We remark that this magnetic transition occurs at $0.05 < x < 0.1$, where the conductivity still behaves like the semiconductor or insulator. This means that the metallic feature in spin dynamics is already visible below the lower doping level than the actual metal-insulator transition appears.

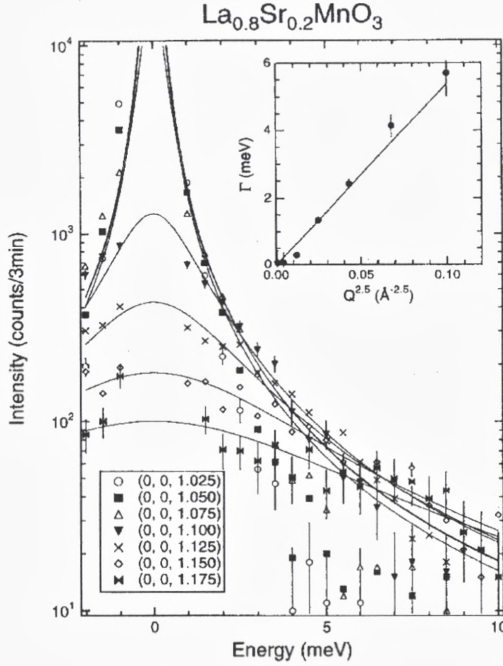Paramagnetic scattering in small q region which has a double Lorentzian func-

Figure 8. Lorentzian fitting of the magnetic critical scattering in $La_{0.8}Sr_{0.2}MnO_3$.

tion with respect to energy and momentum is represented as follows,

$$S(q,\omega) \quad \propto \quad \frac{\hbar\omega/kT}{1-\exp(-\hbar\omega/kT)}kT\chi(0)\frac{\kappa_1^2}{\kappa_1^2+q^2}\cdot\frac{\Gamma}{\Gamma^2+\omega^2}$$

$$\kappa_1 \quad = \quad \kappa_0(1-T/T_c)^{-\nu}$$

$$\Gamma \quad = \quad Aq^{2.5}\left\{1+(\kappa_1/q)^2\right\}$$

where A and κ_0 characterize the dynamical feature. As shown in Fig. 8, the analysis by introducing the double Lorentzian functional form is reasonable and in particular A was determined by the theoretical result of the critical scattering from the Heisenberg ferromagnet (Marshall and Lovesey, 1971). The scattering intensity contour presents a characteristic feature of $\chi''(q,\omega)$ in the Heisenberg ferromagnets. We emphasize here that the paramagnetic scattering just above T_c in the most of typical transition metal ferromagnets like Fe, Ni, Pd_2MnSn, EuO, MnSi or even recently observed CoS_2 obeys the double Lorentzian shape, and importantly the intensity contour map observed in the ferromagnets becomes quite universal when the map is scaled by these two characteristic parameters of A and κ_0. The result

of the scaling analysis is shown in the Table I. From the accumulated values of
ratio of T_C^{MF}/T_C (T_C^{MF} = mean field Curie temperature) and A/T_C or D/T_C we
just phenomenologically argue that these ratios represent a degree of the electron
correlations. Stronger the electron correlation, the smaller the ratio, approaching
unity as is expected. Inversely, when the kinetic energy or transfer energy is large,
consequently the ratio becomes large. The important points addressed here is that
the ratio of metallic $La_{1-x}Sr_xMnO_3$ is the same as that of Fe, as shown in Table I.
Then if we define the metallic $La_{1-x}Sr_xMnO_3$ as the strongly electron correlated
system, how do we think the ferromagnetic nature in metallic Fe? Even it is very
important the fact that almost all the metallic ferromagnets have the similar ratios
with each other.

Table I. Various quantities characterizing the dynamical ferromagnetic properties in
typical transition metals of EuO, Pd$_2$MnSn,Fe, CoS$_2$, MnSi and Ni compared with
the ferromagnetic phases of La$_{1-x}$Sr$_x$MnO$_3$ ($x = 0.3$, and $x = 0.2$). A and A^* in
the table were evaluated by the present author from the original papers. Note that
d^* and A^* are, respectively, inverse nearest neighbour distance and reduced value
of A with respect to d^*.

	T_C (K)	$D(0.8T_C)$ (meVÅ^2)	A (meVÅ$^{2.5}$)	d^* (Å^{-1})	A^*/T_C
EuO	69	7.4	8.3	2.1	0.77
Pd$_2$MnSn	190	70	60	1.7	1.2
Fe	1040	175	140	3.1	2.3
CoS$_2$	121	106	71	2.0	3.1
MnSi	30	50	20	1.9	3.3
Ni	631	330	330	3.1	9.4
La$_{0.7}$Sr$_{0.3}$MnO$_3$	378	114	≈ 70	2.9	≈ 2.7
La$_{0.8}$Sr$_{0.2}$MnO$_3$	316	89	54	2.9	2.5

Finally, as far as spin dynamics is concerned, the spin dynamics in metallic
$La_{1-x}Sr_xMnO_3$ is quite normal in all temperature range we have studied. Con-
comitantly there is no clear evidence that phonon softening occrs in the vicinity of
the magnetic phase transition. It should be noted that the lattice distortion from
the cubic perovskite to either rhombohedral or orthorhombic symmetry is far larger
than the typical (anti-)ferroelectric perovskites like $SrTiO_3$ (Shirane, 1959). Since
the specific mechanism of the colossal magnetoresistance is not fully understood
yet, in particular the relation or the interplay among electron (charge), orbital

(electron-phonon coupling) and spins, further experimental explorations must be very important.

Acknowledgements

References

Aharony A, Birgeneau RJ, Coniglio A, Kastner MA and Stanley HE, 1988: Phys. Rev. Lett. **60**, 1330

Birgeneau RJ and Shirane G, 1989: *Physical Properties of High temperature Superconductors*, ed. by D.M. Ginzburg (World Scientific, Singapore) p. 151

Boni P and Shirane G, 1986: Phys. Rev. B **33**, 3012

de Gennes PG, 1960: Phys. Rev. **118**, 141

Endoh Y, 1989: Phase Transitions **15**, 223

Endoh Y, Yamada K, Matsuda M, Nakajima K, Kuroda K, Hidaka Y, Tanaka I, Kojima H, Birgeneau RJ, Kastner MA, Keimer B, Shirane G and Thurston TR, 1992: Jap. J. Appl. Phys. **7**, 174

Endoh Y, Fukuda T, Yamada K and Takeda M, 1994: J. Phys. Soc. Jpn. **63**, 3572

Fong HF, Keimer B, Anderson PW, Reznik D, Dogan F and Aksay A, 1995: Phys. Rev. Lett. **75**, 316

Fukuda T, Endoh Y, Yamada K, Takeda M, Itoh S, Arai M and Otomo T, 1996: J. Phys. Soc. Jpn. **65**, 1418

Fukuyama H, Kohno H and Tanamoto T, 1994: J. Low. Temp. Phys. **95**, 309

Goodenough JB, 1955: Phys. Rev. **100**, 564

Gutzwiller MC, 1963: Phys. Rev. Lett. **10**, 159

Hayden SM, Aeppli G, Mook HA, Cheong SM and Fisk Z, 1990: Phys. Rev. B **40**, 10220

Hayden SM, Aeppli G, Mook HA, Perring TG, Mason TM, Cheong SM and Fisk Z, 1996: Phys. Rev. Lett. **76**, 1344

Hiraka H, 1996: Thesis (Tohoku Univ.)

Hirota K, Kaneko N, Nishizawa A and Endoh Y, 1996: J. Phys. Soc. Jpn. **65**, Dec. issue

Hosoya S, Lee CH, Wakimoto S, Yamada K and Endoh Y, 1994: Physica C **235-240**, 547

Hubbard J, 1963: Proc. Roy. Soc. **A276**, 238

Ishikawa Y, Noda Y, Uemura, YJ, Majkrzak CF and Shirane G, 1985: Phys. Rev. B **31**, 5884

Itoh S, Yamada K, Arai M, Endoh Y, Hidaka Y and Hosoya S, 1994: J. Phys. Soc. Jpn. **63**, 4542

Kanamori J, 1959: J. Phys. Chem. Solids **10**, 87

Kanamori J, 1963: Prog. Theor. Phys. **30**, 275

Kievelson SA, and Emery VJ, 1994: *Strongly Correlated Electronic Materials*, eds. K.S. Bedell et al. (Addison Wesley, Redwood City) p. 619

Mason TE, Aeppli G, Mook HA, 1992: Phys. Rev. Lett. **68**, 1414

Marshall W and Lovesey SM, 1971: *Theory of Thermal neutron Scattering* (Clarendon Press, Oxford)

Matsuda M, Yamada K, Endoh Y, Thurston TR, Shirane G, Birgeneau RJ, Kastner MA, Tanaka I and Kojima H, 1994: Phys. Rev. B **49**, 6958

Nakajima K, Endoh Y, Hosoya S, Wada J, Welz D, Mayer HM, Graf HA and Steiner M, 1996: (submitted)

Samuelsen EJ, Andersen E and Feder J, 1972: *Proceeding of the NATO Advanced Study on Structural Phase Transitions and Soft Modes* (Plenum, New York)

Shirane G, 1959: Acta Cryst. **12**, 282

Shirane G, Uemura YJ, Wicksted JP, Endoh Y and Ishikawa Y, 1985: Phys. Rev. B **31** 1227

Shirane G, Birgeneau RJ, Endoh Y and Kastner MA, 1994: Physica B **197**, 158

Si Q, Zha Y, Levin K and Lu JP, 1993: Phys. Rev. B **47**, 9124

Steinvoll O, Majkrzak CF, Shirane G and Wicksted J, 1984: Phys. Rev. B **30**, 2377

Tanamoto T, Kohno H and Fukuyama H, J.Phys.Soc.Jpn., 1994: **63**, 2739

Tanamoto T, 1995: Thesis, (Univ. Tokyo)

Tokura Y, Urushibara A, Moritomo Y, Arima T, Asamitsu A, Kido G and Furukawa N, 1995: J. Phys. Soc. Jpn. **63**, 3931

Tranquada JM, Steinlieb BJ, Axe JD, Nakamura Y and Uchida S, 1995: Nature **375**, 561

Urushibara A, Moritomo Y, Arima T, Asamitsu A, Kido G and Tokura Y, 1995: Phys. Rev. B **51**, 14103

Wicksted JP, Boni P and Shirane G, 1984: Phys. Rev. B **30** 3655

Wollan EO and Kohler WC, 1955: Phys. Rev. **100**, 545

Yamada K, Endoh Y, Lee CH, Wakimoto S, Arai M, Ubukata K, Fujita M, Hosoya S and Bennington SM, 1994: J. Phys. Soc. Jpn. **64**, 2742

Yamada K, Wakimoto S, Shirane G, Lee CH, Kastner MA, Hosoya S, Greven M, Endoh Y and Birgeneau RJ, 1995: Phys. Rev. Lett. **75**, 1626

Yamada K, Wada J, Kurahashi K, Lee CH, Kimura Y, Wakimoto S, Endoh Y, Hosoya S, Shirane G, Birgeneau RJ and Kastner MA, 1996: (submitted)

Zhang FC and Rice TM, 1988: Phys. Rev. B **37**, 3759

Routes to Heavy Fermions

Peter Fulde

Max–Planck-Institut für Physik komplexer Systeme

Bayreuther Str. 40, D-01187 Dresden, Germany

Abstract

Heavy-fermion excitations require the presence of a low-energy scale in the system. In recent years it has become clear that these scales can result from rather different physical processes. The Kondo effect is one of them, certainly the one most studied. We describe and discuss in addition to Kondo lattices two other sources of heavy quasiparticles: the Zeeman route to heavy fermions which applies to $Nd_{2-x}Ce_xCuO_4$ ($0.1 \leq x \leq 0.2$) and a scenario of nearly half-filled Hubbard chains which is related to the semimetal Yb_4As_3. It is suggested that these are not the only processes leading to heavy-fermion behaviour.

1   Introduction

The investigation of heavy-fermion systems with heavy-quasiparticle excitations has developed into a new branch of low-temperature physics. Recent reviews have been given of theoretical (Lee et al., 1986; Fulde et al., 1988; Schlottmann, 1984; Zwicknagl, 1993; Norman and Koelling, 1993; Kasuya, 1993; Hewson, 1993) and experimental (Stewart, 1984; Ott, 1988; Grewe and Steglich, 1991; Wachter, 1994) developments in this field. In most cases these compounds contain Ce, Yb, U or Np as one of their constituents, implying that $4f$ or $5f$ electrons are involved. Examples are the metals $CeAl_3$, $CeCu_2Si_2$, $CeRu_2Si_2$, $CeCu_6$, $YbCu_2Si_2$, UBe_{13}, UPt_3, and $NpBe_{13}$. But also the electron-doped cuprate $Nd_{2-x}Ce_xCuO_4$ shows heavy-fermion behaviour (Brugger et al., 1993) in the range of $0.1 \leq x \leq 0.2$. Heavy-fermion excitations have also been found in semimetals like Yb_4As_3, Sm_3Se_4 or in some of the Ce and Yb monopnictides and even in insulators like YbB_{12} or SmB_6 (see, for example, Proc., 1995).

We speak of heavy-fermion behaviour when a system meets the following conditions: (a) The low temperature specific heat $C = \gamma T$ has a coefficient γ of order $1\ Jmol^{-1}K^{-2}$, rather than $1\ mJmol^{-1}K^{-2}$ as, e.g., found for sodium metal; (b) the Pauli susceptibility χ_s is similarly enhanced as γ; (c) the ratio $R = \pi^2 k_B^2 \chi_s / (3\mu_{\text{eff}}^2 \gamma)$

(Sommerfeld–Wilson ratio) is of order unity. Here μ_{eff} is the effective magnetic moment of the quasiparticles. Both quantities γ and χ_s are proportional to the quasiparticle density of states at the Fermi level $N^*(0)$. The latter is proportional to m^*, i.e., the effective mass of the fermionic excitations. Large values of γ and χ_s can therefore be interpreted by ascribing a large m^* to the quasiparticles. When R is calculated, the density of states $N^*(0)$ drops out. For free electrons $R = 1$, while in the presence of quasiparticle interactions $R = (1 + F_0^a)^{-1}$. The Landau parameter F_0^a relates to the interactions and enters χ_s. When conditions (a)–(c) are met, we may assume a one-to-one correspondence between the quasiparticle excitations of the complex system and those of a free electron gas, provided we use the effective mass m^* and, in the case of semimetals or insulators, the effective charge e^*, instead of the corresponding bare quantities.

Heavy-fermion behaviour requires the presence of a low-energy scale in the system. Usually, that scale is characterized by a temperature T^*. As the temperature of the system increases to values above T^*, the quasiparticles lose their heavy-mass character. The specific heat levels off, and the susceptibility changes from Pauli- to Curie-like behaviour. With increasing temperature the rare-earth or actinide ions behave more and more like ions with well-localized f electrons.

One key problem is to understand the physical origin of the low-energy scales. Until few years ago, it was commonly believed that the Kondo effect is the sole source of heavy-fermion behaviour. The physics associated with the Kondo effect is extensively described in a monograph by Hewson (1993) and a number of reviews (Lee at al., 1986; Fulde et al., 1988; Schlottmann, 1984; Zwicknagl, 1993; Norman and Koelling, 1993; Kasuya, 1993). However, more recently it has been found that heavy quasiparticles may result from rather different physical effects. In all cases a lattice of $4f$ (or $5f$) ions is involved. In metallic systems it is coupled to conduction electrons. In that case the conduction electrons can be either weakly correlated like in CeAl$_3$, or they can be strongly correlated like in the high-T_c cuprates. In the latter case the correlations are perhaps not as strong as those of the f electrons, but they may influence substantially the physical properties of the system. This situation is encountered, e.g., in Nd$_{2-x}$Ce$_x$CuO$_4$ and it will be shown later that here the Zeeman effect is responsible for the formation of heavy fermions. In a semimetal like Yb$_4$As$_3$, the heavy quasiparticles result from the $4f$ electron system itself, i.e., without having a coupling to conduction electrons crucially contributing. Thus, instead of having one single physical origin, heavy fermions may have a variety of effects responsible for their existence.

Obviously, the low-lying excitations characterizing heavy-fermion systems involve predominantly spin degrees of freedom. Direct evidence is given by the amount of entropy associated with the excess specific heat. The latter is associated with an entropy of order $S \simeq k_B \ln \nu_f$ per f site, where ν_f denotes the degeneracy

of the crystal-field ground state of the atomic f shell. It is pretty safe to state that in all likelihood yet unknown mechanisms will add to the presently known ones. In the following, a discussion is given of the three routes to heavy-fermion behaviour just outlined.

2   Kondo lattices

The essence of the single-site Kondo effect is the formation of a singlet ground-state due to a weak hybridization of the incomplete $4f$ shell with the conduction electrons. A specific form of the singlet wavefunction is obtained by starting from the Anderson impurity Hamiltonian

$$
\begin{aligned}
H &= \sum_{km} \epsilon(k) c_{km}^+ c_{km} + \epsilon_f \sum_m n_m^f + \frac{U}{2} \sum_{m \neq m'} n_m^f n_{m'}^f + \\
&+ \sum_{km} V(k)(f_m^+ c_{km} + c_{km}^+ f_m) + \tilde{H}_0.
\end{aligned}
\tag{1}
$$

Here f_m^+ denotes the creation operator of an f electron in state m of the lowest J multiplet and $n_m^f = f_m^+ f_m$. The f-orbital energy is ϵ_f and U is the $f - f$ Coulomb repulsion. The c_{km}^+ create conduction electrons with momentum $|\mathbf{k}| = k$ and the three quantum numbers $\ell = 3$, J and m. The hybridization between the f and conduction electrons is given by the matrix element $V(k)$. Finally, $\tilde{H}_0$ contains all those degrees of freedom of the conduction electrons which do not couple to the impurity. The following ansatz for the singlet ground-state wave function is due to Varma and Yafet (1976).

$$
| \psi_0 \rangle = A \left(1 + \frac{1}{\sqrt{\nu_f}} \sum_{km} \alpha(k) f_m^+ c_{km} \right) | \phi_0 \rangle
\tag{2}
$$

where $| \phi_0 \rangle$ represents the Fermi sea of the conduction electrons. The ansatz (2) is closely related to the one suggested by Yoshida (1966; see also Yoshida and Yoshimori, 1973) for the ground state of the Kondo Hamiltonian. The variational parameters A and $A\alpha(k)$ are obtained by minimizing the energy. The energy E_0 of $| \psi_0 \rangle$ is always lower than the one of the multiplet $| \psi_m \rangle = f_m^+ | \phi_0 \rangle$. The difference ϵ is found to be

$$
\epsilon = -D \exp[- | \epsilon_f | /(\nu_f N(0) V^2)]
\tag{3}
$$

and denotes the energy gain due to the formation of the singlet. Here D is half of the bandwidth of the conduction electrons and $N(0)$ is their density of states per spin direction at the Fermi energy. It is customary to associate with this energy gain a temperature T_K, i.e., the Kondo temperature. The singlet-triplet

excitation energy is often of the order of a few meV only, and provides a low-energy scale. When a lattice of f ions is considered like, e.g., CeAl$_3$ the Anderson lattice Hamiltonian replaces Eq. (1). The energy scale $k_B T_K$ is replaced here by $k_B T^*$ which takes into account modifications in the presence of the lattice, i.e., due to interactions between different f sites. The energy gain due to singlet formation competes here with the one due to the RKKY interaction when the f sites are in a magnetic state (Doniach, 1971, 1987). In the limit of small hybridization V the RKKY interaction energy always wins out because it is proportional to V^4 while the singlet-formation energy depends exponentially on V, see Eq. (3), and therefore is smaller. This seems to be the case in systems like CeAl$_2$, CePb$_3$ and NpBe$_{13}$ which become antiferromagnets at low temperatures.

In addition to T^* there exists another characteristic temperature $T_{\mathrm{coh}} < T^*$ below which the local singlet-triplet excitations lock together and form coherent quasiparticles with large effective masses. The details of this coupling are not yet understood, but de Haas–van Alphen measurements demonstrate convincingly that the f electrons behave like delocalized electrons. At the Fermi surface they show strong anisotropies in the effective mass. It is somewhat surprising that one can calculate the Fermi surface of a heavy-electron system and determine the anisotropic masses with one adjustable parameter only. This is achieved by renormalized band-structure calculations (Zwicknagl, 1993, 1990; Razafimandimby et al., 1984; d'Ambrumenil and Fulde, 1985; Sticht et al., 1986; Strange and Newns, 1986; Zwicknagl et al., 1990). Thereby the effective potential seen by a quasiparticle is described by energy-dependent phase shifts $\eta_\ell^A(\epsilon)$ of the different atoms A. The index ℓ refers to the different angular momentum channels.

In the following we consider CeRu$_2$Si$_2$ as an example (Zwicknagl, 1993, 1990; Zwicknagl et al., 1990). The essential point is to use for the phase shifts the ones computed within the local-density approximation (LDA) to density functional theory, with the exception of the $\ell = 3$ phase shift of the Ce ion. This approximation neglects the coupling of conduction electrons to different configurations of the $4f$ or $5f$ shell with *fixed* f electron number. [The mass enhancement of the conduction electrons of Pr metal falls into that category. It results from the virtual transitions between different crystal-field eigenstates of the $4f^2$ system caused by the coupling between conduction and $4f$ electrons (Fulde and Jensen, 1983; see also White and Fulde, 1981)]. Thus, only the $\eta_{\ell=3}^{\mathrm{Ce}}(\epsilon)$ phase shift remains undetermined. According to Hund's rules the ground-state multiplet of the $4f^2$ configuration of Ce is $J = 5/2$ with the $J = 7/2$ multiplet being much higher in energy. Therefore, we may set $\eta_{J=7/2}^{\mathrm{Ce}}(\epsilon_F) = 0$. Of the $J = 5/2$ multiplet, only the Kramers-degenerate crystal-field ground state is considered, because it is the only state occupied at low temperatures. Let τ denote the degeneracy index of that ground state. Only the phase shift $\eta_\tau^{\mathrm{Ce}}(\epsilon_F)$ among the different $\ell = 3$ channels differs then from zero. It

must contain the strong correlations of the $4f$ electrons and is unknown. In the spirit of Landau's Fermi liquid theory we expand this unknown function around the Fermi energy and write

$$\eta_\tau^{Ce}(\epsilon) = \eta_\tau^{Ce}(\epsilon_F + a(\epsilon - \epsilon_F) + O((\epsilon - \epsilon_F)^2). \tag{4}$$

Of the two parameters one, i.e., $\eta_\tau^{Ce}(\epsilon_F)$ is fixed by requiring that the number of $4f$ electrons $n_f = 1$. According to Friedel's sum rule this implies $\eta_\tau^{Cu}(\epsilon_F) = \frac{\pi}{2}$. The remaining parameter a fixes the slope of the phase shift at ϵ_F. The latter determines the density of states and hence the effective mass. We set $a = (k_B T^*)^{-1}$ and determine T^* by requiring that the linear specific heat coefficient γ calculated from the resulting quasiparticle dispersions agrees with the experimental one. The different computational steps are summarized in Fig. 1. Calculations of this form have explained and partially predicted (Zwicknagl, 1993, 1990; Zwicknagl et al., 1990) the large mass anisotropies in CeRu$_2$Si$_2$ (Lonzarich, 1988). For more details on renormalized band theory we refer to comprehensive reviews which are available (Zwicknagl, 1993; Norman and Koelling, 1993).

When the temperature increases beyond $T_{\rm coh}$ the excitations lose their coherence properties and the problem reduces to that of independent impurities. In that regime the specific heat contains large contributions from the incoherent part of the f electron excitations. The noncrossing approximation (NCA) is a valuable tool for treating the coupled $4f$ and conduction electrons in that temperature regime (Aoki et al., 1993; Keiter and Kimball, 1971; Kojima et al., 1984). It leads to a system of coupled equations of the form

$$\Sigma_0(z) = \frac{\Gamma}{\pi} \sum_m \int_{-\infty}^{+\infty} d\zeta\, \rho_m(\zeta) K_+(z - \zeta) \tag{5}$$

$$\Sigma_m(z) = \frac{\Gamma}{\pi} \int_{-\infty}^{+\infty} d\zeta\, \rho_0(\zeta) K_-(z - \zeta).$$

Here $\Gamma = \pi N(0) V^2$ and $K_\pm(z)$ are defined by

$$K_\pm(z) = \frac{1}{N(0)} \int_{-\infty}^{+\infty} d\epsilon\, \frac{N(\pm\epsilon) f(\epsilon)}{z + \epsilon} \tag{6}$$

where $f(\epsilon)$ is the Fermi energy and $N(\epsilon)$ is the energy-dependent conduction-electron density of states. The function $\Sigma_\alpha(z)$ and $\rho_\alpha(z)$ $(\alpha = 0; m)$ are related to each other through

$$\rho_\alpha(z) = -\frac{1}{\pi} \mathrm{Im}\{R_\alpha(z)\} \tag{7}$$

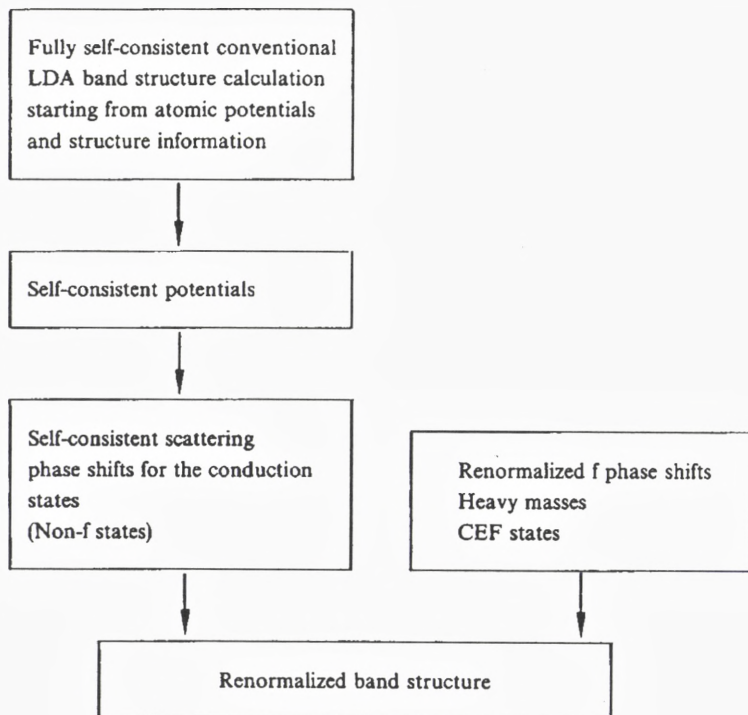$$R_\alpha(z) = \frac{1}{z - \epsilon_\alpha - \Sigma_\alpha(z)}$$

Figure 1. Different computational steps for a renormalized band-structure calculation (Zwicknagl, 1993)).

with $\epsilon_{\alpha=0} = 0$, $\epsilon_{\alpha=m} = \epsilon_{fm}$. The NCA equations have to be solved numerically (Bickers, 1987; Bickers et al., 1985). However, one can find simple, approximate solutions which have the virtue that crystal-field splittings can be explicitly included, a goal which has not been achieved yet by numerical methods. Once the $\rho_\alpha(\epsilon)$ are known, one can determine, e.g., the temperature dependence of the f-electron occupancies $n_{fm} = \langle f_m^+ f_m \rangle$ through

$$n_{fm}(T) = \frac{1}{Z_f} \int_{-\infty}^{+\infty} d\epsilon \, \rho_m(\epsilon) \, e^{-\beta(\epsilon-\mu)}, \tag{8}$$

where μ is the chemical potential and

$$Z_f = \int_C \frac{dz}{2\pi i} \, e^{-\beta z} \left(R_0(z) + \sum_m R_m(z) \right) \tag{9}$$

is the partition function of the f electrons. Knowing the $n_{fm}(T)$ enables us to compute quantities like the temperature dependence of the quadrupole moment of
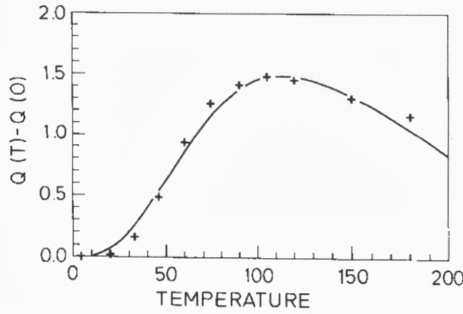
Figure 2. Temperature dependence of the quadrupole moment $Q(T)$ of the $4f$ electrons in YbCu$_2$Si$_2$. Crosses: experimental values; solid line: theoretical results for the parameters $T^* = 200$ K, $\Gamma = 47.4$ meV and a crystal-field parameter $3B_2^0 = -1.67$ meV (Zevin et al., 1988).

the f sites

$$Q(T) = \sum_m \langle m \mid (3J_z^2 - J^2) \mid m \rangle \, n_{fm}(T). \tag{10}$$

In Fig. 2 is shown a comparison between theory and experiments for the quadrupole moment of Yb in YbCu$_2$Si$_2$ (Thomala et al., 1990; Zevin et al., 1988). The input parameters are Γ, T^* and the CEF parameter B_2^0. The latter determines the crystal-field splitting of the $J = 7/2$ ground-state multiplet of Yb^{3+}.

When $T \gg T^*$, the f electrons can be treated as being localized. Their moment is weakly interacting with that of the conduction electrons and perturbation theory can be applied to study the resulting effects. The different temperature regimes are shown in Fig. 3. A beautiful demonstration of the above scenario is the experimentally observed difference in the Fermi surfaces of CeRu$_2$Si$_2$ and CeRu$_2$Ge$_2$ (King and Lonzarich, 1991). When Si is replaced by Ge the distance between Ce and its nearest neighbours is increased. This implies a decrease in the hybridization of the $4f$ electrons with the valence electrons of the neighbouring ions. While in CeRu$_2$Si$_2$ the characteristic temperature is $T^* \simeq 15$ K, it is practically zero in CeRu$_2$Ge$_2$. De
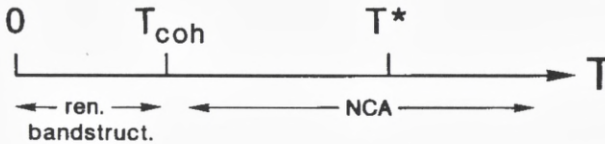

Figure 3. Different temperature regimes and theoretical methods for describing the low-energy excitations of a Kondo-lattice system

Haas–van Alphen experiments are performed at a temperature $T \simeq 1$ K implying $T \ll T^*$ for CeRu$_2$Si$_2$ while $T \gg T^*$ for CeRu$_2$Ge$_2$. Therefore, the $4f$ electron of Ce contributes to the volume of the Fermi sea in the former case, but not in the latter. Indeed, experiments show that the two Fermi surfaces have similar features but differ in volume by one electron (King and Lonzarich, 1991).

3 Zeeman route to heavy fermions

Low-temperature measurements of the specific heat and magnetic susceptibility demonstrate the existence of heavy-quasiparticle excitations in the electron-doped system Nd$_{2-x}$Ce$_x$CuO$_4$ (Brugger et al., 1993). For $x = 0.2$ and temperatures $T \leq 1$ K the linear specific heat coefficient is $\gamma = 4$ J/(mol K^2). The magnetic susceptibility χ_s is approximately T-independent in that temperature regime and the Sommerfeld–Wilson ratio is $R \simeq 1.8$ (see Fig. 4). While these features agree with those of other heavy-fermion systems, there are also pronounced differences. In superconducting heavy-fermion systems like CeCu$_2$Si$_2$ or UPt$_3$ the Cooper pairs are formed by the heavy quasiparticles. This is evidenced by the fact that the jump in the specific heat ΔC at the superconducting transition temperature T_c is directly related to the large γ coefficient, i.e., $\Delta C(T_c)/(\gamma T_c) \approx 2.4$. The low-energy excitations are therefore strongly reduced below T_c. In superconducting Nd$_{1.85}$Ce$_{0.15}$CuO$_4$ the formation of Cooper pairs has no noticeable effect on the heavy-fermion excitations. They remain unaffected by superconductivity.

A crucial difference between Nd$_{2-x}$Ce$_x$CuO$_4$ and, e.g., CeCu$_2$Si$_2$ are the strong electron correlations between the conduction electrons present in the former, but not in the latter material. In the two-dimensional Cu–O planes of Nd$_{2-x}$Ce$_x$CuO$_4$ with $x \geq 0.1$ we have to account for antiferromagnetic fluctuations which are very slow at low temperatures. There is considerable experimental evidence for this. Consider undoped Nd$_2$CuO$_4$, an antiferromagnet with a Néel temperature of $T_N \simeq 270$ K. Since the exchange interactions between a Nd ion and its nearest-neighbour Cu ions cancel because of the antiferromagnetic alignment of the Cu spins, one is left with the next-nearest neighbour Cu–Nd spin interaction. The latter is of the form $\alpha \, \mathbf{s}_{\mathrm{Cu}} \cdot \mathbf{S}_{\mathrm{Nd}}$ and is larger than the Nd–Nd interaction. The Schottky peak in the specific heat seen in Fig. 4 results from the spin flips of the Nd ions in the staggered effective field $\alpha \langle \mathbf{s}_{\mathrm{Cu}} \rangle$ set up by the Cu spins (Zeeman effect). It is also present in doped systems like Nd$_{1.8}$Ce$_{0.2}$CuO$_4$ where antiferromagnetic long-range order is destroyed by doping. This can only be understood if the changes in the preferred direction of the Cu spins occur sufficiently slowly, i.e., slower than 10^{-10} s in the present case, so that the Nd spins can follow those motions adiabatically. Only then is a similar energy to that in Nd$_2$CuO$_4$ required to flip
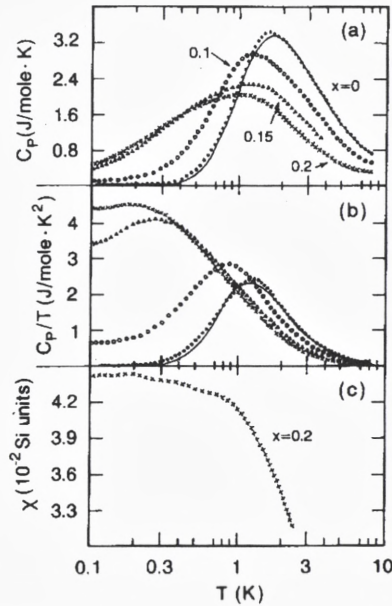
Figure 4. Heavy-fermion behaviour of $Nd_{2-x}Ce_xCuO_4$. (a) specific heat $C_p(T)$; (b) $C_p(T)/T$; (c) spin susceptibility for an overdoped sample with $x = 0.2$ (Brugger et al., 1993).

a Nd spin. This physical picture has been confirmed by recent inelastic neutron-scattering (Loewenhaupt et al., 1996) and μSR experiments (J. Litters, private communication). Spin-glass behaviour can be excluded.

Due to an effective valency of Ce of approximately +3.5 the Cu–O planes are doped with electrons, i.e., a corresponding number of Cu sites are in a $3d^{10}$ configuration. Since these sites have no spin they do not interact with the Nd ions. The extra electrons move freely in the Cu–O planes and therefore, the interaction of a Nd ion with the next-nearest Cu site is repeatedly turned off and on. It is this feature which results in heavy-quasiparticle excitations.

Two model descriptions have been advanced in order to explain the low-energy excitations of $Nd_{2-x}Ce_xCuO_4$. One is based on a Hamiltonian in which the Nd–Cu interaction is treated by a hybridization between the Nd $4f$ and Cu $3d$ orbitals. Usually it is much easier to extract heavy quasiparticles from such a Hamiltonian than from one with a spin–spin interaction obtained after a Schrieffer–Wolff transformation. The slow, antiferromagnetic fluctuations of the Cu spins are replaced by a static staggered field acting on them. This symmetry-breaking field also accounts for the strong correlations in the Cu–O planes because charge fluctuations between
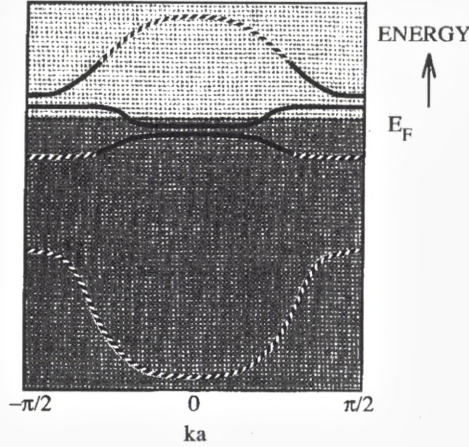
Figure 5.   Schematic drawing of the quasiparticle excitation bands of $Nd_{2-x}Ce_xCuO_4$ for $x > 0$ (electron doping). The Fermi energy is indicated by a dotted line. Dashed lines: d-like excitations and solid lines: f-like excitations.

Cu sites are strongly reduced this way (unrestricted Hartree–Fock). Thus H reads

$$H = -t \sum_{<ij>\sigma} (a_{i\sigma}^+ a_{j\sigma} + \text{h.c.}) + h \sum_{i\sigma} \sigma e^{i\mathbf{Q}\cdot\mathbf{R}_i} a_{i\sigma}^+ a_{i\sigma} \tag{11}$$
$$+ V \sum_{i\sigma} (a_{i\sigma}^+ f_{i\sigma} + \text{h.c.}) + \tilde{\epsilon}_f \sum_{i\sigma} f_{i\sigma}^+ f_{i\sigma}.$$

Here $\mathbf{Q} = (\pi, \pi)$ is a reciprocal lattice vector, $\mathbf{R}_i$ denotes the positions of the Cu ions and h is the size of the staggered field. The operators $a_{i\sigma}^+$, $f_{i\sigma}^+$ create an electron in the Cu $3d_{x^2-y^2}$ and the Nd $4f$ orbital, respectively. For simplicity, only one Nd site per Cu site is considered and one $4f$ orbital with energy $\tilde{\epsilon}_f$ is assumed instead of seven. The energies $\tilde{\epsilon}_f$ and V are strongly renormalized quantities because of the $4f$ electron correlations.

The Hamiltonian (11) is easily diagonalized. Four bands are obtained, two of which are d-like (Cu) and two which are f-like (Nd). The dispersions of the four bands are given by

$$E_\nu(\mathbf{k}) = \frac{\tilde{\epsilon}_f \pm \epsilon_\mathbf{k}}{2} \pm \frac{1}{2}\sqrt{(\epsilon_\mathbf{k} \mp \tilde{\epsilon}_f)^2 + 4V^2} \ , \ \nu = 1,\ldots,4 \tag{12}$$

where $\epsilon_\mathbf{k} = (\epsilon_0^2(\mathbf{k}) + h^2/4)^{1/2}$ and $\epsilon_0(\mathbf{k}) = -2t(\cos k_x + \cos k_y)$. A schematic plot is shown in Fig. 5. At half-filling only the lower f band is filled and the Schottky-peak contributions to $C(T)$ are due to transitions from the filled lower to the empty
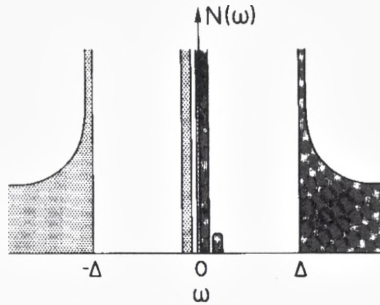
Figure 6. Superconducting density of states for $Nd_{1.85}Ce_{0.15}CuO_4$. A BCS-like model has been assumed. The f-like low-energy excitations remain virtually unchanged by the superconducting order parameter (Courtesy of G. Zwicknagl and S. Tornow).

upper f band. When the planes are doped with electrons the upper f band becomes partially filled resulting in low-energy excitations with large effective mass. The latter follows from the quasiparticle dispersion

$$E_{qp}(\mathbf{k}) \simeq \tilde{\epsilon}_f + \frac{V^2}{(\tilde{\epsilon}_f + \epsilon_\mathbf{k})}. \tag{13}$$

It is noticed that here it is the Zeeman splitting of the f states which is responsible for the occurrence of heavy-electron behaviour. The effect of superconductivity on the heavy quasiparticles can be studied by adding an attractive interaction part H_{attr} for the charge carriers in the Cu–O planes to the Hamiltonian (Fulde and Zevin, 1993). For $V = 0$ the conventional BCS spectrum is recovered for the electrons in the upper Cu band. When $V \neq 0$ the lower Cu band hybridizes with one of the dispersionless f bands. The lower d band remains unaffected by superconductivity because pairing occurs in the upper d band. Therefore, superconductivity has no effect here. The upper d band hybridizes with the second f band. When H is diagonalized one finds a BCS gap in the Cu band while the f band remains virtually unchanged as compared with a vanishing superconducting order parameter. The resulting density of states is shown in Fig. 6. The structure inside the gap stems from the spin degrees of freedom of the Nd ions.

The second model description of the Nd spins coupled to the Cu spin is based on stochastic forces acting on the latter (Igarashi et al., 1995). They mimic the interaction of the Cu spin with its environment, i.e., with the other Cu spins. In that case we start from the Hamiltonian

$$H_{int} = \alpha\, \mathbf{s}_{Cu} \cdot \mathbf{S}_f\,, \qquad \alpha > 0 \tag{14}$$

for the Nd–Cu interaction. For simplicity, both spins are assumed to be of magnitude S. We treat the vector $\mathbf{\Omega} = \mathbf{s}_{Cu}/S$ like a classical variable, subject to a stochastic force. We assume a Gauss–Markov process in which case the distribution function obeys a Fokker–Planck equation. The correlation function is then of the form

$$\langle \mathbf{\Omega}(0)\mathbf{\Omega}(t)\rangle = e^{-2D_r t} \tag{15}$$

where D_r can be obtained from the nonlinear σ model (Chakravarty et al., 1989; Chakravarty and Orbach, 1990). Because there is no long range-order $\langle \mathbf{\Omega}(0)\rangle = \mathbf{0}$. The motion of the Nd spin is governed by the equation

$$\frac{d}{dt}\,\mathbf{n}(t) = \omega_0\big(\mathbf{\Omega}(t)\times\mathbf{n}(t)\big) \tag{16}$$

where $\mathbf{n}(t) = \mathbf{S}_f/S$ and $\omega_0 = \alpha S$. The spectral function

$$I(\omega) = \frac{1}{2\pi}\int_{-\infty}^{+\infty} dt\, e^{i\omega t}\langle\mathbf{n}(0)\mathbf{n}(t)\rangle \tag{17}$$

is evaluated by making use of the corresponding stochastic Liouville equation. We find that $I(\omega)$ is of the form

$$I(\omega) = \frac{1}{3\pi}\,\frac{4D_r}{\omega^2 + (4D_r)^2} + \text{(side peaks at } \omega_0). \tag{18}$$

While $D_r(T)$ vanishes as $T \to 0$ in the presence of long-range order, it remains finite when the latter is destroyed by doping. A linear specific heat contribution of the $4f$ spin is obtained from

$$C(T)_{\mathrm{imp}} = \frac{d}{dT}\langle H_{\mathrm{int}}\rangle = \frac{S(S+1)}{T^2}\int_0^\infty d\omega\,\omega^2\,\frac{I(\omega)}{\cosh^2(\omega/2T)} \tag{19}$$

when $D_r(T = 0) \neq 0$. The side peaks in $I(\omega)$ give raise to a Schottky-type contribution. The calculated specific heat is shown in Fig. 7 and reproduces the experiments reasonable well (compare with Fig. 4). One shortcoming of the theory in its present form is the low-temperature spin susceptibility which follows from

$$\chi_{\mathrm{imp}}(T) = \frac{4}{3}(g\mu_B)^2 S(S+1)\int_0^\infty d\omega\,\frac{I(\omega)}{\omega}\,\tanh\frac{\omega}{2T}. \tag{20}$$

We find $\chi_{\mathrm{imp}}(T) \sim \ln(D_r/T)$ at low T. This is possibly due to the neglect of Nd–Nd interactions. However, when evaluated for $T = 0.4$ K one finds for $Nd_{1.8}Ce_{0.2}CuO_4$ a Sommerfeld–Wilson ratio of $R \simeq 1.4$.
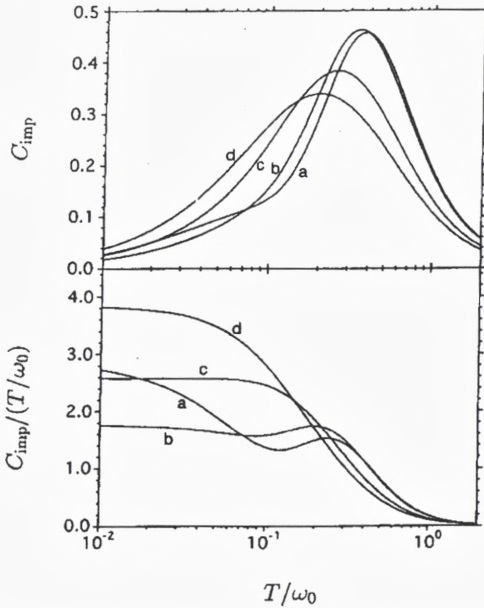
Figure 7. Specific heat contribution of a Nd ion with $S = 1/2$. Curves (a)-(d) correspond to $D_r/\omega_0 = 0.05, 0.1, 0.5, 0.8$, respectively (Igarashi et al., 1995).

4   Hubbard chains - Yb$_4$As$_3$

The intermetallic compound Yb$_4$As$_3$ is of the anti-Th$_3$P$_4$ structure. The Yb ions are situated on chains with directions along the diagonals of a cube. Thus we are dealing with a system of four sets of interpenetrating chains (see Fig. 8). We want to draw attention to the fact that the distance between neighbouring Yb ions on a chain exceeds the one between neighbouring ions on different chains.

Because As has a valency of -3, three of the four Yb ions have a filled $4f$ shell, i.e., a valency $+2$, while one ion is in a $4f^{13}$ configuration (valency $+3$). Since all Yb sites are equivalent, the hole in the $4f$ shell is shared between four Yb ions and the system is metallic. However, at a temperature $T_s \simeq 300$ K the system undergoes a weak first-order phase transition into a trigonal distorted structure (Ochiai et al., 1990; Suzuki, 1993; Ochiai et al., 1993; Reinders et al., 1993; Kasuya, 1994; Bonville, 1994). Thereby one set of chains, e.g., along $[1,1,1]$ is shortened while the other three sets are elongating thereby leaving the volume of the unit cell unchanged. This results in charge ordering because the Yb^{3+} ions have a smaller ionic radius than the Yb^{2+} ones and occupy the chains with smaller Yb–Yb distances (short chains) (Kasuya, 1994). The driving force for the phase transition
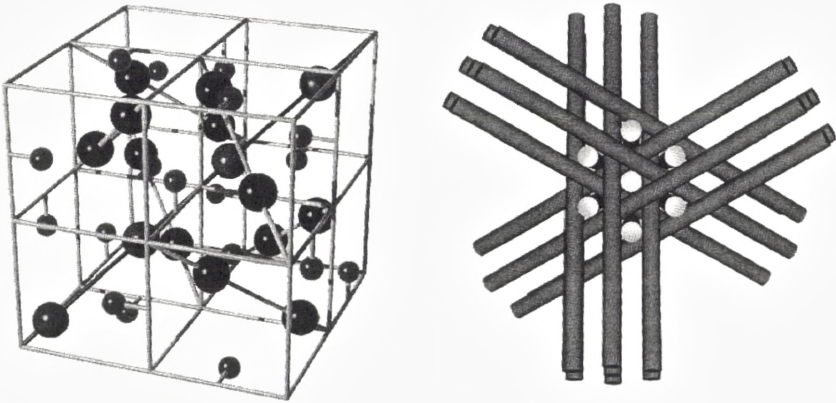
Figure 8. (a) Structure of Yb_4As_3: large and small spheres represent the Yb and As ions, respectively. (b) Four sets of interpenetrating chains on which the Yb ions are located.

is the Coulomb repulsion between Yb^{3+} ions. Measurements of the Hall constant reveal a dramatic increase below T_s, implying a sharp drop in the charge carrier density with decreasing temperature. At low T one is left with one carrier per 10^3 Yb ions. The resistivity increases below T_s with decreasing temperature until it reaches a maximum of approximately 10 mΩ cm. At low T it is of the form $\rho(T) = \rho_0 + AT^2$ and therefore shows Fermi-liquid behaviour. The linear specific-heat coefficient γ is found to be of order $\gamma \simeq 200$ mJ/(mol K^2). The spin susceptibility is Pauli like and equally enhanced as γ, giving raise to a Sommerfeld–Wilson ratio of order unity. No indication of magnetic order is found down to $T = 0.045$ K, but below 2 K the susceptibility increases again which indicates the presence of another low energy scale (Bonville et al., 1994). The above findings strongly suggest heavy-fermion behaviour which is further confirmed by the observation that the ratio A/γ^ν ($\nu \simeq 2$) compares well with that of other heavy-fermion systems (Ochiai et al., 1993). One should appreciate that despite the low-carrier concentration the γ value exceeds that of, e.g., Na by a factor of more than 10^2. This demonstrates that the high density of low-energy excitations must clearly involve spin-degrees of freedom of the Yb^{3+} ions. The Kondo effect can be ruled out as a source of heavy quasiparticles. The low-energy scale which corresponds to the observed γ value is $T^* \simeq 40$ K. But inelastic neutron scattering shows a well resolved crystal-field excitation of Yb^{3+} at a comparable energy which would be impossible if local singlets would form with a binding energy of similar size.

A theory has been developed which can explain rather consistently the above

experimental findings. It is based on interpreting the structural phase transition in terms of a collective band Jahn–Teller (CBJT) effect (Fulde et al., 1995). The transition is caused by a strong deformation-potential coupling which is quite common in mixed-valence systems. It is based on the Coulomb repulsion between different rare-earth ions. The CBJT transition splits the fourfold degenerate quasi-$1d$ density of states into a nondegenerate one corresponding to the short chains and a threefold one due to the long chains. The nondegenerate one is lower in energy and would be half filled if charge ordering were perfect and the holes were uncorrelated fermions. Instead, the holes are strongly correlated. Two holes on a site imply a $4f^{12}$ configuration for Yb and that has a much too high energy to occur. Therefore, we are dealing with an almost full lower (hole) Hubbard band rather than with an almost half-filled band. Therefore, the ideal system should be an insulator. That Yb_4As_3 is a semimetal and not an insulator is probably related to the nonvanishing hopping matrix elements between $4f$ orbitals in the long and short chains. This may result in self-doping with a fraction of holes moving from the short to the long chains. Accurate conditions for self-doping are not easily worked out, but a first step in this direction was recently done (Blawid et al., 1996).

The phase transition can be described by an effective Hamiltonian of the form

$$ H = -t \sum_{\mu=1}^{4} \sum_{<ij>\sigma} (f_{i\mu\sigma}^{+} f_{j\mu\sigma} + \text{h.c.}) + \epsilon_\Gamma \sum_{i,\mu=1}^{4} \Delta_\mu f_{i\mu\sigma}^{+} f_{i\mu\sigma} + 4N_L c_0 \epsilon_\Gamma^2. \tag{21} $$

The operators $f_{i\mu\sigma}^{+}(f_{i\mu\sigma})$ create (destroy) a $4f$ hole at site i of chain μ with effective spin σ (the crystal-field ground state of the $J = 7/2$ multiplet is two-fold degenerate). Interchain hopping matrix elements are neglected and so is the on-site Coulomb repulsion between holes, since near T_s holes are reasonably well separated. The notation $<ij>$ refers to Yb–Yb nearest neighbours in a chain of length N_L. The trigonal-strain order parameter $\epsilon_\Gamma < 0$ corresponds to the bulk elastic constant $4c_0$. The deformation potential Δ_μ is

$$ \Delta_\mu = \Delta \left\{ \begin{array}{ll} 1 & \mu = 1 \\ -\frac{1}{3} & \mu = 2, 3, 4. \end{array} \right. \tag{22} $$

With a choice of $4t = 0.2$ eV obtained from LDA calculations, $c_0 = 10^{11}$ Ω erg/cm³ (Ω is the volume of a unit cell) and $\Delta = 5$ eV we obtain $T_s \simeq 250$ K.

With increasing charge ordering (see Fig. 9), correlations become more and more important because with the increase in concentration of holes in the short chains their average distance decreases. Therefore, at low temperatures T the t–J Hamiltonian or a Hubbard Hamiltonian must be used. Using the former and making use of a slave-boson mean-field approximation we arrive at an effective
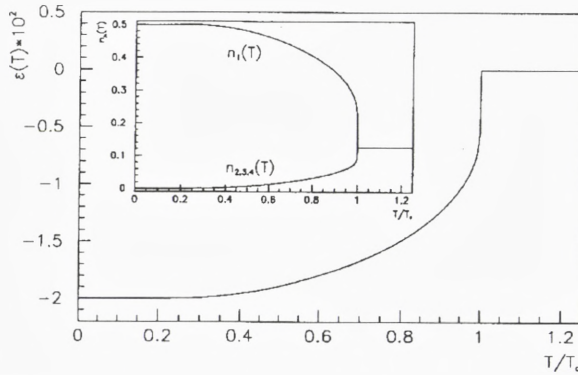
Figure 9. Temperature dependence of the trigonal-strain order parameter $\epsilon_\Gamma(T)$. Shown as an inset are the occupation numbers n_μ of the short ($\mu = 1$) and long ($\mu > 1$) chains (Bonville et al., 1994).

mass enhancement of the form

$$\frac{m^*}{m_b} = \frac{t}{t\delta + (3/4)\chi J}. \tag{23}$$

Here m_b denotes the band mass, $\chi = \chi_{ij} = \langle \sum_\sigma f_{i1\sigma}^+ f_{j1\sigma} \rangle$, δ is the deviation of the short chains denoted by 1 from half filling and $J = 4t^2/U$, where U is the on-site Coulomb repulsion between holes. With $U = 10$ eV one finds $J = 10^{-3}$ eV and using $\chi(T = 0) = (2/\pi)\sin(\pi(1 - \delta)/2)$ with $\delta = 10^{-3}$ one obtains a ratio of $m^*/m_b \simeq 100$. This derivation of the mass enhancement hides somewhat the fact that spin degrees of freedom are responsible for the heavy quasiparticles. A more direct way of understanding the large γ value in the specific heat is by realizing that a spin chain gives rise to a linear specific heat. Although a Heisenberg chain has no long-range order, short-range antiferromagnetic correlations lead to spin-wave like excitations which can be rather well described by linear spin-wave theory. Indeed, Kohgi et al. (private communication) measured the spin-excitation spectrum by inelastic neutron scattering and found a one-dimensional spin-wave spectrum.

Since spin-wave-like excitations are responsible for the fermionic low-energy excitations associated with the specific heat and susceptibility we are dealing here with charge-neutral heavy fermions in distinction to the charged heavy electrons, which appear, e.g., in CeAl$_3$. Therefore, we speak of an uncharged or neutral heavy Fermi liquid.

The physical interpretation given above allows for an explanation of another experiment. It has been previously found that an applied magnetic field of 4 tesla has little influence on the γ coefficient above 2 K, but suppresses γ considerably below

2 K (Helferich, Steglich and Ochiai, private communication). This effect is unexpected, since one would have thought that the changes are of order $(\mu_B H/k_B T^*)^2$ and therefore very small. However, we can explain the experiments by providing for a weak coupling between parallel short chains. When linear spin-wave theory is applied, a ratio between interchain and intrachain coupling of order 10^{-4} opens an anisotropy gap which modifies $C(T)$ in accordance with observation (Schmidt et al., 1996).

5 Conclusions

We have shown that heavy-fermion excitations may be of very different physical origin. Three distinct mechanisms have been discussed which result in low-energy scales required for the heavy quasiparticles. The most, and until recently only one studied so far refers to Kondo lattices and is based on the formation of (local) singlet states. They result from a weak hybridization of the $4f$ electrons with the conduction electrons. In that case the low-energy scale is given by the binding energy associated with the singlets. In distinction to Kondo lattices we are dealing in the case of $Nd_{2-x}Ce_xCuO_4$ with a lattice of Nd ions with a well localized magnetic moment which are coupled to a two-dimensional system of strongly correlated conduction electrons. In that case a low-energy scale is provided by the Zeeman energy of the Nd magnetic moment in the slowly fluctuating molecular field set up by the Cu spins. Finally, in Yb_4As_3 the low-energy scale is due to the band width of the spin-wave like excitations in magnetic chains formed by Yb^{3+} ions. The few carriers, i.e., one per 10^3 Yb ions are unimportant for the low temperature specific heat which is governed exclusively by spin excitations (spinons). The system serves as an example of almost perfect separation between spin and charge degrees of freedom. For the purpose of understanding its low temperature thermodynamic properties it can be considered a neutral or chargeless heavy Fermi liquid. Yb_4As_3 belongs to a class of materials often referred to as low-carrier Kondo systems or Kondo insulators (for recent references see, e.g., Proc., 1996). As we have shown that might be misleading, at least for Yb_4As_3, where the appearance of heavy fermions has nothing to do with the Kondo effect. However, that material is rather distinct to CeNiSn or other members of that class. Therefore, the origin of low-energy scales must be investigated from case to case.

In summary, heavy-fermions behaviour can have a variety of physical origins. It remains a challenge for the future to uncover other processes leading to low-energy scales.

Acknowledgements

References

Aoki H, Uji S, Albessand A and Onuki Y, 1993: Phys. Rev. Lett. **71**, 2120

Bickers NE, 1987: Rev. Mod. Phys. **59**, 845

Bickers NE, Cox DL and Wilkins J.W, 1985: Phys. Rev. Lett. **54**, 230

Blawid S, Hoang AT and Fulde P, 1996: Phys. Rev. B (in print)

Bonville P, Ochiai A, Suzuki T and Vincent E, 1994: J. Phys. I **4**, 595

Brugger T, Schreiner T, Roth G, Adelmann P and Czjzek G. 1993: Phys. Rev. Lett. **71**, 2481

Chakravarty S and Orbach R, 1990: Phys. Rev. Lett. **64**, 224

Chakravarty S, Halperin BI, Nelson DR, 1989: Phys. Rev. B **39**, 2344

d'Ambrumenil N and Fulde P, 1985: J. Magn. Magn. Mater. **47–48**, 1

Doniach S, 1971: Physica B **91**, 231

Doniach S, 1987: *Theoretical and Experimental Aspects of Valence Fluctuations and Heavy Fermions*, eds. L.C. Gupta and S.K. Malik (Plenum Press, New York 1987) p. 179

Fulde P and Jensen J, 1983: Phys. Rev. B **27**, 4085

Fulde P and Zevin V, 1993: Europhys. Lett. **24**, 791

Fulde P, Keller J and Zwicknagl G, 1988: *Solid State Physics*, eds. H. Ehrenreich and D. Turnbull (Academic Press, San Diego) Vol. 41, p. 1

Fulde P, Schmidt B and Thalmeier P, 1995: Europhys. Lett. **31**, 323

Fulde P, Zevin V and Zwicknagl G, 1993: Z. Phys. B **92**, 133

Grewe N and Steglich F, 1991: *Handbook on the Physics and Chemistry of Rare Earths*, eds. K.A. Gschneidner, Jr. and L. Eyring (North-Holland, Amsterdam) Vol. 14

Hewson AC, 1993: *The Kondo Problem to Heavy Fermions* (Cambridge University Press, Cambridge)

Igarashi I, Murayama K and Fulde P, 1995: Phys. Rev. B **52**, 15966

Kasuya T, 1993: *Transport and Thermal Properties of f-Electron Systems*, eds. G. Oomi et al. (Plenum Press, New York)

Kasuya T, 1994: J. Phys. Soc. Jpn. **63**, 2481

Keiter H and Kimball JC, 1971: Int. J. Magn. **1**, 233

King C.A and Lonzarich GG, 1991: Physica B **171**, 161

Kojima H, Kuramoto Y and Tachiki M, 1984: Z. Phys. B **54**, 293

Lee PA, Rice TM, Serene JM, Sham LJ and Wilkins JW, 1986: Comments Condens. Matter Phys. **12**, 99

Loewenhaupt M, Metz A, Pyka NM, McK Paul DM, Martin J, Duijn VHM, Franse JJM, Mutka H and Schmidt W, 1996: Ann. Phys. **5**, 197

Lonzarich GG, 1988: J. Magn. Magn. Mater. **76–77**, 1

Norman M.N, Koelling D, 1993: *Handbook on the Physics and Chemistry of Rare Earths*, eds. K.A. Gschneidner, L. Eyring, G.H. Lander and G.R. Choppin (Elsevier, Amsterdam) Vol. 17, p. 1

Ochiai A, Li DX, Haga Y, Nakamura O and Suzuki T, 1993: Physica B **186–188**, 437

Ochiai A, Suzuki T and Kasuya T, 1990: J. Phys. Soc. Jpn. **59**, 4129

Ott HR, 1987: Prog. Low Temp. Phys. **11**, 215

Proc. of the Inter. Conf. on Strongly Correlated Electron Systems, 1995: Physica B **206–207**

Proc. of the Inter. Conf. on Strongly Correlated Electron Systems, 1996: Physica B **223–224**

Razafimandimby H, Fulde P and Keller J, 1984: Z. Phys. B **54**, 111

Reinders PHP, Ahlheim U, Fraas K, Steglich F and Suzuki T, 1993: Physica B **186–188**, 434

Schlottmann P, 1984: Phys. Rep. **181**, 1

Schmidt, B, Thalmeier P and Fulde P, 1996: Europhys. Lett. **35**, 109

Stewart GR, 1984: Prog. Low Temp. Phys. **56**, 755

Sticht J, d'Ambrumenil N and Kübler 1986: J, Z. Phys. B **65**, 149

Strange P and Newns DM, 1986: J. Phys. F **16**, 335

Suzuki T, 1993: Physica B **186–188**, 347

Thomala K, Weschenfelder G, Czjzek G and Holland-Moritz E, 1990: J. Magn. Magn. Mater. **89**, 143

Varma CM and Yafet Y, 1976: Phys. Rev. B **13**, 2950

Wachter P, 1994: *Handbook on the Physics and Chemistry of Rare Earths*, eds. K. A. Gschneidner, Jr., L. Eyring, G. H. Lander and G.R. Chappin (Elsevier, Amsterdam) Vol. 19

White RM and Fulde P, 1981: Phys. Rev. Lett. **47**, 1540

Yoshida K, 1966: Phys. Rev. **147**, 223

Yoshida K and Yoshimori A, 1973: *Magnetism*, eds. G.T. Rado and H. Suhl (Academic Press, New York) Vol. 5, p. 253

Zevin V, Zwicknagl G and Fulde P, 1988: Phys. Rev. Lett. **60**, 2331

Zwicknagl G, 1988: J. Magn. Magn. Mater. **76–77**, 16

Zwicknagl G, 1993: Adv. Phys. **41**, 203

Zwicknagl G, Runge E and Christensen NE, 1990: Physica B **163**, 97

Itinerant f-Electron Systems

Börje Johansson

Condensed Matter Theory Group, Physics Department,

Uppsala University, Box 530, Uppsala, Sweden

and

Hans L. Skriver

Center for Atomic-scale Materials Physics and Department of Physics,

Technical University of Denmark, DK-2800 Lyngby, Denmark

Abstract

The electronic structures of the earlier lanthanide and actinide elements are considered, and especially cohesive properties and crystal structures are used to demonstrate the deep involvement of the f electrons in the metallic bonding. The recent observation for samarium of a bct structure at a pressure of about 1 Mbar suggests that the $4f$ electrons at these conditions have become itinerant, and, in addition, the observed axial ratio (c/a) is only reproduced from a calculation with a *ferromagnetic* ordering of the itinerant (metallic) $4f$ electrons. As a consequence of this interpretation of the observed data, a thorough experimental investigation of the crystal structure behaviour of the lanthanides in the megabar pressure range, in particular for the elements Nd-Tb, should be very fruitful. For the earlier actinide elements the ground state crystal structures have recently been obtained theoretically and shown to originate from itinerant $5f$ electrons. Thus, for the first time, the crystal structure of Pu has been derived from basic electronic structure calculations. This firmly establishes that there is a profound change in the behaviour of the $5f$ electrons when proceeding from Pu to the next element Am. Recent theoretical work on the pressure-temperature phase diagram of cerium, where the Mott transition picture of the γ–α transformation is extended to finite temperatures, is reviewed. The high pressure phase of praseodymium is also discussed in terms of itinerant $4f$ electrons. This picture fits nicely with the behaviour of highly compressed samarium metal mentioned above. Accordingly, the normally localized $4f$ electrons can be transformed into a radically new electronic configuration by high pressure.

1   Introduction

Since the present symposium is devoted to metallic magnetism it might seem fairly inappropriate to discuss systems with itinerant f electrons, since most of these systems do not order magnetically. Nevertheless, at the planning stage of the conference program, Allan Mackintosh assured us that this topic was central to the

meeting and that no excuses for the subject were necessary. It remains true that the expectations of finding magnetism in these systems are so high, that its very absence creates a special need for an understanding of the underlying reasons for this unexpected behaviour. In the present contribution we will however limit ourselves to some recent developments where we have been involved, but also restrict ourselves to the behaviour of the condensed phase of some pure elements of particular interest. In doing this, we will pay particular attention to the actual crystal structure adopted by the atoms in the solid. We demonstrate that the crystal structure provides us with important data for formulating a deeper understanding of these systems. We also refer to some review articles where a more complete account of the lanthanide and actinide electronic structure has been given (Johansson and Brooks, 1993; Brooks et al., 1984). In another review article by Brooks and Johansson (1993) the magnetic effects are especially stressed. Despite the rather general absence of magnetism in itinerant f systems, the theoretical studies of samarium at high pressure suggest that *a completely new research field of itinerant magnetism* has been discovered, namely lanthanides at a pressure of 1 Mbar.

The electronic structure determines the ground state crystalline atomic arrangement. Consequently, the experimentally observed crystal structures contain important information about the basic nature of the corresponding electronic configuration. This is especially so when one deals with a system displaying an unique crystal structure, not observed for any other system. This is certainly the case for the α-Pu phase, which has 16 atoms per unit cell. In those particular cases where in addition there is also a crystal structure change observed as a function of volume, one is provided with even more detailed facts that have to be matched by theory. This is one of the reasons why high pressure experiments are particularly useful to monitor the accuracy of the theoretical treatment. It so happens that for the $4f$ and $5f$ elements there are a number of crystal structure transformations which take place both as a function of pressure or as a function of alloying. These circumstances provide further input to an accurate study of the lanthanides and the actinides, but have not yet been fully exploited.

There is also another circumstance that makes investigations of the rare-earth systems particularly challenging for theory. Namely that for some systems under compression, most dramatic electronic phase changes might take place, being accompanied by colossal volume collapses when compared to normal crystalline phase transitions in metallic systems. These changes involve the nature of the $4f$ electrons and their transformation between on the one hand localized non-bonding magnetic moments and on the other hand strong metal bonds. This is an example of a Mott transition between an insulating state and a metallic state within the $4f$ shell, a phase transformation that takes place in the presence of a conduction band built up from s, p, and d orbitals occupied by approximately three electrons. The

most well-known example of this is of course the γ–α transition in cerium. The particular significance of the volume collapse in cerium is due to the fact that the transformation does not involve a change of the crystallographic structure, i.e. the crystal structure is fcc on both sides of the transition.

2   Atomic volume

In Fig. 1 we show the atomic volumes of most of the metals in the Periodic Table. The most obvious feature is the similarity between the d transition elements, in particular between the 4d and 5d metals. Also the volume of the 3d elements display an essentially parabolic variation, although there are clear deviations for Mn, Fe and Co, a fact which can be assigned to their magnetic properties. The parabolic behaviour originates from the metallic bonding of the d electrons, where for the earlier elements of the d transition series the bonding part of the d band is being occupied and for the heavier elements the anti-bonding part of the d band is becoming filled. This regularity among the d elements is quite well understood today and indeed electronic structure calculations, utilizing the local density approximation for the exchange and correlation energy, have been very successfully applied to these elements during the last ten years or so. This theory can easily be extended so that magnetism can be treated as well. Thereby the anomalous volumes of the magnetic 3d elements can be explained as a consequence of the magnetization, which removes part of the original metallic bonding. This loss of bonding is partly compensated by a corresponding gain in exchange energy due to polarization of the electron spins.

A most interesting feature in Fig. 1 is the behaviour of the lanthanides. As can be seen there is only a very small volume contraction as one proceeds through the series. The similarity between the individual elements is explained as due to the fact that all the elements have three valence electrons, starting and ending with the two obvious cases lanthanum and lutetium having zero and fourteen 4f electrons, respectively, and therefore three valence electrons filling the conduction band formed from 6s, 6p and 5d orbitals. The two elements Eu and Yb have only two valence electrons and therefore their equilibrium volumes are distinctly higher than for the other trivalent lanthanides. Another point to notice is that the atomic volume for cerium in the α-phase deviates considerably from the general behaviour of the lanthanide elements. Later we will show that this is due to itinerant 4f electrons, a property which is in contrast to all the other lanthanides where the 4f electrons are localized with an integral occupation of the atomic-like f level, 4f^n.

Turning now to the actinide series a most interesting and challenging behaviour can easily be distinguished. In the beginning of the series we notice once more a
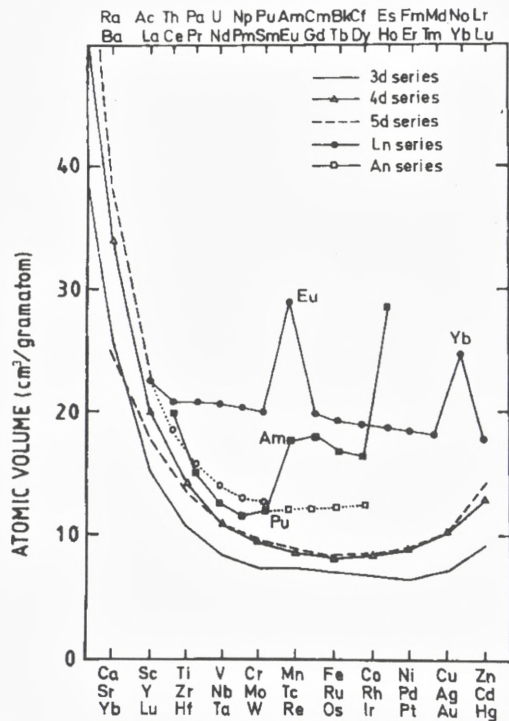
Figure 1. The experimental equilibrium atomic volumes of the $3d$, $4d$ and $5d$ transition metals, the lanthanides and the actinides. The low volume data for the earlier lanthanides and the transplutonium elements are estimations of the equilibrium volumes for the case that the f electrons were itinerant (and paramagnetic).

parabolic decrease of the atomic volume as a function of the atomic number. Then suddenly, between Pu and Am, there is a dramatic change and the volume increases by about 50%. Thus, a drastic transformation of the electronic structure must take place between Pu and Am. This difference has been explained as a transition from metallic to insulating $5f$ electron behaviour and a good account of the volumes for the earlier actinides as well as the volume jump between Pu and Am has already been obtained in the work by Skriver et al. (1978 and 1980).

From Am and onwards the atomic volumes behave very similar to the lanthanides. It is only when we arrive at Es that there is another distinct difference between the lanthanides and actinides, since the deviating Es volume is not observed for the corresponding $4f$ element, Ho. The reason is that several of the late actinide elements will be divalent in the metal phase (Johansson, 1978) in contrast to the heavy lanthanides where only Yb is found to be divalent in the

metallic state. We also notice from Fig. 1 that Am is trivalent, in clear contrast
to its corresponding element among the lanthanides, Eu, which is divalent. This
difference is well understood and has led to the prediction of superconductivity in
Am (Johansson and Rosengren, 1975a), which later was confirmed experimentally
(Smith and Haire, 1978).

Once more we emphasize that at zero pressure there is a profound difference
between the early and late actinide metals, in the sense that the $5f$ electrons are
itinerant (metallic) for the elements up to and including Pu, while they are localized
and non-bonding (atomic-like) for the elements beyond Pu (Johansson, 1975). Thus
in this respect the later (heavier) actinides and their $5f$ electrons behave like most
of the lanthanides with their localized $4f^n$ atomic-like configurations. On the other
hand, among the lanthanides the first element with a substantial occupation of the
$4f$ shell, i.e. cerium, shows already at rather low pressures or at low temperatures a
behaviour very reminiscent of the early actinides (Johansson, 1974). Thus for the
actinides there are five elements (Th-Pu) showing itinerant $5f$ behaviour before
localization sets in when the atomic number is increased from Pu to Am, while for
the lanthanides only one element exhibits $4f$ itinerant properties, i.e. cerium, and
thereafter localization is energetically favoured for all the heavier $4f$ elements. We
illustrate this by arranging the actinides relative to the lanthanides introducing a
displacement in atomic number (Johansson and Rosengren, 1975a):

			Ce	Pr	Nd	Pm	Sm	Eu	Gd
Th	Pa	U	Np	Pu	Am	Cm	Bk	Cf	Es	Fm

(The physical reason for this displacement is the larger spatial extent of the $5f$
orbital as compared to the $4f$ orbital for the corresponding element.) This suggests
a most interesting connection between the $4f$ and $5f$ series, but this has not yet
been fully explored.

Further evidence of the validity of this picture comes from the fact that the
element following cerium, i.e. praseodymium, shows a volume collapse (Smith and
Akella, 1982; Grosshans et al., 1983) of about 10% at 200 kbar and that this dense
phase shows similarities with the early actinides. Thus application of a moderate
pressure moves the division line between itinerant and localized $4f$ behaviour one
atomic number upwards so that now, at these new external conditions (i.e. a pres-
sure of about 220 kbar or so), two lanthanide elements show correspondence to the
early actinides. The important conclusion is that depending on the external pres-
sure, more than one element of the lanthanides can be brought into a state with
close similarities to the early actinides. This relationship between the two f series
was pointed out more than twenty years ago and a generalized phase diagram for
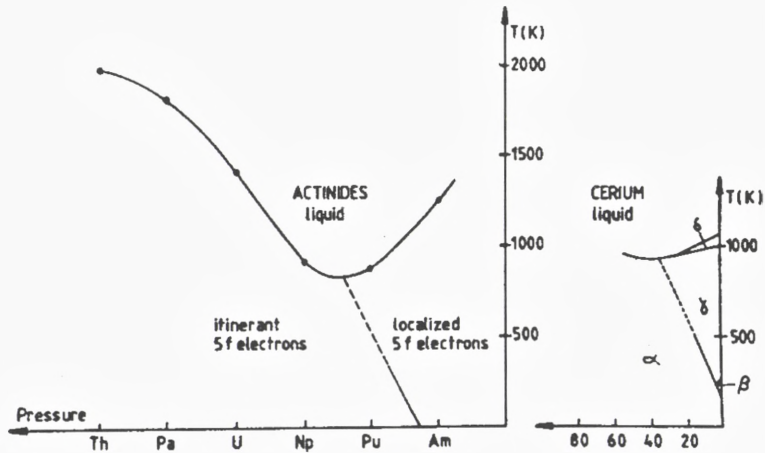the actinides was constructed (Johansson 1974) and compared with the individ-

Figure 2. Melting temperatures for the actinide elements (left) and the $P-T$ phase diagram for cerium (right) (Johansson, 1974). The effect of pressure on an individual element is to make it behave more similarly to its predecessor in the series. This is schematically indicated by a tentative pressure axis on the left. The indicated transition line for the transition between localized and itinerant $5f$ behaviour (Mott transition) as a function of atomic number Z (or pressure for an individual element) has been included schematically. Its extension to the minimum point of the melting curve has been drawn as a suggestive analogy to the behaviour in cerium metal. Also, in the $P-T$ phase diagram for cerium an extension of the γ–α transition line to the minimum of the melting temperature is indicated by a dashed line.

ual pressure-temperature phase diagram for cerium metal (Fig. 2). This diagram for the actinides was later developed further by Kmetko and Smith (1983), who constructed a generalized phase diagram for actinide alloy systems, i.e. for alloys between actinide metals.

3   Crystal structure for itinerant f-electron systems

Turning to the complex structures associated with the itinerant f electrons, there has very recently been some substantial progress in the theoretical understanding. Wills and Eriksson (1992) showed that the ground state crystal structure for Pa is the bct phase, in good agreement with the data available at ambient conditions. For the next element, U, they indeed obtained that α-U is the most stable phase, as required from experiments. However, it is interesting to notice that at high pressures the high symmetry bcc structure is found to become sta-

ble. Söderlind et al. (1994a, 1995a) investigated the Np metal in two papers, the first of which utilized the LDA approximation to the exchange-correlation energy functional, and the second of which applied the more involved GGA approximation. In Fig. 3 we show the energy versus volume diagram for Np obtained by Söderlind et al. (1995a). As can be noticed, the α-Np phase is calculated to be the most stable crystal structure at equilibrium and for small pressures. At high pres-
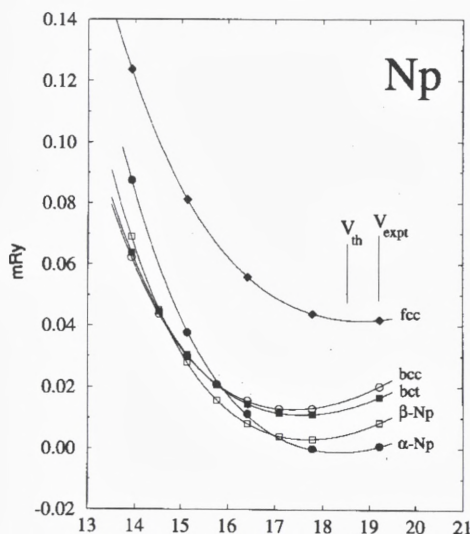

Figure 3. Calculated total energies as a function of volume for the α-Np, β-Np, α-U, bct, bcc, hcp, and fcc crystals of neptunium metal. The points represent calculated values and the solid lines connecting them show the Murnaghan functions as obtained by a least-square fit to the calculated energies.

sures, we again find that the bcc structure is the most stable form. Just recently Söderlind et al. (1997) completed a similar study for Pu metal, where the observed low temperature phase is a monoclinic phase with a wide range of different nearest neighbour distances and as many as 16 atoms per unit cell. Also here the computed theoretical data agree well with known experimental data. Again the bcc structure is found to be the most stable structure at high pressure conditions (Fig. 4). This agreement concerning the equilibrium crystal structure is most satisfactory in view of the complexity of the structure of the plutonium metal. This shows that full-potential electronic structure methods combined with an appropriate density functional treatment of the electron–electron interaction are capable of treating
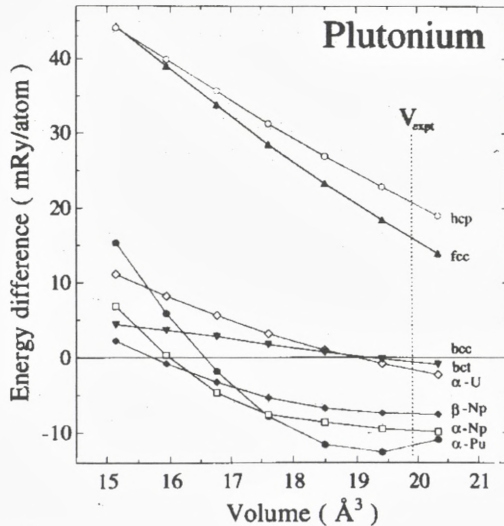
Figure 4. Total energy for plutonium, calculated in the α-Pu, α-Np, β-Np, α-U, bct ($c/a = 0.85$), hcp (ideal c/a), and fcc crystal structures, relative to the bcc structure, as a function of volume.

as heavy elements as the actinides with the same accuracy as for the d transition elements. With this achievement one may conclude that theory has demonstrated its wide versatility as regards the electronic structure of the metallic Elements.

Söderlind et al. (1995a) also analyzed their results in terms of a canonical treatment of the f states and the crystal structure stabilities as a function of f band filling. Such a comparison is only meaningful between the fcc, hcp and bcc structures which have almost identical Madelung energies. This comparison is reproduced in Fig. 5. One notices in particular the strong preference of the bcc structure for the elements beyond uranium. However, this structure is not observed experimentally for volumes close to equilibrium conditions. Instead heavy displacements of the atoms distort the bcc structure into low symmetry phases. This is possible energetically since the states driving these distortions are the narrow f bands close to the Fermi energy. For compressed volumes the f bandwidth will have increased to such an extent that distortions are no longer energetically favoured. From the behaviour of the canonical one-electron energy sums it is obvious that the bcc structure should be the favoured one at these wide-band conditions. Nevertheless, and unfortunately, at present it seems very difficult to produce a theoretical explanation for the occurrence of the actinide structures with the same simplicity as is found for the d transition elements. However, one may still clam that a big step in this direction has been taken for the actinides. Namely, that the equilib-
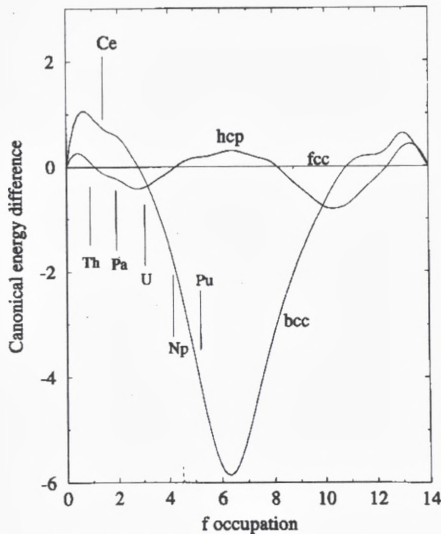
Figure 5. Canonical f band structural energy differences (arbitrary units) as a function of f band occupation. The fcc canonical energy defines the zero energy level of the plot. Calculated equilibrium f band occupations for the light actinides (Th-Pu) are also shown as vertical lines.

rium volume structures can be considered as based upon the bcc structure, which undergoes a substantial distortion due to the narrow f band states. Söderlind et al. (1995b) also performed an interesting study of two d transition metals and one simple metal, which is highly relevant to the present discussion. They expanded the Fe, Nb, and Al metals, and investigated the structure stability as a function of expansion. The most interesting observation was that for all three of these metals, the α-U structure becomes favoured relative to the structure observed at normal conditions. Thus, again the very fact that the dominant bonding states narrow their energy bandwidth upon expansion makes it energetically favourable to undergo distortions away from high symmetry structures. Therefore it is not primarily the f orbital character that determines the crystal structure, but rather the bandwidth of the bonding orbitals is of decisive importance for a distorted metal. The canonical structure sequences as a function of band-filling are however different between for example d and f bands. The difficulty in finding a simple theory for distorted structures depends on the large difference between the Madelung energies for the different structures. For the d transition metals, where, based on experimental data, one may allow oneself to restrict the comparison to the three main metal crystal structures – bcc, hcp, and fcc – one can to a good accuracy neglect the difference between the Madelung sums for the three structures, thereby

gaining enormously in simplicity. Nevertheless, as regards the crystalline forms of the metal elements, we believe that a great step forward has been taken towards a general capability to handle the basic interactions giving rise to the wide range of crystal structures observed among the elements. The fact that we can treat the $5f$ elements and the d elements equally well means that today we essentially cover the whole Periodic Table, and as regards crystal structure studies we see no particular limitation of the present local density approximation.

In this context it is also of interest to consider thorium metal. For a long time the observed fcc crystal structure was taken as evidence for a normal transition metal behaviour dominated by the d electron character. However it was recently shown (Ahuja et al., 1995) that this is not at all the case, since instead a regular tetravalent d transition metal should either have an hcp, bcc or ω-structure. It was only when the presence of some $5f$ character in the conduction band was included in the theoretical treatment that the observed fcc structure could be reproduced. Therefore, actually all the metals Th-Pu can be said to have anomalous crystal structures when compared to the rest of the periodic system. It is most important to notice that these structures can only be explained by the bonding properties of the itinerant $5f$ electrons. Thus, the recent theoretical work regarding the actinide crystal structures has shown that the earlier theory regarding the cohesion of these metals is correct, namely that the lighter elements form a unique series of metals with $5f$ electrons as the dominant part of the metallic bonding and that the heavier elements behave as a second rare-earth series with atomic-like $5f$ electrons (Johansson, 1975; Johansson and Rosengren, 1975b).

4   Local-moment collapse in compressed Sm metal

Recent developments of the experimental high pressure technique have made it possible to study materials at static pressures in the Megabar range (Mao et al., 1989; Vohra and Ruoff, 1990). One can now begin to investigate solids under new experimental conditions, where the volume is reduced to typically half of its normal value ($V/V_0 = 0.5$, where V_0 is the equilibrium volume). It has therefore become a great challenge for theory to cover this new physical regime for various classes of materials.

The magnetic rare-earth metals are especially interesting in connection with extreme compressions. Normally, in most cases the $4f$ electrons are localized and the associated magnetic moments are very well described by atomic theory (Jensen and Mackintosh, 1991). This fact forms the basis for the so-called standard model for rare-earth systems. Furthermore, the lanthanides are well understood from a trivalent picture (Ce, Eu, and Yb are exceptions) and the metallic bond originates

from a rather broad conduction band containing three (*spd*) electrons. The trivalent metals crystallize in hexagonal close packed structures (hcp, Sm-type, and dhcp). Theoretical calculations (Duthie and Pettifor, 1977; Skriver, 1985) show that the crystal structure sequence is correlated with the *d* occupation of the valence band [or to a related quantity, the ratio between the metallic and ionic radii (Johansson and Rosengren, 1975a)]. It has actually been demonstrated that the crystal structure sequence found when traversing the lanthanide series, dhcp → Sm-type → hcp, originates from the decreasing *d* occupation. Also, applying pressure to a late lanthanide metal increases the *d* character of the metallic bond and correspondingly the reversed structure sequence, hcp → Sm-type → dhcp, is observed. At sufficiently high pressure the trivalent lanthanide metals transform first to the fcc structure and then to a trigonal distortion of the fcc structure (Vohra et al., 1991; Staun-Olsen et al., 1991; Grosshans and Holzapfel, 1992). Hence, all previous high pressure work show transitions between close packed structures, and the understanding of this behaviour is based on a trivalent ground state with chemically inert 4*f* electrons (Johansson and Rosengren, 1975). However, relatively recent experimental high pressure work (Vohra et al., 1991) showed that at around 1 Mbar Sm adopts a quite unique body centered tetragonal (bct) structure. Such kind of structures (open, low symmetric) have previously mainly been found in delocalized *f* metals and in the present context it is tempting to associate the bct structure with an onset of *f* bonding (Johansson, 1974).

With this in mind Söderlind et al. (1993) performed a study of Sm at these new extreme conditions. In order to determine when the 4*f* states might become itinerant in Sm, these authors compared the bonding energy associated with delocalized *f* states with the atomic polarization energy (E(pol)) associated with localized *f* states. To do this they had to compare the total energy between two different electronic states for highly compressed samarium, namely the standard localized $4f^5(^6G_{\frac{5}{2}})$ trivalent metallic state and the itinerant 4*f* state, where for the latter not only the *spd* states but also the *f* states are part of the conduction band. The total energies for the two phases were calculated using a full potential linear method (FPLMTO) (Wills and Cooper, 1987). These calculations make no shape approximation for the charge density and potential and are based on the local density approximation of the density functional theory. For the localized phase the 4*f* states were treated as part of the core and with a statistical occupation of the $4f_{\frac{5}{2}}$ and $4f_{\frac{7}{2}}$ levels, which corresponds to the grand barycentre for the atomic-like $4f^5$ manifold. The total energies for the two phases will therefore be directly comparable if the energy difference between the grand barycentre and the lowest atomic multiplet is taken into account for the trivalent state (Johansson et al., 1980; Johansson and Skriver, 1982). This energy, E(pol), is known to be 5.8 eV from analysis of atomic spectra (Nugent, 1970).

At zero pressure the crystal structure of samarium metal is a 9 layer stacking sequence of hexagonal planes (Sm-structure) and the experimental equilibrium atomic volume V_0 is equal to 33.2 Å^3. However, as mentioned above it is well-known that the lighter lanthanides under high pressure transform into the fcc structure (Vohra et al., 1991). Therefore Söderlind et al. (1993) used the fcc structure in the calculations for the standard local moment, trivalent samarium metal and for the itinerant state they used the experimentally reported high pressure structure, bct (with the observed axial ratio $c/a = 1.76$). For the study of the local moment collapse these particular choices of structures are however not crucial.

By introducing the atomic energy, $E(\mathrm{pol})$, Söderlind et al. (1993) could perform a proper energy comparison between the localized and itinerant states from first principles calculations of the total energies as a function of volume (Johansson and Skriver, 1982). This comparison is shown in Fig. 6, where the total energy has been plotted as a function of volume both for the delocalized and localized phases. Notice that there is a transition from the localized fcc phase at 18.3 Å^3
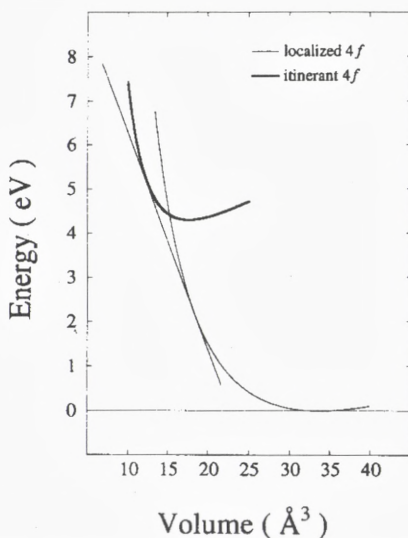

Figure 6. Total energies for Sm with localized (thin line) and delocalized (thick line) $4f$ electrons. The energy for the localized phase is corrected by the polarization energy $E(\mathrm{pol})$ in order to account for the lowest multiplet state of the $4f^5$ configuration (see text). The transition pressure is obtained from the common tangent construction.

to the delocalized bct phase. The transition pressure, obtained from the common tangent shown in Fig. 1, is 0.8 Mbar. This result is consistent with the experimental finding of a bct structure being stable at high compressions, since it is known that chemically bonding f electrons favour open, low symmetry structures (Johansson, 1974). However, experimentally the volume collapse associated with the bct phase is much smaller than the calculated value, a point we will return to below.

The validity of the finding that the highly compressed phase of Sm has delocalized $4f$ states, can be further investigated by consideration of the crystallographic parameters, like for example the c/a axis ratio of the bct structure. This is in fact a very sensitive test, since crystal structure energy differences are very small and sensitive to the details of the electronic structure. Söderlind et al. (1993) treated the $4f$ states as delocalized and calculated the total energies of Sm using three different crystal structures; fcc, bct, and the orthorhombic α-U structure. The α-U structure was included since this structure is found in many delocalized f electron systems [U (Zachariasen, 1952); Ce (Ellinger and Zachariasen, 1974); Pr (Smith and Akella, 1982; Grosshans et al., 1983) and Am (Benedict, 1984)]. This was done at volumes where it is known experimentally that the bct structure is stable, with a c/a ratio of 1.76. For the α-U structure the crystallographic parameters corresponding to α-Ce were used. These calculations covered the volume range $0.3 < V/V_0 < 0.4$. It was found that the bct structure is favoured over the α-U structure (by about 4–8 mRy/atom) as well as over the fcc structure (by 10–30 mRy/atom). It was due to the presence of itinerant f states in the theoretical treatment that the bct structure obtained the lowest energy.

To further illustrate the importance of the f electrons for the crystal structure Söderlind et al. (1993) calculated the energy of the Bain path (total energy as a function of the c/a ratio for the bct structure) for both delocalized and trivalent Sm at a compression $V/V_0 = 0.37$ (Fig. 7). It is worthwhile to remark here that the bct structure is the same as the bcc structure for $c/a = 1$ and the same as the fcc structure for $c/a = \sqrt{2}$. Fig. 7 shows that for the trivalent localized $4f$ configuration the bcc structure is stable, in disagreement with the experimental finding. However, the delocalized (paramagnetic) configuration yields the correct structure, bct. Hence, only for delocalized states could Söderlind et al. (1993) reproduce the correct structure. However, the calculated c/a ratio (1.95) is substantially larger than the experimental data (1.76). This large disagreement indicates that the $4f$ contribution to the bonding is overemphasized. However, in these calculations a paramagnetic state was imposed. Removing this restriction and allowing the system to break the spin degeneracy, a very substantial spin moment was obtained, which is displayed in Fig. 8 as a function of volume for the ferromagnetic state. Notice that at volumes where one finds the delocalized phase to be stable (see Fig. 6) the magnetic moment is changing quite dramatically as a function of volume.
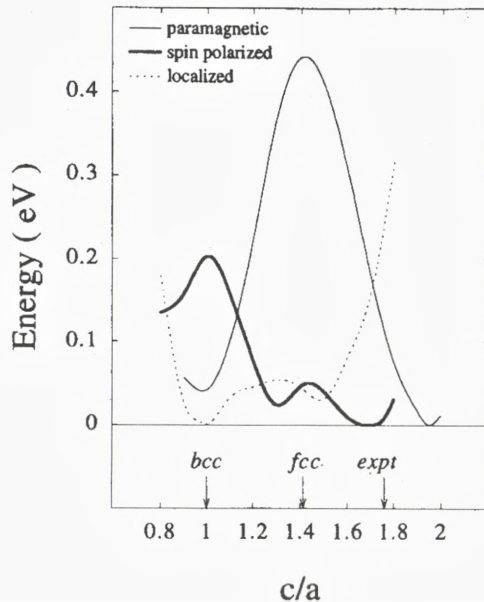
Figure 7. Theoretical Bain path for Sm at 37 % of the experimental volume. The thin full-drawn and bold full-drawn lines refer to a treatment of the $4f$ electrons as itinerant-paramagnetic and itinerant-spin polarized, respectively. The dotted line represents the result for the localized phase, where the $4f$ electrons are considered as part of the inert core.

Nevertheless, at the transition volume the spin moment is substantial, about 4 μ_B. An account of this ferromagnetic state in the theoretical equation-of-state would decrease most significantly the volume collapse ascribed to the delocalization process (compare above). At sufficiently low volumes the moment disappears and Sm metal becomes a $4f$ delocalized paramagnet. Söderlind et al. (1993) also calculated the energy of the Bain path for the ferromagnetic phase of Sm (Fig. 7). Notice that now, for the spin polarized state, the theoretical c/a ratio (1.70) agrees very well with experimental data. Therefore, both direct total energy considerations as well as the more indirect details concerning the atomic structural arrangement suggest that Sm metal at high pressures is a $4f$ itinerant magnet.

Based on the above comparisons with experimental data, it is clear that strong theoretical evidence has been obtained for that the localized $4f$ moment in samarium metal has become itinerant in the Mbar pressure range. This is remarkable since the samarium $4f^5$ moment is normally considered to be extremely stable against external influences. This finding opens the prospects that even the local moments in europium, gadolinium and terbium might become unstable at pressures
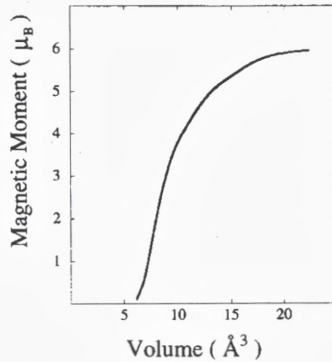
Figure 8. The calculated ferromagnetic spin moment for the itinerant phase of Sm as a function of volume, i.e. the $4f$ electrons are considered as conduction electrons.

attainable at laboratory conditions. The discovery of ferromagnetism in samarium at high compressions strongly suggests that we might have disclosed a *new research area for itinerant magnetism*, namely lanthanides at a pressure of 1 Mbar.

5   Calculated phase diagram for Ce metal

Cerium is one of the most fascinating elements in the Periodic Table. It has, in particular, an extremely rich phase diagram with at least five allotropic forms (Koskenmaki and Gschneidner, 1979). Most attention has been focussed on the γ–α isostructural phase-transition where the high-volume face-centered cubic (fcc) γ phase collapses into the low-volume fcc α-phase at a pressure of about 7 kbar. There is little doubt about the electronic nature of this transition and a great number of theoretical investigations have dealt with the electronic properties of cerium (Coqblin and Blandin, 1968; Ramirez and Falicov, 1971; Hirst, 1974; Johansson, 1974; Glötzel, 1978; Podloucky and Glötzel, 1983; Pickett et al., 1981; Min et al., 1986; Allen and Martin, 1982; Lavagna et al., 1982, 1983; Gunnarsson and Schönhammer, 1983; Liu et al., 1992; Allen and Liu, 1992; Eriksson et al., 1990; Szotek et al., 1994; Svane, 1994).

   The unusual behaviour of Ce has been described within a number of models that may be classified into three groups. However, here we will only consider the Mott transition picture advocated by one of the authors (Johansson, 1974). According to this model the nature of the $4f$ states in Ce changes from local non-bonding in the γ-phase to itinerant bonding in the α-phase. A number of recent ab initio calculations, where one assumes that the $4f$ electron is localized in γ-Ce but delocalized in α- and α'-Ce, have given excellent results for the ground state

properties of γ- and α-Ce (Eriksson et al., 1990; Szotek et al., 1994; Svane, 1994) as well as for the α'-phase (Wills et al.,1991; Eriksson et al., 1992). Moreover, by applying the self-interaction corrected (SIC) local density approximation (LDA) Szotek et al. (1994) and Svane (1994) found that in spite of the dramatic change in the electronic structure at the transition, the difference in total energy between γ- and α-Ce is of the order of mRy. A similar energy difference was found by Eriksson et al. (1990) and this is exactly what is required to describe the transition in the Mott transition model.

Recently the pressure-temperature phase diagram of cerium was calculated by Johansson et al. (1995) based on the Mott transition picture and the thermodynamic
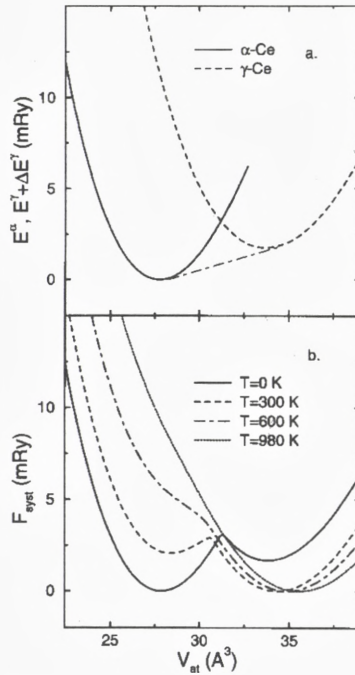
Figure 9. Binding energy curves for α- and γ-Ce (a) and the free energy of the system F_{syst} at different temperatures (b) as a function of atomic volume V_{at}. The energies in (a) are relative to the minimum energy for α-Ce while in (b) they are relative to the minimum value of F_{syst} at the corresponding temperature. The dot-dashed line in (a) corresponds to the extrapolated experimental value of -6 kbar for the (negative) transition pressure at zero temperature. The energy shift ΔE in Eq. (5) has been adjusted to reproduce this transition pressure.

model illustrated in Fig. 9. According to this, there are at zero temperature two phases for Ce, a low volume α-phase which is stable, and a high volume γ-phase which is metastable. The resulting binding energy curve viewed as a function of volume is formed by two branches corresponding to α- and γ-Ce, respectively, which cross at some intermediate volume. The transition between α- and γ-Ce represented by the common tangent in Fig. 1 occurs when the lattice is expanded and from the experimental data reviewed by Koskenmaki and Gschneidner (1979) the transition pressure is deduced to be -6 kbar.

As the temperature increases the state (α or γ) which is metastable may be thermally populated. Hence, there is a probability x of finding a γ-Ce atom in the system and a $1 - x$ probability of finding an α-Ce atom. Therefore, one may consider the cerium metal as a pseudo-alloy between the γ- and α-phases and write its free energy F_{alloy} for any "concentration" x, volume V and temperature T as

$$F_{\text{alloy}}(x, V, T) = E(x, V) - TS(x) + F_{lv}(x, V, T). \tag{1}$$

Here, E is an average internal energy per atom in the pseudo-alloy at $T = 0$, S the entropy, and F_{lv} the free energy of the lattice vibrations.

The configurational mixing entropy is taken into account by using the mean-field (MF) approximation

$$S_{\text{conf}}(x) = -k_B[x \ln x + (1 - x) \ln(1 - x)], \tag{2}$$

where k_B is the Boltzmann constant. In addition to this also the magnetic entropy from the localized magnetic moment on the γ-Ce atoms must be included. Assuming that for temperatures of interest only the ground state multiplet with total angular momentum $J = \frac{5}{2}$ is appreciably populated, the magnetic entropy becomes

$$S_{\text{magn}}(x) = k_B x \ln(2J + 1). \tag{3}$$

Finally, the vibrational free energy $F_{lv}(x, V, T)$ is estimated from the Debye-Grüneisen model (Moruzzi et al.,1988).

Since γ-cerium can transfer into α-cerium and vice versa, the alloy concentration is not a free parameter as in the case of a real alloy system. Instead, the concentration x_{eq} is determined from the value which for a fixed volume and temperature minimizes the free energy. Hence, one arrives at the final expression for the free energy of the system

$$F_{\text{syst}}(V, T) = F_{\text{alloy}}(x_{eq}(V, T), V, T). \tag{4}$$

Having derived F_{syst} as a function of volume one may obtain Gibbs free energy $G = F + PV$, where P is the pressure, and determine the transition pressure of

the γ–α phase change at any temperature. In this way the P–T phase diagram for Ce can be obtained, based on the Mott transition model for the electronic transformation within the $4f$ shell.

To obtain realistic results, a good description is needed for the initial α- and γ-states as well as for the alloy total energy $E(x, V)$. In particular, for the accuracy of the calculated phase diagram it is important that the equilibrium volumes of pure γ- and α-Ce are well reproduced by the total energy calculations. For this purpose Johansson et al. (1995) used the scalar-relativistic linear muffin-tin orbitals (LMTO) method, within the atomic sphere approximation (ASA) and in the tight-binding representation (Andersen et al., 1985; Gunnarsson et al., 1983; Skriver, 1984). This was performed in conjunction with a Green's function technique and a treatment of the alloy utilizing a scheme based on the single-site coherent-potential approximation (SS-CPA) (Johnson et al., 1990; Abrikosov et al., 1993).

To describe paramagnetic α-Ce the $4f$-electron is regarded as a delocalized valence electron. Note that such an assumption together with LDA is known to lead to an underestimate of the equilibrium volume and an overestimate of the bulk modulus compared with the experimental values. However, this is basically an effect of using the LDA rather than an effect associated with any special properties of α-Ce. Moreover, Söderlind et al. (1994) found that the ground state parameters α-Ce are very sensitive to the approximation used for the exchange-correlation functional. When one applies the Becke–Perdew gradient correction (GGA, Perdew, 1986; Becke, 1988) to the exchange-correlation potential one obtains a much better agreement between the calculated and experimental atomic volume and bulk modulus for α-Ce. For this reason, Johansson et al. (1995) chose to describe pure α-Ce and the α-Ce atoms in the alloy within this approximation for exchange and correlation.

The localized $4f$-electron in γ-Ce can be accounted for by means of the SIC-LDA scheme (Szotek et al., 1994; Svane, 1994). However, in an alloy this becomes numerically very complicated and instead an approach used earlier by Min et al. (1986), can be applied. In this scheme the $4f$-electron in γ-Ce is treated as fully localized by including it as part of the inert core, but the f functions are kept in the LMTO valence basis set. Using the Vosko–Wilk–Nusair parametrization (Vosko et al., 1980) of the exchange-correlation energy density and potential the calculations for the equilibrium atomic volume and bulk modulus of γ-Ce show excellent agreement with the results obtained from the SIC-LDA calculations (Szotek et al., 1994; Svane, 1994) as well as with experimental values. These are the set of approximations which Johansson et al. (1995) applied in the description of the pseudo-alloy.

Within the frozen core approximation (Gunnarsson et al., 1983), used in the simplified description of γ-Ce, the contribution to the energy from the localized

$4f$ electron is discarded. The energies of the two phases of Ce must therefore be aligned by an energy shift ΔE added, for instance, to the total energy of γ-Ce. This is the only adjustable parameter in the model and it is only introduced for technical reasons rather than as a matter of principles. The internal energy $E(x, V)$ in Eq. (1) may now be written in the form

$$E(x, V) = (1 - x)E_\alpha(x, V) + xE_\gamma(x, V) + \Delta E, \tag{5}$$

where $E_j(x, V), j = \alpha, \gamma$, is the calculated total energy per α (or γ) atom.
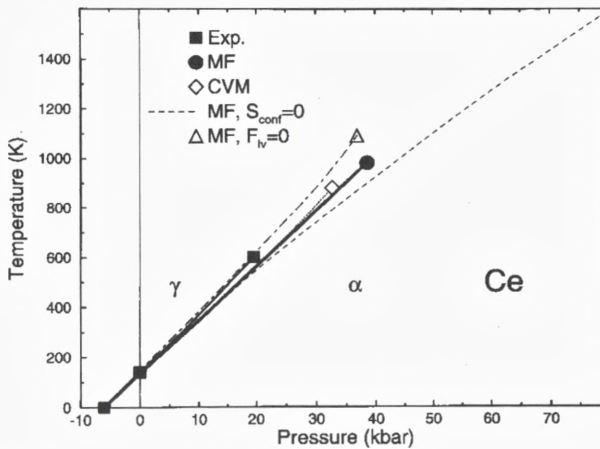
Figure 10. Pseudoequilibrium pressure-temperature phase diagram for Ce. The experimental result is taken from Koskenmaki and Gschneidner (1979) and shown by the full line and filled squares. The zero temperature is obtained by extrapolation. The diagram calculated within the mean-field (MF) approximation and with all the contributions to the free energy included is shown by the heavy line. The corresponding critical point is shown by the full circle. The results obtained by the cluster variation method (CVM) are indicated by the dotted line and the open diamond. The dashed line corresponds to a MF phase diagram where the effect of alloying is neglected, i.e. $S_{conf} = 0$, and the dot-dashed line with the open triangle corresponds to the MF result calculated without the vibrational contribution to the free energy, i.e. $F_{lv} = 0$.

The calculated phase diagram for the γ–α transition in Ce is shown in Fig. 2 together with the experimental phase diagram taken from Koskenmaki and Gschneidner (1979). It is seen, that the theory, correctly describes the salient features of the phase diagram, i.e., the linear dependence of the transition temperature on pressure and the existence of a critical point. The zero pressure transition tem-

perature is calculated to be 135 K in excellent agreement with the experimental value 141 ± 10 K. The critical point is found at 980 K and 38.6 kbar, in fair agreement with experiment (600 ± 50 K, 19.6 ± 2 kbar) (Koskenmaki and Gschneidner, 1979). A small overestimate of the critical temperature and pressure is to be expected because of the application of the mean-field approximation for the entropy. If the more elaborate cluster variation method (CVM) is used in conjunction with the CPA-Connolly–Williams scheme for calculating interatomic interactions (Abrikosov et al., 1993) an even better result for the calculated P–T diagram is obtained (compare Fig. 10).

An analysis of the results shows that the dominating entropy contribution originates from the magnetic moment on the Ce atoms, which is zero in the α-phase and $k_B \ln(2J + 1)$ in the γ-phase. The transition pressure can now easily be estimated as (Johansson et al., 1993)

$$P(T) = P_0 + k_B T (V_{\gamma 0} - V_{\alpha 0})^{-1} \ln(2J + 1), \tag{6}$$

where the subscript 0 refers to properties at $T = 0$. This immediately explains the observed linear dependence of the transition temperature on the pressure. Finally, for the artificial, intermediate volumes the equilibrium concentration x_{eq} is substantial already at relatively low temperatures (about 300 K). This results in a *softening* of the crossover between the two branches of the free energy, as shown in Fig. 9b, and in the end to *the occurrence of the critical point*. When the effect of alloying is completely neglected the low temperature behaviour of the phase diagram is almost identical to that of the complete calculation, but the critical point is lost.

References

Abrikosov IA, Ruban AV, Kats DYa and Vekilov YuH, 1993: J. Phys. Condens. Matter **5**, 1271

Ahuja R, Eriksson O, Wills JM and Johansson B, 1995: Phys. Rev. Lett. **75**, 3473

Allen JW and Martin RM, 1982: Phys. Rev. Lett. **49**, 1106

Allen JW and Liu LZ, 1992: Phys. Rev. B **46**, 5047

Andersen OK, Jepsen O and Glötzel D, 1985: in *Highlights of Condensed-Matter Theory*, eds. F. Bassani, F. Fumi and M.P. Tosi (North Holland, New York)

Becke AD, 1988: Phys. Rev. A **38**, 3098

Benedict U, 1984: J. Phys. Colloq. (Paris) **45**, 145

Brooks MSS, Johansson B and Skriver HL, 1984: *Handbook on the Physics and Chemistry of the Actinides*, eds. A.J. Freeman and G.H. Lander (North-Holland, Amsterdam, 1984) p. 153

Brooks MSS and Johansson B, 1993: *Handbook of Magnetic Materials*, ed. K.H.J. Buschow (Elsevier, Amsterdam) Vol. 7, p. 139

Coqblin B and Blandin A, 1968: Adv. Phys. **17**, 281

Duthie JC and Pettifor DG, 1977: Phys. Rev. Lett. **38**, 564

Ellinger FH and Zachariasen WH, 1974: Phys. Rev. Lett. **32**, 773

Eriksson O, Brooks MSS and Johansson B, 1990: Phys. Rev. B **41**, 7311

Eriksson O, Wills JM and Boring AM, 1992: Phys. Rev. B **46**, 12981

Glötzel D, 1978: J. Phys. F **8**, L163

Grosshans WA, Vohra YK and Holzapfel WB, 1983: J. Phys. F **13**, 14

Grosshans WA and Holzapfel WB, 1992: Phys. Rev. B **45**, 5171

Gunnarsson O and Schönhammer K, 1983: Phys. Rev. B **28**, 4315

Gunnarsson O, Jepsen O and Andersson OK, 1983: Phys. Rev. B **27**, 7144

Hirst LL, 1974: J. Phys. Chem. Solids **35**, 1285

Jensen J, and Mackintosh AR, 1991: *Rare Earth Magnetism: Structures and Excitations* (Clarendon Press, Oxford)

Johansson B, 1974: Philos. Mag. **30**, 469

Johansson B, 1975: Phys. Rev. B **11**, 2740

Johansson B, 1978: J. Phys. Chem. Solids **39**, 467

Johansson B and Rosengren A, 1975a: Phys. Rev. B **11**, 2836

Johansson B and Rosengren A, 1975b: Phys. Rev. B **11**, 1367

Johansson B, Skriver HL, Mårtensson N, Andersen OK and Glötzel D, 1980: Physica B **102b**, 12

Johansson B and Skriver HL, 1982: J. Magn. Magn. Mater. **29**, 217

Johansson B and Brooks MSS, 1993: *Handbook on the Physics and Chemistry of Rare Earths*, eds. K.A. Gschneidner Jr., L. Eyring, G.H. Lander, and G.R. Choppin (Elsevier Science Publishers, Amsterdam) Vol. 1, p. 149

Johansson B, Abrikosov IA, Aldn M, Ruban AV and Skriver HL, 1995: Phys. Rev. Lett. **74**, 2335

Johnson DD, Nicholson DM, Pinski FJ, Gyorffy BL and Stocks GM, 1990: Phys. Rev. B **41**, 9701

Koskenmaki DC and Gschneidner Jr KA, 1979: *Handbook on the Physics and Chemistry of Rare Earths*, eds. K.A. Gschneidner Jr., and L. Eyring (North-Holland, Amsterdam) Vol. 1, p.337

Lavagna M, Lacroix C and Cyrot M, 1982: Phys. Lett. **90A**, 210

Lavagna M, Lacroix C and Cyrot M, 1983: J. Phys. F **13**, 1007

Liu LZ, Allen JW, Gunnarsson O, Cristensen NE and Andersen OK, 1992: Phys. Rev. B **45**, 8934

Mao HK, Wu Y, Hemley RJ, Chen LC, Shu JF and Finger LW, 1989: Science **246**, 649

Moruzzi VL, Janak JF and Schwarz K, 1988: Phys. Rev. B **37**, 790

Min BI, Jansen HJF, Oguchi T and Freeman AJ, 1986: Phys. Rev. B **34**, 369

Nugent LJ, 1970: J. Inorg. Nucl. Chem. **32**, 3485

Perdew JP, 1986: Phys. Rev. B **33**, 8822

Pickett WE, Freeman AJ and Koelling DD, 1981: Phys. Rev. B **23**, 1266

Podloucky R and Glötzel D, 1983: Phys. Rev. B **27**, 3390

Ramirez R and Falicov LM, 1971: Phys. Rev. B **3**, 2425

Skriver HL, 1984: *The LMTO Method* (Springer-Verlag, Berlin)

Skriver HL, 1985: Phys. Rev. B **31**, 1909

Skriver HL, Johansson B and Andersen OK, 1978: Phys. Rev. Lett. **41**, 42

Skriver HL, Johansson B and Andersen OK, 1980: Phys. Rev. Lett. **44**, 1230

Smith GS and Akella J, 1982: J. Appl. Phys. **53**, 9212

Smith JL and Haire RG, 1978: Science **200**, 535

Smith JL and Kmetko EA, 1983: J. Less. Common Metals **90**, 83

Staun-Olsen J, Steenstrup S, Gerward L, Benedict U, Akella J and Smith G, 1990: High Pressure Research **4**, 366

Svane A, 1994: Phys. Rev. Lett. **72**, 1248

Szotek Z, Temmerman WM and Winter H, 1994: Phys. Rev. Lett. **72**, 1244

Söderlind P, Eriksson O, Wills JM and Johansson B, 1993: Phys. Rev. B **48**, 9212

Söderlind P, Wills JM, Boring AM, Johansson B and Eriksson O, 1994a: J. Phys. Condens. Matter **6**, 6573

Söderlind P, Eriksson O, Johansson B and Wills JM, 1994b: Phys. Rev. B **50**, 7291

Söderlind P, Johansson B and Eriksson O, 1995a: Phys. Rev. B **52**, 1631

Söderlind P, Eriksson O, Johansson B, Wills JM and Boring AM, 1995b: Nature **374**, 524

Sösderlind P, Wills JM, Johansson B and Eriksson O, 1997: Phys. Rev. B (in press)

Vohra YK and Ruoff AL, 1990: Phys. Rev. B **42**, 8651

Vohra Y, Akella J, Weir S and Smith G, 1991: Phys. Lett. A **158**, 89

Vosko SH, Wilk L and Nusair M, 1980: Can. J. Phys. **58**, 1200

Wills JM and Cooper BR, 1987: Phys. Rev. B **36**, 3809

Wills JM, Eriksson O and Boring AM, 1991: Phys. Rev. Lett. **67**, 2215

Wills JM and Eriksson O, 1992: Phys. Rev. B **45**, 13879

Zachariasen WH, 1952: Acta Crystallogr. **5**, 19

Photoelectron Spectroscopy of Cuprate Superconductors

David W. Lynch and Clifford G. Olson

Department of Physics and Astronomy and Ames Laboratory, USDOE,

Iowa State University, Ames IA 50011

Abstract

We present a review of the current status of angle-resolved photoelectron spectroscopy of the valence bands of cuprate superconductors, including results from the first half of 1996.

1 Introduction

Photoelectron spectroscopy has contributed significantly to our understanding of the electronic structure of cuprate superconductors in both their normal and superconducting states. In the following, we review the information achieved by the technique of angle-resolved ultraviolet valence-band photoelectron spectroscopy (ARUPS). Some of the most definitive studies have been carried out on $Bi_2Sr_2CaCu_2O_8$ (Bi2212) because its surfaces are more predictable and stable than those of other cuprates. Extensive ARUPS studies have been carried out on $YBa_2Cu_3O_7$ (Y123), which has been more widely studied than Bi2212 by all other physical techniques. Studies have been extended to other members of the Bi2212 and Y123 families, as well as to the $Nd_xCe_{2-x}CuO_4$ and the oxy-chloride systems. As "better" single crystals of other cuprates become available it is certain that extensive ARUPS studies will be made without delay. Some of the important questions photoelectron spectroscopy can address, but usually not answer in a simple direct way, are the nature of the normal state (Fermi liquid or not), wave vector dependence of the energy of the photoexcitations (hole quasiparticles) and sometimes their symmetry, the effects of doping on the electronic structure, and the magnitude, anisotropy, and temperature dependence of the superconducting order parameter. Such studies were not carried out on traditional superconductors because the states of interest are within a few $k_B T_c$ of the Fermi energy, a region too narrow for study by photoelectron spectroscopy. The cuprates had values of

T_c so much larger that resolution improvements made their study feasible.

In the following, we outline briefly experimental techniques, emphasizing present limits on resolution and samples. This is followed by a brief description of the theoretical basis for photoelectron spectroscopy. Good reviews of photoelectron spectroscopy exist (Cardona and Ley, 1978; Ley and Cardona, 1979; Plummer and Eberhardt, 1982; Smith and Himpsel, 1982; Courths and Hüfner, 1984; Kevan, 1992; Hüfner, 1995). The bulk of the paper describes experimental results to date. Some of these have implications for microscopic models of the electronic structures of the cuprates, both in the normal and superconducting states. Detailed interpretation of all aspects of the spectra requires a microscopic model, but at the time of this writing, there is not universal agreement on such models. For this reason, and for lack of space, we do not discuss some of the possible interpretations of the data.

There is an enormous literature on cuprates, and a very large one on photoelectron spectroscopic studies on them. To keep the length of this review manageable we concentrate almost exclusively on ARUPS. Angle-integrated photoelectron studies of valence bands, and the study of core level spectra are mentioned only briefly to justify an occasional statement. Similarly, we cannot reference all ARUPS work, but refer the reader to several reviews (Lindberg et al., 1990; Brenig, 1995; Shen and Dessau, 1995; Lynch and Olson, 1997). Results from photoelectron spectroscopy should not be studied in isolation. There are many related spectroscopies whose results should be melded with those of photoelectron spectroscopy. These include x-ray absorption and emission, and electron energy loss spectroscopies. These have been reviewed elsewhere (Fink et al., 1994; Bozovic and van der Marel, 1996). It is also useful to compare photoelectron spectra of the cuprates with those of related materials, e.g., CuO and NiO, but there is not space in this short review to do so. An excellent review of the electronic structure of 3d-transition-metal oxides exists (Hüfner, 1994).

2   Experimental aspects of angle-resolved photoelectron spectroscopy

Conceptually the experiment is simple. A photon excites an electron in a many-electron system. Ideally it emerges from the sample with no measurable change in energy or direction due to internal scattering processes, and it is detected by an angle-resolving electron energy analyzer. From its measured energy and direction, its wave vector is determined. The component of this wave vector normal to the surface has been altered upon escape by the potential "step" at the surface, but for a "good" surface, the parallel component is conserved, modulo a surface

reciprocal lattice vector. (The other component of **k** sometimes may be obtained through further measurements, but for two-dimensional materials like Bi2212 it is not necessary. Y123 is not adequately two dimensional). Use of the photon energy $h\nu$ and the kinetic energy of a Fermi level electron from a reference metal gives the initial state of the electron (or system - see below) E_i, and, since the photon wave vector is small on the scale of electron wave vectors, the initial-state wave vector is the same as that of the final state, modulo a reciprocal lattice vector.

Because work functions range up to about 5 eV or so, energetic photons are required. The commonest sources are the He I and He II lines at 21.2 and 40.8 eV respectively, and synchrotron radiation dispersed by a monochromator. The latter has the advantage of selectable photon energy, allowing use of the energy dependence of the photoexcitation cross section to select for or against particular subshells of electrons. With current technology, the best resolution achieved to date is about an 8 meV spectral bandpass from a monochromator and 5 meV resolution in electron energy analysis. Taking the square root of the sum of the squares gives an overall resolution of about 10 meV. Most of the work reported below used an overall resolution of 25 meV or larger. The best angular acceptance used to date for studies on cuprates is about 1°. This translates into an uncertainty in the parallel component of the wave vector and in the case of dispersive states degrades the energy resolution.

Photon energy resolution may be limited by aberrations in the monochromator, and electron energy resolution by stray electric or magnetic fields or geometric imperfections in the analyzer. When none of these is the limiting factor, then the acceptable flux imposes a limit. Improving resolution always means reducing the flux of photons on the sample. If the flux is reduced, the time to obtain a spectrum at constant signal to noise ratio increases. If surfaces are not stable for long periods of time, the spectra must be taken quickly. In any case, studies on cuprates require many spectra to be taken, and even with stable surfaces and high-quality vacuum, time is always a factor. In the near future, there will be several new beam lines in operation that should yield overall resolutions of 7-8 meV with angular resolution of about 0.5°. Further improvement appears possible.

ARUPS is very surface sensitive. The mean free path for escape without in-elastic scattering is only of the order of 10 Å, i.e., only about a third of the unit cell height for Bi2212. ARUPS requires single crystals. Surfaces must be prepared and measured in ultrahigh vacuum, pressures in the range of 10^{-10} Torr or below. For cuprates, this has traditionally be done by cleaving. The sample is epoxied to a post, and a tab or another post epoxied on top. In vacuum, the upper post is knocked off, giving a cleavage surface. Some of these surfaces have been adequate for ARUPS studies of several cuprates, but for others, e.g., $Tl_2Ba_2CuO_6$, the surface quality has been poor and no ARUPS peaks have yet been found.

Early work on Eu123 (List et al., 1988) showed that spectra measured at 20 K on a surface cleaved at 20 K, then warmed to about 100 K for a few minutes, then recooled to 20 K showed an irreversible change. This was consistent with the loss of a small amount of oxygen to the vacuum, an effect later used to explain LEED observations of reconstructed Y123 surfaces (Behner et al., 1992) and with the STM observations of Edwards et al. (1992) Since then, nearly all ARUPS studies have used surfaces cleaved at 20 K and held there, except for temperature increases of short duration to take data above T_c.

The quality of the surface is very important. Differences in the results of several groups, especially in the early years, are most likely due to differences in the quality of the sample surfaces, which derive from the quality of the single crystals used. It has not been easy to determine what plane is exposed upon cleaving. Core-level studies by x-ray-induced photoelectron spectroscopy have been used to try to determine this, but the situation is complex. For example, these studies show that Bi2212 cleavage surfaces are Bi–O planes. It is believed the cleave occurs between pairs of adjacent weakly bonded Bi–O planes and both new surfaces are equivalent. STM studies also show this surface. Such is not the case with Y123, where freshly cleaved surfaces are usually said to be Ba–O planes. From Fig. 1 we see that cleaving between Ba–O and Cu–O planes can be done two ways, along dashed planes marked 1 and 2. Only one of these leaves a Ba–O plane for the surface of the bottom half; the Ba–O plane after cleavage 2 falls away. Cleaves 3 and 4 separate a Ba–O plane from a Cu–O chain. Surfaces 3 and 1, both Ba–O surfaces, are not equivalent because different planes lie below them. If cleaves of the type 1 and 2 are easier, the surface may contain a distribution of them, roughly half the area being a Ba-O surface, with numerous steps. In general, up to four different surfaces could be exposed upon cleaving. There is even a suggestion that in some unusual cleaves an Y surface may be exposed (Schroeder et al., 1993). One way to determine the cleavage surface is to compare photoelectron spectra with those calculated for all possible terminating planes (Calandra and Manghi, 1992, 1994). Bansil et al. (1992) carried out such a calculation of the ARUPS spectra expected for all six possible (1 0 0) surfaces after cleaving. Comparison with experimental spectra led them to conclude that the surface measured was a Ba–O plane with a Cu–O_2 plane just below it. However, Edwards et al. (1992), cleaved surfaces of Y123 in ultrahigh vacuum at low temperature. They observed by STM the cleavage plane to be between a Ba–O plane and the plane of the Cu–O chains. This surface lost oxygen upon being heated to 70 K. (Y123 crystals are also twinned, altering their apparent symmetry. They can be "detwinned", but the breakage rate is very high.)

In addition to the primary photoelectron spectrum, there are secondary electrons, electrons which have lost a measurable amount of energy before escaping (in
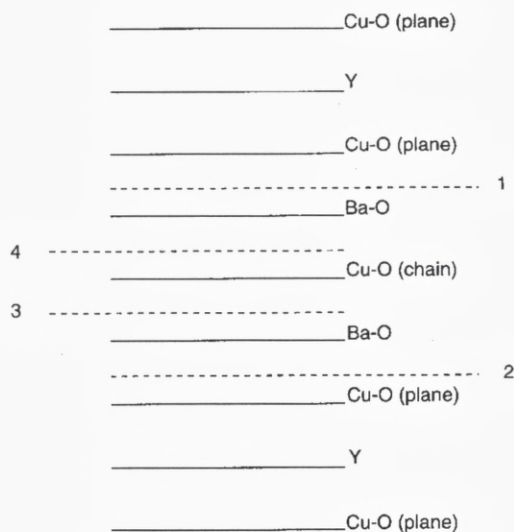
Figure 1. Schematic of the atomic layers in Y123. The numbered dashed lines indicate possible cleaves. See text.

one model of photoemission). These form a nearly structureless background spectrum at kinetic energies lower than those of the primaries, i.e., at greater apparent binding energies. It would be useful to strip this from the measured spectrum, but this has rarely been attempted in ARUPS for several reasons. The inelastic scattering is usually assumed to be due to electron–electron scattering, and for electrons of relatively low energy, any single-scattering model should not be accurate. The electron wavelength exceeds the distance between scattering centers and a multiple scattering formalism should be used. Also, the methods used to remove inelastic backgrounds from XPS spectra require either a part of the spectrum where no primaries are expected to exist or electron energy loss spectra for the material. High-resolution ARUPS scans take considerable time and rarely extend far enough to reach the region of excitation below the bottom of the valence band, and the requisite electron energy loss measurements as a function of both energy and momentum with adequate energy resolution do not exist.

A striking feature of ARUPS spectra of cuprates compared with spectra of other materials is the very large "background". The peaks near the Fermi energy in Bi2212 ARUPS spectra are only about twice as large as the background 300–500 meV below the Fermi energy. This ratio is about the same for spectra taken by several groups on crystals grown by several groups over a period of 7 years. Figure 2 shows spectra taken under comparable conditions for Bi2212 and $TiSe_2$, illus-

trating the difference in apparent backgrounds. Over the past 7 years, the visual quality of the cleaved surfaces has improved, but the background has not changed. One interpretation of this is that for the cuprates this is not a background of in-elastically scattered electrons but rather an intrinsic feature of the photoelectron spectrum due to leaving the system in a continuum of excited states (see below). Another is that the surface is intrinsically defective due to the oxygen vacancies introduced by doping to produce the metallic superconductor from the insulating parent compound. Defects spaced an average distance Λ apart can create a wave vector uncertainty of the order of Λ^{-1}. Kevan (1986) has shown that the addition of 1–2% of a monolayer of K atoms to a Cu surface had a broadening effect on the photoelectron spectrum from a surface state. (The inelastic background was not studied). The expected oxygen vacancy concentration in an optimally doped cuprate is comparable to that in Kevan's work. However, there is yet no experimen-tal proof for the origin of the large background found in cuprate spectra. Figure 2 also illustrates how weak a feature one is dealing with in studying the near-Fermi edge photoemission in cuprates. Under comparable conditions, the count rate for the TiTe$_2$ spectrum is about 20 times that of the Bi2212 spectrum. At larger bind-ing energies, the count rate for Bi2212 increases considerably, but this region is of less interest.

3   Theoretical aspects of angle-resolved photoelectron spectroscopy

Although a "three-step" model (excite, transport to the surface, escape) has been used for many years, and is still in use for some purposes, the correct picture is of a one-step process. Initially one has an N-electron system and a photon (which can be treated classically), and at the end, there is an $N - 1$ electron system, an electron in the detector, and no photon. The $N - 1$ electron system need not be left in its own ground state. The Hamiltonians for the two systems are thus not the same, although if the independent-electron approximation is made, as in band theory, they are the same, and the energy of any one eigenstate is independent of the occupancy of other eigenstates. The energy and momentum of the detected electron are then related to the energy and momentum of the hole in the $N - 1$ electron system. The interaction of an electron with the electromagnetic field is effected by the perturbation Hamiltonian, $H' = (e/mc)(\mathbf{A} \cdot \mathbf{p} + \mathbf{p} \cdot \mathbf{A})$, where $\mathbf{A}$ and $\mathbf{p}$ are the vector potential and momentum operators, respectively. The in-teractions with the surface and with the other electrons (inelastic scattering) are handled in the Green's function G of the final state electron. The photocurrent in the detector is proportional to the product of the square of the electric dipole
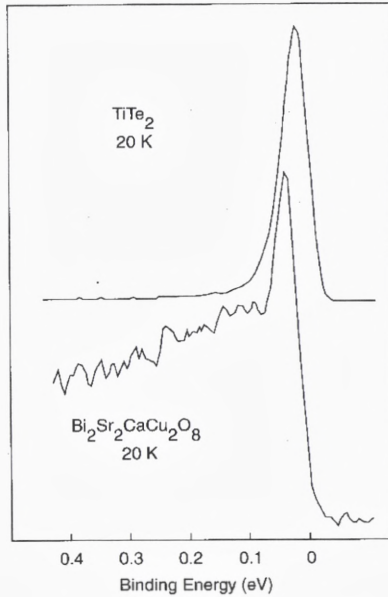
Figure 2. Photoelectron spectra of Bi2212 and $TiTe_2$. These spectra were taken at comparable energy and angle resolutions and photon fluxes. The peak count rate for $TiTe_2$ is about 20 times that of Bi2212. The rising edge in the Bi2212 spectrum is shifted away from the Fermi level because the sample is superconducting.

(momentum) matrix element between initial and final states and the spectral density $A(E, \mathbf{k}) = (1/\pi)\mathrm{Im}G(E, \mathbf{k})$. For negative energies $A(E, \mathbf{k})$ is the spectrum for electron removal, as in photoemission, and for positive E, the spectrum for electron addition, as in inverse photoemission. The proportionality between photocurrent and $A(E, \mathbf{k})$ is valid only if the sudden approximation is valid, and a priori, one does not know above what final state energy this is a good approximation for a given system. Since the early photoemission studies it has been assumed to be valid for valence band electrons photoexcited with 15–25 eV photons. Recently Randeria et al. (1995) put to rest the fears of those concerned by showing that for Bi2212 the sudden approximation was indeed valid for such spectra, a result presumably extendible to all cuprates.

The widths of the peaks in the photoelectron spectra often are interpreted as arising from the lifetime of the photoelectron and photohole, after the removal of instrumental broadening. In a strictly two-dimensional system, the photoelectron lifetime contribution drops out. The photohole width, if its energy dependence can be measured close enough to E_F, would give an important test for many-

body models for the quasiparticles. Unfortunately, the reliable extraction of the photohole lifetime from data is very difficult (Smith et al., 1993). Moreover, Y123 probably is not sufficiently two dimensional to allow such extraction.

4   Early results

Many of the earliest photoelectron studies on cuprates, primarily Y123, were aimed at demonstrating the presence of Cu^{3+} due to the hole doping but these were not very successful. Often the samples were pressed sintered pellets and fresh surfaces were prepared *in situ* by scraping, which may have exposed intergranular material. All work was at room temperature, except for unsuccessful attempts by UPS to detect the opening of a gap. Photoelectron spectra of the valence bands in these samples rarely showed a Fermi edge, although the bulk samples were known to be metallic. The angle-integrated valence-band photoelectron spectra often resembled those from LDA calculations, but the few features often were shifted to greater binding energy, and there was an unexpected peak at around 9 eV binding energy. Both of these are now believed to be due to the effect of the loss of oxygen to the vacuum, making the surfaces somewhat insulating so they become charged positively upon photoemission. The 9 eV peak is now taken as the signature of a deteriorated surface.

Attempts to see a gap open up upon entering the superconducting phase eventually were successful (Olson et al., 1989). These required single crystal samples cleaved at low temperatures. Bi2212 was the sample of choice, for its cleaved surfaces were much more stable in vacuum than those of Y123, and they could be studied even at room temperature. This early work, at 28–32 meV overall resolution, established a number features of the ARUPS spectra. A peak was tracked from below the Fermi surface till it crossed the Fermi surface along the ΓX line at the wave vector predicted by LDA calculations. (The Brillouin zone is shown in Fig. 4, which illustrates more recent data.) The effective mass was about twice that of the LDA calculation. There seemed to be no effect of the superlattice along the b-direction, but better crystals later showed this result to be spurious. The bands just below E_F along the $\Gamma \bar{M}$ line were rather complicated and not resolved. Finally, the width of the peak along ΓX, decidedly non-Lorentzian, depended strongly on binding energy, and the dependence was linear, not quadratic. However, the quadratic dependence is expected for a Fermi liquid only in a very limited energy range spanning E_F, and the finite energy and momentum resolution causes an effective integration over a region even wider than that for which the quadratic dependence is expected. Moreover, the extraction of a lifetime width from a measured width is extremely difficult to do reliably (Smith et al., 1993). Finally, upon

cooling below T_c, the photoelectron peak "at" E_F was seen to retreat, not rigidly, with a pileup of intensity at the new edge. Fitting to a BCS model gave a gap energy Δ of about 20 meV. There are now different and better ways to extract the gap from the data. The value of 20 meV is probably still correct to within 5 meV, but it represents only the maximum gap at 20 K. This gap was found originally not to depend on wave vector in the basal plane, but more recent work finds considerable anisotropy in good samples. More extensive recent work with improved samples and improved resolution by several groups has confirmed a number of these features, and found many new features. Crystals grown more recently have given some results that are different from those just described. These crystals presumably have better crystallinity and homogeneity. (However the background described above is not smaller).

Similar early work on Y123 also established that the LDA Fermi surface was close to the experimental one, although one part of it was not seen in the experiment. The Fermi edge was weaker than in Bi2212, and no reliable estimates of the gap were published.

5   Current status

Most work has been done on samples near optimal doping. This will be assumed in the following, unless stated otherwise. Photon energies in the 15–25 eV range are usually used because of the broad maximum in the O $2p$ photoexcitation cross section. The structures of interest have widths comparable to the best resolution used to date. The intrinsic spectral shapes then appear in the measured spectra only after convolution with the instrument function, which depends on energy and angle. Assuming these can be factored, the energy part can be determined by measuring the Fermi edge on metal like Pt. The angle dependence is normally not known, and a Gaussian is substituted with a width given by the nominal angular acceptance of the analyzer. Absolute line shapes, or parameters in an assumed line shape are thus not very precisely known. Many conclusions can be drawn without such precise knowledge, however. More important is whether the spectra have been reproduced by at least two groups.

5.1   Bi2212

Band mapping has been carried out in the normal state. Because of the complexity of the bands, only the first 0.5 eV below the Fermi energy has been studied intensely. Earlier work mapped a number of deeper valence bands, but identification with theoretical band structure was difficult. There was initial disagreement in the results of different groups even in the number of bands observed crossing the Fermi

level along a line in reciprocal space. This probably was the result of actual sample differences, both the bulk samples and in the quality of the cleaved surfaces. Figure 3 shows a series of typical scans such as now have been recorded by several groups. One can see a peak that disperses with wave vector, passing through the Fermi level and disappearing. This gives one point on the Fermi surface. Such scans have been carried out for wave vectors covering the ΓXY plane of the Brillouin zone to produce a Fermi surface in good agreement with that from LDA band calculations (Fig. 4). Spectra with peaks below E_F are used to map the quasiparticle band. Along some regions of the Brillouin zone, e.g., ΓX, the experimental band is close to parabolic, but its effective mass is about twice that of the LDA calculation. Along $\Gamma \bar{M}$ the bands are more complex, running rather parallel to the surface. By scanning perpendicular to the $\Gamma \bar{M}$ line along lines passing through this flat region, a line of critical points (near critical points, if we consider experimental resolution), saddle points, has been found. This is a persistent feature, found in many cuprate superconductors.
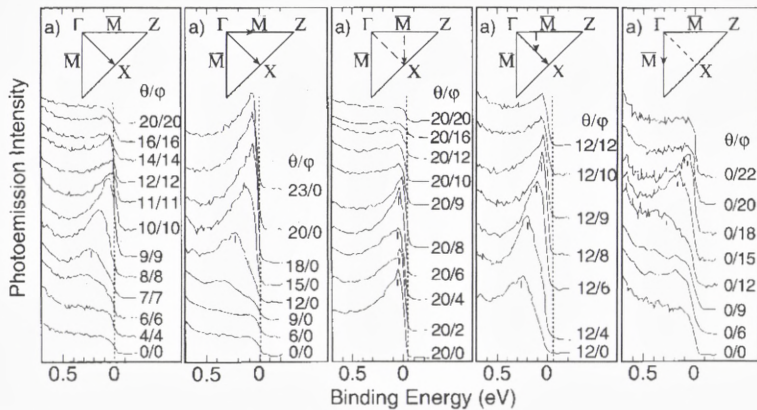
Figure 3. ARUPS scans on Bi2212 at 100 K. The locations of the points in reciprocal space are marked in Fig. 4. (Dessau et al., 1993).

The ΓX and ΓY lines should be nearly equivalent, for the a and b lattice parameters are nearly the same. However, they are not nearly equivalent. There is a superlattice with a repeat distance along the b axis of about 27 Å. The new orthorhombic unit cell is approximately a $\sqrt{2} \times 5\sqrt{2} - 45°$ cell in the tetragonal lattice, a larger unit cell with a smaller Brillouin zone. The bands remap and
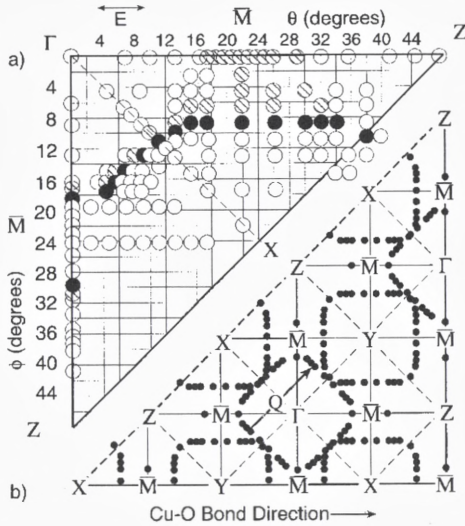
Figure 4. (a) Fermi surface of Bi2212 marked by filled circles. The points where a band crosses E_F were determined from the data in Fig. 3. Empty circles mark locations in the Brillouin zone with no states observed at E_F. Shaded circles mark spectra with states at E_F that do not clearly pass through it in nearby scans. The circle diameters indicate angle resolution. (b) The Fermi surface of (a) repeated in the extended zone by the use of symmetry. **Q** denotes a nesting wave vector. (Dessau et al., 1993).

gaps open at band crossings. Singh and Pickett (1995) have calculated the effect of a similar reconstruction in Bi2201 on the LDA band structure and find rather large effects. Bands based on Bi–O states (the Bi–O planes distort the most in the reconstruction) shift up to 0.4 eV and the Fermi surface is altered. Still, to date, most ARUPS data on Bi2212 are compared with the results calculated for a tetragonal, not orthorhombic, unit cell.

Aebi et al. (1994, 1995) and Osterwalder et al. (1995) measured the photocurrent originating from the Fermi level of Bi2212 over a very fine mesh in angle, taking several thousand spectra over almost 2π steradians. This was done at 300 K. They also examined a Pb-doped sample for which the superlattice does not occur. In addition to the previously known Fermi surface, they found some parts of the Fermi surface exhibiting two-fold symmetry which gave weak signals not present in the Pb-doped samples, see Fig. 5. These were attributed to the effect of the superlattice. They also found several sets of weak "shadow bands" crossing the Fermi surface. These were attributed to antiferromagnetic correlations, rather than Umklapp processes. Kelley et al. (1993) reported differences in dispersion
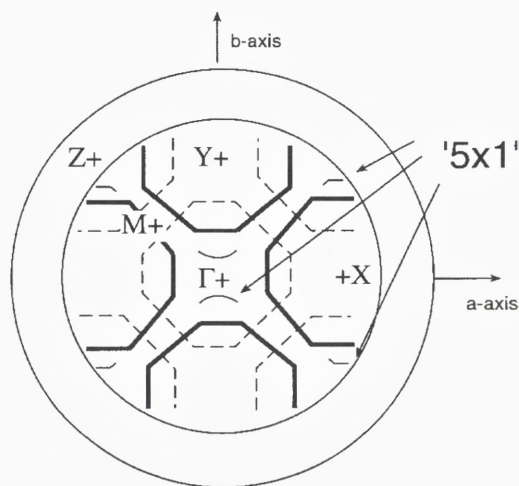
Figure 5. Stereographic projection of the Fermi surface of Bi2212 obtained by Osterwalder et al. (1995). The heavy lines mark the trace of large photocurrents from the normal Fermi surface, as in Fig. 4. The dashed lines are the weaker "shadow bands". The small arcs marked 5 × 1 result from the superlattice. The outer ring of the stereogram represents photoemission parallel to the surface.

between the band crossing E_F along ΓX and along ΓY due to the superlattice. The superlattice and shadow bands were also studied by Ding et al. (1996).

Bi2212 contains two pairs of Cu–O_2 planes, each of which contributes a degenerate set of bands near E_F. Weak interaction between these planes should produce bonding-antibonding pairs of bands, but this has not been found (Ding et al., 1996a) in one recent set of measurements. LDA calculations indicate a splitting of about 0.25 eV near the $\bar{M}$ point (Massida et al., 1988) which would be reduced by many-body effects. Liechtenstein et al. (1996) showed that many body effects reduced the LDA splitting from 300 meV to 40 meV in a model calculation. Depending on dipole matrix elements, a 40 meV splitting might or might not be expected to have been detected in the data Ding et al. took at 13 K.

The ARUPS band maps all indicated a flat band just below E_F along the $\Gamma\bar{M}$ direction. Such a flat region has been found in many cuprates, not just Bi2212, but its distance below E_F varies from material to material, and with doping for any one material. For all the hole-doped cuprates, this flat region is close enough to E_F to be important in any model for the superconductivity.

The original report (Olson et al., 1990) of the photohole lifetime varying as $(E - E_F)^1$ has been controversial, with several discussions of better fitting proce-

dures having appeared subsequently. In fact, it was measured on too coarse an energy scale to related directly to Fermi liquid theory. Moreover, the line shape was not Lorentzian and the width was not small with respect to the photohole energy. At this time, this result remains a tantalizing curiosity. More can be done with higher resolution spectrometers, better knowledge of the final states, and, especially, an understanding of the inelastic background in the ARUPS spectra, if indeed that is what it is.

The first hints of anisotropy in the superconducting order parameter Δ ("the gap") came in 1992 (Wells et al., 1992). The most recent measurements indicate that it has $d_{x^2-y^2}$ symmetry (Shen et al., 1993; Yokoya et al., 1996), see Fig. 6. This has now been found by several groups, and seems to be a secure result. The largest value for Δ, one half the gap, is about 25 meV $\pm$ 5 meV, about 6 $k_B T_c$, and the largest value occurs along the $\Gamma\bar{M}$ line, which corresponds to the direction of the Cu–O bond in real space. The minimum value is 0 with about the same uncertainty, and the minima occur along ΓX and ΓY, 45° from the maxima. (Photoelectron spectra give only the absolute magnitude of the gap). The early determinations of the gap fit the spectral peak in the normal phase to a Lorentzian multiplied by a Fermi-Dirac function convolved with an instrument function. In the superconducting phase, the Lorentzian width was reduced and it was multiplied by the BCS "density of states" although the latter is not appropriate for such a limited volume of reciprocal space. Later work often used the shift of the 50% point on the initial edge near the Fermi energy to obtain Δ. Fehrenbacher (1996) has shown how difficult it is to extract Δ from experimental data with finite energy and angle resolution. The angle dependence of the instrument function is rarely known well.

The temperature dependence of Δ has been measured often, but rarely published because the error bars grow very large as T_c is approached from below. All groups find Δ decreases with increasing T less rapidly than the well-known BCS result $\Delta(T)/\Delta(0) \sim (1 - T/T_c)^{1/2}$ near T_c, in accord with strong coupling theories. There is one report (Ma et al., 1995) of a different temperature dependence for different directions in reciprocal space, but this has not been reported by more than one group.

Below T_c in many parts of the Brillouin zone there is a dip at about 90 meV (about 3–4 Δ) below E_F, followed by a peak at about 100 meV (Dessau et al., 1991, 1992), see Fig. 6. This peak is most prominent for spectra taken along directions in the Brillouin zone associated with larger values of Δ, e.g., $\Gamma\bar{M}$, and small or missing where Δ is small, e.g., ΓX. Ding et al. (1996a) indicate that this structure is not the result of two independent peaks with a valley between. The spectral intensity on both sides of the dip varies in the same way as the photon polarization is changed. The current explanation of this dip is that the opening of
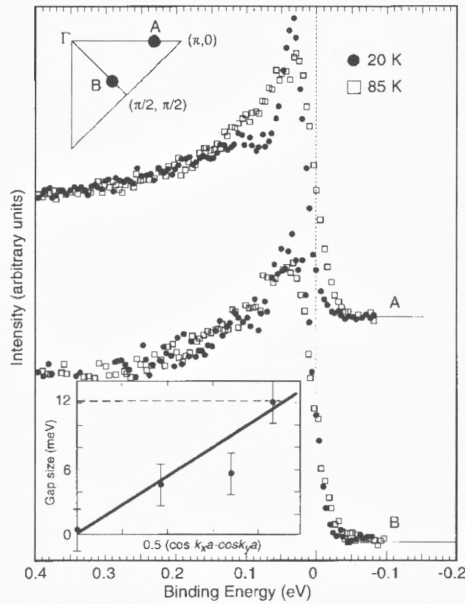
Figure 6. Angle-resolved photoelectron spectra of B12212 below and above T_c at two points in the Brillouin zone, marked in the upper left corner. The shift of the edge and pileup below the edge can be seen in A, where the gap is relatively large. At point B the gap is much smaller. Note also the dip at about 90 meV binding energy for $T < T_c$. The inset shows the dependence of the gap on angular position in the Brillouin zone. (Shen et al., 1995).

a gap suppresses the line width for $E < 3\Delta$, sharpening the structure between 0 and 70 meV (Varma and Littlewood, 1992; Coffey and Coffey, 1993).

Campuzano et al, (1996) recently published an esthetically satisfying study of the approach and retreat of the edge of the Bi2212 ARUPS spectrum. At low temperatures, the BCS spectra function is $A(\mathbf{k}, \omega) = (\pi/2)\Gamma(1 - \epsilon_{\mathbf{k}}/E_{\mathbf{k}})/[(\omega + E_{\mathbf{k}})^2 + \Gamma^2]$, where $\epsilon_{\mathbf{k}}$ is the normal state energy and $E_{\mathbf{k}} = (\epsilon_{\mathbf{k}}^2 + |\Delta(\mathbf{k})|^2)^{1/2}$ is the quasiparticle energy, both measured from E_F. Γ is a line width. The normal state spectrum results if $\Delta = 0$, and any spectral peak, followed as a function of $\mathbf{k}$, should pass through E_F from below and disappear. Below T_c, the closest a peak in $A(\mathbf{k}, \omega)$ can come to E_F is Δ. Scanning from below E_F, the peak in $A(\mathbf{k}, \omega)$ should follow the curve shown in Fig. 7, approaching E_F, but then retreating from it with decreasing intensity, as the quasiparticle amplitude for these $\mathbf{k}$ values is predominantly above E_F. Such behavior was seen in the spectra of Campuzano et al. (Figs. 8 and 9).
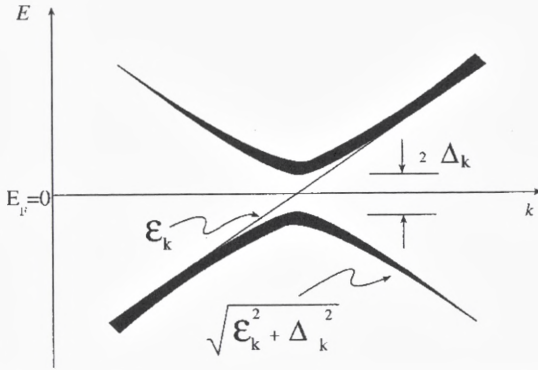
Figure 7. Behaviour of expected quasiparticle dispersion in the normal (thin straight line) and superconducting state. The line width of the lower curve for the super-conducting state indicates the intensity expected in the photoelectron spectrum. (Campuzano et al., 1996).
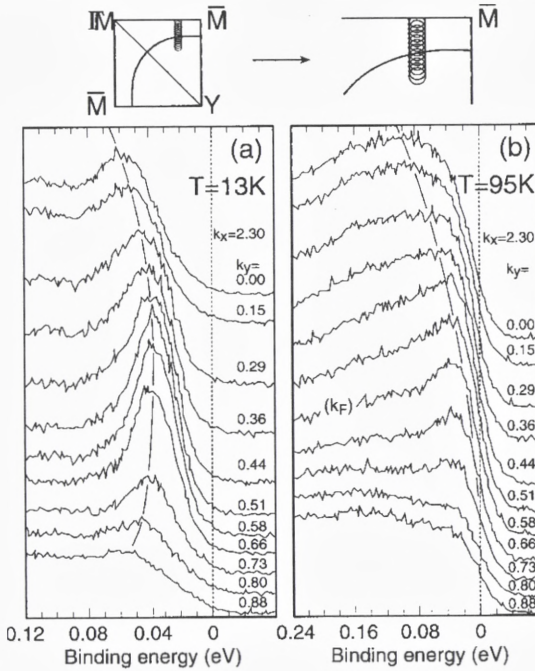
Figure 8. Photoelectron spectra from Bi2212 above and below T_c. The solid curve is a guide to the eye. In the normal state, the curve approaches close to the Fermi level while in the superconducting state, it approaches, then retreats. The wave vectors are in units of $(1/a)$. (Campuzano et al., 1996).
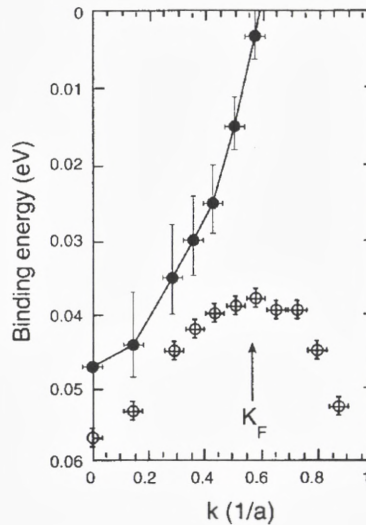
Figure 9. Distribution of maxima in the spectra of Fig. 7, plotted as a dispersion curve. Solid points: normal state; open points: superconducting state. Compare with Fig. 7. (Campuzano et al., 1996).

Photoemission studies on underdoped Bi2212 samples with lower values of T_c recently revealed a surprise (Marshall et al., 1996; Loeser et al., 1996; Ding et al., 1996b). Above T_c, parts of the Fermi surface were missing. It was suggested that this was the result of the opening of a gap, even at $T > T_c$. A gap with $d_{x^2-y^2}$ symmetry was then found. There are several possibilities for the origin of this gap. That the sample was no longer superconducting could be attributed to the lack of long-range coherence in the system of pairs (Emery and Kivelson, 1995).

5.2   Y123

Band mapping of Y123 has been carried out less frequently. Crystals cleaved at low temperature, then warmed above T_c often are not stable, though different groups have reported that some samples or cleaves are more stable than others. Band mapping can be carried out below T_c, however (Tobin et al., 1992; Liu et al., 1992). The LDA Fermi surface is shown in Fig. 10 along with experimental points from ARUPS . The calculated Fermi surface shown is a projection of the actual three-dimensional surface on the plane normal to the k_z axis, the widths of the shaded regions indicating the degree of k_z dependence of the Fermi surface. The contributions of bands from both the Cu–O chains and the Cu–O planes were

found, and agreement with the LDA calculations appears rather good. Liu et al. varied the oxygen stoichiometry between 6.3 and 6.9 per formula unit and found approximately the same Fermi surface for the two metallic samples. The insulating sample ($x = 6.3$) had a very small Fermi surface. This was an early hint of the difference between metallic and insulating samples in the cuprates. Thinking of cuprates as doped insulators leads to a small Fermi surface, with volume (area) proportional to the number of holes added to the half-full valence band. This is what is suggested in the data of Liu et al., and in the recent work on Bi2212 by Marshall et al. The metallic cuprates have a larger Fermi surface, with volume proportional to the number of electrons in the band, as expected from Luttinger's theorem. Photoemission studies of Y123 have been reviewed by Veal and Gu (1994).
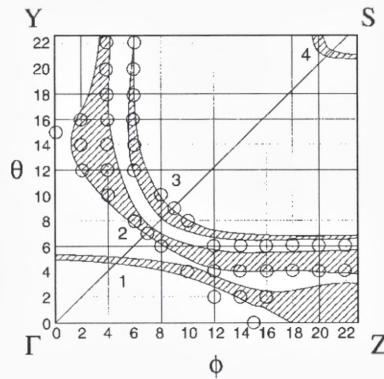
Figure 10. Calculated Fermi "surface" (shaded) and Fermi surface points determined by ARUPS for Y123. The ARUPS data were taken on a twinned single crystal. The points from the Cu–O plane bands have reflection symmetry about the ΓS line. The points from the chain bands do not. (Liu et al., 1992).

Further study (Abrikosov et al., 1993; Gofron et al., 1994) by scanning through the flat band along ΓY just below E_F, but scanning perpendicular to the ΓY line, revealed the presence of a line of saddle points (Figs. 11 and 12). Such an extended saddle point gives a stronger divergence in the density of states than does a simple saddle point.

The Fermi edge is rather weak, and most studies going below T_c did not report a peak, although there have been some reports of a shift of about 20 meV upon going from about 100 to 20 K. All studies reported a very sharp peak at about 1 eV binding energy. This peak, sometimes considered to be from a surface state,
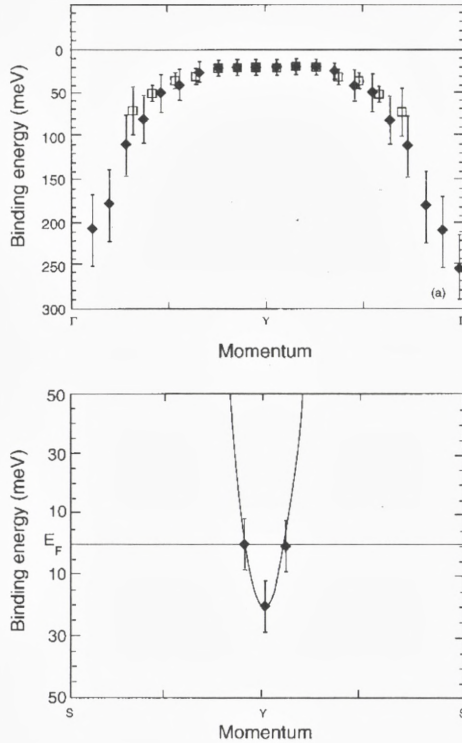
Figure 11. Position of ARUPS peaks from Y123 along the ΓY line in the Brillouin zone and along a line, YS, perpendicular through it, illustrating the extended saddle point. (Abrikosov et al., 1993).

disperses measurably (Tobin et al., 1992). Schroeder et al. (1993) described some "anomalous" cleaves, the surfaces of which had a larger edge at E_F and a smaller peak at 1 eV. These samples showed a clearer edge shift and pileup around E_F when cooled below T_c, leading to an estimate of a gap of about 20 meV.

5.3 n-type cuprates

$Nd_{2-x}Ce_xCuO_4$ goes superconducting with its highest T_c around 25 K for $x = 0.15$. In the normal state the carriers are electrons, not holes. Many of its properties in the normal phase are not "anomalous" like those of the other cuprates whose charge carriers are holes. ARUPS measurements (Sakisaka et al., 1990; King et al., 1993; Anderson et al., 1993) produced a Fermi surface in good agreement with
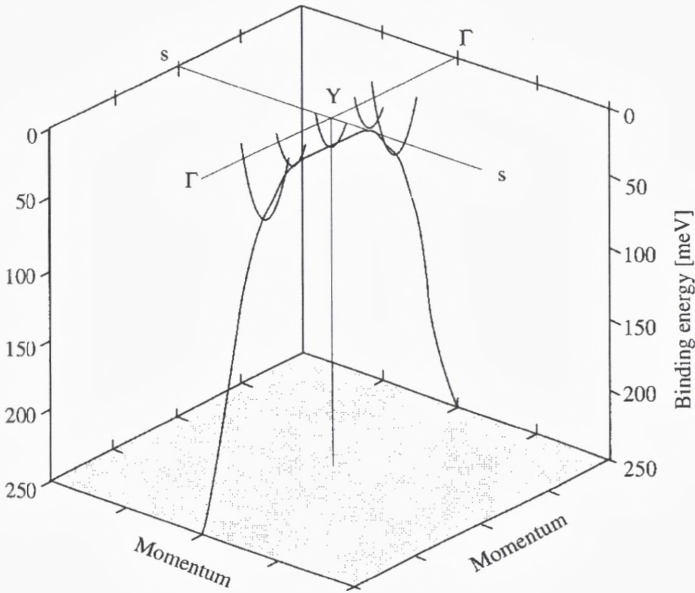
Figure 12. Three-dimensional representation of the extended saddle point in Y123. (Abrikosov et al., 1993).

the LDA calculated surface. This is a hole surface, despite the sign of the Hall coefficient. However, Lindroos and Bansil (1995) calculate that for some (0 0 1) surface terminations, there is a band of surface states which crosses the Fermi level which is easily confused with the bulk band crossing E_F. King et al., also determined a part of the Fermi surface for an overdoped sample ($x = 0.22$), and the hole surface was smaller, as expected for fewer holes. The effect of doping on surface states has yet to be examined. $Nd_{2-x}Ce_xCuO_4$ has an extended flat band, like those found in p-type cuprates, but it was much further, about 300 meV, below E_F.

6   Interpretation and summary

There are several microscopic models for the normal state of cuprates and several models for the formation of the superconducting state. ARUPS studies usually cannot so much as verify a model as eliminate one or more models, and place limits on surviving models. The theoretical literature is very large, and many photoelectron spectra have been calculated with several models. Almost all have

shown some agreement with experiment! Even the recent finding of a gap above T_c and the loss of part of the large Fermi surface have several possible explanations. Rather than try to explain all the accepted aspects of the ARUPS spectra in terms of each model, we list below the important features of such spectra that all models must account for. For the sake of brevity, we make the assumption that results found on one type of hole-doped cuprate, e.g., Bi2212, eventually will be found on the other n-type cuprates. This may not be true in detail, and perhaps not in one or more gross features.

1. For metallic cuprates, the Fermi surface is "large" and very close to that of the LDA calculations. Luttinger's theorem is valid. Correlation effects appear as an increased effective mass of the bands crossing the Fermi level. Detailed agreement with the LDA bands below the Fermi level has not yet been found. Some parts of predicted Fermi surfaces have not been found.

2. For underdoped, but still metallic, cuprates it appears that part of the large Fermi surface is lost.

3. There is an extended line of saddle critical points just below E_F, the position depending on which cuprate and on the doping level.

4. Below T_c a gap with $d_{x^2-y^2}$ symmetry, or something which effectively produces a symmetry of this form, appears. Its maximum magnitude is about 25 meV which occurs for a wave vector directed along the Cu–O bond. Above T_c a similar gap appears in underdoped samples.

5. There is a dip in the spectrum at about 90 meV below E_F that appears to correlate with the gap parameter Δ.

Recent theoretical work has tied together some of these features. The shadow bands were first predicted by Kampf and Schrieffer (1990), a result of coupling states **k** and **k** + **Q** by antiferromagnetic fluctuations where **Q** = (π, π). The calculation required for observable shadow bands a magnetic correlation length considerably longer than that measured. Langer et al. (1996) were able to compute the self energy for a one-band, two-dimensional Hubbard model with realistic dispersion. The resultant spectral density exhibited both shadow bands and the "90 meV dip", while the correlation length was small. The calculated dependence of the Fermi surface on hole doping, and the energy and doping dependence of the quasiparticle lifetime were in qualitative agreement with experimental results.

Acknowledgements

The work reported herein has been carried out over seven years by a number of groups of changing composition. We acknowledge interesting conversations and the receipt of preprints from many individuals, including J.W. Allen, A.J. Arko, J.C. Campuzano, J. Fink, R. Liu, G. Margaritondo, M. Onellion, Z.X. Shen, M. Skibowski, T. Takahashi and B.W. Veal. The Ames Laboratory is operated by Iowa State University for the U.S. DOE under contract No. 7405-ENG-82.

The late Professor A.R. Mackintosh played a role in this work, for we have discussed, much to our benefit, this and other research work with him over the years.

References

Abrikosov AA, Campuzano JC and Gofron K, 1993: Physica C **214**, 73

Aebi P, Osterwalder J, Schwaller P, Schlapbach L, Shimoda M, Mochiku T and Kadowaki K, 1994: Phys. Rev. Lett. **72**, 2757

Aebi P, Osterwalder J, Schwaller P, Berger H, Beeli C and Schlapbach L, 1995: J. Phys. Chem. Solids **56**, 1845

Anderson RO, Claessen R, Allen JW, Olson CG, Janowitz C, Liu LZ, Park JH, Maple MB, Dalichaouch Y, de Andrade MC, Jardim RF, Early EA, Oh SJ and Ellis WP. 1993: Phys. Rev. Lett. **70**, 3163

Bansil A, Lindroos M, Gofron K, Campuzano JC, Ding H, Liu R and Veal BW, 1992: J. Phys. Chem. Solids **53**, 1541

Behner H, Rauch W and Gornik E, 1992: Appl. Phys. Lett. **61**, 1465

Bozovic I and van der Marel D, 1996: *Spectroscopic Studies of Superconductors* (SPIE, Bellingham)

Brenig W, 1995: Phys. Repts. **251**, 153

Calandra C and Manghi F, 1992: Phys. Rev. B **46**, 3600

Calandra C and Manghi F, 1994: J. Electron Spectrosc. Relat. Phenom. **66**, 453

Campuzano JC, Ding H, Norman MR, Randeria M, Bellman AF, Yokoya T, Takahashi Y, Katayama-Yoshida H, Mochiku T and Kadowaki K, 1996: Phys. Rev. B **53**, R14737

Cardona M and Ley L, eds., 1978: *Photoemission in Solids* (Springer Verlag, Berlin) Vol. 1

Coffey L and Coffey D, 1993: Phys. Rev. B **48**, 4184

Courths R and Hüfner S, 1984: Phys. Repts. **112**, 53

Dessau DS, Wells BO, Shen ZX, Spicer WE, Arko AJ, List RS, Mitzi DB and Kapitulnik A, 1991: Phys. Rev. Lett. **66**, 2160

Dessau DS, Shen ZX, Wells BO, King DM, Spicer WE, Arko AJ, Lombardo LW, Mitzi DB and Kapitulnik A, 1992: Phys. Rev. B **45**, 5095

Dessau DS, Shen ZX, King DM, Marshall DS, Lombardo LW, Dickinson PH, DiCarlo , Park CH, Loeser AG, Kapitulnik A and Spicer WE: 1993, Phys. Rev. Lett. **71**, 2781

Ding H, Bellman AF, Campuzano JC, Randeria M, Norman MR, Yokoya T, Takahashi T, Katayama-Yoshida H, Mochiku Y, Kadowaki K, Jennings G and Brivio GP: 1996a, Phys. Rev. Lett. **76**, 1533

Ding H, Yokoya T, Campuzano JC, Takahashi T, Randeria M, Norman MR, Mochiku T, Kadowaki K and Giapintzakis J: 1996b, Nature **382**, 51

Edwards HL, Markert JT and de Lozanne AL, 1992: Phys. Rev. Lett. **69**, 2967

Emery VJ and Kivelson SA, 1995: Nature **374**, 434

Fehrenbacher R, 1996: preprint (submitted to Phys. Rev. B)

Fink J, Nücker N, Pellegrin E, Romberg H, Alexander M and Knupfer M: 1994, J. Electron Spectrosc. Rel. Phenom. **66**, 395

Gofron K, Campuzano JC, Abrikosov AA, Lindroos M, Bansil A, Ding H, Koelling D and Dabrowski B, 1994: Phys. Rev. Lett. **73**, 3302

Hüfner S, 1994: Adv. Phys. **43**, 183

Hüfner S, 1995: *Photoelectron Spectroscopy* (Springer Verlag, Berlin)

Kampf AP and Schrieffer JR, 1990: Phys. Rev. B **42**, 7967

Kelley RJ, Ma J, Onellion M, Marsi M, Almeras P, Berger H and Margaritondo G, 1993: Phys. Rev. B **48**, 3534

Kevan SD, 1986: Phys. Rev. B **33**, 4364

Kevan SD, ed., 1992: *Angle-resolved Photoemission – Theory and Current Applications* (Elsevier Science Publishers, Amsterdam)

King DM, Shen ZX, Dessau DS, Wells BO, Spicer WE, Arko AJ, Marshall DS, DiCarlo J, Loeser AG, Park CH, Ratner ER, Peng JL, Li ZY and Greene RL, 1993: Phys. Rev. Lett. **70**, 3159

Langer M, Schmalian J, Grabowski S and Bennemann KH, 1996: Phys. Rev. Lett. **75**, 4508

Ley L and Cardona M, eds., 1979: *Photoemission in Solids* (Springer Verlag, Berlin) Vol. 2

Liechtenstein AI, Gunnarsson O, Andersen OK and Martin RM, 1996: preprint (submitted to Phys. Rev. B)

Lindberg PAP, Shen ZX, Spicer WE and Lindau I, 1990: Surface Science Reports **11**, 1

List RS, Arko AJ, Fisk Z, Cheong SW, Conradson SD, Thompson JD, Pierce CB, Peterson DE, Bartlett RJ, Shinn ND, Schirber JE, Veal BW, Paulikas AP and Campuzano JC, 1988: Phys. Rev. B **38**, 11966

Lindroos M and Bansil A, 1995: Phys. Rev. Lett. **75**, 1182

Liu R, Veal BW, Paulikas AP, Downey JW, Kostic PJ, Fleshler S, Welp U, Olson CG, Wu X, Arko AJ and Joyce JJ, 1992: Phys. Rev. B **46**, 11056

Loeser AG, Shen ZX, Dessau DS, Marshall DS, Park CH, Fournier P and Kapitulnik A, 1996: Science **273**, 325

Lynch DW and Olson CG, 1997: *Photoemission of High-Temperature Superconductors* (to be published)

Ma J, Quitmann C, Kelley RJ, Berger H, Margaritondo G and Onellion M, 1995: Science **267**, 862

Marshall DS, Dessau DS, Loeser AG, Park CH, Matsuura AY, Eckstein JN, Bozovic I, Fournier P, Kapitulnik A, Spicer WE and Shen ZX, 1996: Phys. Rev. Lett. **76**, 4841

Massida S, Yu J and Freeman AJ, 1988: Physica C **152**, 251

Olson CG, Liu R, Yang AB, Lynch DW, Arko AJ, List RS, Veal BW, Chang YC, Jiang PZ and Paulikas AP, 1989: Science **245**, 731

Olson CG, Liu R, Lynch DW, List RS, Arko AJ, Veal BW, Chang YC, Jiang PZ and Paulikas AP, 1990: Phys. Rev. B **42**, 381

Osterwalder J, Aebi P, Schwaller P, Schlapbach L, Shimoda M, Mochiku T and Kadowski K, 1995: Appl. Phys. A **60**, 247

Plummer EW and Eberhardt W, 1982: in *Advances in Chemical Physics*, eds. I. Prigogine and S.A. Rice (John Wiley and Sons, New York) Vol. XLIV, p. 533

Randeria M, Ding H, Campuzano JC, Bellman AF, Jennings G, Yokoya T, Takahashi T, Katayama-Yoshida H, Mochiku T and Kadowaki K, 1995: Phys. Rev. Lett. **74**, 4951

Sakisaka Y, Maruyama T, Morikawa Y, Kato H, Edamoto K, Okusawa M, Aiura T, Yanashima H, Terashima T, Bando Y, Iijima K, Yamamoto K and Hirata K, 1990: Phys. Rev. B **42**, 4189

Schroeder N, Böttner R, Ratz S, Dietz E, Gerhardt U and Wolf T, 1993: Phys. Rev. B **47**, 5287

Shen ZX and Dessau DS, 1995: Phys. Repts. **253**, 1

Shen ZX, Dessau DS, Wells BO, King DM, Spicer WE, Arko AJ, Marshall D, Lombardo LW, Kapitulnik A, Dickinson P, Doniach S, DiCarlo J, Loese, AG and Park CH, 1993: Phys. Rev. Lett. **70**, 1553

Shen ZX, Spicer WE, King DM, Dessau DS and Wells BO, 1995: Science **267**, 343

Singh DJ and Pickett WE, 1995: Phys. Rev. B **51**, 3128

Smith NV and Himpsel FJ, 1982: in *Handbook of Synchrotron Radiation*, eds. D.E. Eastman, Y. Farge and E.-E. Koch (North-Holland Publishing Co., Amsterdam) Vol. I b, chapt. 9

Smith NV, Thiry P and Petroff Y, 1993: Phys. Rev. B **47**, 15476

Tobin JG, Olson CG, Gu C, Liu JZ, Solal FR, Fluss MJ, Howell RJ, O'Brien JC, Radousky HB and Sterne PA, 1992: Phys. Rev. B **45**, 5563

Varma CM and Littlewood PB, 1992: Phys. Rev. B **46**, 405

Veal BW and Gu C, 1994: J. Electron Spectrosc. Relat. Phenom. **66**, 321

Wells BO, Shen ZX, Dessau DS, Spicer WE, Mitzi DB, Lombardo LW, Kapitulnik A and Arko AJ, 1992: Phys. Rev. B **46**, 11830

Yokoya T, Takahashi T, Mochiku T and Kadowaki K, 1996: Phys. Rev. B **53**, 14055

Neutron Scattering Studies of
Heavy Fermion Systems

T. E. Mason

Department of Physics, University of Toronto, Toronto, ON, Canada M5S 1A7

and

G. Aeppli

NEC Research Institute, 4 Independence Way, Princeton, NJ, U.S.A. 08540

Abstract

We review the results of recent studies of the elastic and inelastic neutron scattering from a variety of heavy fermion compounds. This class of materials exhibits a rich variety of ground states: antiferromagnetically ordered, superconducting, semiconducting, and paramagnetic. Neutron scattering from single crystals and powders has been a productive tool for probing the magnetic order and fluctuations in all four cases. This review deals with work on UPt_3, UPd_2Al_3, UNi_2Al_3, UNi_4B, $CeNiSn$, $Y_{1-x}U_xPd_3$, and $UCu_{5-x}Pd_x$.

1 Introduction

1.1 Overview

Heavy fermion compounds, typically alloys containing U or Ce, are characterised by the small energy scale associated with the hybridization of nearly localised f-electrons with conduction electrons. This small energy scale means that properties such as band structure, which are normally not considered temperature dependent, can vary with temperature and are sensitive to small perturbations. This sensitivity gives rise to a rich variety of low temperature states in these materials; for a review see Grewe and Steglich (1991).

At high temperatures heavy fermion systems behave as Kondo lattices and the unpaired f-electrons have a local magnetic moment that interacts with the conduction electrons in the same way as an isolated Kondo impurity in a metal. As the temperature is lowered, however, the magnetic moments no longer behave as isolated, localised impurities and the system enters the coherent state which is characterised by the large effective mass (and enhanced electronic specific heat)

associated with the quasiparticles of a strongly interacting band of carriers. In this coherent, heavy fermion state there are substantial antiferromagnetic spin fluctuations which can be studied in great detail by magnetic neutron scattering from single crystals. This has been the topic of a recent review (Aeppli and Broholm, 1994). The present paper presents highlights of some experiments which have occurred since then.

1.2   Neutron scattering cross section

Because of its magnetic moment the neutron can couple to moments in solids via the dipolar force. The energy and wavelengths of thermal and subthermal neutrons are well matched to the energy and length scales of most condensed matter systems and this is particularly true for heavy fermions. We will briefly review the formalism which describes the magnetic neutron scattering. For a detailed treatment of the neutron scattering cross-section there are some excellent texts which can serve as an introduction (Squires, 1978) or more comprehensive exposition (Lovesey, 1984).

The partial differential cross section for magnetic neutron scattering, which measures the probability of scattering per solid angle per unit energy, is

$$\frac{d^2\sigma}{d\Omega dE'} = \frac{k'}{k}\frac{N}{\hbar}(\gamma r_o)^2 |f(\boldsymbol{Q})|^2 \sum_{\alpha\beta}(\delta_{\alpha\beta} - \hat{Q}_\alpha\hat{Q}_\beta)S^{\alpha\beta}(\boldsymbol{Q},\omega) \tag{1}$$

where $k(k')$ is the incident (scattered) neutron wavevector, N is the number of moments, $\gamma r_o = 5.391$ fm is the magnetic scattering length, $f(\boldsymbol{Q})$ is the magnetic form factor (analogous to the electronic form factor appearing in the x-ray scattering cross section), $\boldsymbol{Q}$ is the momentum transfer, ω is the energy transfer, and the summation runs over the Cartesian directions. $S^{\alpha\beta}(\boldsymbol{Q},\omega)$ is the magnetic scattering function which is proportional to the space and time Fourier transform of the spin-spin correlation function.

If the incident and scattered neutron energies are the same (elastic scattering) then the correlations at infinite time are being probed and, in a magnetically ordered material, the scattering function will contain delta functions at the wavevectors corresponding to magnetic Bragg reflections. The $(\delta_{\alpha\beta} - \hat{Q}_\alpha\hat{Q}_\beta)$ term in the cross section means that neutrons probe the components of spin perpendicular to the momentum transfer, $\boldsymbol{Q}$. If there is no analysis of the scattered neutron energy then (within the static approximation) the measured intensity is proportional to the Fourier transform of the instantaneous correlation function which is essentially a snapshot of the spin correlations in reciprocal space. At non-zero energy transfers the spin dynamics of the system under study are probed. In a magnetically ordered system of localised spins the elementary magnetic excitations are spin waves.

The fluctuation dissipation theorem relates the correlations to absorption, in other words the scattering function is proportional to the imaginary part of a generalised (Q and ω dependent) susceptibility, $\chi''(Q, \omega)$. In the zero frequency, zero wavevector limit, the real part of the generalised susceptibility is the usual DC susceptibility measured by magnetisation. In a metal the elementary excitations are electron-hole pairs. Since it is possible to excite an electron-hole pair by promoting a quasiparticle from below the Fermi surface to above the Fermi surface, and at the same time flipping its spin, neutrons can be used to probe the low energy excitations of a metal. The generalised susceptibility (for a non-interacting metal) is just the Lindhard susceptibility which can be calculated from the band structure.

2   Antiferromagnetism and superconductivity

2.1   UPt$_3$

UPt$_3$ has remained a very popular system because it is both the quintessential strongly renormalized Fermi liquid, as revealed especially by de Haas–van Alphen experiments, and the quintessential unconventional superconductor, displaying an array of properties ranging from multiple superconducting phases to anisotropies not likely predicated on normal state anisotropies. While the broad outlines of the UPt$_3$ problem were clear several years ago, the past two years have witnessed scattering experiments which have answered important outstanding questions. These experiments all have to do with the weak antiferromagnetic order whose Bragg signal is reduced by passing into the superconducting state, and which is greatly enhanced – while superconductivity is eliminated – upon Th substitution for U or Pd substitution for Pt (Ramirez et al., 1986; de Visser et al., 1986; Goldman et al., 1987; Frings et al., 1987). In particular, Isaacs et al. (1995) performed a combination of x-ray and neutron diffraction experiments which showed the following (see Fig. 1): (i) The reduction in the magnetic Bragg scattering found in an earlier experiment (Aeppli et al., 1989) is due to a reduction in the magnitude of the corresponding magnetic moment, and not to rotation of the moments, e.g., in the basal planes of the material. (ii) There seems to be little difference between the behaviours of the magnetic order exhibited in the near surface region probed by resonant x-ray scattering and the bulk probed by neutrons. (iii) The magnetic coherence length in quite heavily doped and non-superconducting U$_{0.95}$Th$_{0.05}$Pt$_3$ is resolution-limited. This again emphasizes that a special local disorder is the most likely cause of the magnetism in pure UPt$_3$.

The second new scattering experiment also addressed the vector nature of the ordered moment. In particular, Lussier et al. (1996) investigated whether an external magnetic field parallel to the basal planes – the 'easy' direction as inferred
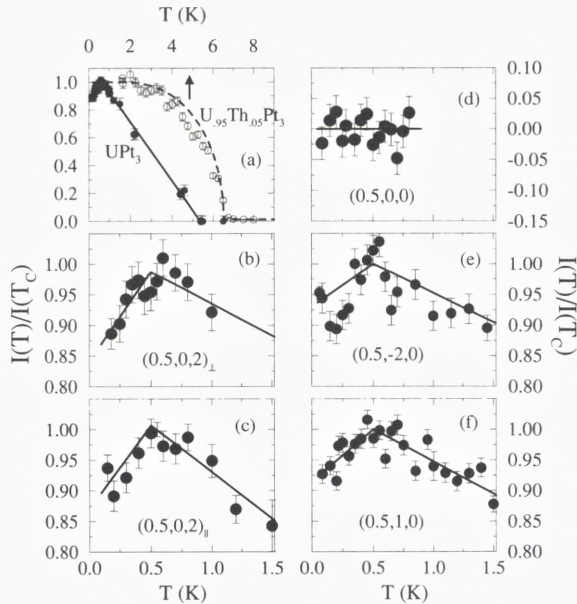
Figure 1. Temperature dependence of the antiferromagnetic Bragg peaks for UPt$_3$. (a)–(c) show the intensity measured with x-rays (with neutron data for isostructural U$_{0.95}$Th$_{0.05}$Pt$_3$ shown in (a) [open circles] for comparison). (d)–(f) show the neutron scattering intensity for three different Bragg reflection entering the superconducting state. From Isaacs et al. (1995).

from bulk measurements – could rotate the moments. A field of up to 3.2 T was not able to either rotate the moments or select a single domain (see Fig. 2). Given that such a limiting field is beyond H_{c2} for the superconductor, finding (i) of Isaacs et al. (1995) is not surprising. Thus there are anisotropies, possibly random, which strongly pin the small ordered moment in pure UPt$_3$. It will be interesting to see whether the same result is obtained in the more coherent antiferromagnetic state induced by Th and Pd impurities. The finding that a single magnetic domain is not produced implies that either the magnetic structure is not single-Q or all measurements of the superconducting phase diagram have been in multi domain samples, requiring a re-evaluation of theories based on the symmetry breaking of antiferromagnetic ordering.

2.2   UPd$_2$Al$_3$ and UNi$_2$Al$_3$

In 1991 two new heavy fermion compounds were discovered which displayed the coexistence of antiferromagnetic order and superconductivity. UPd$_2$Al$_3$ has an
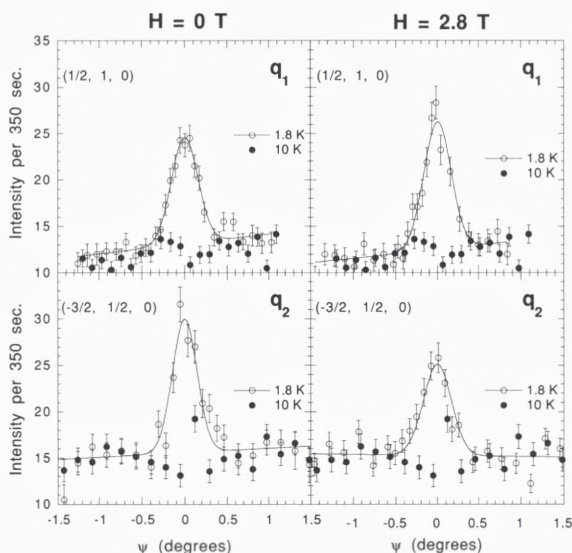
Figure 2. Magnetic Bragg peaks for two different domains in UPt$_3$ for $H = 0$ and 2.8 tesla. Complete selection of a single domain by the 2.8 T field would eliminate the $\mathbf{q}_2$ Bragg peak and increase the $\mathbf{q}_1$ peak by a factor of three. From Lussier et al. (1996).

antiferromagnetic transition at 14.4 K and, in the best samples, a superconducting T_c of 2 K, the highest of any heavy fermion compound at ambient pressure (Geibel et al., 1991a). UNi$_2$Al$_3$ has a somewhat lower T_N (5.2 K) and T_c (1 K) (Geibel et al., 1991b). Both share the same hexagonal crystal structure (space group P6/mmm).

Powder neutron diffraction has shown that, in the antiferromagnetic state, UPd$_2$Al$_3$ has moments of 0.85 μ_B lying in the hexagonal basal plane with the moments in a given layer ferromagnetically aligned and alternating up the c axis (Krimmel et al., 1992a). Initial reports of a suppression of the ordered moment in the superconducting state by Krimmel et al. (1992a) have not been reproduced (Kita et al., 1994). Measurements of the magnetisation density in the paramagnetic state using polarized neutrons have shown that the magnetic moment resides on the U site with no spin transfer to the Pd ions (Paolasini et al., 1993), comparison with magnetisation data suggest that there is an additional (12% contribution) from the polarisation of the conduction electrons. A determination of the magnetic phase diagram up to 5 T (Kita et al., 1994) has shown that the moment lies along the a axis in the basal plane. Application of a magnetic field perpendicular to one of the a axes (along $[\bar{1}\,1\,0]$) favours that magnetic domain and as the field is increased
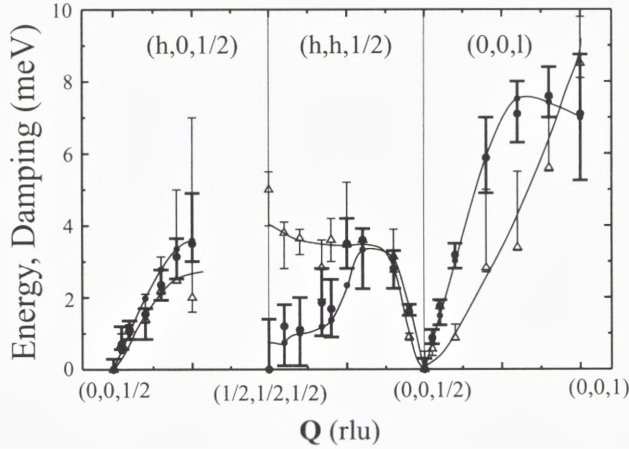
Figure 3. Wavevector dependence of the energy (filled circles) and damping (open triangles) of the spin waves in the ordered state of UPd_2Al_3. There are well defined spin waves along the c^* axis however, in the basal plane, the response is overdamped making it difficult to independently determine Γ_Q and ω_Q.

above a critical field of order 0.5 T the fraction of the sample with moments aligned along the a axis perpendicular to H increases from 33% to 100%. If the field is applied parallel to [0,1,0] then a two step process occurs: first above 0.5 T the two domains at $\pi/3$ are selected, then above 4 T the moments are constrained to lie perpendicular to the field along the next nearest direction in the basal plane. As the temperature is increased towards T_N the fields for domain selection and reorientation approach zero.

The inelastic neutron scattering from UPd_2Al_3 has been studied using powder, time-of-flight (Krimmel et al., 1996) and single crystal, triple-axis techniques (Petersen et al., 1994; Mason et al., 1995). The powder measurements in the paramagnetic state show a strong quasi-elastic response which is peaked at the wavevector corresponding to the $(0,0,\frac{1}{2})$ Bragg peak. The single crystal studies have shown that in the antiferromagnetically ordered state this response evolves into spin waves which, within the limits of the experimental resolution of 0.35 meV, have no gap at the ordering wavevector. The full dispersion surface extracted from these measurements is shown in Fig. 3 along with the wavevector dependence of the spin wave lifetime. These quantities correspond to the energy and damping of an inelastic Lorentzian response corrected for spectrometer resolution. The structure of the dispersion requires a model of the magnetic interactions with at least four groups of next neighbours implying long range interactions. Moreover, it is not
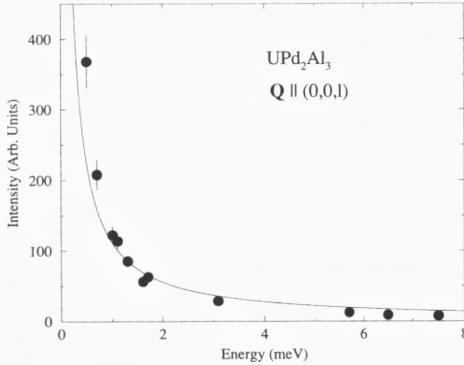
Figure 4. Spin wave intensity as a function of energy for UPd_2Al_3 obtained for momentum transfers displaced from $(0, 0, \frac{1}{2})$ along the c axis. The intensity is the amplitude for an inelastic Lorentzian response convolved with the spectrometer resolution. The line is the $1/\omega$ dependence expected for conventional spin waves.

possible to describe both energies and lifetimes in a localised moment spin wave model (Lindgård et al., 1967) because damping arising from off-diagonal terms in the Hamiltonian results in a zone centre gap inconsistent with the data. This suggests the damping is of extrinsic (conduction electron) origin. The damping is generally comparable to the spin wave energy although for wavevectors displaced along the c axis there are well resolved modes with a linear dispersion. The intensity of the spin waves along the c axis, obtained from the same fits, is shown in Fig. 4 in comparison with the $1/\omega$ expected for conventional spin waves. Measurements of the spin wave intensities in a single domain sample (produced as described in the preceding paragraph) have shown the excitations are transverse to the moment direction. It appears that UPd_2Al_3 is unique among U compounds in that it possesses conventional spin wave excitations with a very small or no gap at the ordering wavevector. These spin waves are strongly damped due to interaction with the conduction electrons but, at energies less than a few multiples of $k_B T_c$, show no change on entering the superconducting state (Petersen et al., 1994). This is consistent with the results of heat capacity (Caspary et al., 1993) and muon spin rotation measurements (Feyerherm et al., 1994) which have been interpreted as evidence for two coexisting electronic systems, localised $5f$ magnetic states and delocalised states which are responsible for superconductivity (Steglich et al., 1996).

Initial powder diffraction studies of UNi_2Al_3 failed to observe any magnetic Bragg peaks below T_N and placed an upper bound on the ordered moment of 0.2
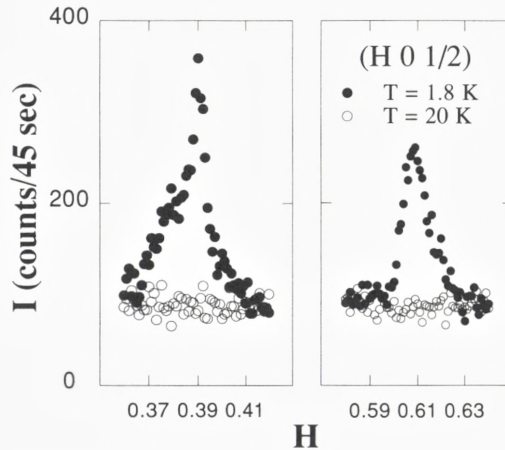
Figure 5. Scans through the incommensurate peaks in UNi_2Al_3 along the $(h, 0, \frac{1}{2})$ direction above (open circles) and below (closed circles) $T_N \sim 5.2$ K. From Schröder et al. (1994)

μ_B (Krimmel et al., 1992b). μSR experiments indicated that the ordered moment was likely of order 0.1 μ_B (Amato et al., 1992). Schröder et al. (1994) performed neutron diffraction measurements on a single crystal of UNi_2Al_3 and found that it ordered incommensurately below 5.2 K with an ordered moment of 0.24 ± 0.1 μ_B. Figure 5 shows scans through two of the incommensurate wavevectors, $(\frac{1}{2} \pm \delta, 0, \frac{1}{2})$ with $\delta = 0.110 \pm 0.003$, above and below T_N. The intensities of six magnetic Bragg peaks measured at 1.8 K are best described by a model structure which is a longitudinal spin density wave within the hexagonal basal plane with the moments parallel to a^*. The moment direction in UNi_2Al_3 is therefore rotated $\pi/6$ compared to UPd_2Al_3 but the observation of an incommensurate modulation within the basal plane is perhaps not surprising given the long range interactions manifested in the spin wave measurements in UPd_2Al_3.

2.3 UNi_4B

One of the most intriguing new compounds which have been studied in recent years is UNi_4B which has a structure based on the hexagonal $CaCu_5$ structure. There is a small distortion which modifies the local environment of $\frac{2}{3}$ of the U ions through their collective motion towards the remaining sites (Mentink et al., 1996a). As a result $\frac{1}{3}$ of the uranium moments are on six-fold symmetric sites while the remainder are on two-fold symmetric sites. The resistivity, susceptibility, and
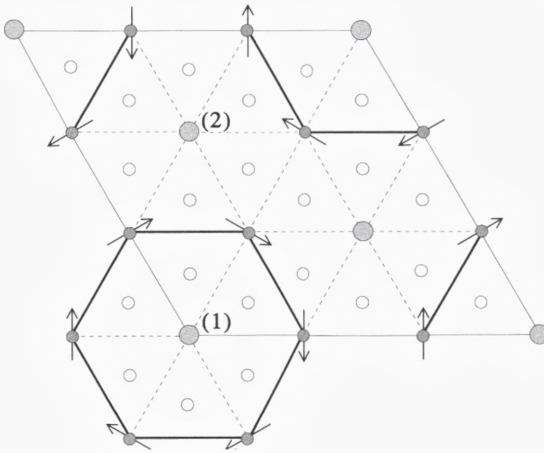
Figure 6. Magnetic structure of UNi_4B projected onto the hexagonal basal plane. The magnetic layers are stacked ferromagnetically along the c axis. The solid circles, labelled (1) and (2), represent the paramagnetic U moments. From Mentink et al. (1994).

specific heat of UNi_4B all show anomalies typical for antiferromagnetic ordering at 21 K and this has been confirmed by single crystal neutron diffraction (Mentink et al., 1994). The magnetic structure, shown in Fig. 6, is very unusual. The moments on the outer, two-fold, sites of hexagonal plaquets form a pinwheel-like structure while the moments on the central six-fold sites, which are frustrated due to the cancellation of interactions with nearest neighbours, do not order. The moments are ferromagnetically aligned along the c axis.

Immediately below the phase transition there is a significant increase in the DC and AC susceptibility (Mentink et al., 1996a) which is quenched by the application of a modest magnetic field (< 1 T). This is likely the signature of the ferromagnetically correlated chains on the non ordering sites. At low temperatures (< 2 K), however, this effect is eliminated, the resistivity passes through a maximum and c/T increases dramatically to over 500 mJ/(mole K^2) at 0.3 K (Mentink et al., 1996b). It appears that the frustration is being alleviated by the formation of heavy itinerant states without a moment in the presence of the localised moments which order at 21 K. This is similar to what occurs in $DyMn_2$ (Nuñez Regueiro and Lacroix, 1994) and CeSb (Ballou et al., 1991) and is the consequence of the combination of lattice frustration, a proximity to a magnetic-nonmagnetic transition and strong anisotropy.
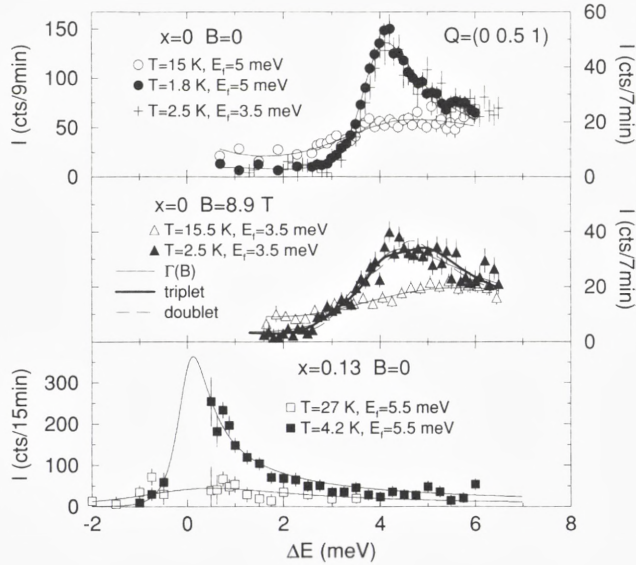
Figure 7. Constant-Q scans in CeNiSn for (upper panel) $B = 0$, (middle panel) $B = 8.9$ T and (lower panel) $CeNi_{0.87}Cu_{0.13}Sn$ at $Q = (0, 0.5, 1)$ showing the effect of increasing temperature and magnetic field on the inelastic response. From Schröder et al. (1996).

3 Semiconductors and Non-Fermi Liquids

3.1 CeNiSn

CeNiSn is interesting because it is the only Ce-based 'Kondo insulator' (for a review see Aeppli and Fisk, 1992) which can be readily fabricated in (large) single crystal form. Since the review of Aeppli and Broholm (1994), the material has received considerable attention from various groups throughout the world. The principal new results are:

(i) The discovery of a clean gapped signal at wavevectors of type $(0, 0.5, l)$ where l is an integer in addition to those equivalent to $(0,0,1)$ (Kadowaki et al., 1994; Sato et al., 1995). Figure 7 shows the new peak, especially striking in its much more intense manifestation after the new Risø cold neutron guide tubes were installed (for a comparison between this spectrum and that taken before the installation of the new guides see Lebech (1993)). While the gap is larger (4 meV) at the former point than the latter (where it is 2 meV (Mason et al., 1992)), the property that $\chi''(Q, \omega)$ is a strong function of Q, while $\chi'(Q, \omega = 0)$ is not, remains. Thus, the

puzzle of the 'shielded' RKKY interactions in Kondo insulators remains, although Varma (1995) has advanced arguments as to its resolution.

(ii) The discovery of long range magnetic order in CeNiSn samples doped by Cu substitution for Ni to achieve metallic heavy fermion behaviour. The magnetic ordering vector is close to the (0.5,1,0) vectors found to exhibit the higher gap frequency. Thus, in addition to producing a (dirty) metal, doping apparently eliminates the shielding phenomenon seen in the parent compound as well as the other celebrated single crystal Kondo insulator, FeSi.

(iii) The discovery that a magnetic field strongly affects the shape of the magnetic gap spectra (see Fig. 7). In particular, the gap appears less sharp, although one cannot judge whether this is due to field-induced splitting of some degeneracy or a true reduction in the lifetime of excitations at the gap energy. In spite of the considerable spectral change as well as the fact that the sample is rapidly approaching a metallic condition with increasing field, the shielding phenomenon mentioned in (i) and (ii) remains. In summary, the most important consequence of the new work on CeNiSn and its relatives is that there are dramatically different routes to metallic behaviour in heavy fermion systems, the first (doping) of which leads to substantial RKKY interactions while the second (external field) does not.

3.2 $Y_{1-x}U_xPd_3$ and $UCu_{5-x}Pd_x$

The properties of heavy fermion metals are a dramatic example of the success of Fermi liquid theory in the sense that the low temperature transport and thermodynamics, as well as the excitation spectra and quantum oscillations in a magnetic field are all in accord with predictions for a metal with a well defined Fermi surface (albeit with an extremely large effective mass due to electronic interactions). Similarly in Kondo insulators such as CeNiSn several distinct energy scales are directly manifested in the size of the gap and the properties of these materials are understandable in the framework of a band type picture even though more careful examination of the neutron data reveal important failings of band theory (Mason et al., 1992). There has been a great deal of interest recently in compounds, typically random alloys, which exhibit weak power law and logarithmic divergences in their low temperature properties at odds with the predictions of Fermi liquid theory, generically referred to as non-Fermi liquid (NFL) behaviour.

One such material is $Y_{1-x}U_xPd_3$ with $x = 0.2$ (Seaman et al., 1991; Andraka and Tsvelik, 1991) which has a logarithmically diverging electronic specific heat below 20 K, a power law divergence of the susceptibility, and a resistivity which varies as $(1 - (T/T_o))^{1.13}$. This behaviour has been attributed to a two channel quadrupolar Kondo effect (Seaman et al., 1991), proximity to a novel zero temperature phase transition (Andraka and Tsvelik, 1991) or the suppression of the Kondo
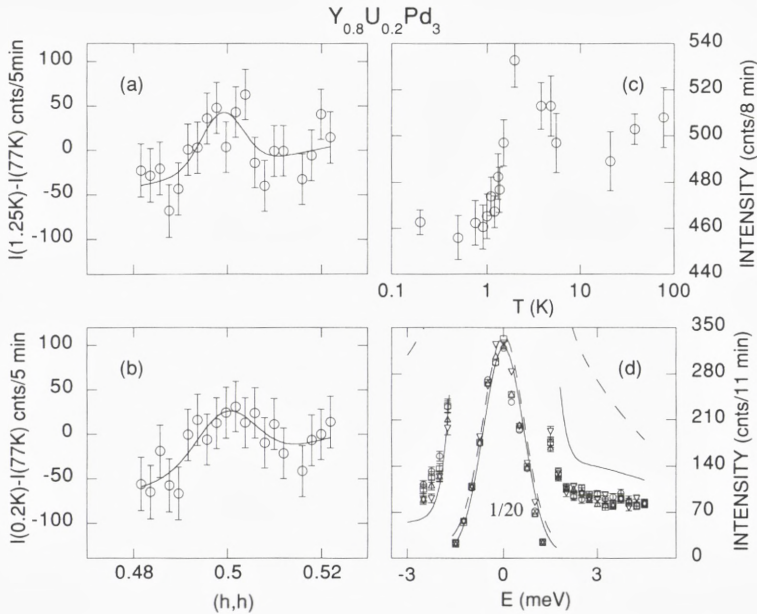
Figure 8. Magnetic correlations in $Y_{0.8}U_{0.2}Pd_3$. (a) $\mathbf{Q}$ dependence of the energy integrated $S(\mathbf{Q}, \omega)$ obtained by taking the difference in intensities at 1.25 K and 77 K. (b) The same difference between 0.2 K and 77 K. (c) Temperature dependence of the scattering at 0.5 meV for $\mathbf{Q} = (0.49, 0.49, 0)$. (d) Constant-$\mathbf{Q}$ scan at (0.5,0.5,0) at 70 K. From Dai et al. (1995)

temperature due to disorder and the associated proximity to a metal insulator transition (Dobrosavljević et al., 1992). Recent neutron scattering measurements by Dai et al. (1995) on polycrystalline samples with $x = 0.2$ and 0.45 have shed considerable light onto the ground state for this material. Figure 8 summarizes some of the results. Panels (a) and (b) show the weak peak in the energy integrated cross section which develops at low temperatures at the same antiferromagnetic wavevector at which long range order develops in the $x = 0.45$ compound (which had previously thought to be a spin glass). A temperature scan at 0.5 meV (panel (c)) shows a suppression of these fluctuations as the characteristic energy moves to lower energies below about 2 K. If the logarithmic increase in the resistivity in this material were due to the conventional Kondo effect then a quasielastic peak with a characteristic energy of $k_B T \sim 3.6$ meV would result in a constant-$\mathbf{Q}$ response shown as solid and dashed lines in panel (d), inconsistent with the data. Polarized beam measurements have shown that the dominant contribution to the magnetic scattering for both the $x = 0.2$ and $x = 0.45$ samples is a resolution limited re-
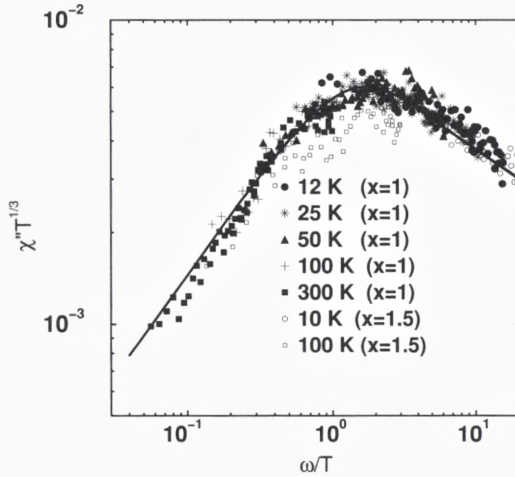
Figure 9. $UCu_{5-x}Pd_x$ exhibits scaling for both $x = 1$ and 1.5. The solid line corresponds to $\chi''(\omega, T)T^{1/3} \sim (T/\omega)^{1/3} \tanh(\omega/1.2T)$. From Aronson et al. (1995).

sponse centred on zero frequency. This indicates that in both cases the ground state for the U ions is the Γ_5 triplet. This magnetic ground state, suggested by the observation of weak critical scattering, rules out the quadrupolar two-channel mechanism for NFL behaviour in $Y_{1-x}U_xPd_3$.

Another instance of NFL behaviour occurs in $UCu_{5-x}Pd_x$. In this case there is randomness due to alloying as in $Y_{1-x}U_xPd_3$ however there is no site dilution of the U. The novel low temperature behaviour observed for $x = 1.5$ has been ascribed to the suppression of a spin glass transition to $T = 0$. Using time-of-flight powder measurements Aronson et al. (1995) have observed a magnetic excitation spectrum which, below a cross over of about 25 meV, is characterised by a scale which is determined by the temperature. At energies lower than T the dynamic susceptibility is proportional to ω/T, exactly cancelling the temperature factor and leading to a temperature independent cross section, $S(\omega)$ similar to what has been seen in lightly doped cuprates (Hayden et al., 1991). This scaling behaviour, which is the same for $x = 1$ and 1.5, is explicitly shown in Fig. 9. Surprisingly for a dense Kondo lattice, there is no observable Q dependence other than the overall form factor dependence. This could suggest a single ion origin for the observed scaling although it may also be due to the directional averaging which occurs in any powder measurement. As in $Y_{1-x}U_xPd_3$, the quasielastic response indicates a magnetic ground state which has an instability driven towards $T = 0$.

The novel effects seen in these materials are not limited to alloys with compositional disorder. Similar effects are seen in URh_2Ge_2 (Süllow et al., 1996) although substitutional disorder between Rh and Ge likely plays a role. In that case there is clearly a competition between spin glass and antiferromagnetic order which may drive the low temperature properties.

Acknowledgements

References

Aeppli G and Broholm C, 1994: *Handbook on the Physics and Chemistry of Rare Earths*, eds. K.A. Gschneidner, L. Eyring, G.H. Lander and G.R. Choppin (Elsevier, Amsterdam) Vol. **19**, p. 123

Aeppli G and Fisk Z, 1992: Comments Cond. Mat. Phys. **16**, 155

Aeppli G, Bishop D, Broholm C, Bucher E, Siemensmeyer K, Steiner M and Stüsser N, 1989: Phys. Rev. Lett. **63**. 676

Amato A, Geibel C, Gygax FN, Heffner RH, Knetsch E, MacLaughlin DE, Schank C, Schenk A, Steglich F and Weber M, 1992: Z. Phys. B **86**, 159

Andraka B and Tsvelik A, 1991: Phys. Rev. Lett. **67**, 2886

Aronson MC, Osborn R, Robinson RA, Lynn JW, Chau R, Seaman CL and Maple MB, 1995: Phys. Rev. Lett. **75**, 725

Ballou R, Lacroix C and Nuñez Regueiro MD, 1991: Phys. Rev. Lett. **66**, 1910

Caspary R, Hellmann P, Keller M, Sparn G, Wassilew C, Köhler R, Geibel C, Schank C, Steglich F and Phillips NE, 1993: Phys. Rev. Lett. **71**, 2146

Dai P, Mook HA, Seaman CL, Maple MB and Koster JP, 1995: Phys. Rev. Lett. **75**, 1202

Dobrosavljević V, Kirkpatrick TR and Kotliar G, 1992: Phys. Rev. Lett. **69**, 1113

Feyerherm R, Amato A, Gygax FN, Schenk A, Geibel C, Steglich F, Sato N and Komatsubara T, 1994: Phys. Rev. Lett. **73**, 1849

Frings PH, Renker B and Vettier C, 1987: J. Magn. Magn. Mater. **63-64**, 202

Geibel C, Schank C, Theiss S, Kitazawa H, Bredl CD, Böhm A, Rau M, Grauel A, Caspary R, Helfrich R, Ahlheim U, Weber G and Steglich F, 1991a: Z. Phys. B **84**, 1

Geibel C, Thies S, Kaczororowski D, Mehner A, Grauel A, Seidel B, Ahlheim U, Helfrich R, Petersen K, Bredl CD and Steglich F, 1991b: Z. Phys. B **83**, 305

Goldman AI, Shirane G, Aeppli G, Bucher E and Hufnagl J, 1987: Phys. Rev. B **36**, 8523

Grewe N and Steglich F, 1991: *Handbook on the Physics and Chemistry of Rare Earths*, eds. K.A. Gschneidner and L. Eyring (Elsevier, Amsterdam) Vol. **14**, p. 343

Hayden SM, Aeppli G, Mook H, Rytz D, Hundley MF and Fisk Z, 1991: Phys. Rev. Lett. **66**, 821

Holland-Moritz E and Lander GH, 1994: *Handbook on the Physics and Chemistry of Rare Earths*, eds. K.A. Gschneidner, L. Eyring, G.H. Lander and G.R. Choppin (Elsevier, Amsterdam)

Vol. **19**, p. 1

Isaacs ED, Zschack P, Broholm CL, Burns C, Aeppli G, Ramirez AP, Palstra TTM, Erwin RW, Stücheli N and Bucher E, 1995: Phys. Rev. Lett. **75**, 1178

Kadowaki H, Sato T, Yoshizawa H, Ekino T, Takabatake T, Fuji H, Regnault LP and Isikawa Y, 1994: J. Phys. Soc. Japan **63**, 2074

Kita H, Dönni A, Endoh Y, Kakurai K, Sato N and Komatsubara T, 1994: J. Phys. Soc. Japan **63**, 726

Krimmel A, Fischer P, Roessli B, Maletta H, Geibel C, Schank C, Grauel A, Loidl A and Steglich F, 1992a: Z. Phys. B **86**, 161

Krimmel A, Loidl, A., Eccleston R, Geibel C and Steglich F, 1996: J. Phys. Condens. Matter **8**, 1677

Lebech B, 1993: Neutron News **4**, 31

Lingård PA, Kowalska A and Laut P, 1967: J. Phys. Chem. Solids **28**, 1357

Lovesey SW, 1984: *Theory of Neutron Scattering from Condensed Matter* (Clarendon Press, Oxford)

Lussier B, Taillefer L, Buyers WJL, Mason TE and Petersen T, 1996: Phys. Rev. B **54**, R6873

Mason TE, Aeppli G, Ramirez AP, Clausen KN, Broholm C, Stücheli N, Bucher E and Palstra TTM, 1992: Phys. Rev. Lett. **69**, 490

Mason TE, Petersen T, Aeppli G, Buyers WJL, Bucher E, Garrett JD, Clausen KN and Menovsky AA, 1995: Physica B **213&214**, 11

Mentink SAM, Drost A, Nieuwenhuys GJ, Frikkee E, Menovsky AA and Mydosh JA, 1994: Phys. Rev. Lett. **73**, 1031

Mentink SAM, Mason, TE, Drost A, Frikkee E, Becker B, Menovsky AA and Mydosh JA, 1996a: Physica B (in press)

Mentink SAM, Amitsuka H, de Visser A, Slanič Z, Belanger DP, Neumeier JJ, Thompson JD, Menovsky AA, Mydosh JA and Mason TE, 1996b: Physica B (in press)

Nuñez Regueiro MD and Lacroix C, 1994: Phys. Rev. B **50**, 16063

Paolasini L, Paixão JA, Lander GH, Delapalme A, Sato N and Komatsubara T, 1993: J. Phys. Condes. Matter bf 47, 8905

Petersen T, Mason TE, Aeppli G, Ramirez AP, Bucher E and Kleiman RN, 1994: Physica B **199&200**, 151

Ramirez AP, Batlogg B, Cooper AS and Bucher E, 1986: Phys. Rev. Lett. **57**, 1072

Sato TJ, Kadowaki H, Yoshizawa H, Ekino T, Takabatake T, Fuji H, Regnault LP and Isikawa Y, 1995: J. Phys. Condens. Matter **7**, 8009

Schröder A, Lussier JG, Gaulin BD, Garrett JD, Buyers WJL, Rebelsky L and Shapiro M, 1994: Phys. Rev. Lett. **72**, 136

Schröder A, Aeppli G, Mason TE, Stücheli N and Bucher E, 1996: (to be published)

Seaman CL, Maple MB, Lee BW, Ghamaty S, Torikachvili MS, Kang J-S, Liu LZ, Allen JW and Cox DL, 1991: Phys. Rev. Lett. **67**, 2882

Steglich F, Geibel C, Modler R, Lang M, Hellman P and Gegenwart P, 1996: *Proc. Int. Euroconf. on Magnetic Correlations, Metal-insulator Transitions and Superconductivity*, J. Low Temp. Phys. (in press)

Squires GL, 1978: *Introduction to the Theory of Thermal Neutron Scattering* (Cambridge University Press, Cambridge)

Süllow S, Mentink SAM, Mason TE, Buyers WJL, Nieuwenhuys GJ, Menovsky AA and Mydosh JA, 1996: Physica B (submitted)

de Visser A, Klaase SCP, van Sprang M, Franse JJM, van den Berg J and Nieuwenhuys GJ, 1986: Phys. Rev. B **34** 8168

The Normal States of Magnetic Itinerant Electron Systems

G. J. McMullan and G. G. Lonzarich

Cavendish Laboratory, University of Cambridge, Cambridge CB3 0HE

Abstract

The normal state of ferromagnetic d metals such as MnSi and ZrZn$_2$ with small or vanishing Curie temperatures may be described over a wide range in temperature and pressure in terms of a quantitative model of a marginal Fermi liquid based on dispersive spin fluctuations spectra inferred from inelastic neutron scattering data. The behaviour of antiferromagnetic f metals such as CePd$_2$Si$_2$ and CeNi$_2$Ge$_2$ with low or vanishing Néel Temperatures (T_N) also appears unconventional, but the normal state above T_N has not yet been interpreted consistently in terms of an elementary extension of the spin-fluctuation model employed for the d-metal systems.

1 Introduction

The normal states of itinerant electron systems at low temperatures are normally described in terms of the Fermi liquid model. In perhaps the narrowest definition of this framework, the low-lying propagating modes of the interacting electron assembly are regarded as having a finite "overlap" with the non-interacting one-particle excitations (Anderson, 1995). This condition may be satisfied in the simple metals, but it has been called into question in particular for magnetic metals above small or vanishing Curie or Néel temperatures and more recently for the short-coherence-length superconductors (Anderson, 1995; Coleman, 1995a; Millis, 1993). In these strongly correlated electron systems, fluctuations of the order parameter may strongly suppress the transition temperature and give rise to a normal state with some unconventional properties.

Perhaps the simplest example of such behaviour may be found in pure ferromagnetic d metals such as MnSi and ZrZn$_2$ which have low Curie temperatures (T_C) that may be suppressed towards absolute zero with modest applied hydrostatic pressures. The temperature and pressure dependences of the resistivity and magnetic susceptibilities of these systems, together with the properties of the underlying spin fluctuation spectra, strongly suggest that the normal state may be

usefully viewed in terms of a model of a marginal Fermi liquid (Moriya, 1985; Lonzarich, 1997). In this framework the usual fermion quasiparticle picture is retained, but the effective interaction between quasiparticles becomes long range and gives rise to low temperature behaviour not usually associated with the simplest Fermi liquid model.

In particular, the marginal Fermi liquid model relevant to this problem for $T_C \to 0$ leads to a logarithmic divergence $\ln(T^*/T)$ of the linear coefficient of the heat capacity C/T and a $T^{-1/3}$ divergence in the quadratic coefficient of the resistivity ρ/T^2 at low temperatures. This behaviour may be traced to a logarithmic divergence of the quasiparticle masses arising from the long-range quasiparticle interaction, and to a concomitant linear variation in the quasiparticle scattering rate as a function of energy or temperature near the Fermi surface. The divergence of the quasiparticle masses on the Fermi surface as $T \to 0$ suggests a breakdown of the Fermi liquid state as defined at least in the narrow sense given above.

The marginal Fermi liquid represents, as the name implies, the weakest breakdown of the usual description of the normal metallic state. In more extreme cases, the starting picture of interacting fermion excitations on a conventional Fermi surface may itself have to be revised. This cannot be ruled out for some of the nearly magnetic or almost localised f-electron systems described below and the very short-coherence-length superconductors.

2   The quasiparticle–quasiparticle interaction

The breakdown of the simplest Fermi liquid description can be anticipated in some cases via an examination of the form of the quasiparticle–quasiparticle interaction. We may think of a quasiparticle excited near the Fermi level as interacting with various fields set up by other quasiparticles. Of particular interest, for an electron system near a ferromagnetic instability, is the exchange field essentially proportional to the local magnetisation, which couples to the spin moment of a quasiparticle. If we take this field acting on a given quasiparticle as a wave generated by another quasiparticle at some other point in space and time, we are led to an induced quasiparticle–quasiparticle interaction which is given, in the linear response approximation, by the space- and time-dependent magnetic susceptibility.

The spatial range of this interaction is then evidently the magnetic correlation length which diverges at the Curie temperature T_C. Thus, the quasiparticle interaction can become long range at low T as $T_C \to 0$. This leads to a singular scattering of quasiparticles near the Fermi surface which can qualitatively alter the character of the quasiparticle relaxation rate and, hence, of the low temperature properties in general.

For the standard model developed for the nearly ferromagnetic d metals, the qualitative temperature dependences of these properties depends chiefly on the dimension of space d (taken to be 3 for the cubic metals such as MnSi or $ZrZn_2$) and the dynamical exponent z which characterises the propagation frequency spectrum for waves which carry the quasiparticle interaction (Millis, 1993; Moriya, 1985; Hertz, 1976; Lonzarich, 1997).

For our problem, this interaction is carried by magnetisation waves which tend to decay in time for $T > T_C$. Thus, the propagation spectrum is purely imaginary and characterised by the relaxation rate, $\Gamma_q \propto q^z$, of a magnetic wave of small wavevector q. For an isotropic and homogeneous metal with $T_C \to 0$, we expect $z = 3$ at low T (at least for $d > 4 - z$), a result consistent with inelastic neutron scattering measurements of the spin relaxation spectrum for a number of nearly ferromagnetic cubic d metals (Bernhoeft et al., 1989; Ishikawa et al., 1985).

3 Consequences of the long-range interaction in nearly ferromagnetic metals

In the limit $T_C \to 0$, the above model with $d = z = 3$ leads to the quasiparticle properties described in the introduction which are normally associated with the marginal Fermi liquid state. Thus, the quasiparticles on the Fermi surface are described by an effective mass diverging as $\ln(T^*/T)$ and a scattering rate proportional to T. This implies a heat capacity of the form $C \propto T \ln(T^*/T)$ and a resistivity $\rho \propto T^{5/3}$ to leading order in T. In the resistivity, one factor of T comes from the underlying linear quasiparticle relaxation rate and an additional factor of $T^{2/3}$ arises from the fact that high q fluctuations are more effective than those at low q in reducing the current. This leads to a weighting factor of q_T^2 in ρ, where q_T is a characteristic wavevector satisfying $T \propto \Gamma_{q_T} \propto q_T^z$. For $z = 3$, this leads to $q_T^2 \propto T^{2/3}$ as required. Note that for the corresponding problem of the electron–phonon interaction, we have $T \propto q_T$ and hence the temperature dependences of ρ and of the quasiparticle relaxation rate differ by a factor of T^2 instead of $T^{2/3}$. The electron–phonon scattering problem differs in other important respects; in particular, the propagation frequency is real rather than imaginary and the phonon spectrum is normally much less strongly temperature dependent than that of magnetic fluctuations.

The above results for C and ρ hold strictly only in leading order in T and for $T_C \to 0$. At elevated temperatures corrections arise from (i) the temperature dependence of $\Gamma_q \propto q(\kappa^2 + q^2)$, where $\kappa(T)$ is the inverse of the magnetic correlation length, and (ii) from the high q form of Γ_q or, effectively, from a cut-off Γ_{sf} in Γ_q.

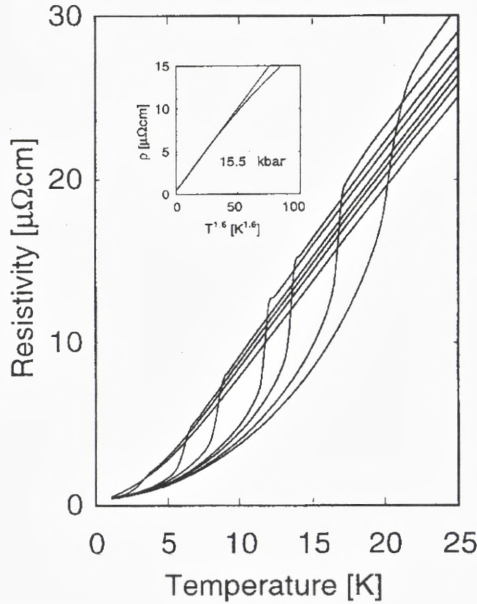Numerical analyses based on the standard model for $\rho(T)$ suggests that the low

Figure 1. The resistivity for MnSi vs temperature at different pressures (5.55 kbar, 8.35 kbar, 10.40 kbar, 11.40 kbar, 12.90 kbar, 13.55 kbar, 14.30 kbar and 15.50 kbar going down starting from the top curve at the far right). The magnetic ordering temperature T_C (marked by the shoulder in ρ vs T) decreases towards absolute zero at $p_c \cong 14.6$ kbar. For $p > p_c$ a non-Fermi liquid form of ρ vs T (i.e. a variation T^β with $\beta \simeq 1.6 < 2$) is seen to extend over a wide range (Pfleiderer et al., 1997).

temperature exponent of $5/3$ is reached only for T well below (typically two orders of magnitude below) the scale set by the cut off $T_{sf} = \hbar\,\Gamma_{sf}/k_B$. The effective exponent $\partial\ln\rho/\partial\ln T$ tends to fall monotonically from $5/3$ towards 1 due to the effect of the cut-off in Γ_q (see (ii) above) and decreases smoothly towards zero at high T/T_{sf} due (additionally) to the temperature dependence of Γ_q (see (i) above).

The predictions of this model have been compared with experimental measurements of $\partial\ln\rho/\partial\ln T$ in the cubic d metal MnSi at the critical pressure ($p_c \cong 15$ kbar) where $T_C \to 0$ (Pfleiderer et al., 1997). The calculations are based solely on the form of Γ_q inferred from inelastic neutron scattering data at ambient pressures, but with $\kappa^2(T) \propto 1/\chi(T)$ derived from the temperature dependence of the susceptibility $\chi(T)$ as measured at p_c.

The general features of the calculations, including an anomaly at low temperatures which may be traced to the low T peak in $\chi(T)$, appear to be in reasonable agreement with the observed behaviour of MnSi (Figs. 1 and 2). We stress, how-
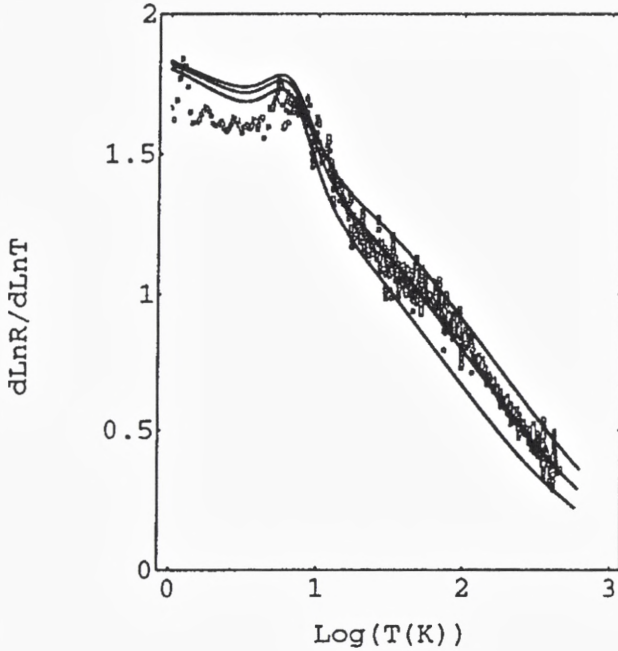
Figure 2. Comparison of measured (points) and calculated (solid lines) logarithmic derivative of the resistivity in MnSi, $\partial \log \rho / \partial \log T$ plotted vs $\log_{10}(T(K))$ at the critical pressure. The calculation involves only the measured temperature dependence of the static susceptibility (Pfleiderer et al., 1997), the parameters of the spin fluctuation spectrum inferred from neutron scattering data (Ishikawa et al., 1985) as discussed in the text, and a cut-off wavevector set equal to the Brillouin zone dimension (ΓX) for the middle line and, respectively, 80% and 120% of ΓX for the lower and upper lines.

ever, that the direct effects of phonon scattering which may be important at high T have been ignored throughout. Also neglected is the phenomenon analogous to phonon drag which may modify the form of ρ vs T due to spin fluctuations at sufficiently low T. Furthermore, we note that since $\chi(T)$ in MnSi is not strictly singular at p_c (Pfleiderer et al., 1997), we expect that the exponent $\partial \ln \rho / \partial \ln T$ will gradually increase towards 2 with decreasing temperature. The experimental exponent, however, appears to fall somewhat below the predicted value as the temperature is decreased. But within the present experimental accuracy, there is no dramatic or unambiguous discrepancy between the prediction of the above model and the observed form of $\partial \ln \rho / \partial \ln T$ in MnSi (Pfleiderer et al., 1997) or in the related cubic d metal ZrZn$_2$ (Grosche et al., 1995).

4   Nearly antiferromagnetic f metals

In a search for the limits of applicability of the above standard model for the spin-fluctuation mediated quasiparticle interaction, we now turn to the heavy fermion f metals on the border of magnetic transitions at low T. In particular, we consider $CePd_2Si_2$ and $CeNi_2Ge_2$ which crystallise in a body-centred tetragonal structure that characterises a large family of Ce ternary compounds, including the first of the heavy-fermion superconductors $CeCu_2Si_2$ (Steglich et al., 1979). At ambient pressure and below 10 K, $CePd_2Si_2$ orders in an antiferromagnetic structure with a weak static moment at low T (Grier et al., 1984).

$CeNi_2Ge_2$ has a slightly smaller lattice constant than $CePd_2Si_2$ and at ambient pressure exhibits no well-defined magnetic transition. It is reasonable to expect that its behaviour at ambient pressure is similar to that of $CePd_2Si_2$ at a pressure somewhat above that required to suppress antiferromagnetic order (Knopp et al., 1988; Fukuhara et al., 1995; Diver, 1996). $CeNi_2Ge_2$ therefore provides us with the opportunity to expand the effective range in pressure over which we may explore the behaviour of essentially the same stoichiometric heavy-fermion system close to the boundary of antiferromagnetic order.

As in the case of MnSi, we find that the transition temperature in $CePd_2Si_2$ falls continuously towards absolute zero and at the critical pressure ($p_c \cong 28$ kbar) the temperature dependence of the resistivity is again found to be significantly slower than quadratic (Grosche et al., 1996) (Fig. 3). But in sharp contrast to the case for MnSi, not only T_N, but also the shoulder of ρ versus T, shifts rapidly with pressure and in a direction opposite to T_N (Thompson et al., 1986). At the critical pressure, the shoulder has shifted by nearly an order of magnitude above its position at ambient pressure.

In the wide range opened up between these two characteristic temperatures near p_c, ρ exhibits a remarkable temperature dependence. The resistivity is linear in $T^{1.2\pm0.1}$ over nearly two decades in temperature down to approximately 0.4 K where our samples with the lowest residual resistivity become superconducting (Fig. 4).

The superconducting regime extends over a relatively narrow pressure range following (and perhaps slightly overlapping with) a regime where T_N falls towards absolute zero. From the temperature variation of the superconducting upper critical field near p_c, we infer a low temperature BCS coherence length of approximately 150 Å, a magnitude characteristic of heavy-fermion superconductivity. Related high pressure results have been reported for $CeCu_2Ge_2$ (Jaccard et al., 1992) and $CeRh_2Si_2$ (Movshovich et al., 1996). What is important in the case of $CePd_2Si_2$, however, is that the normal state above the superconducting transition temperature T_s does not exhibit a temperature dependent resistivity normally associated
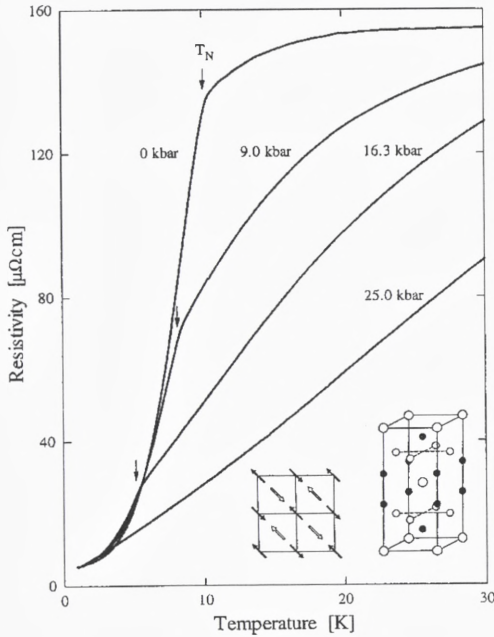
Figure 3. The temperature dependence of the resistivity along the a axis of $CePd_2Si_2$ at different pressures (Grosche et al., 1996). The Néel temperatures T_N, marked by arrows, are visible as significant changes in the slope of ρ vs T. The $ThCr_2Si_2$ lattice structure of $CePd_2Si$ and spin configuration below T_N are illustrated in the insets (Grier et al., 1984). The Ce atoms are on the corners and centre of the tetragonal unit cell, and the Pd atoms are on the cell faces.

with a Fermi liquid state. In some sense, this then represents a form of "high temperature" superconductivity; not high in absolute terms, but in relation to some low temperature scale apparently not yet reached on cooling to T_s. Among the heavy fermion systems, another extreme but qualitatively different examples of such "high temperature" superconductivity is found in UBe_{13} (Ott et al., 1983).

At sufficiently high pressures, we expect to recover a Fermi liquid (quadratic) form of ρ versus T which is ubiquitous in other paramagnetic heavy fermion metals at low T. As stated earlier, $CeNi_2Ge_2$, with a slightly smaller cell volume than $CePd_2Si_2$, but otherwise with a similar lattice and starting electronic structure, provides us with the opportunity to examine the crossover to the Fermi liquid form of ρ versus T without the use of very high applied pressures. Initial studies in $CeNi_2Ge_2$ suggested a more or less unexceptional behaviour. In particular, ρ versus T was thought to have a conventional form characteristic of many normal heavy
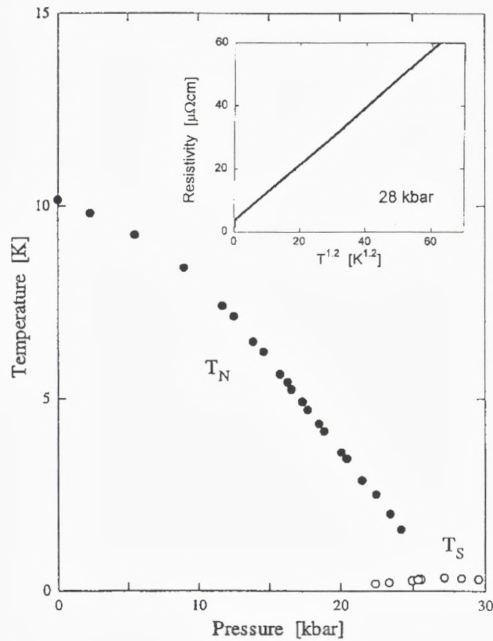
Figure 4. The temperature-pressure phase diagram of CePd$_2$Si$_2$. The Néel temperature T_N falls monotonically towards zero and is nearly linear in pressure before entering a relatively narrow region where superconductivity appears in the millikelvin range (Grosche et al., 1996). The magnetic field dependence of the superconducting transition temperature T_s exhibits a high slope characteristic of heavy fermion superconductors. Near the critical pressure where $T_N \to 0$, the resistivity is seen to be linear in $T^{1.2\pm0.1}$ over nearly two decades in temperature (inset) (Grosche et al., 1996).

fermion systems. But more detailed studies in samples with low residual resistivities have revealed that ρ does not exhibit a simple quadratic temperature variation except perhaps below one or two hundred mK and in fact varies as $\rho \sim T^{1.4\pm0.1}$ over a decade below several degrees K (Steglich, 1996; Diver, 1996). This anomalous behaviour of the temperature dependence of the resistivity appears to extend up to 10 kbar and beyond where a new superconducting instability is observed (Grosche, 1997; Carter et al., unpublished). Also, we note that in both compounds the value of the anomalous exponent of ρ versus T appears to be quite sensitive in particular to sample perfection (Carter et al., unpublished).

The nature of the anisotropic spin fluctuation spectra of CePd$_2$Si$_2$ and CeNi$_2$Ge$_2$ are not yet sufficiently well known to enable us to carry out a quantitative analysis

analogous to that presented for the d-metal ferromagnets in the previous section. Further, the validity of the naive extension of this model to antiferromagnetic systems (for which z is taken to be 2 instead of 3) is not clearly self evident (Hlubina and Rice, 1995). For the very simplest case with $d = 3$ and $z = 2$, the exponent $\partial \ln \rho / \partial \ln T$ falls monotonically from $3/2$ for $T \gg T_{sf}$ towards zero for $T \ll T_{sf}$. The observation of a low temperature exponent of less than $3/2$ in $CePd_2Si_2$ at p_c is not necessarily inconsistent with this model since convergence of $\partial \ln \rho / \partial \ln T$ to $3/2$ is found to be very slow. But the locking in of the experimental exponent to a fixed value over a wide temperature range is not a feature of the present spin fluctuation model. Also difficult to understand within this same framework is the non-Fermi liquid form of ρ versus T at still higher pressures above p_c in $CePd_2Si_2$, or in the smaller volume relative $CeNi_2Ge_2$ at ambient or low pressures and above one or two hundred mK.

It is not yet clear whether a consistent description of the above findings can be given in terms of a refined version of the model developed for the d-metal ferromagnets or whether a radically different approach is required. In the f heavy fermion systems, in contrast to typical d metals, there may be an ambiguity in the spin-fluctuation theory as it is conventionally formulated. It is perhaps unclear in our systems whether the Fermi surface close to which the relevant quasiparticles are excited is that formed by the "conduction electrons" together with the f electrons, as suggested by de Haas–van Alphen studies on a number of normal heavy fermion compounds, or by the conduction electrons alone as is often assumed in "intermediate temperature" descriptions. What is more, the usual assumption that the strength of the coupling of the quasiparticles to the exchange field is weakly temperature dependent may in these highly correlated systems seriously break down in the temperature range of interest.

5   Conclusions

The idealised model for describing nearly ferromagnetic d metals, such as MnSi and $ZrZn_2$, near the critical point $T_C \to 0$, appears to be that of a marginal Fermi liquid which has also been invoked in theoretical treatments of the coupling of electrons to transverse photons and in the study of nuclear matter (Baym and Pethick, 1991). In both cases, the starting picture remains that of fermion quasiparticles excited above a normal Fermi surface. In more extreme cases, an altogether different starting point may be required.

It is conceivable that this is the case in some of the more strongly correlated electron systems among the heavy fermion compounds (see also Morin et al., 1988; Löhneysen et al., 1994; Seaman et al., 1991; Andraka and Stewart, 1993; Tsvelik

and Reizer, 1993; Coleman, 1995b). In particular, we have noted that a naive extension of the spin fluctuation model used for the d-metal ferromagnets cannot readily account for the curious locking into a fixed exponent $\partial \ln \rho / \partial \ln T$ over nearly two decades in temperature in $CePd_2Si_2$ near the critical pressure nor in $CeNi_2Ge_2$ at ambient pressure.

Acknowledgements

References

Anderson PW, 1995: Phys. World **18**, 37; and forthcoming book on "high temperature superconductivity"

Andraka B and Stewart GR, 1993: Phys. Rev. B **47**, 3208

Baym G and Pethick C, 1991: *Landau–Fermi Liquid Theory* (Wiley, New York) Chap. 3

Bernhoeft NR, Hayden SM, Lonzarich GG, McK Paul D and Lindley EJ, 1989: Phys. Rev. Lett. **62**, 657; Lonzarich GG, Bernhoeft NR and McK Paul D, 1989: Physica B **156 & 157**, 699

Coleman P, 1995a: Phys. World **18**, 29

Coleman P, 1995b: Physica B **206 & 207**

Diver A, 1996: Thesis (University of Cambridge); Gray IR, 1989: Thesis, (University of Cambridge)

Fukuhara T, Maezawa K, Ohkuni H, Sakurai J and Sato H, 1995: J. Magn. Magn. Mater. **140–144**, 889

Grier BH, Lawrence JM, Murgai V and Parks RD, 1984: Phys. Rev. B **29**, 2664

Grosche FM, Pfleiderer C, McMullan GJ, Lonzarich GG and Bernhoeft NR, 1995: Physica B **206 & 207**, 20

Grosche FM, Julian SR, Mathur ND and Lonzarich GG, 1996: Physica B **223 & 224**, 50; Julian SR, Mathur ND, Grosche FM and Lonzarich GG, 1997: (to be published)

Grosche FM et al., 1997: Physica B (in press)

Hertz J, 1976: Phys. Rev. B **14**, 1164

Hlubina R and Rice TM, 1995: Phys. Rev. B **51**, 9253

Ishikawa Y, Noda Y, Wemura WJ, Majhrazah CF and Shirane G, 1985: Phys. Rev. B **31**, 5884; Brown SA, Bernhoeft NR, Hayden SM and Lonzarich GG (to be published)

Jaccard D, Behnia K and Sierro J, 1992: Phys. Lett. A **163**, 475

Knopp G, Loidl A, Caspary R, Gottwick U, Bredl CD, Spille H, Steglich F and Murani AP, 1988: J. Magn. Magn. Mater. **74**, 341

Lonzarich GG, 1997: *The Magnetic Electron* in *The Electron*, ed. M. Springford (Cambridge University Press, Cambridge); *Magnetic Phase Transitions at Low Temperature*, unpublished lectures (College on Quantum Phases, ICPT, Trieste, 1994)

Löhneysen, H.v. Pietrus T, Portisch G, Schlager HC, Schröder A, Sieck M and Trappmann T, 1994: Phys. Rev. Lett. **72**, 3262

Millis AJ, 1993: Phys. Rev. B **48**, 7183

Morin P, Vettier C, Flouquet J, Konczykowski M, Lassailly Y, Mignot JM and Welp U, 1988: J. Low Temp. Phys. **70**, 377

Moriya T, 1985: *Spin Fluctuations in Itinerant Electron Magnetism* (Springer Verlag, Berlin)

Movshovich R, Graf T, Mandrus D, Thompson JD, Smith JL and Fisk Z, 1996: Phys. Rev. B **53**, 8241

Ott HR, Rudingier H, Fisk Z and Smith JL, 1983: Phys. Rev. Lett. **50**, 1595

Pfleiderer C, McMullan GJ, Julian SR and Lonzarich GG, 1997: Phys. Rev. B (in press)

Seaman CL, Maple MB, Lee BW, Ghamaty S, Torikachvili MS, Kang JS, Liu LZ, Allen JW and Cox DL, 1991: Phys. Rev. Lett. **67**, 2882

Steglich F, 1996: J. Phys. Condens. Matter **8**, 9909; (private communications)

Steglich F, Aarts J, Bredl CD, Lieke W, Meschede D, Franz W and Shäfer J, 1979: Phys. Rev. Lett. **43**. 1892

Thompson JD, Parks RD and Borges H, 1986: J. Magn. Magn. Mater. **54–57**, 377

Tsvelik A and Reizer M, 1993: Phys. Rev. B **48**, 4887

Magnetism in Heavy-Electron Metals

H. R. Ott

Laboratorium für Festkörperphysik, ETH Hönggerberg,

CH 8093 Zürich, Switzerland

Abstract

Originally it was believed that the presence of heavy-mass charge carriers at low temperatures in some special rare-earth or actinide compounds was simply the result of a suppression of magnetic order in these materials. Various experiments reveal, however, that magnetic order may occur from a heavy-electron state or that a heavy-electron state may also develop within a magnetically ordered matrix. It turned out that pure compounds without any sign of a cooperative phase transition down to very low temperatures are rare but examples are known where microscopic experimental probes give evidence for strong magnetic correlations involving moments of much reduced magnitude ($\leq 0.1\mu_B$) in such cases. It appears that electronic and magnetic inhomogeneities, both in real and reciprocal space occur which are not simply the result of chemical inhomogeneities. Long range magnetic order among strongly reduced magnetic moments seems to be a particular feature of some heavy-electron materials. Other examples show, that disorder may lead to a suppression of cooperative phase transitions and both macroscopic and microscopic physical properties indicate that conservative model calculations are not sufficient to describe the experimental observations. The main difficulty is to find a suitable theoretical approach that considers the various interactions of similar strength on an equal footing. Different examples of these various features are demonstrated and discussed.

1 Introduction

The stability of magnetic moments in a metallic environment has been the subject of many theoretical and experimental studies but the ideas considered in the early works of Friedel (1956), Blandin (1958), Anderson (1961) and Kondo (1964) still provide the essential background for discussing recent and new experimental observations. The low temperature behaviour of simple metals is believed to be well understood on the basis of Landau's (1956) Fermi liquid model. The often observed transition to a superconducting state can be well explained by the BCS theory (Bardeen et al., 1957) and a pairing potential that is due to the interaction between conduction electrons and lattice excitations (phonons). Less transparent is the behaviour of d- and f-electron transition metals and compounds. Particular recent interest is connected with a class of substances for which electron-electron

interactions and correlations are dominating factors, the so called heavy-electron systems. For the description of the properties of these metallic systems, many-body effects can no longer be neglected or treated with simple approximation schemes. Materials that we discuss here contain ions with incompletely occupied atomic f-electron orbitals, leading to well defined ionic moments containing both orbital and spin components. These ions occupy regular lattice sites and their moments interact with the ensemble of itinerant charge carriers. In most cases it may be expected that the adopted ground state of these materials is of some magnetically ordered variety, a result of the coupling of these moments via the Ruderman–Kittel–Kasuya–Yosida (RKKY) interaction mediated by the conduction electrons (Ruderman and Kittel, 1954 ; Kasuya, 1956; Yosida, 1957). As is well known from the above cited work, a metallic environment may also lead to a partial or complete compensation of a single magnetic moment. Instead of considering the stability of only a single magnetic moment in a metallic environment, the new developments that are considered here necessitate the same treatment for a regular array of magnetic moments in three dimensions. Various new schemes to treat this type of problem have recently been employed (Jones, 1991; Sheng et al., 1994; Keiter et al., 1995; Wölfle, 1995) and, in particular, the possibility of new types of metallic ground states, different from that of a Fermi liquid, has received considerable attention in the last few years (Cox, 1987; Coleman et al., 1994; Ludwig, 1994).

Below we intend to discuss a few experimental observations which indicate that due to competing interactions of similar magnitude, ground states that are more complex than previously envisaged may be adopted. The main purpose of this presentation and discussion is to provide experimental evidence for the new aspects that were mentioned above, but this short review is certainly not exhaustive. The selected series of examples, however, may serve as a guideline for future explorations in this field, both experimentally and hopefully also theoretically.

2   Magnetic inhomogeneities in real space

A well documented case for this type of feature has been established for the compound CeAl$_3$. This compound has for a long time been considered as a standard example for which well defined localized magnetic moments at low temperatures donate their degrees of freedom to a new kind of state whose properties are characteristic for a Fermi liquid with strongly renormalized parameters and is formed by quasiparticles with considerably enhanced effective masses. This view was based on the results of experiments probing thermal- and transport properties at high and low temperatures, i.e., between 0.05 and 300 K (Andres et al., 1975; Ott et al., 1984a).
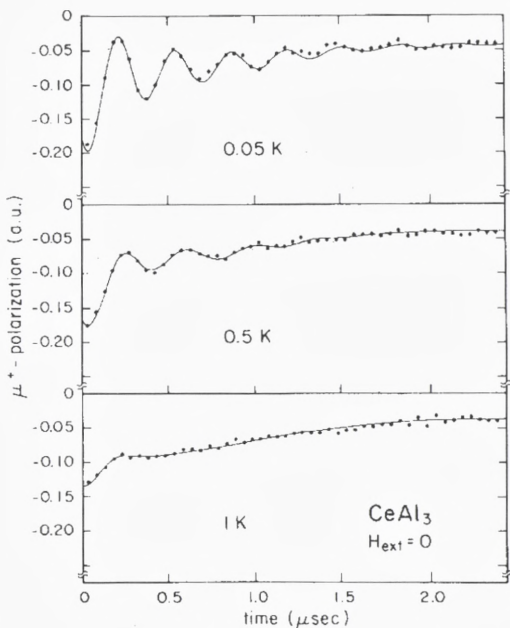
Figure 1. Time dependence of the zero-field μ^+ polarization in CeAl$_3$ at low temperatures. The solid lines are fits to the data (see Barth et al., 1989).

Subsequent microscopic studies involving μSR and NMR experiments revealed a more complicated situation, however. At very low temperatures and in zero magnetic field an oscillatory component in the μSR spectra shown in Fig. 1 indicated the presence of at least quasistatic magnetic correlations inducing a corresponding local field at the muon site (Barth et al., 1987). The temperature dependence of the oscillation frequency in the range of observation between 0.05 and 0.7 K is rather weak and above this temperature the oscillatory component is no longer discernible. The observation of a single frequency proves that all the muons experiencing the corresponding local field, which doesn't vary much with temperature, are trapped and decay on equivalent sites. The temperature dependence of the μ^+-decay asymmetry indicates that the number of trapping sites exposed to the quasistatic magnetic field increases with decreasing temperature. As T approaches 0, a large part of the sample is magnetically correlated (Barth et al., 1989). The growth of the correlated regions occurs without any manifestation of a cooperative phase transition, compatible with all observations when probing macroscopic properties.
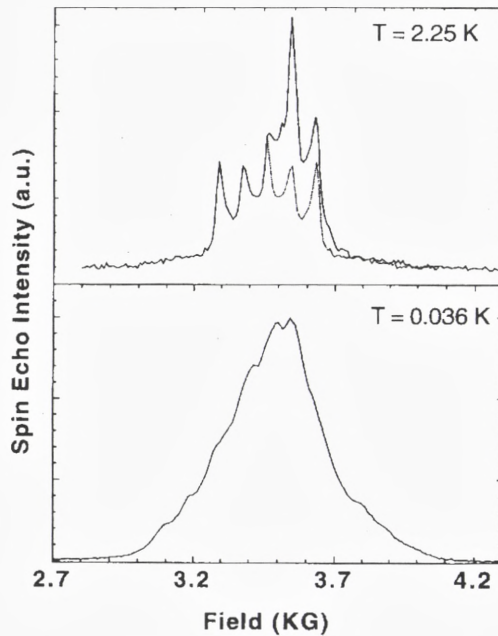
Figure 2. Low frequency NMR spectra of CeAl₃ at low temperatures. The dotted line indicates the quadrupolar split spectrum of the oriented part of the powder sample.

Additional μSR experiments in non-zero magnetic fields were intended to iden-tify with some reliability the μ^+-decay site in the crystal lattice. Accompanying simulation calculations and a thorough analysis of all the available data indicate a magnetic moment of only 0.05 μ_B residing on the Ce^{3+} ions within the correlated regions below 0.7 K (Schenck, 1993). It seems obvious that both the small value of the moments involved in the correlated regions and the unusual, spatially inhomo-geneous increase of magnetically correlated volume with decreasing temperature deserved more attention. Subsequent low-field NMR experiments (Gavilano et al., 1995a) on the same material and at temperatures between 0.04 and 20 K to a large extent confirmed the previous microscopic observations. Above 3 K, sharp and quadrupole-split resonance lines of ^{27}Al nuclei reveal a normal paramagnetic envi-ronment. Below 3 K, however, a broad background intensity in these spectra grows with decreasing temperature and at the lowest temperatures the NMR spectrum consists of a broad and only faintly structured peak with a width of a few hundred gauss (see Fig. 2). The growing background intensity may be interpreted as being
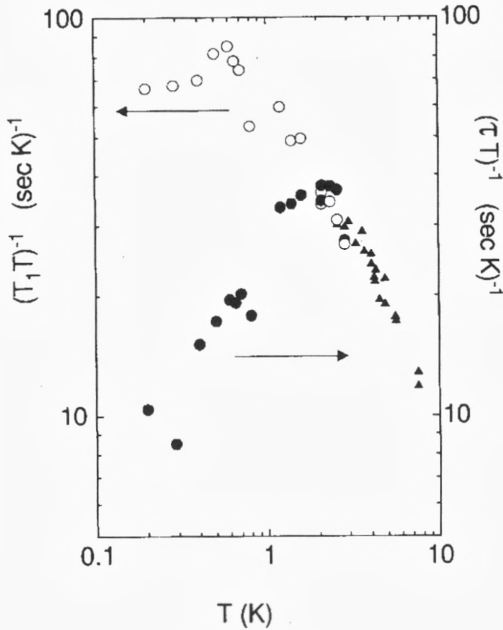
Figure 3. Temperature dependence of the NMR relaxation rates related to the two different parts of the spectra of CeAl$_3$.

due to an increase of the number of nuclei which are exposed to an internal field barely changing with temperature and of the order of 500 gauss. Considering this field value and the geometrical arrangement of Ce and Al atoms in the hexagonal crystal structure of CeAl$_3$, again an average moment of the order of 0.05 μ_B/Ce ion may be deduced. The broadening of the quadrupole split lines of nuclei in a paramagnetic environment is thought to arise from the fact that the correlated regions are dispersed and rather small in volume, thereby allowing a large number of the nuclei in the paramagnetic parts of the sample to be close to a boundary between a correlated and a paramagnetic region.

Measurements of the spin–lattice relaxation time T_1 revealed that the coupling of the nuclear magnetisation to its environment is quite different for either the correlated or the paramagnetic regions (see Fig. 3). Above 3 K, the relaxation occurs via a single channel characterized by a single value for T_1 which increases considerably with decreasing temperature. Below 3 K, two different relaxation rates may be distinguished. The rate related with the paramagnetic regions increases further with decreasing temperature and finally, below 0.7 K, the product $(T_1T)^{-1}$

saturates at a much enhanced value of 65 K^{-1}. For pure Al, this value is 0.56 K^{-1}. The temperature dependence of the relaxation rate associated with the correlated regions is completely different and the corresponding values of $(T_1 T)^{-1}$ decrease considerably with temperature. At the lowest temperatures of observation the difference in these relaxation rates is about one order of magnitude.

All these microscopic observations indicate that the low temperature state of CeAl$_3$ cannot simply be identified as a strongly renormalized Fermi liquid state. There is strong evidence for the coexistence of two magnetically and electronically inequivalent phases at very low temperatures. Although in retrospect some of the features of thermal properties (specific heat, magnetic susceptibility) below 1 K might be considered as indicative for the behaviour described above, the transport properties certainly reveal no such manifestation. Additional recent experiments on small single crystals (Lapertot et al., 1993) and material with small amounts of non magnetic impurities on the Ce sites (Andraka et al., 1995) confirm that the ground state of CeAl$_3$ is very close to being magnetically ordered.

3 Electronic inhomogeneities in momentum space

As we pointed out in the introduction, long range magnetic order in metals is very often the result of the RKKY interaction, a coupling of magnetic moments mediated by conduction electrons. The oscillatory nature of this interaction is a result of the Fermi–Dirac type of occupation probability of the electronic states in k-space and we intend to demonstrate that different parts of the Fermi surface may be involved in quite different ways in the formation of the ground state of a metal. As an example we choose the case of UCu$_5$.

Experimental studies of the low temperature properties of this compound gave the first evidence that a heavy-electron state may also develop in the environment of a magnetically ordered matrix (Ott et al.,1985), a feature that was not anticipated in early discussions concerning the formation of massive states of itinerant electrons. Various macroscopic and microscopic measurements established the rather conventional antiferromagnetic order that develops among the U magnetic moments of the order of 1 μ_B/U ion in UCu$_5$ below 15 K (van Daal et al., 1975; Murasik et al., 1974; Schenck et al., 1990). The phase transition is clearly manifested by anomalies in the temperature dependence of the specific heat $C_p(T)$ and the electrical resistivity $\rho(T)$. The feature of this latter anomaly implies that the phase transition induces a partial gapping of the Fermi surface thereby reducing the amount of available itinerant charge carriers (Bernasconi et al., 1994). The formation of this gap has more recently been confirmed by measurements of the optical reflectivity, indicating that the transition is at least partially due to
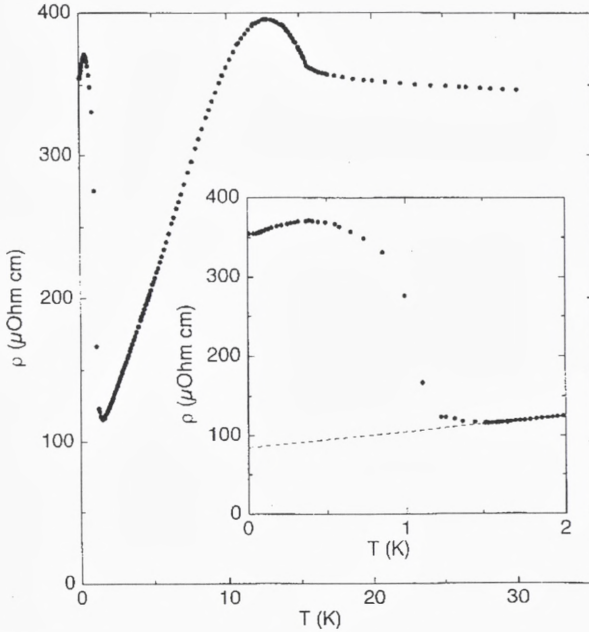
Figure 4. Temperature dependence $\rho(T)$ of the electrical resistivity of UCu$_5$ between 0.02 and 30 K. The inset emphasizes $\rho(T)$ below 2 K.

a magnetic Fermi surface instability (Degiorgi et al., 1994). The temperature dependence of ρ between 0.03 and 30 K is shown in Fig. 4. It may be seen that the remaining free carriers experience a drastic reduction in scattering below about 12 K, most likely due to the combined effect of less magnetic scattering and the onset of coherence due to electronic correlation effects with decreasing temperature.

These correlation effects lead to a distinct increase of the $C_p(T)$ ratio with decreasing temperature below 4 K, reaching a value exceeding 300 mJ/mole K^2 below 2 K (Ott et al., 1985). The correlated electron system now by itself loses its stability and another cooperative phase transition at approximately 1 K is indicated by, again, anomalies in $C_p(T)$, shown in Fig. 5, and $\rho(T)$ (see Fig. 4). Below 1 K, $\rho(T)$ reaches a maximum at 0.4 K and subsequently decreases somewhat as T approaches 0. The anomaly of $C_p(T)$ is small but distinct, the corresponding entropy change is negligible compared to $R \ln 2$. Below 0.7 K, C_p decreases linearly with temperature to zero and the ratio $\gamma = C_p/T$ is 80 mJ/mole K^2. Both these observations are again compatible with a sizeable reduction of occupied electronic states at the Fermi energy induced by the 1 K transition. Additional transport
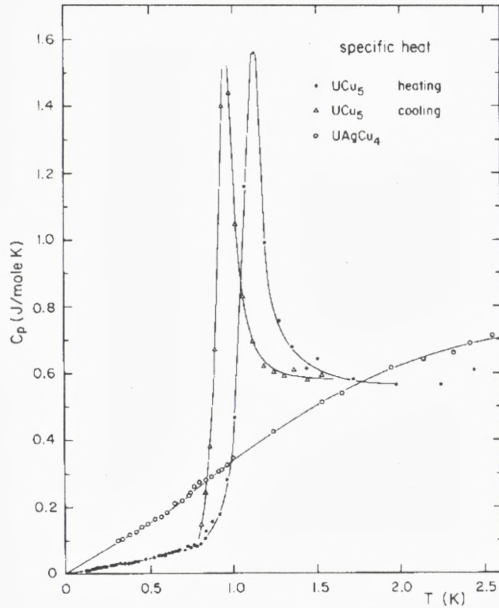
Figure 5. Specific heat of UCu$_5$ and UAgCu$_4$ between 0.1 and 2.5 K.

experiments (Bernasconi et al., 1994) and spectroscopic measurements (Nakamura et al., 1991) support the conclusion that the remaining itinerant charge carriers form a state with the features of a renormalized Fermi liquid. This state, however, coexists with an antiferromagnetically ordered state which is partly due to a spin-wave-type instability and yet another ordered state developing below 1 K whose order parameter has not been established yet.

This coexistence is indicated because the 1 K transition in zero magnetic field has very little influence on the ordered state that has been established to form below 15 K. At the 1 K transition the magnetic susceptibility shows only a minute increase with decreasing temperature (Chernikov et al., 1995). The microscopic probing of the magnetism of UCu$_5$ invoking μSR and neutron scattering experiments (Schenck et al., 1990) revealed that within experimental resolution no change of the ordered structure nor in the magnitude or orientation of the ordered moments can be inferred. The only noticeable manifestation of this transition in μSR or neutron scattering data is an increase in the relaxation rate inferred from μ^+-decay spectra. An example for one of the decay channels is shown in Fig. 6. A possible implication of this result could be the formation of some order among tiny
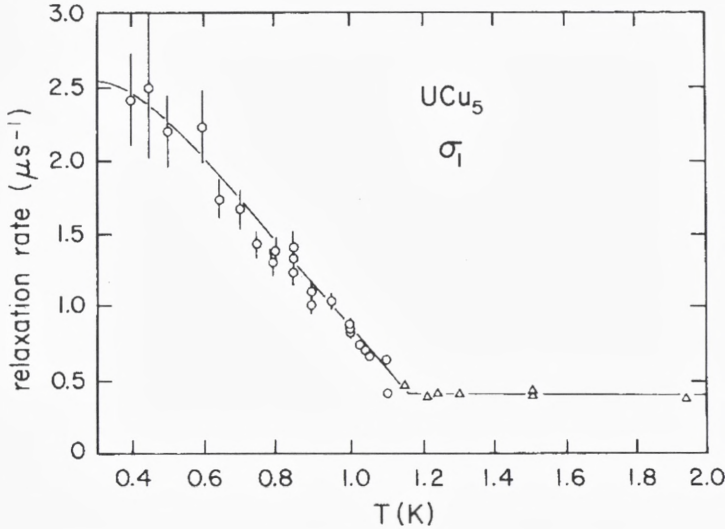
Figure 6. Temperature dependence of the μSR relaxation rate in one of the decay channels of UCu$_5$ below 2 K.

moments, not detectable by neutron scattering, again due to a Fermi surface instability involving states with enhanced effective masses. The estimated magnitude of such moments from μSR data is definitely less than 0.01 μ_B. Other conjectures such as the formation of a small internal distortion of the crystal lattice or the transition from a multi-q to a single-q state of magnetic order (Nakamura et al., 1994; Lopez de la Torre et al., 1995) seem incompatible with the combined data of both macroscopic and microscopic experiments. The 1 K transition is extremely sensitive to impurities and imperfections in general (Ott et al., 1989), a feature that is often observed for heavy-electron systems, particularly also in connection with superconducting transitions in such materials and the formation of a correlated state, as in this case (Ott et al., 1987). For some deliberately introduced impurities, especially those which occupy Cu sites, also the 15 K transition is considerably affected, in not the same excessive way, however (Ott et al., 1989).

The main question of how this subdivision of the electronic subsystem has to be addressed theoretically is not easily answered. Estimates based on band structure calculations reproduce both the Néel temperature of 15 K and the magnitude of the ordered moment of the antiferromagnetic order quite well (Norman et al.,1988). Any description of the features at very low temperatures, however, are clearly beyond the capacity of such approaches. Considering the crystal structure of UCu$_5$

it may be noted that cation and anion sites are well separated and this may lead to an intrinsic anisotropy of possible interactions which are all, judging from the experimental observations, rather small and not very different in magnitude. Most importantly, the fact that a heavy-electron state may also form even within a lattice of antiferromagnetically aligned f-electron moments seems of some significance in view of theoretical models describing corresponding correlated systems.

More recently it has been speculated that the low-temperature properties of alloys of the form $UCu_{5-x}Pd_x$ with $x \sim 1$ indicate a non Fermi liquid type behaviour, both from macroscopic and microscopic investigations (Andraka et al., 1993; Maple et al., 1995; Bernal et al., 1996). Recent optical measurements (Degiorgi et al., 1996) confirm that at low temperatures T and for low frequencies ω, the charge transport relaxation rate varies almost linearly with T and ω, and not with T^2 and ω^2, the expected functional dependencies claimed for a Fermi liquid.

4   Magnetic ordering in the presence of heavy electrons

The possibility of magnetic order in the presence of heavy electrons may be demonstrated very well by discussing the low temperature properties of the compound U_2Zn_{17}. In Fig. 7 we show results of the electronic part of the low-temperature specific heat of U_2Zn_{17} which was obtained by subtracting from the total specific heat the lattice contribution as evaluated from corresponding measurements on the isostructural compound Th_2Zn_{17} (Ott et al., 1984b). The very large C_p^{el}/T ratio of 550 mJ/mole K^2 indicates the anomalously enhanced electronic specific heat above T_N. As evidenced by the discontinuous change of C_p/T around 9.7 K the phase transition is very sharp. The electronic part of the specific heat below 5 K can very well be approximated by $C_p^{el} = \gamma T + \beta T^3$ where the prefactor of the linear term is about 1/3 of the C_p^{el}/T ratio above T_N. Since recent optical experiments (Degiorgi et al., 1994) have shown that this reduction cannot be traced back to the formation of a partial gap at the Fermi surface, a reduction of the effective mass of the charge carriers induced by the onset of magnetic order seems to be the cause for this observation. The second term is typical for a contribution due to magnetic excitations in the ordered state. The solid line in Fig. 7 indicates that a BCS type curve, taking into account the remaining electronic specific heat below T_N, does not describe the experimental results. In view of the absence of a gap formation in the electronic spectrum this may not be too surprising. In connection with this phase transition we also note that the entropy loss due to the transition is anomalously small, i.e. much less than $2R \ln 2 = 11.52$ J/mole K, the entropy that would be released by lifting the degeneracy of a doubly degenerate ground state of
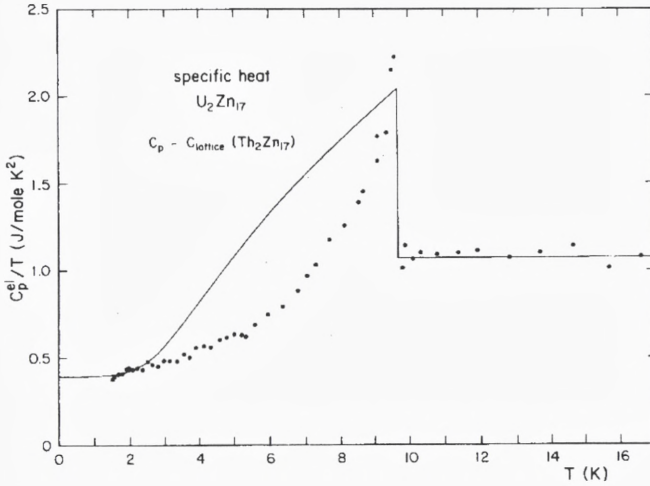
Figure 7. C_p^{el}/T versus T for U_2Zn_{17} between 1.5 and 16 K. The solid line is a BCS-type curve taking into account a non-zero electronic contribution below T_N.

the U ions.

The temperature dependence of the magnetic susceptibility $\chi(T)$ suggests that the transition is to an antiferromagnetically ordered state. Although the high temperature part of $\chi(T)$ cannot really be described by a simple Curie–Weiss type law, the general features, nevertheless, indicate a rather strong antiferromagnetic coupling via a seemingly negative paramagnetic Curie temperature. At low temperatures, $\chi(T)$ reveals a maximum at approximately 17 K and a discontinuous slope change at the temperature where the specific heat varies discontinuously. Very similar features have also been observed for the temperature dependence of the electrical resistivity $\rho(T)$.

Measurements employing microscopic techniques confirm the antiferromagnetic character of the ordered state. Neutron diffraction experiments (Cox et al., 1986) and μSR measurements (Barth et al., 1986) have been made to probe the phase transition and the ordered state of U_2Zn_{17}. The neutron results suggest a rather simple magnetically ordered structure below T_N. Because the chemical unit cell contains two U atoms, it is identical with the magnetic unit cell. For the saturated ordered moment in zero magnetic field a value of 0.8 μ_B/U has been deduced and its orientation is claimed to lie in the basal plane of the rhombohedral crystal lattice. The magnitude of the staggered moment is distinctly smaller than expected for either free U^{3+} or U^{4+} ions. Somewhat different conclusions were drawn from the experimental μSR data. They seem to reveal a magnetically inhomogeneous

state (Schenck et al., 1991) and do not confirm the relatively simple picture that is imposed by the neutron results, although both types of experiments have been made using exactly the same single-crystalline sample.

Rather unusual features emerged from a study employing inelastic neutron scattering (Broholm et al., 1987a). First, no evidence for propagating spin waves could be identified, although a scattering intensity due to magnetic excitations is clearly observed. The observation of only a single ridge of intensity parallel to the ω axis and the failure to identify two branches commonly associated with propagating spin waves is not a resolution problem. This follows from considering the T^3 term in the specific heat and the available instrumental resolution. We also note that the broad magnetic excitation spectra persist to energies considerably exceeding kT_N. For the analysis of constant $\mathbf{q}$ and constant ω scans, a rather simple model for the generalized susceptibility has been used successfully. The susceptibility $\chi_{\mathbf{q}}(\omega)$ was approximated by assuming an effective single-ion susceptibility $\chi_0(\omega)$ and a nearest neighbour RKKY coupling J'. Fitting the neutron data on the basis of this model suggests that the phase transition is driven by the temperature dependence of J' rather than by a strong increase of χ_0, as is usually the case. Concomitant with the transition a sizeable increase of the fluctuation rate is observed, compatible with the decrease of the specific heat γ parameter.

Finally we should like to point out that the antiferromagnetic ordering of U_2Zn_{17} is extremely sensitive to impurities replacing Zn on the anion sites (Ott et al., 1989), much more than what is encountered for conventional antiferromagnets. This may be seen from specific heat data that are shown in Fig. 8 and which were obtained by substituting about 2% of the Zn atoms by Cu. Susceptibility measurements down to 0.02 K indicate that this variation of chemical composition is sufficient to suppress magnetic order above this rather low temperature(Willis et al., 1986). The large electronic specific heat above T_N, however, is not much affected by the presence of these impurities. Because of the absence of magnetic order, the C_p^{el}/T ratio stays large down to very low temperatures, with a distinct trend to further enhancement close to $T = 0$. This observation, together with many others, also stated in the previous section, confirms the general conclusion that properties of heavy electron materials are very often sensitive to even tiny changes in their chemical composition.

5   Magnetic order involving small moments

One of the outstanding new phenomena in heavy-electron physics is the occurrence of drastically reduced magnetic moments and the cooperative ordering of such tiny moments at low temperatures. Particularly intriguing is the fact that these small
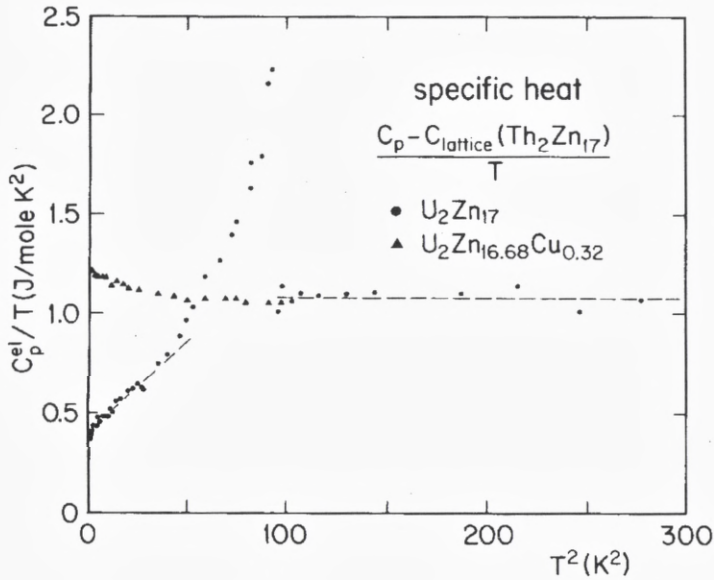
Figure 8. Comparison of C_p^{el}/T versus T^2 between pure and Cu-doped U_2Zn_{17} between 1.5 and 16 K.

moments usually derive from ionic moments of expected normal magnitude. The presence of these normal size moments is manifested in the magnitude and temperature dependence of the magnetic susceptibility at elevated temperatures. Even when considering crystal electric field effects, the low-temperature magnetic moments of rare-earth and actinide ions of interest here, are expected to be of the order of 1 μ_B per ion. It has been found, however, that moments of much smaller magnitude exist as mentioned, for example, in Sect. 2 for $CeAl_3$. Even more surprisingly it has been established that long range magnetic order involving very small moments is possible, first discovered by neutron scattering experiments for URu_2Si_2 (Broholm et al., 1987b) and by μSR measurements for UPt_3 (Heffner et al., 1987). In both cases this magnetic order appears to coexist with a superconducting state that sets in at a critical temperature T_c of about one tenth of the antiferromagnetic transition temperature T_N. As an example we show the anomalies in the temperature dependence of the specific heat manifesting the transitions of URu_2Si_2 in Fig. 9. Neutron diffraction results reveal antiferromagnetic order in this compound below 17 K, among moments with values of a few hundredth of a Bohr magneton (Broholm et al., 1987b). The development of the elastic magnetic scattering intensity with decreasing temperature is shown in Fig. 10. The moments
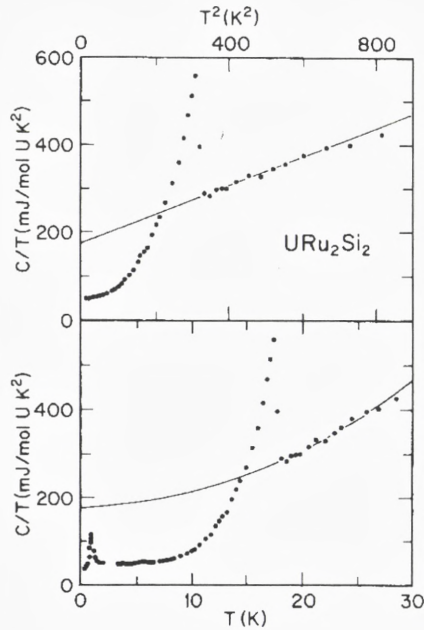
Figure 9. Low-temperature specific heat of URu_2Si_2 as C/T versus T^2 (upper part) and versus T (lower part) (see Palstra, 1986).

are aligned parallel to the tetragonal c axis of the crystal lattice. While for UPt_3 the onset of magnetic order among moments of a few hundredth of a Bohr magneton (Aeppli et al., 1988) finds no manifestation in the temperature dependence of thermal or transport properties, as might be expected, the situation is quite different for URu_2Si_2. The transition at 17 K is very well discernible by a large C_p anomaly at T_N, as shown in Fig. 9. The entropy loss in this phase transition is obviously not compatible with the measured size of the staggered moments and in spite of many efforts it is still a puzzle how this discrepancy can be explained. From Fig. 9 it may also be seen that via this phase transition, again the C_p/T ratio measured above T_N is sizeably reduced at temperatures well below T_N. The resulting electronic subsystem with this reduced effective mass of the quasiparticles has been found to undergo a transition to a superconducting state at approximately 1 K (Schlabitz et al., 1986; Palstra et al., 1985). This superconducting state coexists with the magnetic order, the same situation is met for UPt_3.

Theoretically the issue of how these very small moments may develop and be stable seems quite challenging. Some suggestions have been made (Coleman et al.,
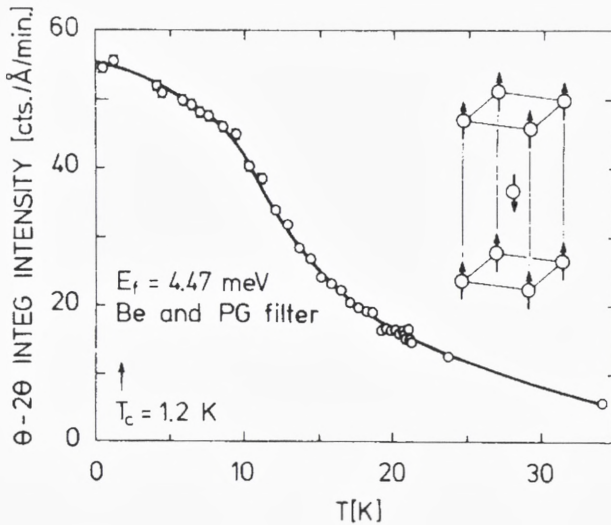
Figure 10. Integral elastic scattering at (100) as a function of temperature for URu_2Si_2 (see Broholm et al., 1987b).

1991; Cooper et al., 1992; Barzykin et al., 1993; Santini et al., 1994; Miranda, 1996) but it is not certain that the correct answer has been found yet. At any rate, the increasing number of examples where these very small moments are claimed to have been observed should be motivation enough to pursue this problem further.

In this section we have mentioned the coexistence of antiferromagnetic order involving strongly reduced moments and an electronic subsystem whose excitations are described by quasiparticles with fairly enhanced effective masses. Below we discuss the case of $CePd_2In$, an example where weak interactions of similar magnitude but with opposite influence lead to distinct features in physical properties at low temperatures for which a fairly complete set of data exists.

$CePd_2In$ crystallizes with the hexagonal $GdPt_2Sn$ structure with two formula units per unit cell (Xue et al., 1993). A phase transition at 1.23 K is indicated by anomalies of the specific heat, the magnetic susceptibility and the electrical resistivity (Bianchi et al., 1995) The temperature dependence of the magnetic susceptibility suggests that the transition is to an antiferromagnetically ordered state. At temperatures well below T_N, both $C_p(T)$ and $\rho(T)$ reveal the presence of quasiparticles with an enhanced effective mass. In the electronic contribution γT to $C_p(T)$ of $CePd_2In$ above T_N the γ parameter is of the order of 30 mJ/mole K^2, about five times larger than that of $LaPd_2In$. In spite of the intermediary transi-
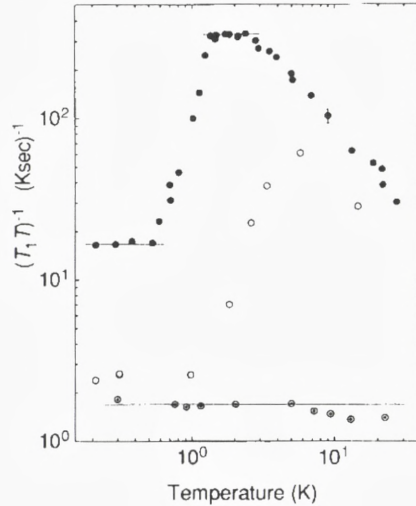
Figure 11. Temperature dependence of the NQR spin–lattice relaxation times of CePd$_2$In (full circles) and LaPd$_2$In (dotted circles), plotted as $(T_1T)^{-1}$ versus T on logarithmic scales. Open circles denote NMR data for CePd$_2$In in a field of 4 T. The dotted lines indicate Korringa type behaviour.

tion to a magnetically ordered state, the γ parameter of CePd$_2$In well below T_N is about 140 mJ/mole K^2. This suggests that the electronic correlations in the itinerant charge-carrier system increase substantially with decreasing temperature and persist down to $T = 0$ K although magnetic order sets in at T_N in this temperature range. Thus we meet an obviously quite different situation than that we discussed above for U$_2$Zn$_{17}$.

More recent NQR and NMR experiments (Gavilano et al., 1995b; Vonlanthen et al., 1996) confirm the antiferromagnetic order and suggest that the ordered moment is only of the order of 0.1 μ_B/Ce. Above T_N the NQR spin–lattice relaxation rate T_1^{-1} is extremely high and obviously due to strong magnetic fluctuations but is reduced by about 95% through the transition (see Fig. 11).

Compared to T_1^{-1} of LaPd$_2$In below 1 K, the value for the Ce compound is still enhanced by a factor of 10 and the Korringa-type temperature dependence suggests that this is due to the above mentioned electronic correlation effects. It is interesting to note that this enhancement can almost be neutralized by the application of an external magnetic field of the order of 4 T (see Fig. 11). It appears that a magnetic field of this magnitude quenches both the antiferromagnetic order and the interaction that leads to the suppression of the magnetic moments, implying

that these different interactions are indeed of about the same order of magnitude and rather weak. Therefore a clear separation of their individual influences is not possible, an obvious nightmare for any theoretical treatment of this situation.

6 Magnetism and superconductivity in heavy-electron materials

The large enhancement of the effective masses of quasiparticles in heavy-electron materials is intimately related with the presence of electronic states with f-symmetry. Depending on not well understood circumstances, electrons occupying these states can either contribute to the formation of magnetic moments or may be involved in the formation of Cooper pairs and hence superconductivity. It is therefore not surprising that magnetism and superconductivity of these materials are intimately related, at least phenomenologically.
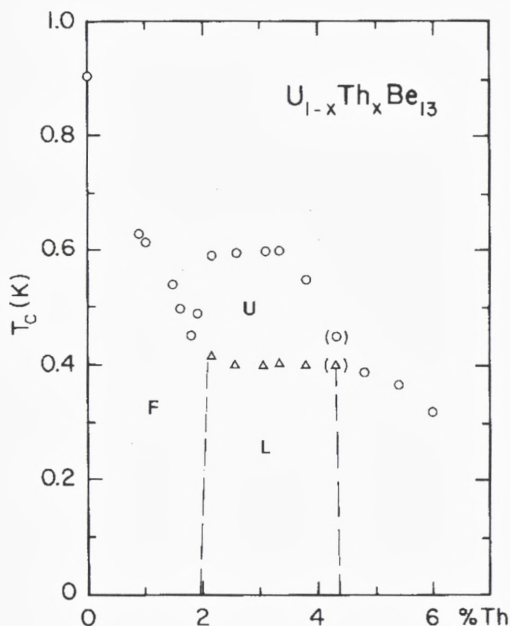
Figure 12. $[x, T]$ phase diagram for superconducting $U_{1-x}Th_xBe_{13}$.

Two examples, UPt_3 and URu_2Si_2, where magnetic order, although among tiny moments only, and superconductivity appear to coexist have been mentioned in Sect. 5. Coexistence of magnetic order and superconductivity has been claimed to occur also in $CeCu_2Si_2$ in a narrow range of chemical composition, but recent μSR experiments (Feyerherm et al., 1995) seem to indicate that the two ordering phenomena rather exclude each other, i.e., some sort of phase separation occurs. If we consider non-unitary states of superconductivity, in which time reversal symmetry is broken, as a manifestation of an exotic form of magnetism, we may mention that some experimental observations and their analysis indicate that such states are realized in superconducting $U_{1-x}Th_xB_{13}$ and, again, UPt_3 (Sauls, 1994). In Fig. 12, we show the $T_c(x)$ phase diagram of superconducting $U_{1-x}Th_xB_{13}$, mapped out by measurements of the specific heat (Ott et al., 1986). Various experiments indicate that the three identified phases F, U and L exhibit indeed different physical properties implying three distinct superconducting phases (Lambert et al., 1986; Heffner et al., 1990; Zieve et al., 1994).

Based on the assumption of unconventional superconductivity with an odd parity order parameter that allows for point nodes of the gap function, a Ginzburg-Landau type analysis reproduces the boundaries of this phase diagram quite well (Sigrist et al., 1989), and predicts a non-unitary superconducting state in the region of the L phase. Experimental support that such a state is indeed physically realized in phase L has been provided by μSR experiments (Heffner et al., 1990).

7 Summary

We have selected and presented a few cases that should demonstrate the outstanding magnetic properties of heavy-electron materials. Most of the features that are observed experimentally are not really well understood. The question concerning the stability of magnetic moments in these metallic substances is quite tricky and a comprehensive theoretical description of the features of these materials meets with considerable difficulties because the potential magnetic moments cannot be treated as single impurities since they reside, periodically arranged, on regular crystal lattice sites. In addition, the important interactions which determine the low-temperature behaviour of these substances are usually small and all of about the same order of magnitude. Therefore, common perturbation type approximations seem of little value from the outset.

Acknowledgements

References

Aeppli G, Bucher E, Broholm C, Kjems JK, Baumann J and Hufnagl J, 1988: Phys. Rev. Lett. **60**, 615

Anderson PW, 1961: Phys. Rev. **124**, 41

Andraka B and Stewart G, 1993: Phys. Rev. B **47**, 3208

Andraka B, Jee CS and Stewart GR, 1995: Phys. Rev. B **52**, 9462

Andres K, Graebner JE and Ott HR, 1975: Phys. Rev. Lett. **35**, 1979

Bardeen J, Cooper LN and Schrieffer JR, 1957: Phys. Rev. **108**, 1175

Barth S, Ott HR, Gygax FN, Schenck A, Rice TM and Fisk Z, 1986: Hyperfine Interactions **31**, 397

Barth S, Ott HR, Gygax FN, Hitti B, Lippelt E, Schenck A, Baines C, van den Brandt B, Konter T and Mango S, 1987: Phys. Rev. Lett. **59**, 2991

Barth S, Ott HR, Gygax FN, Hitti B, Lippelt E, Schenck A and Baines C, 1989: Phys. Rev. B **39**, 11695

Barzykin and Gor'kov LP, 1993: Phys. Rev. Lett. **70**, 2479

Bernal OO, MacLaughlin DE, Amato A, Feyerherm R, Gygax FN, Schenck A, Heffner RH, Le LP, Niewenhuys GJ, Andraka B, v. Löhneisen H, Stockert O and Ott HR, 1996: Phys. Rev. B (in print)

Bernasconi A, Mombelli M, Fisk Z and Ott HR, 1994: Z. Phys. B **94**, 423

Bianchi AD, Felder E, Schilling A, Chernikov MA, Hulliger F and Ott HR, 1995: Z. Phys. B **99**, 69

Blandin A and Friedel J, 1958: J. Phys. Radium **19**, 573

Broholm CJ, Kjems JK, Aeppli G, Fisk Z, Smith JL, Shapiro SM, Shirane G and Ott HR, 1987a: Phys. Rev. Lett. **58**, 917

Broholm CJ, Kjems JK, Buyers WJ, Palstra TTM, Menovsky AA and Mydosh JA, 1987b: Phys. Rev. Lett. **58**, 1467

Chernikov MA and Ott HR, 1995: (unpublished)

Coleman P and Gan J, 1991: Physica B **171**, 3

Coleman P, Miranda E and Tsvelik A, 1994: Physica B **199 & 200**, 197

Cooper BR, Sheng QG, Lim SP, Sanchez-Castro C, Kioussis N and Wills JM, 1992: J. Magn. Magn. Mater. **108**, 10

Cox DE, Shirane G, Shapiro SM, Aeppli G, Fisk Z, Smith JL, Kjems JK and Ott HR, 1986: Phys. Rev. B **33**, 3614

Cox DL, 1987: Phys. Rev. Lett. **59**, 1240

Degiorgi L, Ott HR, Dressel M, Grüner G and Fisk Z, 1994: Europhys. Lett. **26**, 221

Degiorgi L and Ott HR, 1996: J. Phys. Condens. Matter (in print)

Feyerherm R, Amato A, Geibel C, Gygax FN, Hellmann P, Heffner RH, MacLaughlin DE, Müller-Reisener R, Nieuwenhuys G, Schenck A and Steglich F, 1995: Physica B **206&207**, 596

Friedel J, 1956: Can. J. Phys. **34**, 1190

Gavilano JL, Hunziker J and Ott HR, 1995a: Phys. Rev. B **52**, R13106

Gavilano JL, Vonlanthen P, Ambrosini B, Hunziker J, Hulliger F and Ott HR, 1995b: Europhys. Lett. **32**, 361

Heffner RH, Cooke DW and MacLaughlin DE, 1987: *Theoretical and Experimental Aspects of Valence Fluctuations and Heavy Fermions*, eds. L.C. Gupta and S.K. Malik (Plenum, New York) p. 319

Heffner RH, Smith JL, Willis JO, Birrer P, Baines C, Gygax FN, Hitti B, Lippelt E, Ott HR, Schenck A, Knetsch EA, Mydosh JA and MacLaughlin DE, 1990: Phys. Rev. Lett. **65**, 2816

Jones BA, 1991: Physica B **171**, 53

Kasuya T, 1956: Progr. Theor. Phys. **16**,45

Keiter HFG, Lenders T and Schönenberg, 1995: J. Low Temp. Phys. **99**, 607

Kondo J, 1964: Progr. Theor. Phys. **32**, 37

Lambert SE, Dalichauch Y, Maple MB, Smith JL and Fisk Z, 1986: Phys. Rev. Lett. **57**, 1619

Landau LD, 1956: Zh. Eksp. Theor. Fiz. **30**, 1058 [Sov. Phys. JETP **3**, 920]

Lapertot G, Calemczuk R, Marcenat C, Henry JY, Boucherle JX, Flouquet J, Hammann J, Cibin R, Coss J, Jaccard D and Sierro J, 1993: Physica B **186-188**, 454

Lopez de la Torre MA, McEwen KA, Ellerby M, Haworth C and Springford M, 1995: J. Phys. Condens. Matter **7**, 9235

Ludwig AWW, 1994: Physica B **199 & 200**, 406

Maple MB, de Andrade MC, Herrmann J, Dalichaouch Y, Gajewski DA, Seaman CL, Chan R, Movshovich R, Aronson MC and Osborn R, 1995: J. Low Temp. Phys. **99**, 223

Miranda E, 1996: *Physical Phenomena at High Magnetic Fields II*, eds. Z. Fisk, D. Meltzer , L.P. Gor'kov and J.R. Schrieffer (World Scientific, Singapore) p. 227

Murasik A, Ligenza S and Zygmunt A, 1974: Phys. Stat. Sol. **a23**, K163

Nakamura H, Kitaoka Y, Asayama K and Onuki Y, 1991: Physica B **171**, 329

Nakamura H, Kitaoka Y, Asayama K, Onuki Y and Shiga M, 1994: J. Phys.: Condens. Matter **6**, 10567

Norman MR, Min BI, Oguchi T and Freeman AJ, 1988: Phys. Rev. B **38**, 6818

Ott HR, Marti O and Hulliger F, 1984a: Solid State Commun. **49**, 1129

Ott HR, Rudigier H, Delsing P and Fisk Z, 1984b: Phys. Rev. Lett. **52**, 1551

Ott HR, Rudigier H, Felder E, Fisk Z and Batlogg B, 1985: Phys. Rev. Lett. **55**, 1595

Ott HR, Rudigier H, Felder E, Fisk Z and Smith JL, 1986: Phys. Rev. B **33**, 126

Ott HR, Rudigier H, Felder E, Fisk Z and Thompson JD, 1987: Phys. Rev. B **35**, 1452

Ott HR and Fisk Z, 1989: *The Challenge of d- and f-Electrons*, ACS Symposium Series **394**, eds. P.R. Salahub and M.C. Zerner (Am. Chem. Soc., Washington) p. 260

Palstra TTM, 1986: Thesis (Leiden)

Palstra TTM, Menovsky AA, van den Berg J, Dirkmaat AJ, Kes PH, Nieuwenhuys and Mydosh JA, 1985: Phys. Rev. Lett. **55**, 2727

Ruderman MA and Kittel C, 1954: Phys. Rev. **96**, 99

Santini P and Amoretti G, 1994: Phys. Rev. Lett. **73**, 1027

Sauls J, 1994: J. Low Temp. Phys. **95**, 153

Schenck A, Birrer P, Gygax FN, Hitti B, Lippelt E, Weber M, Böni P, Fischer P, Ott HR and Fisk Z, 1990: Phys. Rev. Lett. **65**, 2454

Schenck A, Amato A, Birrer P, Gygax FN, Hitti B, Lippelt E, Barth S, Ott HR and Fisk Z, 1992: J. Magn. Magn. Mater. **108**, 97

Schenck A, 1993: *Frontiers in Solid State Sciences*, eds. L.C. Gupta and M.S. Multani (World Scientific, Singapore) Vol. II, p. 269

Schlabitz W, Baumann J, Politt B, Rauchschwalbe U, Mayer HM, Ahlheim U and Bredl CD, 1986: Z. Phys. B **62**, 171

Sheng QG and Cooper BR, 1994: Phys. Rev. B **50**, 9216

Sigrist M and Rice TM, 1989: Phys. Rev. B **39**, 2200

van Daal HJ, Buschow KHJ, van Aken PB and van Maaren MH, 1975: Phys. Rev. Lett. **34**, 1457

Vonlanthen P, Gavilano JL, Ambrosini B, Heisenberg D, Hulliger F and Ott HR, 1996: (unpublished)

Willis JO, Fisk Z, Stewart GR and Ott HR, 1986: J. Magn. Magn. Mater. **54-57**, 395

Wölfle P, 1995: J. Low Temp. Phys. **99**, 625

Xue B, Hulliger F, Baerlocher C and Estermann M, 1993: J. Alloys Compounds **191**, L9

Yosida K, 1957: Phys. Rev. **106**, 893

Zieve RJ, Jin DS, Rosenbaum TF, Kim JS and Stewart GR, 1994: Phys. Rev. Lett. **72**, 756

Magnetism of Cuprate Oxides

G. Shirane

Brookhaven National Laboratory, Upton, NY 11973, USA

Abstract

A review is given of the current neutron scattering experiments on cuprate oxides. We first discuss the extensive neutron measurements on high T_c oxides; $La_{2-x}Sr_xCuO_4$ and related $La_{1.6-x}Nd_{0.4}Sr_xCuO_4$. The second topic is the spin-Peierls system $Cu_{1-x}Zn_xGeO_3$, where a new type of antiferromagnetic phase has been discovered.

1   Introduction

It has been ten years since the discovery of high T_c superconductors by Bednorz and Müller (1986). Very extensive neutron scattering studies have been carried out both on $La_{2-x}Sr_xCuO_4$ (214-type) and $YBa_2Cu_3O_{6+d}$ (123-type). In this review, we limit our discussions only to the 214 type oxides and report some of the recent advances by the neutron scattering techniques.

The high T_c discovery prompted an extensive search for other copper oxides for new compounds of superconductivity. This resulted in opening a new field of magnetism not directly related to superconductivity. One of the most interesting copper oxides in this category is the spin-Peierls oxide $CuGeO_3$, discovered by Hase et al. (1993). This oxide goes into the singlet dimer state below $T_{sp} = 14$ K and is the first example of a simple oxide exhibiting a spin-Peierls transition. Again, the doping of Cu or Ge reveals very interesting phenomena, just like the doping of the high T_c oxides.

2   High T_c oxides: $La_{2-x}Sr_xCuO_4$ type

The antiferromagnetic spin fluctuations in these copper oxides have been studied extensively and a review was given by Shirane et al. (1994). The double peaks in q scan across the 2D ridge was first reported by Birgeneau et al. (1989) and the exact locations of satellite peaks were later mapped out by Cheong et al. (1991). Despite extensive neutron scattering studies of $La_{1.85}Sr_{0.15}CuO_4$, the existence of energy
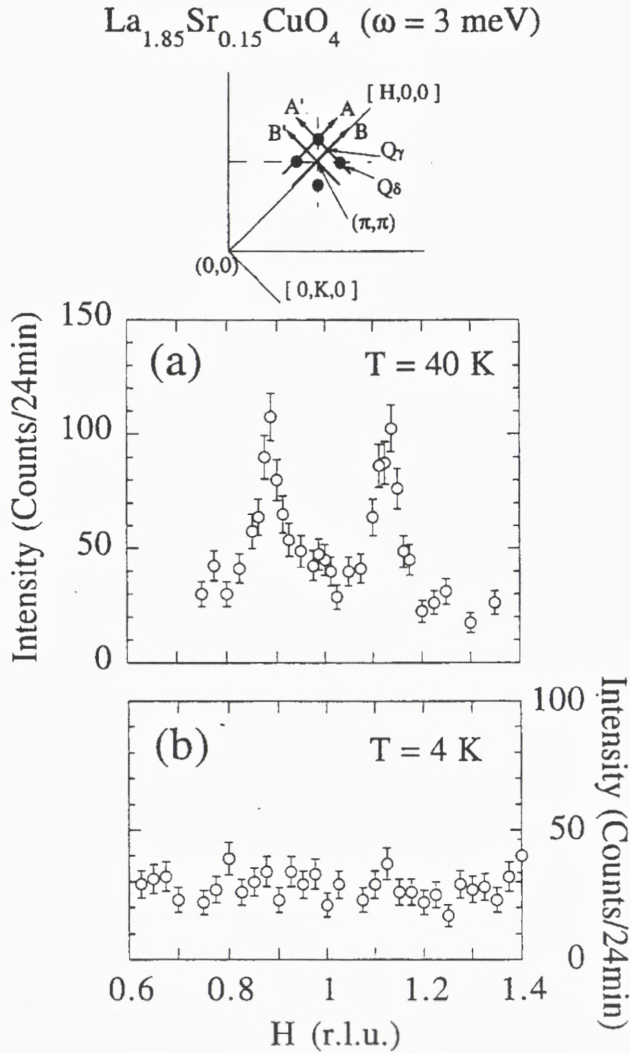
Figure 1. Neutron inelastic scattering spectra at 3 meV for Sendai crystal 1 at $T = 40$ K ($> T_c$) (a) and $T = 4$ K (b) taken by scan A. At the top is a schematic drawing of reciprocal space near the (π, π) position; typical scan directions are denoted by A, A', B, and B'. The closed circles denote the peak positions of the incommensurate magnetic fluctuations. In the $[HHL]$ zone, scans A and B can be performed with tilts of the crystal around the c^* axis equal to $6°$ and $10°$, respectively. After Yamada et al. (1995).
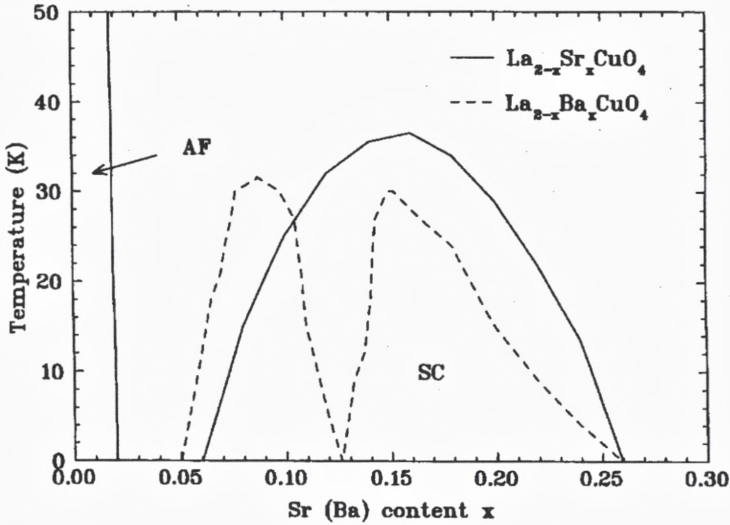
Figure 2. Phase diagram of $La_{2-x}Sr_xCuO_4$ (solid line). AF denotes antiferromagnetic order and SC indicates superconductivity. Dashed line indicates the superconducting regime in $La_{2-x}Ba_xCuO_4$.

gap in magnetic excitation spectrum has only been demonstrated very recently (Yamada et al., 1995).

The progress of the neutron scattering study of high T_c oxides has always been dictated by the successful crystal growth of better (and larger) crystals. The latest step along this line for $La_{1.85}Sr_{0.15}CuO_4$ was accomplished by Hosoya et al. (1994). These crystals are called Sendai, where they were grown, and they show the highest onset of T_c at 37.3 K. Improved quality of the crystals is also reflected in the sharp phase transition between orthorhombic and tetragonal phases. Very recently, Yamada et al. (1996) extended the study for a wide range of x in $La_{2-x}Sr_xCuO_4$. These very interesting experimental results are discussed extensively by Y. Endoh in this conference. Thus, we limit ourselves only to the special topics related to the incommensurate peaks around (π, π) position.

The neutron data shown in Fig. 1 were taken with a large (1.5 cm^3) and nearly perfect single crystal. In contrast to the results reported on lower T_c-crystals, the intensity below 3.5 meV dramatically decreases as the temperature decreases below T_c, and vanishes into the background below 15 K. The clear cut gap is observed only at the optimal doping $x = 0.15$ with $\delta = 0.12$. The important relation between $\delta(x)$ and T_c is discussed by Endoh.
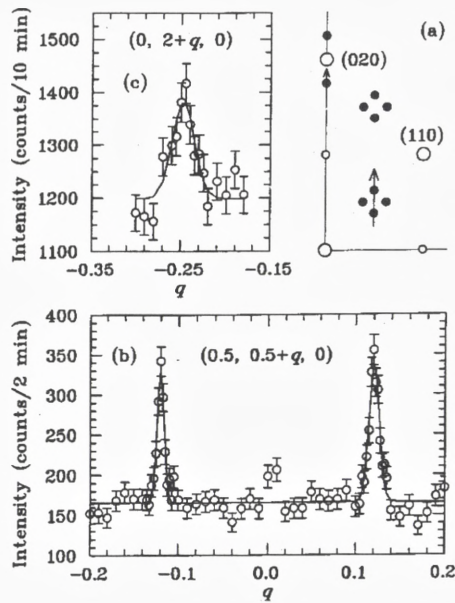
19*

Figure 3. Elastic scans with 2.4 Å neutrons of superlattice peaks consistent with the proposed spin and charge stripes, in $La_{1.48}Nd_{0.4}Sr_{0.12}CuO_4$ at 11 K. (a) Diagram of the $(h\,k\,0)$ zone of reciprocal space. Open circles indicate locations of Bragg peaks for the LTT structure; solid circles denote spin- and charge-ordering superlattice peaks. Arrows indicate the regions scanned. (b) Scan along, $(\frac{1}{2}, \frac{1}{2} + q, 0)$ through the $(\frac{1}{2}, \frac{1}{2} \pm \epsilon, 0)$ peaks. The small peak width indicates that the in-plane correlation length is greater than 150. (c) Scan along $(0, 2+q, 0)$ through the $(0, 2-2\epsilon, 0)$ peak. The lines in (b) and (c) are the result of least-squares fits to gaussian peak shapes plus a flat background. After Tranquada et al. (1995).

3   The 1/8 problem

One of the long-standing puzzles in high T_c research is depicted in Fig. 2. An amazing dip of T_c vs. composition in $La_{2-x}Ba_xCuO_4$ was discovered by Moodenbaugh et al. (1988). Axe et al. (1989) then demonstrated that this dip is related to the phase transition from the low temperature orthorhombic (LTO) to low temperature tetragonal (LTT) structure. It is not possible to grow large enough single crystals of $La_{2-x}Ba_xCuO_4$ to study this feature, but crystals are available for $La_{2-x-y}Nd_ySr_xO_4$, which exhibits a similar dip in T_c as a function of x. This is called the 1/8 problem because the dip in T_c (see Fig. 2) corresponds to the x value of 1/8.

Very recently Tranquada et al. (1995) have carried out an elegant and com-

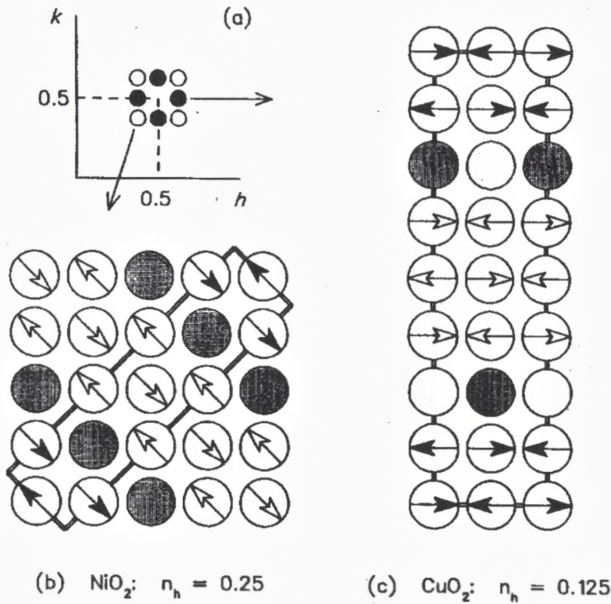(b) NiO$_2$: n$_h$ = 0.25   (c) CuO$_2$: n$_h$ = 0.125

Figure 4. (a) Sketch of the $(h\,k\,0)$ zone of the reciprocal lattice showing the positions of the magnetic scattering peaks observed for hole-doped La$_2$CuO$_4$ (filled circles) and La$_2$NiO$_4$ (open circles). (b) Idealized diagram of the spin and charge stripe pattern within an NiO$_2$ plane observed in hole-doped La$_2$CuO$_4$ with $n_h = 1/4$. (c) Proposed stripe pattern in a CuO$_2$ plane of hole-doped La$_2$CuO$_4$ with $n_h = 1/8$. In both (b) and (c), only the metal atoms are represented; the oxygen atoms, which surround the metal sites in a square planar array, have been left out. After Tranquada et al. (1995).

prehensive neutron scattering experiments on La$_{1.48}$Nd$_{0.4}$Sr$_{0.12}$CuO$_4$. Their key results are shown in Fig. 3, which also depicts the scattering geometry. Incommensurate dynamical spin correlations have been known in La$_{2-x}$Sr$_x$CuO$_4$ (see Fig. 1) for sometime. What is new in Fig. 3 is that these magnetic peaks at δ are elastic Bragg peaks. Moreover, the 2δ peak is observed around $(2\,0\,0)$ (tetragonal notation), and this represents the charge modulation. The LTT structure plays the key role for this special type of stripe phase (see Fig. 4).

This development of the charge density wave (CDW) is the cause of depression of T_c. The phase transition from LTO to LTT phase occurs at 70 K. The transition to the CDW phase takes place around 60 K, which is 10 K higher than the magnetic transition near 50 K. In this system, the phase transition is driven by charge and it is quite different from the case of Cr when the charge part is the secondary effect of the spin ordering. Further study of these fascinating phase transitions continues.
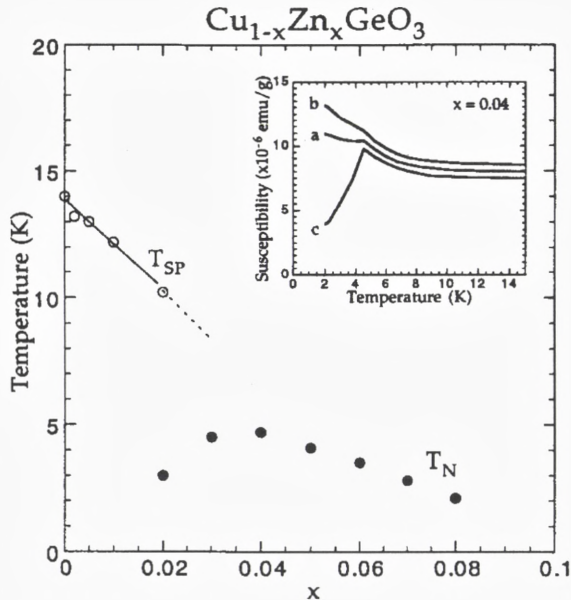
Figure 5. The previously reported phase diagram for $Cu_{1-x}Zn_xGeO_3$ as deduced from magnetic susceptibility measurements of powders. The inset shows the susceptibility measurement of an $x = 0.04$ single crystal in the a, b and c crystallographic directions as labeled. After Hase et al. (1993, 1995).

4   Doped spin-Peierls system Cu(Zn)GeO$_3$

The spin-Peierls (SP) transition in CuGeO$_3$ at $T_{sp} = 14$ K was discovered by Hase et al. (1993). Previous examples of spin-Peierls systems were all organic compounds and this simple inorganic oxide, gives us the first chance for full understanding of the detailed mechanism of the phase transition into a singlet state mainly because large single crystals can be produced. Comprehensive measurements have already been carried out on important physical properties of CuGeO$_3$; energy gap and magnetic excitations by Nishi et al. (1994) dimerized atomic configuration by Hirota et al. (1994). The structure below 14 K is the simple combined displacements of coppers and oxygen to form alternate dimers in the crystal.

Immediately after the discovery of CuGeO$_3$, the effect of substitution of Zn for Cu was reported by Hase et al. (1993). Then followed several papers on Cu(Zn) and Ge(Si) doping. I shall discuss in some detail our current neutron scattering studies at Brookhaven on Zn doped CuGeO$_3$. This topic may be somewhat out of place for a conference on Magnetism in "Metals", but the coexistence of antiferromagnetic
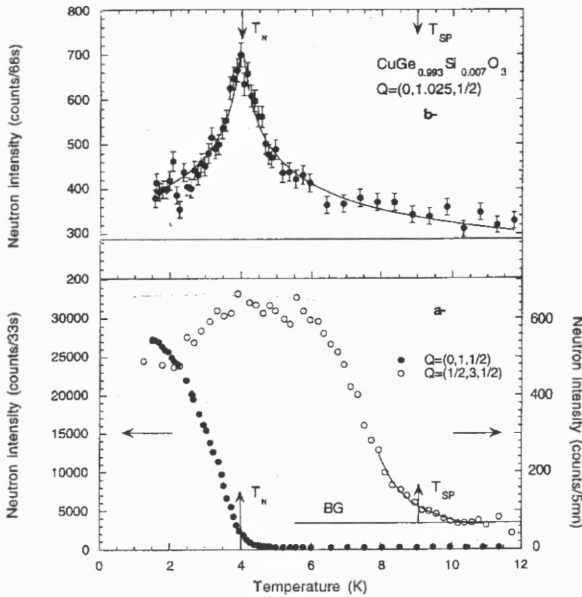
Figure 6. Temperature dependencies of elastic contributions at scattering vectors (a) $\mathbf{Q} = (\frac{1}{2}, 3, \frac{1}{2})$ and $\mathbf{Q} = (0, 1, \frac{1}{2})$ and (b) $\mathbf{Q} = (0, 1.025, \frac{1}{2})$, showing the occurrence of an antiferromagnetic phase transition at $T_N = 4$ K. After Regnault et al. (1995).

(AF) order with spin-Peierls dimerization is a new and exciting physics, which may have future implications on other branches of magnetism and phase transitions. From measurements on powder samples, it is now well established that a new AF ordered phase appears as shown in the phase diagram of Fig. 5. The SP transition is near 14.2 K for the undoped oxide, decreases in temperature with increased Zn concentration, and seemed to disappear around 2% Zn. At 4% Zn, the magnetic susceptibility no longer shows a SP transition, but only a Néel temperature $T_N \sim 4$ K.

A very surprising result was then reported by Regnault et al. (1995) in their neutron scattering study of 0.7% Si-doped CuGeO$_3$. As shown in Fig. 6 Regnault et al. demonstrated the successive SP (9 K) and AF (4 K) transitions with two separate branches of magnetic excitations below T_N. Note that the dimer peak $(\frac{1}{2} 3 \frac{1}{2})$ decreases below T_N but does not disappear. The co-existence of the SP and AF state was first demonstrated in this work. The coexistence of two order parameters, in this fashion, is extremely rare in structural and magnetic phase transitions.

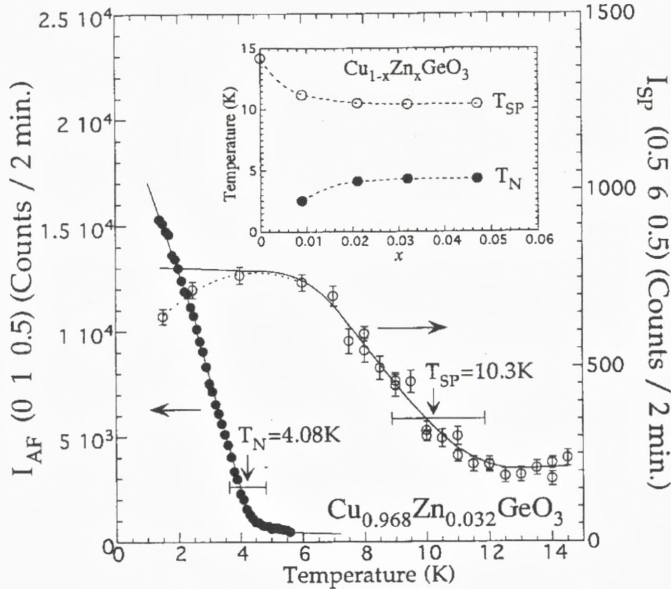The phase diagram of doped Cu(Zn)GeO$_3$, was re-examined by Sasago et al.

Figure 7. Intensities of the SP and AF superlattice peaks as functions of temperature for a 3.2% Zn-doped crystal. The intensity of the SP lattice dimerization peak is seen to decrease below T_N, however the states are clearly coexisting. The inset shows T_{sp} and T_N measured on samples of 0, 0.9, 2.1, 3.2, and 4.7% Zn-doped crystals. After Sasago et al. (1996).

(1996) and, as shown in Fig. 7, the co-existence of AF and SP phases is also demonstrated in this system. As shown in the inset of Fig. 5, the T_{sp} at 10 K in the 4% Zn sample does not reveal itself in the magnetic susceptibility measurement. However, this is clearly seen in neutron scattering by the appearance of the dimer line ($\frac{1}{2}$ 6 $\frac{1}{2}$) in Fig. 7.

The SP transition persists up to nearly 5% Zn concentration. Fukuyama et al. (1996) proposed a theoretical model for antiferromagnetic order in disordered spin-Peierls systems. They suggest that, surprisingly, long range lattice distortions will actually enhance the degree of the long range coherence of the antiferromagnetism. This model is quite different from the conventional "percolation" type idea in which islands of activated AF copper moments around Zn dopants eventually form "connected" AF order. Fukuyama et al. proposes explicit shape of both order parameters (Cu moment and dimer shift) as a function of dopant concentration. A particularly intriguing question is the lowest limit of concentration x for the appearance of the AF phase. This problem is now being pursued by Martin et al.
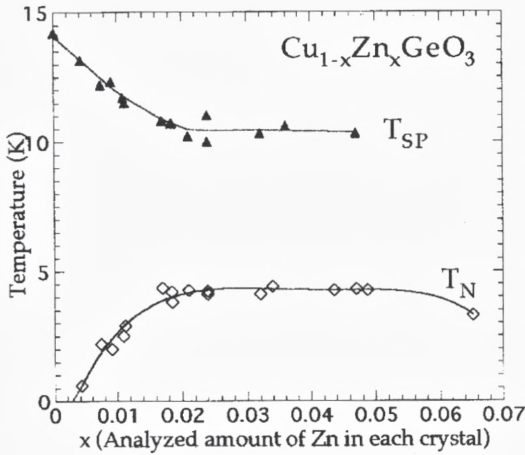
Figure 8. The current phase diagram of Cu(Zn)GeO$_3$ constructed by Martin et al. (1996) for neutron and susceptibility measurements.

(1996). They recently observed a long range AF peak below 0.6 K for Zn concentration of 0.4%. It is rather unbelievable that such a small concentration of Zn substitution does create true long range magnetic order. The phase diagram of the Cu$_{1-x}$Zn$_x$GeO$_3$ system is constructed by Martin et al. (1996) and shown in Fig. 8. The data combined both neutron and susceptibility measurements. How about the magnetic excitations? Regnault et al. (1995) reported the existence of separate low energy extensions in small q regions from AF peak $(0\,1\,\frac{1}{2})$. Extensive neutron scattering measurements are now being carried out by Martin et al. (1996) and they have extended AF mode measurements to much wider range in q space. Further neutron scattering studies are needed to complete the picture of this fascinating system.

Acknowledgements

References

Axe JD, Moudden AH, Holwein D, Cox DE, Mohanty KM, Moodenbaugh A, Yu Y, 1989: Phys. Rev. Lett. **62**, 2751

Bednorz JG, and Müller KA, 1986: Z. Phys. B **64**, 189

Birgeneau RJ, Endoh Y, Hidaka Y, Kakurai K, Kastner MA, Murakami T, Shirane G, Thurston TR and Yamada K, 1989: Phys. Rev. B **39**, 2868

Cheong S-W, Aeppli G, Mason TE, Mook HA, Hayden SM, Canfield PC, Fisk Z, Clausen KN and Kojima H, 1991 (unpublished)

Fukuyama H, Tanimoto T and Saito M, 1996: J. Phys. Soc. Jpn. **65**, 1182

Hase M, Terasaki I, Uchinokura K, 1993a: Phys. Rev. Lett. **70**, 3651

Hase M, Terasaki I, Sasago Y, Uchinokura K and Obara H, 1993b: Phys. Rev. Lett. **71**, 4059

Hase M, Uchinokura K, Birgeneau RJ, Hirota K and Shirane G, 1996: J. Phys. Soc. Jpn. **65**, 1392

Hirota K, Cox DE, Lorenzo JE, Shirane G, Tranquada JM, Hase M, Uchinokura K, Kojima H, Shibuya Y and Tanaka I, 1994: Phys. Rev. Lett. **73**, 736

Hosoya S, Lee CH, Wakimoto S, Yamada K and Endoh Y, 1994: Physica C **235**, 547

Martin M, Hase M, Hirota K, Shirane G, Sasago Y, Koide N and Uchinokura 1996: (unpublished)

Moodenbaugh AR, Xu Y, Suenaga M, Folkerts TJ and Shelton RN, 1988: Phys. Rev. B **38**, 4596

Nishi M, Fujita O and Akimitsu J, 1994: Phys. Rev. B **50**, 6508

Regnault LP, Renard JP, Dhalenne G and Revcolevschi A, 1995: Europhys. Lett. **32**, 579

Sasago Y, Koide N, Uchinokura K, Martin MC, Hase M, Hirota K and Shirane G, 1996: Phys. Rev. B (to be published)

Shirane G, Birgeneau RJ, Endoh Y, Kastner MA, 1994: Physica B **197**, 158

Tranquada JM, Sternlieb BJ, Axe JD, Nakamura Y and Uchida S, 1995: Nature **375**, 561

Yamada K, Wakimoto S, Shirane G, Lee CH, Kastner MA, Hosoya S, Greven J, Endoh Y and Birgeneau RJ, 1995: Phys. Rev. Lett. **75**, 1626

Yamada K, Wada J, Kurahashi K, Lee CH, Kimura Y, Wakimoto S, Endoh Y, Hosoya S, Shirane G, Birgeneau RJ and Kastner MA, 1996: (submitted)

Conduction Electrons in Magnetic Metals

M. S. S. Brooks

European Commission, Joint Research Centre, Institute for Transuranium Elements,

Postfach 2340, D-76125 Karlsruhe, Germany

Abstract

The conduction electrons in magnetic metals are sometimes themselves responsible for the magnetism, as in the $3d$ transition metals, and sometimes are magnetic intermediaries, as in the rare earths. In both cases the calculated magnitude of the exchange interactions is now in good agreement with experiment. The effect of magnetism upon the crystal structure of the $3d$ transition metals is reviewed. In the rare earths the manner in which the conduction electrons mediate the interactions between the $4f$ states is examined by using constrained calculations. The actinides present a more complex problem since there are large orbital contributions to the magnetic moments which are not, as in the rare earths, determined by Russel–Saunders coupling and the Wigner–Eckart theorem.

1 Introduction

Most atoms loose their magnetic moments in the metallic state; the exceptions are some transition metals, the rare earths, and the actinides. The $3d$, $4d$ and $5d$ transition metals, when not magnetically ordered, have relatively large paramagnetic susceptibilities. The magnetism is primarily due to the d-states close to the Fermi energy which are also involved in the determination of cohesion and structure (Friedel, 1969; Pettifor, 1970, 1972). Nearly all of the rare earths are magnetic, the magnetism arising from the orbitally degenerate localized open $4f$-shell (Duthie and Pettifor, 1977; Skriver, 1983a). The rare earth metals are early $5d$-transition metals since the $5d$ shell is less than half-filled and the $4f$ shell chemically inert the bonding and structure being due to the conduction electrons (Jensen and Mackintosh, 1991). The actinides are more complex. The light actinides are $5f$-transition metals while the heavy actinides have an essentially chemically inert $5f$-shell and are therefore early $6d$-transition metals (Skriver, 1985; Wills and Eriksson, 1992; Söderlind et al., 1995).

The $4f$ shell in metallic rare earths is similar to the $4f$ shell of the isolated atom, modified only weakly by interaction with the environment in the solid (Duthie and Pettifor, 1977; Skriver, 1983a). But the exchange interactions between the $4f$ and

conduction, principally $5d$, electrons are responsible for the induced conduction electron spin density through which the $4f$-shells interact. Free rare earth and $3d$ transition metal ions are normally described by Russell–Saunders coupling scheme in which Coulomb correlation is the largest part of the ionic valence electron Hamiltonian. Spin–orbit interaction is projected onto eigenstates characterized by total spin and total orbital angular momentum which it couples to give a total angular momentum of $\mathbf{J} = \mathbf{L} + \mathbf{S}$. The saturated ground state $4f$ moment, μ_s^{4f}, is then the product of J with the Landé factor, g_J and the orbital degeneracy of the ground state is partially or fully removed by the crystalline electric field in the solid. One of the most interesting characteristics of rare earths is the interaction between the induced itinerant electron magnetism of the conduction electrons and the localized and anisotropic $4f$ magnetism of the rare earth ions in the elemental metals. Similarly, in rare earth transition metal intermetallics, the nature of the interaction between the transition metal $3d$ magnetism and the localized $4f$ magnetism of the rare earth ions is of primary interest. This has naturally led to investigations of the site-resolved moments which have been studied in neutron diffraction experiments (Boucherle et al., 1982; Givord et al., 1980, 1985) and by theory (Yamada and Shimizu, 1986; Brooks et al., 1989, 1991b) and the coupling between the transition metal and rare earth magnetic moments (Brooks et al., 1991c; Liebs et al., 1993) which transfers magnetic anisotropy to the transition metal.

The magnetic moments of the $3d$ transition metals, in contrast, are due to splitting of the up and down spin states at the Fermi energy which must be calculated self-consistently since both magnetic and kinetic energies are involved (Christensen et al., 1988). In contrast to the rare earth magnetism the orbital magnetism in the $3d$ transition metals is very weak since itinerant states responsible for the magnetism are orbitally non-degenerate, almost totally quenching the orbital moments (Singh et al., 1976; Ebert et al., 1988; Eriksson et al., 1990b).

The light actinide metals are Pauli paramagnets (Skriver et al., 1978, 1980). The heavy actinides (Cm and beyond) are probably localized magnets, similar to the rare earth metals although sound experimental data is sparse. Many actinide compounds, however, order magnetically and there are critical An–An spacings in actinide compounds above which ground state ordered moments are stable (Hill, 1970). The systematic absence of magnetism in compounds with small An–An separation suggests that magnetic ordering is due to the competition between kinetic and magnetic energies and actinide transition metal intermetallics provide several examples of the magnetic transition as a function of either the actinide or the transition metal. But the magnetic actinide compounds have – in contrast to normal transition metals – very large orbital moments (Brooks and Kelly, 1983; Brooks, 1985; Eriksson et al., 1990a,c) since the $5f$ spin-orbit interaction in the actinides is far larger than that of the $3d$ spin–orbit interaction in the much lighter $3d$

transition metals. Figure 1 shows the relative size of the spin–orbit interaction and bandwidths for the transition metals, rare earths and actinides. The bandwidths of the actinides are less than those of the $3d$ transition metals, whereas the spin–orbit interaction is far larger and it mixes an orbital moment into the ground state. This involves mixing states from across the energy bands, and when the bandwidth is large the mixing is small and vice versa. The narrow $5f$ bands and the large spin–orbit interaction in actinides produces the ideal situation for itinerant electrons to support the strong orbital magnetism which is one of the remarkable features of actinide magnetism.
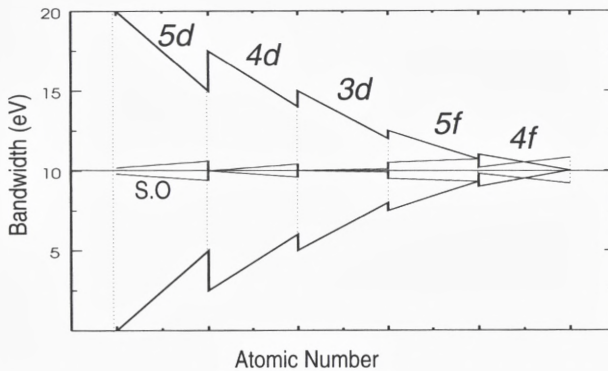

Figure 1. Widths of the d and f bands compared with spin-orbit splitting for the transition metals, rare earths and actinides.

2   Exchange interactions

Density functional theory (Hohenberg and Kohn, 1964; Kohn and Sham, 1965; von Barth and Hedin, 1972) transforms the many-electron problem into an effective one particle problem. Most electronic structure calculations for real materials use a very simple approximation to density functional theory, the local spin density approximation (LSDA), where the exchange and correlation energy is approximated by the sum of local contributions which are identical to those of a homogeneous electron gas at that local density. In LSDA the spin up and spin down states have different potentials which self-consistently arise from the different spin up and spin down densities if the system is magnetic, just as in unrestricted Hartree Fock theory. An approximation to the self-consistent theory is to restrict the spin up and down potentials to the same shape, from which Stoner theory follows with

the band splitting at the Fermi energy the product of the magnetic moment and an exchange integral. The exchange integral is simplest if just one angular momentum component contributes, which is a reasonable approximation for transition metals where d-states dominate (Gunnarsson, 1976, 1977). The calculated d–d exchange integrals for transition metals are shown in Fig. 2 (Christensen et al., 1988). The
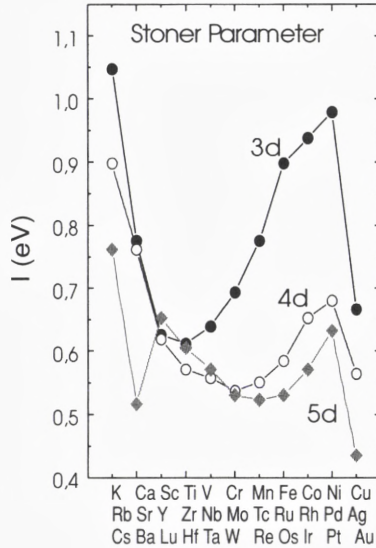

Figure 2. Exchange integrals for the transition metals.

exchange integrals have a minimum inside the series because they are proportional to the integral of the the two thirds power of the reciprocal of the density which leads to a decrease and to the fourth power of the d-wave function which increases due to wave function contraction across the series.

In the Hartree–Fock approximation that part of the exchange energy which depends upon the total spin may be approximated by (Severin et al., 1993)

$$E_{\rm SP}^{\rm HF} = -\frac{1}{4} \sum_{ll'} V_{ll'} \mu_l \mu_{l'} \tag{1}$$

in terms of the partial spin moments, μ_l. The exchange integrals $V_{ll'}$ are linear combinations of products of radial Slater exchange integrals and Clebsch–Gordan

coefficients. The isotropic exchange interactions $V_{ll'}$ therefore depend only upon the orbital quantum number of the shell and radial integrals. The calculated HF f–d and f–p exchange integrals of free rare earth and actinide atoms are shown in Fig. 3. In LSDA the spin polarization energy may also be expressed in terms of
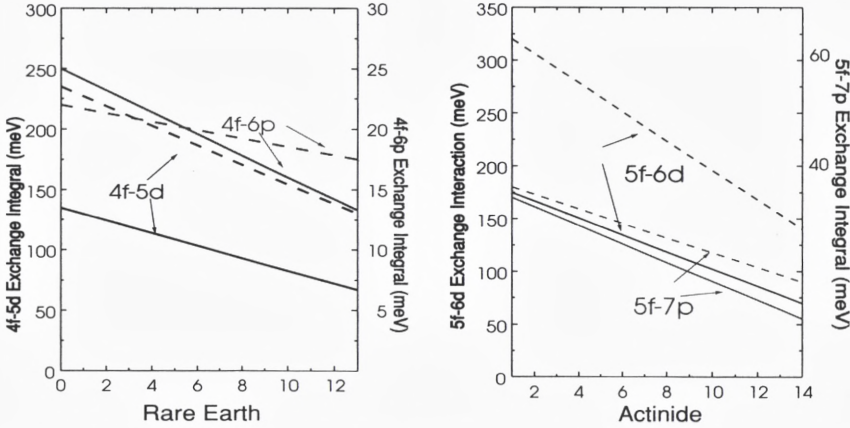

Figure 3. Exchange integrals for free rare earth and actinide atoms from HFA and LSDA.

radial exchange integrals (Severin et al., 1993)

$$E_{\mathrm{SP}}^{\mathrm{LSDA}} = -\frac{1}{4} \sum_{ll'} J_{ll'} \mu_l \mu_{l'} .$$ (2)

The f–p and f–d LSDA exchange integrals for the f states of rare earth and actinide atoms are also shown in Fig. 3. The reason that the f–d exchange integrals decrease across each series is the contraction (Lanthanide and Actinide) of the f-shell, which decreases the overlap with the d-states. The overlap between $4f$ and $5d$ densities occurs over a relatively small region of space corresponding to the outer part of $4f$ density and the inner part of the $5d$ density (Fig. 4). As the $4f$ shell contracts the region of overlap decreases. HFA and LSDA yield quite different magnitudes for the f–d exchange integrals which determine the induced conduction electron polarization. Experience has shown that the LSDA integrals lead to splittings of energy bands and calculated magnetic moments that are in better agreement with measurements than if the HF approximation is used.

In the standard model (Duthie and Pettifor, 1977; Skriver, 1983a) for rare earths
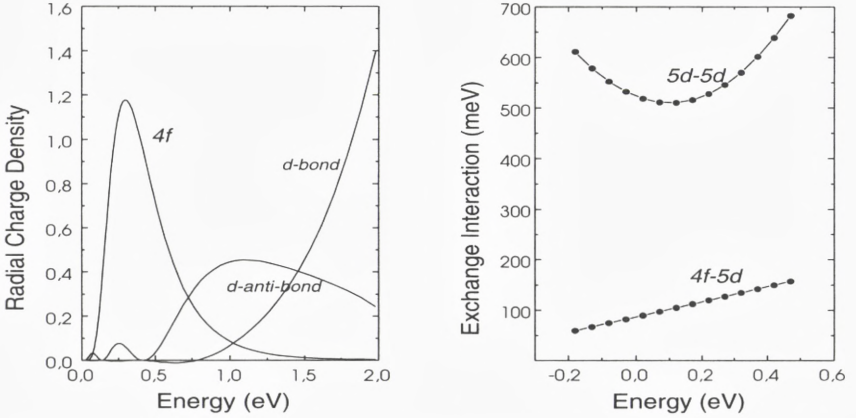
Figure 4. Overlap of the $4f$ and $5d$ charge densities in Gd metal for bonding and anti-bonding $5d$-states.

the exchange interaction Hamiltonian between conduction electrons and local $4f$ moments is

$$H_{s\text{-}f} = -2\tilde{J}_{4f\text{-}c}\mathbf{S}_{4f} \cdot \mathbf{s_c} = -\tilde{J}_{4f\text{-}c}(g_J - 1)\mathbf{J}_{4f} \cdot \boldsymbol{\mu}_c \tag{3}$$

where $\tilde{J}_{4f\text{-}c}$ is an average taken over the ground state J multiplet, $\mathbf{J}_{4f}$ is the total $4f$ angular momentum and $\mathbf{s}_c$ is the conduction electron spin and $\boldsymbol{\mu}_c$ its moment. In rare earth metals and compounds the $5d$ and $6p$ states make larger contributions to the exchange interactions than do the $6s$ states. The exchange integrals are always positive. The spin up and spin down conduction bands are split by the exchange interactions

$$\epsilon_{nk}^{\pm} = \epsilon_{nk} \mp \langle J_{4f}^z \rangle (g_J - 1)\tilde{J}_{4f\text{-}c}(n\mathbf{k}, n\mathbf{k}) \tag{4}$$

leading to an approximate conduction electron moment

$$\langle \mu_c^z \rangle = \mu_B N(\epsilon_F)(g_J - 1)\langle J_{4f}^z \rangle \tilde{J}_{4f\text{-}c} \tag{5}$$

where $N(\epsilon)$ is the state density per f.u. in the paramagnetic phase.

In density functional theory the exchange integrals between $4f$ states and conduction electrons of partial l character are

$$J_{4f\text{-}l}(n\mathbf{k}, n\mathbf{k}) = \frac{2}{3} \int r^2 \phi_{4f}^2(r)\phi_l^2(r, E_{nk}) A[n(r)]/n(r)dr \,, \tag{6}$$

where $A(r)$ is a well known (Hohenberg and Kohn, 1964; Kohn and Sham, 1965; von Barth and Hedin, 1972) function of the density. In the solid state where the conduction electron bands are continuous functions of energy and the exchange integrals are energy dependent. The magnitude of $J_{4f\text{-}5d}$ depends upon the small overlap region of the $4f$ and $5d$ densities (Fig. 4) which varies enormously as the bonding $5d$ density is moved outwards away from the $4f$ density.

The total energy of a system which is allowed to polarize may be separated into a part depending upon the electron density, $E[n]$, and a part depending upon both the density and spin density, $\Delta E[n, \mu]$. Changes in spin density induce changes in the total electron density and in the components of $E[n]$ such as the kinetic energy but $E[n]$ is at a variational minimum in the paramagnetic state therefore the individual components cancel to $o(\delta n^2)$ and make a negligible contribution to the magnetic energy. The remaining energy, $\Delta E[n, \mu]$, may be split into two contributions one of which is the exchange interaction energy and the other is the change in the kinetic energy arising from polarization of the conduction bands. The latter contribution is just $\mu_c^2/2\chi_0$ and is always positive. In transition metals the balance between these two contributions to the magnetic energy is responsible for the Stoner criterion. In the rare earths χ_0 is small and the conduction bands are polarized by the $4f$ states as they would not by themselves polarize. The conduction electron band splitting in the field of the $4f$ states is then given in LSDA by replacing $\tilde{J}_{4f\text{-}c}$ in the standard model by $J_{4f\text{-}c}$. The effective energy splitting at the Fermi energy is (Brooks and Johansson, 1993)

$$\Delta\epsilon(E_F) = \sum_l \left[\frac{N_l(E_F)}{N(E_F)} \sum_{l'} J_{ll'}(E_F)\mu_{l'} + J_{4f\text{-}l}(E_F)\mu_{4f}^s \right], \qquad (7)$$

where the sum over l, l' excludes $l = 3$ and q labels the atom. The integrals, $J_{ll'}(E_F)$, for the hcp Gd are calculated to be $J_{5d5d} = 39$ mRy, $J_{5d6p} = 40$ mRy and $J_{5d6s} = 42$ mRy and are more or less constant across the series. The integrals $J_{4f\text{-}d}(E_F)$ varies from 8.6 mRy for Pr to 6.5 mRy for Gd. Since rare earth contraction, which changes $4f$–$5d$ overlap, is fairly smooth the integrals may reasonably be interpolated by $J_{4f\text{-}5d} \approx 8.6 - 0.42(x - 2)$ mRy where x is the number of $4f$ electrons.

Self-consistent calculations for Gd using the linear muffin tin orbital (LMTO) method (Andersen, 1975; Skriver, 1983b) in which the $4f$ spin is varied between 0 and 7 confirm that the $5d$ moment is approximately a linear function of the $4f$ spin. The $5d$ conduction electron moments may be estimated from the corresponding exchange splitting of the $5d$ bands at the Fermi energy, at various levels of approximation. If it is assumed that the partial $5d$ state state density dominates the $5d$ moment at a site is given by

$$\mu_{5d} = J_{4f5d}\mu_{4f}^s \frac{N_{5d}(E_F)/2}{[1 - J_{5d5d}N_{5d}(E_F)/2]}, \tag{8}$$

where J_{5d5d} is calculated to be 531 meV for Gd and $\mu_{4f}^s = 7$ is the $4f$ spin. This approximation yields results to within a few percent of the actual $5d$ moments obtained in the self-consistent spin polarized LMTO calculations (Fig. 5). The partial
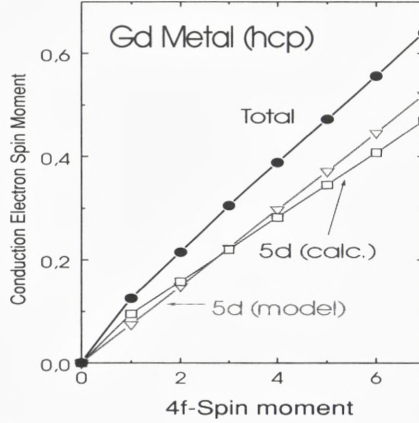

Figure 5. The calculated conduction electron moment in Gd metal as a function of $4f$ spin moment. Also shown are the $5d$ contribution and the $5d$ contribution calculated using the model with exchange interactions.

$5d$ state density at the Fermi energy is calculated to be about 16 states/Ry/atom in the paramagnetic state and is more or less constant across the heavy rare earth series. The $5d$ moment for Gd is calculated to be $\mu_{5d} = 0.53$ μ_B from Eq. (8) and to be $\mu_{5d} = 0.48$ μ_B self-consistently. Self-consistent spin polarized LMTO calculations yield a total conduction electron moment for Gd of 0.65 μ_B which compares well with the measured value of 0.63 μ_B (Roeland et al., 1975) and suggests that LSDA gives reasonable values for the conduction band

Wulff et al. (1988) deduced an effective exchange interaction of about 9 mRy from dHvA data for Pr. The calculated exchange interactions are $J_{4f\text{-}5d} = 8.6$ mRy and $J_{5d5d} = 38$ mRy. The partial $5d$ state density is 50 states/cell/Ry compared with a total of 66 states/cell/Ry. The effective $4f\text{-}5d$ interaction is

$$\bar{J}_{4f\text{-}5d}(E_F) = J_{4f\text{-}5d}(E_F)\frac{N_{5d}(E_F)}{N(E_F)} \tag{9}$$

which is only 6.6 mRy. This interaction is then enhanced by the effective $5d$–$5d$ interaction which, from Eq. (8), is 29 mRy. The enhanced $5d$–$5d$ exchange interaction then becomes 8 mRy, if the $6s$ and $6p$ contributions are neglected.

3   Transition metal magnetism and crystal structure

The crystal structures of the transition metals follow the same structural sequence hcp $\to$ bcc $\to$ hcp $\to$ fcc through the series as a function of atomic number. The origin of the crystal structure sequence is the influence of crystal structure upon the total energy. Although it is difficult to analyse the total energy the force theorem (Pettifor, 1976; Mackintosh and Andersen, 1979) enables total energy differences to be analysed in terms of single electron contributions to the total energy. In particular, structural energy differences are related directly to differences in band contributions to the total energy and therefore to the differences in state densities for the different structures (Pettifor, 1986). The partial d-state densities of the transition metals have a characteristic shape, which follows from canonical band theory and depends only upon structure, independent of series or atomic number (Andersen, 1975; Skriver, 1983b). The shape of a state density, or eigenspectrum, may be characterized – as for any distribution function – by its energy moments (Cyrot-Lackmann, 1967)

$$\mu_m = \mathrm{Tr}\, H^m = \sum_{l_1,l_2,\ldots l_n} H_{l_1 l_2} H_{l_2 l_3} \ldots H_{l_n l_1} \, . \tag{10}$$

The mth moment is therefore obtained from all paths of length m which begin and end at a particular atom. Moments up to the second influence the grosser cohesive properties such as cohesive energy and lattice constant. The second moment, for example, is directly related to the width of a rectangular (or constant) density of states which enters Friedel's model of metallic cohesion. The structure in the density of states which is characteristic of a particular lattice enters through the higher moments which differ significantly between bcc, fcc and hcp structures. If two state densities have identical moments up to the nth moment then the energy difference as a function of band filling must have $(n-1)$ nodes within the bands (Ducastelle and Cyrot-Lackmann, 1971). The bcc state density splits into distinct bonding and anti-bonding regions with a minimum for 6 states (Fig. 6). The fcc and hcp state densities have less pronounced bonding and anti-bonding regions and are broadly similar but differ in that the hcp state density has local minima for 4 and 8 states. The bimodal character of the bcc state density is due to its relatively small fourth moment and it implies that the band energy contribution of the bcc
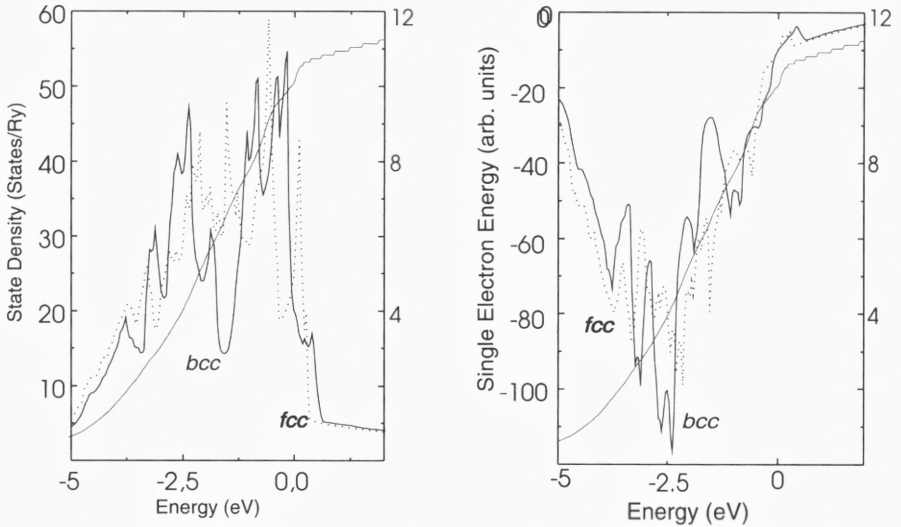
Figure 6. State densities for fcc and bcc transition metals, calculated from a self-consistent potential for Ni, and the difference in the sum energy eigenvalues as a function of band filling.

structure relative to that of the bcc and hcp structures is negative in the middle of the transition metal series (Pettifor, 1995). The much smaller energy difference between the fcc and hcp structures is due to the difference in their sixth moments. After the beginning of the series and for between 6 and 8 states the energy of the hcp structure lies lower whereas the energy of the fcc structure is lower than hcp (but higher than bcc) in the middle of the series and is again the lowest for between about 8 and 9 states and right at the beginning of the series (Pettifor, 1995).

The elements V, Nb, Ta, Cr, Mo and W ($n = 5$ - 6) therefore have the bcc structure. The elements Ti, Zr, Hf , Mn, Tc, Re, Fe, Ru ,Os ($n = 4$ and 8) should have the hcp structure and the bcc structure of Fe and the α-Mn structures are anomalous. The elements Co, Rh and Ir ($n = 9$) should have the fcc structure and the hcp structure of Co is also anomalous. The crystal structures of several magnetic transition metals are therefore anomalous compared with their isovalent counterparts. Fe, Co and Ni are magnetic because, with $3d$-bandwidths of about 5 eV and Stoner exchange integrals of about 1 eV they obey the Stoner criterion for ferromagnetism (albeit in the case of Fe this is due to an anomalously large peak at the Fermi energy for the bcc structure). The elements Cr and Mn obey the criterion for anti-ferromagnetism which is less stringent towards the centre of a series. Fe, Co and Ni are known from self-consistent calculations to have about 7.4,

8.4 and 9.4 3d-electrons, respectively. They are essentially saturated ferromagnets with moments of 2.2, 1.4 and 0.6, respectively, corresponding to a filled spin up band with the moments equal to the number of holes in the spin down band. The fact that the spin up band is filled removes its contribution to bonding and the bonding contribution to both the cohesive energy and crystal structure. The cohesive energies of these three metals are therefore anomalously small and the crystal structures are altered since the ratio of the number of spin down electrons to the total number of spin down states differs from the ratio of the total number of electrons to the total number of states. In Fe and Co the effective fractional d-band occupancy becomes 2.4/5 and 3.4/5 which puts them in the bcc and hcp regions, respectively. Under pressure Fe undergoes a transition to a non-magnetic hcp phase as the increasing bandwidth reduces the magnetic moment and with it the magnetic energy which stabilizes the bcc phase. Although more complicated, the α-Mn phase is also stabilized by magnetism (Pettifor, 1995). Accurate, self-consistent, calculations yield a paramagnetic fcc ground state with a lower energy than a bcc magnetic ground state for Fe although the energy difference is very small (Wang et al., 1985). Detailed studies of the elastic shear constant, which is related to the structural energy difference between bcc and fcc phases, for Fe have also shown that the absence of a spin up contribution is responsible for the anomalously low bulk modulus and shear elastic constant of Fe (Söderlind et al., 1994).

4   Conduction electrons in rare earth metals

Four approaches have been made to the calculation of conduction electron band structure in the rare earths. In the first, the 4f states have been treated as part of the band structure (Harmon, 1979; Norman and Koelling, 1993; Temmerman and Sterne, 1990). This treatment is most suitable for Gd where the seven filled spin-up 4f-states lie self-consistently below, and the empty spin down f-states above, the Fermi energy. The splitting between these two sets of 4f-states is easily estimated to be 7 times the 4f–4f exchange integral ($J_{4f4f} \approx 0.69$ eV) or 4.8 eV. The spin down 4f-bands are quite close to the Fermi level, raise the state density at the Fermi energy through hybridization with the 5d states, and they increase the calculated state density at the Fermi energy to 27 states/Ry compared with a value deduced from measurements (Wells et al., 1974) and assuming no enhancement, of 21.35 states/Ry. The 4f character at the Fermi energy in Gd is 5 states/Ry (Singh, 1991) which corresponds to the difference between theory and measurement. The situation is far worse for the other metals since the 4f-bands always cut the Fermi level.

The second approach has been to treat the $4f$ states as part of the core. Since the $4f$ shell is open the occupation number must be input to the calculations and the electronic structure is calculated self-consistently subject to this constraint. This approach has been used very successfully for the computation of cohesive properties (Skriver, 1985; Wills and Eriksson, 1992; Söderlind et al., 1995). The calculated partial $5d$ occupation numbers were found to increase across the series with increasing atomic number leading to the structural sequence hcp $\rightarrow$ dhcp $\rightarrow$ Sm-structure $\rightarrow$ fcc as is to be expected for a $5d$ transition metal series. The $4f$ spin occupation numbers are determined by applying the standard Russell–Saunders coupling scheme to the $4f$ shell and the magnetic moment is given by $\mu_{4f} = g_J J$. The ground state spin component of the total $4f$ moment, μ_{4f}^s, is obtained from the projection of the spin along the direction of total angular momentum

$$\mu_{4f}^s = 2(g_J - 1)J. \tag{11}$$

The $4f$ spin up and spin down occupation numbers are then determined by

$$n_{4f} = n_{4f}^+ + n_{4f}^-$$
$$\mu_{4f}^s = n_{4f}^+ - n_{4f}^- \tag{12}$$

where $n_{4f}^\pm$ are the up and down spin occupation numbers and n_f is the total number of $4f$ electrons. The occupation numbers n_{4f}^+, n_{4f}^- are part of the input to the calculations and are not determined ab initio as are the partial occupation numbers of the conduction electron states.

The third approach, which is more recent, is to incorporate the self-interaction correction (Heaton et al., 1983) (SIC) in the energy band calculations. The result is that localized states are localized further, and the energies of occupied and un-occupied states are split. Svane and Gunnarsson (1990) have applied SIC to the transition metal oxides, obtaining a drastic improvement in band gaps and calcu-lated moments compared with the results of LSDA. The most favourable aspect of SIC in its application to rare earths is the existence of separate occupied and unoccupied states. Szotek et al. (1993) have applied SIC to praseodymium metal where the occupied $4f$ states are pulled well below the conduction bands and the unoccupied $4f$ bands lie about 1 eV above the Fermi energy.

The fourth approach (Thalmeier and Falikov, 1979; Anisimov et al., 1993; Liechtenstein et al., 1994) has become known as 'LDA+U' since it is an attempt to add some aspects of the Hubbard model to self-consistent energy band calcula-tions. An additional interaction of the Hubbard form, which is dependent upon the occupation of the individual orbitals is added. The effect is to make the energies of the individual orbitals dependent upon their occupation, introducing an additional

symmetry breaking. This approximation can therefore lead to a large energy separation between occupied and unoccupied states. The electron–electron interaction parameter U which enters the theory may be estimated from constrained density functional calculations.

Most of the LSDA calculations have been for Gd metal. For calculations with the $4f$-states polarized in the bands (Harmon, 1979; Norman and Koelling, 1993; Temmerman and Sterne, 1990; Sticht and Kübler, 1985; Krutzen and Springelkamp, 1989; Richter and Eschrig, 1989) there is agreement that the state density at the Fermi energy is 25–37 states/Ry/atom/spin, to which there is a $4f$ contribution of about 5–6 states/Ry/atom/spin. From calculations with a paramagnetic ground state and the $4f$ states in the core (Harmon, 1979; Norman and Koelling, 1993; Temmerman and Sterne, 1990; Lindgård, 1976; Brooks et al., 1992) the state density at the Fermi energy per atom was found to be between 22 and 28 states/Ry/atom/spin. From calculations with the $4f$ states polarized in the core (Brooks et al., 1992) or an exchange splitting applied (Skriver and Mertig, 1990) the state density at the Fermi energy was calculated to be 12 states/Ry/atom/spin. The latter calculations yield results that are on the correct side of experiment. The calculated magnetic moments are in good agreement with measurements (Roeland et al., 1975) of 7.63 μ_B lying between 7.65 μ_B and 7.68 μ_B (Sticht and Kübler, 1985; Krutzen and Springelkamp, 1989; Temmerman and Sterne, 1990; Richter and Eschrig, 1989; Brooks et al., 1992).

Fermi surface calculations for Gd (Harmon, 1979; Norman and Koelling, 1993; Temmerman and Sterne, 1990; Singh, 1991; Ahuja et al., 1994) are in reasonable agreement with measurements (Young et al., 1973; Schirber et al., 1976; Young et al., 1976; Mattocks and Young, 1977; Sondhelm and Young, 1985) except that some measured smaller orbits provide some difficulty. Detailed dHvA experiments (Wulff et al., 1988) on dhcp praseodymium have led to calculations (Wulff et al., 1988; Auluck and Brooks, 1991) of its Fermi surface for which there is reasonable agreement with the frequencies of the measured orbits.

5 Rare earth transition metal intermetallics

5.1 The ReFe$_2$ series

Most studies have been for lutetium or yttrium compounds (Coehoorn, 1991; Cyrot and Lavagna, 1979; Yamada, 1988; Szpunar and Jr, 1990; Jaswal, 1990; Sellmyer et al., 1988) which simulate the conduction electron band structure of many rare earth compounds well. Fig. 7 shows the calculated total conduction electron spin moment through the RFe$_2$ series and its decomposition into $3d$ and $5d$ contributions (Brooks et al., 1991a). The individual $5d$ and $3d$ moments depend much more
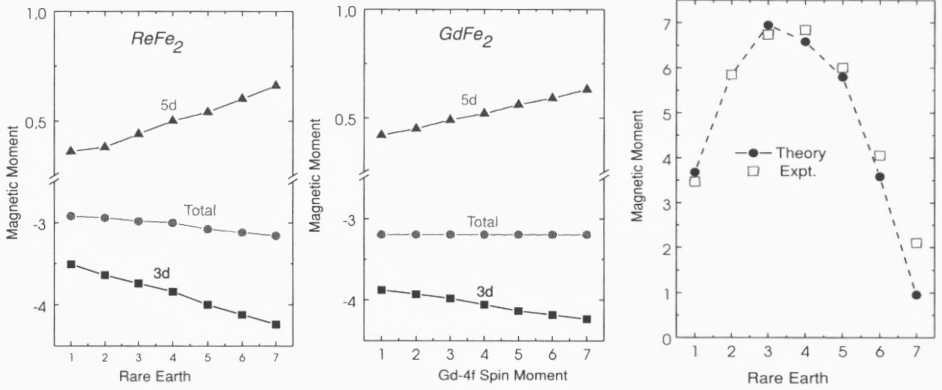
Figure 7. Calculated and measured moments of the ReFe$_2$ series plus the conduction electron contributions analysed into $3d$ and $5d$ contributions.

strongly upon atomic number than does the total moment. Also shown are the results of calculations for GdFe$_2$ when the magnitude of the $4f$ spin moment is constrained to vary from seven to zero. The calculated number of $5d$ electrons is found to be independent of the size of the $4f$ spin. Both the $5d$ and $3d$ moments increase when the $4f$ spin moment is increased but, as they are of opposite sign, the changes cancel and the total conduction electron moment remains constant, suggesting that the total conduction electron moment is saturated. The good agreement between the calculated total (including $4f$) moments and measurements is also shown in Fig. 7.

A simple model illustrates the origin of the ferrimagnetic interaction. In the free atom the energy of the $3d$ states lies far lower than that of the $5d$ states. When the solid is formed the $5d$ and $3d$ states hybridize, yielding the bonding-antibonding level scheme illustrated in Fig. 8. The bonding level is primarily of $3d$ character while the antibonding level has mainly $5d$ character. The degree of mixing between the $3d$ and $5d$ states depends on the overlap matrix element and on the energy separation between the $3d$ and $5d$ levels. When the $3d$ electrons polarize the energy difference between the bonding and antibonding sub-bands differs for the two spin directions, changing the $3d$–$5d$ hybridization for the majority and minority spins. The $5d$ content in the spin-up $3d$ bonding band decreases and that of spin-down $3d$ bonding band increases. Therefore the $3d$ and $5d$ spins must be in anti-parallel.

When there is a localized $4f$ spin it must be parallel to the $5d$ spin and $4f$–$5d$ exchange enhances the total $5d$ moment by moving the $5d$ spin up band further
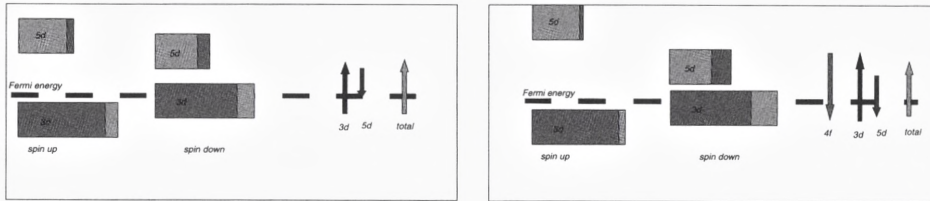
Figure 8. Model partial $3d$ and $5d$ state densities for RT_2 compounds showing the effect of the introduction of a $4f$ moment which polarizes the $5d$ states. The electron contributions analysed into $3d$ and $5d$ contributions.

away from the spin-up $3d$ bonding band, reducing $3d$–$5d$ spin-up hybridization. The opposite occurs for the spin-down bands the net result of which is that spin is transferred to the $3d$ sites and the $3d$ moment increases. However, if the total conduction electron moment is saturated, only its distribution between the R and Fe atoms changes. Therefore the presence of the $4f$ spin redistributes the conduction electron spin between the rare-earth and iron sites, while the total moment remains constant. This cancellation explains the successful interpretation of experimental magnetic moment data in terms of a constant conduction electron spin and an atomic $4f$ moment through a series of compounds.

5.2   Rare earth–transition metal exchange interactions

The $3d$–$5d$ hybridization not only produces significant $5d$ density at the R-sites but is also responsible for the crucial coupling between the R and M moments. The essential point to realize is that the R–$4f$ and R–$5d$ spins are coupled by local exchange interactions (which are always ferromagnetic) and that the interaction between R–$4f$ and M–$3d$ spins is mediated entirely by the R–$5d$ M–$3d$ hybridization (Brooks et al., 1991c).

The energy of the conduction electrons is at a variational minimum for a self-consistent calculation in which the $4f$ moment is constrained. The total energy change due to changes in conduction electron moment is therefore $o(\delta\mu_c^2)$ since individual contributions from exchange, kinetic and potential energies must cancel to $o(\delta\mu_c)$. This cancellation due to the variational principle allows the molecular field from the transition metal at the rare earth site to be calculated particularly simply. A change of $4f$ spin induces changes in conduction electron moment as the conduction electrons move to shield the disturbance, but the resulting total energy change is dominated by the explicit change of $4f$–$5d$ spin polarization energy due to

the change of $4f$ spin which is the only contribution of $o(\delta\mu_c)$. The spin polarization energy between $4f$ and $5d$ states is

$$E_{4f5d} = -\frac{1}{2}J_{4f5d}\mu_{4f}^s\mu_{5d}.$$ (13)

Neutron scattering experiments on the RFe_2 series have resolved the low lying spin wave modes and the generic form of the spectra is shown in Fig. 9. The lowest
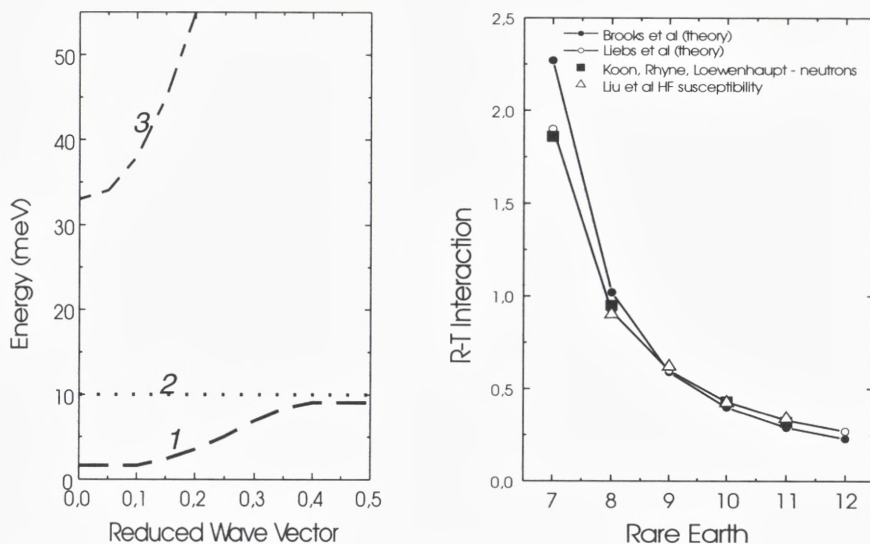

Figure 9. Schematic spin wave spectrum for a RFe_2 compound and the calculated and measured inter-atomic exchange interaction.

mode (labelled 1) at zero wave vector is the uniform mode and the highest (labelled 3) the exchange resonance mode of a ferrimagnet. The mode of interest here is the dispersionless mode (labelled 2) which corresponds to the precession of the R–$4f$ moments in the molecular field due to the M-moments. The molecular field is therefore about 10 meV. Contact between Eq. (13) and experiment is established through this spin wave gap. Equation (13) may be re-written in terms of the total $4f$ angular momentum via the Wigner–Eckart theorem

$$E_{4f5d} = -2(g_J - 1)J_{4f5d}\bar{J}_{4f}\bar{S}_{5d}$$ (14)

and, since the selection rule for spin waves is $\Delta J = \pm 1$, the change in total energy

is the gap. Due to the above mentioned cancellation theorem the change of total energy to $o(\delta m)$ is

$$\Delta = 2(g_J - 1)J_{4f5d}\bar{S}_{5d}. \tag{15}$$

The results are compared with experiment in Fig. 9. The experimental results were from neutron scattering (Koon and Rhyne, 1980; Nicklow et al., 1976), high field susceptibility (Liu et al., 1991) or Curie temperature (Belorizky et al., 1988) measurements. The values of the decrease in exchange interaction is due to both a decrease in the bare exchange integrals – caused by lanthanide contraction – and the decrease in $5d$ spin across the series, which itself is caused by the decrease in $4f$ moment. Although the parameters in Eq. (13) appear to be properties of the R atoms, in fact the R–$5d$ density arises from hybridization with the M–$3d$ states and this is the origin of the interatomic interactions.

5.3   Other rare earth compounds

Several electronic structure calculations for $Nd_2Fe_{14}B$ have been made (Coehoorn, 1991; Cyrot and Lavagna, 1979; Yamada, 1988; Szpunar and Jr, 1990; Jaswal, 1990; Sellmyer et al., 1988; Nordström et al., 1991; Hummler and Fähnle, 1992) and both the $4f$ states of Nd and the $3d$ states of Fe have been spin polarized. The total moment of the unperturbed $4f^3$ shell of Nd is 3.27 μ_B/atom. This consists of a projected orbital part of 5.72 μ_B/atom and a projected spin contribution of -2.45 μ_B/atom. The size of the conduction electron rare-earth moment increases by about 50 per cent due to the $4f$ spin moment.

The conduction bands in RCo_2 compounds (Coehoorn, 1991; Cyrot and Lavagna, 1979; Yamada, 1988; Szpunar and Jr, 1990; Jaswal, 1990; Sellmyer et al., 1988; Wohlfarth and Rhodes, 1962; Shimizu, 1964; Schwarz and Mohn, 1984) are metamagnetic. The state density of the RCo_2 compounds is almost identical to the state density of YCo_2. The Fermi energy lies in a dip in the state density with a large double peak just below and a somewhat broader peak above. The criterion for the local stability of a metamagnetic state is given in terms of the high field unenhanced susceptibility by

$$\frac{1}{2I}\left[\frac{1}{N^+(E_F)} + \frac{1}{N^-(E_F)}\right] \leq 1.$$

At a finite splitting of the energy bands both spin up and spin down state densities become large enough to satisfy this criterion. A similar situation occurs for $Y(Fe_{1-x}Co_x)_2$ alloys.

The exchange enhanced paramagnetism of the Co $3d$-bands in RCo_2 compounds was studied (Coehoorn, 1991; Cyrot and Lavagna, 1979; Yamada, 1988; Szpunar

and Jr, 1990; Jaswal, 1990; Sellmyer et al., 1988; Bloch et al., 1975) in an attempt to explain the trend in Curie temperatures across the heavy rare earth series, the first order magnetic transitions observed for $ErCo_2$, $HoCo_2$ and $DyCo_2$, and the second order magnetic transitions observed for $TbCo_2$ and $GdCo_2$, in terms of a molecular field theory in which the $3d$ band susceptibility is enhanced by the field from the localized $4f$-moment. The d-band susceptibility was calculated (Nordström et al., 1992a) to be about 10 States/Ry/atom in $GdFe_2$ and fairly constant across the series. The calculated Curie temperature of $GdCo_2$ is then 413 K compared with a measured value of 395 K.

5.4   Cerium compounds

Several cerium compounds have anomalously small lattice constants, Curie temperatures that are low in comparison with the other isostructural rare-earth compounds and magnetic moments that deviate from the values one would expect for normal trivalent ions at the cerium sites. Self-consistent LMTO calculations (Eriksson et al., 1988) for the CeM_2 (M = Fe, Co and Ni) cubic Laves phases with the $4f$ states treated as itinerant reproduce the trends in lattice constant. Only $CeFe_2$ is calculated to satisfy the Stoner criterion, in agreement with experiment, with a calculated total spin moment of 2.16 μ_B/f.u. which is about 1 μ_B less than the calculated total conduction electron moment for $GdFe_2$ of 3.15 μ_B/f.u. When the $4f$ electrons are itinerant a $4f$ electron is transferred from the core to the valence band states. If the conduction band moment is saturated the extra valence electron must enter the spin down states, reducing the total moment by 1 μ_B/f.u. The reduction of the moment is probably the reason for the anomalously low Curie temperatures of many of the cerium intermetallic ferromagnets. A similar moment reduction was found for (Nordström et al., 1990) $CeCo_5$. This reduction for $CeCo_5$ is caused by the hybridization between the Ce–$4f$ and the Co–$3d$ states which induces a $4f$ spin moment antiparallel to the cobalt moment and reduces the cobalt moment which is less than for $LaCo_5$, as is observed experimentally The Curie temperature for $CeCo_5$ is about 200 K less than would be expected from comparison with the other RCo_5 compounds.

6   Orbital magnetism of conduction electrons

The orbital contribution to the magnetic moment is 0.08 μ_B, 0.14 μ_B and 0.05 μ_B in Fe, Co and Ni, respectively (Stearns, 1986; Bonnenberg et al., 1986). The orbital moments are parallel to the spin contributions of 2.13 μ_B, 1.52 μ_B and 0.57 μ_B for Fe, Co and Ni, respectively (Fig. 10). The orbital moment belongs almost entirely to the $3d$ electrons. The spin contributions to the magnetic moments are
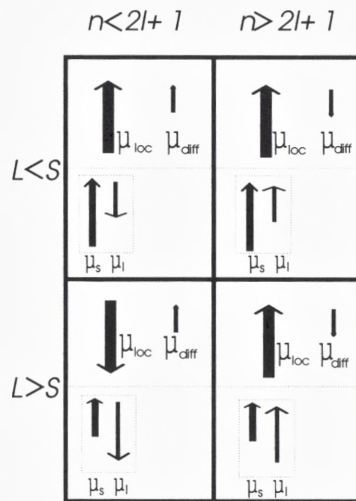
Figure 10. The relative signs of the local, spin and orbital, and diffuse moments of early and late transition metals.

resolved into local, or 3d, and diffuse, or sp, parts in Fig. 10. The *diffuse* part of the moment lies mainly in the interstitial region of the crystal and is not detected in neutron diffraction experiments. In Fe, Co and Ni the diffuse part of the moment is antiparallel to the local part. The origin of the relative signs of the diffuse and local moments is hybridization between the 3d and sp electrons. The Fe, Co and Ni 3d band is more than half-filled and the Fermi energy lies close to the bottom of the broad, free electron like, sp bands. The hybridization is therefore similar to that between early and a late transition metals and results in the relative sign of the local and diffuse moments being antiparallel (Terakura, 1977; Anderson, 1961; Heine and Samson, 1980).

Magnetism in actinide compounds is characterized by two unusual features. The first is the presence of correlations associated with very narrow bands and the second is the effect of relatively large spin–orbit interaction for the 5f electrons. In contrast to the theory for the transition metals, spin–orbit interaction plays a first-order role in the theory of magnetism and moment formation in the actinides. The actinides are early transition metals and the 4f moments are polarized parallel to the 5d moments which constitute nearly all of the diffuse moment. Exchange interactions between the local and diffuse moments are always positive and would always lead to parallel polarization in the absence of hybridization. In Fe, Co and Ni the spin moments are not large and the exchange interactions between local and diffuse moments small enough that hybridization dominates. In the actinides both

mechanisms lead to parallel polarization of the local and diffuse moments, Fig. 10.

In Fe, Co and Ni the orbital contributions to the moments are parallel to the spin contributions since the $3d$ bands are more than half filled, Fig. 10. Light actinides have a less than half-filled $5f$ band, therefore the induced orbital moment is antiparallel to the $5f$ spin moment, Fig. 10. Therefore there are two sign changes – for both diffuse and orbital moments – occurring between the right and left hand sides of Fig. 10.

Relativistic energy band calculations yield orbital contributions which are larger than the spin contributions to the moments in compounds containing actinides (Brooks and Kelly, 1983; Brooks, 1985; Eriksson et al., 1990a,c; Severin et al., 1991; Norman and Koelling, 1986; Norman et al., 1988). The induced orbital moment is sensitive to the ratio of bandwidth to spin–orbit interaction which is far smaller in the actinides than transition metals. The spin–orbit splitting of the $5f$ states in uranium is about 0.77 eV, which is comparable with the Stoner splitting. However, although the calculated orbital moments are very large in actinides, they are smaller than measured. This is also true in Fe, Co and Ni, although the larger discrepancies for the actinides are more obvious.

In the homogeneous electron gas for which the interactions in LSDA are derived, there is no spin–orbit interaction as there is no localized nuclear charge. The orbital exchange interactions, Coulomb in nature, which occur in atoms do not occur in the free electron gas. Orbital exchange interactions lead to interactions between the atomic orbital moments which are responsible for Hund's second rule. Hund's first rule, the exchange interaction between spins, is reproduced in LSDA where it leads to spin polarization. The interaction between the orbital moments is absent in LSDA. One way to approximate orbital interactions which has had some success has been suggested (Brooks, 1985; Eriksson et al., 1990a). A Hund's second rule energy which peaks for quarter filled shells and is zero for half-filled shells is added to the Hamiltonian. Its functional dependence upon occupation number may be approximated quite well, but not perfectly, by $-(1/2)E^3 L_z^2$ where E^3 is a Racah parameter (a linear combination of Slater Coulomb integrals). Although the orbital polarization energy in this approximation is not a functional of the density it is a function, through L^z – the total orbital angular momentum of the shell, of the orbital occupation numbers. The differential of the orbital polarization energy with respect to occupation number leads to different energies for the orbital levels $|m\rangle$ when there is an orbital moment. E^3, the Racah parameter, may be re-evaluated during the iterative cycles of a self-consistent calculation along with the orbital occupation numbers, so that no free parameters are introduced. Therefore orbital interactions arise by consideration of a series of Hund's rule ground states with single determinant wave functions. The orbital interactions are exchange interactions just as are the spin interactions and they arise from preferential filling

of orbitals. This approximation has been applied to a number of systems where it improves agreement between theory and experiment. Applications to non-actinides such as Fe, Co and Ni and some cobalt compounds have also improved agreement with experiment for the orbital moments.

The magnetic anisotropy energy is usually calculated by making two sets of calculations with the quantization axis along hard and easy axes and subtracting the total energies for the two directions. For Fe, Co and Ni the calculation of magnetic anisotropy has been only partially successful (Daalderop et al., 1990; Jansen, 1990). Part of the difficulty is because the magnetic anisotropy energy for these systems is of the order of μeV, which demands extremely accurate numerical treatment. The magnitude of the MAE is calculated to be too small and in Ni the sign is wrong. Inclusion of the orbital polarization correction term improves the results, except for Ni. For rare earth compounds (Daalderop et al., 1992; Nordström et al., 1992b) and, for actinide compounds (Brooks et al., 1986) the situation is better. For example, the anisotropy of US was about double that measured. The anisotropy energy of US is about two orders of magnitude greater than that of a rare earth metal.

Acknowledgements

References

Ahuja R, Auluck S, Johansson B and Brooks MSS, 1994: Phys. Rev. B **50**, 5147

Andersen OK, 1975: Phys. Rev. B **12**, 3060

Anderson PW, 1961: Phys. Rev. **124**, 41

Anisimov VI, Soloyev IV, Korotin MA, Czyzyk MT and Sawatzky GA, 1993: Phys. Rev. B **48**, 16929

Auluck S and Brooks MSS, 1991: (unpublished)

Belorizky E, Gavigan JP, Givord D and Li HS, 1988: Europhys. Lett. **5**, 349

Bloch D, Edwards DM, Shimizu M and Voiron J, 1975: J. Phys. F **5**, 1217

Bonnenberg D, Hempel KA and Wijn HPJ, 1986: in *3d, 4d and 5d Elements, Alloys and Compounds*, ed. H. Wijn (Springer Verlag, Berlin) Landolt–Börnstein, New Series, group 3, Vol. 19a

Boucherle JX, Givord D and Schweizer J, 1982: J. Phys. (Paris) C **7**, 199

Brooks MSS, 1985: Physica B **130**, 6

Brooks MSS and Johansson B, 1993: in *Handbook of Magnetic Materials*, ed. K. Buschow (Elsevier Science Publishers) Vol. 7, p. 139

Brooks MSS and Kelly PJ, 1983: Phys. Rev. Lett. **51**, 1708

Brooks MSS, Johansson B, Eriksson O and Skriver HL, 1986: Physica B **144**, 1

Brooks MSS, Eriksson O and Johansson B, 1989: J. Phys. Condens. Matter **1**, 5861

Brooks MSS, Gasche T, Auluck S, Nordström L, Severing L, Trygg L and Johansson B, 1991a: J. Appl. Phys. **79**, 5972

Brooks MSS, Nordström L and Johansson B, 1991b: J. Phys. Condens. Matter **3**, 2357

Brooks MSS, Nordström L and Johansson B, 1991c: J. Phys. Condens. Matter **3**, 3393

Brooks MSS, Auluck S, Gasche T, Trygg L, Nordström L, Severing L and Johansson B, 1992: J. Magn. Magn. Mater. **104-107**, 1496

Christensen NE, Gunnarsson O, Jepsen O and Andersen OK, 1988: J. Phys. (Paris) C **8**, 17

Coehoorn R 1991: in *Supermagnets, Hard Magnetic Materials*, eds. G. Long and F. Grandjean, (Kluwer Academic, Dordrecht)

Cyrot M and Lavagna M, 1979: J. Phys. (Paris) **40**, 763

Cyrot-Lackmann F, 1967: Adv. Phys. **16**, 393

Daalderop GHO, Kelly PJ and Schuurmans MFH, 1990: Phys. Rev. B **42**, 11919

Daalderop GHO, Kelly PJ and Schuurmans MFH, 1992: J. Magn. Magn. Mater. **104-107**, 737

Ducastelle F and Cyrot-Lackmann F, 1971: J. Phys. Chem. Solids **32**, 285

Duthie JC and Pettifor DG, 1977: Phys. Rev. Lett. **38**, 564

Ebert H, Strange P and Gyoffry BL, 1988: J. Phys. F **18**, L135

Eriksson O, Nordström L, Brooks MSS and Johanson B, 1988: Phys. Rev. Lett. **60**, 2523

Eriksson O, Brooks MSS and Johansson B, 1990a: Phys. Rev. B **41**, 9087

Eriksson O, Johansson B, Albers RC, Boring AM and Brooks MSS, 1990b: Phys. Rev. B **42**, 2707

Eriksson O, Johansson B and Brooks MSS, 1990c: Phys. Rev. B **41**, 9095

Friedel J, 1969: in *The Physics of Metals*, ed. J. Ziman, (Cambridge Univ. Press) p. 341

Givord D, Gregory AR and Schweizer J, 1980: J. Magn. Magn. Mater. **15-18**, 293

Givord D, Li HS and Tasset F, 1985: J. Appl. Phys. **57**, 4100

Gunnarsson O, 1976: J. Phys. F **6**, 587

Gunnarsson O, 1977: Physica B **91**, 329

Harmon BN, 1979: J. Phys. (Paris) C **5**, 65

Heaton RA, Harrison JG and Lin CC, 1983: Phys. Rev. B **28**, 5992

Heine V and Samson JH, 1980: J. Phys. F **10**, 2609

Hill HH, 1970: in *Plutonium 1970*, ed. W. Miner (Met. Soc. AIME, New York) p. 2

Hohenberg P and Kohn W, 1964: Phys. Rev. **136**, 864

Hummler K and Fähnle M, 1992: Phys. Rev. B **45**, 3161

Jansen HJF, 1990: J. Appl. Phys. **67**, 4555

Jaswal SS, 1990: Phys. Rev. B **41**, 9697

Jensen J and Mackintosh AR, 1991: *Rare Earth Magnetism: Structures and Excitations* (Clarendon Press, Oxford)

Kohn W and Sham LJ, 1965: Phys. Rev. A **140**, 1133

Koon NC and Rhyne JJ, 1980: in *Crystalline Electric Field and Structural Effects*, eds. J. Crow, P. Guertin and T. Mihalisin, (Plenum, New York) p. 125

Krutzen BCH and Springelkamp F, 1989: J. Phys. Chem. **1**, 8369

Liebs M, Hummler K and Fähnle M, 1993: J. Magn. Magn. Mater. **124**, 239

Liechtenstein AI, Antropov VP and Harmon BN, 1994: Phys. RevB **49**, 10770

Lindgård PA, 1976: in *Metals and Metallic Compounds*, eds. J. Lopuzanski, A. Pekalsky and J. Przystawa (Plenum, New York) p. 203

Liu JP, de Boer FR and Buschow KHJ, 1991: J. Magn. Magn. Mater. **98**, 291

Mackintosh AR and Andersen OK, 1979: (Cambridge Univ. Press) p. 149

Mattocks PG and Young RC, 1977: J. Phys. F **7**, 1219

Nicklow RM, Koon NC, Williams CM and Milstein JB, 1976: Phys. Rev. Lett. **36**, 532

Nordström L, Eriksson O, Brooks MSS and Johansson B, 1990: Phys. Rev. B **41**, 911

Nordström L, Johansson B and Brooks MSS, 1991: J. Appl. Phys. **69**, 5708

Nordström L, Brooks MSS and Johansson B, 1992a: J. Magn. Magn. Mater. **104-107**, 1378

Nordström L, Brooks MSS and Johansson B, 1992b: J. Magn. Magn. Mater. **104-107**, 1942

Norman MR and Koelling DD, 1986: Phys. Rev. B **33**, 3803

Norman MR and Koelling DD, 1993: in *Handbook of Physics and Chemestry of Rare Earths*, eds. K.A. Gsneidner, L. Eyring, G. Lander and G. Choppin (North Holland, Amsterdam) Vol. 17, p. 1

Norman MR, Min BI, Oguchi T and Freeman AJ, 1988: Phys. Rev. B **38**, 6818

Pettifor DG, 1970: J. Phys. C **C3**, 367

Pettifor DG, 1972: in *Metallurgical Chemestry*, ed. O Kubashewsky, (H.M. Stationary Office, London)

Pettifor DG, 1976: Commun. Phys. **1**, 141

Pettifor DG, 1986: J. Phys. Chem. **19**, 285

Pettifor DG, 1995: *Bonding and Structure of Molecules and Solids* (Clarendon Press, Oxford) p. 223

Richter M and Eschrig H, 1989: Solid State Commun. **72**, 263

Roeland LW, Cock GJ, Muller FA, Moleman CA, McEwen KA, Jordan RC and Jones DW, 1975: J. Phys. F **5**, L233

Schirber JE, Schmidt FA, Harmon BN and Koelling DD, 1976: Phys. Rev. Lett. **36**, 448

Schwarz K and Mohn P, 1984: J. Phys. F **14**, L129

Sellmyer DJ, Engelhardt MA, Jaswal SS and Arko AJ, 1988: Phys. Rev. Lett. **60**, 2077

Severin L, Nordström L, Brooks MSS and Johansson B, 1991: Phys. Rev. B **44**, 9392

Severin L, Brooks MSS and Johansson B, 1993: Phys. Rev. Lett. **71**, 3214

Shimizu M, 1964: Proc. Phys. Soc. **86**, 147

Singh DJ, 1991: Phys. Rev. B **44**, 7451

Singh M, Callaway J and Wang CS, 1976: Phys. Rev. B **14**, 1214

Skriver HL, 1983a: in *Systematics and Properties of the Lanthanides*, ed. S. Sinha (Reidel, Dordrecht) p. 213

Skriver HL, 1983b: *Muffin Tin Orbitals and Electronic Structure* (Springer Verlag, Heidelberg)

Skriver HL, 1985: Phys. Rev. B **31**, 1909

Skriver HL and Mertig I, 1990: Phys. Rev. B **41**, 6553

Skriver HL, Andersen OK and Johansson B, 1978: Phys. Rev. Lett. **41**, 42

Skriver HL, Andersen OK and Johansson B, 1980: Phys. Rev. Lett. **44**, 1230

Söderlind P, Ahuja R, Eriksson O, Willis JM and Johansson B, 1994: Phys. Rev. B **50**, 5918

Söderlind P, Wills JM, Johansson B and Eriksson O, 1995: Nature **374**, 524

Sondhelm SA and Young RC, 1985: J. Phys. F **15**, L261

Stearns MB, 1986: in *3d, 4d and 5d Elements, Alloys and Compounds*, ed. H. Wijn (Springer Verlag, Berlin) Landolt–Börnstein, New Series, group 3, Vol. 19a

Sticht J and Kübler J, 1985: Solid State Commun. **53**, 529

Svane A and Gunnarsson O, 1990: Phys. Rev. Lett. **65**, 1148

Szotek Z, Temmerman WM and Winter H, 1993: Phys. Rev. B **47**, 1124

Szpunar B and Jr VHS, 1990: J. Solid State Chem. **88**, 217

Temmerman WM and Sterne PA, 1990: J. Phys. Chem. **2**, 5529

Terakura K, 1977: J. Phys. F **7**, 1773

Thalmeier P and Falikov LM, 1979: Phys. Rev. B **20**, 4637

von Barth U and Hedin L, 1972: J. Phys. Chem. **5**, 1629

Wang CS, Klein B and Krakauer H, 1985: Phys. Rev. Lett. **54**, 1852

Wells P, Lanchester PC, Jones WD and Jordan RG, 1974: J. Phys. F **4**, 1729

Wills J and Eriksson OK, 1992: Phys. Rev. B **45**, 13879
Wohlfarth P and Rhodes P, 1962: Phil. Mag. **7**, 1817
Wulff M, Lonzarich GG, Fort D and Skriver HL, 1988: Europhys. Lett. **7**, 629
Yamada H, 1988: Physica B **149**, 390
Yamada H and Shimizu M, 1986: J. Phys. F **16**, 1039
Young RC, Jordan RG and Jones DW, 1973: Phys. Rev. Lett. **31**, 1473
Young RC, Jordan RG and Jones DW, 1976: J. Phys. F **6**, L37

Dilute Magnetic Alloys

B. R. Coles

Physics Department, Imperial College, London, SW7 2BZ, UK.

Abstract

A survey is given of the major strands in the development of the study of the magnetic behaviour and related properties in dilute alloys of elements capable of possessing magnetic moments in appropriate hosts. While the main emphasis is on the growth of the experimental information and the theoretical concepts needed for adequate explanations, indications will be given of significant recent developments. Specific topics include the Kondo effect, superconductivity in dilute alloys, spin glasses and the onset of long-range magnetic order.

1   Introduction

This is a topic (one with which I was first concerned 44 years ago) that has had an impact in a number of areas of metal physics and one to which Allan Mackintosh and his coworkers made significant contributions. It has been argued that theoretical work in this area provided important insights for more general areas of metallic magnetism, and a review of the topic (Morandi et al., 1981) has even used its history as a model system for the examination of aspects of the sociology of science.

The present paper will trace the main lines of development in this field and indicate some recent developments where new concepts have emerged or old ones revived.

2   The early roots

I have in other places (Coles, 1984, 1985) given some historical musings on the origins of later intensive studies of the results of interactions between magnetic moments in dilute alloys (the spin glass problem), but this followed a period where these interactions were seen as complications in efforts to understand the single impurity problem (Rizzuto, 1974). The earliest manifestation of interesting effects in the electronic properties of dilute alloys were found in the electrical resistivity

at low temperatures, but it was not immediately clear that these were associated only with impurities of magnetic character, since it seemed that that the resistivity minimum found in gold containing some impurities (see van den Berg, 1964, 1965) could be produced by additions of elements like tin to copper that did not have such a minimum. However, that effect was explained when it was realized (Gold et al., 1960) that in alloying the tin could reduce particles of iron oxide to introduce Fe into solid solution. Theoreticians (Korringa and Gerritsen, 1953) had early suggested a role for magnetic impurities and resonant scattering, but it was a little while before it became clear that the resistivity minimum in dilute alloys of $3d$ elements in Cu or Au was a single impurity effect while the resistivity maximum below it found at only slightly larger concentrations was the result of long-range interactions between moment-bearing impurities through the conduction electrons. During the period that then elapsed ($\sim$1954 to 1964), before the basic theory of the minimum was enunciated by Kondo (1964) and baptized into the church of physics with his name, important developments had taken place in our understanding of the basic question "under what circumstances does a $3d$ atom possess or fail to possess a magnetic moment in solid solution in another metal ?" In most such work the criterion for the existence of a moment was the manifestation of a Curie–Weiss susceptibility and it was not at first recognized that in some systems that criterion could give different answers at high and low temperatures. The first significant breakthrough was by Friedel (1956), who came to the problem via his concern with the scattering produced by transition metal solutes in various hosts, especially Cu and Al, introducing the concept of the virtual bound state produced by $3d$-conduction electron mixing. He recognized the possibility that this, like the $3d$ band of a pure transition metal, could be magnetic or non-magnetic depending on whether a criterion like the Stoner criterion was satisfied. This at once explained why some alloys (e.g. **Au**Fe) could behave like a dilute magnetic salt (e.g. (**Zn,Mn**)SO_4) while others like **Al**Fe had temperature-independent susceptibilities, although the $3d$ shell was clearly not full. At the end of the $3d$ series it seemed possible that the collective band model successful for **Ni**Cu (Wohlfarth, 1949) might be applied to **Cu**Ni with Ni filling its $3d$ shell as Pd does in Ag, but it became clear (Coles, 1952) that at the Cu-rich end also empty Ni($3d$) states existed without Curie–Weiss susceptibilities, and the approach of Friedel solved this problem. A little later the intuition of Matthias (Matthias et al., 1960), that the different effects of Fe on the superconductivity of host metals were associated with whether or not it carried a moment, directly stimulated the important work of Anderson (1961) who put the $3d$–conduction electron hybridization on a firm theoretical basis with the Hamiltonian that bears his name. I was pleased, with Matthias's encouragement, to be able to show (Coles, 1963) that Fe produced a resistance minimum in Mo but not in Nb. That, incidentally, led to the serendipitous

discovery of the strange resistivity behaviour of **Rh**Fe which became a useful low temperature thermometer. During the same period a very important study was made by Owen et al. (1957) of the "good" moment system **Cu**Mn, a system later shown (Hirshkoff et al., 1971) to maintain, in the dilute limit, a good Curie–Weiss behaviour down to 10 mK, in contrast to **Cu**Fe where it is lost below about 10 K. The **Cu**Mn study was important for two reasons. First the good spin-resonance behaviour showed that Mn carried into the alloy the intra-atomic correlations that made it possible to speak of it as essentially $3d^5$, $S = \frac{5}{2}$, $g = 2$ and the importance of on-site Hund's rule correlations was later emphasized in the work of Hirst (1970). (The importance of these "ionic" aspects was even greater in later work on the rare earth solutes, where additional structure in the resonant levels is due to crystalline electric field effects, normally assumed to be strong enough in $3d$ materials to quench orbital contributions to the moments). Second, the observation of susceptibility maxima in quite dilute alloys was reminiscent of antiferromagnetism and showed clearly that interactions between these moments were important. At about the same time a number of people were demonstrating large extra contributions to the specific heat in such alloys at low temperatures (see Coles, 1984), effects which led to the concept of a distribution of effective fields seen by the solute moments. Blandin in his thesis (1961) (see Blandin and Friedel, 1959) seems to have been the first to recognize that the origin of this distribution had its roots in the very on-site mixing of the $3d$ and conduction electron states that had created the virtual bound states, but an intriguing suggestion was that of Overhauser (1959) that the local moments stabilized a spin-density wave in the conduction electrons of Cu, a situation later found to hold for dilute solutions of heavy rare earths in yttrium (Sarkissian and Coles, 1976).

3   The Kondo effect

At this point it seems appropriate to look at the developments in our understanding of the single magnetic impurity before returning to the treatment of the interactions between them. Kondo's (1964, 1969) breakthrough work on the origin of the resistivity minimum opened the floodgates to theoretical work on the nature of the ground state of a system consisting of a local moment coupled by exchange interaction to the conduction electrons. (This J_{sd} term is often called the Kondo exchange Hamiltonian but it had been used earlier by workers in USSR, USA and Japan). The irony was that to produce the resistivity minimum J had to be negative and it was fortunate that earlier he (Kondo, 1962), de Gennes (1962) and Anderson and Clogston (1961) had shown that the local state-conduction electron mixing led to an effective (not classical) exchange that was negative.

Not only was there, in the description of the ground state, a fascinating and difficult problem but it was one on which the condensed matter theorists could exercise their recently developed many-body muscles. As it became clear that the ground state became non-magnetic by the compensation of hybrid up-spins with hybrid down-spins (not a simple antiferromagnetic coupling of a local spin with a conduction electron spin) the range above T_K and the range $0 < T \ll T_K$ could be treated with reasonable approximations, but no treatment was available to take the system through T_K until the breakthrough provided by Wilson's (1975) use of renormalization group methods. (It may be noted that although the binding energy $k_B T_K$ was similar in form – $D \exp(1/N(0)J)$ – to that for the BCS superconductor there could be no phase transition in this essentially zero-dimensional system.) More recently analytical treatments founded on a Bethe ansatz have underpinned this approach (Andrei, 1980; Wiegman, 1980; Wiegman and Tsvelik, 1983), and it is possible in principle to calculate T_K for different systems. Few such calculations have been made and I suspect that it would be very difficult to justify the very low T_K in **Cu**Mn without carefully taking into account the hybridization that has already taken place in the $l = 2$ channel in pure Cu. Similarly the "good" moment Fe shows in Mo (where $n(E_F)$ is larger than that of Al, although small for a transition metal, and with dominately d character) seems difficult to reconcile on any simple approach with the absence of such a moment for Fe in Al. The full story of the developments of the theory of the Kondo effect and our present state of understanding of it have been presented in a recent book by Hewson (1994).

Later in the dilute alloy story interesting effects of Kondo-related character were found for some alloys containing Ce and Yb, elements known to have unstable valencies, and these were of particular interest when the host was superconducting, see Sect. 4. These effects also proved to be important in the heavy fermion industry since compounds of these elements were the early players, and a sort of taxonomy has developed where Kondo lattices are distinguished from homogeneous mixed valence compounds rather as one distinguishes "good" moment solutes with Kondo effect from non-magnetic virtual bound states with local spin fluctuations in the dilute alloy story.

Little work has been done on dilute alloys containing U, although these should be of interest, partly because of the large number of heavy fermion compounds of U and partly because the radial extent of the $5f$ wave functions for U and Pu can be expected to be intermediate between that of the $3d$ states of Fe and that of the $4f$ states of Ce. Correspondingly the behaviour of U varies greatly with the character of the host in its dilute alloys. Thus in Au it shows a "good" moment and a resistivity minimum (Hillebrecht et al., 1989), in Th strong local spin fluctuation character (Maple et al., 1970) where the superconducting behaviour is of interest, but in Nb and Mo non-magnetic virtual bound state character (Coles et al., to be

published). Interestingly there is no indication of the marked contrast for these two hosts that they show for Fe as solute; certainly U has little effect on the superconductivity of Nb, but meaningful measurements on the superconductivity of **Mo**U await the availability of high purity iron-free Mo.

4 Superconductivity in dilute magnetic alloys

This also is a topic that has been reviewed in a number of places (see especially Maple, 1973) and reference has been made above to the role of Matthias's intuition in stimulating both experimental and theoretical work on the dilute alloy problem. Quite early in this era, when the topic was escaping from the pejorative "dirty superconductors" label, Anderson (1959) made clear the reason for the sharp difference between the effects of simple and moment-bearing solutes on superconducting transition temperatures: although in the former k and $-k$ are no longer strictly good quantum numbers because of scattering there is no objection to pairing a scattered state with its time reversed conjugate; but when spin dependent scattering occurs time reversal symmetry is broken and pair-breaking takes place. The consequences for systems like **La**Gd were calculated by Abrikosov and Gor'kov (1961), and for rare earth systems free from intermediate valence tendencies the situation is fairly well understood, although consideration of crystal field effects is required. These and the modifications for solutes with finite Kondo temperatures or spin-fluctuation temperatures are discussed in detail by Maple (1973). That crystal field split levels could be clearly defined enough and weakly enough coupled to the conduction electrons was demonstrated by the observation of non-S-state paramagnetic resonances. These levels and their role in the magnetic, electrical and thermal properties of dilute alloys of the heavy rare earths are now fairly well understood, especially following the work of the Danish groups (Høg and Touborg, 1974; Rathmann et al., 1974) which was greatly aided by Allan Mackintosh's deep understanding of the rare earths.

5 Spin glasses

Although the term spin glass has been applied to a wide range of systems without long-range magnetic order, the concept had its roots in the dilute alloy problem. When it was recognized that interactions between solute atoms were taking place at quite low concentrations unless frustrated by Kondo, general arguments such as those of Blandin (1961) and the character of the specific heat made it clear that no straightforward antiferromagnetic transition was taking place. (I have referred elsewhere to the ironies that the negative θ-values that led Néel to his great

theory of antiferromagnetism never took him back to explore the low temperature properties of the alloys manifesting them, and that Kittel failed initially to invoke for **Cu**Mn his own RKKY interaction).

The experimental situation for spin glasses in dilute alloys is now fairly clear and has been set out by Mydosh (1993), whose demonstration (Cannella and Mydosh, 1972) of sharp peaks in the ac susceptibility had played a major role in attracting the attention of theorists, and led to an explosion of sessions on the topic at magnetism conferences. (On a personal note I find it interesting that my own suggestion of an analogy between such spin glasses and conventional "atomic position" glasses was developed in the context of dilute alloys with by-no-means good moments in the systems **Au**Co and **Rh**Fe). The competition in dilute alloys between a Kondo or Friedel–Anderson spin compensation and spin glass freezing has a close relationship to the delicate balance between magnetic and non-magnetic ground states for atomically ordered heavy fermion compounds; the problem of this balance was first addressed by Doniach (1977).

However the fundamental character of the spin glass transition has taken a long time to resolve and the theoretical techniques used to address it have become less clear to the experimentalist. The current situation is well reviewed by Fisher and Hertz (1991), and the consensus seems to be that in Ising systems a phase transition does exist in 3 dimensions, although that is below the critical dimensionality for Heisenberg systems, which then require anisotropies to yield a phase transition.

6 The onset of long-range order

In some dilute alloys with good moments it had seemed from Mössbauer and high field magnetization measurements that ferromagnetism occurred at quite dilute concentrations, but it later became apparent (Murani, 1974; Murani et al., 1974; Coles et al., 1978) that **Au**Fe is, in fact, a spin glass with strong ferromagnetic bias to the competing interactions, and that long-range ferromagnetism only sets in above a percolation concentration (~18% Fe) where nearest neighbour interactions dominate. Just above that concentration, however, the effects of co-existing finite clusters gave rise to a situation often described (not quite accurately) as a re-entrant spin glass (see Roy and Coles, 1993).

Long-range order can set in quite rapidly at quite low solute concentrations when the host is strongly exchange-enhanced and the onset of ferromagnetism has been intensively studied in both **Pd**Ni and **Pd**Fe. In the former the local extra enhancement associated with the Ni atoms (which do not carry a moment in the dilute limit) fairly rapidly leads to ferromagnetism at ~2.4% (Murani, 1974; Murani et al., 1974) but there is evidence from neutron scattering (Aldred et al., 1970) that

close pairs of Ni atoms play a significant role in producing the polarization clouds that over-lap to give long-range, although inhomogeneous, ferromagnetism. In **Pd**Fe the solute does possess a good moment and at very dilute concentrations ($\sim$ 0.01%) giant polarization clouds overlap to give ferromagnetism. In most other $4d$–$3d$ alloys the first magnetic freezing that occurs is clearly of spin glass character, and there are indications that at very low temperatures for very small concentrations **Pd**Fe also has a spin glass regime.

A fascinating, but rather neglected aspect of dilute alloy magnetism is the occurrence of ferromagnetism for small substitutions of Mn for Ge in GeTe (Cochrane et al., 1974) where the small carrier concentration ($\sim 10^{21}$ cm^{-3}) yields a value of the Fermi wave vector so small that up to large distances the RKKY interaction has not crossed zero and no competing interactions exist to give a spin glass. (This is not the case for all magnetic semiconductors however).

7 Recent developments

Two inter-related aspects of the dilute alloy problem that have attracted attention in recent years are the multichannel Kondo effect, originally introduced by Nozières and Blandin (1980) but rather neglected since, and the quadrupolar Kondo effect (Cox, 1988). Much attention has been focussed on substitutions of U for Y in YPd$_3$ where the effective Kondo temperature changes rapidly with U concentration (an effect sometimes called Fermi level tuning) from values above room temperature to values small enough for antiferromagnetic order to dominate over Kondo above 20% (Dai et al., 1995). This makes it difficult to be sure that the undoubted deviations in the susceptibility, resistivity and specific heat (Seaman et al., 1991) from the expectations of Fermi liquid theory require these new approaches or follow from the decline of characteristic temperatures towards 0 K. (For the resistivity, at least, related deviations are found close to the critical concentration for ferromagnetism in **Pd**Ni and for spin glass formation in **Rh**Fe. The suppression of any T^2 regime to very low temperatures in the latter is what makes it a useful low temperature thermometer).

For dilute U alloys, as emphasized by Coleman (1995), the role of Hund's rule effects have yet to receive a satisfactory treatment, and this makes them more difficult to discuss than those of Ce.

In conclusion it seems clear that, as predicted many years ago, the understanding of the single solute atom behaviour will continue to make important contributions to attempts to provide a sound basis for discussing magnetism in strongly correlated systems, including both heavy fermions and high temperature superconductors.

References

Abrikosov AA and Gor'kov LP, 1961: Sov. Phys. JETP **12**, 1243

Aldred AR, Rainford BD and Stringfellow MW, 1970: Phys. Rev. Lett. **24**, 297

Anderson PW, 1959: J. Phys. Chem. Solids **11**, 26

Anderson PW, 1961: Phys. Rev. **124**, 41

Anderson PW and Clogston AH, 1961: Bull. Am. Phys. Soc. **6**, 124

Andrei N, 1980: Phys. Rev. Lett. **45**, 379

Blandin A, 1961: Ph.D. thesis (University of Paris)

Blandin A and Friedel J, 1959: J. Phys. Rad. **20**, 160

Cannella A and Mydosh JA, 1972: Phys. Rev. B **6**, 4220

Cochrane RW, Plishke M and Ström-Olsen JO, 1974: Phys. Rev. B **9**, 3013

Coleman P, 1995: Physica B **206–207**, 872

Coles BR, 1952: Proc. Phys. Soc. B **65**, 221

Coles BR, 1963: Phil. Mag. **8**, 335

Coles BR, 1984: in *Multicritical Phenomena*, eds. R. Pynn and A. Skjeltorp (Plenum, New York) p. 363

Coles BR, 1985: Ann. Phys. (Paris) **10**, 63

Coles BR, Sarkissian BVB and Taylor RH, 1978: Phil. Mag. **37**, 489

Cox DL, 1988: Physica C **153**, 1442

Dai P, Mook HA, Seaman CL, Maple MB and Koster J, 1995: Phys. Rev. Lett. **75**, 1202

de Gennes PG, 1962: J. Phys. Rad. **23**, 510

Doniach S, 1977: Physica B **91**, 231

Fisher K and Hertz JA, 1991: *Spin Glasses* (Cambridge University Press, Cambridge) p. 375

Friedel J, 1956: Can. J. Phys. **34**, 1190

Gold AV, MacDonald DKC, Pearson WB and Templeton IV, 1960: Phil. Mag. **5**, 765

Hewson AC, 1994: *The Kondo Problem to Heavy Fermions* (Cambridge University Press, Cambridge)

Hillebrecht FU, Trodahl HJ, Sechovsky V and Thole BJ, 1989: Z. Phys. B **77**, 373

Hirshkoff E, Symko O and Wheatley J, 1971: J. Low Temp. Phys. **5**, 155

Hirst LL, 1970: Phys. Kondens. Mat. **11**, 255

Høg J and Touborg P, 1974: Phys. Rev. B **9**, 2920

Kondo J, 1962: Proc. Theor. Phys. **28**, 846

Kondo J, 1964: Proc. Theor. Phys. **32**, 37

Kondo J, 1969: *Solid State Physics* **23**, 183

Korringa J and Gerritsen AN, 1953: Physica **19**, 357

Maple MB, 1973: in *Magnetism V*, ed. H. Suhl (Academic Press, New York) p. 289

Maple MB, Huber JG, Coles BR and Lawson AC, 1970: J. Low Temp. Phys. **3**, 137

Matthias BT, Peter M, Williams HJ, Clogston AH, Corenzwit EC and Sherwooc RC, 1960: Phys. Rev. Lett. **5**, 542

Morandi G, Napoli F and Ratto CR, 1981: *Theoretical Review of the Friedel–Anderson model* (Universitaria, Ferrara)

Murani AP, 1974: J. Phys. F **4**, 757

Murani AP, Tari A and Coles BR, 1974: J. Phys. F **4**, 1769

Mydosh JA, 1993: *Spin Glasses* (Taylor and Francis, London)

Nozières P and Blandin A, 1980: J. Phys. (Paris) **41**, 193

Overhauser A, 1959: Phys. Rev. Lett. **4**, 414

Owen J, Browne ME, Arp V and Kip AF, 1957: J. Phys. Chem. Solids **2**, 85

Rathmann O, Als-Nielsen J, Bak P, Høg J and Touborg P, 1974: Phys. Rev. B **10**, 3983

Rizzuto C, 1974: Rep. Prog. Phys. **37**, 147

Roy SB and Coles BR, 1993: in *Selected Topics in Magnetism*, eds. L.C. Gupta and M.S. Multani (World Scientific, Singapore) p. 375

Sarkissian BVB and Coles BR, 1976: Commun. Phys. **1**, 17

Seaman CL, Maple MB, Lee BW, Ghamaty S, Torikachvili MS, Kang JS, Liu LZ, Allen JW and Coc DL, 1991: Phys. Rev. Lett. **67**, 2882

van den Berg GJ, 1964: Prog. Low Temp. Phys. **IV**, 194

van den Berg GJ, 1965: *Low Temperature Physics, LT9* (Plenum, New York) p. 955

Wiegman PB, 1980: Phys. Lett. **80A**, 163

Wiegman PB and Tsvelik AM, 1983: J. Phys. C **16**, 2281; *ibid.*, 2321

Wilson K, 1975: Rev. Mod. Phys. **47**, 773

Wohlfarth EP, 1949: Proc. Roy. Soc. **195**, 434

Spin-Density-Wave Antiferromagnetism in the Chromium System I: Magnetic Phase Diagrams, Impurity States, Magnetic Excitations and Structure in the SDW Phase

Eric Fawcett

Physics Department, University of Toronto,

Toronto M5S 1A7, Canada

Abstract

The chromium system, comprising pure Cr and alloys with most transition metals and some non-transition metals, is the archetypical spin-density-wave (SDW) system. This paper supplements, with a brief summary and extension to include recent work, two previous comprehensive reviews on Cr (Fawcett, 1988) and Cr alloys (Fawcett et al., 1994). The magnetic phase diagrams are reviewed. Impurity states in CrFe and CrSi, when suitably doped with V or Mn, produce dramatic effects in the electrical resistivity, including a low-temperature resistance minimum due to impurity-resonance scattering. Curie–Weiss paramagnetism appears just above the Néel temperature in dilute CrV alloys. Recent work on inelastic neutron scattering in pure Cr is reviewed: the apparent absence of dispersion of the spin-wave modes at the wave vectors of the incommensurate SDW where the Bragg satellite peaks occur; the energy-dependent anisotropy of the excitations in the longitudinal-SDW phase; the commensurate magnetic scattering at the centre of the magnetic zone, which at higher energy and temperature dominates the inelastic scattering at the satellites; the Fincher–Burke excitations seen at low-energy in the transverse-SDW phase; and the silent satellites seen in single-Q Cr at off-axis incommensurate points as temperature increases towards the Néel transition. X-ray scattering with synchrotron radiation has illuminated the relation between the SDW in Cr and the incommensurate charge-density wave that accompanies it.

1 Introduction

Chromium is the archetypical itinerant antiferromagnet, whose incommensurate spin-density wave (SDW) has a wave vector Q determined by the nesting properties of its Fermi surface. At the same time, the persistence of antiferromagnetism in Cr alloys over a wide range of compositions, when considered in the light of its absence in Mo and W, whose Fermi surfaces are very similar to that of pure Cr,

indicates that the 3d character of this metal is of fundamental importance to its being magnetic.

The beauty and the mystery of Cr and its alloys do not derive from their being antiferromagnets, of which there are many, but from the fact that they constitute a SDW antiferromagnetic system. The richness of the magnetic phenomena observed in the Cr system is a consequence of the SDW's being a truly many-body effect.

The present paper, and the companion papers (Fawcett et al., 1997; Fawcett, 1997, which are referred to as Papers II and III, respectively) summarize the reviews of SDW antiferromagnetism in Cr, by Fawcett (1988: referred to as RMP I), and in Cr alloys, by Fawcett et al. (1994: referred to as RMP II), with discussion especially of those areas where significant new advances have since been made. Some of the most active workers in the field presented papers at the 1996 Yamada Conference in a symposium having the same title as the present paper, which will accordingly summarize only very briefly their findings and refer the reader to the 1996 Yamada Conference Proceedings for a more complete account and further references (Alberts and Smit, 1997; Fishman et al., 1997; Hayden et al., 1997; Tsunoda, 1997; see also Fishman and Liu, 1993, 1994, 1996).

Section 2 reviews magnetic phase diagrams in the composition-temperature x–T plane. Impurity states, discussed in Sect. 3, offer new possibilities for understanding interesting properties of some Cr alloys. Recent experiments, which exploit the enhanced sensitivity of the SQUID magnetometer in studies of the temperature and field dependence of their magnetic susceptibility, show that Curie–Weiss paramagnetism occurs in dilute CrV alloys just above the Néel temperature; and that spin-glass behaviour occurs in CrMn and ternary alloys of Cr containing Mn (see Paper II, Fawcett et al., 1997). In both cases, presumably, a moment exists on the impurity atom, but there is no theoretical understanding of these phenomena.

The final Sect. 4 deals with inelastic neutron scattering in pure Cr. The magnetic excitation spectra of Cr and its SDW alloys are so rich in unusual phenomena that they continue to elude our understanding, despite considerable experimental efforts by several groups. We shall discuss here briefly, but with generous illustrations of the original data, so that the reader will have a fairly comprehensive picture of the behaviour: the energy-dependent anisotropy of the excitations in the longitudinal-SDW phase; the so-called "Fincher–Burke" excitations seen at low energy, $E \leq 8$ meV, in the transverse-SDW phase; the so-called "commensurate magnetic scattering" (CMS) at the centre of the magnetic zone, which grows with energy and temperature until it dominates the spin-wave scattering at the incommensurate satellite points in both the longitudinal- and transverse-SDW phases; and the so-called "silent satellites", which are low-energy critical fluctuations that grow rapidly close to the Néel temperature at the off-axis incommensurate points in single-Q Cr, thus leading to the return to cubic symmetry in the paramagnetic

phase with the disappearance of the SDW at the weakly first-order Néel transition.

Critical scattering in the paramagnetic phase in pure Cr and dilute CrV alloys (Noakes et al., 1990), and the so-called "SDW paramagnons" that occur close to the quantum critical point in the paramagnetic alloy $Cr_{95}V_5$ (Fawcett et al., 1988; Hayden et al., 1997) are discussed in relation to new high-temperature thermal expansion results in Paper II (Fawcett et al., 1997).

The remarkable similarity of the magnetic phase diagrams in the composition-temperature and composition-pressure planes is discussed in Paper III (Fawcett, 1997) in relation to the strong volume-dependence of the magnetism in the Cr system. This is reflected in dramatic effects in the temperature dependence of the physical properties of Cr and its SDW alloys, which persist to temperatures much greater than the Néel transition, as discussed in Paper II. A striking example of this parallelism between the effects of composition change and pressure in ternary CrFeV alloys is described in Paper III.

2   Magnetic phase diagrams

Chromium alloys exhibit four magnetic phases: longitudinal SDW (AF_2), transverse SDW (AF_1), commensurate SDW (AF_0), and paramagnetic magnetic (P). The general features of the phase diagram may be explained in terms of the canonical model for SDW antiferromagnetism in the Cr alloy system, which comprises nesting electron and hole octahedra, with a reservoir of electrons corresponding to the rest of the Fermi surface. This model was first worked out in detail by Shibatani et al. (1969), following the idea of the SDW proposed originally by Overhauser (1960, 1962). The model was further developed by Kotani (a new name for Shibatani), in a series of papers referenced in RMP II, to include the effects of the charge-density wave and of scattering of electrons by impurities. These two effects have featured large in recent theoretical work by Fishman et al. (1997, and references therein).

Figure 1 illustrates the systematics of the phase diagram for most alloys of Cr with transition metals. The metals from Group IB (Au), Group IV (Ti) and Group V (V, and also Nb and Ta not shown here) depress the Néel temperature T_N with increasing concentration, and eventually destroy the SDW at a concentration of a few atomic percent. Group VII (Mn, Re) and Group VIII (all the other elements shown in Fig. 1), apart from the ferromagnetic metals Fe, Co and Ni (and also Pd), raise T_N, with the appearance at a concentration of a fraction of a percent (see Table IV in RMP II) of the commensurate SDW phase AF_0. With changing composition x of the solute metal, T_N rises rapidly beyond the triple point, while the transition temperature T_{IC} between the AF_0 and AF_1 phases drops rapidly to
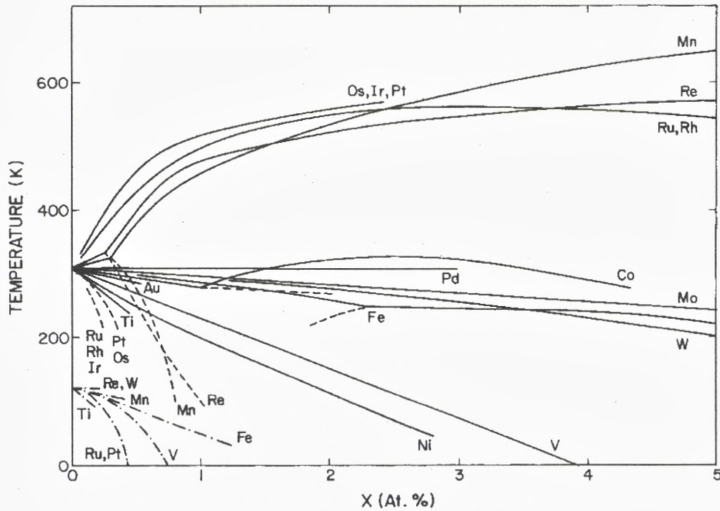
Figure 1. Schematic magnetic phase diagram for alloys $Cr_{1-x}A_x$ of chromium with transition metals A. ———— T_N, Néel temperature; — — — — T_{IC}, transition temperature from the incommensurate SDW AF_1 phase to the commensurate SDW AF_0 phase; — · — · — T_{SF}, spin-flip temperature from the transverse-SDW phase AF_1 to the longitudinal-SDW phase AF_2.

zero. Thus, when $x > 1$ to 2 at.%, the SDW remains commensurate all the way from T_N to zero temperature.

This behaviour is well understood qualitatively in terms of the canonical model and a rigid band picture for which transition metals in Groups IV and V lower the Fermi level, thereby decreasing the nesting between the electron and hole octahedra, and conversely for Group VII and VIII metals. The pioneer experimental work in this field was done by Allan Mackintosh and his co-workers (Møller and Mackintosh, 1965, Møller et al., 1965; Koehler et al., 1966) and the Japanese group (Hamaguchi and Kunitomi, 1964) using neutron diffraction.

The typical behaviour for larger concentrations of a Group VIII transition metal dissolved in Cr is illustrated in Fig. 2. Interest in the nature of the phase boundary between the SDW phase and the superconducting phase, and the possible coexistence of the two states goes back to the study of CrRe by Muheim and Müller (1964). Subsequent work on both CrRe and CrRu, both of which systems are superconducting for compositions close to the SDW phase, have however been inconclusive (see Sect. VI.E in RMP II).

The depression of T_N by the Group VI metals Mo and W, which are isoelectronic with Cr and have a very similar Fermi surface, with however increasing width of the
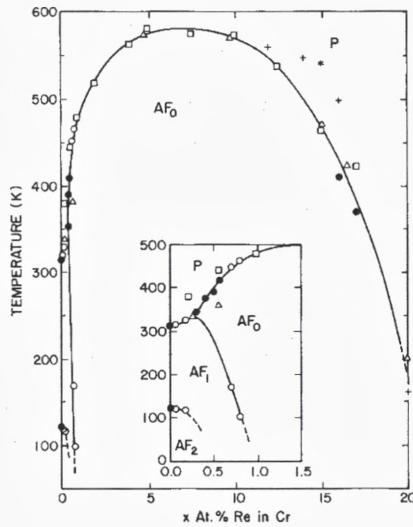
Figure 2. Magnetic phase diagram for the $Cr_{1-x}Re_x$ alloy system (see Fig. 13 in RMP II for sources of the experimental data).

d-bands from $3d$ to $4d$ to $5d$, is presumably due to their reduction of the exchange and correlation interactions responsible for the occurrence of the SDW rather than to change in the Fermi level (see also Fig. 3b and comments on it below).

Inspection of Fig. 1 shows that the systems CrFe, CrNi and CrPd do not follow these simple rules. Considerable efforts have been made to understand, in particular, the unique phase diagram of CrFe, in which the AF_1 phase occurs at higher temperature than the AF_0 phase, i.e., the dash-line showing $T_{IC}(x)$ goes to the left towards lower values of x in Fig. 1 (Galkin et al., 1997b). A similar effect occurs in CrSi also (Endoh et al., 1982), but very soon the $T_{IC}(x)$ line turns back to the normal behaviour giving a re-entrant AF_0 phase very close to the triple point (see Fig. 17 in RMP II). The model of Nakanishi and Kasuya (1977) was most successful in explaining this effect in CrFe (see Fig. 57b in RMP II), but it relies upon an arbitrary magnetoelastic term in the free energy, and a fundamental explanation is lacking. This term however reproduces the large magnetostriction that is seen at the strongly first order Néel transition to the AF_0 phase in CrFe (Butylenko, 1989; see Fig. 1 in Fawcett and Galkin, 1992). CrSi also exhibits a large first order magnetostriction at the Néel transition to the AF_0 phase (Suzuki, 1977), but it is difficult to understand the commonality between the two alloy systems.

For several alloys of Cr with non-transition metals the phase diagram is rather similar to that for Cr with Group VIII transition metals, as shown in Fig. 3. These
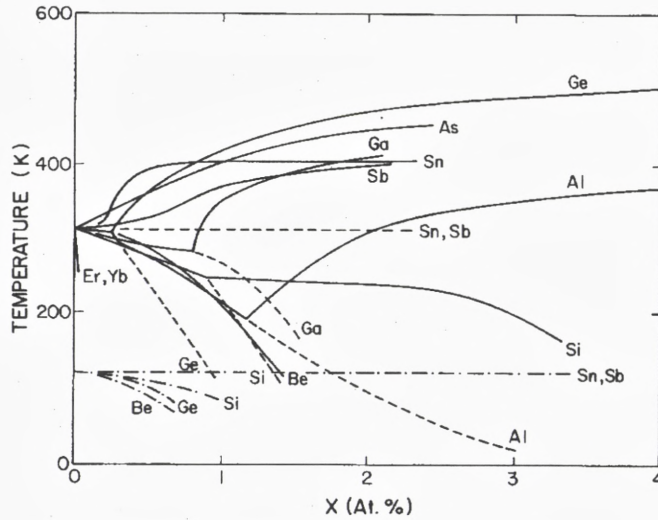
Figure 3. Schematic magnetic phase diagram for alloys $Cr_{1-x}A_x$ of chromium with non-transition metals A. ———— T_N, Néel temperature; — — — — T_{IC}, non-transition temperature from the incommensurate SDW AF_1 phase to the commensurate SDW AF_0 phase; — · — · — T_{SF}, spin-flip temperature from the transverse-SDW phase AF_1 to the longitudinal-SDW phase AF_2.

are all substitutional alloys, but there is no reason whatsoever to believe that the effect of a non-transition metal like Ge on the band structure of Cr is similar to that of Ru, for example. One looks in vain for an alternative to the canonical model to explain the behaviour of alloys of Cr with non-transition metals.

We select for more detailed discussion the CrAl alloy system, whose magnetic phase diagram is shown in Fig. 4. Alternative interpretations of the experimental data are shown, but the dash-line is now thought to be incorrect and serves only to illustrate the difficulties encountered sometimes in mapping out the phase diagram, in this case probably due to errors in determining the alloy compositions.

The behaviour of the $Cr_{1-x}Al_x$ alloy system for x up to 30 at.% Al shown in Fig. 4a is quite remarkable. The value of T_N approaches 800 K, a value higher than that for any other system. There is some evidence that for the higher concentrations, $x > 15$ at.% Al, CrAl is a narrow-gap semiconductor, which would mean that the moments are localized rather than existing in a SDW (Fawcett et al., 1994).

Figure 4b shows how the introduction of 5 at.% Mo so dilutes the Cr host, thereby reducing the exchange and correlation interactions, that the SDW disappears in the ternary alloys for $2 \leq x \leq 5$ at.% Al (Smit and Alberts, 1987).

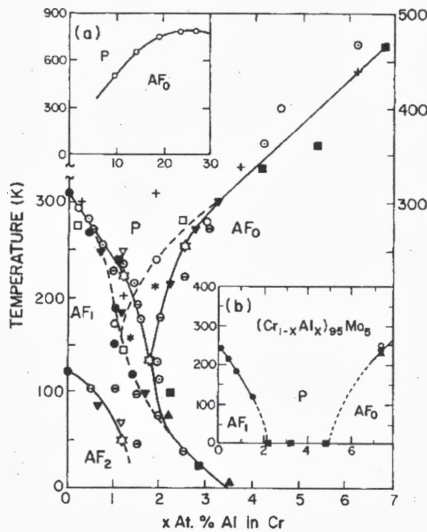Finally we note in Figs. 1 and 3 that the spin-flip transition temperature de-

Figure 4. Magnetic phase diagram for the $Cr_{1-x}Al_x$ alloy system. Insert (a) shows the phase diagram for higher concentrations of Al, and insert (b) shows the phase diagram for the ternary alloy system $(Cr_{1-x}Al_x)_{95}Mo_5$ (see Fig. 16 in RMP II for sources of the experimental data).

creases rapidly to zero with increasing solute concentration for all alloy systems (except CrSn and CrSb, but for these the experimental data are suspect). A satisfactory explanation of the spin-flip transition in pure Cr is still wanted (RMP I).

3 Impurity states

Allan Mackintosh and his co-workers (Møller et al., 1965; Trego and Mackintosh, 1968) performed the first systematic study of the temperature dependence of the electrical resistivity $\rho(T)$ and the thermopower $S(T)$ of SDW alloys of Cr with V, Mn, Mo, W, and Re (and also neutron diffraction in the same alloys, Koehler et al., 1966). As well as finding qualitative agreement between the variation of the Néel temperature with electron concentration and an early version of the canonical model for the Cr system, they observed effects associated with the electron-hole condensation responsible for the formation of the SDW in Cr (Overhauser, 1962). Their results for CrV alloys are shown in Fig. 5. The increase of $\rho(T)$ with decreasing T below the Néel transition seen in Fig. 5a is largely due to the formation of an energy gap on the nesting parts of the Fermi surface, where the electron–hole
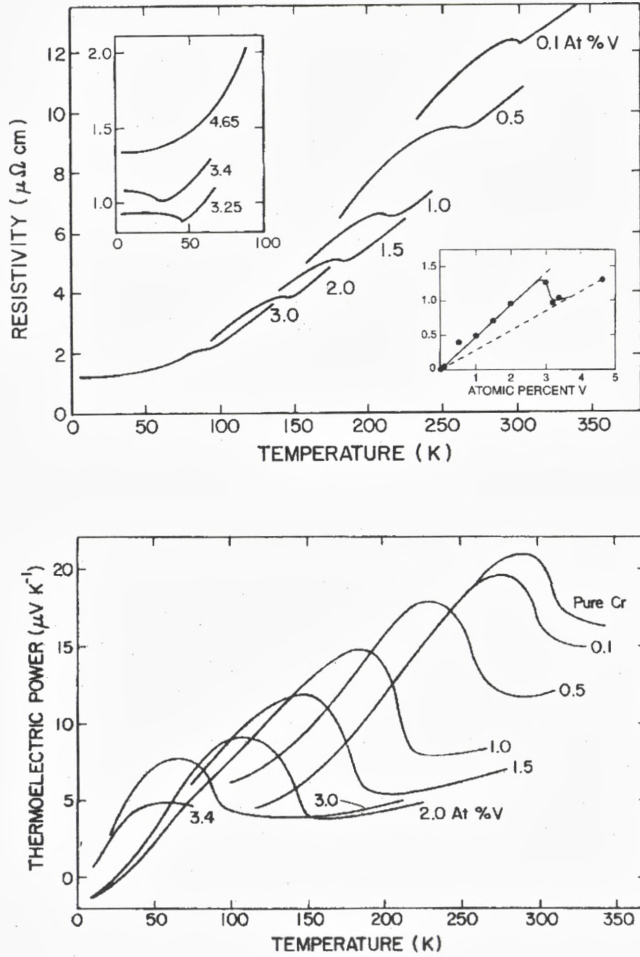
Figure 5. (a) Temperature dependence of the resistivity of $Cr_{1-x}V_x$ alloys, for compositions ranging from $x = 0.1$ to 4.65 at.% V in Cr. The inset shows the residual resistivity at temperature 4.2 K as a function of V concentration. (b) Temperature dependence of the thermoelectric power of the same CrV alloys (after Trego and Mackintosh, 1968)

pairs do not contribute to electrical conduction. The effect is seen in pure Cr and it is anisotropic in a single-Q sample (see Fig. 47 in RMP I) because the nesting occurs along and thus defines the wave vector Q of the SDW. The condensation of the electrons and holes also changes the scattering of single-particle carriers, which is largely due to phonons in the temperature region of interest. The hump in $\rho(T)$ below T_N results from a combination of these two factors, and in some alloys is much larger than in pure Cr (see Table VI in RMP II).

The anomaly in $S(T)$ shown in Fig. 5b is similar in form to that of $\rho(T)$, but is more pronounced. The explanation (Trego and Mackintosh, 1968) is that the thermopower is proportional to the derivative of the resistivity with respect to energy of electrons/holes at the Fermi surface, $S \sim -d\ln\rho/dE$. Thus, while the decrease in the scattering almost cancels the increase in resistivity due to the condensation with decreasing temperature, giving rise to only a small hump in $\rho(T)$ below T_N, as seen in Fig. 7a, the energy dependence of the two effects that determine the thermopower results in two terms that have the same sign and together give the large hump in $S(T)$. In dilute $Cr_{1-x}Mn_x$ alloys ($x \leq 3.4$ at.% Mn), Trego and Mackintosh (1968) found that $S(T)$ exhibits a low-temperature hump, which increases in amplitude relative to the value in the paramagnetic phase as x increases, and showed that the form of the temperature dependence provides clear evidence that it is due to phonon drag.

Although there is a vast literature on impurity states in normal metals, ferromagnetic metals and semiconductors, this aspect of the theory and practice for SDW alloys in the Cr system has been neglected. The use of local probes, principally the Mössbauer effect, diffuse neutron scattering, perturbed angular correlation and nuclear magnetic resonance, to explore a limited number of Cr alloys has provided desultory information about a few impurity atoms dissolved in Cr and in the SDW phase (RMP II).

The theory of local impurity states within the antiferromagnetic energy gap opened up by the electron-hole condensation (Volkov and Tugushev, 1984; Tugushev, 1992) offered new possibilities for understanding the behaviour of SDW Cr alloys with non-magnetic as well as magnetic metals. Until now these possibilities have been little explored, though the potential for discovering new phenomena is no doubt as rich as it was for impurity states in the forbidden energy band of semiconductors. Those predicted by Tugushev's theory include: resonant scattering by the impurity state, which gives rise to an additional term in the residual resistivity at zero temperature, and a negative temperature-dependent contribution $\rho_{\mathrm{res}}(T) \sim -T^2$, when the Fermi level is close to one of the pair of impurity levels predicted by the theory; and a negative magneto-resistance in the case when the pair of impurity levels are spin-polarized.

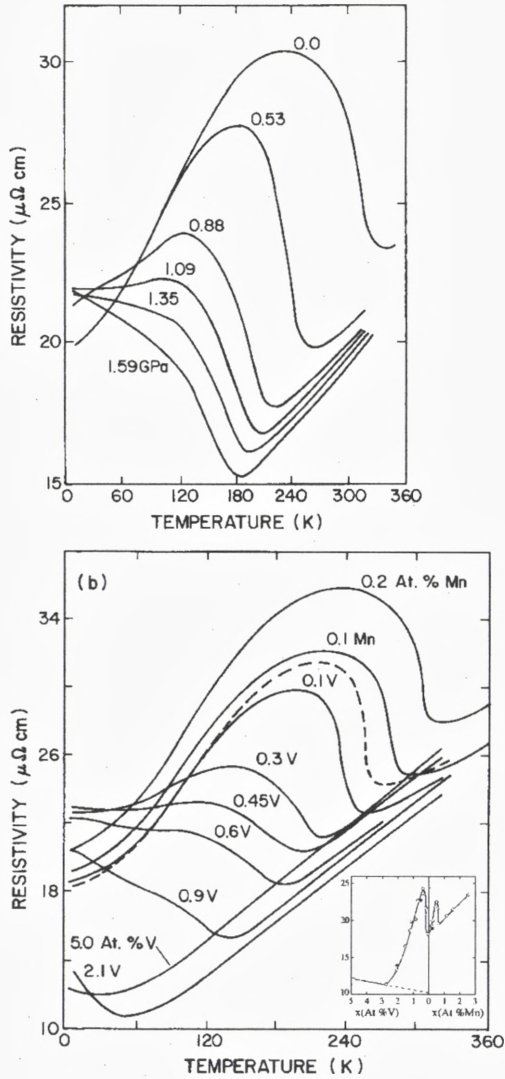The best evidence to support the theory of local impurity states is illustrated

Figure 6. (a) Pressure dependence of the resistivity of Cr+2.7 at.% Fe+0.27% Mn (from Galkin, 1989). (b) Temperature dependence of the resistivity of ternary alloys (Cr+2.7 at.% Fe)$_{1-x}$(V,Mn)$_x$, with the concentrations x of V or Mn shown on the curves, the curve for undoped Cr+2.7 at.% Fe being dashed (after Galkin and Fawcett, 1993). The inset shows the residual resistivity at temperature 4.2 K as a function of alloy composition (from Galkin, 1989).

in the inset to Fig. 6b. The two peaks in the concentration dependence of the residual resistivity are believed to correspond to the energy levels of the pair of impurity states of the Fe atom, with doping by (V,Mn) being employed only to tune the Fermi level. Fawcett and Galkin (1991) have analyzed this data and also measurements by Galkin (1987) on $(Cr+1.3 \text{ at.}\% \text{ Si})_{1-x}(V,Mn)_x$, and find that the splitting between the pair of energy levels is about the same, 24 to 28 meV, of the order of 10% of the energy gap in a commensurate SDW Cr alloy (see Fig. 70 in RMP II).

It seems likely that the resistance minimum seen in several Cr alloy systems (see Table VI in RMP II) is due to the predicted negative term in the resistivity, $\rho_{res}(T) \sim -T^2$. Katano and Mori (1979) attribute the minimum in $\rho(T)$ seen in CrFe alloys (see Fig. 29 in RMP II) to the Kondo effect associated with the moment on the Fe impurity that gives rise to the Curie–Weiss temperature dependence of the susceptibility in the SDW phase, but none of the other Cr alloys that exhibit a low-temperature resistivity minimum have a moment according to this criterion. When the term $\rho_{res}(T)$ is combined with other temperature-dependent terms in the resistivity, the behaviour of $\rho(T)$ becomes rather complex, and the curves in Figs. 6a and 6b, for example, still have not been analyzed. Paper III (Fawcett, 1997) describes work by Galkin et al. (1997c) that shows convincingly that the minimum in CrFeV alloys in the SDW phase is due to impurity-resonance scattering, but when the system is brought into the paramagnetic phase by doping or the application of pressure it becomes a shallower Kondo minimum.

V and Mn have been generally regarded, ever since the construction of the canonical model, which together with a rigid-band model explained very nicely the dependence of the wave vector Q and the Néel temperature T_N on the composition of dilute Cr(V,Mn) alloys, as doing nothing more than tune the Fermi level by adding (Mn) or removing (V) electrons from the host Cr. It turns out in fact that V strongly affects many other physical properties, including (Fawcett, 1992) inelastic neutron scattering, nuclear magnetic relaxation time, the nature of the Néel transition, electrical resistivity in the paramagnetic phase, and the magneto-elastic properties. We shall consider here only the appearance with V doping of a component of the susceptibility $\chi(T)$ in the paramagnetic phase having a temperature dependence that obeys a Curie–Weiss law (Hill et al., 1994). CrMn alloys, on the other hand, have been found to exhibit remarkable spin-glass properties at low temperatures (Galkin et al., 1995, 1996a, 1996b, 1997a). The absence of a Curie–Weiss law for $\chi(T)$ in the SDW phase had been generally assumed to mean that the Mn atom carries no moment in SDW $Cr_{1-x}Mn_x$ alloys for $x \leq 10$ at.% Mn (Maki and Adachi, 1979).

Figure 7 shows the data for $\chi(T)$ in two dilute CrV alloys in comparison with that for pure Cr. The Curie–Weiss paramagnetism evident here is not seen in CrV
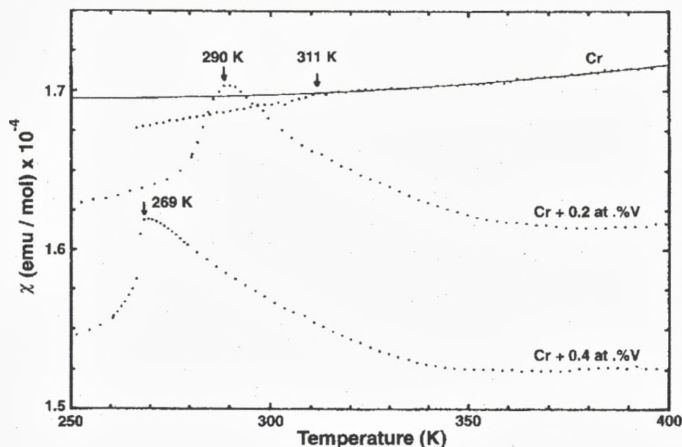
Figure 7. Temperature dependence of the magnetic susceptibility $\chi(T)$ of pure Cr and two dilute CrV alloys. The line through the data points above the Néel temperature, $T_N = 311$ K, for Cr is a quadratic fit to $\chi(T)$ (from Hill et al., 1994).

alloys containing more than $x \geq 0.67$ at.% V, and is suppressed in a measuring field, $H = 6$ kOe (de Oliviera et al., 1996b).

No theory is available to explain any of these unexpected experimental results. They have been made possible, like the discovery of spin-glass behaviour in CrMn alloys, by the advent of highly sensitive methods of measuring the magnetic susceptibility with low measuring fields, either by use of a SQUID magnetometer (Hill et al., 1994) or of an AC susceptometer (de Oliviera et al., 1996a). It is quite likely that other alloys of Cr with non-magnetic metals will be found, when re-examined more carefully by use of these methods, to exhibit Curie–Weiss paramagnetism. It is well-known that Fe and Co, as well as Mn, carry a moment in the paramagnetic phase of their alloys with Cr (see Table V in RMP II). In the case of CrRe, CrRh and CrSi there may already be some evidence for the existence of local moments above T_N, in that, for concentrations high enough to be well into the AF_0 phase, there are some compositions for which $\rho(T)$ decreases with increasing temperature above T_N (see the references in Table V in RMP II).

4   Neutron scattering in the SDW phase

The spectrum of magnetic excitations in Cr is rich in modes that are still largely not explained at even the most rudimentary level. The so-called "spin-wave" modes are
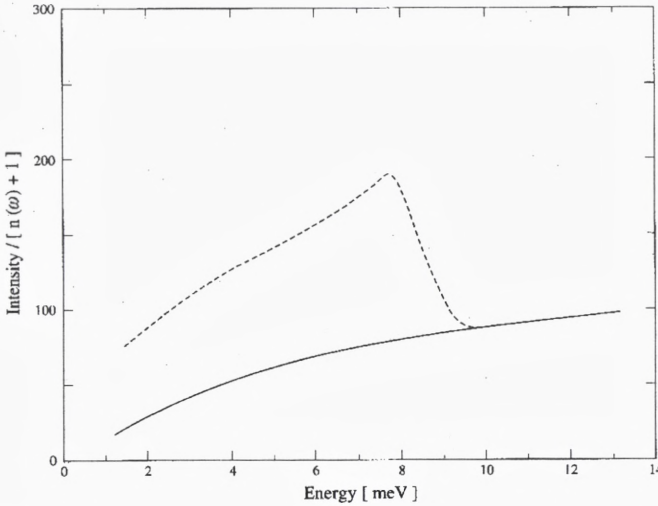
Figure 8. Anisotropy of spin fluctuations in the longitudinal-SDW phase of Cr: peak intensity for single-Q Cr in the longitudinal-SDW AF_2 phase at temperatures from 10 to 100 K, normalized by the thermal factor $[n(\omega) + 1]^{-1}$: ———— at $(2\pi/a)$ $(1-\delta, 0, 0)$ from longitudinal q-scans (see Fig. 11b); – – – – at $(2\pi/a)(\delta, 1, 0)$ from transverse q-scans (after Lorenzo et al., 1994).

conceived as lying on a a dispersion cone emanating, in the case of a single-Q sample with wave vector Q along x, from the incommensurate points at $\pm Q_x = (2\pi/a)$ $(1 \pm \delta)$, δ being the incommensurability parameter, as illustrated in the inset (b) of Fig. 11. Theory predicts that their velocity will be of the same order of magnitude as the Fermi velocity of the electrons and holes that condense to form the triplet pairs constituting the SDW. Experiments on CrMn alloys having a commensurate SDW seem to support this idea (see Table I in RMP I). There is, however, no clear evidence for such dispersion in pure Cr, though the inelastic scattering peaks at the satellites do increase in width roughly linearly with increasing energy (see Fig. 5 in Fukuda et al., 1996).

The spin-wave modes in the longitudinal-SDW phase have an unusual energy-dependent anisotropy, as illustrated in Fig. 8. For energy below, $E \leq 8$ meV, the excitations are predominantly longitudinal, while for higher energy they are isotropic. The intensity scaled by the thermal factor, $[n(\omega) + 1]^{-1}$, $n(\omega = E/\hbar)$ being the Bose-Einstein distribution function, is independent of temperature in the longitudinal-SDW phase. The analysis can be taken further (Lorenzo et al., 1994) by assuming a linear dispersion relation for the spin-wave mode, with the result that the longitudinal and transverse components of the dynamic susceptibility, $\chi_L(E)$
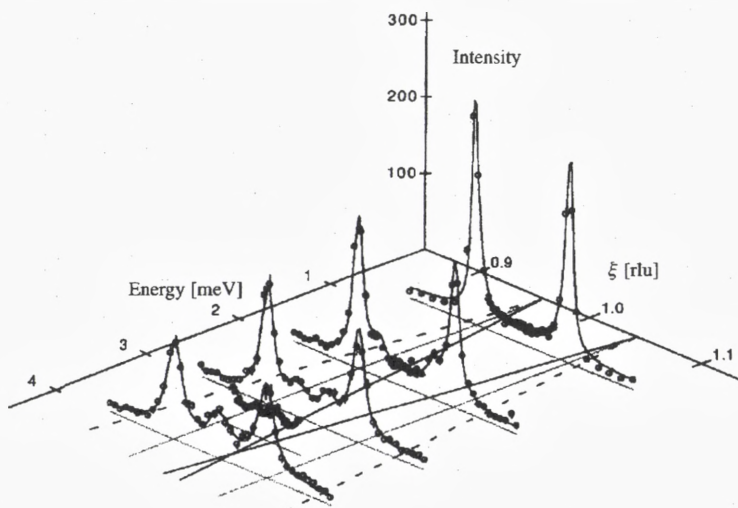
Figure 9. Fincher–Burke modes: longitudinal q-scans at constant energy, $E =$ 0.75, 2 ,3, 3.5 and 4 meV, along $(\xi, 0, 0)$ (the solid arrow in Fig. 3b) for single-Q Cr in the transverse-SDW phase at temperature 230 K. The peaks of intensity I (arbitrary units) are projected into the E–ξ plane: ——— the SDW satellites at $(2\pi/a)(1 \pm \delta, 0, 0)$; ——— the modes seen between the SDW satellites; – – – – the modes *not* seen outside the SDW satellites (after Sternlieb et al., 1993).

and $\chi_T(E)$, respectively, vary as the reciprocal of E. This is the same as for $\chi_T(E)$ for spin waves in an antiferromagnet having localized moments, but in this case, $\chi_L(E) = 0$. Burke et al. (1983) pointed out that longitudinal excitations, in the form of propagating crystal-field modes, are found in many rare-earth metals and compounds, but that no other case is known in 3d metals and alloys.

In the transverse-SDW phase, modes of excitation appear between the unresolved spin-wave peaks at $\pm Q_x = (2\pi/a)(1 \pm \delta)$ in a single-Q sample. These Fincher–Burke modes were first thought to have dispersion relations that are symmetric about $\pm Q_x$, having a velocity the same as that of the $(\xi, 0, 0)$ longitudinal phonons (Burke et al., 1983). As illustrated in Fig. 9, however, there is no evidence for inelastic scattering peaks for $\xi < -Q_x$ or $\xi > +Q_x$. Thus their identification as magneto-vibrational modes is incorrect.

Pynn et al. (1992) also found that the intensity of the 4 meV peak at $(2\pi/a)$ $(1, 0, 0)$, where the two modes intersect (see Fig. 9), increases in intensity with increasing temperature much faster than one would expect for a mode involving phonons. They used polarized neutrons and found that the scattering at this 4

meV peak involves spin fluctuations parallel to the polarization direction of the transverse SDW. The susceptibility $\chi_{FB}(E)$ of these modes, like the spin-wave modes in the longitudinal-SDW phase, varies as the reciprocal of the energy E (Lorenzo et al., 1994). These clues may help us to understand the origin of the Fincher–Burke modes.

Fishman and Liu (1996) have analyzed the low-energy magnetic excitations of the incommensurate-SDW phase of Cr. They find two Goldstone modes evolving from the incommensurate points, transverse spin waves, and longitudinal phasons. But their velocity is of the same order of magnitude as the Fermi velocity, about two orders larger than the Fincher–Burke modes. Thus the origin of the low-energy excitations remains a mystery.

At higher energies, in both the longitudinal- and transverse-SDW phase, a broad scattering peak develops at the commensurate point, $(2\pi/a)(1,0,0)$. Fukuda et al. (1996) find that this commensurate magnetic scattering (CMS), as illustrated in Fig. 10, increases with both energy E and temperature T, until it overwhelms the incommensurate scattering due to the spin-wave modes by $E = 40$ meV at $T = 54$ K in the longitudinal-SDW phase (Fig. 10a), or by $T = 235$ K at $E = 15$ meV in the transverse-SDW phase (Fig. 10h). In the longitudinal-SDW AF_2 phase the integrated intensity of the CMS increases roughly linearly with energy, whereas the intensity of the spin-wave mode peaks at $E \approx 20$ meV (see Fig. 6a in Fukuda et al., 1996).

This magnetic scattering at the magnetic-zone centre was first studied by the BNL group (Fincher et al., 1981; Grier et al., 1985), who described it as "commensurate-diffuse scattering" (CDS). It appeared to increase in intensity very rapidly as temperature approached the Néel transition, but this feature of the behaviour has been shown to be an instrumental artifact associated with the existence of the silent satellites (Sternlieb et al., 1995). The characteristic energy, $E \approx 4$ meV, of the CDS should also rather be considered as a feature of the Fincher–Burke modes (see Fig. 9). Thus we prefer to use the new acronym CMS, rather than CDS, to describe the broad high-energy scattering peak at the magnetic-zone centre. The latter may still however be the appropriate term for the scattering at the commensurate point seen in the paramagnetic phase at high temperatures, up to and beyond $2T_N$ (see Figs. 13 and 14 in Grier et al., 1985). Whether or not CMS and CDS are manifestations in different temperature regimes of the same modes of excitation will not be known until we have an explanation of commensurate scattering in Cr, whose origin is still a complete mystery.

Sternlieb et al. (1995) realized the significance for pure Cr of the existence in the paramagnetic alloy, Cr+5 at.%V, of spin fluctuations at the incommensurate points corresponding to the nesting vector Q' of the Fermi surface (Fawcett et al., 1988). One might expect to find a peak in the wave-vector dependent susceptibility $\chi(q)$ at
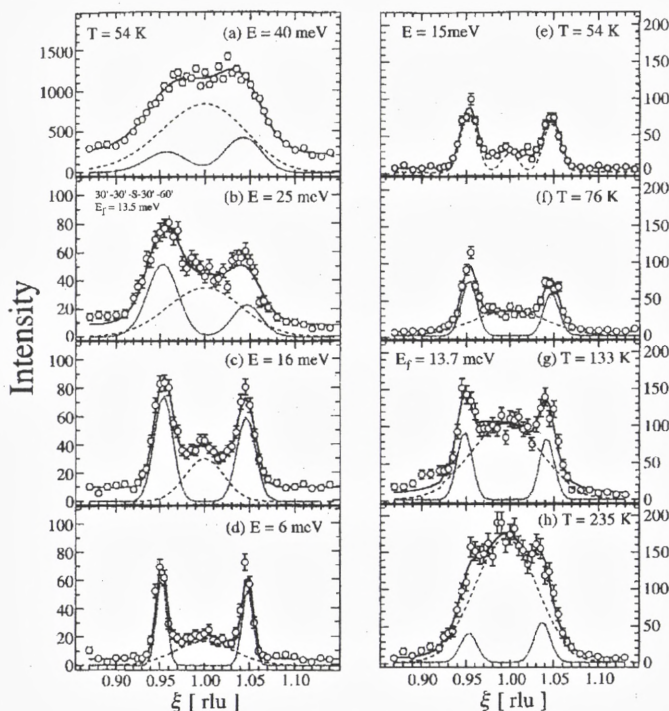
Figure 10. Commensurate Magnetic Scattering (CMS): longitudinal constant-E scans (the solid arrow in Fig. 3b) for single-Q Cr at various energies E at temperature, $T = 54$ K (panels a, b, c and d), and for various T at $E = 15$ meV (panels e, f, g and h). The dash and light lines are the CMS and incommensurate SDW components, respectively, which together with a constant background give the resultant solid line fit to the data (from Fukuda et al., 1996).

Q', which becomes a singularity corresponding to the onset of long-range magnetic order, i.e., a SDW with $Q \approx Q'$, when the V content is reduced to less than about 4 at.%V (RMP II). Thus, in a single-Q sample of Cr with $Q = (2\pi/a)(1 \pm \delta, 0, 0)$, the other two pairs of off-axis satellites at $(2\pi/a)(1, \pm\delta, 0)$ and $(2\pi/a)(1, 0, \pm\delta)$ might be expected to give rise to peaks in $\chi(q)$, with corresponding modes of excitation giving inelastic scattering at these points.

Figure 11 illustrates the experimental evidence for these silent satellites. As temperature increases towards the Néel temperature T_N, their intensity increases rapidly from very low values, until at T_N a discontinuous jump (corresponding to the first-order nature of the Néel transition in Cr) results in equal scattering at all six satellites corresponding to the cubic symmetry of the paramagnetic phase. Thus
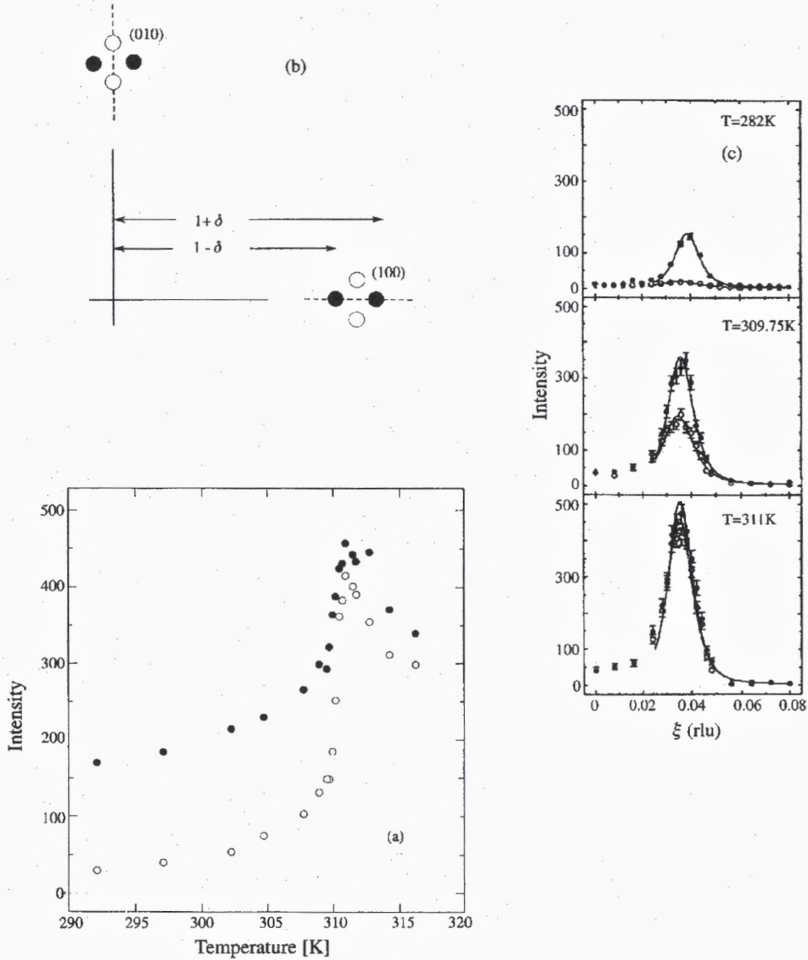
Figure 11. Silent satellites: (a) temperature dependence of the peak intensity for longitudinal scans at constant energy, $E = 0.5$ meV, for single-Q Cr: • corresponds to the q-scan ———— in inset (b); ○ corresponds to the q-scan — — — — in inset (b). Inset (c) shows the data for the complete q-scan close to the Néel temperature, $T_N = 310.3$ K, and at a temperature 28 K below T_N (after Sternlieb et al., 1995).

the Néel transition is driven by critical fluctuations at all six satellites, not just at the two at the wave vectors $\pm Q_x$ of the SDW. This picture of the relation between the spin-wave excitations and the critical fluctuations is unique to Cr, but its theoretical analysis should enlarge our general understanding of phase transitions.

The Chalk River group first recognized that the apparent commensurate-diffuse scattering in the paramagnetic phase, at least close to the Néel temperature and at low energies, is in fact an instrumental artifact (Noakes et al., 1990). Thus a constant-energy scan through the satellites at $Q = (2\pi/a)(1 \pm \delta, 0, 0)$ will pick up the off-axis satellites (the silent satellites in the case of a single-Q sample) if the momentum resolution transverse to the $(1, 0, 0)$ axis is poor as usually is the case. This does not of course preclude the existence of genuine commensurate modes of excitation at high energies in the ordered phase (Fig. 10) or at high temperatures in the paramagnetic phase (Grier et al., 1985).

Synchrotron radiation is a powerful tool for studying the charge-density wave that is present in Cr (Tsunoda et al., 1974; Pynn et al., 1976) and Cr alloys (RMP II). When x-rays of energy $\approx$ 10 keV are used, the technique is limited to the study of the surface of the sample, since they penetrate only to a depth of about 1 μm. This may account for the fact that in the measurements of Hill et al. (1995) the results corresponded to there being a single Q-direction, normal to the (100) surface of the sample, since residual strain from the mechanical polishing may have been sufficient to cause this effect. It may also have something to do with the failure thus far to see the CDW in any Cr alloys.

Conceptually there are two mechanisms a density wave in the charge distribution. First, the lattice may be periodically distorted, with each ion retaining its equilibrium charge: a strain wave. Second, there may be a periodic excess and deficit of charge on the sites of an undistorted lattice. In the CDW literature, these two effects are collectively referred to as a charge-density wave. Both produce x-ray diffraction peaks at $2Q$ and $4Q$. The dominant contribution to the x-ray scattering intensity arises from the core electrons of the ion, and thus corresponds to the strain wave. Mori and Tsunoda (1993) attempted to separate the two contributions, and claim that they found a small conduction-electron density wave in addition to the dominant contribution from the strain wave.

Hill et al. (1995) found that in Cr the intensities of elastic scattering due the the fundamental SDW and the second and fourth harmonic CDW had temperature dependence throughout both the AF_1 and AF_2 phases corresponding to mean-field theory.

Acknowledgements

References

Alberts HL and Smit P, 1997: Proceedings of the 1996 Yamada Conf., Physica B (In press)

Burke SK, Stirling WG, Ziebeck KRA and Booth JG, 1983: Phys. Rev. Lett. **51**, 494

Butylenko AK, 1989: Fiz. Met. Metalloved. **68**, 873 [Phys. Met. Metallogr. (USSR) **68**, 37 (1989)]

de Oliviera AJA, Ortiz WA, de Camargo PC and Galkin VYu, 1996a: J. Magn. Magn. Mater. **152**, 86

de Oliviera AJA, de Lima OF, de Camargo PC, Ortiz WA and Fawcett E, 1996b: J. Phys. Condens. Matter **8**, L403

Endoh Y, Mizuki J and Ishikawa Y, 1982: J. Phys. Soc. Jpn. **51**, 263

Endoh Y, 1996: (private communication)

Fawcett E, 1988: Rev. Mod. Phys. **60**, 209

Fawcett E, Werner SA, Goldman A and Shirane G, 1988: Phys. Rev. Lett. **61**, 558.

Fawcett E, and Galkin VYu, 1991: J. Phys. Condens. Matter **3**, 7167

Fawcett E, 1992: J. Phys. Condens. Matter **4**, 923

Fawcett E and Galkin VYu, 1992: J. Magn. Magn. Mater. **109**, L139

Fawcett E, Alberts HL, Galkin VYu, Noakes DR and Yakhmi JV, 1994: Rev. Mod. Phys. **66**, 25

Fawcett E, de Camargo PC, Galkin VYu and Noakes DR, 1997: Proceedings of the 1996 Yamada Conf., Physica B (In press)

Fawcett E, 1997: Proceedings of the 1996 Kumamoto Conf., Physica B (In press)

Fert A, Grunberg P, Barthelemy A, Petroff F and Zinn W, 1995: J. Magn. Magn. Mater. **140-144**, 1

Fincher JCR, Shirane G and Werner SA, 1979: Phys. Rev. Lett. **43**, 1441

Fishman RS and Liu SH, 1993: J. Phys. Condens. Matter **5**, 3959

Fishman RS and Liu SH, 1994: Phys. Rev. B **50**, 4240

Fishman RS and Liu SH, 1996: Phys. Rev. Lett. **76**, 2398

Fishman RS, Liu SH and Viswanath VS, 1997: Proceeding of the 1996 Yamada Conf., Physica B (In press)

Fukuda T, Endoh Y, Yamada K, Takeda M, Itoh S, Arai M and Otomo T, 1996: J. Phys. Soc. Jpn. **65**, 1418

Galkin VYu, 1987: Fiz. Met. Metalloved. **624**, 1199 [Phys. Met. Metallogr. (USSR) **64**, 150 (1987)]

Galkin VYu, 1989: J. Magn. Magn. Mater. **79**, 327

Galkin VYu and Fawcett E, 1993: J. Magn. Magn. Mater. **119**, 321

Galkin VYu, de Camargo PC, Ali N, Schaf J and Fawcett E, 1995: J. Phys. Condens. Matter **7**, L649

Galkin VYu, de Camargo PC, Ali N, Schaf J and Fawcett E, 1996a: J. Magn. Magn. Mater. **159**, 1

Galkin VYu, de Camargo PC, Ali N and Fawcett E, 1996b: J. Phys. Condens. Matter (in press)

Galkin VYu, de Camargo PC, Ali N and Fawcett E, 1997a: Proceedings of the 1996 Yamada Conf., Physica B

Galkin et al., 1997b: Proceedings of the 1996 MMM Conf., J. Appl. Phys. (In press)

Galkin et al., 1997c: Proceedings of the 1996 MMM Conf., J. Appl. Phys. (In press)

Grier BH, Shirane G and Werner SA, 1985: Phys. Rev. B **31**, 2882

Hayden SM, Doubble R, Aeppli G, Fawcett E, Perring TG, Lowden J, and Mitchell PW, 1997: Proceedings of the 1996 Yamada Conf., Physica B (In press)

Hamaguchi Y, and Kunitomi N, 1964: J. Phys. Soc. Jpn. **19**, 1849

Heinrich B, and Bland JAC (ed.), 1994: *Ultrathin Magnetic Structures* (Springer-Verlag, Berlin), Chapter 2

Hill P, Ali N, de Oliveira AJA, Ortiz WA, de Camargo PC and Fawcett E, 1994: J. Phys. Condens. Matter **6**, 1761

Hill JP, Helgesen G and Gibbs D, 1995: Phys. Rev. B **51**, L77

Katano S and Mori N, 1979: J. Phys. Soc. Jpn. **46**, 691

Koehler WC, Moon RM, Trego AL and Mackintosh AR, 1966: Phys. Rev. **151**, 405

Lorenzo JE, Sternlieb BJ, Shirane G and Werner SA, 1994: Phys. Rev. Lett. **72**, 1762

Maki S and Adachi K, 1979: J. Phys. Soc. Jpn. **46**, 1131

Møller HB and Mackintosh AR, 1965: Phys. Rev. Lett. **15**, 623

Møller HB, Trego AL and Mackintosh AR, 1965: Solid State Commun. **3**, 137

Mori M and Tsunoda Y, 1993: J. Phys. Condens. Matter **5**, L77

Muheim S and Müller, 1964: Phys. Kondens. Mater. **2**, 377

Nakanishi K, and Kasuya T, 1977: J. Phys. Soc. Jpn. **42**, 833

Noakes DR, Holden TM, Fawcett E and de Camargo PC, 1990a: Phys. Rev. Lett. **65**, 369

Overhauser AW, 1960: Phys. Rev. Lett. **4**, 226

Overhauser AW, 1962: Phys. Rev. **128**, 1437

Pynn R, Press W, Shapiro SM and Werner SA 1976: Phys. Rev. B **13**, 295

Pynn R, Stirling WG and Savering A, 1992: Physica B **180-181**, 203

Shibatani A, Motizuki K and Nagamiya T, 1969: Phys. Rev. **177**, 984

Smit P and Alberts HL, 1987: J. Phys. Chem. Solids **48**, 887

Sternlieb BJ, Shirane G, Werner A and Fawcett E, 1993: Phys. Rev. B **48**, 10217

Suzuki T, 1977: J. Phys. Soc. Jpn. **43**, 869

Trego AL and Mackintosh AR, 1968: Phys. Rev. **166**, 495

Tsunoda Y, Mori M, Kunitomi N, Teraoka Y and Kanamori J, 1974: Solid State Commun. **14**, 287

Tsunoda Y, 1997: Proceedings of the 1996 Yamada Conf., Physica B (In press)

Tugushev VV, 1992: in *Electronic Phase Transitions*, eds. by W. Hanke and Yu.V. Kipaev (Elsevier, New York/Amsterdam) p. 237

Volkov BA and Tugushev VV, 1984: Fiz. Tverd. Tela (Leningrad) **26**, 2428 [Sov. Phys. Solid State **26**, 1471 (1984)]

Two Recent Examples of X-Ray Magnetic Scattering Studies

Doon Gibbs

Department of Physics, Brookhaven National Laboratory,

Upton, New York, USA

Abstract

Recent results concerned with x-ray resonant magnetic scattering studies of the induced Lu magnetization in Dy-Lu alloys (Everitt et al., 1995) and of magnetic disordering of UO_2 surfaces (Watson et al., 1996) are reviewed.

1   Introduction

During the last 10 years, x-ray magnetic scattering techniques using synchrotron radiation have blossomed, especially in studies of rare earth metals and actinides, including bulk materials, thin films and compounds. These studies have especially benefited from the use of the resonance and polarization properties of the cross-section when the incident x-ray energy is tuned near an L or M absorption edge. Brief reviews of these techniques and recent applications may be found in Gibbs (1992) and Stirling and Lander (1992). Non-resonant magnetic scattering has also continued to develop, most notably in studies of transition element magnetism using incident photons of ≥ 40 keV (Schneider, 1995). In this case the enhancement to the signal comes from the increased penetration (up to cms) possible with high energy photons. Although the strengths of x-ray magnetic scattering techniques sometimes overlap those of neutron diffraction, they are generally complementary, and include high Q resolution, sensitivity to lattice modulations, small beam size and useful polarization and resonance properties. In the last 10 years x-ray magnetic scattering studies of the magnetic structure of rare earth and actinide materials (including thin films) have almost become routine (Hill et al., 1996; Detlefs et al., 1996; Helgesen et al., 1994, 1995). New kinds of experiments have been concerned with critical properties, characterized near magnetic ordering transformations (Nuttall et al., 1996; Thurston et al., 1994) and with the use of circularly polarized incident beams (Sutter et al., 1997).

In this proceedings, we briefly review recent experiments concerned with the induced Lu magnetization in Dy–Lu thin films (Everitt et al., 1995) and with the observation of surface magnetism in UO_2 (Watson et al., 1996; Ferrar et al., 1996).

2   Species sensitivity in Dy–Lu thin films

It is generally accepted that exchange interactions in the heavy rare-earth metals (Gd to Er) are indirect, arising through the agency of spin-density oscillations induced in the $5d$–$6s$ conduction bands by the localized $4f$ moments (Freeman, 1972). The conduction electron response peaks at a wave vector determined by nesting features in the Fermi surface and, in competition with the hexagonal crystal field, leads to the complex antiferromagnetic structures observed at low temperatures, including c-axis modulated, helical, cycloidal, and conical configurations (Cooper, 1972; Jensen and Mackintosh, 1991). Band structure calculations, indeed, give a good account of the periodicities observed near T_N (Evenson and Liu, 1969; Liu et al., 1971). However, direct evidence for the induced spin-density wave is sparse.

In early experimental work, Moon et al. (1972) were able to determine the conduction electron polarization in ferromagnetic Gd by subtracting from the observed neutron scattering intensity the component attributable to the half-filled $4f$ shell of Gd. Extra intensity was observed in low-order peaks which, when combined with the excess moment measured at saturation, yielded a map of the conduction electron polarization around each Gd ion and revealed its oscillatory nature. Similar methods have been used to map the magnetic response of non-magnetic Sc (Koehler and Moon, 1976) and Lu (Stassis et al., 1977) in a uniform field of order 6 T. In the case of Dy, which is of interest here, it is well known (Rhyne, 1972) that the saturation moment in the low-temperature ferromagnetic phase exceeds the 10 μ_B expected for the $^6H_{15/2}$ ground configuration by approximately 0.33 μ_B. The excess is usually attributed to the conduction electron polarization, and has been detected by means of x-ray resonant scattering (Hannon et al., 1988; Isaacs et al., 1989). However, the induced polarization of a non-magnetic atom has never been measured in the helimagnetic phase. These experiments demonstrate that it is possible to detect the conduction electron polarization induced on a non-magnetic atom in the helical phase of a rare-earth alloy by means of the resonant scattering of x-rays.

X-ray resonant magnetic scattering (XRES) (Hannon et al., 1988) is an element-specific technique that exploits the anomalous cross-section for x-ray scattering at an absorption edge. The XRES intensity is much larger, in general, than that of off-resonant scattering; the two processes also have different polarization characteristics. In the lanthanide series, the L_{III} edge lies in an energy range (7–10 keV)

that is convenient for diffraction studies. Near the edge energy, both dipole transitions from the $2p_{3/2}$ core level to unoccupied $5d$ states and quadrupole transitions to unoccupied $4f$ levels contribute significantly to the atomic form factor for x-ray scattering. Sensitivity to magnetic order arises from the differential occupancy of spin-up and spin-down states in the vicinity of the Fermi surface. Recently, studies of the binary magnetic-magnetic rare-earth alloys $Ho_{0.5}Er_{0.5}$ (Pengra et al., 1994) and $Ho_{0.5}Tb_{0.5}$ (Stunault et al., 1995) using this technique have been reported. For this work, the helimagnetic alloy $Dy_{0.6}Lu_{0.4}$ was chosen, which has been found via neutron scattering (Everitt et al., 1994) to order in a basal-plane spiral below 120 K. This alloy affords the opportunity to study the diffraction profiles at both the Dy (7.79 keV) and Lu (9.24 keV) L_{III} edges. Because Lu has a filled $4f$ shell, any scattered intensity that is resonant at the L_{III} edge must arise from magnetization of the $5d$ levels at the Lu site, and will therefore be a measure of the induced conduction electron polarization at the helimagnetic wave vector.

The elastic scattering cross-section for x-ray scattering from a single crystal is given by

$$\frac{d\sigma}{d\Omega} = r_0^2 \left| \sum_j e^{i\mathbf{Q}\cdot\mathbf{R}_j} f_j(\mathbf{Q}, \omega) \right|^2, \tag{1}$$

where r_0 is the classical radius of the electron; $\mathbf{Q} = \mathbf{k}_{in} - \mathbf{k}_{out}$, the photon momentum transfer; and $\hbar\omega$, the x-ray energy. The atomic scattering amplitude f_j consists of the usual Thomson contribution plus magnetic terms. The non-resonant magnetic amplitude may be written as

$$f_j^{\text{nonres}} = \frac{i\hbar\omega}{2mc^2}[\mathbf{L}_j(\mathbf{Q}) \cdot \mathbf{A} + 2\mathbf{S}_j(\mathbf{Q}) \cdot \mathbf{B}]; \tag{2}$$

the vectors $\mathbf{A}$ and $\mathbf{B}$ depend on the polarizations of the incoming and outgoing photons relative to their respective wave vectors. $\mathbf{L}_j(\mathbf{Q})$ and $\mathbf{S}_j(\mathbf{Q})$ are the Fourier components of the orbital and spin magnetization densities due to the jth atom (Blume, 1985; Blume and Gibbs, 1988). In a helimagnet, it has been shown (Gibbs et al., 1991) that the signal scattered from the σ to the π channel is due to the sum of orbital and spin densities.

The resonant scattering contributions are more complex (Hannon et al., 1988; Luo et al., 1993). The electric dipole contribution at the L_{III} edge has been treated in detail by Hannon et al. (1988) and can be approximated by

$$f_j^{E1,\text{xres}} = \frac{F_0}{E_{L_{III}} - \hbar\omega - i\Gamma/2} \left[\hat{\mathbf{e}}_{out} \cdot \hat{\mathbf{e}}_{in} \, n_h + i(\hat{\mathbf{e}}_{out} \times \hat{\mathbf{e}}_{in}) \cdot \hat{\mathbf{z}}_j P/4 \right]. \tag{3}$$

Here, F_0 includes the $2p_{3/2} \rightarrow 5d$ radial matrix element, $E_{L_{III}}$ is the edge energy, and Γ is the width of the resonance. The magnetic moment of the jth ion is parallel

to $\hat{\mathbf{z}}_j$. The first term, which depends on the number n_h of holes of both spins, does not reflect the magnetic order. The polarization factor can be written as

$$P = (n_{d\uparrow} - n_{d\downarrow}) - n_h\delta - \frac{n_h\Delta/2}{E_{L_{III}} - \hbar\omega - i\Gamma/2}, \qquad (4)$$

where $n_{d\uparrow} - n_{d\downarrow}$ is the net number of magnetized $5d$ electrons, δ depends on the difference in radial matrix elements for spin-up and spin-down electrons, and Δ is the exchange splitting. At this level of approximation, the magnetic reflections appear only as first-order satellites of the main Bragg peaks, and only in the $\sigma \to \pi$ channel.
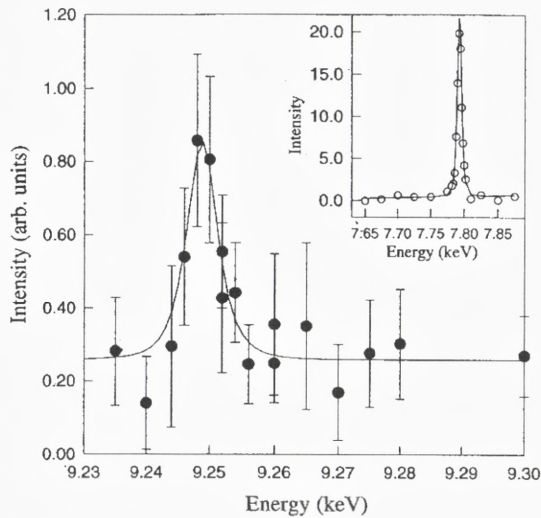
Figure 1. Q-integrated intensity of the $(0002+\tau)$ magnetic peak vs energy through the Lu L_{III} edge. Residual intensity is attributed to the non-resonant scattering from the Dy moments. Inset: The same, measured through the Dy L_{III} edge. An MgO(420) analyzer was used for both measurements. Lorentzian-squared curves with a FWHM of 7 eV have been fit to both data sets.

X-ray resonant magnetic scattering was observed at both the Dy and Lu edges in the $\sigma \to \pi$ geometry, consistent with dipole selection rules. The same crystal was used at both energies in order to compare directly the magnitudes of the resonant intensities. First-order helimagnetic satellites were detected about the (0002), (0004), and (0006) Bragg reflections of the alloy; they are designated as $(000\ell\pm\tau)$.

At low temperatures, these were separated from the Bragg peaks by $\tau \simeq 0.24$ reciprocal lattice unit (rlu), in agreement with earlier neutron scattering data from the same sample (Everitt et al., 1994). We focus mainly on the $(0002+\tau)$ magnetic reflection, since the resonant scattering is more intense than at the $(0004\pm\tau)$ or $(0006\pm\tau)$ reflections and the background is lower than at the $(0002-\tau)$ reflection. Figure 1 shows the Q-integrated intensity of the $(0002+\tau)$ peak at 10 K as the energy was scanned through the Lu L_{III} edge (main figure) and the Dy L_{III} edge (inset). The data are normalized to monitor counts, with the energy dependence of the monitor efficiency taken into account, and are corrected for the Lorentz factor. Polarization and Debye–Waller corrections, which amount to $\cong 1\%$ of the intensity each, were not applied. Absorption was also not taken into account. The presence of resonant magnetic scattering at the Lu edge demonstrates the existence of an induced moment on the Lu atoms. The $\sigma \to \pi$ character of the scattering shows that it occurs within the Lu $5d$ band. Estimates of the induced Lu moment obtained using Eqs. (3) and (4) give an SDW amplitude of ~ 0.2 μ_B.
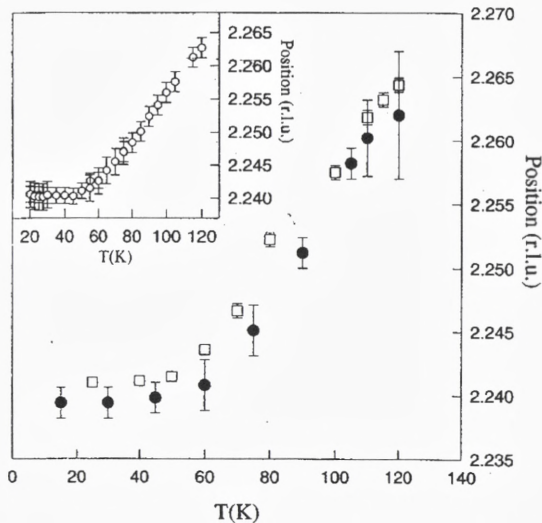
Figure 2. Magnetic wave vector τ in units of the c-axis reciprocal lattice vector, determined from the $(0002+\tau)$ peak. Solid circles: XRES data at the Lu edge in the $\sigma \to \pi$ configuration; squares: previous neutron scattering data. Inset: XRES data at the Dy edge, measured in the scattering plane, using a Ge analyzer for higher resolution. Below 60 K, a lock-in occurs to a value near 0.240 rlu.

Figure 2 shows the position of the $(0002+\tau)$ magnetic peak (filled circles) as a function of temperature, with the neutron scattering data of Everitt et al. (1994) superposed. The helimagnetic wave vector is $\cong 0.265$ $\mathbf{c}^*$ at the Néel temperature $T_N = 120$ K, and decreases with temperature before appearing to lock in to 0.240 ± 0.001 $\mathbf{c}^*$ ($\cong 6/25$) below $\simeq 60$ K. This may be seen more clearly in the inset to Fig. 2, where the position of the same reflection, measured at the Dy edge using a Ge(111) analyzer for better resolution, is plotted. This is a considerably tighter spiral than observed (Koehler, 1972) in bulk Dy, where the wave vector is 0.239 $\mathbf{c}^*$ at T_N decreasing to 0.147 $\mathbf{c}^*$ at the Curie temperature $T_C = 89$ K.

The temperature dependence of the $(0002+\tau)$ magnetic peak is shown in Fig. 3. In this figure, the Dy data were taken in the high-resolution mode (Ge analyzer) and the Lu data in the $\sigma \rightarrow \pi$ mode (MgO analyzer). Neutron scattering data are shown in the inset, for reference. Lines are drawn as a guide to the eye. These results show that the temperature dependence of the $5d$ magnetization density induced at the Lu and Dy sites follows that of the Dy $4f$ moments in the alloy.
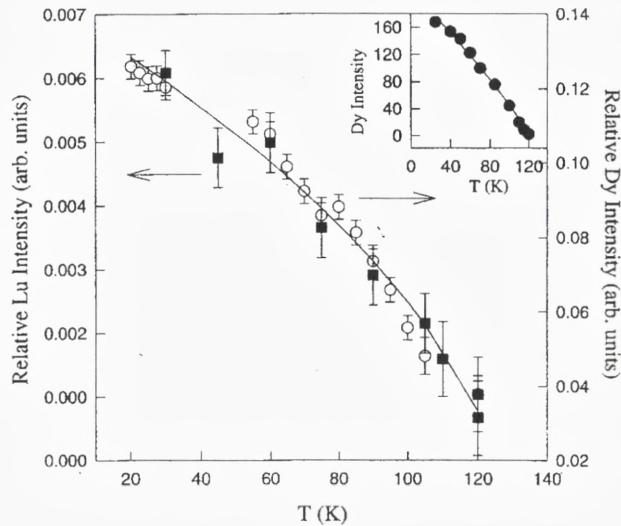
Figure 3. Temperature dependence of the $(0002+\tau)$ magnetic peak. Squares: Lu-edge data taken in the $\sigma \rightarrow \pi$ geometry; circles: Dy-edge data, taken in high resolution mode. Inset: Neutron diffraction data for the same sample.

3   UO$_2$ surfaces

In the last several years, there have been continuing efforts to probe long ranged magnetic order at surfaces by x-ray and neutron diffraction (Felcher et al., 1984; Usta et al., 1991; Kao et al., 1990; Fasolino et al., 1993; Bernhoeft et al., 1996; Stunault et al., unpublished; Watson et al., 1996), following many earlier studies by low energy electron diffraction (Palmberg et al., 1968; Dewames and Wolfram, 1969; Celotta et al., 1979; Alvarado et al., 1982; Dauth et al., 1987). The main motivation has been to discover how bulk magnetic structures are modified near a surface, where the crystal symmetry is broken. In this section, we describe synchrotron-based x-ray scattering studies of magnetic ordering near the (001) surface of the type-I antiferromagnet UO$_2$. Our aim in choosing UO$_2$ was twofold: first, to take advantage of its chemical inertness, which simplifies the preparation and handling of the surface; and second, to take advantage of the large resonant enhancements of the magnetic cross-section which occur when the incident photon energy is tuned near the uranium M_{IV} absorption edge (McWahn et al., 1990). We have found that it is possible to observe x-ray magnetic scattering from UO$_2$ surfaces at glancing incident angles (Watson et al., 1996) near the critical angle for total external reflection, with counting rates as high as 200 s^{-1} on a wiggler beam line. This has allowed characterization of the momentum transfer dependence of several magnetic (and charge) truncation rods along the surface normal. By tuning the incident x-ray energy through the M_{IV} edge, we have verified that the observed scattering is magnetic, and extracted forms for the variation of f' and f'' with x-ray energy. A most interesting result is that within about 50 Å of the surface, the temperature dependence of the magnetic scattering intensity decreases continuously near the Néel temperature $T_N = 30.2$ K and is well described by a power law in reduced temperature. In contrast, the bulk magnetic order parameter is well known to be discontinuous (Frazer et al., 1965; Willis and Taylor, 1965).

UO$_2$ has the face-centered cubic fluorite structure with a lattice constant of 5.47 Å at 300 K. The allowed chemical Bragg reflections are defined by H, K, and L either all even or all odd. The diffraction pattern of a crystal supporting a surface is characterized by rods of scattering (called truncation rods) which pass through the allowed bulk Bragg points and are parallel to the surface normal (see Fig. 4(a)). The variation of the x-ray intensity along the chemical truncation rods is determined by the decay of the electronic charge density near the surface (Feidenhans'l, 1989). The bulk magnetic structure of UO$_2$ is triple **Q**, consisting of ferromagnetic (001)-type planes stacked antiferromagnetically along each of the ⟨001⟩ directions. The magnetic bulk reflections are obtained by adding a ⟨001⟩ wave vector to each allowed chemical Bragg wave vector (see Fig. 4(a)). We may similarly define magnetic truncation rods (Fasolino et al., 1993), which pass through
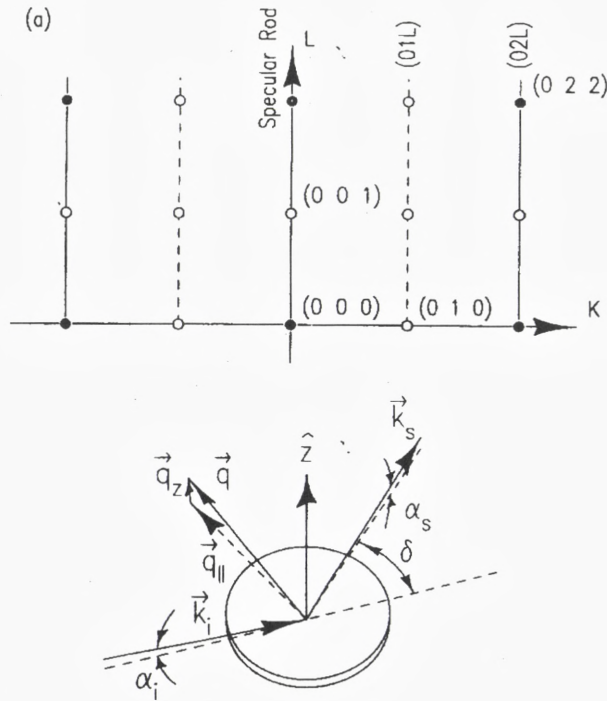
Figure 4. (a) Reciprocal space map for the UO$_2$ (001) surface showing chemical (solid circles) and magnetic (open circles) bulk Bragg reflections and mixed (solid lines) and magnetic (dashed lines) truncation rods. (b) Glancing-incidence scattering geometry. $\hat{z}$ is the surface normal direction, $\vec{k}_i$, $\vec{k}_s$, and $\vec{q}$ are the incident, scattered, and transferred wave vectors, respectively. $\vec{q}_z$ is the component of the momentum transfer normal to the surface.

the bulk magnetic reflections, and whose intensity variation depends on the decay of the magnetization density near the surface. For an antiferromagnet, this leads both to magnetic contributions to the chemical rods as well as to the existence of pure magnetic truncation rods when H and K are mixed (see Fig. 4(a)). The primary aim of the present experiments was to observe the (01L) magnetic rod.

The scattering geometry is illustrated in Fig. 4(b). Most of the experiments were carried out at glancing incidence, where the incident and exit angles of the x-ray beam to the surface are near the critical angle $\alpha_c \sim 0.75°$ for total external reflection. Near α_c, the refraction effects become important and lead to an enhancement of the transmitted beam. These effects are well understood (Feidenhans'l, 1989) and illustrated in the top of Fig. 5(a) where the intensity dependence
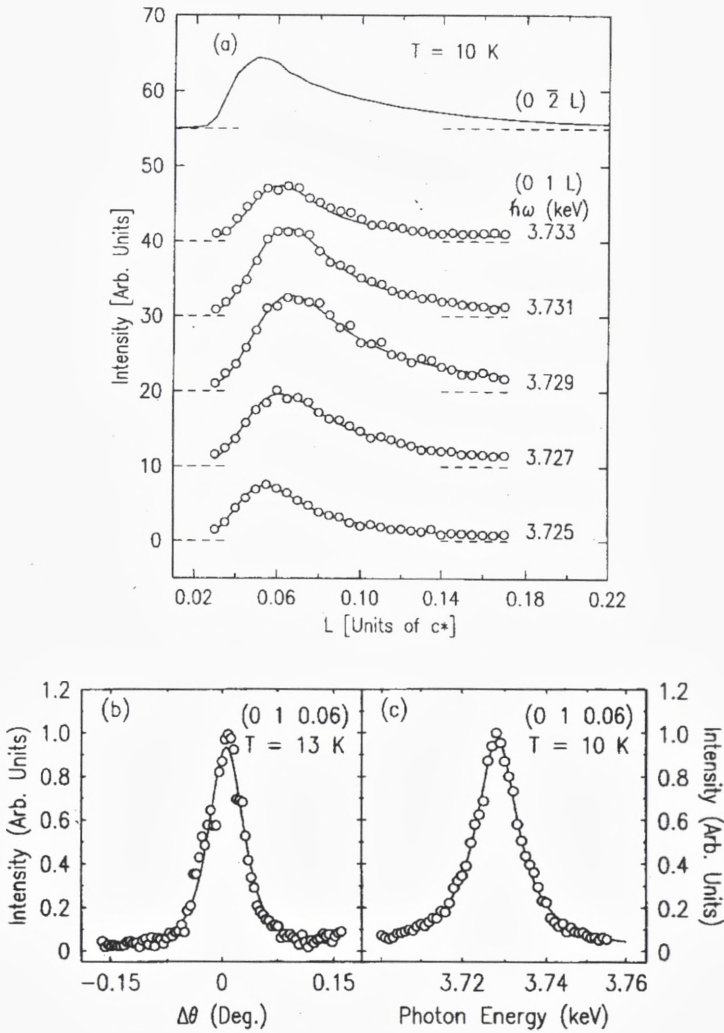
Figure 5. Intensity of the $(0\bar{2}L)$ charge (solid line, and $(01L)$ magnetic (open points) truncation rods as a function of L. The magnetic rod was obtained at five photon energies. The $(0\bar{2}L)$ rod was obtained with an incident photon energy of 3.728 keV. (b) Rocking curve of the magnetic truncation rod at $L = 0.06$. (c) Energy dependence of the intensity of the magnetic truncation rod at $L = 0.06$.

of the $(0\bar{2}L)$ charge scattering rod is shown. The intensity along the rod may be described by

$$I(k_i, k_s)/I_0 = (I/A_0) \mid T(\alpha_i) \mid^2 \mid T(\alpha_s) \mid^2 \left(\frac{d\sigma}{d\Omega}\right), \tag{5}$$

where A_0 and I_0 are the area and flux of the incident beam and $T(\alpha)$ is the usual Fresnel transmission amplitude for x rays at an angle α to the surface. $d\sigma/d\Omega$ is the cross-section for x-ray scattering and depends on the Fourier transform of the electronic charge density. Near the critical angle, the transmission coefficients exhibit maxima which lead to the peak observed in Fig. 5(a).

The lower curves in Fig. 5(a) show the intensity dependence of the pure magnetic scattering along the $(01L)$ rod, obtained as a function of incident photon energy. Their shapes are all qualitatively similar to that of the charge scattering. Rocking curves taken through the magnetic rod at $L = 0.06$ (see Fig. 5(b)) give full widths of $0.06°$, identical to that of the charge scattering rod, and close to the bulk mosaic. No variation in rocking width was observed along the rods. All of this indicates that the in-plane magnetic structure near the surface is well ordered at 10 K. The energy dependence of the magnetic intensity at fixed L is summarized in Fig. 5(c). The observed resonance is identical to that obtained in other uranium compounds and shows that the observed scattering is magnetic in origin.

We turn now to the temperature dependence of the magnetic scattering. Figure 6 shows the intensity plotted versus temperature as obtained at two positions along the magnetic truncation rod, (0,1,0.075) and (0,1,0.15), and at the bulk (001) reflection. From the measured dispersion corrections to the atomic form factors, it may be shown that these values of (HKL) correspond to penetration depths of ~ 50, ~ 120, and ~ 850 Å, respectively. The temperature dependence of the magnetic scattering at the (001) reflection exhibits the discontinuity at T_N expected from previous studies (Frazer et al., 1965; Willis and Taylor, 1965). In contrast, the magnetic scattering intensities obtained on the truncation rod fall more slowly to zero as T_N is approached from below. Indeed, they appear continuous. It is worth noting that the width of the magnetic truncation rods are temperature independent and, to within ± 0.5 K, the bulk and near surface ordering temperatures are equal. These results suggest that the magnetic structure *begins* to disorder at lower temperatures near the surface than in the bulk. This conclusion is similar to that obtained by Dosch and co-workers in their x-ray structural studies of the order-disorder transition in Cu_3Au (Dosch et al., 1988; Dosch and Peisl, 1989; Dosch et al., 1991; Reichert et al., 1995). In those experiments, the near-surface superlattice peak of the ordered alloy was found to decay continuously near T_0 (the order-disorder temperature), whereas the bulk behaviour was discontinuous. They interpreted their results in terms of surface-induced disordering, wherein a
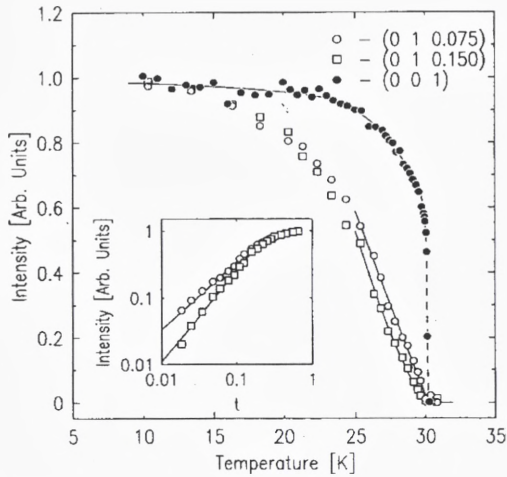
Figure 6. Magnetic intensities obtained at the (001) specular Bragg reflection (solid circles) and along the (01L) magnetic truncation rod at $L = 0.075$ (open circles) and 0.15 (open squares). They have been normalized to 1.0 at low temperatures. The solid lines represent best fits to a power law dependence on reduced temperature. The solid line for the (001) reflection is a guide for the eye. Inset: log–log plot of the magnetic scattering intensity at (0,1,0.075) and (0,1,0.15) vs reduced temperature.

partially disordered layer of crystalline phase wets the near-surface volume below T_0 and grows logarithmically in thickness as T approaches T_0. Surface-induced disorder was introduced for first-order transitions by Lipowsky (Lipowsky, 1982; Lipowsky and Speth, 1983) and has been discussed in many contexts since (Dietrich, 1988; Mecke and Dietrich, 1995, and references therein). Within Landau theory, these calculations yield regions of the phase diagram for which the order parameter at the surface is predicted to follow a power law in reduced temperature.

Motivated by these ideas, we have attempted a similar analysis in UO_2. Fits of the magnetic scattering intensity to a power law in reduced temperature, $I = At^{2S}$, where $t = (T_N - T)/T_N$, are shown for two values of L by the solid lines in Fig. 6. The fits are clearly satisfactory and yield exponents $S = 0.5 \pm 0.1$ at $L = 0.075$ and $S = 0.7 \pm 0.15$ at $L = 0.150$. Evidently, the exponents exhibit an L dependence, *increasing* for increasing δL (δL referred to the nearest Bragg peak), which differs from trends observed in Cu_3Au and from the predictions of Lipowsky's theory. More sophisticated models, for example, including a temperature-dependent width to the interface between the ordered and disordered magnetic regions (Lipowsky, 1987), have not resolved this distinction. In this regard, it is important to note

that the intensity measured along a truncation rod depends on the order parameter profile along the surface normal and reduces to the square of the average order parameter only when the atomic planes scatter in phase. Thus while our results are qualitatively consistent with the ideas of surface-induced disordering, a quantitative description of UO_2 remains lacking.

4   Conclusions

This proceedings has briefly reviewed two recent developments in x-ray scattering studies of magnetic materials. Ongoing efforts continue both in thin films and on surfaces, as well as in other areas not mentioned here for lack of space. The long term prospects for these techniques seem very exciting indeed.

5   Acknowledgements

References

Al Usta K et al., 1991: Physica B **173B**, 65
Alvarado SF, 1982: Phys. Rev. Lett. **48**, 51
Bernhoeft N et al., 1995: J. Magn. Magn. Mater. **140**, 1421
Blume M, 1985: J. Appl. Phys. **57**, 3615
Blume M and Gibbs Doon, 1988: Phys. Rev. B **37**, 1779
Celotta RJ, 1979: Phys. Rev. Lett. **43**, 728
Cooper BR, 1972: *Magnetic Properties of Rare-Earth Metals*, ed. R.J. Elliott (Plenum Press, London) Chap. 2
Dauth B et al., 1987: Surf. Sci. **189/190**, 729
Detlefs C et al., 1996: Phys. Rev. B **53**, 6355
Dewames RE and Wolfram T, 1969: Phys. Rev. Lett. **22**, 137
Dietrich S, 1988: *Phase Transitions and Critical Phenomena*, eds. C. Domb and J.L. Lebowitz (Academic, New York) **12**
Dosch H et al., 1988: Phys. Rev. Lett. **60**, 2382
Dosch H and Peisl J, 1989: Colloq. Phys. **50**, C7-257
Dosch H et al., 1991: Phys. Rev. B **43**, 13172

Evenson WE and Liu SH, 1969: Phys. Rev. **178**, 783

Everitt B et al., 1995: Phys. Rev. Lett. **75**, 3182

Everitt BA, Salamon MB, Flynn CP, Park BJ, Borchers JA, Erwin RW and Tsui F, 1994: J. Appl. Phys. **75**, 6592

Fasolino A et al., 1993: Phys. Rev. B **47**, 3877

Feidenhans'l R, 1989: Surf. Sci. Rep. **10**, 105

Felcher GP et al., 1984: Phys. Rev. Lett. **52**, 1539

Ferrar S et al., 1996: Phys. Rev. Lett. **77**, 747

Frazer BC et al., 1965: Phys. Rev. **140**, 1448

Freeman AJ, 1972: *Magnetic Properties of Rare-Earth Metals*, ed. R.J. Elliott (Plenum Press, London) Chap. 6

Gibbs D, 1992: Synchrotron Radiation News **5**, 18

Gibbs D et al., 1991: Phys. Rev. B **43**, 5663

Hannon JP, Trammel GT, Blume M and Gibbs D, 1988: Phys. Rev. Lett. **61**, 1245

Helgesen G, Hill JP, Thurston TR, Gibbs D, Kwo J and Hong M, 1994: Phys. Rev. B **50**, 2990

Helgesen G et al., 1996: Phys. Rev. B **52**, 9446

Hill JP, Sternlieb B, Gibbs D, Detlefs C, Goldman A, Stassis C, Canfield P and Cho B, 1996: Phys. Rev. B **53**, 3487

Isaacs ED, McWhan DB, Siddons DP, Hastings JB and Gibbs D, 1989: Phys. Rev. B **40**, 9336

Jensen J and Mackintosh AR, 1991: *Rare Earth Magnetism: Structures and Excitations* (Clarendon Press, Oxford)

Kao CC et al., 1990: Phys. Rev. Lett. **65**, 373

Koehler WC, 1972: *Magnetic Properties of Rare-Earth Metals*, ed. R.J. Elliott (Plenum Press, London) p. 81

Koehler WC and Moon RM, 1976: Phys. Rev. Lett. **36**, 616

Lipowsky R, 1987: Ferroelectrics **73**, 69

Lipowsky R, 1982: Phys. Rev. Lett. **49**, 1575

Lipowsky R and Speth W, 1983: Phys. Rev. B **28**, 3983

Liu SH, Gupta RP and Sinha SK, 1971: Phys. Rev. B **4**, 1100

Luo Jin, Trammell GT and Hannon JP, 1993: Phys. Rev. Lett. **71**, 287

McWahn DB et al., 1990 Phys. Rev. B **42**, 6007

Mecke KR and Dietrich S, 1995: Phys. Rev. B **52**, 2107

Moon RM, Koehler WC, Cable JW and Child HR, 1972: Phys. Rev. B **5**, 997

Nuttall WJ, Langridge S, Stirling WG, Lander GH, Lebech B and Vogt O, 1996: Phys. Rev. B (in press)

Palmberg PW et al., 1968: Phys. Rev. Lett. **21**, 682

Pengra DB, Thoft NB, Wulff M, Feidenhans'l R and Bohr J, 1994: J. Phys. Condens. Matter **6**, 2409

Reichert H et al., 1995: Phys. Rev. Lett. **74**, 2006

Rhyne JJ, 1972: *Magnetic Properties of Rare-Earth Metals*, ed. R.J. Elliott (Plenum Press, London) p. 131.

Schneider J, 1995: Synchrotron Radiation News **8**, No. 2, 26

Stassis C, Kline BR, Loong CK and Harmon BN, 1977: Solid State Commun. **23**, 159

Stirling WG, and Lander GH, 1992: Synchrotron Radiation News **5**, 17

Stunault A, Vettier C, de Bergevin F, Maier F, Grübel G, Galéra RM and Palmer SB, 1995: J. Magn. Magn. Mater. **140-144**, 753

Stunault A, Langridge S, Vettier C, Gibbs D and Bernhoeft N, 1996: Phys. Rev. B (in press)

Sutter C, Grübel G, Vettier C, de Bergerin F, Stunault A, Gibbs D and Giles C, 1997: Phys. Rev. B (in press)

Thurston T, Helgesen G, Hill JP, Gibbs D, Gaulin BD and Simpson P, 1994: Phys. Rev. B **49**, 15730

Watson GM et al., 1996: Phys. Rev. Lett. **77**, 751

Watson GM et al., 1996: Physica B **221**, 405

Willis BTM and Taylor RI, 1965: Phys. Lett. **17**, 188

Neutron Scattering from Disordered and Fractal Magnets

Hironobu Ikeda

Booster Synchrotron Utilization Facility,

National Laboratory for High Energy Physics,

Oho 1-1, Tsukuba 305, Japan

Abstract

Over a period of twenty years, studies concerning disordered magnets, in which transition metals
are considered to carry magnetic moments, have been performed using neutron-scattering tech-
niques. This research field has been rich for testing theories of phase transitions and excitations
in random magnetic systems; neutron experiments continue to provide crucial tests of theories
and new challenges for theoretical work. We describe recent neutron-scattering studies on these
system, which reveal the properties of the excitations and phase transitions of disordered systems.
Special attention is paid to the very recent neutron-scattering studies on percolating magnets with
a fractal geometry.

1   Introduction

In recent years random or disordered magnetic systems have attracted great interest
among theoretical and experimental physicists. These are spin glasses, amorphous
magnets, diluted magnets, random-field magnets, mixed antiferromagnets with two
different magnetic species, and random systems of two magnetic species with com-
peting spin anisotropies. In all these problems neutron scattering has played an
important role, since from observations of the scattering function, which is the
space-time Fourier transform of the spin pair-correlation function, one can obtain
detailed information concerning the structural and dynamical properties of these
systems, such as the order parameter, critical fluctuations, collective or localized
magnetic excitations and diffusive spin motions.

Very recently, much attention has been paid to the static and dynamical prop-
erties of diluted magnets, whose magnetic concentration is very close to the per-
colation concentration. It is generally accepted that the atomic connectivity of
a percolating cluster takes the form of a fractal (Stanley, 1977). The theory of

percolation has been formulated by many authors, and can now be used to interpret an exceptionally wide variety of physical and chemical phenomena, such as the gelation process (de Gennes, 1979), transport in amorphous materials (Zallen, 1983), and hopping conduction in a doped semiconductor (Shklovskii and Efros, 1984). The concept of fractals has contributed significantly to our understanding of percolation (Nakayama et al., 1994). The simplest ideal percolating networks are realized by substitutionally diluting magnetic systems by non-magnetic atoms. At a critical magnetic concentration c_p, a single infinite cluster (a percolating network) spans the full space; with a further decreasing concentration of magnetic atoms, the system splits into an assembly of only finite clusters. The percolating networks exhibit a self-similarity, and can be characterized by a non-integer mass dimension, i.e., a fractal dimension D_f. In a square and a simple cubic lattice, it has been numerically estimated that the D_f of the percolating network is 1.896 and 2.48 respectively, i.e., D_f is less than the Euclidian dimension D (Nakayama et al., 1994).

In this report, we present recent results concerning neutron-scattering experiments on two- and three-dimensional (2D and 3D) percolating antiferromagnets: a direct observation of the self-similarity of the magnetic order in a percolating cluster (Ikeda et al., 1993), and investigations of the magnetic fracton excitations in a percolating Heisenberg antiferromagnet (Ikeda et al., 1994), the observation of anomalous spin diffusion in a percolating cluster (Ikeda et al., 1995), and the observation of the ordering kinetics in a percolating Ising antiferromagnet (Ikeda et al., 1990).

2 Fractal structure and magnetic Bragg scattering

The scattering law for the fractal structure, which is observed by neutrons or photons, is quite simple. The small-angle neutron scattering intensity $I(q)$ is simply proportional to q^{-D_f}, where q is the wave vector. This relationship was actually observed by small-angle neutron scattering from silica aerogels (Vacher et al., 1988). However, an experimental observation of the self-similarity of the percolating network in diluted magnets was successful only recently.

Very recently, we achieved the first experimental observation of the fractal structure in diluted antiferromagnets (Ikeda et al., 1994). In the vicinity of the percolation threshold, the geometrical correlation length ξ_G is defined as $\xi_G = a_0 |c - c_p|^{-\nu_G}$, where ν_G is a numerical constant which depends on the lattice shape, and a_0 is the nearest-neighbour lattice spacing. It is now believed that this system is a fractal at length scales smaller than ξ_G; conversely, the system appears to be homogeneous at length scales larger than ξ_G. The geometrical corre-

lation length ξ_G is related to the crossover wave vector by $q_c = \xi_G^{-1}$. The systems in which the magnetic concentration c is very close to, or just above, the percolation threshold, order antiferromagnetically at low temperatures. The magnetic elastic scattering of neutrons from an infinite cluster in these systems, at the antiferromagnetic superlattice position, can be written as: $I(q) \propto \delta(\mathbf{Q} - \boldsymbol{\tau})$ for $q < q_c$, and $I(q) \propto q^{-D_f}$ for $q > q_c$; here, $\mathbf{q} = \mathbf{Q} - \boldsymbol{\tau}$, and $\mathbf{Q}$ and $\boldsymbol{\tau}$ are the scattering vector and the antiferromagnetic reciprocal vector, respectively. Below the transition temperature, spins belonging to the infinite network order magnetically, while those belonging to only finite clusters do not order, even at 0 K. It is important to note that magnetic correlations between an infinite cluster and finite clusters are absent due to a lack of magnetic interactions between them. This makes possible an observation of the fractal structure of an infinite cluster by a high-resolution measurement of the elastic-scattering profile near to the magnetic reciprocal point.

Our experiments were performed on a 2D diluted Ising antiferromagnet $Rb_2Co_cMg_{1-c}F_4$ ($c = 0.60$), whose magnetic concentration (0.60) is very close to the percolation threshold of a square lattice (0.593). The pure Rb_2CoF_4 system becomes antiferromagnetic at $T_N = 102.96$ K with the spin direction along the c-direction and alternating in the basal c-plane (Hutchings et al., 1982). The magnetic-exchange interaction dominates within the plane and is limited to the nearest neighbours. The measured Néel temperature of a $c = 0.60$ sample was 20.0 K, and the observed rounding of the transition was less than 1 K; hence, variations in the Co concentration are within $0.599 < c < 0.601$. Using the value of ν_G (1.33) for a square lattice system we can estimate the geometrical correlation length $\xi_G \approx 730\ a_0$ for $c = 0.60$, which implies a crossover wave vector q_c of 3.1 $\times 10^{-4}\ 2\pi/a$, where a ($\sqrt{2}\,a_0$) is taken as the unit length of the [1 0 0] direction. This sample is then expected to reveal a crossover at q_c, from a homogeneous structure at low q to a self-similar fractal structure at large q. Neutron elastic scattering experiments were performed on a triple-axis spectrometer (T1-1) installed at the thermal-neutron beam guide of the JRR-3M reactor at JAERI, Tokai. This was used in the triple-axis operation mode with the energy transfer fixed at 0 meV and with pyrolytic graphite crystals used as both the monochromator and analyzer. Collimations were open-10'-10'-20' with incident energies of 13.7 meV. Higher-order contamination was eliminated by using a pyrolytic graphite filter. The crystal was oriented with its [0 0 1] axis vertical; the magnetic elastic scattering as a function of the wave vector along the [1 0 0] direction was measured at the (1 0 0) magnetic reciprocal position. The momentum-resolution width along the [1 0 0] direction was 0.0095 $2\pi/a$ at the full width at half maximum (FWHM). The scattered intensities $I(q)$ were corrected for a small, but constant, instrumental background.

Figure 1 shows the magnetic intensity distribution (plotted in a semi-logarithmic scale) measured from $Rb_2Co_{0.60}Mg_{0.40}F_4$. The intensity is shown as a function of

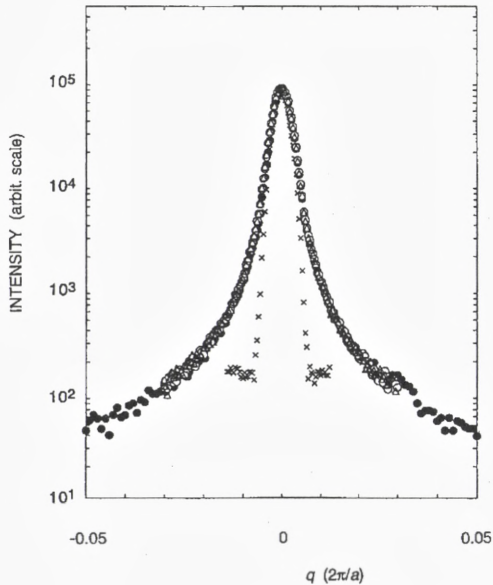Figure 1. Scattered neutron intensities for $Rb_2Co_{0.60}Mg_{0.40}F_4$ near to the $(1\,0\,0)$ antiferromagnetic reciprocal position measured at 4.5 K (solid circles), 7.5 K (open circles), 10 K (triangles) together with the instrumental resolution (crosses) in a semi-logarithmic plot.

q at $T = 7.5$ K (open circles) together with the instrumental resolution function (crosses). Below the transition temperature ($T_N = 20$ K) of this sample, three kinds of scattering contribute to the observed intensity. One is from the ordered pattern of the infinite network; the others are both from the critical magnetic fluctuations in an infinite cluster and thermal fluctuations in finite clusters. The line shape of the former is independent of the temperature, and takes the form of a δ-function if the system is homogeneous. The latter contribution is strongly temperature dependent with regard to both the intensity and the line width, as is well established. The absence of a temperature dependence in the scattering well below T_N (data at 4.5, 7.5 and 10 K in Fig. 1) indicates that the measured intensity is only from the ordered magnetic structure. This is due to the fact that the critical scattering in a 2D Ising system decreases very rapidly with decreasing temperature, and is clearly negligible at these temperatures. A remarkable feature of the line shape observed in the near-percolating system, $Rb_2Co_{0.60}Mg_{0.40}F_4$, is the very large width of the peak. This should be compared with the intrinsic δ-function peak arising from the antiferromagnetic long-range order (LRO) convoluted by the Gaussian resolution function (crosses in Fig. 1).

The data taken at 7.5 K were plotted in a double-logarithmic scale. The slope of the observed intensity versus the wave vector at $q > 0.01 \, 2\pi/a$ is 1.95 ± 0.07. This value is in good agreement with the fractal dimension ($D_f = 1.896$) of an infinite cluster in a 2D percolating network. In the $c = 0.60$ sample, since the length scale expands to 730 a_0, a very large intensity from the self-similar fractal structure is observed over a large q region, as shown in Fig. 1. At q less than 0.005 $2\pi/a$, the Gaussian peak shape due to the magnetic long-range order is evident. Crossover from a homogeneous structure at small q to a fractal structure at large q is clearly seen in this figure. From similar experiments with different magnetic concentrations, we observed that the q values at which the scattering deviates from the Gaussian shape increases with increasing Co concentration. The observed crossover region in each sample with different concentrations is consistent with the estimated value of q_c mentioned earlier. This provides the first direct experimental observation of the self-similar structure of an infinite cluster in a diluted magnet close to the percolation threshold.

From the present experimental results we can directly conclude that the magnetic LRO below the second-order phase transition temperature is not always described by a δ-functional form in reciprocal lattice space. The self-similar fractal structure can be observed within a reasonable length scale in the simplest physical realization of a fractal system: a diluted antiferromagnet close to the percolation threshold.

3   Fracton excitations in a Heisenberg antiferromagnet

In recent years, considerable attention has been directed towards the dynamical properties of highly ramified percolating networks that exhibit a fractal geometry (Orbach, 1986). Recent theories and computer simulations of these systems predict the existence of highly localized fracton excitations with huge oscillation amplitudes (Alexander and Orbach 1982; Nakayama et al., 1994). A random site-diluted Heisenberg antiferromagnet is an ideal system for probing the existence of these excitations. In such a system and at concentrations close to, but just above, the percolation threshold there should be a crossover from long-wavelength spin-wave excitations to short-wavelength fracton excitations. The origin of this crossover is the fact that the fractal geometry is realized only at length scales shorter than the geometrical correlation length ξ_G (Stauffer, 1979). Magnetic excitations in diluted magnetic systems have been extensively studied using neutron inelastic scattering techniques (Cowley, 1981). However, a renewed experimental effort has recently been initiated to characterize the fractal component of the dynamics in these di-

luted magnetic systems. For this, it is important to distinguish fracton excitations from other localized excitations, such as Ising-like cluster excitations.

We have recently performed an experiment aimed to give the first quantitative measurement of fracton excitations in near-percolating Heisenberg systems (Ikeda et al., 1994). For this experiment we have chosen a diluted pure-Heisenberg antiferromagnet ($RbMn_{0.39}Mg_{0.61}F_3$), in which the Mn concentration (0.39) is very close to the percolation threshold ($c_p = 0.312$). The corresponding cross-over wave vector is $q_c = \xi_G^{-1} = 0.024$ reciprocal lattice units (rlu). The excitations with wave vectors smaller than q_c are expected to be spin waves, while the excitations with wave vectors larger than q_c are expected to be fractons. Since q_c in the present system is very small, the fracton region is observable in such an experiment.

Our experiment was performed on a single crystal (about 1 cm^3 in volume) of $RbMn_{0.39}Mg_{0.61}F_3$. The pure system $RbMnF_3$ has a cubic perovskite structure and becomes antiferromagnetic at $T_N = 82$ K with the spin directions alternating along the cubic edges. The $RbMn_{0.39}Mg_{0.61}F_3$ sample orders at 18 ± 1 K with the same magnetic configuration as in the pure system. The inelastic scattering measurements were performed on a triple-axis spectrometer installed at the HFIR reactor at the Oak Ridge National Laboratory (ORNL). The crystal was oriented with its [0 1 -1] axis vertical. The magnetic excitations were measured for wave vectors along the [0 1 1] direction from the ($\frac{1}{2}$ $\frac{1}{2}$ $\frac{1}{2}$) zone center ($q = 0$), to the zone boundary ($q = 0.375$ rlu).

Figure 2 shows the energy spectrum of the magnetic response, taken at 4.5 K, at the zone boundary corrected for instrumental background. As depicted in the figure, a fine structure due to the Ising-cluster excitations in this system appears. The vertical bars in the figure give the probability density of random populations of magnetic neighbors for $c = 0.39$. The energy values at the peaks agree with the Ising-cluster energies of Mn^{2+} ions when an exchange constant of $J = 0.30$ meV is used. No measurable intensity is expected at the highest position of 9.0 meV ($z = 6$) due to the small probability for 6 magnetic neighbors. It should be noted, however, that the observed magnetic response extends beyond 8 meV where no magnetic intensities from the cluster excitations are expected. This observation indicates that the energy spectrum at the zone boundary, in this system, cannot be described solely by a simple Ising-cluster model. Since the energy resolution (1.0 meV FWHM) is finer than the peak interval (1.5 meV), the contribution from the cluster excitations can be resolved from the additional magnetic scattering. This additional magnetic contribution is indicated by the dotted line in Fig. 2.

The energy spectra obtained at several wave vectors from $q = 0$ to 0.375 rlu (ZB) reveal that the observed line shapes are not smooth, but have some small structure, originating from the cluster excitations, throughout the Brillouin zone. Also, over the entire Brillouin zone the energy spectrum of the additional contribution shows
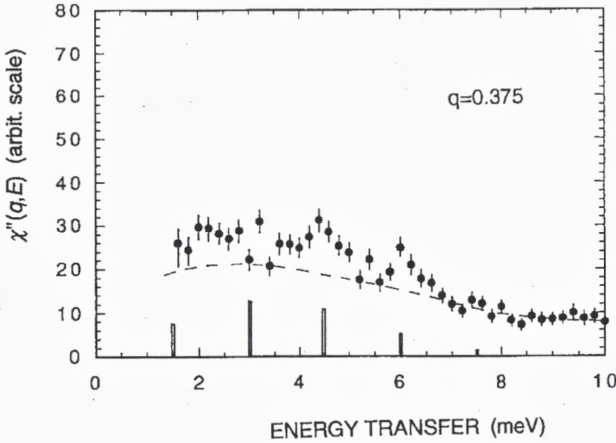
Figure 2. Magnetic response $\chi''(q, E)$ of $RbMn_{0.39}Mg_{0.61}F_3$ observed at the zone boundary at 4.5 K with an energy resolution of 1.0 meV. The vertical bars indicate the probability density of random populations of magnetic neighbours. The dotted line represents the additional magnetic contribution and also the fitted scattering function described in the text. Vertical bars represent error bars.

a very broad, smooth shape, and its magnetic response extends to the highest energies measured in our experiment (10 meV). The energy width of this spectrum is much broader than the energy resolution. As the wave vector increases, the intensity of the scattered neutrons decreases rapidly.

We have analysed the line shape of the magnetic response of an additional magnetic contribution obtained at 4.5 K. From a physical point of view, a damped harmonic oscillator (DHO) would be the most reasonable model to fit these excitations. We therefore fitted the broad excitation data to the functional form $\chi''(q, E) = A\Gamma(q)E/[(E^2 - E_p(q)^2)^2 + (\Gamma(q)E)^2]$, where A is a constant. This form was successfully fitted to all of the data. The fitted values of $E_p(q)$ and $\Gamma(q)$ as a function of q satisfy the power-law relationship with the same exponent, i.e., $E_p(q) \propto \Gamma(q) \propto q^{1.1\pm0.2}$. It should be noted that since the value of $\Gamma(q)$ is much larger than $E_p(q)$, the excitations are strongly over-damped over the entire Brillouin zone. It has been recently reported that the single length-scale postulate (SLSP) holds for the magnetic response from fractons (Nakayama et al., 1994). This postulate states that the peak energy and the energy width should have the same wave-number dependence as q^{z_a}, i.e., $E_p(q) \propto \Gamma(q) \propto q^{z_a}$. The present result is in accord with this theory.

A similar analysis using a DHO form has been performed in the nearly perco-
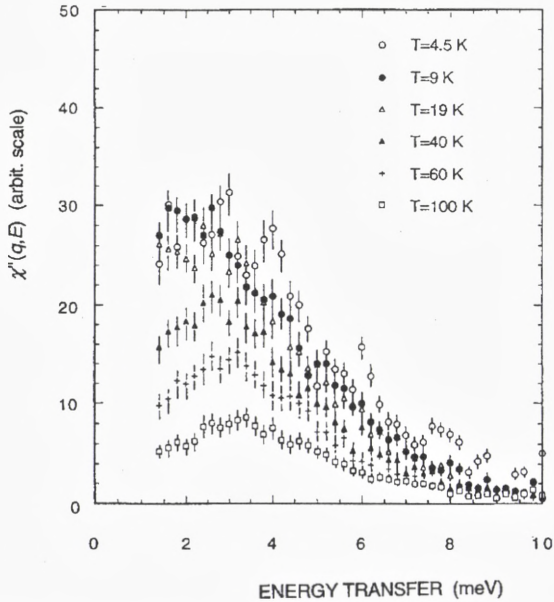
Figure 3. Temperature variation of $\chi''(q, E)$ at $q = 0.2$ as a function of energy transfer observed at $T = 4.5$ K (open circles), 9 K (closed circles), 19 K (open triangles), 40 K (closed triangles), 60 K (crosses) and 100 K (open squares). Vertical bars represent error bars.

lating antiferromagnet $Mn_{0.32}Zn_{0.68}F_2$ by Coombs et al. (1976). We presume that their over-damped signal might have contained contributions from both fracton and Ising-cluster excitations, although a separation of these was not pursued.

Another evidence for fractons is seen in the temperature variation of $\chi''(q, E)$ at wave vectors larger than q_c. In Fig. 3, the energy spectra at $q = 0.2$ rlu obtained from $T = 9$ K to 100 K are shown. At $T = 9$ K ($T_N/2$), peaks from Ising-cluster excitations almost disappear due to the much more enhanced thermal fluctuations of the molecular fields than at $T = 4.5$ K. On the other hand, the over-damped component is predominant at this temperature, and the line shape is the same as that measured at $T = 4.5$ K. In this figure we observe the remarkable fact that the over-damped component can survive even at $T = 100$ K ($> 5\ T_N$), and the peak energy slightly shifts towards higher energies with increasing T. These are completely different from the traditional spin-wave excitations in the Heisenberg system. The increase in the peak energy could be related to the localized nature of fractons, and thus the excitation energy (oscillating frequency) could be increased by obtaining the thermal energy.

On the other hand, high-resolution inelastic neutron-scattering studies have recently been performed on a three-dimensional (3D) diluted near-Heisenberg anti-ferromagnet ($Mn_{0.5}Zn_{0.5}F_2$) by Uemura and Birgeneau (1986, 1987). They ascribed the asymmetry of the obtained spectra and the double-peak structure at small wave vectors to the coexistence of magnons and fractons, and its wave-vector dependence to the magnon-fracton crossover. This interpretation should be taken with caution, however, because the magnetic concentration of the system that they studied (0.5) is far above the percolation threshold ($c_p = 0.245$ or less for a body-centered tetrag-onal lattice). At this relatively high magnetic concentration it is difficult to obtain conclusive evidence of fractons, since the system is not self-similar, even at small length-scales.

Our arguments, based on the DHO function, are qualitatively in good agreement with the current theory for fractons, although a quantitative description of the physical properties of the antiferromagnetic fractons in a Heisenberg system has not yet been completely resolved. We hope that an accurate description, even for the magnetic response function itself, will be available in the near future from analytic theories and/or computer simulations.

4 Anomalous diffusion and self-correlation function

The observation of a single-spin diffusive motion on a percolating network hav-ing fractal geometry has been a long-standing problem concerning the dynamical properties of percolation (Aeppli et al., 1984). In uniform systems, the mean-square displacement of a random walker $\langle R^2(t) \rangle$ is proportional to the time t, $\langle R^2(t) \rangle \propto t$, for any Euclidean dimension. In percolating systems with fractal ge-ometry, the diffusion is anomalous, and the mean-square displacement is described by $\langle R^2(t) \rangle \propto t^{2/(2+\Theta)}$ ($\Theta > 0$) (Gefen et al., 1983). Here, Θ is defined using the critical exponents β, ν and μ, where β describes the probability of a site belonging to the infinite network and ν and μ represents the average size and the average mass (number of sites) of finite clusters as a function of the concentration, respec-tively. These exponents were numerically estimated and for a 2D system Θ is 0.871 (Havlin and Bunde, 1991). This causes a slowing down of the diffusion of a spin due to the irregular path-structure of a fractal.

In order to observe anomalous spin diffusion using neutron scattering, the fol-lowing considerations were made: (1) The diffusion of spins on percolating net-works can be observed by neutron magnetic scattering. (2) Slow diffusion requires a very high energy-resolution, particularly in a 2D system. (3) An observation of the self-correlation function $\langle S_0(0)S_0(t) \rangle$ (where the subscript 0 refers to the

lattice site) is essential for studying anomalous diffusion due to the single-spin nature of motions. This quantity is inversely proportional to the volume $V(t)$ which can be occupied by a single spin during time t. That is, $\langle S_0(0)S_0(t)\rangle \propto V(t)^{-1} \propto R(t)^{-D_f} \propto t^{-D_f/(2+\Theta)}$, where D_f is the fractal dimension; for a square-lattice system it has been numerically estimated that D_f of a percolating network is 1.896. A Fourier transform of this quantity gives the following relationship: $S(E) = \int \langle S_0(0)S_0(t)\rangle \, e^{-iEt} \, dt \propto E^{D_f/(2+\Theta)-1}$. This quantity is obtained by integrating the generalized scattering function $S(q, E)$ over q. (4) Since $D_f/(2+\Theta) - 1 = -0.34$ the form of $S(E)$ exhibits a long tail, which makes it distinguishable from the tail of the Lorentzian lineshape, which is typical for critical magnetic scattering.

Neutron inelastic-scattering experiments were performed using the IRIS spectrometer at the ISIS pulsed spallation neutron source in Rutherford Appleton Laboratory (RAL), UK (Ikeda et al., 1995). IRIS is an inverted geometry spectrometer in which the neutrons scattered from the sample are energy-analyzed by being Bragg diffracted by large-area arrays of single crystals of mica and pyrolytic graphite (Carlile and Adams, 1992). For the experiment detailed here the $(0\,0\,4)$ reflection of the mica analyzer bank was used with an energy resolution of 4 μeV and a fixed final energy of 0.832 meV. The mica detector bank has 51 separate elements covering a 2θ-range of 25° to 155°. Inelastic signals can thus be observed simultaneously over a wide-range of momentum transfer with a high energy-resolution. The energy-transfer range covered in these experiments was -0.15 meV (neutron energy gain) to $+0.15$ meV (neutron energy loss).

The sample used in the present experiments was a 2D square-lattice antiferromagnetic insulator diluted by non-magnetic Mg atoms, $Rb_2Co_{0.6}Mg_{0.4}F_4$. The spins ($S = 1/2$) in the material are localized, and it is the diffusion which is observed. The Co concentration is very close to, but slightly above, the percolation threshold (0.593). The magnetic-exchange interaction dominates within the plane, and is limited to the nearest neighbors. A large single-crystal (diameter 30 mm and height 12 mm) sample of $Rb_2Co_{0.6}Mg_{0.4}F_4$ having a cylindrical shape was successfully grown using the Bridgman method. The c axis coincides exactly with the cylindrical axis. The Néel temperature T_N measured with a magnetic susceptometer was 17.0 ± 0.2 K, and no appreciable rounding of the transition was observed. The mosaic spread of the sample was less than 0.5°. Lattice constants a_0 and c_0 were 5.78 and 13.71 at $T = 5$ K, respectively.

The sample was mounted in a liquid-helium cryostat with its c axis vertical to the neutron scattering plane. The detectors at 2θ-angles between 68.8° and 145.5° were used for integrating the intensity $S(q, E)$ over the momentum. These detectors covered a wide momentum space centered at the $(1\,0\,0)$ magnetic reciprocal point. No magnetic scattering was observed in the other detectors, at any tem-
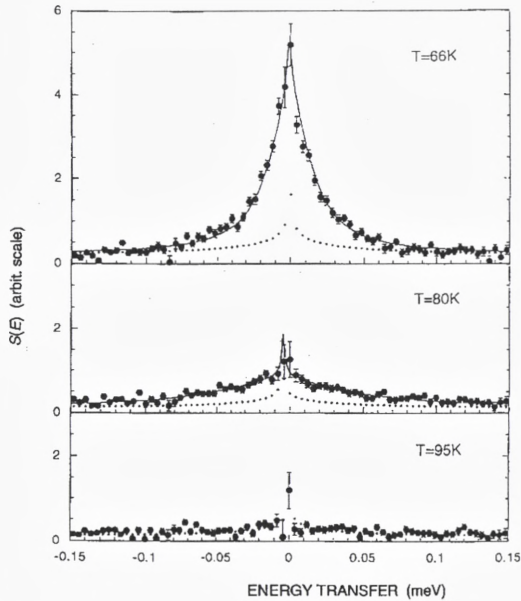
Figure 4. Self-correlation function $S(E)$ of $Rb_2Co_{0.6}Mg_{0.4}F_4$ as a function of the energy transfer observed at 66, 80 and 95 K. The solid lines indicate the results of a fit to the sum of the Lorentzian and $E^{-0.35}$ form. The dotted lines represent the contribution from only the $E^{-0.35}$ form. The vertical bars represent error bars.

perature measured, because these detectors viewed a region of momentum space well away from the magnetic reciprocal lattice point. Effectively, each detector element was associated with an area of the mica analyzer of dimensions 30 mm wide and 200 mm high. The large height of the analyzer provided a high counting rate without compromising the momentum resolution, because the 2D nature of the sample means that the momentum transfer in the vertical direction at a particular scattering angle 2θ, is identical.

Experiments were performed at several temperatures above and below T_N. Figure 4 shows the self-correlation function as a function of the energy-transfer, measured at $T = 66$, 80 and 95 K. As depicted, a long-tailed spectrum extending towards a high energy-transfer is clearly observed. The overall spectrum is quite different from the lineshape of the critical magnetic scattering. Fitting the data with a Lorentzian lineshape was of course not successful. Since the system has a Néel temperature of 17 K, strong critical scattering with a Lorentzian lineshape is expected; we therefore fitted the data with the sum of the Lorentzian and E^{-x}-form. The best result was obtained with x being between 0.3 and 0.4

($x = 0.35 \pm 0.06$), suggesting that the long-E tail comes from anomalous diffusion, which predicts the $E^{-0.34}$-form in the scattering function. The best results of a fitting with $x = 0.35$ are shown by the solid lines in Fig. 4, where the dotted lines describe the contribution from only $E^{-0.35}$. This fitting was successful for all of the data taken above and below T_N. Although the fitting to the sum of two functional forms is successful at any temperature, on approaching T_N the critical scattering is more dominant, as was expected. On approaching T_N, the thermal correlation length becomes large, and the picture of single-spin diffusion does not hold. This causes the decrease in amplitude of $E^{-0.35}$ near to T_N.

This experiment provides evidence for the anomalous diffusive motions of spins in a near-percolating Ising antiferromagnet, $Rb_2Co_{0.6}Mg_{0.4}F_4$. The scattering function integrated over momentum space in the paramagnetic phase reveals a long-tailed spectrum with the form of $E^{-(0.35\pm0.06)}$ superimposed on the Lorentzian lineshape, which originates from the normal critical magnetic scattering.

5   Ordering kinetics in fractal networks

The ordering kinetics of a pure Ising model with a nonconserved order parameter has been extensively studied both theoretically and experimentally (Gunton et al., 1983). The order develops from the initial disordered state to the final long-range ordered (LRO) state after rapid quenching from a high-temperature paramagnetic state to an ordered state below its transition temperature. Theories as well as computer simulations and experimental observations in metallic binary alloys have proved that the temporal development of the order obeys $t^{1/2}$ law during the last stage. However, it has been unclear how the order develops in a highly diluted magnet in which the magnetic concentration is close to the percolation threshold; the ordered cluster is therefore highly ramified and takes the form of a fractal. We have recently succeeded in observing the ordering kinetics of a highly diluted anti-ferromagnet, $Rb_2Co_{0.60}Mg_{0.40}F_4$, with a fractal geometry by both neutron elastic scattering and magnetization measurements (Ikeda et al., 1990).

In order to observe how a system develops in going from a disordered initial state to a final LRO state, one may cool the sample very rapidly from a high-temperature paramagnetic state to an ordered state at low temperature. In magnetic substances, however, the LRO is quickly stabilized when passing through the phase transition temperature and, hence, it was too difficult to observe a temporal growth of the domain size on a real time scale. In the present experiments, we utilized a new idea to realize the initial disordered state. As has been extensively argued during the last decade, the LRO in 2D diluted Ising antiferromagnets is destroyed by a uniform magnetic field applied along the spin direction and the
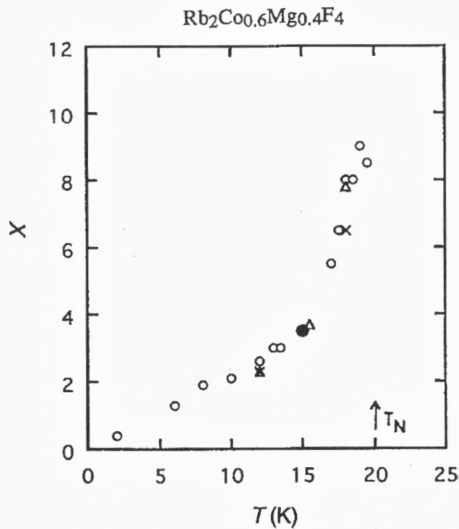
Rb₂Co₀.₆Mg₀.₄F₄

Figure 5. x versus T for data taken with external field cooling of 1 tesla (open circles), 2 tesla (triangles), and 3 tesla (crosses). x was found from fits of the magnetization by $[\log_{10}(t)]^{-x}$. The neutron data point is denoted by the solid circle.

system is broken into a micro-domain state (random-field effect) (Birgeneau et al., 1984; Belanger 1988; Nattermann and Villain, 1988). Experiments have verified that the equilibrium domain size in an external field decreases with increasing field and with decreasing magnetic concentration. Our observation of the equilibrium domain size of $Rb_2Co_{0.60}Mg_{0.40}F_4$ in a field of 4.8 tesla showed only 12 a_0. This value is actually microscopic. Furthermore, we found that after removing the field the LRO recovers within a macroscopic time scale, typically from several hours to several days. These facts have enabled us to observe the ordering kinetics on a real time scale.

For the time-resolved experiments, we performed both neutron-scattering and magnetization measurements. In both pure and diluted antiferromagnets, a system having a LRO has no net magnetization at all. However, in a cluster having a finite size a ferromagnetic moment arises along the magnetic field due to a statistical excess of the number of up-spins. Simple argument gives rise to a relationship between the micro-domain size R and the induced ferromagnetic moment M as $R \propto 1/M$, even in a system with fractal geometry. Therefore, the temporal decrease in $M(t)$ corresponds to the time evolution of the domain size $R(t)$.

For magnetization measurements a small piece of 0.0550 g mass was cut out of the single crystal and mounted in a SQUID susceptometer. The crystal was
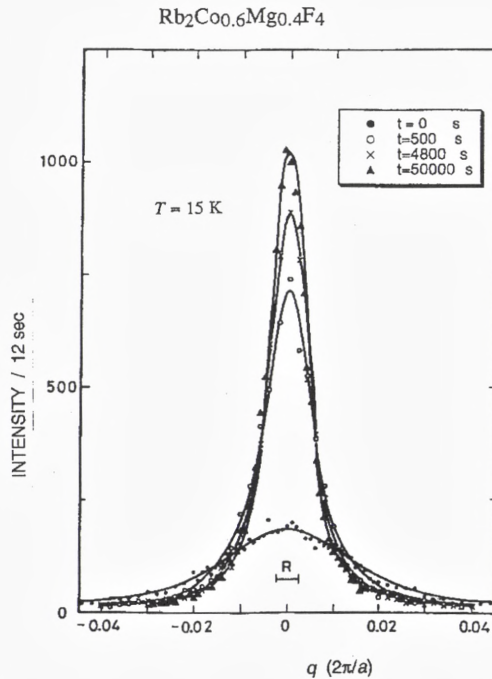
Rb$_2$Co$_{0.6}$Mg$_{0.4}$F$_4$

Figure 6. Temporal variation of transverse scans across the (1 0 0) superlattice po-
sition at $T = 15$ K; the cooling field was 4.8 tesla. The solid lines represent fit by a
single Lorentzian convoluted with the instrumental resolution function. R represents
the resolution width.

cooled down to several designated temperatures below T_N (20 K) while an exter-
nal magnetic field was applied along the c axis. The applied field was turned off
after reaching the desired temperature and the magnetization measurement was
performed in a zero field. The temporal decay rate of the magnetization is clearly
temperature dependent. This suggests that the growth rate of the order is governed
by thermally activated magnetic fluctuations. In order to analyze the magnetiza-
tion data, we made fits with several different functional forms, including a simple
power law; in the end, however, we obtained the best results using a logarithmic
power law, $M(t)^{-1} = A + B[\log_{10}(t)]^x$, where A, B, and x are adjustable parame-
ters. We plot x as a function of temperature in Fig. 5, where the results for 1 T,
2 T and 3 T cooling are depicted. Note that x goes to zero as T approaches zero,
indicating that the kinetics are frozen at $T = 0$. This provides further support for
our conjecture of thermally driven kinetics.

    In order to directly observe the domain size as a function of time, neutron-

scattering experiments using a TUNS spectrometer installed at JRR-2, JAERI, were performed. We used a triple-axis mode of operation with the transferred energy fixed at zero using incident neutron of 13.7 meV. An external field up to 5 tesla in magnitude was applied in the vertical direction, so that the single crystal was mounted in a cryostat with the c axis (spin direction) vertical. In order to obtain the best instrumental resolution possible, transverse scans across the $(1\,0\,0)$ superlattice Bragg point were performed. The resolution of the spectrometer under these conditions was typically 0.0050 FWHM in reciprocal lattice units (rlu) (1 rlu $= 2\pi/a = 1.097$ Å^{-1}). The time dependence of the line shape with the transverse scan was measured at 15 K for 4.8 T field cooling of the sample and was directly compared with the magnetization measurements. The scan was repeated over a period of 15 hours. Each scan takes approximately 15 min. Typical line shapes at different times are shown in Fig. 6. The line shape was fitted with several functions of the structure factor: a Lorentzian, a squared Lorentzian and the form $(\kappa^2 + \mathbf{q}^2)^{-1.5}$. The sum of mean square deviations (χ^2) in the Lorentzian fitting for 62 scans is less than the other two. The average domain size as determined from fits by a single Lorentzian gives an exponent x of 3.5 at 15 K. This value is in good agreement with the magnetization result. From these results we found that in the above time intervals the observed domain size satisfies the self-similarity condition $R(t) < \xi_G$, where the geometrical correlation length ξ_G in the present sample is 730 a_0, and, therefore, large enough.

Although the logarithmic time dependence of the domain size $R(t)$ has been discussed in earlier theoretical works (Grest and Slorivitz, 1985: Slorovitz and Grest, 1985; Huse and Henley, 1985; Chawdhury et al., 1987), to the best of our knowledge this is the first experiment which actually shows the $\log(t)$ power-law behaviour and kinetics which exhibits freezing at $T = 0$.

In a magnet with quenched impurities, the impurities act as energy barriers to domain growth; the pinning walls are therefore localized in energetically favourable positions, drastically slowing down the ordering kinetics. In particular, freezing in the percolating magnets should involve domain motion, which should be dependent on R; in other words, the energy barrier is dependent on R: $E(R) = (1/F)(R - R_0)^{1/x}$ (Lai et al., 1988). Here, R_0 and F are only weakly temperature dependent. Since the time necessary to overcome such barriers will have an activated temperature dependence, $t \approx \tau_1 \exp[E(R)/T]$, the growth law for the domain size in this model will have a logarithmic dependence, $R(t) = R_0 + FT[\ln(t/\tau_1)]^x$. Our experiment shows that x is dependent on the temperature and that it drastically increases as the temperature approaches T_N (20 K). We believe that although this behaviour might be related to critical fluctuations, thermally controlled domain-wall motion dominates the ordering kinetics.

Acknowledgements

References

Aeppli G, Guggenheim HJ and Uemura YJ, 1984: Phys. Rev. Lett. **52**, 942

Alexander S and Orbach R, 1982: J. Phys. Lett. (Paris) **43**, L625

Belanger DP, 1988: Phase Transitions **11**, 53

Birgeneau RJ, Cowley RA, Shirane G and Yoshizawa H, 1984: J. Stat. Phys. **34**, 817

Carlile CJ and Adams MA, 1992: Physica B **182**, 431

Chawdhury D, Grant M and Gunton JD, 1987: Phys. Rev. B **35**, 6792

Coombs GJ, Cowley RA, Buyers WJL, Svensson EC, Holden TM and Jones DA, 1976: J. Phys. C **9**, 2167

Cowley RA, 1981: *Excitations in Disordered Systems*, ed. M.F. Thorpe (Plenum, New York)

de Gennes PG, 1979: *Scaling Concepts in Polymer Physics* (Cornell Univ. Press, Ithaca)

Gefen Y, Aharony A and Alexander S, 1983: Phys. Rev. Lett. **50**, 77

Grest GS and Slorovitz DJ, 1985: Phys. Rev. B **32**, 3014

Gunton JD, San Miguel M and Sahni PS, 1983: in *Phase Transitions and Critical Phenomena*, eds. C. Domb and J.L.L. Lebowitz (Academic, New York) Vol. 8

Havlin S and Bunde S, 1991: in *Fractals and Disordered Systems*, eds. A. Bunde and S. Havlin (Springer-Verlag, Berlin)

Huse DA and Henley CL, 1985: Phys. Rev. Lett. **54**, 2708

Hutchings MT, Ikeda H and Janke E, 1982: Phys. Rev. Lett. **49**, 86

Ikeda H, Endoh Y and Itoh S, 1990: Phys. Rev. Lett. **64**, 1266

Ikeda H, Iwasa K and Andersen KH, 1993: J. Phys. Soc. Jpn. **62**, 3832

Ikeda H, Fernandez-Baca JA, Nicklow RM, Takahashi M and Iwasa K, 1994: J. Phys. Condens. Matter **6**, 10543

Ikeda H, Itoh S and Adams MA, 1995: Phys. Rev. Lett. **75**, 4440

Lai Z, Mazenko GF and Valls OT, 1988: Phys. Rev. B **37**, 9481

Nakayama T, Yakubo K and Orbach R, 1994: Rev. Mod. Phys. **66**, 381

Nattermann T and Villain J, 1988: Phase Transitions **11**, 5

Orbach R, 1986: Science **251**, 814

Shklovskii BI and Efros AF, 1984: *Electronic Properties of Doped Semiconductors* (Springer-Verlag, Berlin)

Slorovitz DJ and Grest GS, 1985: Phys. Rev. B **32**, 3021

Stanley HE, 1977: J. Phys. A **10**, L211

Stauffer D, 1979: Phys. Rep. **54**, 2

Uemura YJ and Birgeneau RJ, 1986: Phys. Rev. Lett. **57**, 1947

Uemura YJ and Birgeneau RJ, 1987: Phys. Rev. B **36**, 7024

Vacher R, Woignier T, Pelois J and Courtens E, 1988: Phys. Rev. B **37**, 6500

Zallen R, 1983: *The Physics of Amorphous Solids* (John Wiley & Son, New York)

Magnetism and Superconductivity Sharing a Common Border in Organic Conductors

D. Jérome

Laboratoire de Physique des Solides,

Université Paris-Sud, 91405, Orsay, France

Abstract

The class of organic solids based on cation radical salts deriving from the parent molecule TTF provides one- and two-dimensional conductors (superconductors) in which the electron delocalization proceeds via a strong overlap between neighbouring molecules. Their magnetic properties reveal in both series a common border between magnetism and superconductivity. Furthermore, the existence of antiferromagnetic fluctuations in the conducting phase is clearly established by susceptibility and NMR experiments. Magnetism is also relevant in the alkali-doped fullerene A_1C_{60} and gives rise to an antiferromagnetic ground state and strong ferromagnetic fluctuations at high temperature.

1 Introduction

The development of itinerant magnetism in organic conductors is tightly linked to the history of organic superconductivity. Magnetism is indeed found in the same materials, where conductivity and superconductivity can be stabilized at low temperature, although under different conditions. The actual start of the research on organic conductors was 1972 when a metallic-like conduction and a huge increase of conductivity down to 60 K was reported in the organic charge compound TTF-TCNQ before a Peierls transition (Jérome and Schulz, 1982). In this material, conduction proceeds very much like in a regular metal although no metal atoms are present in the molecules. This is the characteristics for organic conductivity. Soon after the discovery of organic superconductivity, itinerant magnetism appeared to be a frequently accompanying phenomenon. Contrasting with conventional molecular crystals made of neutral organic molecules held together by weak Van der Waals forces, organic conductors contain molecules with unpaired carriers in π-molecular orbitals presenting an open shell configuration. Such a situation originates from a partial oxidation (reduction) of donor (acceptor) molecules in the formation of a salt with an inorganic anion (cation). In addition, a strong inter-

molecular overlap of π-orbitals allows the electron delocalization over all molecular sites in the crystal. However, in most cases the delocalization occurs preferentially along selected crystallographic directions. Such a packing optimizes the overlap
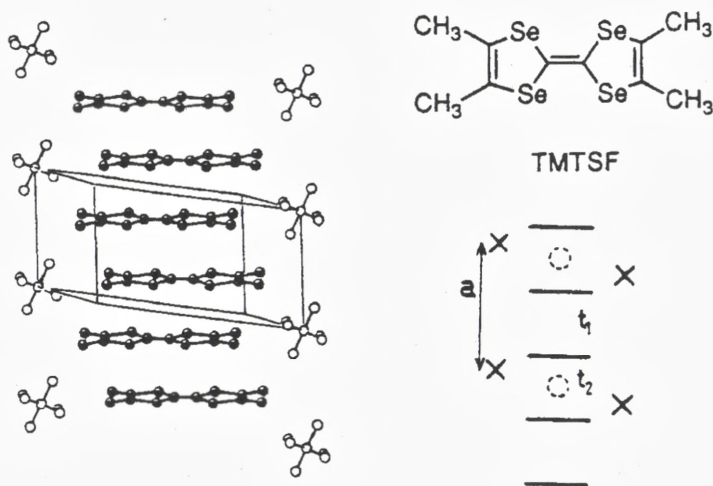

Figure 1. Donor molecule TMTSF, entering the Q-1D structure of $(TM)_2X$ compounds. The structure is dimerized with an alternating intermolecular distance (overlap integrals).

between molecular orbitals along the stacking direction. As long as the on-site Coulomb repulsion U does not overcome the energy gained by the band formation, conducting properties can be observed with a very pronounced one dimensional character along the stacking axis. The planar TMTSF (tetramethyl-tetraselena fulvalene) donor molecule with the TTF skeleton forms loosely connected stacks of molecules in the crystalline state of $(TMTSF)_2X$ salts (Fig. 1, where the organic molecule is oxidized in the presence of an inorganic acceptor $X = PF_6$, ClO_4, NO_3,...) (Bechgaard et al., 1980).

Other derivatives of the TTF molecule also give rise to higher dimensionality conductors. These are the planar donor molecules BEDT-TTF (ET) (Williams et al., 1991). The κ-type packing of ET molecules is unique in that the molecules first form dimers and then adjacent dimers are arranged in planes in an almost orthogonal order (Urayama et al., 1988), Fig. 2. Intra and interdimer interactions are nearly equal in amplitude. Secondly, the planes are packed in a 3D structure
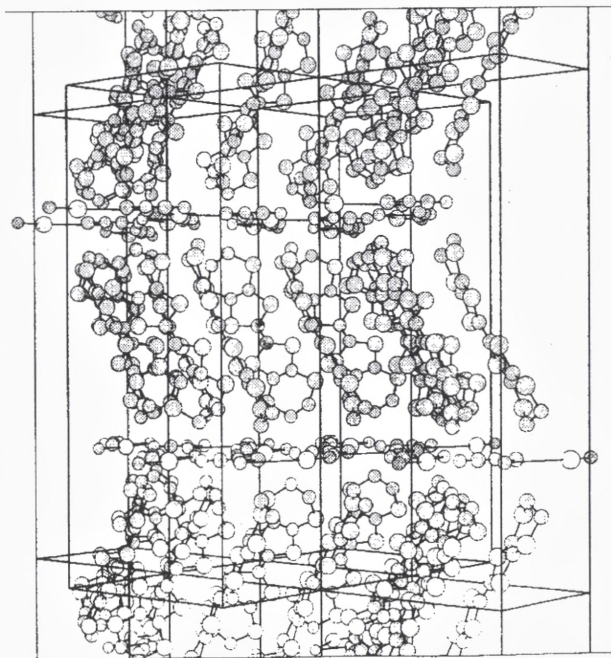
Figure 2. Transverse view of the 2D organic superconductor κ-$(ET)_2Cu[N(CN)_2]Br$.

of $(ET)_2X$ materials with an alternation of organic and inorganic planes of anions $X = Cu(NCS)_2$, $Cu[N(CN)_2]Br$ (or Cl), etc.... .

This crystal structure gives rise to a large metal-like conduction within the molecular layers and a very loose coupling between layers. In both 1- and 2D series, the negatively charged anions adopt a closed-shell configuration and do not contribute to the electrical conduction. So far, we have introduced organic compounds displaying 1- or 2D conducting properties. However, the recent discovery of the C_{60} molecule (Kroto et al., 1985) has allowed the synthesis of isotropically conducting organic solids. Unlike the TMTSF molecule (called TM from now on), neutral C_{60} molecule is a good electron acceptor molecule. Hence, when electrons are added to the LUMO of individual molecules through their reduction by an alkali cation the strong intermolecular interaction between π-orbitals makes a salt such as A_3C_{60}, $A = K$, Rb, Cs a 3D conductor and even a superconductor (Hebbard et al., 1985), Fig. 3. We shall restrict the subject of this review to the three families of organic conductors which have been mentioned above. They all exhibit
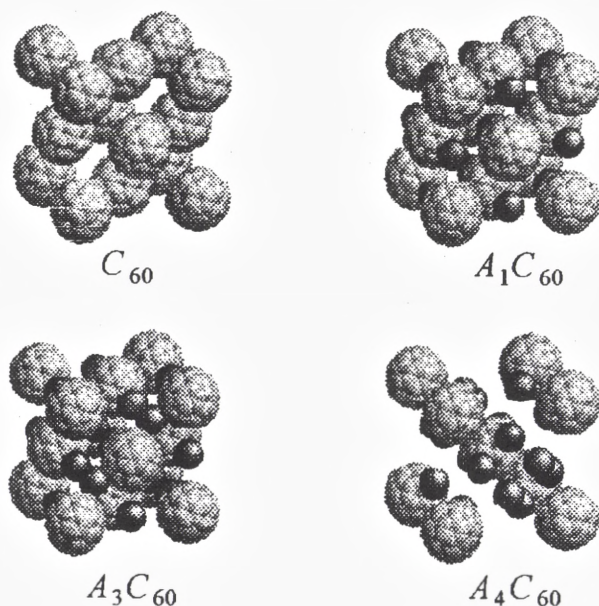
Figure 3. Crystal structures of C_{60} and various alkali-doped fullerides, after Goze (1996).

superconductivity with critical temperatures ranging between 1 and 30 K in the 1-, 2- and 3D series. They can also exhibit itinerant antiferromagnetic ground states instead of superconductivity and strong magnetic fluctuations at high temperature. A conduction band formed by the intermolecular overlap of π-molecular orbitals giving rise to bandwidths of the order of 1 eV, Fig. 4.

The family of organic conductors extends far beyond those discussed in this short survey but the interplay between magnetism and superconductivity is best illustrated by the restricted choice made in this article.

2 One dimensional conductors

2.1 Materials

Practically all properties that can be anticipated from the theory of 1D conductors (Solyom, 1979) are observed in the prototypic family $(TM)_2X$ where TM means the symmetrical TMTSF molecule or its sulfur analogue TMTTF and X is a monoanion such as an halogen or PF_6, ClO_4, etc$\cdots$. This brief review will not discuss the prop-
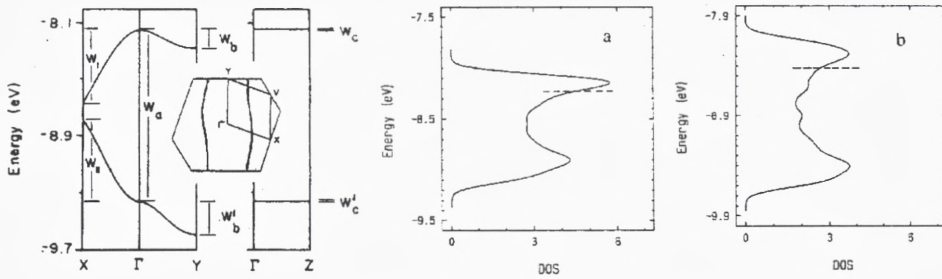
Figure 4. Energy dispersion of $(TMTSF)_2PF_6$ using the double ζ calculation and density of states or $(TMTTF)_2Br$ (a) and $(TMTSF)_2PF_6$ (b) (E. Canadell, 1995). The interchain coupling is responsible for the small warping of the Fermi surface. The dimerization gap is visible at the point X of the zone boundary. The minimum near the center the density of states is a reminiscence of the dimerization.

erties related to structural disorder introduced by non symmetrical molecules such as TMDTDSF (Auban, 1989), DMET (Ishiguro and Yamaji, 1990), or by alloying the organic stack. According to the 2 : 1 stoichiometry of the salt, oxidation of the neutral TM molecule should lead to the presence of half a hole per TM molecule. However, the intermolecular distance along the stacking direction in the crystal exhibits a dimerization with the important consequence of opening a dimerization gap in the 1D electron dispersion (Ducasse et al., 1986), hence, the 1D conduction band becomes half-filled instead of 3/4-filled as can be inferred from chemical considerations only. The conduction band is about 1 and 0.5 eV wide for TMTSF and TMTTF salts respectively, Fig. 4. It will become clear that the half-filling character is one of the crucial parameters which governs the electronic properties of these materials at low temperature. This property can be related to the gap δ_G (the dimerization gap) which is opened in the middle of the originally 3/4 filled band and gives rise to full (empty) lower (upper) bands. The dimerization gap is related to the alternation of the intra stack transfer integral. Structure determinations and band calculations show that the relative bond alternation is large for sulfur based molecules 38% in $(TMTTF)_2PF_6$ and smaller in selenium compounds 19% and 15% in $(TMTSF)_2PF_6$ and $(TMTSF)_2ClO_4$ respectively with a further decrease under pressure and (or) at low temperature due to thermal contraction. There exists a finite (although small) interstack coupling $t_\perp$ which makes these 1D conductors actually quasi-1D (Q-1D) when the temperature is smaller than a cross-over temperature T_x. In a non-interacting electron gas T_x reads $T_x^0 = t_\perp/\pi$ (Emery, 1983). However the cross-over temperature is influenced by Coulombic intrachain interactions and T_x could very well be much smaller than the bare cross-over temperature T_x^0 (vide-infra). Consequently, we may anticipate that sulfur compounds in the $(TM)_2X$ series with large dimerization gaps and low cross-over temperatures

should exhibit more pronounced 1D features than the selenium-based conductors. Such an expectation is corroborated by the examination of the $(TM)_2X$ phase diagram.

2.2   High temperature regime

Electronic, magnetic and structural properties of $(TM)_2X$ compounds are now fairly well understood in a quasi-one dimensional (Q-1D) theoretical framework where the band-filling character, the amplitude of the Coulomb repulsion and intra (inter) chain overlaps are the relevant parameters. The generic diagram in Fig. 5 displays the variety of regimes than can be observed among $(TM)_2X$ compounds (Jérome, 1991). Special attention has been paid to key compounds on which transport, magnetic, NMR and structural experiments have been performed varying the temperature or pressure. They are labeled by letters in Fig. 5. The transport in the high temperature domain ($T \geq 300$ K) is governed by the strength of the 1D lattice dimerization. This dimerization makes the half-filling of the band a particularly relevant concept for compounds at the left of the diagram but much less pertinent (although non zero) where moving towards the right. The band structure of these 1D conductors is relatively simple as it comprises two nearly planar and open Fermi surfaces, Fig. 4. The interactions between electrons are usually taken as three constants g_1, g_2 and g_3 modeling the backward, forward and Umklapp scattering of two electrons respectively. When the band is half-filled, the scattering of two electron from one side of the Fermi surface to the other via the Umklapp repulsion $g_3 = g_1 \frac{\delta_G}{E_F}$ contributes to localize the 1D carriers (Barisič and Brazovskii, 1979) since the momentum transfer in this scattering is a reciprocal lattice vector. The transport becomes activated below a temperature with an activation energy $\Delta_\rho = \pi T_\rho$ (Emery et al., 1982). $(TMTTF)_2PF_6$ (a) provides a good example for the strong Mott-Hubbard localization $\Delta_\rho \approx 600$ K of carriers in a half-filled band. The magnetism of such a Mott-Hubbard localized phase is that of a 1D Heisenberg chain. The uniform susceptibility ($q = 0$ fluctuation modes) follows a Bonner-Fisher behaviour with a maximum at a temperature inversely proportional to Δ_ρ. The $2k_F$ fluctuations modes are also low lying excitation mode of this AF chain. They can be probed by the measurement of the hyperfine spin-lattice relaxation rate T_1^{-1} (Moriya, 1963) which reads for a 1D conductors (Bourbonnais, 1987),

$$T_1^{-1} = C_0 T \chi_S^2(T) + C_1 T^{K_\rho} \tag{1}$$

where $q = 0$ ($2k_F$) spin fluctuations contribute to the first (second) term in Eq. (1). K_ρ is the exponent related to the spatial dependence of the charge-charge correlation function in 1D theory (Schulz, 1991). It also enters the power law temperature dependence of the density wave (DW) response at $2k_F$, namely
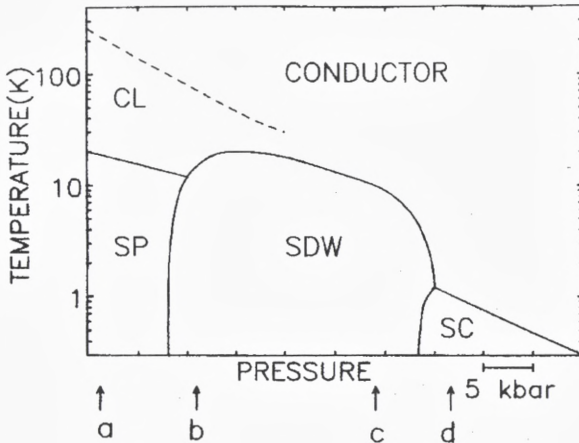
Figure 5. Generalized phase diagram for the $(TM)_2X$ series. Spin-Peierls (SP), spin density wave (SDW) and superconductivity (SC) are indicated together with the zero pressure location of prototypical compounds $(TMTTF)_2PF_6$ (a), $(TMTTF)_2Br$ (b), $(TMTSF)_2PF_6$ (c) and $(TMTSF)_2ClO_4$ (d). The dotted line represents the temperature T_ρ separating the metallic phase at high temperature from the charge localized phase (CL) at low temperature.

$\chi_{DW}(2k_F) \approx T^{K_\rho - 1}$. If 1D charge localization comes into play, $K_\rho \to 0$, and the $2k_F$ contribution to T_1^{-1} should become T-independent according to Eq. (1).

The temperature dependence of T_1^{-1} of $(TM)_2X$ compounds provides a remarkable illustration for the evolution between Mott-Hubbard localized electrons in (a) and delocalized 1D electrons in selenium compounds (c) and (d), Fig. 6. In those selenium compounds, because of the weakness of the half-filling character, 1D Mott-Hubbard (localization is not efficient until a cross-over towards a 2- or 3D electron gas is reached at the cross-over temperature T_x). It has been pointed out that the cross-over temperature can be strongly suppressed by intrachain Coulombic interaction in the Q-1D electron gas and should read (Bourbonnais and Caron, 1986)

$$T_x = T_x^0 \left(\frac{t_\perp}{E_F} \right)^{\frac{1 - K_\rho}{K_\rho}} \tag{2}$$

According to Eq. (2), a single particle cross-over temperature is either non relevant or at most very small whenever the Mott-Hubbard localization is developed. This is the situation which is encountered for sulfur compounds with $K_\rho \to 0$. For selenium compounds, Umklapp can no longer be a strong localizing mechanism although strong $2k_F$ fluctuations are still seen by NMR experiments and a metal-
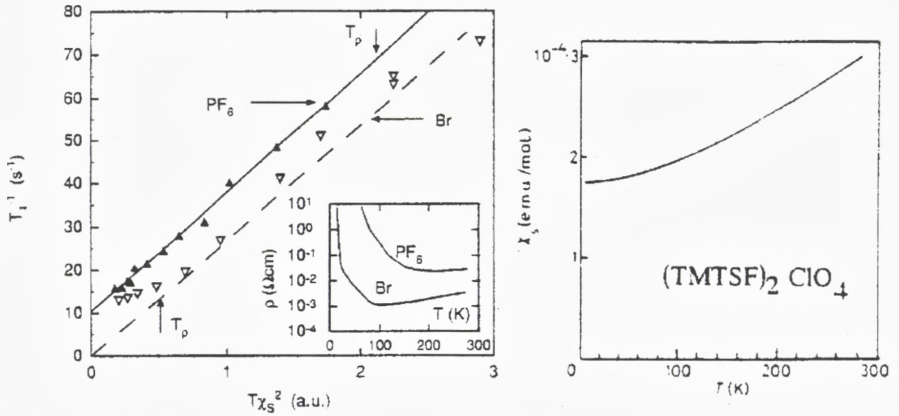
Figure 6. ^{13}C-relaxation rate of two compounds of $(TMTTF)_2X$ series versus $T\chi_S^2$, $X = PF_6$ and Br. T_ρ is the temperature showing the charge localization. The localized limit is reached at low temperature in all sulfur compounds. The finite intercept of T_1^{-1} at $T = 0$ is attributed to the role of 1D AF-fluctuations. These fluctuations, although present in selenium compounds as well cannot be detected on such a plot, see the dashed line for the schematic behaviour of $(TM)_2X$ compounds. The T-dependence of the spin susceptibility is similar throughout the $(TM)_2X$ series.

like behaviour survives down to a critical temperature where the conducting state undergoes a transition towards an itinerant magnetic ground state (Bechgaard et al., 1980; Jérome and Schulz, 1982). The extensive NMR investigation conducted in various compounds of the $(TM)_2X$ series (Wzietek, 1993) has led to a determination of the intrachain interactions governing the magnetic and transport properties of the 1D metallic phases (Jérome, 1994).

Table I: Parameters describing the behaviour of transport (K_ρ, g_3) and magnetic properties (g_1) of some $(TM)_2X$ compounds in the conducting (or localized) phase at high temperature.

Compounds	T_ρ	K_ρ	$\frac{g_1}{\pi v_F}$	$\frac{g_3}{\pi v_F}$	T_x	E_F
$(TMTTF)_2PF_6$	> 250 K	0 $(T < 250$ K$)$	1	0.4	< 20 K	1600 K
$(TMTTF)_2Br$	100 K	0 $(T < 50$ K$)$	0.9	0.35	< 20 K	1900 K
$(TMTSF)_2PF_6$	No	0.15 $(T < 100$ K$)$	1.1	0.16	10 K	3100 K

2.3   (TM)$_2$X ground states

At the left side of the diagram Fig. 5(a) (TMTTF)$_2$PF$_6$ presents an insulating spin-Peierls ground state in which the electrons of a uniform Heisenberg chain at high temperature are dimerized and form a non-magnetic singlet ground state with a $2k_F$-lattice distortion below $T_{SP} = 19$ K (Pouget et al., 1982). The spin-Peierls instability is slightly depressed under pressure (Jérome, 1991) and above 10 kbar a ground state with an internal magnetization is stabilized; a spin-density wave (SDW) phase with a commensurate wave vector (Brown et al., 1997). That is also the situation encountered in (TMTTF)$_2$Br at ambient pressure (a) (Barthel et al., 1993). Increasing pressure, the Néel temperature increases and the commensurate antiferromagnetic Néel state becomes incommensurate above a critical pressure of 10 and 5 kbar for (a) and (b) respectively with a concomitant maximum of the AF transition temperature (Klemme et al., 1995), Fig. 7. The 3D coupling which promotes the existence of long-range order at low temperature is the intrachain interaction between $2k_F$ bond CDW for the spin-Peierls ground state and the interchain exchange coupling for the commensurate Néel instability (Bourbonnais, 1987). When the conducting phase is stable below T_x, it is the nesting properties of the 2D Fermi surface which triggers the establishment of the Overhauser ground state at T_N given by $1 - g_1(T_x)\chi_{SDW}(\mathbf{Q}, T) = 0$ where $g_1(T_x)$ stands for the amplitude of the electron interaction renormalized down to T_x and $\mathbf{Q}$ is the best nesting vector of the 3D Fermi surface (Ishiguro and Yamaji, 1990). With a 2D model for the Fermi surface (FS), $\mathbf{Q} = (2k_F, \pi/b)$ when only nearest neighbour interchain interactions are included in the energy dispersion, namely

$$\varepsilon(k) = 2t_\| \cos k_\| a + 2t_\perp cos k_\perp b. \tag{3}$$

Deviations to perfect nesting are taken into account by adding a contribution $2t'_\perp \cos 2k_\perp b$ to Eq. (3). Thus, the nesting vector becomes incommensurate with the underlying lattice. This is the situation which prevails in (TMTSF)$_2$PF$_6$ (c) at ambient pressure or in (TMTTF)$_2$PF$_6$ and (TMTTF)$_2$Br under high pressure. Evidences for the incommensurability of the magnetic modulation have been given by NMR and transport properties experiments. The ^{13}C-NMR single crystal line-shape of (TMTSF)$_2$PF$_6$ reveals a continuous distribution of local fields (Barthel et al., 1993) instead of the narrow lines related to the finite number of magnetically inequivalent nuclei at high temperature.

At first sight, the field distribution can be explained by a sinusoidal modulation with amplitude (0.06–0.08 μ_B). This spectrum is at variance with the discrete NMR spectrum observed in the commensurate SDW of (TMTTF)$_2$Br at ambient pressure using ^{13}C and ^{1}H-NMR.

Other evidences for the incommensurability of the SDW ground state are given
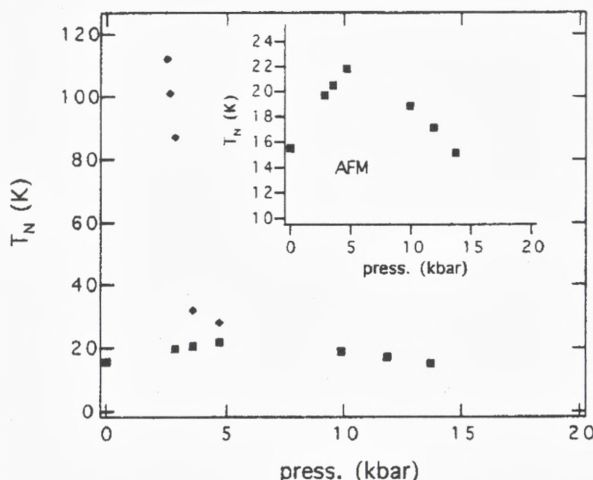
Figure 7. The SDW ground state of $(TMTTF)_2Br$ under pressure. 5 kbar is a critical pressure between a commensurate SDW ($P < 5$ kbar) and an incommensurate SDW at $P > 5$ kbar.

by the consequence of the existence of a low lying long wavelength phason mode in the excitation spectrum corresponding to the sliding of the modulation. This mode gives rise to a hyperfine relaxation of the nuclear spins which is T-independent when the SDW effective mass is not enhanced by a coupling to phonons (Barthel, 1994). This behaviour has been clearly identified in the SDW state of $(TMTSF)_2PF_6$ (Barthel et al., 1993a) and also in $(TMTTF)_2Br$ under 12 kbar (Klemme et al., 1996), Fig. 8. The behaviour of $(TMTTF)_2Br$ at 1 bar or $(TMTTF)_2PF_6$ at 10 kbar is in striking contrast. There, the gapless phason mode is suppressed by commensurability and nuclear relaxation is induced by the thermal excitation of magnon modes with an activation energy of ≈ 12 K at $H = 9.4$ T.

Another consequence of the SDW incommensurability can be observed in the transport properties of the Overhauser state. The magnetic incommensurate structure has no preferential position with respect to the lattice; it can slide and contribute to a collective conducting channel similar to the Fröhlich mode of CDW systems (Grüner, 1994). This mode consists in the joint displacement of both spin polarized CDW modulations building up the SDW ground state. Hence, the conductivity of the SDW state becomes electric field dependent. However, a non linear conductor is only observed above a threshold field E_T (of the order of 5 mV/cm (Tomič and Jérome, 1989)). The threshold field is related to the breaking of the translational invariance of the SDW by the existence of randomly distributed im-
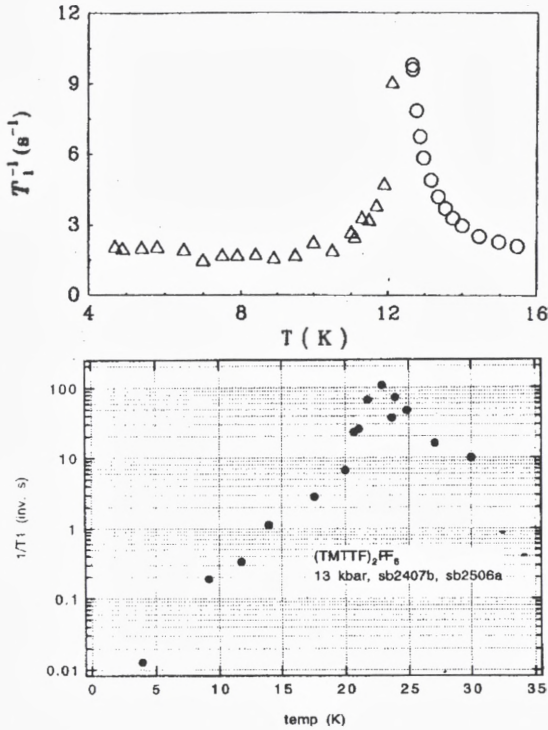
Figure 8. Temperature dependence of the ^{13}C-relaxation in the incommensurate SDW phase of $(TMTSF)_2PF_6$. The T-independent relaxation below the peak due to 3D fluctuations at T_N is attributed to the gap less phason mode. The relaxation is activated in $(TMTTF)_2PF_6$ under 13 kbar as the ground state is expected to be a commensurate SDW.

purities acting as pinning centers on the condensate, Fig. 9. The oscillation of the SDW condensate around its equilibrium position can contribute to the AC conductivity (at $E < E_T$) and gives rise to a resonance in the far infrared regime. This is the pinned mode resonance. The very large electrical polarizability of the condensate gives rise to a large static dielectric constant which in turn is related to the threshold field by the equation

$$\varepsilon(0)E_T = \text{constant.} \qquad (4)$$

The validity of Eq. (4) has been proven for a variety of CDW phases (Grüner, 1988). It is also followed over a wide domain of threshold fields in the $(TMTSF)_2[AsF_6]_{(1-x)}[SbF_6]_x$ series as E_T is varied by several orders of magni-
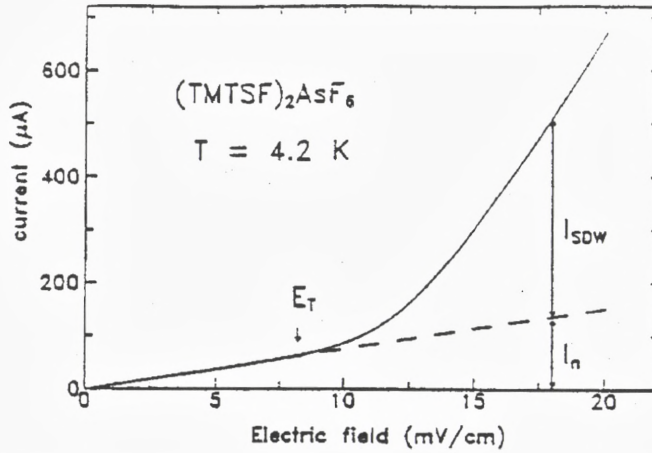
Figure 9. Non linear conduction in the SDW phase of $(TMTTF)_2AsF_6$ at $T = 4.2$ K.

tudes throughout the solid solution (Traetteberg et al., 1994). The DC collective motion of the SDW condensate generates an AC component at a frequency ν_n which is linearly related to the collective current. The existence of the oscillating current is well established in $(TMTSF)_2PF_6$ by looking at the interference between an external AC driging source and the internal AC current (Kriza et al., 1991). This is the equivalent of the Shapiro steps in the physics of Josephson junctions. Furthermore, the rigid motion of the magnetic modulation induces a local magnetic field modulation at a frequency ν_ϕ as observed from the magnetic motional narrowing of the NMR lineshape (Barthel et al., 1993b). There still remains a controversy about the relation between ν_n and ν_ϕ (at a given SDW current) in a SDW state. The origin of the AC current oscillation, rigid motion of the condensate or single particle to collective conversion at the electrodes is not settled for a SDW state (Clark, 1996).

A recent claim has been made about the existence of CDW x-ray scattering satellites (extremely weak) in the $(TMTSF)_2PF_6$ ground state at a wave vector $\mathbf{Q}$ corresponding to the wave-vector of the magnetic modulation (Pouget, 1996). The coexistence between magnetic and electric modulations implies that the two spin polarized CDW building up the SDW modulation are not exactly out of phase, as expected for a pure SDW. This mixture between degrees of freedom could possibly explain the weakly first-order character of the transition revealed in transport and magnetic measurements. The 2D nesting becomes frustrated when $2t'_\perp$ is increased (changing the anion or under pressure). Consequently the SDW ground state is rapidly suppressed. The possible divergence of the Cooper channel at low temper-
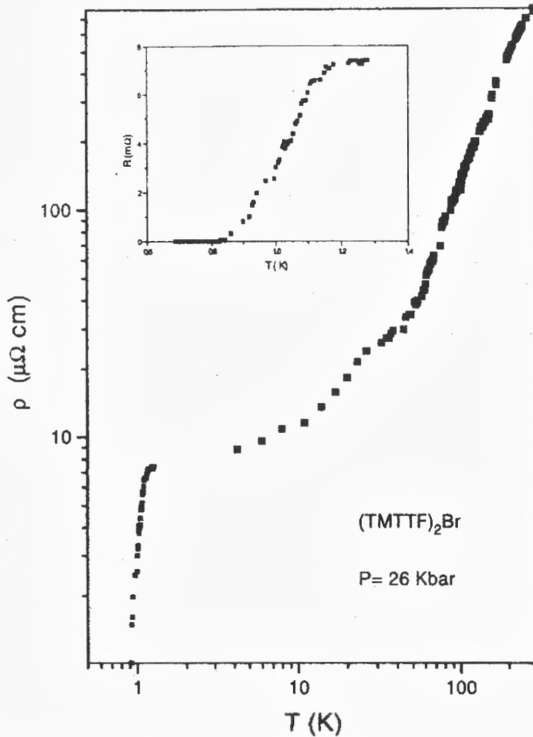
Figure 10. Superconducting transition in $(TMTTF)_2Br$ under 26 kbar.

ature is unaffected by the increase of $2t'_\perp$ since inversion symmetry $\epsilon(k) = \epsilon(-k)$ is preserved for very general energy dispersion laws. A superconducting ground state can thus be stabilized for $(TM)_2X$ compounds. The critical temperature never exceeds 2 K. High pressure is required for the superconductivity of sulfur compounds $(TMTTF)_2Br$ (Balicas et al., 1994), Fig. 10, and selenium compounds $(TMTSF)_2PF_6$ (Jérome et al., 1980), Fig. 11. $(TMTSF)_2ClO_4$ is the only member of the $(TM)_2X$ series in which superconductivity exists under ambient pressure (Bechgaard et al., 1981). What has emerged from the study of $(TM)_2X$ superconductors is the strong competition existing between superconducting and DW instabilities governed by the FS nesting. Attempts to raise T_c (superconductivity) in $TMTSF_2ReO_4$ using a pressure cycling procedure to prevent the formation of an anion ordered insulating phase has led to the stabilization of the more stable SDW phase (Tomič and Jérome, 1989). Therefore, T_c cannot be raised above 1.3 K but superconductivity in the $(TM)_2X$ series develops in a background of AF

spin fluctuations. Unlike 2D superconductors which are the subject of the next section, the properties of the anisotropic 1D superconducting state have not yet been studied in details.

3   Two dimensional conductors

3.1   Ground states

When 2D organic superconductors first appeared, they became very popular for a lot of reasons. Rather high superconducting T_c (as compared to the $(TM)_2X$ series) could be stabilized in the phase β_H-$(ET)_2I_3$ ($T_c = 8$ K) (Laukhin et al., 1985; Creuzet et al., 1985) and $T_c = 9.4$ K in κ-$(ET)_2Cu(NCS)_2$ (Urayama et al., 1988), Fig. 11, or even 11.4 and 12.8 K in κ-$(ET)_2Cu[N(CN)_2]Br$ (Kini, 1990) and κ-$(ET)_2Cu[N(CN)_2]Cl$ under 0.3 kbar (Williams et al., 1990) respectively. Owing to the very pronounced 2D character of the FS, textbook examples for quantum oscillations of the magnetization and resistivity have been observed in κ-$(ET)_2Cu(NCS)_2$ (Oshima et al., 1988) and β_H-$(ET)_2I_3$ (Kang et al., 1989) leading to a detailed determination of the FS (Wosnitza, 1995). The importance of magnetism in 2D conductors is less apparent than for Q-1D conductors since the absence at first sight of any nesting feature on the FS precludes the stabilization of SDW phases. Consequently, several 2D conductors remain metallic down to low temperatures. At variance with Q-1D conductors, what is exceptional for 2D conductors is the absence of magnetism under ambient pressure. There are, however, some indications that in these systems too, superconductivity is located close to an insulating state which shows magnetic properties. The relevance of magnetism becomes clear from the phase diagram in Fig. 12 displaying the different ground states which can be stabilized in the κ-$(ET)_2CuX$ series varying the nature of the anion CuX or the pressure parameter. The origin of pressure has been fixed at the compound κ-$(ET)_2Cu[N(CN)_2]Cl$ undergoing the onset of a magnetic modulation below 26 K (Miyagawa et al., 1995). The magnetic nature of the ground state is also supported by the observation of an antiferromagnetic resonance in ESR experiments. Furthermore, ^{13}C and ^1H-NMR data suggest the stabilization of a commensurate magnetic structure with an amplitude of 0.4–1 μ_B which is about ten times the amplitude measured in the $(TM)_2X$ series. The origin for such a commensurate magnetic ground state is not clear at the moment as the FS of these 2D conductors does not reveal any obvious commensurate nesting vectors. In spite of its unknown origin the interplay between magnetism and superconductivity is obvious in Fig. 12. A minute pressure of 0.3 kbar is enough to suppress the magnetic ground state and stabilize superconductivity below 12.8 K (Sushko et al., 1993).
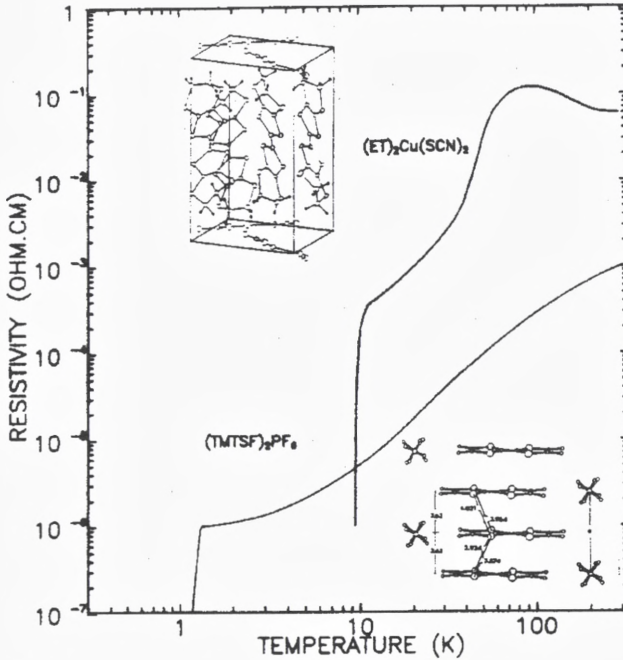
Figure 11. Superconductivity at 1 K in $(TMTSF)_2PF_6$ under 9 kbar and at 9 K in κ-$(ET)_2Cu(NCS)_2$ at ambient pressure.

3.2   Magnetic fluctuations at high temperature

Although the role of Coulomb repulsions in 2D conductors could be anticipated from the early data of frequency dependent optical conductivity leading to $U/W \approx 1$ (Jacobsen, 1987; Jérome, 1994). This is the NMR investigation of κ-phase conductors which confirm that magnetic fluctuations govern the electronic properties of the conducting phase at high temperature. First, the pressure dependence of the Knight shifts (KS) in κ-Br is large (-6% kbar^{-1}) and can only be explained if the on-site Coulomb repulsion to bandwidth ratio is of the order unity (Mayaffre et al., 1994). Secondly, an anomalous temperature dependence was found for the Knight shift and the spin-lattice relaxation rate (Mayaffre et al., 1994), Fig. 13. At ambient pressure, the Knight shift shows a smooth T-dependence between 300 and 50 K which can be understood by the thermal contraction but below 50 K a further pronounced drop of the susceptibility is observed (Kataev et al., 1992). Concomitantly, $(T_1T)^{-1}$ reveals near 50 K an important enhancement which obviously departs from the usual Korringa relation (Mayaffre et al., 1994; Kawamoto
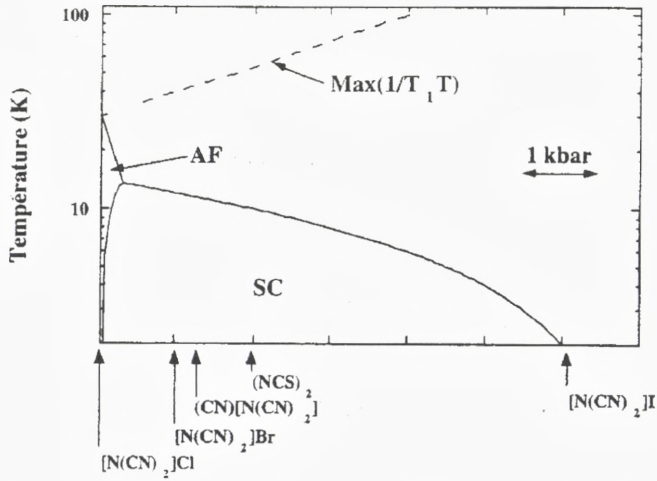
Figure 12. Generalized phase diagram for the κ-(ET)$_2$CuX 2D conductors.

et al., 1995). This behaviour of the relaxation rate seems to be general for most κ-phase materials. At a pressure of 4 kbar, all anomalies of KS and $(T_1 T)^{-1}$ are removed and a Korringa law is recovered (Mayaffre et al., 1994). The temperature profile of both $(T_1 T)^{-1}$ and KS suggest the existence of a pseudo-gap in the density of states and of strong spin fluctuations at a wave vector nesting the 2D Fermi surface. Besides magnetic properties there exists an anomalous behaviour for the resistivity as well in the same temperature range. The temperature of 50 K is the temperature where a peak of dR/dT is observed (Sushko, 1991). As for $(T_1 T)^{-1}$ or KS, a regular behaviour of the metallic conductivity is recovered under a pressure of $\approx$ 4 kbar (Sushko, 1991).

3.3   Comparison with high T_c cuprates

The temperature profiles of $(T_1 T)^{-1}$ and KS show a striking similarity with those reported in underdoped cuprates, for example via ^{63}Cu-NMR in YBa$_2$Cu$_3$O$_{6.63}$ (Takigawa et al., 1991). This relaxation behaviour in HTSC has often been explained by the existence of short range AF correlations in the CuO$_2$ planes giving rise to a gap in the spin excitations (Kampf and Schrieffer, 1990). However, for κ-ET$_2$X materials, the tight correlation between the relaxation peak and the temperature dependence of the resistivity makes it difficult to consider a decoupling between the spin and charge degrees of freedom. The origin of enhanced relaxation and transport scattering rate could be due to some nesting properties of the
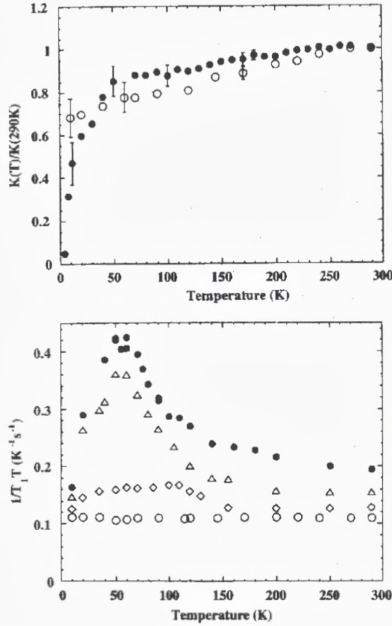
Figure 13. κ-$(ET)_2Cu[N(CN)_2]Br$ NMR under pressure. Temperature dependence of the Knight shift at 1 bar ($\bullet$) and 4 kbar ($\circ$) normalized to the 300 K value (a) and of $(T_1T)^{-1}$ at different pressures 1, 1.5, 3 and 4 kbar from top to bottom (b).

2D Fermi surface with two possible incommensurate wave vectors connecting the flat portions (Oshima et al., 1988), Fig. 14. Both nuclear relaxation and electron scattering depend on the imaginary part of the spin susceptibility. Thus,

$$(T_1T)^{-1} \approx \sum_q \frac{\chi''(\mathbf{q}, \omega_n)}{\omega_n} \tag{5}$$

If $\mathbf{Q}$ is the vector nesting the Fermi surface even partially, this features leads to an enhancement of the real part of the bare susceptibility $\chi_0'(\mathbf{q}, \omega)$ at $\mathbf{q} = \mathbf{Q}$ and with the RPA $(T_1T)^{-1}$ reads (Charfi-Kaddour et al., 1992).

$$(T_1T)^{-1} \cong \sum_q \frac{1}{(1 - U\chi_0'(\mathbf{q}, \omega_n))^2} \frac{\chi_0''(\mathbf{q}, \omega_n)}{\omega_n} \tag{6}$$

Therefore, a maximum of $(T_1T)^{-1}$ could derive from the nesting at the wave vector $\mathbf{Q}$ enhancing $\chi_0'(\mathbf{q}, \omega_n)$ in Eq. (6). Going beyond the RPA, the Fermi liquid theory in the presence of nesting properties explains the development of the pseudo gap in
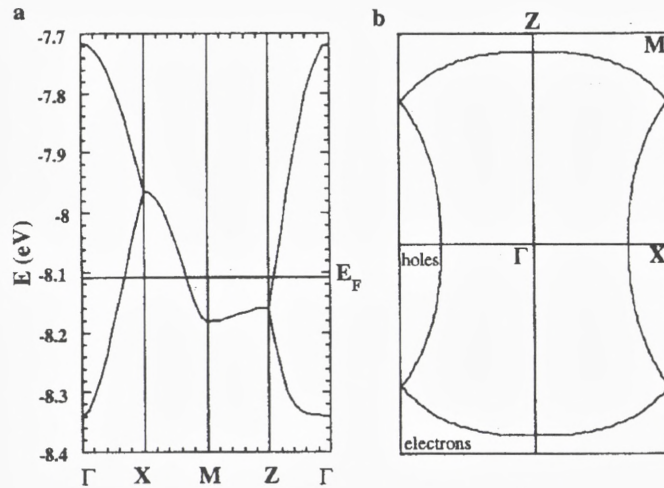
Figure 14.   Calculated band structure (a) and Fermi surface (b) of κ-(ET)$_2$Cu[N(CN)$_2$]Br, after Canadell (1996).

the density of states at the Fermi level. Such pseudo-gap would affect the static and dynamic susceptibility explaining both the drop of KS and the peak of relaxation. Furthermore, the peak of resistivity can be attributed to the enhanced scattering against AF fluctuations. The high pressure work shown how the various manifestations of AF fluctuations on magnetism and transport vanish very quickly. T_1 or the pseudo gap, being related to the nesting properties are much more sensitive to pressure than the high temperature Knight shift (or susceptibility). Furthermore, as observed in Q-1D superconductors the suppression of AF fluctuations under pressure goes together with the disappearance of superconductivity. This observation emphasizes the experimental relation between spin fluctuations and superconductivity in both 1D and 2D series of organic superconductors (Wzietek et al., 1996).

4   Fullerides

4.1   Phase 3 fullerides

Among the various kinds of $A_x C_{60}$ fullerides superconducting compounds $A_3 C_{60}$ (A = K, Rb, Cs) are probably those in which magnetism plays the smallest role. The metallic character of $A_3 C_{60}$ is fairly well understood in terms of a half filling of a band deriving from the six threefold-degenerate lowest unoccupied molecular

orbital (LUMO) of C_{60}. The study of the spin susceptibility of K_3C_{60} via ^{13}C Knight shift and T_1 measurements (Kerkoud et al., 1994) reveals a very small pressure coefficient ($\approx -1\%$ kbar^{-1}) which is in fair agreement with the pressure dependence of the band structure neglecting Coulomb interaction. In addition, the superconducting transition of phase 3 compounds with different alkali atoms or under pressure supports an interpretation in terms of a weak coupling BCS model with a pairing interaction mediated by intramolecular electron-phonon coupling (Haddon, 1992).

4.2   Phase 4 fullerides

In A_4C_{60} compounds, four levels among the six threefold-degenerate t_{1u} orbitals are occupied by alkali metals electrons implying a partial filling of the band in the solid. However, the metallic character which could be expected from the partial band filling is not observed from photoemission spectra (Benning et al., 1992) optical conductivity (Iwasa et al., 1993) and thin film resistivity (Haddon et al., 1994) data. Furthermore, ESR susceptibility (Kosaka et al., 1993) and T_1^{-1} data (Zimmer et al., 1994) show the non-magnetic and insulating nature of the ground state, Fig. 15. However the nuclear spin-lattice relaxation is very fast at room temperature and cannot be explained by a straightforward semiconducting band structure model. Following an NMR investigation under pressure (Kerkoud et al., 1996), an interplay between the molecular Jahn-Teller and the energy dispersion has been proposed for the interpretation of the electronic properties of A_4C_{60}. The t_{1u} manifold is split into three components with two lower degenerate components filled by the four alkali atom electrons and one empty higher component. Moreover, the molecular interaction gives rise to the broadening of the molecular level into a semiconducting band scheme. If the Jahn-Teller effect Δ_{JT} is strong enough to overcome the band broadening an insulating material is obtained. The fast relaxation at room temperature has been explained by intrinsic localized paramagnetic centers provided by local excitations of the C_{60}^{4-} molecules. The lowest excited state $(C_{60}^{4-})^*$ differs from C_{60}^{4-} by the inverse arrangement of the doubly degenerate and non degenerate Jahn-Teller levels. The lower level is completely filled by two electrons and the higher is half-filled by the two residual electrons. The latter, according to the Hund's rule form a triplet state giving rise to thermally activated localized paramagnetic centers with an activation energy which amounts to $\Delta_{JT}/2$. A Jahn-Teller splitting of 140 meV has been derived from the activated temperature dependence of T_1^{-1} in Rb_{60}^{4-}. The exciton level at $\Delta_{JT}/2$ lies within the Jahn-Teller gap and at increasing pressure the bandwidth increases with a concomitant merging of the localized states into the itinerant states. The material evolves from a narrow gap semiconductor with localized paramagnetic excitations
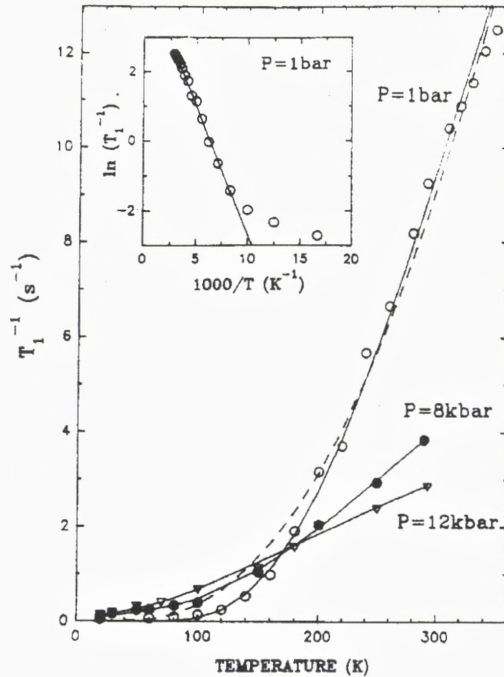
Figure 15. Temperature dependence of ^{13}C-T_1^{-1} in Rb$_4$C$_{60}$ for different pressures. The fit with the model of localized triplet excitons (Kerkoud et al., 1996) is shown by the continuous line at 1 bar. The relaxation of thermally activated carriers in a semiconductor would follow the dashed line.

at ambient pressure to a semimetal under a pressure of 12 kbar as shown from the recovery of the Korringa behaviour for T_1^{-1}, Fig. 15.

4.3   Phase 1 fullerides

A$_1$C$_{60}$ forms a remarkable system where the stabilization of an itinerant magnetic ground state has been identified for the first time in the A$_x$C$_{60}$ series (Chauvet et al., 1994). A$_1$C$_{60}$ undergoes a first-order structural transition around 350 K between a fcc phase at high temperature and an orthorhombic phase at low temperature (Stephens et al., 1994). The orthorhombic phase is particular as it exhibits a polymerized structure along chains of C$_{60}$ molecules. ESR (Pekker, 1994) and optical conductivity (Bommelli et al., 1995) data support the conducting nature of A$_1$C$_{60}$ down to 50 K. However, the progressive opening of a pseudo-gap in $N(E_F)$ is observed at low temperatures (Chauvet et al., 1994) and a magnetic ground state
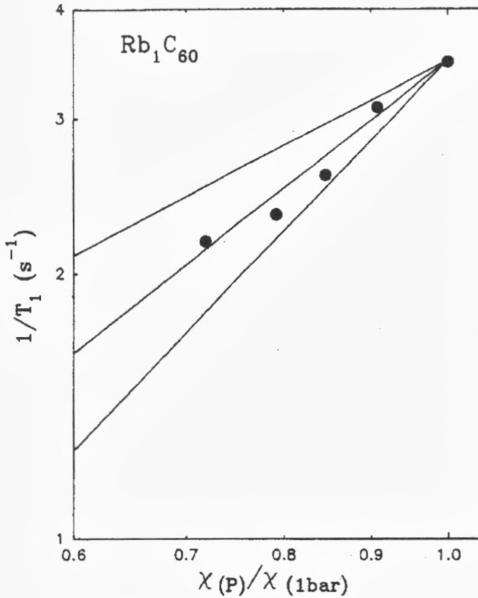
Figure 16. Relation between ^{13}C-T_1^{-1} and χ_S in Rb_1C_{60} when the pressure is varied between 1 bar and 4.5 kbar. The best fit is obtained for $T_1^{-1} \approx \chi^{3/2}$.

sets in below 20 K (Uemura et al., 1995; Mac Farlane et al., 1995). The unusually large pressure coefficient of the susceptibility ($\approx -9\%$ kbar^{-1}) (Forro et al., 1996) reveals the importance of the exchange enhancement in these materials with a Stoner factor of about 3 under ambient conditions (Auban-Senzier et al., 1996). The magnitude of the enhancement may be explained by two specific features for phase 1 fullerides. First, the calculation of the effective Coulomb repulsion taking into account the Jahn-Teller energy and the bare on-site repulsion provides a value of 0.2 eV for Rb_1C_{60} but nearly negligible for A_3C_{60} (Victoroff et al., 1995). Secondly, a large contribution to $N(E_F)$ can be expected from a singularity in the density of states located in the vicinity of the Fermi energy (Victoroff and Héritier, 1996).

The nature of magnetic fluctuations is still very controversial. One-dimensional AF fluctuations, related to the polymerized structure have been claimed to persist up to room temperature on the basis of a temperature independent nuclear relaxation (Brouet et al., 1996). However, this suggestion is in agreement neither with the conducting character of the compound nor with the experimental relation between T_1 and χ_S leading to $1/T_1 \approx \chi_S^{3/2}$ or χ_S^2 which is followed (Moriya, 1995),

Fig. 16, as the pressure is increased up to 6 kbar (Auban-Senzier et al., 1996). What has been proposed instead is the model of ferromagnetic fluctuations within chains or planes of the body centered orthorhombic structure of A_1C_{60}. AF-fluctuations between planes grow below 50 K and provide a two-sublattice magnetic ground state at 15-20 K (Erwin et al., 1995). The band structure calculation (Erwin et al., 1995) has shown that the 3D AF-modulation opens a gap at the Fermi level and makes the ground state insulating. The magnetic ground state is suppressed under pressure as shown by NMR data under pressure, Fig. 17, but at 6 kbar even in the absence of long range ordered magnetism strong 3D AF-fluctuations remain, in the incipient antiferromagnet as indicated by the temperature dependence of the relaxation, $1/T_1 \approx T^{1/4}$ (Moriya, 1995). Under 12 kbar, the existence of a Korringa relaxation down to the lowest temperatures supports the existence of a weakly correlated metallic phase bearing much resemblance with the conducting phases of Rb_3C_{60} at ambient pressure or Rb_4C_{60} under pressure.
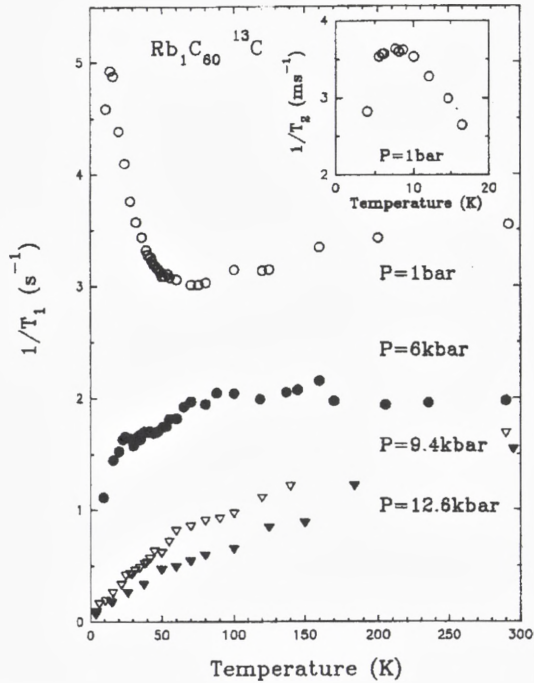

Figure 17. Temperature dependence of $^{13}C\text{-}T_1^{-1}$ at different pressures.

5   Conclusion

Organic superconductivity has been around for the last 15 years. Remarkable progresses have been achieved in terms of increasing the stability of the superconducting state from 1K in one dimensional organic conductors pertaining to the $(TM)_2X$ series up to 30 K in the fullerides. The systematic study of isostructural series of either 1D or 2D conductors has shown that the phase diagrams exhibit magnetic phases in close proximity to the superconducting state. Furthermore, superconductivity emerges out of a "normal conducting" state in which the presence of magnetic fluctuations has been clearly identified by a wealth of NMR data. As far as 1D conductors are concerned, the U/W ratio is close to unity and the interplay between the half-filling character (the Umklapp scattering term) and the interchain overlap (the cross-over temperature T_x) makes the generalized phase diagram remarkably diversified with spin-Peierls, SDW and superconducting ground states. Proximity between superconductivity and magnetism is also observed in high T_c superconductors with a noticeable difference since the critical temperature reaches zero at the borderline. The anisotropic character of the pairing interaction in 2D organics is inferred from the gapless character of the quasi particle energy spectrum. However, the symmetry of the order parameter is still waiting for phase-sensitive experiments. In this context the role of magnetic fluctuations in pair formation of organic superconductors has to be clarified (Mayaffre et al., 1995). In spite of the narrow bandwidth, magnetism is less present in the series of A_xC_{60} fullerides. Only in A_1C_{60} uniform spin fluctuations are observed at high temperature and the AF coupling between ferromagnetic planes allows the stabilization of an AF ground state at low temperature. High pressure decreases the importance of magnetic fluctuation and suppresses the stability of the AF ground state.

Acknowledgements

References

Auban P et al., 1989: J. Phys. (Paris) **50**, 2727

Auban-Senzier P et al., 1996: J. Phys. (Paris) I, in press

Balicas L et al. 1994: J. Phys. (Paris) I, **4**, 1539

Barišič S and Brazovskii S, 1979: in *Recent Development in Condensed Matter Physics*, ed. JT
        Devreese (Plenum Press, New York) p. 327

Barthel E et al., 1993a: Europhys. Lett. **21**, 87

Barthel E, Kriza G, Quirion G, Wzietek P, Jérome D, Christensen JB, Jørgensen M and Bechgaard
        K, 1993b: Phys. Rev. lett. **71**, 2825

Barthel E, 1994: Thesis (Université Paris-Sud, Orsay)

Bechgaard K et al., 1980: Solid State Commun. **33**, 1119

Bechgaard K et al., 1981: Phys. Rev. Lett. **46**, 852

Benning PJ et al., 1992: Phys. Rev. B **45**, 6899

Bommeli F et al., 1995: Phys. Rev. B **51**, 14794

Bourbonnais C and Caron L, 1986: Physica B **143**, 451

Bourbonnais C, 1987: in *Low dimensional Conductors and Superconductors*, eds. D. Jérome and
        LG Caron (Plenum Press, New York) p. 155

Brouet V et al., 1996: Phys. Rev. Lett. **76**, 3638

Brown S et al., 1997: to be published

Canadell E, 1995, private communication

Canadell E, 1996, private communication

Charfi-Kaddour S et al., 1992: J. Phys. I **2**, 1853

Chauvet O et al., 1994: Phys. Rev. Lett. **72**, 2721

Clark WG, 1996: private communication

Creuzet F et al., 1985: J. Phys. Lett. (Paris) **46**, L-1079

Ducasse L et al. 1986: J. Phys. C **19**, 3805

Emery V et al., 1982: Phys. Rev. Lett. **48**, 1039

Emery V, 1983: J. Phys. (Paris) Coloq. **44** C3-977

Erwin SC et al., 1995: Phys. Rev. B **51**, 7345

Forro L. et al., 1996: Proceedings of the Kirchberg Conference

Goze C, 1996: Thesis (Univ. Montpellier)

Grüner G, 1988: Rev. Mod. Phys. **60**, 1129

Grüner G, 1994: Rev. Mod. Phys. **66**, 1

Haddon R 1992: Acc. Chem. Res. **25**, 127

Haddon R et al., 1994: Chem. Phys. Lett. **218**, 100

Hebbard A.F. et al., 1985: Nature **350**, 600

Ishiguro T and Yamaji K, 1990: *Organic Superconductors*, (Springer-Verlag, Berlin) Vol. 88

Iwasa Y et al., 1993: J. Phys. Chem. Solids **54**, 1795

Jacobsen CS, 1987: in *Low Dimensional Conductors and Superconductors*, eds. D. Jérome and
        L. Caron (Plenum Press, New York)

Jérome D, 1994: in *Organic Conductors*, ed. J.P. Farges (Dekker, New York) p. 405,

Jérome D and Schulz HJ, 1982: Adv. Phys. **31**, 299

Jérome D et al., 1980: J. Phys. Lett. (Paris) **41**, L-95

Jérome D, 1991: Science **252**, 1509

Kampf A and Schrieffer R, 1990: Phys. Rev. B **41**, 6399

Kang W et al., 1989: Phys. Rev. Lett. **62**, 2559

Kataev V et al., 1992: Solid State Commun. **83**, 435

Kawamoto A et al., 1995: Phys. Rev. Lett. **74**, 3455

Kerkoud R et al., 1994: Europhys. Lett. **25**, 379

Kerkoud R et al., 1996: J. Phys. Chem. Solids **57**, 143

Kini AM et al., 1990: Solid State Commun. **69**, 503

Klemme BJ et al., 1995: Phys. Rev. Lett. **75**, 2408

Klemme BJ et al., 1996: J. Phys. (Paris) I, **6**, 1745

Kosaka M et al., 1993: Chem. Phys. Lett. **203**, 429

Kriza G et al., 1991: Phys. Rev. Lett. **66**, 1922

Kroto HW et al. 1985: Nature **318**, 162

Laukhin VN et al. 1985: Sov. Phys. JETP Lett. **41**, 81

Mac Farlane WA et al., 1995: Phys. Rev. B **52**, R 6995

Mayaffre H et al., 1994: Europhys. Lett. **28**, 205

Mayaffre H et al., 1995: Phys. Rev. Lett. **75**, 4122

Miyagawa K et al., 1995: Phys. Rev. lett. **75**, 1174

Moriya T, 1963: J. Phys. Soc. Jpn. **18**, 516

Moriya T, 1995: in *Spectroscopy of Mott insulators and Correlated Metals*, eds. A. Fujimori and
    Y. Tokura (Springer-Verlag, Berlin) p. 66

Oshima K et al., 1988: Phys. Rev. B **38**, 938

Pekker S 1994: Solid State Commun. **90**, 349

Pouget JP et al., 1982: Mol. Cryst. Liq. Cryst. **79**, 129

Pouget JP, 1996: J. Phys. (Paris) I, **6**, 1501

Schulz HJ, 1991: Int. J. Mod. Phys. B **5**, 57

Solyom J, 1979: Adv. Phys. **28**, 201

Stephens PW et al., 1994: Nature **370**, 636

Sushko YV et al., 1991: J. Phys. (Paris) I **1**, 1375

Sushko YV et al., 1993: Solid State Commun. **87**, 997

Takigawa M et al., 1991: Phys. Rev. B **43**, 247

Tomič S and Jérome D, 1989: J. Phys. Condens. Matter **1**, 4451

Traetteberg O et al., 1994: Phys. Rev. B **49**, 409

Uemura YJ et al., 1995: Phys. Rev. B **52**, R 6991

Urayama H, et al., 1988: Chem. Lett. **55**, 1988

Victoroff W and Héritier M, 1996: J. Phys. (Paris) I, **6**, 2175

Victoroff W et al., 1995: Synthetic. Metals **71**, 1489

Williams JM et al., 1991: Science **252**, 1501

Williams JM et al. 1990: Inorg. Chem. **29**, 3272

Wosnitza J, 1995: in Springer Series in Solid State Science (Springer-Verlag, Berlin)

Wzietek P, 1993: J. Phys. (Paris) I **3**, 171

Wzietek P et al., 1996: J. Phys. (Paris) I, **6**,2011

Zimmer G et al., 1994: Europhys. Lett. **27**, 543

Nuclear Magnetism in Copper, Silver, and Rhodium Metals at Positive and Negative Spin Temperatures in the Nano- and Picokelvin Regimes

Olli V. Lounasmaa

Hahn–Meitner Institut, 14019 Berlin, Germany

and

Low Temperature Laboratory, Helsinki University of Technology, 02150 Espoo, Finland

Abstract

This paper reviews magnetic susceptibility and neutron diffraction studies of metallic copper, silver, and rhodium. I shall start by giving a short historical introduction, followed by a simple theoretical discussion. The concept of negative spin temperatures will then be explained. Next, I shall describe the experimental techniques. The results of measurements will then be presented, first on copper, then on silver, and lastly on rhodium. My review ends with a few concluding remarks.

1 Introduction

Electronic magnetism shows a wide spectrum of different ordering phenomena, extending from room temperature and above in iron to a few millikelvins in cerium magnesium nitrate. Because the nuclear magnetic moments are three orders of magnitude smaller than their electronic counterparts and because dipolar interactions are proportional to the respective magnetic moments squared, spontaneous ordering phenomena can be expected to occur in a nuclear spin system only at microkelvin temperatures and below. Solid ^{3}He is an exception owing to the strong quantum mechanical exchange force, augmented by the large zero-point motion, and so are Van Vleck paramagnets, like $PrNi_5$, in which considerable hyperfine enhancement of the magnetic field occurs. In these systems, the transition temperature is relatively high, around 1 mK (Andres and Bucher, 1968).

Experiments on nuclear magnetic ordering in metals are based on the pioneering investigations of Nicholas Kurti and his collaborators (Kurti et al., 1956). They established the feasibility of the "brute force" nuclear demagnetization method.

The basic formula for nuclear cooling is given by the relationship

$$B_1/T_1 = B_2/T_2 \,, \tag{1}$$

where B_1 and T_1 are the initial and B_2 and T_2 the final magnetic field and temperature before and after demagnetization, respectively. In spite of the limitations imposed by cryogenic techniques forty years ago, the Oxford group succeeded in reaching 1 μK in the nuclear spin system of copper. Subsequent improvements in experimental procedures, much of it done in Helsinki after the advent of powerful dilution refrigerators and superconducting magnets in the late sixties, have made nuclear cooling a reality even below 1 nK (Lounasmaa, 1989).

It is important to note that very near the absolute zero it is meaningful to speak about two distinct temperatures in the same specimen and at the same time; these are the nuclear spin temperature T and the lattice and conduction electron temperature T_e. During nuclear refrigeration experiments, these two quantities can differ by many orders of magnitude. The nuclei reach local thermal equilibrium among themselves in a time characterized by τ_2, the spin–spin relaxation time, whereas the approach to equilibrium between nuclear spins and conduction electrons is governed by the spin–lattice relaxation time τ_1. At low temperatures, $\tau_2 \ll \tau_1$, which makes a separate nuclear spin temperature meaningful and real.

According to Korringa's law (Korringa, 1950),

$$\tau_1 T_e = \kappa \,, \tag{2}$$

where κ is Korringa's constant. For copper $\kappa = 1.2$ sK, in silver and rhodium $\kappa = 10$ sK, and in platinum $\kappa = 0.03$ sK. For example, at the conduction electron temperature of 50 μK, relevant to experiments on copper, the relaxation time $\tau_1 = 7$ h. In silver and rhodium the conduction electrons have been cooled to 100 μK; 28 h are then needed to reach equilibrium between electrons and nuclei in these metals. In low applied fields ($B < B_{\mathrm{loc}}$), the relaxation is faster at least by a factor of two and even quicker in the presence of electronic magnetic imputities. For example, in silver at 100 μK, $\tau_1 \approx 8$ h was actually observed after demagnetization. In platinum, conduction electrons and the nuclei are usually at the same temperature because of the very quick spin–lattice relaxation process.

Purcell and Pound (1951) first produced negative spin temperatures by rapid magnetic field reversal, using LiF as the working substance. The implications of these early NMR experiments have been discussed by Ramsey (1956) and by Van Vleck (1957). Two decades later, beginning in 1968, studies of nuclear co-operative phenomena at positive and negative spin temperatures were started by Abragam and Goldman (Abragam, 1987; Goldman, 1970; Bouffard et al., 1994); the Saclay group investigated the dielectric materials CaF_2, LiF, and LiH.

The Helsinki investigations of spontaneous nuclear magnetic ordering were started in the mid 1970's by constructing a two-stage nuclear demagnetization cryostat, a pioneer of its kind (Ehnholm et al., 1979, 1980). The first really important results were obtained in 1982 when magnetic susceptibility measurements showed that copper orders antiferromagnetically below the Néel temperature $T_N = 58$ nK (Huiku and Loponen, 1982). In 1984, three antiferromagnetic phases were discovered in a single crystal specimen below the critical field $B_c = 0.25$ mT (Huiku et al., 1984, 1986).

In order to investigate, in more detail, the antiferromagnetically ordered spin structures of copper, neutron diffraction experiments were initiated in 1985 by a collaboration between the Risø National Laboratory in Denmark (Kurt Clausen and Per-Anker Lindgård), the Hahn–Meitner Institut in Berlin and the University of Mainz (Michael Steiner), and the Low Temperature Laboratory in Helsinki (Olli Lounasmaa). These measurements, carried out in Risø, extended by an order of magnitude the temperature regime at which neutron diffraction had been employed previously. In 1987, the first results were obtained when the (1,0,0) Bragg reflection was observed in copper confirming, indeed, antiferromagnetic order (Jyrkkiö et al., 1988). In 1989 another Bragg reflection, at $(1, \frac{1}{3}, \frac{1}{3})$, was found (Annila et al., 1990, 1992). The three antiferromagnetic phases, discovered by susceptibility measurements, were reproduced.

The work on silver started in Helsinki in 1987 (Oja et al., 1990). By employing magnetic susceptibility measurements, positive and negative spin temperatures of 0.8 nK and -4.3 nK were recorded. In the middle of 1990, antiferromagnetic order was found below 560 pK at positive temperatures (Hakonen et al., 1991). And, in 1991, the ferromagnetically ordered spin structure at negative temperatures was observed in silver, with ordering at $T_C = -1.9$ nK (Hakonen et al., 1992). In 1993 the Danish-Finnish-German team started preparations for neutron diffraction work at $T > 0$ on silver at the Hahn–Meitner Institut in Berlin. In 1995 the antiferromagnetic Bragg peak at $(0,0,1)$ was seen (Tuoriniemi et al., 1995). A structure with the ordering vector $\mathbf{k} = (\pi/a)(0,0,1)$ developed when the ordered phase was entered by adiabatic demagnetization along the $[0,0,1]$ axis. The observed Bragg peak proves decisively spontaneous antiferromagnetic nuclear spin ordering in silver at $T > 0$. So far the neutron diffraction work has not been extended to negative spin temperatures, but such experiments should be technically feasible.

In rhodium, spin temperatures of 280 pK and -750 pK were produced in 1993 (Hakonen et al., 1993). These are the current world records on each side of the absolute zero. Spontaneous magnetic ordering has not been seen in rhodium so far.

The present paper is very short on theory but a comprehensive review (Oja and Lounasmaa, 1997), including an extensive theoretical section, will appear in the

January 1997 issue of Reviews of Modern Physics. I also refer to short articles by Hakonen et al. (1991) and by Hakonen and Lounasmaa (1994). I discuss the theory and practice of neutron diffraction experiments only very briefly (see the begining of Sect. 8); for a more complete treatment the publications by Steiner (1993) and by Nummila et al. (1997) should be consulted.

2 Theoretical remarks

Nuclear spins in metals provide good models to investigate magnetism. The nuclei are well localized, their spins are isolated from the electronic and lattice degrees of freedom at low temperatures, and the interactions between nuclei can often be calculated from first principles. Therefore, these systems are particularly suitable for testing theory against experiments. Comparisons with ab initio calculations allow rather deep new insights into the interactions leading to spontaneous nuclear ordering.

The Hamiltonian of the nuclear spin system can be written

$$H = H_{\mathrm{dip}} + H_{\mathrm{RK}} + H_Z + H_{\mathrm{psd}} \,. \tag{3}$$

In this expression the dipolar force between the magnetic moments of the nuclei is given by

$$H_{\mathrm{dip}} = \frac{\mu_0 \hbar^2}{4\pi} \sum_{i<j} \gamma_i \gamma_j r_{ij}^{-3} \left[\mathbf{I}_i \cdot \mathbf{I}_j - 3 r_{ij}^{-2} (\mathbf{r}_{ij} \cdot \mathbf{I}_i)(\mathbf{r}_{ij} \cdot \mathbf{I}_j) \right] . \tag{4}$$

The form of the dipolar interaction is known exactly. In Eq. (4), μ_0 is the permeability of free space, $\hbar$ is Planck's constant divided by 2π, γ is the gyromagnetic ratio (proportional to the nuclear magnetic moment μ), r_{ij} is the distance between spins i and j, and $\mathbf{I}$ is the nuclear spin. The appearance of the lattice vector $\mathbf{r}_{ij}$ in the second term in braces shows that the dipolar force is direction dependent, i.e., the interaction is anisotropic.

The so-called Ruderman–Kittel (1954) exchange force, caused by polarization of conduction electrons by the magnetic nuclei, is given by

$$H_{\mathrm{RK}} = -\sum_{i<j} J_{ij}(r_{ij}) \, \mathbf{I}_i \cdot \mathbf{I}_j \,,$$

where

$$J(x) \propto [\cos x - (\sin x)/x]/x^3 \,. \tag{5}$$

The expression for H_{RK} shows that the RK-force is isotropic. Calculations of H_{RK} requires detailed knowledge of the electronic band structure of the metal. The form

function $J_{ij}(r_{ij})$ is expanded in Eq. (5) using the free-electron approximation, but it has been calculated for copper and silver from first principles (Lindgård et al., 1986; Harmon et al., 1992). The RK exchange interaction, which oscillates with distance between neighbouring nuclei, can be ferro- or antiferromagnetic, depending on the lattice parameter and crystal symmetry.

The Zeeman interaction with the external magnetic field B is

$$H_Z = -\hbar\gamma \mathbf{B} \cdot \sum_i \mathbf{I}_i \,. \tag{6}$$

In copper, the ferromagnetic dipolar force is almost equal to the antiferromagnetic Ruderman–Kittel interaction, whereas in silver the latter dominates by a factor of 2.5. This leads to a complicated magnetic phase diagram (see Sects. 7 and 8) in Cu. Owing to the strong exchange force, the spin system in silver bears a close resemblance to an fcc Heisenberg antiferromagnet which has been the object of much theoretical interest owing to "frustration" (Binder and Young, 1986). With ferromagnetic forces between neighbours, there is no problem. Because the nuclear spin $I = 1/2$ in silver and rhodium, quantum effects are expected to be prominent.

In rhodium the d-electron-mediated anisotropic exchange forces, characteristic of transition metals, contribute as well (Bloembergen and Rowland, 1955). These can be taken into account, approximately, by a pseudodipolar term

$$H_{\mathrm{psd}} = \sum_{i<j} B_{ij} [\mathbf{I}_i \cdot \mathbf{I}_j - 3r_{ij}^{-2}(\mathbf{r}_{ij} \cdot \mathbf{I}_i)(\mathbf{r}_{ij} \cdot \mathbf{I}_j)] \tag{7}$$

in the Hamiltonian of Eq. (3).

Nuclear ordering in scandium metal has been investigated by Suzuki and his coworkers (Koike et al., 1995); they claim to have seen the transition to an ordered phase but the experimental data so far are not convincing. Pobell and his group at Bayreuth have studied thallium metal (Schröder-Smeibidl et al., 1991) and the cubic intermetallic compound $AuIn_2$; in these two substances the spin–lattice relaxation time is so short that conduction electrons and the nuclei are always in thermal equilibrium with each other. Recent data (Herrmannsdörfer et al., 1995) on $AuIn_2$ show that the ^{115}In nuclei order ferromagnetically at the surprisingly high Curie temperature $T_C = 35 \ \mu K$. For a discussion of hyperfine enhanced materials, such as $PrNi_5$, I refer to Andres and Lounasmaa (1982).

All experiments on insulators, by Abragam, Goldman, and their coworkers (Bouffard et al., 1994) and by Wenckebach and his team (Van der Zon et al., 1990), have been performed using dynamic nuclear polarization, followed by adiabatic demagnetization in the rotating frame. The main weakness of the dynamic method of cooling is the inevitable presence of electronic paramagnetic impurities,

introduced purposely to polarize the nuclei by the "solid effect"; the strong local fields produced by the impurities probably blur, to a certain extent, some of the features of the nuclear long-range order. Copper, silver, and rhodium provide more general systems for experimental and theoretical studies of nuclear magnetism at positive and negative spin temperatures. These metals can be cooled by the brute force adiabatic nuclear demagnetization technique, without recourse to electronic impurities.

3   Negative spin temperatures

Much of the theoretical discussion in this section is based on the early work of Ramsey (1956) and Van Vleck (1957).

Energy level diagram for an assembly of silver or rhodium nuclei, at positive and negative spin temperatures, is shown schematically in Fig. 1; the spin $I = 1/2$,
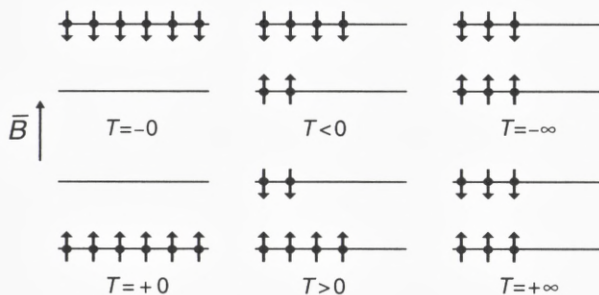

Figure 1. Energy-level diagram of nuclear spins in silver or rhodium at selected temperatures when $B = $ constant (Hakonen and Lounasmaa, 1994).

so there are just two levels, corresponding to $\boldsymbol{\mu}$ parallel and antiparallel to the external field **B**.

The distribution of the nuclei among the Zeeman energy levels is determined by the Boltzmann factor,

$$\exp(-\varepsilon/k_B T) = \exp(\boldsymbol{\mu} \cdot \mathbf{B}/k_B T). \tag{8}$$

At positive temperatures the number of nuclei in the upper level, with $\boldsymbol{\mu}$ antiparallel to **B**, is always smaller than in the lower level. At the absolute zero, all nuclei are in the ground state with $\boldsymbol{\mu}$ parallel to the external magnetic field **B**. At $T < 0$

there are more spins in the upper than in the lower level.

Ordinarily, the temperature describes the average energy which is either connected with the free motion of the particles or with their vibrations about the lattice sites. In both cases the energy per particle is on the order of $k_B T$. The kinetic energy has no upper bound. Thus, if the temperature were raised towards infinity, the energy of the system would increase without limit. This is an unphysical situation and means that conduction electrons and the crystalline lattice cannot be brought to $T = \pm \infty$, even less to $T < 0$.

Negative temperatures, however, are possible when the energies of the particles are bound from above. In such cases, the absolute temperature is closely connected with the amount of disorder, i.e., with entropy. Let us consider nuclei in a constant external field **B**. The magnetic moment $\boldsymbol{\mu}$ of each nucleus tends to orient itself along the field, but thermal motion produces disorder. When the temperature approaches zero, the entropy decreases. At $T = +0$, this causes complete order among the nuclei. In principle, one can also remove the nuclear disorder and approach the absolute zero from the opposite, negative side, $T \to -0$, by having the nuclear moments fully aligned antiparallel to the external field.

The theorems and procedures of statistical mechanics, such as the use of the partition function and the quantum mechanical density matrix, apply equally to systems at negative temperatures. By examining the statistical theory by which the Boltzmann distribution is derived, there is nothing objectionable a priori for the parameter $1/k_B T$ being negative; $T < 0$ simply means that the mean energy of the system is higher, instead of being lower than the energy corresponding to equal populations among the energy levels at $T = \pm \infty$.

The thermodynamic functions can be computed from the partition function, given for a 2-level system, with energy $\varepsilon = \pm \mu B$ (see Fig. 1), by the expression

$$Z = [\exp(\mu B/k_B T) - \exp(-\mu B/k_B T)]^N = [2\sinh(\mu B/k_B T)]^N \,, \tag{9}$$

where N is the number of spins in the assembly. Polarization p and entropy S are given by the relations

$$p = \tanh(\mu B/k_B T) \,, \tag{10}$$

$$S/R = \ln 2 - \tfrac{1}{2}[(1+p)\ln(1+p) + (1-p)\ln(1-p)] \,. \tag{11}$$

The thermodynamic quantities are functions of B/T only.

Near the absolute zero, $1/T$ or $\log T$ is sometimes used as the temperature function but, when $T < 0$, $\log T$ is not suitable. However, on the inverse-negative scale $\beta = -1/T$, the coldest temperature, $T = +0$, corresponds to $\beta = -\infty$ and the hottest temperature, $T = -0$, to $\beta = +\infty$. On this scale the algebraic order of β and

the order from cold to hot are identical; the system passes from positive to negative Kelvin temperatures through $\beta = -0 \rightarrow +0$. The choice, $\beta = -1/T$, ensures that a colder temperature is always to the left side of a hotter one along the β-axis. This inverse-negative scale thus runs in an "orderly" fashion from the coldest to the hottest temperature. The third law of thermodynamics appears "naturally" by the impossibility to reach the positive or negative ends of the β-axis infinitely far.

Figure 2 illustrates the entropy S, the specific heat at constant field C_B, and the internal energy U, suitably normalized, of a two-level spin assembly as a function of $\beta = -1/T$. The external field B and the energy level separation $2\mu B$ are
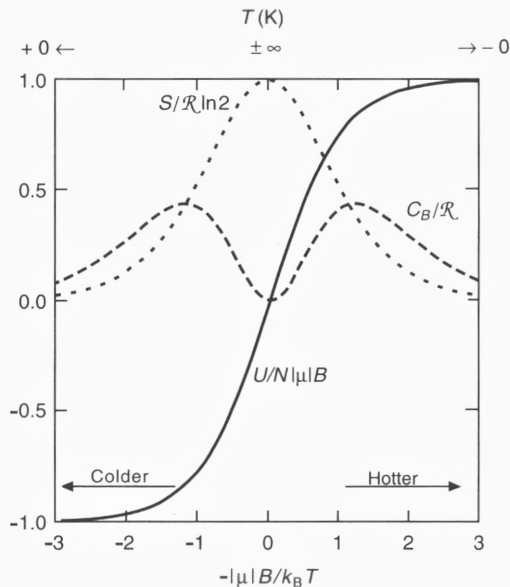

Figure 2. Entropy (dotted curve), internal energy (full curve), and specific heat (dashed curve) plotted as a function of $-|\mu|B/k_B T$ at $B = $ constant for a nuclear spin system of two energy levels separated by $2\mu B$ ($I = 1/2$, $|\mu| = \frac{1}{2}\hbar|\gamma|$, and R is the gas constant).

assumed constant. The entropy has its maximum value $S = R\ln 2$ at $\beta = \pm 0$, i.e. at $T = -\infty$ or $T = +\infty$, because both energy levels are equally populated and polarization is zero. The specific heat C_B is zero at $\beta = -\infty$ and at $\beta = +\infty$ since all spins occupy their lowest or highest energy level at $T = \pm 0$ and no more heat

can be removed or absorbed, respectively. At $\beta = \pm 0$, $C_B = 0$ as well because a very large change in T corresponds to a very small change in the spin configuration. The internal energy U has its lowest value at $T = +0$ and its highest value when $T = -0$.

At $T < 0$, adiabatic demagnetization heats the spin system, instead of cooling it as happens when $T > 0$. Similarly, for experiments on polarized nuclei, at $T < 0$ the spin system must be heated to the hottest negative temperature to achieve maximum polarization, while at positive temperatures the spins must be cooled.

From the thermodynamic point of view, an essential requirement for the existence of a negative temperature is that the entropy S is not a monotonically increasing function of the internal energy U. In fact, whenever $(\partial S/\partial U)_B < 0$, $T = 1/(\partial S/\partial U)_B < 0$ as well. It was mentioned already that for negative temperatures to occur, there must be an upper limit to all allowed energy states of the system, otherwise the Boltzmann factor of Eq. (8) does not converge for $T < 0$. Nuclear spins satisfy this requirement since there are $2I + 1$ Zeeman levels and, indeed, $(\partial S/\partial U)_B$ changes sign at $T = \pm\infty$.

In addition, the elements of the spin assembly must, of course, be in internal thermodynamic equilibrium so that the system can be described by the Boltzmann distribution and thereby assigned a temperature. The thermal equilibrium time τ_2 among the nuclear spins themselves must be short compared to the time τ_1 of appreciable "leakage" of energy to or from other systems. In silver, for example, $\tau_1 = 28$ h at $T_e = 100$ μK, while $\tau_2 = 10$ ms.

We now return to the nuclear energy level diagram of Fig. 1. As the temperature is increased from $T = +0$, nuclei flip into the upper energy level and, at $T = +\infty$, there is an equal number of spins in both levels; the infinite temperature, however, does not cause any problems in this case since the energy spectrum has an upper bound. When the energy is increased further by lifting more spins to the higher level, the inversed spin distribution can still be described by the Boltzmann factor, see Eq. (8), but now with a negative temperature. Finally, when approaching the absolute zero from the negative side, $T \to -0$, eventually only the upper energy level is populated. Since heat is transferred from the warmer to the colder body when two systems are brought into thermal contact, negative temperatures are actually "hotter" than positive ones.

At $T = +0$, an isolated nuclear spin assembly has the lowest and, at $T = -0$, the highest possible energy. This important fact can be put on a more general basis. During demagnetization, the external magnetic field B at first completely controls the nuclear spin system. Entropy, a function of B/T, stays constant. However, when the field has been reduced sufficiently, approaching the internal local field B_{loc}, 0.25 mT in copper and 35 μT in silver and rhodium, the dipole–dipole and exchange forces gradually take over and the spin order begins to change from that

forced by $\boldsymbol{B}$ to an arrangement determined by mutual interactions. During this spontaneous adjustment of spins the entropy increases, according to the general principles governing thermodynamic equilibrium, until S reaches a maximum while the magnetic enthalpy

$$H = U - BM \,, \tag{12}$$

where M is the magnetization, stays constant because the system is isolated. If the entropy does not exceed a critical value, about 45% of its maximum $R\ln(2I+1)$, spontaneous spin order will occur.

In order to find the equilibrium spin configuration, one has to consider the variation of entropy under the restriction of a constant enthalpy, i.e., one must seek an extremum of $S + \lambda H$ where, by differentiation, Lagrange's multiplier $\lambda = -dS/dH = -1/T$. Therefore, one obtains $S - H/T = -G/T$ for the thermodynamic potential reaching an extremum; G is the Gibbs free energy. When temperature is positive,

$$G = H - TS \tag{13}$$

and the extremum is a minimum since S assumes its largest value at equilibrium. When the temperature is negative,

$$G = H + |T|S \tag{14}$$

and the Gibbs free energy obviously reaches a maximum.

The tendency to maximize the energy, instead of minimizing it, is the basic difference between negative and positive temperatures. In silver, the nearest-neighbour antiferromagnetic Ruderman–Kittel exchange interaction, three times stronger than the dipolar force, favours antiparallel alignment of the nuclear magnetic moments and thus leads to antiferromagnetism at positive spin temperatures. At $T < 0$, since the Gibbs free energy now must be maximized, the very same interactions tend to produce ferromagnetic nuclear order. This has been observed in experiments (see Sect. 9).

4   Achieving population inversion in practice

The Helsinki group has produced negative spin temperatures in silver and rhodium (see Sects. 9 and 11). In these metals, the spin–spin relaxation time $\tau_2 = 10$ ms; therefore, the nuclei can quickly equilibrate among themselves to a common spin temperature. On time scales 10 ms $\ll t \ll$ 10 h, two separate temperatures exist: one, T_e for the lattice and conduction electrons, and another, T for the nuclei. The

spin–lattice relaxation time, $\tau_1 = (10 \text{ sK})/T_e$ in silver and rhodium, is inversely proportional to the conduction electron temperature, see Eq. (2). For good thermal isolation between electrons and nuclei, a low T_e is thus needed; this is why the experiments must be carried out at ultra low temperatures.

Population inversion from positive to negative spin temperatures is rather hard to generate in metallic samples for two reasons: First, substantial effort is needed to reach the high initial spin polarizations, and second, eddy currents make the production of inverted spin populations a difficult task. In spite of these problems, a team in Helsinki (Oja et al., 1990) decided to try such an experiment on silver: A small external magnetic field was reversed quickly, in about 1 ms, so that the nuclei had no chance to rearrange themselves among the energy levels.

This simple idea worked: Negative temperatures were produced in the nuclear spin system of silver but the loss of polarization was large. After improvements and refinements of the technique, fully satisfactory results were obtained; first on silver (Hakonen et al., 1990) and later on rhodium (Hakonen et al., 1993). In copper, $\tau_2 = 0.1$ ms, 100 times shorter than in silver and rhodium. Therefore, production of negative temperatures has not succeeded in copper, because the external magnetic field could not be reversed fast enough without causing massive eddy current heating in the specimen.

Indeed, it is important to realize that the field flip must be rapid in comparison to τ_2, the Larmor period of the spins in the local field B_{loc}. If this condition is not met, the spins are able to follow adiabatically the field reversal, and negative temperatures will not result. Demagnetization will just be followed by remagnetization to the positive starting temperature. In fact, during the quick field flip the Boltzmann distribution of the spins breaks down and, for a short moment, the system cannot be assigned a temperature. In a certain sense, the spin assembly passes from positive to negative temperatures via $T = +\infty \rightarrow -\infty$, without crossing the absolute zero. Therefore, the third law of thermodynamics is not violated. The needed increase in the energy of the spin system is supplied by the external magnetic field.

The rapid reversal of a small magnetic field, typically 400–500 μT, always resulted in a loss of polarization, i.e. increase of entropy of the spin system. The inversion efficiency from p_1 to p_2 was about 95% at small polarizations but decreased to 80% for $p_1 > 0.8$. Therefore, the studies at $T < 0$ in silver were limited to negative polarizations up to $p_2 \approx -0.6$.

The increase of entropy is, at least partially, explained by the heat that must flow to the spin–spin interaction "reservoir" to warm it to a negative temperature after population inversion, which reverses only the sign of the Zeeman temperature T_Z (Oja et al., 1990). Owing to the magnetic dipolar forces between the spins and other interactions, the Zeeman levels actually form bands which have an energy

distribution and a temperature T_{ss} of their own.

Contrary to the Zeeman energy, the spin–spin interaction energy does not depend on B. By changing the external magnetic field, a difference can thus be produced between T_Z and T_{ss}. When B is much higher than B_{loc} (35 μT in silver), the separation of the two Zeeman energy levels is large in comparison with the width of the spin–spin bands. This means that the latter system has a very small possibility to absorb an energy quantum produced when a spin is flipped. It then takes a long time for T_Z and T_{ss} to equalize. When $B \approx B_{loc}$, equilibrium is reached quickly. This process, leading to $T = T_Z = T_{ss}$, is probably an important reason for the polarization loss during the field reversal.

Before the field flip, $T_Z = T_{ss} = 10$ nK. After the 400 μT field is quickly reversed to -400 μT, $T_Z \approx -10$ nK but T_{ss} first stays at $+10$ nK. Since $B \gg B_{loc}$, the heat capacity of the Zeeman reservoir is much larger than the heat content of the spin–spin system, which guarantees that, after equilibrium, the spin temperature $T < 0$, but "colder" than -10 nK. As soon as $B \approx B_{loc}$, dipole–dipole and exchange interactions become important and, at the Curie temperature $T_C = -1.9$ nK, produce ferromagnetic order in silver (see Sect. 9).

5   Cryogenic techniques

To obtain nuclear temperatures in the nano- and picokelvin regimes, a sophisticated "brute force" cooling apparatus, with two nuclear refrigeration stages in series, has been employed in Helsinki, Risø and Berlin. The cryostats have, of course, undergone many important changes over the years. Precooling is done by a dilution refrigerator, and the large first nuclear stages have been manufactured from copper rods weighing over 1 kg. The second nuclear stage is the sample itself, made of a 2 g piece of bulk copper or of many 25 to 75 μm thick strips of silver or rhodium.

The specimen is connected to the precooling first nuclear stage without a heat switch. This means that the conduction electron temperature T_e is the same in both nuclear stages and that, for thermal isolation of the nuclear spin system in the sample, one relies entirely on the slowness of the spin–lattice relaxation process. The latest of these cascade nuclear refrigerators, operating at the Hahn–Meitner Institut in Berlin, is illustrated in Fig. 3. Cooling techniques below 1 K are discussed in detail by Lounasmaa (1974).

In copper the spin–lattice relaxation time is too short for experimental convenience, but for silver and rhodium τ_1 is inconveniently long, 28 h at 100 μK in a high magnetic field. Therefore, precooling a silver sample to 50 μK is a tedious process requiring two days. Owing to the limited capacity of the liquid ^{4}He bath, it was not feasible in the experiments on silver to wait long enough; this frequently
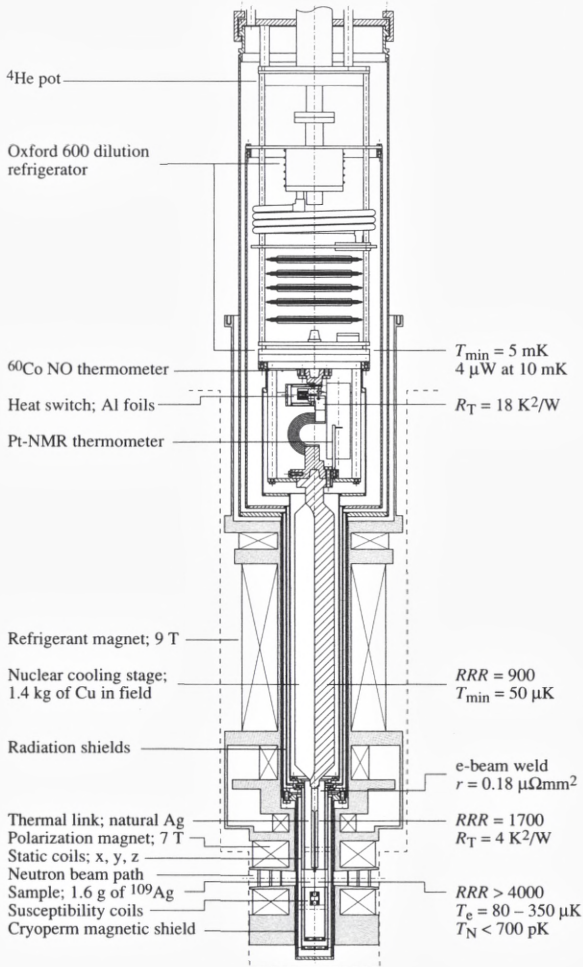
Figure 3. Cascade nuclear demagnetization cryostat designed for neutron scattering experiments on silver in Berlin (Nummila et al., 1997). The apparatus has a 9 T magnet surrounding the 1.4 kg copper nuclear cooling stage and a 7 T magnet for the sample. The copper refrigerant, demagnetized to 60 mT, keeps the lattice temperature at about 100 μK while the ^{109}Ag nuclei are polarized to 95%. The spins are further cooled into the picokelvin range by reducing the 7 T external field to zero. Before the end of demagnetization, an additional field of 400–500 μT is applied on the sample by a set of small coils, so that the ordered state can later be entered from any field direction. The Oxford 600 dilution refrigerator has a cooling power of 4 μW at 10 mK.

prevented the use of starting temperatures lower than 100 μK.

Figure 4 is a schematic illustration, on a temperature vs. entropy diagram, of the procedure for cooling an assembly of silver or rhodium nuclei to negative nano-kelvin temperatures. Numerical values refer to the YKI cryostat in Helsinki. One proceeds as follows:

- (A → B) Both nuclear stages are cooled to 10 mK by the dilution refrigerator and, simultaneously, the nuclei in the first stage are polarized in a strong magnetic field of 8 T.

- (B → C) The first stage, made of 1400 g of copper, is adiabatically demagnetized to 100 mT, which produces a low temperature of ≈ 100 μK. Towards the end of demagnetization, the second nuclear stage, i.e. the sample, is magnetized to 8 T.

- (B → D) The 2 g silver or rhodium specimen of thin foils then slowly cools, in the high magnetic field of 8 T, by thermal conduction to ≈ 100 μK.

- (D → E) As the next step, the sample is adiabatically demagnetized from 8 T to 400 μT, whereby the spins reach approximately 10 nK. They are thermally isolated by the 28 h spin–lattice relaxation process from the conduction electrons which are anchored to 100 μK by the first nuclear stage at C.

- (E → F) Finally, the negative spin temperature is produced in the system of silver or rhodium nuclei by reversing the 400 μT magnetic field in about 1 ms. The increase in the energy of the spin system is absorbed from the external magnetic field. The rapid inversion causes some loss of polarization, i.e. increase of entropy. By continuing demagnetization to $B = 0$, the record temperature of -750 pK was reached in rhodium. In silver, dipole–dipole and exchange interactions produced ferromagnetic order at the Curie temperature $T_C = -1.9$ nK.

- (F → G → A) The system then begins to lose its negative polarization, crossing in a few hours, via infinity, from negative to positive temperatures. The measurements must be carried out in about 10–30 min after the final demagnetization, since the nuclear spin temperature starts immediately to relax towards $T_e = 100$ μK with the time constant τ_1, determined by the spin–lattice relaxation process.

- (C → A) The first nuclear stage warms slowly, under the 100 mT field, from 100 μK towards 15 mK. A new experimental sequence can then be started.
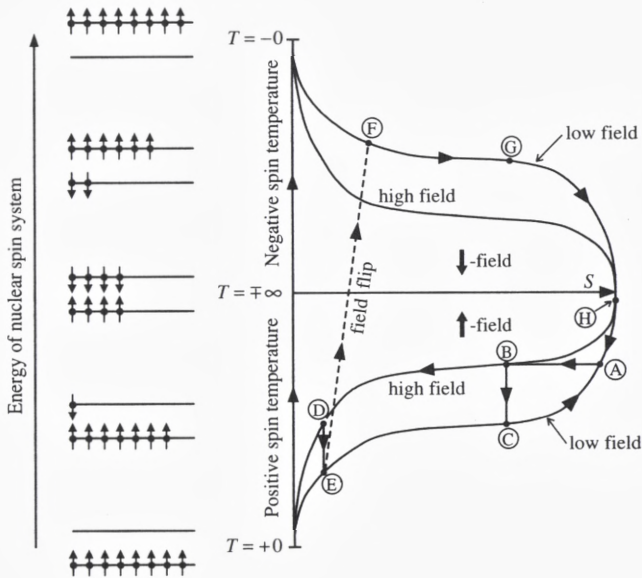
Figure 4. Schematic illustration of the cascade nuclear cooling process to produce negative spin temperatures (Lounasmaa et al., 1994).

If production of negative spin temperatures was not intended, demagnetization from 400 μT was continued at E to zero field, resulting in the record temperature of 280 pK in rhodium. In silver, dipole–dipole and exchange interactions produced antiferromagnetic order at the Néel temperature $T_{\mathrm{N}} = 560$ pK.

6   Measurement of spin temperature

One of the difficult tasks in these experiments was to measure the absolute temperature of the thermally isolated nuclei. The usual technique employs directly the second law of thermodynamics, viz.

$$T = \Delta Q / \Delta S \,. \tag{15}$$

At positive temperatures, the nuclear spin system is supplied with a small amount of heat ΔQ and the ensuing entropy increase ΔS is calculated from the measured loss of nuclear polarization (see below). The method works equally well at negative spin temperatures: $\Delta Q < 0$ when entropy increases. The system radiates some of its energy at the nuclear Larmor frequency while the populations of the two energy

levels tend to equalize.

The primary observable in these experiments is the nuclear magnetic resonance signal (Slichter, 1990), recorded by a SQUID. We measured $\chi(\nu) = \chi'(\nu) + i\chi''(\nu)$ using frequency sweeps across the resonance in a constant magnetic field. This was done at low frequencies where the skin effect does not prevent the magnetic field from penetrating into the metalic specimen. The experimental setup for recording the susceptibility has evolved over the years. One of the later SQUID-NMR systems is described by Hakonen et al. (1993).

From χ'', applying the Kramers–Kronig relation

$$\chi'(0) = (2/\pi) \int (\chi''(\nu)/\nu)d\nu \,, \tag{16}$$

one can calculate χ' which, at the low frequencies, is equal to the static susceptibility $\chi'(0)$; ν is the NMR excitation frequency. Furthermore, from the measured χ'' it is possible to deduce the nuclear polarization using the well known relationship

$$p = A \int \chi''(\nu)d\nu; \tag{17}$$

the proportionality constant A can be calibrated against the platinum-NMR temperature scale around 1 mK. Equation (17) is valid when $B \gg B_{\text{loc}}$. When the polarization has been determined, one can compute the entropy, Eq. (11), because, at these ultralow temperatures, the only contribution to S is from the nuclear spins.

One of the drawbacks in measuring the nuclear temperature directly by means of the second law, Eq. (15), is that the applied ΔQ warms the spins substantially because a large heat pulse is needed to allow an accurate determination of ΔS. Only a small number, 7 to 9 points per run, could be obtained, but more data are needed for studies of ordering, which was revealed both by changes in the shape of the NMR line and by a plateau in the static susceptibility vs. time curve. For this reason, Hakonen et al. (1991) developed another method of thermometry by first investigating the connection between polarization and temperature. By equating the second order expansion of entropy in terms of polarization, viz.

$$S/R \ln 2 = 1 - p^2/(2 \ln 2) \,, \tag{18}$$

with the $1/T^2$-expansion of entropy, one obtains a linear dependency between $1/p$ and T. The low temperature end is also known approximately: By neglecting quantum fluctuations, one expects that $p \to 1$ when $T \to 0$. In fact, an almost linear relationship was found below $|T| < 10$ nK, namely

$$1/|p| - 1 = 0.55(|T|/\text{nK}), \tag{19}$$

both at $T > 0$ and $T < 0$. The accuracy of the measured temperatures is $\pm 20\%$.

During neutron diffraction experiments it is possible to employ the transmission of a polarized neutron beam as a primary thermometer. The paper by Lefmann et al. (1997) describes this convenient and accurate method in some detail. Even unpolarized neutrons can be used for absolute thermometry without calibration. An important advantage of neutron thermometry is that the technique can be applied in any magnetic field and on bulk metal samples, unlike the NMR method. The neutron technique was used recently in studies of nuclear magnetic ordering of ^{109}Ag nuclei at nanokelvin temperatures (see Sect. 10). Transmission of thermal neutrons provided a convenient tool for monitoring the state and evolution of the spin assembly (Tuoriniemi et al., 1997).

7   Susceptibility measurements on copper

The Helsinki investigations of spontaneous nuclear magnetic ordering were started in the mid 1970's by constructing a two-stage nuclear demagnetization cryostat. Evidence for antiferromagnetic order in copper was found in 1978 (Ehnholm et al., 1979, 1980) but it took four years before magnetic susceptibility measurements showed that the actual transition is at $T_N = 58$ nK (Huiku and Loponen, 1982). In two more years experiments were made using a single-crystal specimen (Huiku et al., 1984, 1986). By an elaborate coil system one could measure the susceptibility in all three Cartesian directions.

Figure 5 shows an important result, the spin entropy of copper; $S_{max} = R \ln 4$ for Cu because the nuclear spin $I = 3/2$. There is a clear jump in entropy which signifies a first order change to an antiferromagnetic phase. $T_N = 58$ nK was, at the time, the lowest transition temperature ever observed or measured. S_{c1} is the lower and S_{c2} the higher critical entropy. This measurement was done on a polycrystalline copper sample.

Figure 6 illustrates the x-, y-, and z-components of the susceptibility in three external fields. For analyzing the data, one must first recall how the longitudinal and transverse susceptibilities behave below the Néel point in electronic antiferromagnets: $\chi_\perp$, the susceptibility transverse to sublattice magnetization, is constant while $\chi_\parallel$, the susceptibility parallel to sublattice magnetization, approaches zero as $T \to 0$. Consequently and by analogy, when $B = 0$, the magnetization is mainly along the y-axis since changes in χ are largest in this direction.

At $B = 0.15$ mT, the sublattice magnetization has its biggest component in the z-direction but it also has a smaller component in the y-direction. At $B = 0.20$ mT, the spins are leaning towards the external magnetic field because there is no longer antiferromagnetism in the z-direction. Furthermore, in contrast to
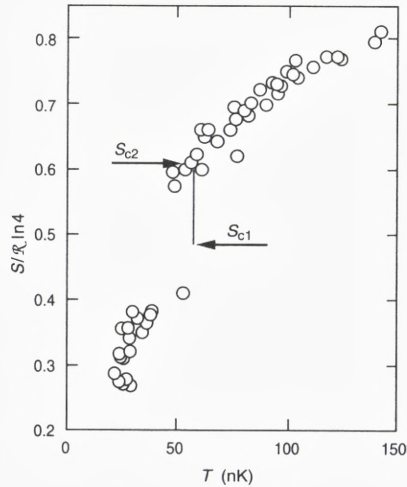
Figure 5. Reduced nuclear entropy $S/R\ln 4$ of copper vs. the spin temperature in nanokelvins (Huiku et al., 1986).

the "paramagnetic" behaviour of χ_z, a small increase in χ_y indicates an antiferro-magnetic y-component of magnetization. Since χ_x is approximately constant in all fields, the sublattice magnetization is always perpendicular to the x-direction. These characteristically different behaviours indicate three separate, antiferromag-netically ordered regions in the nuclear spin system of copper.

Figure 7 shows the B–S phase diagram of copper; it was constructed by demag-netizing from different initial values of entropy, between 10% and 35% of $R\ln 4$, i.e., by moving down on the diagram, and then by letting the specimen to warm up, thus moving horizontally to the right while the susceptibility was being measured. The low field phase is marked by AF1, the middle field phase by AF2, and the high field phase by AF3; the paramagnetic phase P is at right. The shaded regions indicate where one characteristic behaviour changes to another and a latent heat is being supplied; $\Delta S \approx 0.12R\ln 4$. The spin arrangements are again drawn into the figure.

A phase diagram in the magnetic field vs. temperature plane was not con-structed because temperatures could be measured reliably only in zero field. Never-theless, surprisingly many interesting results were obtained from these simple but technically very difficult susceptibility measurements.
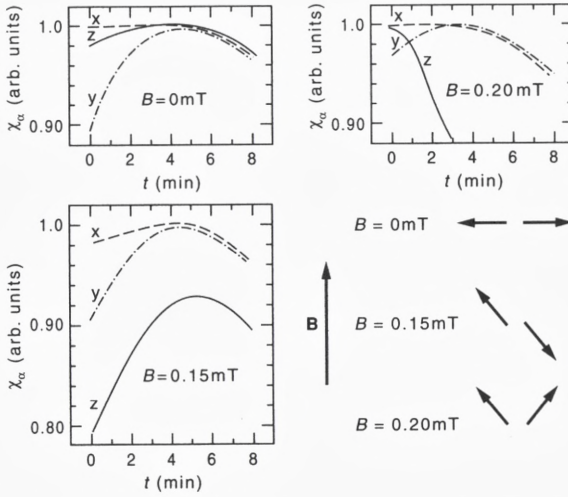
Figure 6. Susceptibility χ_α of a Cu single crystal, along the three Cartesian directions ($\alpha = x, y, z$) as a function of time in external fields $B = 0$, 0.15, and 0.20 mT. The originally suggested spin arrangements are illustrated in the lower right corner. The sample was a slab of dimensions $0.5 \times 5 \times 20$ mm^3 along the x-, y- and z-directions, respectively (Huiku et al., 1986).

8   Neutron diffraction on copper

However, no detailed information about the ordered spin structures can be extracted from susceptibility data. The appropriate technique is neutron diffraction, which is the most powerful method for microscopic structural studies of magnetic systems because the neutron-nucleus scattering length a is spin dependent (Price and Sköld, 1986; Windsor, 1986; Steiner, 1990). The relevant equation is

$$a = b_0 + b\,\mathbf{I} \cdot \mathbf{S}\,, \tag{20}$$

where b_0 and b are constants, $I = 3/2$ is the nuclear spin of copper, and $S = 1/2$ is the spin of the neutron. The observed scattered neutron intensity is proportional to the square of the sublattice polarization. Likewise, the nuclear absorption cross section is also spin dependent. In both cases, the sensitivity is increased significantly by the use of a polarized beam.

Successful neutron diffraction experiments on copper were undertaken by a Danish-Finnish-German collaboration at the Risø National Laboratory in Denmark. Copper has an fcc structure which means that only reflections with all Miller indices (h, k, l) even or all odd are allowed. Long-range antiferromagnetic order in
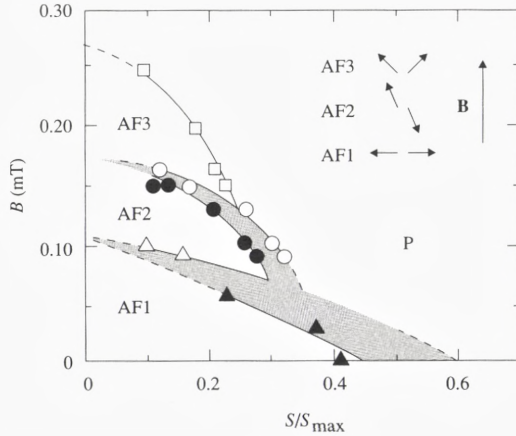
Figure 7. External magnetic field vs. entropy diagram of copper nuclear spins (Huiku et al., 1986). The critical field $B_c \approx 0.25$ mT. The Néel temperature $T_N \approx 60$ nK.

the nuclear spin system gives rise to additional Bragg peaks with (h, k, l) mixed, which yield the translational symmetry of the magnetic superstructure. However, nuclear scattering, which results from the strong interaction, but not from dipolar forces as in electronic neutron diffraction experiments, is isotropic in the spin space which makes it impossible to assign directions to the magnetic moments relative to the lattice axes. Polarized neutrons with a full polarization analysis would provide this information. So far, however, the magnetic shields (see Fig. 3), needed around the sample for the ordering experiments below $B_c \approx 0.25$ mT, depolarized the neutron beam in low fields.

In zero external magnetic field, theoretical calculations predicted antiferromagnetic structure (Lindgård, 1988), exemplified by the modulation vector $\mathbf{k} = (\pi/a)(1,0,0)$, which yields a $(1,0,0)$ Bragg peak (Kjäldman and Kurkijärvi, 1979). In copper, the lattice constant $a = 3.61$ Å. In high fields, especially along the $[1,1,0]$ direction, a 3-$\mathbf{k}$ state, in which the modulation is a superposition of all three $\{1,0,0\}$ vectors, was predicted (Heinilä and Oja, 1993).

The experiments were carried out in the neutron guide hall next to the DR-3 reactor in Risø using a standard two-axis spectrometer (Jyrkkiö et al., 1988, 1989). A two-stage nuclear demagnetization cryostat, especially designed for studies of nuclear magnets by neutron diffraction, was constructed in Helsinki for these experiments. Instead of natural copper, which is an almost equal mixture of ^{63}Cu and ^{65}Cu and which was used in the susceptibility measurements (see Sect. 7), ^{65}Cu was chosen as the sample material because a factor of six is gained in the scattered

neutron intensity this way. Figure 8 shows a block diagram of the experimental arrangement. The neutron beam is first reflected by a graphite monochromator
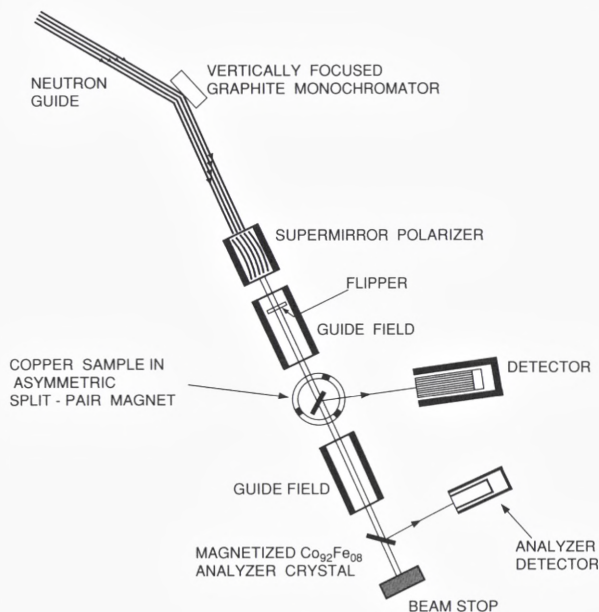

Figure 8. Neutron diffraction setup at Risø for studies of copper using a polarized beam (Jyrkkiö et al., 1988). The cryostat is mounted on the spectrometer turntable. Polarization of the beam is maintained by a constant vertical guide field of 1–2 mT outside the cryostat and by the large field of the asymmetric second stage magnet inside. The flipper coil is used to reverse the beam polarization. A typical flux at the site of the sample is $2 \cdot 10^5$ neutrons $\mathrm{cm}^{-2}\mathrm{s}^{-1}$.

crystal. It then passes through a supermirror polarizer and hits the sample in the cryostat; the scattered neutrons are counted by the detector and the beam polarization is measured from transmitted neutrons by the analyzer.

The cryostat, mounted on a turntable, and the detector attached to it could be moved independently in the scattering plane before an experiment was started. The sample must be positioned so that the particular plane in the reciprocal space, which is accessible to neutron diffraction measurements, contains the **k**-vectors of

the most probable spin structures in the magnetically ordered states. Because of the limited time available for experiments in the ordered state, a single crystal specimen is neccessary for a reasonable statistical accuracy. It should be noted that the external magnetic field during the initial neutron diffraction experiments on copper was in the $[0, -1, 1]$ direction of the crystal, whereas the susceptibility measurements in Helsinki were made with the field in the $[0, 0, 1]$ direction.

Heating caused by the neutron beam is, of course, a drawback in these experiments. The target nuclei are warmed mainly through processes following neutron capture, i.e. by prompt γ-rays and by β-emission from the radioactive intermediate nuclei. Much of the energy released by γ-radiation escapes since the penetration depth is typically a few centimeters; for thin specimens (< 1 mm) the fraction of the absorbed energy is usually less than 5%. In contrast, the charged β-particles dissipate their kinetic energy very effectively in solids; the fraction of β-energy absorbed is typically 50–80% of the total.

In the autumn of 1987, a clear antiferromagnetic (1,0,0) Bragg peak, characteristic of simple Type-I order in an fcc lattice, was observed below $T_N = 60$ nK. The neutron intensity and the static longitudinal susceptibility $\chi_\parallel$, as functions of time after the field had been reduced to zero, are shown in Fig. 9. And there were, indeed, neutrons, and plenty of them during the first few minutes! Since the counter
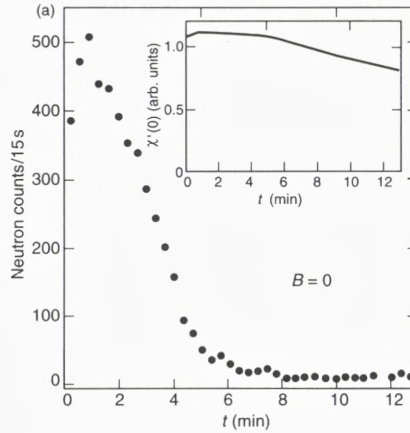

Figure 9. Neutron diffraction and susceptibility data on the nuclear spin system of copper (Jyrkkiö et al., 1988).

was in the $(1,0,0)$ Bragg position of mixed indices (h, k, l) antiferromagnetism in copper had been proven by the neutron diffraction data beyond all doubt!

During the first 4–5 min $\chi_\parallel$, illustrated in the insert of Fig. 9, showed almost a plateau, indicating an antiferromagnetic state; this agrees with the susceptibility experiments in Helsinki (see Fig. 6). The neutron signal displayed, for the first minute, a small increase. After this, during the susceptibility plateau, the neutron count diminished rapidly, indicating a fast decrease in the antiferromagnetic sub-lattice polarization as the nuclei warmed up owing to the spin–lattice relaxation process. The susceptibility settled to an exponential decrease, characteristic of the paramagnetic state, in about 7 min after the end of the final demagnetization. By this time the temperature had increased above $T_N = 60$ nK and the remaining neutron signal had disappeared.

To obtain more information about the phase diagram of nuclearly ordered copper, intensities of scattered neutrons were measured at many non-zero fields. The data, showing variations of the neutron count and of the nuclear susceptibility as functions of time after reaching the final field, are presented in Fig. 10.

At $B = 0.04$ mT, the qualitative behaviour of the neutron count is similar to that at $B = 0$, but the intensity is less. The susceptibility, too, is similar in both fields. At $B = 0.08$ mT, the neutron intensity was further reduced; the susceptibility had a small maximum at 1 min, but it then reached a plateau and started to bend after 6 min towards its final paramagnetic behaviour. At $B = 0.10$ mT, the susceptibility shows, in contrast, a clear increase for the first 4 min, whereas the neutron intensity is almost zero during the entire experiment.

At $B = 0.12$ mT, the neutron data are drastically different from the results at lower fields. The intensity was very high immediately after the final field had been reached and showed no increase but a very rapid decrease at the beginning of the experiment; after about 2.5 min no neutron signal was observable. The susceptibility increased almost 20% during the first 4 min. The neutron count thus disappeared clearly before the system was at T_N, which was reached approximately at the susceptibility maximum.

At $B = 0.16$ mT the characteristics were similar to those at zero field. The neutron intensity was very high initially, as at $B = 0.12$ mT, but it now decreased much more slowly. The disappearance of the count was coexistent with the maximum of $\chi_\parallel$. The behaviour of the susceptibility was qualitatively the same as at $B = 0.10$ and 0.12 mT, showing first a clear increase. In still higher fields no drastic changes happened: At $B = 0.20$ and 0.24 mT, the neutron signal was qualitatively the same as at $B = 0.16$ mT, but the intensity was smaller, especially at 0.24 mT. The susceptibility increase at $B = 0.16$ mT was reduced to a plateau at $B = 0.20$ mT and at $B = 0.24$ mT, only a decreasing slope was observed. Finally, at $B = 0.30$ mT (not shown in Fig. 10), no signs of ordering were seen, neither in
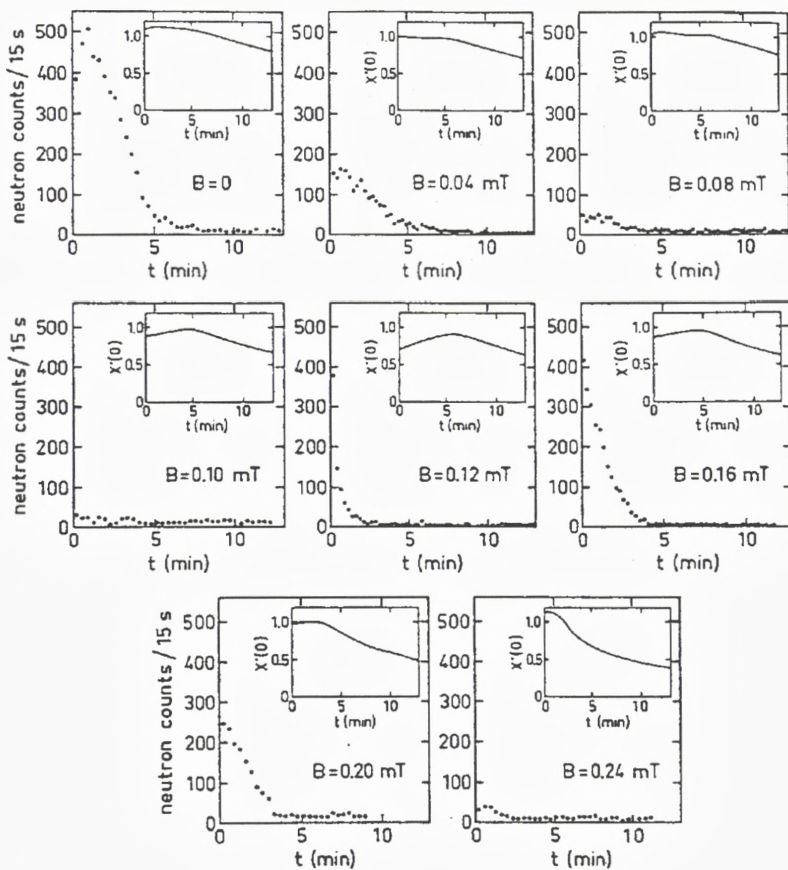
Figure 10. Integrated neutron intensity measured for copper at the (1,0,0) Bragg position and the static susceptibility $\chi'(0)$ (in arbitrary units) as functions of time after final demagnetization to the field indicated on each frame (Jyrkkiö et al., 1988).

the neutron intensity nor in the susceptibility signal.

The neutron data above $B \geq 0.16$ mT suggest that, at elevated fields, the nuclear spins tilt towards B and that, thereby, the contribution to the antiferromagnetic peak becomes weaker. By extrapolating to the field at which the neutron intensity disappeared, the critical field $B_c = 0.25$ mT was obtained; this value is the same as was observed in the susceptibility measurements (Huiku et al., 1986). The drastic change in the neutron intensity between $B = 0.08$ and 0.12 mT indicates a phase transition at about $B = 0.10$ mT.

The most interesting observation was that at the (1,0,0) Bragg reflection a lot of neutrons were seen in low fields and also in fields near 0.16 mT but that in-between, around 0.10 mT, there were very few scattered neutrons. At 0.12 mT many counts were recorded at first but the neutrons disappeared rapidly. The intriguing question was: What about neutrons of the in-between region, where the spins clearly were ordered according to susceptibility measurements?

So the Risø group decided to start looking at other positions in the reciprocal lattice for the missing neutron intensity. But this was not so easy! In conventional neutron diffraction experiments one can scan the reciprocal space automatically for days and observe the peaks as they go by, but in this case the total time available for measurements was about 5 min after demagnetization. And it took at least two days before the sample was ready again for the next experiment! So one had to think carefully where to look for the missing neutrons; it would have taken much too long to map out all regions of the reciprocal space. Fortunately, theoretical calculations by Lindgård (1988) helped in planning the experiments.

Success came in 1989 when four new but equivalent antiferromagnetic Bragg peaks, $(1, \frac{1}{3}, \frac{1}{3})$, $(1, -\frac{1}{3}, -\frac{1}{3})$, and $\pm(0, -\frac{2}{3}, -\frac{2}{3})$, were found (Annila et al., 1990, 1992). It was unexpected that the order proved to be simply commensurate with a three-sublattices structure, not observed previously in any fcc antiferromagnets. The discovery was made when the reciprocal lattice was searched along the high symmetry directions; this is the first time that conventional scanning was employed at nanokelvin temperatures.

From the neutron count vs. time curves an intensity contour diagram was constructed; the result is shown in Fig. 11. Three maxima were found: at $B = 0.09$ mT for the $(1, \frac{1}{3}, \frac{1}{3})$ reflection and at $B = 0$ and $B = 0.15$ mT for the $(1, 0, 0)$ reflection. The $(1, \frac{1}{3}, \frac{1}{3})$ signal was strongest when the $(1,0,0)$ signal was weakest and vice versa, implying the presence of three distinct antiferromagnetic phases in copper. The neutron data are thus in excellent agreement with earlier susceptibility measurements (see Fig. 7). The reason for the rapid disappearance of the $(1,0,0)$ neutron signal at 0.12 mT (see Fig. 10) was probably that the high field $(1,0,0)$ phase, formed immediately after the field had been reduced to $B_C = 0.25$ mT, was still changing to the $(1, \frac{1}{3}, \frac{1}{3})$ phase. A remarkable reature of the phase diagram of
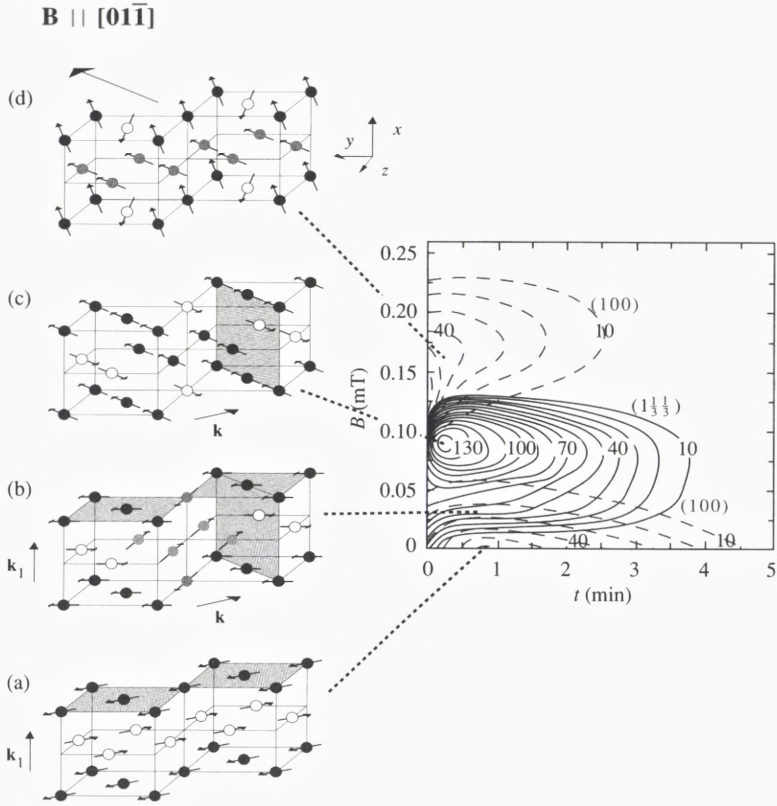
Figure 11. At right: Neutron intensity contour diagram of copper for the $(1, \frac{1}{3}, \frac{1}{3})$ (solid curves) and $(1, 0, 0)$ (dashed curves) Bragg reflections as functions of time (i.e. of temperature) and the external magnetic field. The number of neutrons collected per second is marked on the contours (Annila et al., 1990). At left: Spin structures of copper for the $[0, 1, -1]$ alignment of the magnetic field. (a) $B = 0$: antiferromagnetic $\mathbf{k}_1 = (\pi/a)(1, 0, 0)$ structure consisting of alternating ferromagnetic planes. (b) $0 < B < B_c/3$: Coexistence of structures with ordering vectors $\mathbf{k}_1 = (\pi/a)(1, 0, 0)$ and $\mathbf{k} = \pm(\pi/a)(0, \frac{2}{3}, \frac{2}{3})$, illustrated for $B = 0.17 B_c$. The $(0, \frac{2}{3}, \frac{2}{3})$ and $(1, \frac{1}{3}, \frac{1}{3})$ reflections are equivalent under fcc symmetry. (c) $B = B_c/3$: Left-left-right structure with $\mathbf{k} = \pm(\pi/a)(0, \frac{2}{3}, \frac{2}{3})$ order. (d) High field configuration with three ordering vectors: $(\pi/a)(1, 0, 0)$, $(\pi/a)(0, 1, 0)$, and $(\pi/a)(0, 0, 1)$. The spin structures, which are consistent with the neutron diffraction data, were drawn according to theoretical calculations by Viertiö and Oja (1992).

copper is its complexity.

An obvious extension to the experiments described so far was to examine the phase diagram when the external magnetic field was aligned along the other main crystallographic axes, besides the $[0, -1, 1]$ direction. A number of very successful experiments were made at different field alignments in Risø (Annila et al., 1992). The observed antiferromagnetic states were bounded by the second order critical field line; the $B_c(T)$ curve was determined from the neutron diffraction and susceptibility data. In fields between 0.10 and 0.20 mT, the $(1,0,0)$ order was strong over a wide span of directions around $\mathbf{B} \parallel [1,0,0]$ and over a narrower angular region about $\mathbf{B} \parallel [0,1,1]$. There was also pure $(1,0,0)$ order near the origin in fields below 0.01 mT.

The susceptibility measurements in Helsinki were made along the $[0,0,1]$ field direction; the three phases, AF1, AF2, and AF3, predicted by the data (see Fig. 7), were reproduced by the experimental neutron diffraction results. The $(1, \frac{1}{3}, \frac{1}{3})$ phase had strong maxima around 0.07 mT, both in the $[1,0,0]$ and the $[0,1,1]$ field directions, but in between the intensity was somewhat less. The ordering vector for the $\mathbf{B} \parallel [1,1,1]$ direction was the main puzzle: There was a large antiferromagnetic region with no neutron intensity! In spite of considerable efforts to find a new Bragg reflection in this field direction, no neutrons were discovered.

In order to determine the spin structure from the neutron diffraction experiments one needs theoretical guidance. This is, as was mentioned already, because the scattering cross section, unfortunately, does not depend on the direction of the spins in relation to the crystalline axes; only the periodicity of the magnetic lattice can be deduced from neutron diffraction data on antiferromagnetically ordered nuclei. The anisotropic dipolar interaction is too weak to be of use because of the small nuclear magnetic moments. A successful calculation of the selection rules between the various antiferromagnetic phases in copper has been made by Viertiö and Oja (1992, 1993).

A thorough discussion of the many theoretical calculations, by Oja and his group (Oja and Viertiö, 1993; Viertiö and Oja, 1987, 1990, 1993; Heinilä and Oja, 1993, 1996), by Lindgård (Lindgård et al., 1986; Lindgård, 1988, 1992), and by Frisken and Miller (1986, 1988), is given in the long review of Oja and Lounasmaa (1997). A striking feature of the phase diagram of copper is the strong coexistence of the $(1,0,0)$ and $(1, \frac{1}{3}, \frac{1}{3})$ phases along the boundaries. A very clear time and history dependence accompanied every passage through the phase diagram. Oja and Lounasmaa (1997) discuss in detail the kinetics of the phase transitions in copper (see Sect. VII.F. of their review).

9 Susceptibility measurements on silver

The susceptibility measurements on silver, at positive and negative spin temper-
atures, were carried out in Helsinki (Oja et al., 1990; Hakonen et al., 1991, 1992).
The magnetic moment μ of Ag nuclei is about 20 times smaller than that of copper,
which means, since the dipolar interaction goes as μ^2, that more than two orders
of magnitude lower transition temperatures are expected. Figure 12 illustrates the
NMR absorption and emission spectra of silver nuclei measured at $T = 1.0$ nK and
at $T = -4.3$ nK. The imaginary component of susceptibility χ'' has been plotted
against the NMR frequency ν. The data show that instead of absorption, as at
positive temperatures, the system is emitting energy at the Larmor frequency when
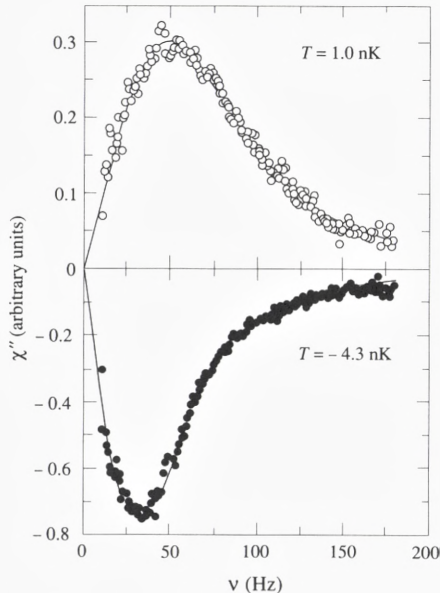the temperature is negative.

Figure 12. NMR absorption and emission spectra for silver, measured in zero mag-
netic field (Hakonen et al., 1990); solid curves are Lorentzian lineshapes. Note the
different vertical scales for the $T = 1.0$ nK and $T = -4.3$ nK data.

In Fig. 13 the absolute value of the inverse magnetic susceptibility $|1/\chi'(0)|$ of
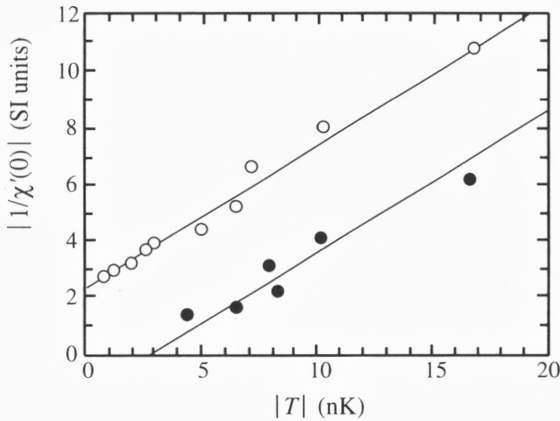silver, calculated from the Kramers–Kronig relation, see Eq. (16), is plotted as a

Figure 13. Absolute value of the inverse static susceptibility $|1/\chi'(0)|$ vs. absolute value of temperature for silver, measured at $T > 0$ (o) and at $T < 0$ (•) (Hakonen et al., 1990).

function of $|T|$ in nanokelvins. We note that at positive temperatures one obtains a straight line with an intercept on the left side of the $|1/\chi'(0)|$-axis. This behaviour is typical and indicates that silver tends to antiferromagnetic order when $T \to +0$. At negative temperatures the intercept is on the right side of the $|1/\chi'(0)|$-axis which shows that, when $T \to -0$, the spin system of silver nuclei prefer ferro-magnetic order, as expected (see Sect. 3); the Néel and Curie points, however, were not reached in these first experiments. The data, both at $T > 0$ and at $T < 0$, followed the Curie–Weiss law

$$\chi = C/(T - \theta) \tag{21}$$

down to the lowest experimental temperatures.

Final success came in 1991. When the static susceptibility was measured as a function of time, a small maximum or, at least, a kink was seen. Such data, depicted in Fig. 14, showed that the nuclear spin system of silver had reached the antiferromagnetic state. In zero field, the measured Néel point was $T_N = 560$ pK. This is the lowest transition temperature that has ever been recorded.

Subsequently, spontaneous nuclear order was produced at negative spin tem-peratures as well. This is shown in Fig. 15 which illustrates the static susceptibility of silver as a function of the nuclear spin polarization measured in zero field (o) and at a 5 μT field oriented perpendicular ($\triangle$) and parallel ($\times$) to the sample foils. The crossing of the two lines is identified as the transition point to the ferromagnetic
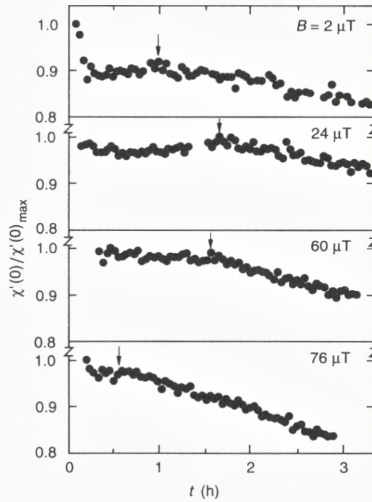
Figure 14. Static susceptibility $\chi'(0)$ of silver nuclei as a function of time after demagnetization to four different external magnetic fields (Hakonen et al., 1991). Each set of data is scaled by the maximum susceptibility $\chi'(0)_{max}$ for that run. Small arrows indicate the transition point from the ordered to the paramagnetic phase.

state. Owing to the rounding of the $\chi(p)$ vs. p curve, one obtains for the critical polarization, in zero field and in 5 μT, the value $p_c = 0.49 \pm 0.05$ which corresponds to $S_c/(R \ln 2) = 0.82 \pm 0.035$.

At $B = 0$, the magnetic susceptibility of silver spins was found to saturate at $\chi_{sat} = -1.05$ (see Fig. 15), which is a typical value for ferromagnetic ordering into a domain state, caused by dipolar interactions. Within the scatter of the data, the critical spin polarization was constant below 5 μT, both for magnetic fields parallel and perpendicular to the sample foils. Using the linear, experimentally observed relationship of Eq. (19) between the inverse polarization and temperature, the Curie point $T_C = -1.9 \pm 0.4$ nK was obtained.

The magnetic field vs. entropy diagram of silver, for positive and negative spin temperatures, is shown in Fig. 16. The critical entropy is lower for $T > 0$ than for $T < 0$. The difference reflects frustration (Binder and Young, 1986) of anti-ferromagnetic interactions as well as the influence of dipolar forces which favour ferromagnetism. The critical field B_c of the ferromagnetic phase is determined by the strength of dipolar forces, while B_c of the antiferromagnetic state is caused by the magnitude of the exchange energy. At negative spin temperatures it was
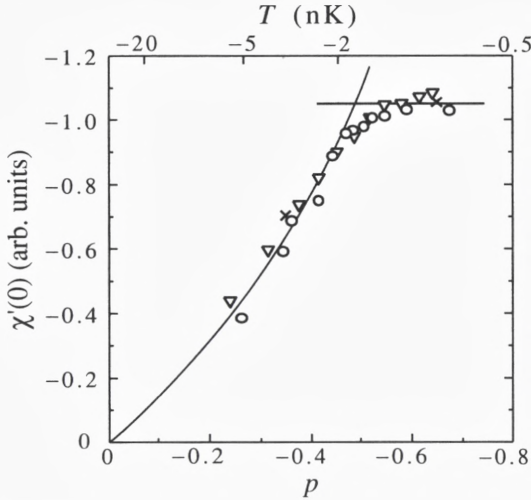
Figure 15. Static susceptibility $\chi'(0)$ of silver vs. polarization p at $T < 0$ (Hakonen et al., 1992). The fitted curve represents the Curie–Weiss law and the straight horizontal line corresponds to the saturation value of susceptibility in the ordered state as predicted by the mean-field theory. An approximate temperature scale is shown at top.

estimated that the critical field $B_c = -\mu_0 M_{\mathrm{sat}}/\chi_{\mathrm{sat}} = 40\ \mu$T at zero temperature; this value was used when drawing the low entropy end of the transition curve for the ferromagnetic phase. At $T = +0$, $B_c \approx 100\ \mu$T.

The saturation of susceptibility to -1 (see Fig. 15) in the ordered state at $T < 0$ can be explained only by the formation of domains, since otherwise χ_{sat} would diverge at T_{C} (Viertiö and Oja, 1992). Instead of needles, as at $T > 0$, plate-like domains are expected when energy is maximized at $T < 0$. The size of the domains is large compared to the interatomic spacing but small with respect to the dimensions of the sample. The direction of magnetization $\mathbf{M}$ is degenerate, but the tangential component of $\mathbf{M}$ has to be continuous and the perpendicular component must change sign across a domain wall. Moreover, the total magnetization has to satisfy the condition $\chi_{\mathrm{sat}} \approx -1$.

The measured critical entropy, $S_c = 0.82R\ln 2$ at $T < 0$, is higher than the value for the Heisenberg model, $S_c = 0.66R\ln 2$, which indicates that, even though the Ruderman–Kittel exchange is dominating in silver, the dipolar interaction substantially aids in the ordering process at $T < 0$.
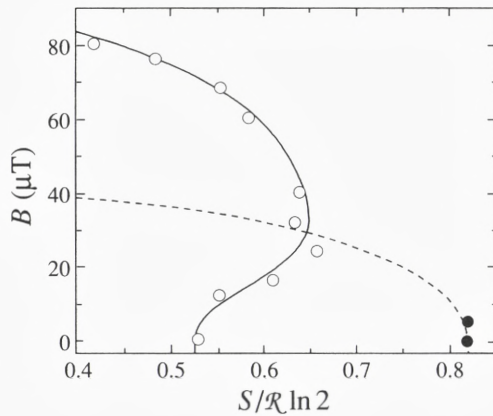
Figure 16. Magnetic field vs. reduced entropy diagram of silver at positive (full curve) and at negative (dashed curve) spin temperatures (Hakonen et al., 1992). At $T > 0$, a long extrapolation to $S = 0$ gives $B_c \approx 100~\mu T$; the forward "bulge" has not been explained so far.

10   Neutron diffraction on silver

Again, by means of NMR measurements it is not possible to verify the details of the spin structure in silver. Experiments employing scattering of neutrons are necessary, as in copper (see Sect. 8), for this purpose. Tuoriniemi et al. (1995) have recently observed long-range nuclear antiferromagnetic order by neutron diffraction in a single crystal of silver at $T > 0$. For this research the sample again had to be isotopically pure, since [107]Ag (51.8%) and [109]Ag (48.2%) in natural silver have opposite signs of the spin dependent scattering coefficient b, see Eq. (20), strongly depressing the coherent neutron signal indicating alignment of nuclear spins. 99.7% enriched material of [109]Ag was used to grow the $0.7 \times 12 \times 25$ mm[3] single crystal. The $[1, -1, 0]$ axis was parallel to the longest edge of the specimen, which was mounted upright in the cryostat. The plane accessible for neutron diffraction studies was thus spanned by the crystallographic axes $[0, 0, 1]$ and $[1, 1, 0]$.

The experiments were performed at the BER II reactor of the Hahn–Meitner Institut in Berlin (Steiner et al., 1996; Lefmann et al., 1997; Nummila et al., 1997). The setup for these measurements was similar to that used earlier in Risø (see Fig. 8). The diffracted neutrons ($\lambda = 4.4$ Å) were recorded at a fixed scattering angle by a single counter or by a position-sensitive detector. Another counter measured the transmitted neutrons. Experiments could be performed either with unpolarized or

polarized beams.

The sample was cooled in the cascade nuclear demagnetization cryostat illustrated in Fig. 3. New methods of neutron thermometry, based on Eq. (10) which gives the relation between p and T, were developed for these experiments (Lefmann et al., 1997). The neutron beam was the main source of heat, reducing τ_1 to 3 h. Prior to demagnetizations, the diffractometer was aligned to the $(0, 0, 1)$ Bragg position of a Type-I antiferromagnet in an fcc lattice. The build-up of the nuclear polarization could be monitored in situ by measuring transmission of polarized neutrons through the sample (Tuoriniemi et al., 1997).

Figure 17 shows two sets of neutron diffraction data on silver. The nuclei were demagnetized into the ordered state with the final external field $B = 500\ \mu$T along the $[0, 0, 1]$ or $[0, 1, 0]$ directions, and neutron counts were monitored while the spin system warmed up. A clear $(0, 0, 1)$ reflection appeared when demagnetization was
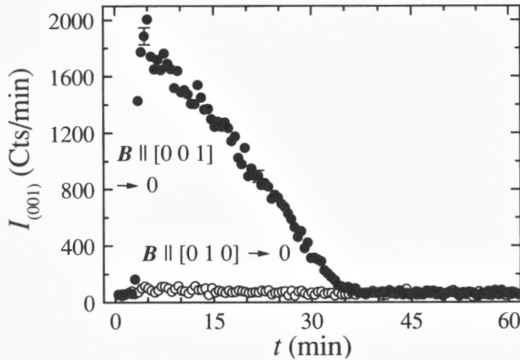

Figure 17. Time dependence of neutron intensity at the $(0, 0, 1)$ Bragg position (Tuoriniemi et al., 1995). The initial polarization $p = 0.91 \pm 0.02$ was first recorded in a 500 μT field in the paramagnetic phase, whereafter **B**, in the $[0, 0, 1]$ or $[0, 1, 0]$ direction (filled and open circles, respectively), was reduced to zero at $t = 3$ min. The $(0, 0, 1)$ neutron signal appeared immediately below $B_c = 100\ \mu$T, but only when **B** $\parallel [0, 0, 1]$ during demagnetization. The silver spins warm up more slowly than the spins of copper (see Fig. 9) because τ_1 is longer in Ag than in Cu.

made with **B** parallel to the corresponding ordering vector $\mathbf{k} = (\pi/a)(0, 0, 1)$. The presence of this signal, with mixed Bragg indices, again provided clear proof for Type-I antiferromagnetic order in silver. But the neutron peak was essentially absent when the ordered state was entered from the perpendicular direction $[0, 1, 0]$,

although in zero field the three **k**-vectors, producing the $\{1,0,0\}$ reflections, are equivalent owing to the cubic symmetry. In this respect, the situation in silver was different from that observed in copper. In Ag, no domains of the other two symmetry-equivalent **k** vectors, $(\pi/a)(0,1,0)$ and $(\pi/a)(1,0,0)$, formed during warmup in zero field. It was concluded that the observed antiferromagnetic state had a simple single-**k** structure and that the stable spin configuration was created during demagnetization. The phase transition was apparently of second order.

To demonstrate that the observed intensity indeed was a Bragg peak a position-sensitive detector was used. Time development of the neutron diffraction pattern is shown in Fig. 18. The lineshape of the antiferromagnetic peak is Gaussian, and its width is comparable to that of the $(0,0,2)$ second-order lattice reflection. The critical entropy of ordering was found from the data on transmitted neutrons. Polarization could be deduced from the count rate when the nuclei were aligned
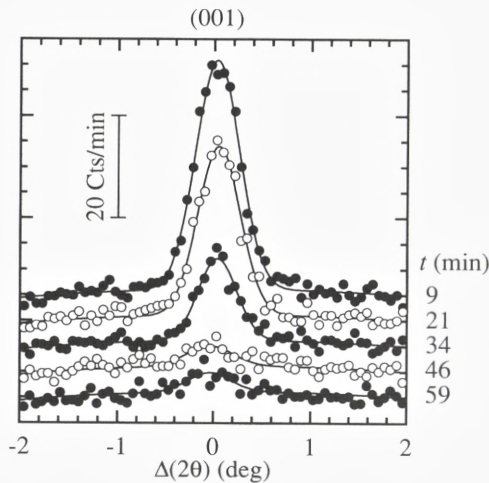

Figure 18. Time evolution (from top to bottom) of the antiferromagnetic Bragg peak of silver in a 30 μT field (Tuoriniemi et al., 1995). The 2θ-dependence of scattered neutrons is plotted as a function of deviation from the $(0,0,1)$ position. The bell-shaped curves are Gaussian fits to counts collected during 6 min intervals; only every second spectrum is shown. For clarity, the successive curves are offset vertically by 5 cts/min. As long as neutrons were observed the spin temperature was below $T_N \approx 700$ pK.

by a magnetic field in the paramagnetic state, because the neutron absorption is spin-dependent. For this purpose the 500 μT field was applied at the beginning of each experiment. The orientation of this field also determined the direction along which the ordered state was entered. Polarization was measured again a few times after the disappearance of the antiferromagnetic signal, and the critical value p_c was found by interpolation. The nuclear entropy S could then be calculated from the paramagnetic polarization in 500 μT, see Eq. (11). The field changes were nearly adiabatic ($\Delta S \approx 0.01 R \ln 2$ for each sweep between $B = 0$ and 500 μT), whereby the entropy was known in all fields. In the zero-field experiment of Fig. 18, $p_c = 0.75 \pm 0.02$ was obtained, corresponding to $S_c = (0.54 \pm 0.03) R \ln 2$. The Néel temperature was estimated as $T_N = (700 \pm 80)$ pK. This is higher than 560 pK for natural silver (see Sect. 9) because the strength of the mutual interactions is scaled by the magnetic moment squared, i.e. by a factor of 1.15.

It was interesting to examine the response of the spin system to an applied magnetic field and to its alignment. With **B** $\parallel [0,0,1]$, the antiferromagnetic intensity decreased smoothly when approaching the critical field of 100 μT. The spins thus lined up continuously towards the increasing field, as in the spin-flop phase of a weakly anisotropic antiferromagnet. No field-induced phase transitions within the ordered state could be identified. Repetitive field cyclings across the phase boundary to the paramagnetic state did not produce any appreciable hysteresis nor deviations from adiabaticity; therefore, the transition was presumably of second order.

The effect of field orientation was investigated by rotating **B** ($B = 50$ μT) with respect to the crystalline axes. In a turn extending from $[-1, -1, 0]$ to $[1, 1, 0]$, the $(0, 0, 1)$ neutron signal was visible when the magnetic field was aligned between the axes $[-1, -1, 1]$ and $[1, 1, 1]$. Within this arc, the intensity did not vary much. An additional field rotation was made in a perpendicular plane; the neutron signal disappeared about $10°$ beyond the $[0, -1, 1]$ axis. These experiments showed that an antiferromagnetic spin structure with **k** $= (\pi/a)(0, 0, 1)$ was formed when **B** was around the $[0, 0, 1]$ direction within a cone of $110°$ full opening. Further measurements were made for $B \parallel [0, 0, 1]$ and for $B \parallel [-0.8, -0.8, 1]$; the latter direction is close to the edge of the cone. The allowed field directions thus span a double cone, barely reaching all eight of the $\{1, 1, 1\}$ directions. Apart from the $(0,0,1)$ reflection, the $(\frac{1}{2}, \frac{1}{2}, \frac{1}{2})$ Bragg peak of Type-II order and the $(0, \frac{2}{3}, \frac{2}{3})$ neutron signal seen in copper were also searched for, but with negative results.

On the basis of these experiments, the magnetic field vs. entropy diagram of silver was constructed. The result is shown in Fig. 19. There is good agreement with earlier susceptibility data (see Sect. 9) on a polycrystalline sample of natural silver. The critical entropy was systematically higher when **B** was near the edge of the cone than when the field was parallel to the central axis. The general features

of the NMR experiments on silver were reproduced with the setup at the Hahn–Meitner Institut in the absence of neutrons, but it is somewhat disturbing that the characteristic susceptibility plateau (see Fig. 14) totally disappeared when the neutron beam was on.

The neutron diffraction data on silver can be compared with theoretical work. The observed Type-I ordering vector had been predicted on the basis of measured and calculated interaction parameters (Harmon et al., 1992). The spin structure of the ground-state has been determined by perturbation analysis (Heinilä and Oja, 1993) and by Monte Carlo simulations (Viertiö and Oja, 1992). Both methods indicate that, when $\mathbf{B} \parallel [0,0,1]$, a single-$\mathbf{k}$ configuration is stable in low magnetic fields $B \leq 0.5B_c$. A structure with $\mathbf{k} = (\pi/a)(0,0,1)$ was expected, in perfect agreement with the experimental observations. In higher fields, however, a triple-$\mathbf{k}$ configuration had been predicted. According to the simulations this structure is stable only if $\mathbf{B}$ is within a narrow cone around the $[1,0,0]$-type axes. The measurements, however, did not provide any evidence for the triple-$\mathbf{k}$ state, although it was searched for in field-sweep and field-rotation experiments (Tuoriniemi et al., 1995). In contrast to the complex situation in copper (see Fig. 11), the ordered phase in silver seems to consist of a single Type-I antiferromagnetic structure.

It is not clear which mechanism prevented domains with equivalent $\mathbf{k}$-vectors from forming in $\mathbf{B} = \mathbf{0}$. The fact that the results depended on the direction of the external magnetic field during demagnetization shows that the small dipolar force is strong enough in silver to break isotropy of the RK interaction, see Eqs. (4) and (5), and lock the nuclear spins perpendicular to the corresponding $\mathbf{k}$-vector (Viertiö and Oja, 1992). Perhaps the intermediate $(1, \frac{1}{3}, \frac{1}{3})$-phase in copper (see Fig. 11) effectively "mixed" the spins during demagnetization, allowing different $(0,0,1)$ domains to form.

Neutron diffraction studies of silver at negative spin temperatures have not been attempted so far.

11 Experiments on rhodium

The Helsinki results on rhodium metal, at $T > 0$ and at $T < 0$, are quite interesting as well (Hakonen et al., 1993; Vuorinen et al., 1995). The absolute value of the inverse static susceptibility, as a function of $|T|$, is plotted in Fig. 20. The upper line represents, at $T > 0$, the antiferromagnetic Curie–Weiss law, see Eq. (21), with $\theta = -1.4$ nK. At $T < 0$, the corresponding ferromagnetic dependence is displayed by the dashed line. At low temperatures the Curie–Weiss approximation is known to deviate, especially when $I = 1/2$, from the more accurate results based on high-T series expansions. For negative temperatures, the measured data show
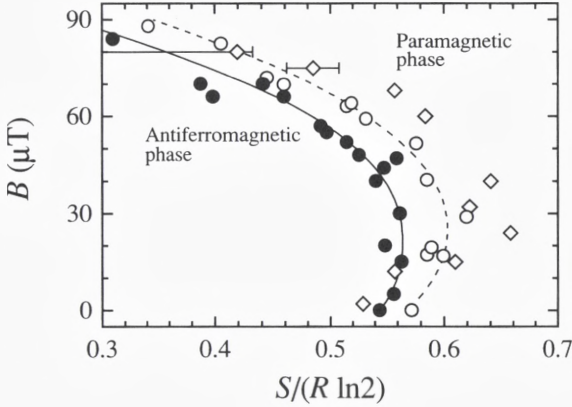
Figure 19. Magnetic field vs. entropy diagram of silver at $T > 0$, based on neutron data (Tuoriniemi et al., 1995). The counts were recorded with $B \parallel [0,0,1]$ (•) and $B \parallel [-0.8, -0.8, 1]$ (∘). Previous NMR data (Hakonen et al., 1991) are included for comparison (◇). The critical temperature $T_N \approx 700$ pK in zero field.

a crossover from ferro- to antiferromagnetic behaviour at about -5 nK. This indicates that the energy of nuclear spins in rhodium is both minimized and maximized by antiferromagnetic order.

The NMR data on rhodium at $T > 0$ and at $T < 0$ extend to roughly a factor of two closer to the absolute zero than the temperatures reached in the experiments on silver (see Fig. 13). Phase transitions, however, were not seen in rhodium, even though the experimentally achieved polarizations, $p = 0.83$ and $p = -0.60$ at $T > 0$ and at $T < 0$, respectively, were higher than those needed for spontaneous ordering in silver. This is an indication that in Rh the nearest and next-nearest neighbour interactions are of almost equal magnitude but of opposite sign. The transition temperature is thus very low, which explains why no ordering was detected in spite of the record-low, 280 pK, and "record-high", -750 pK, spin temperatures produced in rhodium.

The susceptibility data on Rh can be used to extract the nearest and next-nearest neighbour Heisenberg interaction coefficients J_1 and J_2; the values obtained from experimental results are $J_1/h = -17$ Hz and $J_2/h = 10$ Hz. Molecular-field calculations have been employed to predict the regions of different types of magnetic ordering in the J_2 vs. J_1-plane. This is illustrated in Fig. 21. In an fcc lattice, ferromagnetism is present only when $J_1 > 0$ and $J_2 > -J_1$. The antiferromagnetic part is divided to AF1, AF3, and AF2 regions at $J_2 = 0$ and at $J_2 = J_1/2$, so that
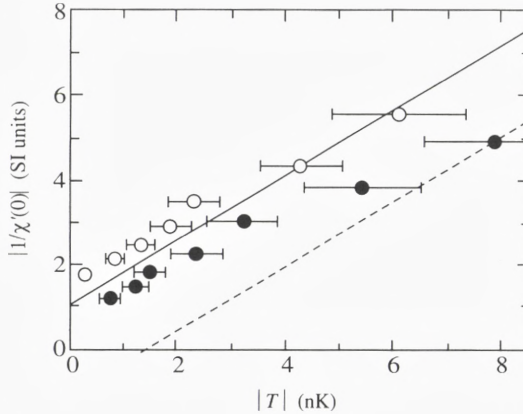
Figure 20. Absolute value of the inverse static susceptibility $|1/\chi'(0)|$ vs. absolute value of temperature for rhodium nuclei, measured at $T > 0$ (○) and at $T < 0$ (●) (Hakonen et al., 1993). The error bars denote the 20% uncertainty in the measurements of temperature.

rhodium lies well inside the AF1 region at $T > 0$. At $T < 0$ the signs of the J's are effectively reversed, and the corresponding point in Fig. 21 is located in the ferromagnetic sector, but rather close to the AF2 antiferromagnetic border.

Spin–lattice relaxation times, measured at positive and negative temperatures, have been investigated in Helsinki on rhodium (Hakonen et al., 1994): Iron impurities shorten substantially τ_1 in small magnetic fields. Previously, this effect has not been studied much in the microkelvin range and below (see, however, Tuoriniemi et al., 1997), in spite of the significance of τ_1 for reaching the lowest nuclear temperatures. A clear difference in τ_1 at $T > 0$ and $T < 0$ was observed.

The spin–lattice relaxation time τ_1 is defined by the relationship

$$d(1/T)/dt = -(1/\tau_1)(1/T - 1/T_e). \tag{22}$$

Since $T_e \gg T$ and $p \propto 1/T$, one finds the exponential time dependence $d\ln p/dt = -(1/\tau_1)$, i.e., $p \propto \exp(-t/\tau_1)$. Experimental data are shown in Fig. 22. The spin–lattice relaxation time was found by fitting a straight line to about 10 successive data points on the $\log p$ vs. t plot. The results show clearly that τ_1 is longer at $T < 0$ than at $T > 0$ and that the spin–lattice relaxation slows down with decreasing polarization when $T > 0$. The most striking result of these relaxation time measurements is that τ_1 is longer when $T < 0$. This finding is difficult to explain since all theories predict equal behaviour on both sides of the absolute zero.
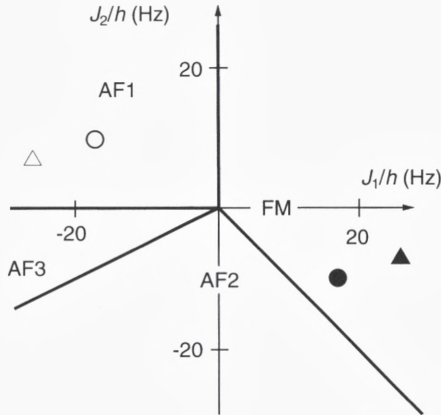
Figure 21. Molecular field calculations for Ag and Rh spins (Vuorinen et al., 1995). Antiferromagnetic regions are denoted by AF1, AF2, and AF3, respectively, whereas FM refers to ferromagnetic ordering. Interaction parameters for rhodium (o) and silver (△) spins are plotted in the figure; open and filled symbols refer to positive and negative temperatures, respectively.

The next step is reaching the ordering transitions at $T > 0$ and at $T < 0$ in rhodium. This should not be too difficult a task with the new YKI cryostat.

12 Concluding remarks

The weakest interactions in solids, by far, are between nuclear spins. Consequently, the time scales for the onset of order or changes therein are long, compared to electronic magnets. Many new phenomena thus become experimentally accessible in studies of nuclear magnets. Determination of the ordered ground state requires special low temperature techniques, extending to nano- and even picokelvin temperatures. The magnetic susceptibility and neutron diffraction and transmission experiments on copper and silver, and NMR measurements on rhodium, have revealed the intricacies of spontaneous magnetic ordering phenomena in these simple metals. It has become obvious that nuclear magnets are not just another class of magnetic materials, but represent systems whose properties add new insights to our knowledge of magnetic ordering and the kinetics of phase transitions.

In copper the phase diagram is surprisingly complex (see Fig. 7); hysteresis and time dependent phenomena have been detected. The close competition between the antiferromagnetic exchange interaction and the ferromagnetic dipolar force is
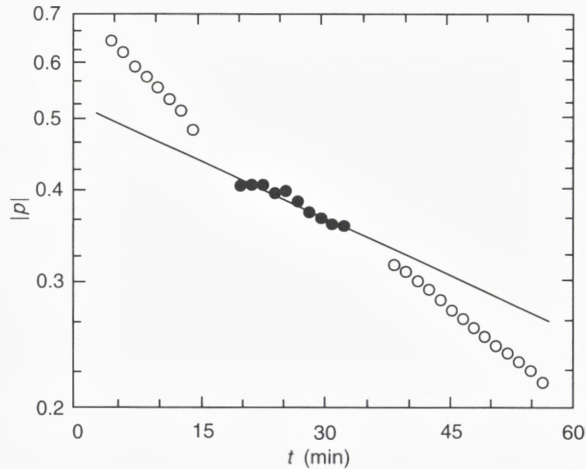
Figure 22. Polarization $|p|$ of rhodium spins as a function of time measured in a magnetic field of 40 μT at $T > 0$ (o) and at $T < 0$ (•) (Hakonen et al., 1994). The straight line is a least-squares fit to the data at $T < 0$.

probably responsible for the complex behaviour of copper. In silver the phase diagram is simpler (see Fig. 16), remarkably stable, but with an unexpected "bulge" at $T > 0$. Successful magnetic susceptibility measurements at negative spin temperatures in silver and rhodium have clarified thermodynamics at $T < 0$.

Research on nuclear magnetism in metals at nano- and picokelvin temperatures continues. With copper there is the mystery (see Sect. 8) of the missing $(1, 0, 0)$ Bragg reflection along the $\{1, 1, 1\}$ field directions. The neutron diffraction work on silver, described in Sect. 10, is not completed; experiments at the Hahn–Meitner Institut continue. More measurements are due in the high symmetry directions $\{1, 1, 0\}$ and $\{1, 1, 1\}$ over the whole range of fields. The stability of magnetic domains in zero field will be investigated as well. Experiments using polarized neutrons, with a full polarization analysis, will be made to determine the directions of the ordered nuclear spins in relation to the crystallographic axes. An ambitious project, also involving polarized neutrons, is to investigate the ferromagnetic structure of silver at negative spin temperatures.

The next goal for the susceptibility measurements in Helsinki is to observe nuclear spin ordering in rhodium. Another experiment which is on the agenda is susceptibility measurements on gold. Here one has the additional bonus that superconductivity might be observed. According to earlier experiments (Buchal et

al., 1982) on alloys rich in noble metals, the superconducting transition temperature for pure gold should be about five orders of magnitude higher than for silver or copper. The problem is to obtain a sufficiently pure specimen so that electronic magnetic impurities would not destroy superconductivity.

Another very promising system is platinum. In this metal there is only one magnetic isotope, ^{195}Pt; the other stable isotopes are nonmagnetic. This means that it is possible to prepare platinum specimens in which the magnetic component varies between zero and 100%. In copper and silver, one cannot change the magnetic concentration because in these metals all stable isotopes have non-integral nuclear spins and, besides, the magnetic moments of the two stable isotopes in both metals are within 7% and 13% of each other, respectively.

In platinum a study of ordering as a function of the magnetic constituent is interesting because the system would provide a very pure model of a spin glass. Unfortunately, however, the properties of platinum are strongly influenced by small concentrations of electronic magnetic impurities. In addition, because of the small value of Korringa's constant, see Eq. (2), $\kappa = 0.03$ sK in Pt, nuclear spins and conduction electrons reach thermal equilibrium quickly, so one might need a three-stage nuclear refrigerator for these experiments.

There are other possibilities as well. For example, the interplay between superconductivity and magnetism could be investigated: By reversing the sign of temperature, the nuclear spin order might be changed from antiferro- to ferromagnetism or vice versa, and the effect of this transformation on the superconducting properties could be investigated. Unfortunately, owing to supercooling, measurements of this type did not succeed in rhodium, even though the conduction electron and lattice temperature in the Helsinki experiments was considerably lower than 325 μK, the critical temperature for superconductivity in rhodium. In AuIn$_2$, superconductivity did not affect nuclear ordering (Herrmannsdörfer et al., 1995). There are several other simple metals for which one can expect important progress in studies of nuclear ordering; these include thallium, scandium, and yttrium. The new YKI cryostat, which has just started operating in Helsinki, and the improvements made in the neutron diffraction setup at the Hahn–Meitner Institut in Berlin will open new possibilities for still more ambitious experiments.

It has been argued, sometimes, that negative temperatures are fictitious quantities because they do not represent true thermal equilibrium in a sample consisting of nuclei, conduction electrons, and the lattice. However, the experiments on silver, in particular, show conclusively that this is not the case. The same interactions produce ferro- or antiferromagnetic order, depending on whether the spin temperature is negative or positive. In fact, the realm of negative spin temperatures offers interesting new possibilities for studies of magnetism in metals.

Acknowledgements

References

Abragam A, 1987: Proc. Roy. Soc. London **412**, 255

Andres K, and Bucher E, 1968: Phys. Rev. Lett. **21**, 1221

Andres K and Lounasmaa OV, 1982: Prog. Low. Temp. Phys. **8**, 221

Annila AJ, Clausen KN, Lindgård PA, Lounasmaa OV, Oja AS, Siemensmeyer K, Steiner M, Tuoriniemi JT and Weinfurter H, 1990: Phys. Rev. Lett. **64**, 1421

Annila AJ, Clausen KN, Oja AS, Tuoriniemi JT and Weinfurter H, 1992: Phys. Rev. B **45**, 7772

Binder K and Young AP, 1986: Rev. Mod. Phys. **58**, 801

Bloembergen N and Rowland TJ, 1955: Phys. Rev. **97**, 1679

Bouffard V, Fermon C, Gregg JF, Jacquinot JF and Roinel Y, 1994: *NMR and More in Honour of Anatole Abragam*, eds. M. Goldman and M. Porneuf (Les Editions de Physique, France) p. 81

Buchal Ch, Mueller RM, Pobell F, Kubota M and Folle HR, 1982: Solid State Commun. **42**, 43

Ehnholm GJ, Ekström JP, Jacquinot JF, Loponen MT, Lounasmaa OV and Soini JK, 1979: Phys. Rev. Lett. **42**, 1702

Ehnholm GJ, Ekström JP, Jacquinot JF, Loponen MT, Lounasmaa OV and Soini JK, 1980: J. Low Temp. Phys. **39**, 417

Frisken SJ and Miller DJ, 1986: Phys. Rev. Lett. **57**, 2971

Frisken SJ and Miller DJ, 1988: Phys. Rev. Lett. **61**, 1017

Goldman M, 1970: *Spin Temperature and Nuclear Magnetic Resonance in Solids* (Clarendon Press, Oxford)

Hakonen PJ and Lounasmaa OV, 1994: Science **265**, 1821

Hakonen PJ, Lounasmaa OV and Oja AS, 1991: J. Magn. Magn. Mater. **100**, 394

Hakonen PJ, Nummila KK, Vuorinen RT and Lounasmaa OV, 1992: Phys. Rev. Lett. **68**, 365

Hakonen PJ, Vuorinen RT and Martikainen JE, 1993: Phys. Rev. Lett. **70**, 2818

Hakonen PJ, Vuorinen RT and Martikainen JE, 1994: Europhys. Lett. **25**, 551

Hakonen PJ, Yin S and Lounasmaa OV, 1990: Phys. Rev. Lett. **64**, 2707

Hakonen PJ, Yin S and Nummila KK, 1991: Europhys. Lett. **15**, 677

Harmon BN, Wang XW and Lindgård PA, 1992: J. Magn. Magn. Mater. **104-107**, 2113

Heinilä MT and Oja AS, 1993: Phys. Rev. B **48**, 7227

Heinilä MT and Oja AS, 1996: Phys. Rev. B **54**, 1

Herrmannsdörfer TP, Smeibidl P, Schröder-Smeibidl B and Pobell F, 1995: Phys. Rev. Lett. **74**, 1665

Huiku MT, Jyrkkiö TA, Kyynäränen JM, Loponen MT, Lounasmaa OV and Oja AS, 1986: J. Low Temp. Phys. **62**, 433

Huiku MT, Jyrkkiö TA, Kyynäränen JM, Oja AS and Lounasmaa OV, 1984: Phys. Rev. Lett. **53**, 1692

Huiku MT and Loponen MT, 1982: Phys. Rev. Lett. **49**, 1288

Jyrkkiö TA, Huiku MT, Lounasmaa OV, Siemensmeyer K, Kakurai K, Steiner M, Clausen KN and Kjems JK, 1988: Phys. Rev. Lett. **60**, 2418

Jyrkkiö TA, Huiku MT, Siemensmeyer K and Clausen KN, 1989: J. Low Temp. Phys. **74**, 435

Kjäldman LH and Kurkijärvi J, 1979: Phys. Lett. **71A**, 454

Koike Y, Suzuki H, Abe S, Karaki Y, Kubota M and Ishimoto H, 1995: J. Low Temp. Phys. **101**, 617

Kurti N, Robinson FN, Simon FE and Spohr DA, 1956: Nature **178**, 450

Lefmann K, Tuoriniemi JT, Nummila KK and Metz A, 1997: Z. Phys. (in press)

Lindgård PA, 1988: Phys. Rev. Lett. **61**, 629

Lindgård PA, 1992: J. Magn. Magn. Mater. **104-107**, 2109

Lindgård PA, Wang XW and Harmon BN, 1986: J. Magn. Magn. Mater. **54-57**, 1052

Lounasmaa OV, 1974: *Experimental Principles and Methods Below 1 K* (Academic Press, London)

Lounasmaa OV, 1989: Physics Today **42**, 26

Lounasmaa OV, Hakonen P, Nummila K, Vuorinen R and Martikainen J, 1994: Physica B **194-196**, 291

Nummila KK, Tuoriniemi JT, Vuorinen RT, Lefmann K, Metz A and Rasmussen FB, 1997: (to be published).

Oja AS, Annila AJ and Takano Y, 1990: Phys. Rev. Lett. **65**, 1921

Oja AS and Lounasmaa OV, 1997: Rev. Mod. Phys. **69**

Oja AS and Viertiö HE, 1993: Phys. Rev. B **47**, 237

Price DL and Sköld K, 1986: in *Neutron Scattering: Methods of Experimental Physics*, eds. K. Sköld and D.L. Price (Academic Press, London) Vol. 23, Part A, p. 1

Purcell EM and Pound RV, 1951: Phys. Rev. **81**, 279

Ramsey NF, 1956: Phys. Rev. **103**, 20

Schröder-Smeibidl B, Smeibidl P, Eska G and Pobell F, 1991: J. Low Temp. Phys. **85**, 311

Slichter, C.P., 1990: *Principles of Magnetic Resonance* (Springer Verlag, Berlin) p. 219

Steiner M, 1990: Physica Scripta **42**, 367

Steiner M, 1993: Int. J. Mod. Phys. B **7**, 2909

Steiner M, Metz A, Siemensmeyer K, Lounasmaa OV, Tuoriniemi JT, Nummila KK, Vuorinen RT, Clausen KN, Lefmann K and Rasmussen FB, 1996: J. Appl. Phys. **79**, 5078

Tuoriniemi JT, Nummila KK, Lefmann K, Vuorinen RT, and Metz A, 1997: Z. Phys. (in press)

Tuoriniemi JT, Nummila KK, Vuorinen RT, Lounasmaa OV, Metz A, Siemensmeyer K, Steiner M, Lefmann K, Clausen KN and Rasmussen FB, 1995: Phys. Rev. Lett. **75**, 3744

Van der Zon CM, Van Velzen GD and Wenckebach WTh, 1990: J. Phys. (Paris) **51**, 1479

Van Vleck JH, 1957: Nuovo Cimento Suppl. **6**, 1081

Viertiö HE and Oja AS, 1987: Phys. Rev. B **36**, 3805

Viertiö HE and Oja AS, 1990: Phys. Rev. B **42**, 6857

Viertiö HE and Oja AS, 1992: J. Magn. Magn. Mater. **104-107**, 915

Viertiö HE and Oja AS, 1993: Phys. Rev. B **48**, 1062

Vuorinen RT, Hakonen PJ, Yao W and Lounasmaa OV, 1995: J. Low Temp. Phys. **98**, 449

Windsor CG, 1986: in *Neutron Scattering: Methods of Experimental Physics*, eds. K. Sköld and D.L. Price (Academic Press, London) Vol. 23, Part A, p. 197